



Bulletin of the Mineral Research and Exploration

<http://bulletin.mta.gov.tr>



ONE OF THE MAIN NEOTECTONIC STRUCTURES IN THE NW CENTRAL ANATOLIA: BEYPAZARI BLIND THRUST ZONE AND RELATED FAULT-PROPAGATION FOLDS

Gürol SEYİTOĞLU^{a*}, Korhan ESAT^a and Bülent KAYPAK^b

^aAnkara University, Dept. of Geological Eng., Tectonics Research Group, Tandoğan, Ankara

^bAnkara University, Dept. of Geophysical Eng., Gölbaşı, Ankara

Research Article

Keywords:

Beypazarı, Blind Thrust, Neotectonics, Earthquake, Central Anatolia, Turkey

ABSTRACT

This paper suggests that the structure known as “Beypazarı flexure / monocline” in the Turkish geology literature should be named as “Beypazarı fault-propagation folds”. Beypazarı, Kilci and Başören blind thrusts together with Erenler back thrust constitute the Beypazarı Blind Thrust Zone which is an active neotectonic structure as indicated by earthquake activity. NW-SE contraction created by the interaction between the North Anatolian Fault Zone, the Kırıkkale-Erbaa Fault Zone and the Eskişehir Fault Zone produced the Eldivan-Elmadağ Pinched Crustal Wedge, the Abdüsselam Pinched Crustal Wedge and the Beypazarı Blind Thrust Zone. These structures take up the internal deformation of the Anatolian Plate.

Received: 27.04.2016

Accepted: 08.09.2016

1. Introduction

Beypazarı flexure (Rondot, 1956; Kalafatçıoğlu and Uysallı, 1964; Kavuşan, 1993a), later known as Beypazarı monocline (Yağmurlu et al., 1988; Demirci, 2000) is one of the important structures in NW central Anatolia. The region between Beypazarı and Çayırhan were mainly investigated by geochemistry oriented studies due to lignite, trona and geothermal resources (Helvacı et al., 1981; Özpeker et al., 1991; Suner, 1993; Kavuşan, 1993b; Karadenizli 1995; Orti et al., 2002; Özçelik, 2002; Özgüm et al., 2003; Özçelik and Altınsoy, 2005; Diker et al., 2006; Şener, 2007; Garcia-Veigas et al., 2013; Bechtel et al., 2014; Pehlivanlı et al., 2014). During trona mining, the problems about rock mechanics and hydrogeology were also investigated (Aksoy et al., 2006; Apaydın, 2010). Structural geology / tectonics oriented studies, however, are very limited (Yağmurlu et al., 1988; İnci, 1991; Kavuşan, 1993a; Demirci, 2000).

Yağmurlu et al. (1988) suggested that the Beypazarı-Çayırhan Neogene basin was initiated in Early Miocene under extensional tectonic regime. After Pliocene the basin deformed under NW-SE contraction that is created by the interaction between

the right lateral North Anatolian Fault and the Eskişehir Fault. This NW-SE contraction produces the NE-SW trending thrust faults, folding axes and monoclines that most prominent one is named as the Beypazarı-Çayırhan monocline.

Kavuşan (1993a), however, proposed that in every stage of the Beypazarı-Çayırhan basin, NW-SE contraction was operational. It is noted that the effect of fractures is fading towards the young strata and turns to folding. Demirci (2000) determined three different regional tectonic phases, E-W contraction, N-S contraction and final extension. It is also noted that the final extension is not observed around Beypazarı (Demirci, 2000, p.142).

Esat and Seyitoğlu (2010), Esat (2011), Esat et al. (2016) and Esat et al. (2017) suggested that the NW-SE contractional tectonic regime is developed in the triangle-like area between the North Anatolian Fault Zone, the Eskişehir Fault Zone and the Kırıkkale-Erbaa Fault Zone (Figure 1). Due to the interaction of these fault zones, the Eldivan-Elmadağ Pinched Crustal Wedge (EPCW) is developed and mapped in detail (Seyitoğlu et al., 2000; 2009). Abdüsselam Pinched Crustal Wedge (APCW) is recognized more

* Corresponding author: Gürol Seyitoğlu, seyitoglu@ankara.edu.tr
<http://dx.doi.org/10.19111/bmre.42566>

recently (Esat, 2011; Esat et al., 2017). The third structure observed in the triangle-like area is the Beypazarı Blind Thrust Zone (BBTZ) which is the subject of this paper (Figure 1).

2. The Stratigraphy of Beypazarı-Çayırhan Neogene Basin

According to Helvacı (2010) who updated previous studies with new data, Late Cenozoic stratigraphy starts with Paleocene Kızılçay Group having red conglomerates and claystones. Unconformably overlain Çoraklar formation having lower and upper lignite layers is composed of volcanoclastic conglomerates, sandstones, siltstones and mudstones. Overlying Hırka formation contains mudstone, claystone, bituminous shale, trona, grey shale, calcareous shale, dolomitic limestone, siltstone, intraformational conglomerate and tuff. The tuff in the Hırka formation has been dated (K-Ar) as

21.5 ± 0.9 Ma (Early Miocene). Hırka formation interfingers with Akpınar formation having alternation of siliceous limestone, chert, tuff, claystone and mudstone. Conformably overlain Çayırhan formation is composed of greenish claystone, mudstone, marl and sandstone layers. Mudcracks and salt crystals are observed to be common. Bozbelen formation is made up of reddish conglomerate, sandstone and mudstone. Kirmir formation, having green claystone with gypsum layers and bedded gypsum, laterally and vertically pass into Bozbelen formation and Sarıyer Limestone which are white, thick-bedded micritic limestone. Teke volcanics interfinger with Beypazarı sequence (Helvacı, 2010) (Figure 2).

3. Fault-Propagation Folding

It would be useful to give a brief summary about fault-propagation folding before presenting the field observations in the Beypazarı area. There are two

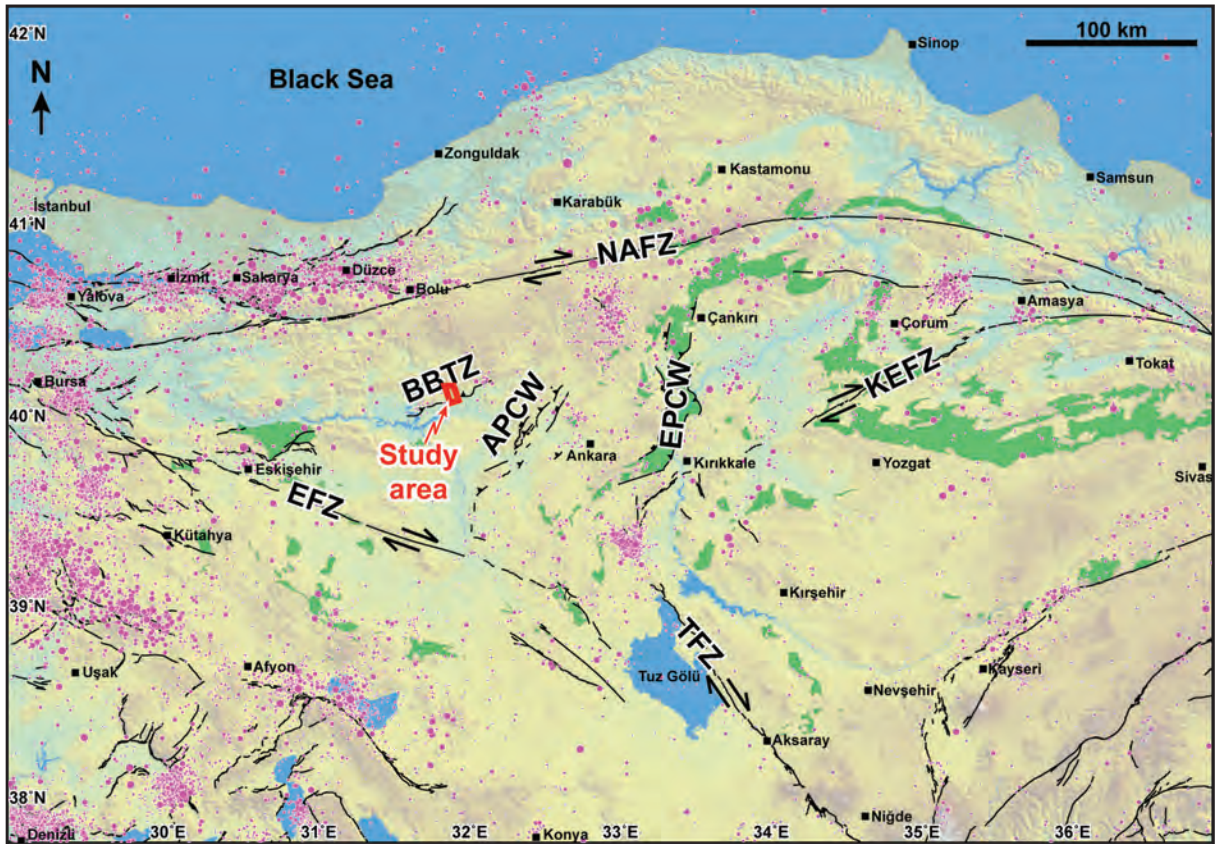


Figure 1- Main neotectonic elements of NW central Anatolia and seismicity. NAFZ: North Anatolian Fault Zone; BBTZ: Beypazarı Blind Thrust Zone; APCW: Abdüsselam Pinched Crustal Wedge; EPCW: Eldivan-Elmadağ Pinched Crustal Wedge; KEFZ: Kırıkkale-Erbaa Fault Zone; EFZ: Eskişehir Fault Zone; TFZ: Tuzgölü Fault Zone. Fault lines adapted from Emre et al., (2013), Seyitoğlu et al., (2000; 2009; 2015), Özsayın and Dirik (2007; 2011), Esat and Seyitoğlu (2010), Esat (2011), Esat et al., (2014; 2016). Pink circles represent the earthquakes from 1900 to 2013 with magnitude 3 or greater (Data was taken from B.U. Kandilli Observatory and Earthquake Research Institute). Green areas show the ophiolitic mélangé rocks of the suture zone.

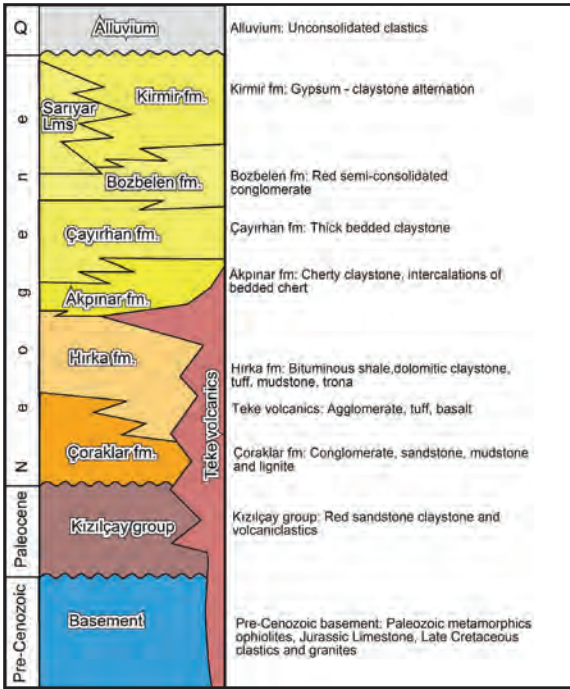


Figure 2- Stratigraphy of the Beypazarı-Çayırhan basin with no scale (Helvacı, 2010).

fault-related folding mechanisms in the thrust belts; (1) fault-bend folding: It develops in response to ramp-flat geometry of the thrust surface (Suppe, 1983) and (2) fault-propagation folding: which develops on the tip of a blind thrust where shortening is transferred to the folding (Suppe, 1985; Mitra, 1990; Suppe and Medwedeff, 1990). In the fault-bend folding, the forelimb has low dip angle compared to the fault-propagating folds with the highly dipping forelimb angle which is sometime even overturned (Calamita et al., 2012). Three models has been proposed for the fault-propagating folds in a fold-thrust belt (Jabbour et al., 2012). In the self-similar model, it is accepted that there is no rotation on the forelimb during folding. Fold geometry would be unchanged while anticline is growing. The interlimb angle remains constant (Suppe, 1985). In the time variant model, forelimb is rotated and the angle between limbs is not consistent (Mitra 1990). In the trishear model, fold developed gradually within the triangle zone on a tip of thrust fault (Erslev, 1991; Hardy and Ford, 1997; Allmendinger, 1998) (Figure 3).

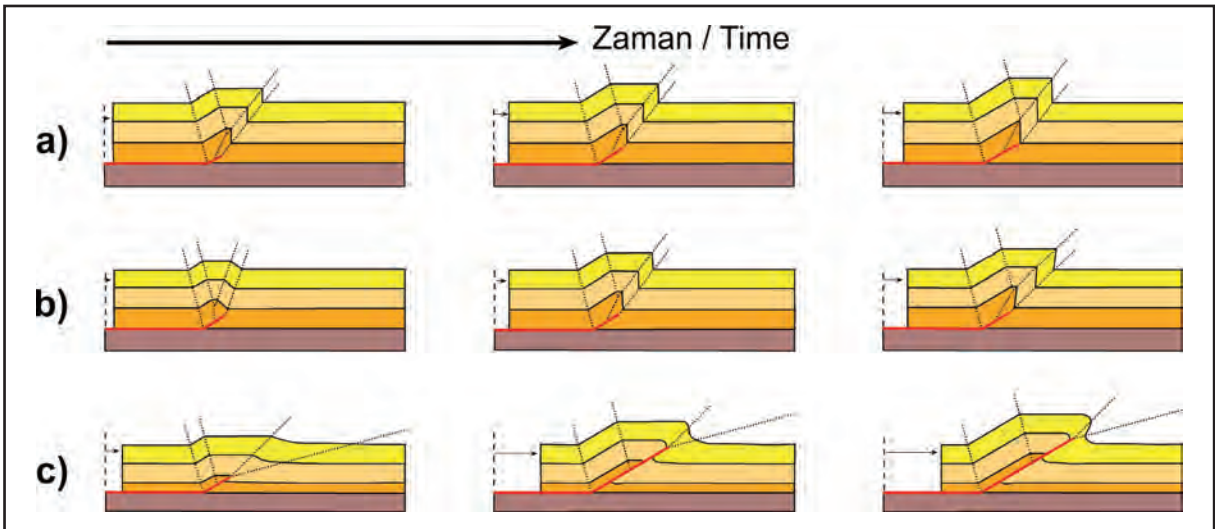


Figure 3- Three models of fault-propagation fold (Jabbour et al., 2012).

4. Field Observations

In the north of Beypazarı town, along the İnözü valley, detailed geological mapping demonstrates that so called Beypazarı - Çayırhan or Beypazarı Monocline is a fault-propagating fold related to blind thrusting (Figure 4). In the geological map of northern Beypazarı, the dark yellow, well lithified, easily distinguished volcanoclastic unit is particularly chosen to show overall structure of the area. The volcanoclastic

unit is composed of poorly sorted lava blocks in tuff matrix and also contains sand size volcanic material. The unit is competent and well bedded. The upper and lower part of the volcanoclastic unit is made up of white marl, claystone, siliceous limestone and tuff. According to the previous description of the formations (Helvacı, 2010; Apaydın, 2010) it can be said that the volcanoclastic unit overlies the Hirka formation (Figure 4).

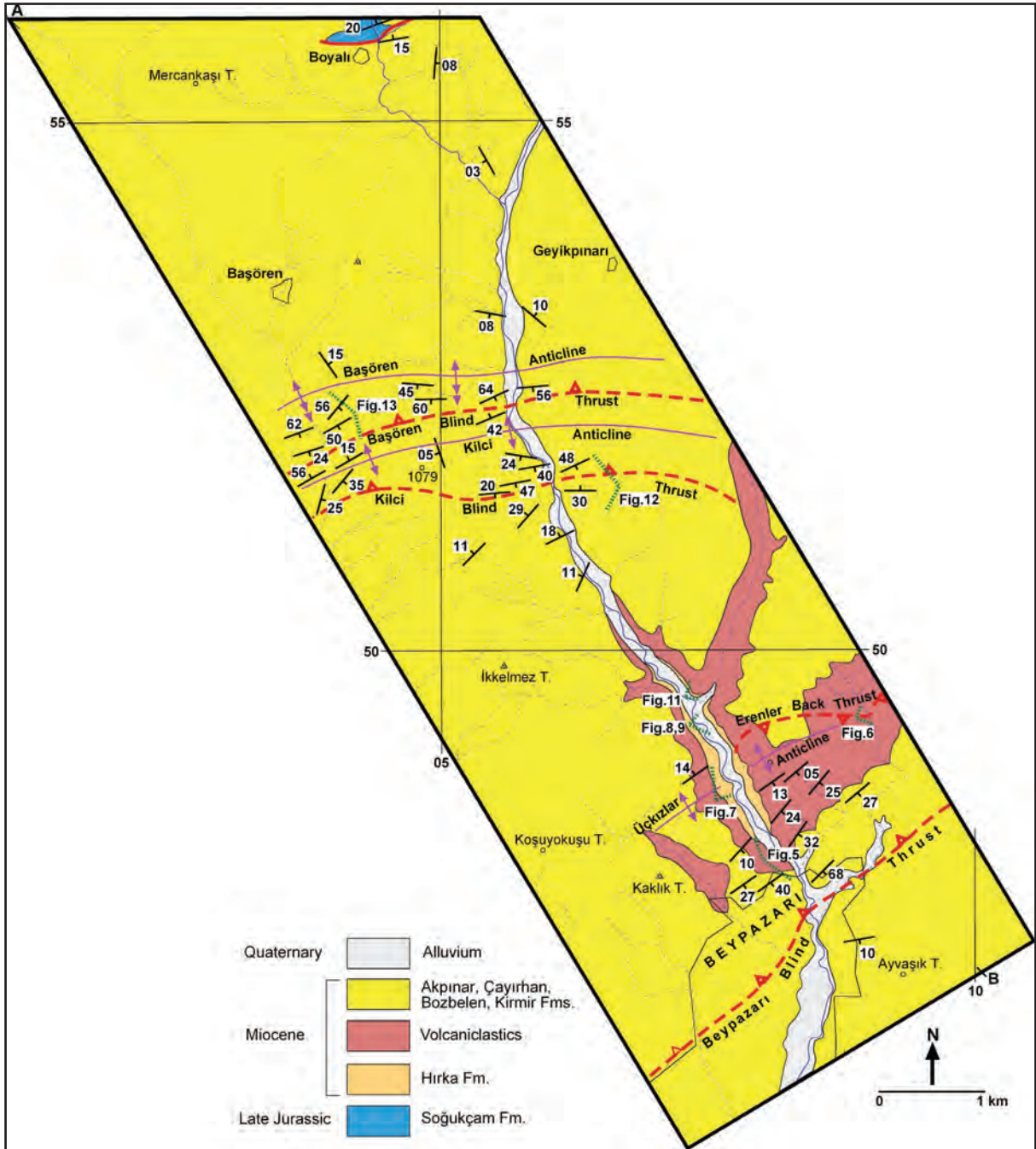


Figure 4- Detailed geological map of the NW Beypazarı.

In the Beypazarı town, Neogene sequence is inclined up to 70° towards SE, but this inclination gradually becomes less (30°) towards north and reach 10° around Üçkızlar Tepe (Figures 4 and 5). In the north of Üçkızlar Tepe, beds are dipping 15° NW. These observations show that the structure reported previously as Beypazarı monocline in the literature is an asymmetric anticline. There is no horizontal limb of fold to interpret the structure as monocline.

We propose the formation of asymmetric anticline is related to a fault propagation system, which can be observed clearly on the western slope of the Erenler Tepe (Figure 6), where the hanging wall moved towards NW on the SE dipping fault surface as indicated by drag folds. The continuation of this fault towards WNW can be traced on the eastern slopes of the road located in the İnözü valley as at least three semi-parallel SE dipping fault surfaces (Figure 7).



Figure 5- a) Panoramic view of the Üçkızlar anticline in the SE of İnözü valley and (b) location of the Beyoazarı blind fault. For location see figure 4.

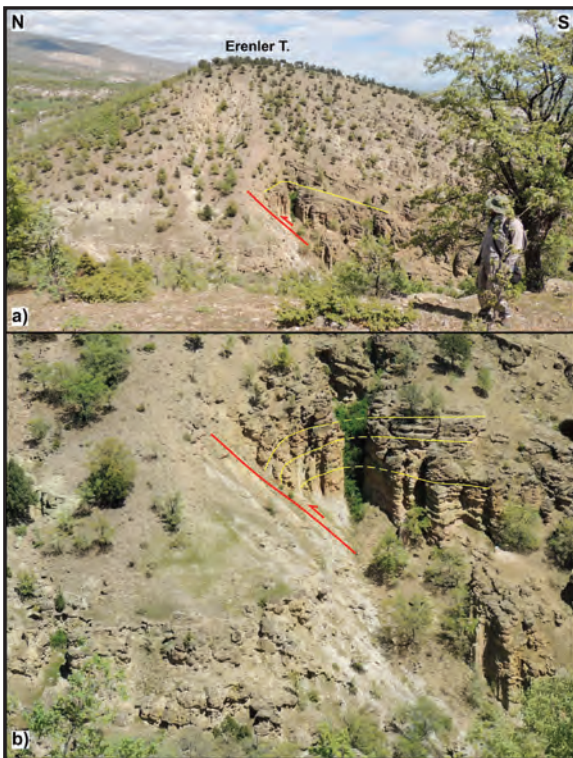


Figure 6- a) The effect of the Erenler back-thrust on volcanoclastic unit. b) detail view of drag folds. For photo locations see figure 4.

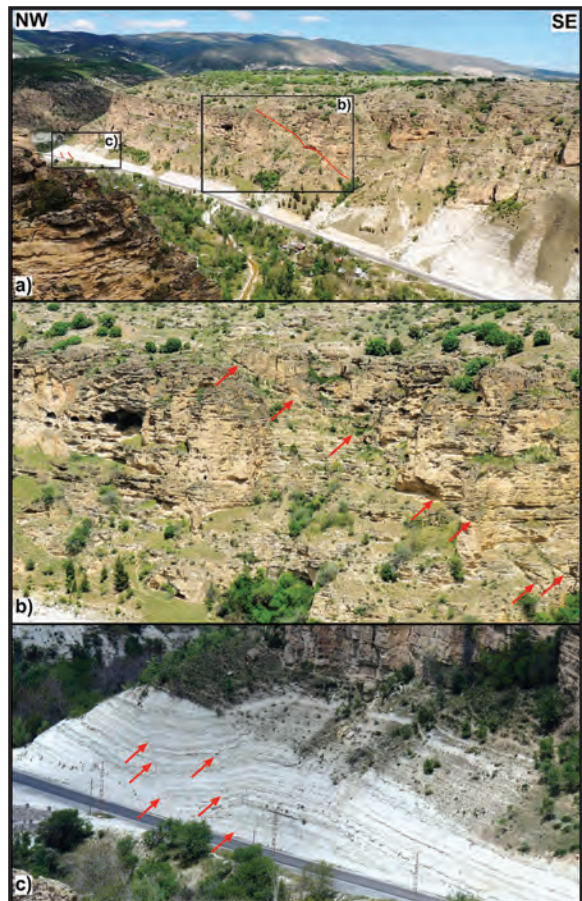


Figure 7- a) The back-thrusts in the İnözü valley. b) The continuation of the Erenler back-thrust in the İnözü valley effects the volcanoclastic unit. c) On the footwall of the Erenler back-thrust, location of semi-parallel back-thrusts. Red arrows indicate thrust surfaces. For details see figures 8 and 9, for location see figure 4.

The drag folds developed in the white marl, tuff and claystone under the volcanoclastic unit clearly indicate that hanging wall movement is towards NW (Figure 8). Upward continuation of these thrust faults cannot be observed and they were developed as blind thrusts (Figure 9). In the north of Beypazarı, main structure is an asymmetric anticline with SE vergence. For this reason, observed NW movement on the SE dipping thrust surfaces can be evaluated as back-thrusts. One can reach a conclusion that the Üçkızlar asymmetric anticline is a fault-propagation fold related to the NW dipping blind thrust (Figure 10), named as Beypazarı blind thrust. This thrust cannot be seen on the surface but its back-thrusts are clearly observed on the road cut of the İnözü valley and western slope of the Erenler Tepe as mentioned above. Therefore the term “Beypazarı monocline” should be changed to “Beypazarı fault-propagation folds” (Figure 10).

Inside the İnözü valley, around Yediler Türbesi, miniature structures of siliceous layers in the marl unit indicate that the movement is towards SE in the N70°E, 15°NW thrust system (Figure 11). These miniature structures mimic the main structure of Beypazarı blind thrust.

Further to north in the İnözü valley, near to the Beypazarı mineral water factory, Neogene sequence is folded again. There are two different anticlines following each other very closely. The smaller southern one is called Kilci anticline (Figures 10 and 12), while the northern one is named as Başören anticline and its southern limb dips more steeply relative to northern limb. These asymmetric anticlines can be traced on the valley of Alan dere, which is located on the west of the İnözü valley (Figures 10 and 13). In the Alan dere,

when we closely examine steeply dipping southern limb, it can be recognized that the bedding in the inner part of the anticline has relatively higher angle than the outer part. In other words, dip values of bedding gradually decrease from inner part to outer part of the anticline (Figure 14). This demonstrates that a blind fault is responsible for the formation of the Başören asymmetrical anticline. In the deeper part, the amount of displacement on the thrust fault is higher therefore, we would expect more steep dipping at the inner part of an anticline, but near the surface, the amount of displacement on the blind thrust gradually decreases that in turn creates gentle dipping bedding towards the outer part of the anticline. In the upper section of the sedimentary sequence the effect of deformation gradually disappears. This feature demonstrates that the structures can be attributed to a fault-propagation folding (Figures 10 - 14).

In the investigated area, Beypazarı blind thrust, Erenler back thrust, Kilci blind thrust and Başören blind thrust constitute the Beypazarı Blind Thrust Zone (BBTZ) (Figure 10).

Further to north, in the Boyalı village, the basement, Jurassic-Cretaceous limestone, shows a normal faulted / overlapped relationship with the Neogene sequence. Although its primary position is altered, this relationship can be evaluated as an evidence for normal fault controlled deposition of Neogene sedimentary unit as suggested by Yağmurlu et al. (1988) (Figure 10).

5. Seismicity and Focal Mechanism Solutions

Beypazarı Blind Thrust can be followed easily from SW of Çayırhan to the NE of Beypazarı due

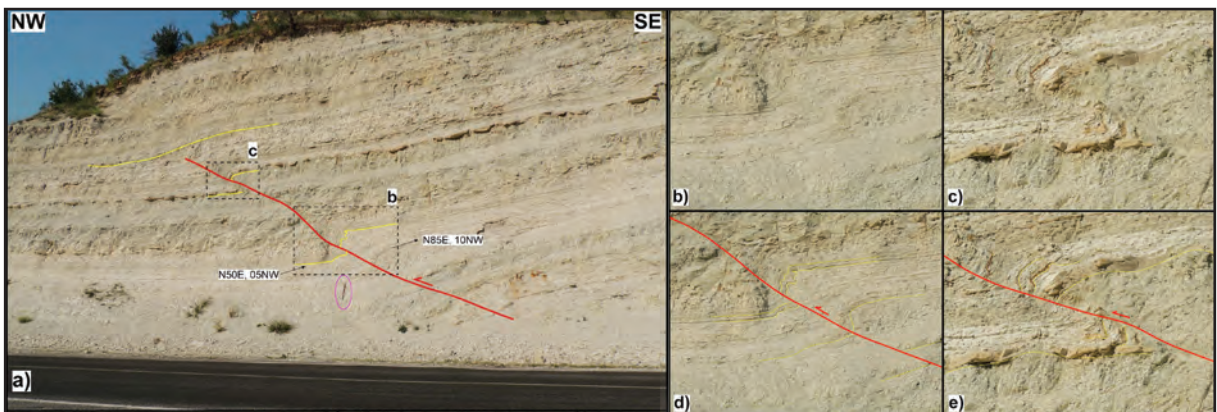


Figure 8- a) In the İnözü valley, the semi-parallel blind thrust developed on the footwall of the Erenler back-thrust. Length of pickaxe is 80 cm. b) and c) The details of drag folds on the blind back-thrusts. d) and e) interpretation of drag folds.

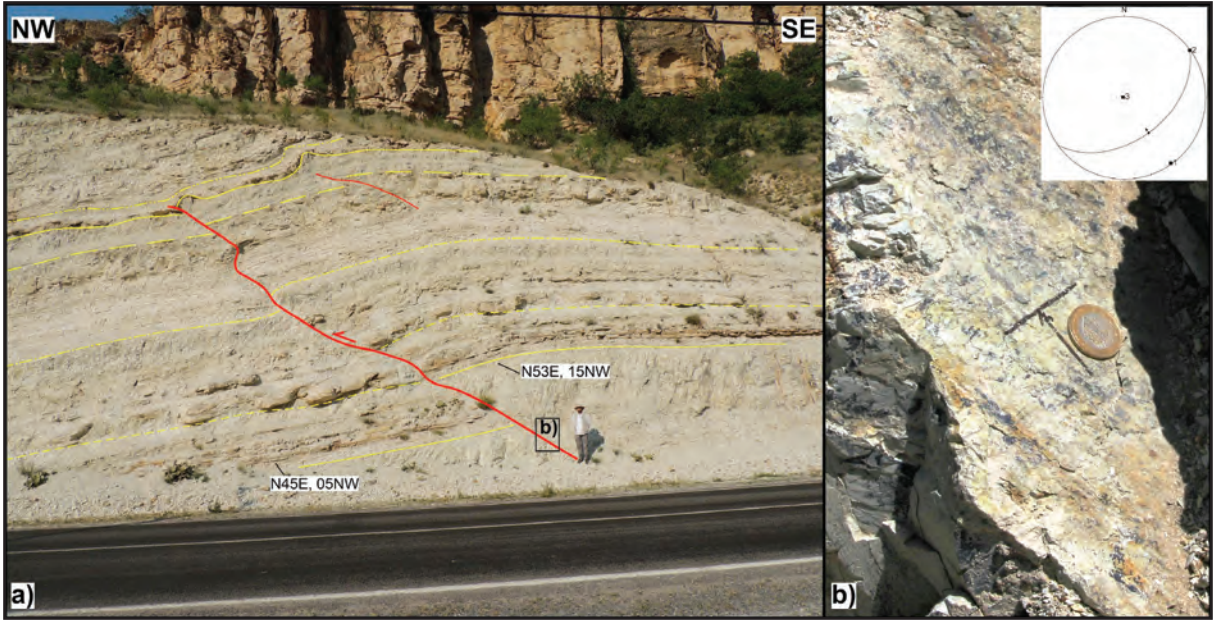


Figure 9- a) In the İnözü valley, the semi-parallel blind thrust developed on the footwall of the Erenler back-thrust. b) The fault surface and slicken lines of the thrust and their lower hemisphere stereographic projection.

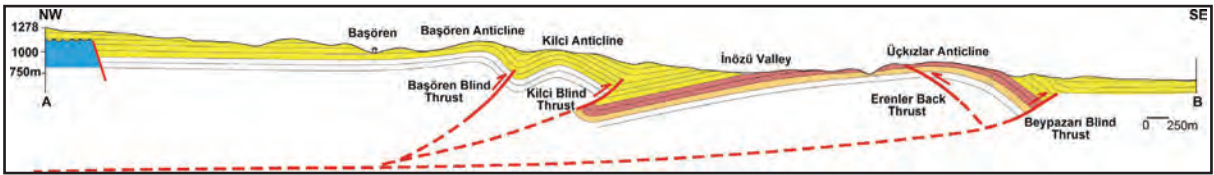


Figure 10- The geological cross section of NW Beypazarı. The position of basal thrust is interpretive. For location see figure 4.

to different dips of bedding in the sedimentary units (Figure 15a). The trending of BBTZ, which consists of the Beypazarı, Kılıcı and Başören blind thrusts and the Erenler back thrust, and the earthquake activity of the region overlap each other (Figure 15a). Based on the data provided by Boğaziçi University Kandilli Observatory and Earthquake Research Institute (KOERI) the earthquake activity contains seismic events having a range of magnitudes 2.5 and 4.2. The focal mechanism solutions of the events occurred between 2002-2013 (their locations and magnitudes were calculated by KOERI) are determined from P-wave first motion polarities in this study. Therefore the PPFIT algorithm (Reasenber and Oppenheimer, 1985) based on the first motion polarity was used. The focal mechanism parameters of the events computed in this study are given in table 1.

The focal mechanisms of the recent earthquakes show that some of the seismic activity is related to thrust faulting (event no: 10, 12, 15, 16, 19, 20) (Table 1; Figure 15a). The other focal mechanism solutions indicate strike-slip faulting with both right and left

lateral movements (event no: 1, 4, 5, 7, 8, 11, 13, 18). For this reason, it is interpreted that these strike-slip focal mechanism solutions may be related to the tear faulting in the thrust systems. Unmeasured strike slip fault surfaces remotely observed on the steep slopes of the İnözü valley must be related to these tear faults. The third group of focal mechanism solutions are related to normal faulting (event no: 3, 9, 17). These normal faults, semi-parallel to the thrusts are similar to the western margin of Eldivan-Elmadağ Pinched Crustal Wedge (Seyitoğlu et al., 2000; 2009) that were interpreted as compression induced normal faults (Ring and Glodny, 2010).

Result of the structural analysis of overall focal mechanism solutions is compatible with the Beypazarı Blind Thrust Zone. The strike of overall thrust surface obtained from kinematic analysis of the fault-slip data of the focal mechanism solutions is parallel to the blind thrusts shown in this paper and the principle stress direction is perpendicular to the fold axes (Figure 15b).

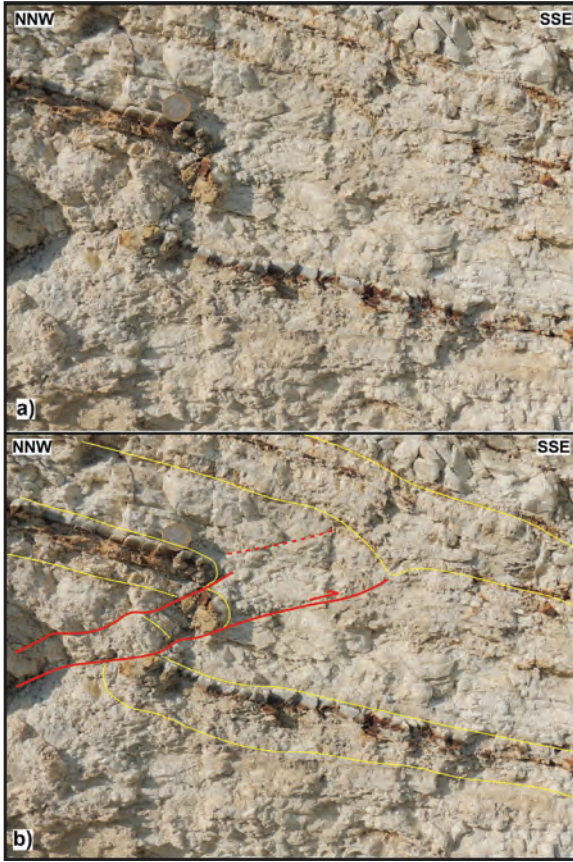


Figure 11- In the İnözü valley around Yediler türbesi, small scale blind thrusts and fault-propagation folds. This small scale structure gives a clue about large scale Bey pazarı blind thrust zone. Please make a correlation for the large scale structure on figure 10.

6. Discussions

“Bey pazarı Monocline” vs. “Bey pazarı fault-propagation folds”: Almost all definitions of a monocline mentioned nearly horizontal bedding on both sides of steeply dipping beds. These definitions indicate that previous “Bey pazarı flexure or Bey pazarı monocline” terminology used in the Turkish geology literature do not represent the structure in the Bey pazarı town. Because detailed geological mapping presented in this paper documents that steeply dipping bedding belongs to a limb of asymmetrical anticline. The other limb is not horizontal as in the definition of monocline but dipping opposite side up to 15° (Üçkızlar anticline). This paper also documents that the Üçkızlar anticline is located between Bey pazarı blind thrust and its back-thrusts. Additionally, the Kilci and Başören anticlines are recognized in this study and their relationship with the blind thrusting is demonstrated. Therefore, regional structure should be defined as “Bey pazarı fault-propagation folds”.

The causes of deformation: In the NW central Anatolia, recently determined Eldivan-Elmadağ Pinched Crustal Wedge (EPCW) indicate that the deformation effected Neogene units have neotectonic character and they are developed as a result of interaction between the North Anatolian Fault Zone and Kırıkkale-Erbaa Fault Zone that creates NW-SE contraction (Seyitoğlu et al., 2000; 2009). Later, a

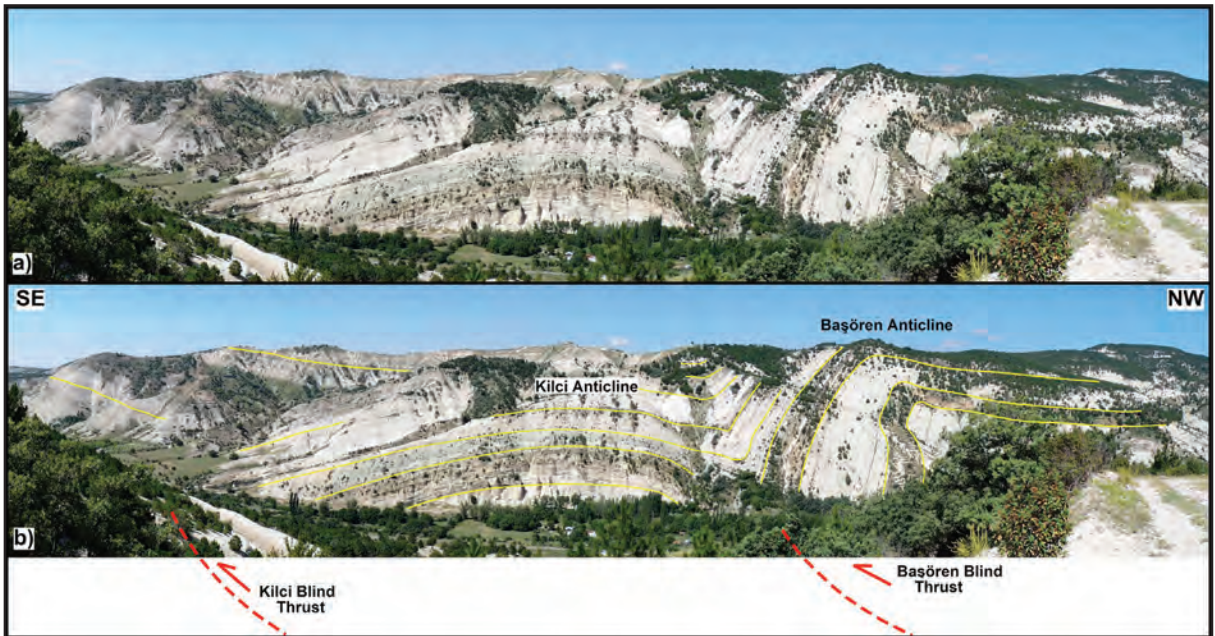


Figure 12- Panoramic photograph of Başören and Kilci anticlines in İnözü valley near to the Bey pazarı mineral water factory. a) un-interpreted b) interpreted. Dipping of beds are decreasing to the up section. The position of blind thrusts are drawn by the help of small scale structures in figure 11. For location of the photo see figure 4.

Table 1- The hypocentral and focal mechanism solutions of the seismic events between Bey pazari and Çayırhan.

| # | Date (yyyy. mm.dd) | Time (hh:mm:ss) | Latitude N (°) | Longitude E (°) | Depth (km) | Mag. | Ns | Gap (°) | Dmn (km) | Rms (s) | Erh (km) | Erz (km) | Nfm | FOCAL MECHANISM SOLUTIONS | | | | | | | | | | | | | | | | | |
|----|--------------------------|--------------------|-------------------|--------------------|---------------|------|----|------------|-------------|------------|-------------|-------------|-----|---------------------------|----|--------|-----|--------|------|---------|----|------|----|--------|--|---------|--|------|--|--------|--|
| | | | | | | | | | | | | | | HYPOCENTRAL SOLUTIONS | | | | | | Plane 1 | | | | | | Plane 2 | | | | | |
| | | | | | | | | | | | | | | P-axis | | T-axis | | Strike | | Dip | | Rake | | Strike | | Dip | | Rake | | Strike | |
| 1 | 2002.11.27 | 02:06:05.66 | 40.2692 | 32.0803 | 12.17 | 3.20 | 13 | 130 | 77.0 | 0.42 | 2.6 | 0.8 | 11 | 295 | 75 | 150 | 33 | 61 | 17 | 347 | 9 | 251 | 32 | | | | | | | | |
| 2 | 2006.08.28 | 18:54:19.97 | 40.2622 | 32.1530 | 12.91 | 3.19 | 13 | 142 | 70.0 | 0.60 | 2.4 | 0.4 | 9 | 5 | 70 | 100 | 158 | 22 | 64 | 87 | 24 | 291 | 64 | | | | | | | | |
| 3 | 2006.12.07 | 22:59:21.50 | 40.2637 | 32.1140 | 5.00 | 3.14 | 22 | 60 | 73.0 | 0.48 | 1.2 | 0.4 | 13 | 350 | 10 | -20 | 100 | 87 | -99 | 360 | 48 | 199 | 41 | | | | | | | | |
| 4 | 2008.01.26 | 04:00:22.62 | 40.2485 | 32.1133 | 5.00 | 3.32 | 31 | 49 | 68.0 | 0.34 | 0.8 | 0.3 | 20 | 125 | 65 | 0 | 35 | 90 | 155 | 83 | 17 | 347 | 17 | | | | | | | | |
| 5 | 2009.01.11 | 01:51:40.29 | 40.2988 | 32.1360 | 5.00 | 4.00 | 77 | 51 | 70.0 | 1.05 | 2.0 | 0.9 | 23 | 85 | 75 | 140 | 187 | 52 | 19 | 141 | 15 | 39 | 38 | | | | | | | | |
| 6 | 2009.01.11 | 02:04:46.43 | 40.2500 | 32.1133 | 5.00 | 3.30 | 32 | 49 | 68.0 | 0.76 | 1.8 | 0.7 | 22 | 50 | 70 | 130 | 162 | 44 | 30 | 112 | 15 | 3 | 49 | | | | | | | | |
| 7 | 2009.01.11 | 02:21:34.95 | 40.2478 | 32.1142 | 5.00 | 3.52 | 45 | 49 | 68.0 | 0.61 | 1.2 | 0.5 | 16 | 0 | 90 | 40 | 270 | 50 | 180 | 127 | 27 | 233 | 27 | | | | | | | | |
| 8 | 2009.01.30 | 15:43:14.02 | 40.2452 | 32.0817 | 6.81 | 3.18 | 26 | 49 | 70.0 | 0.37 | 1.1 | 0.2 | 13 | 40 | 55 | -10 | 136 | 82 | -145 | 4 | 30 | 263 | 18 | | | | | | | | |
| 9 | 2009.02.09 | 00:06:31.69 | 40.2962 | 32.1603 | 9.12 | 3.30 | 15 | 70 | 69.0 | 0.31 | 1.0 | 0.3 | 8 | 120 | 65 | -90 | 300 | 25 | -90 | 30 | 70 | 210 | 20 | | | | | | | | |
| 10 | 2009.02.09 | 08:23:25.26 | 40.2542 | 32.1298 | 5.00 | 3.50 | 41 | 50 | 68.0 | 0.68 | 1.5 | 0.6 | 22 | 200 | 25 | 40 | 73 | 74 | 110 | 147 | 27 | 8 | 56 | | | | | | | | |
| 11 | 2009.06.09 | 01:56:08.45 | 40.1448 | 31.6782 | 5.00 | 3.18 | 32 | 44 | 55.0 | 0.24 | 0.6 | 0.2 | 13 | 130 | 80 | 150 | 226 | 61 | 12 | 181 | 13 | 84 | 28 | | | | | | | | |
| 12 | 2009.07.19 | 00:54:51.92 | 40.2075 | 32.1205 | 5.00 | 2.77 | 16 | 92 | 65.0 | 0.31 | 1.2 | 0.4 | 8 | 75 | 85 | 90 | 255 | 5 | 90 | 165 | 40 | 345 | 50 | | | | | | | | |
| 13 | 2009.07.21 | 19:01:25.24 | 40.1157 | 31.6732 | 8.05 | 3.07 | 21 | 80 | 57.0 | 0.47 | 1.5 | 0.3 | 10 | 180 | 55 | -30 | 288 | 66 | -141 | 148 | 44 | 52 | 7 | | | | | | | | |
| 14 | 2010.08.28 | 01:03:19.67 | 40.1777 | 31.8363 | 5.00 | 3.29 | 12 | 132 | 63.0 | 0.81 | 3.9 | 1.3 | 7 | 345 | 85 | 80 | 229 | 11 | 153 | 84 | 39 | 244 | 49 | | | | | | | | |
| 15 | 2010.11.11 | 23:03:27.42 | 40.0487 | 31.6355 | 7.70 | 2.97 | 12 | 125 | 60.0 | 1.08 | 4.9 | 0.9 | 6 | 160 | 50 | 110 | 310 | 44 | 68 | 236 | 3 | 135 | 74 | | | | | | | | |
| 16 | 2010.11.20 | 17:23:03.15 | 40.1820 | 31.7265 | 5.00 | 2.91 | 11 | 165 | 55.0 | 0.32 | 1.8 | 0.6 | 7 | 135 | 50 | 130 | 262 | 54 | 53 | 18 | 2 | 112 | 60 | | | | | | | | |
| 17 | 2010.12.02 | 23:01:46.32 | 40.1240 | 31.6802 | 9.83 | 2.92 | 13 | 81 | 56.0 | 0.35 | 1.7 | 0.3 | 6 | 75 | 30 | -120 | 289 | 64 | -74 | 228 | 67 | 7 | 18 | | | | | | | | |
| 18 | 2011.01.12 | 10:31:34.60 | 40.1482 | 31.7363 | 5.00 | 3.30 | 20 | 85 | 58.0 | 0.28 | 0.8 | 0.3 | 9 | 145 | 65 | 170 | 239 | 81 | 25 | 10 | 11 | 105 | 24 | | | | | | | | |
| 19 | 2011.09.20 | 07:34:59.26 | 40.3032 | 32.1113 | 8.52 | 3.20 | 27 | 91 | 72.0 | 0.61 | 1.7 | 0.4 | 18 | 145 | 55 | 120 | 280 | 45 | 54 | 214 | 6 | 112 | 65 | | | | | | | | |
| 20 | 2013.11.17 | 20:28:00.36 | 40.1967 | 32.1308 | 5.00 | 3.10 | 25 | 48 | 64.0 | 0.42 | 1.0 | 0.4 | 13 | 25 | 45 | 70 | 232 | 48 | 109 | 309 | 2 | 212 | 76 | | | | | | | | |

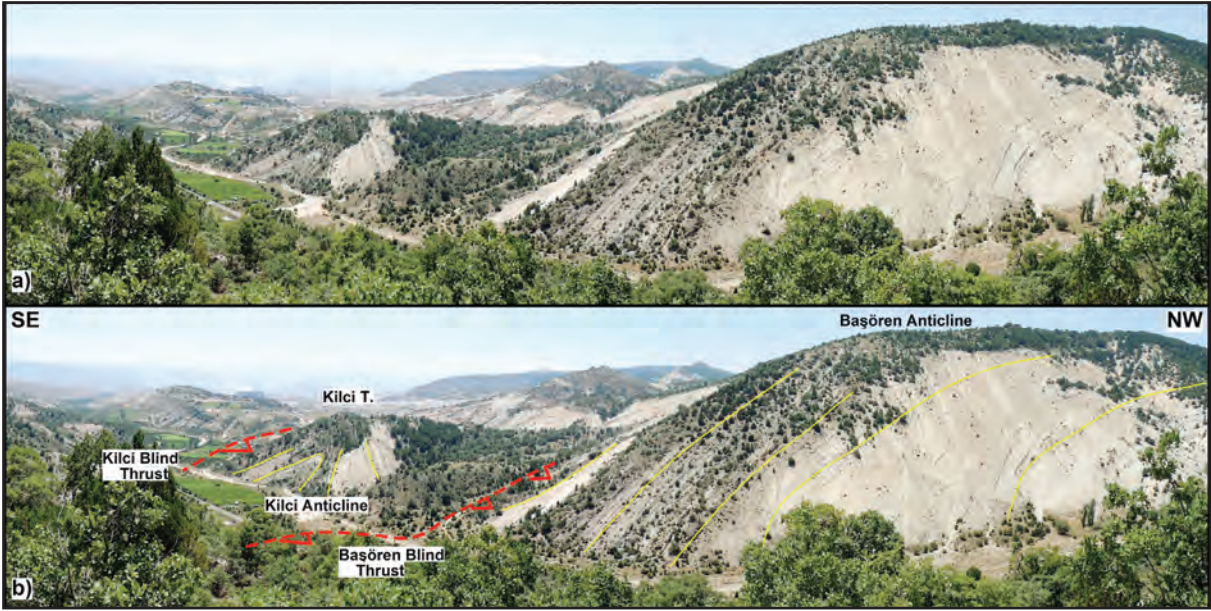


Figure 13- Panoramic photograph of Başören and Kilci anticlines at the north of Eti Soda factory in Alandere. a) un-interpreted b) interpreted. For the location of photo see figure 4.

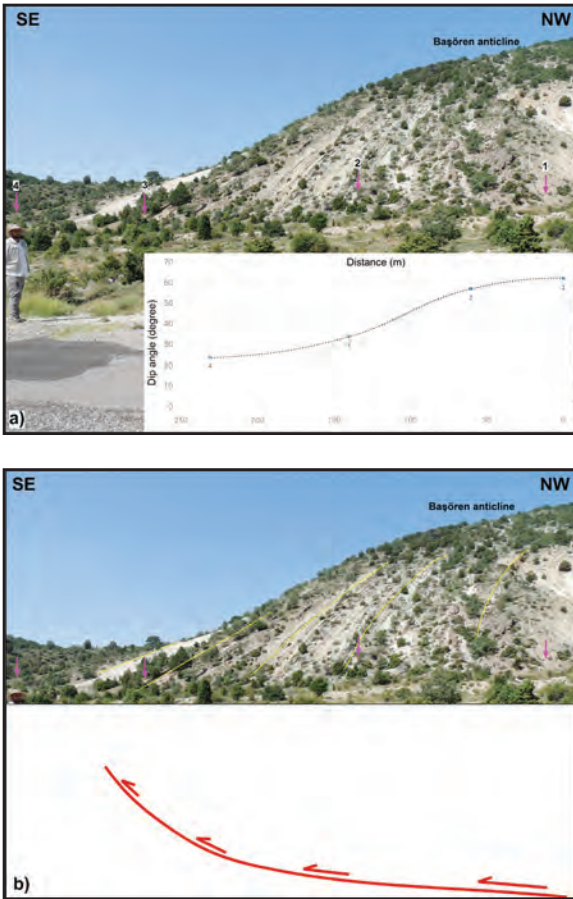


Figure 14- a) The dipping of beds is gradually decreased towards SE at the forelimb of asymmetric Başören anticline in Alan dere. b) The possible relationship between displacement differences on blind thrusting and dipping of beds. Please find that length of arrows indicates displacement differences.

similar Abdüsselam Pinched Crustal Wedge (APCW) is defined and it is stated that triangle-like area between the North Anatolian Fault Zone, Eskişehir Fault Zone and the Kırıkkale-Erbaa Fault Zone is under NW-SE contraction (Esat and Seyitoğlu, 2010; Esat, 2011; Esat et al., 2016; Esat et al., 2017). Inside the triangle-like area, positions of main contractional structures are different (Figure 1). EPCW, is located between Ankara and Çankırı and has a NNE-SSW trend (Seyitoğlu et al., 2009). In the west of Ankara, APCW has NE-SW trend (Esat, 2011; Esat, et al., 2017). The Beypazarı blind thrust zone (BBTZ, its details given in this paper) has ESE-WSW trend. In the NW central Anatolia, the strikes of main contractional structures gradually change from NNE to WSW, this situation must be related to a triangle-like area getting narrower towards west. It is considered that the interaction between the North Anatolian Fault and the Eskişehir Fault created deformation around Beypazarı as previously suggested by Yağmurlu et al. (1988).

The relationship between the earthquake activity and Beypazarı Blind Thrust Zone: The focal mechanism solutions presented in this paper indicate that Beypazarı Blind Thrust Zone (BBTZ) is an active structure (Figures 15a and b). There is an epicenter distribution on the SE of BBTZ. These data indicate that BBTZ is continuing towards SE with a basal thrust. As indicated by the focal mechanism solution of earthquake number 12 (Table 1; Figure 15a), the basal thrust must be shallow dipping towards NW.

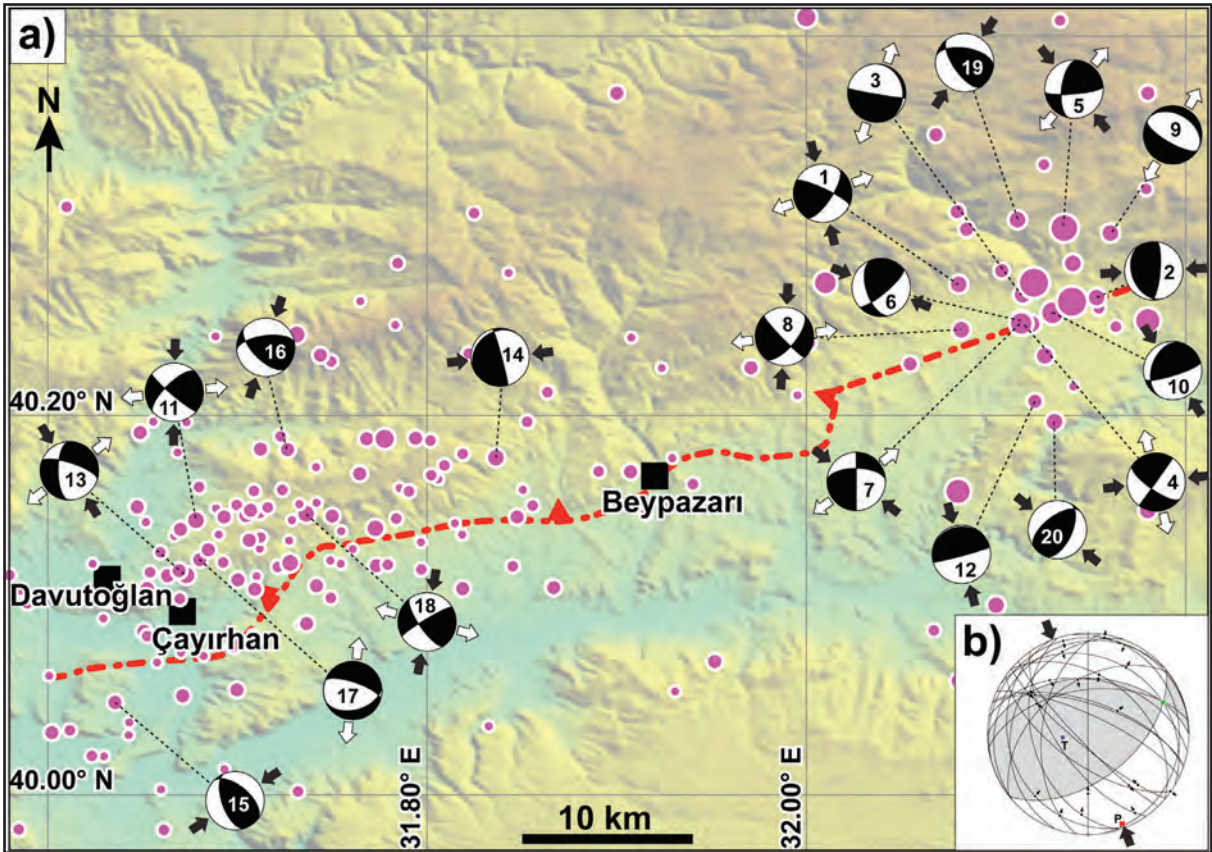


Figure 15- The focal mechanism solutions produced in this study and the seismic activity around Beypazari . Pink circles represent the earthquakes in the instrumental period. The magnitudes vary between 2.5 and 4.2. Data was taken from Boğaziçi University Kandilli Observatory and Earthquake Research Institute. For details of the focal mechanism solutions see table 1. Red dotted line indicates Beypazari Blind Thrust b) A structural analysis of the fault-slip data obtained from the focal mechanism solutions. P and T represent the contraction and extension axes, respectively.

The focal mechanism solutions are related to both thrust and strike-slip faulting. The lacking of dominantly right and left lateral strike-slip solutions may indicate that they are related to tear faulting. Similarly, in the NE of the study area, the main and aftershocks of 2000.08.22 Uruş earthquake (M: 4.3) provide solutions of both thrust and strike-slip faulting. Kaplan (2004) attributed these focal mechanism solutions to the NE-SW trending left lateral Uruş (Çeltikçi) fault zone, but these seismic events may well be related to Beypazari Blind Thrust Zone and related NW-SE trending right lateral tear faulting.

7. Conclusions

The structure known as “Beypazari flexure” or “ Beypazari monocline” in the Turkish geology literature is in fact a fault-propagation folds related to blind thrusting. For this reason, the name of “Beypazari fault-propagation folding” is proposed in this paper. All of the blind thrusts that played a role

to create this structure are named as the Beypazari Blind Thrust Zone (BBTZ). Seismic activity and focal mechanism solutions show that BBTZ is an active neotectonic structure. BBTZ is an important element with EPCW and APCW which take up the internal deformation of Anatolian plate between NAFZ, EFZ and KEFZ (Figure 1).

Acknowledgement

Field observations in this paper were performed during the Advanced Geological Mapping lecture. We thank to the Faculty of Engineering, Ankara University for their support. We are grateful to all MSc students (2014-2015), particularly Anıl Ardahanlıoğlu and Efe Demirci from the Tectonics Research Group for fruitful discussions in the field. Thanks to Gültekin Kavuşan who generously shared his experience on the geology of Beypazari basin. Earthquake data used in this study were obtained from Boğaziçi University

Kandilli Observatory and Earthquake Research Institute Regional Earthquake-Tsunami Monitoring Center. The manuscript is benefited critical reviews of Dr. Shah Faisal and other anonymous referees for which we are grateful.

References

- Aksoy, C.O., Onargan, T., Yenice, H., Küçük, K., Köse, H. 2006. Determining the Stress and Convergence at Beypazarı Trona Field by Three- dimensional Elastic-Plastic Finite Element Analysis: A Case Study. *International Journal of Rock Mechanics and Mining Sciences* 43, 166-178.
- Allmendinger, R.W. 1998. Inverse and Forward Numerical Modeling of Trishear Fault-Propagation Folds. *Tectonics* 17, 640-656.
- Apaydın, A. 2010. Relation of Tectonic Structure to Groundwater Flow in the Beypazarı Region, NW Anatolia, Turkey. *Hydrogeology Journal* 18, 1343-1356.
- Bechtel, A., Karayığit, A.İ., Sachsenhofer, R.F., İnaner, H., Christanis, K., Gratzner, R. 2014. Spatial and Temporal Variability in Vegetation and Coal Facies as Reflected by Organic Petrological and Geochemical Data in the Middle Miocene Çayırhan Coal Field (Turkey). *International Journal of Coal Geology* 134/135, 46-60.
- Bürküt, Y., Suner, F., Esenli, V. 1998. Çayırhan-Beypazarı Bölgesi (Ankara) Tenardit-Trona Yatakları Oluşum Koşulları. *Yerbilimleri Geosound* 32, 191-198.
- Calamita, F., Pace, P., Satolli, S. 2012. Coexistence of Fault-Propagation and Fault-Bend Folding in Curve-Shaped Foreland Fold-and-Thrust Belts: Examples From the Northern Apennines (Italy). *Terra Nova* 24, 396-406.
- Demirci, C.Y. 2000. Structural Analysis in Beypazarı-Ayaş-Kazan-Peçenek Area, NW of Ankara (Turkey). PhD thesis Middle East Technical University.
- Diker, S., Çelik, M., Kadioğlu, Y.K. 2006. Fingerprints of the Formation of Geothermal Springs on the Granitoids: Beypazarı-Ankara, Turkey. *Environmental Geology* 51, 365-375.
- Emre, Ö., Duman, T.Y., Özalp, S., Elmacı, H., Olgun, Ş., Şaroğlu, F. 2013. Active Fault Map of Turkey with an Explanatory Text 1:1,250,000 scale. Special Publication Series 30, General Directorate of Mineral Research and Exploration, Ankara-Turkey. ISBN: 978-605-5310-56-1
- Erslev, E.A. 1991. Trishear Fault-Propagation Folding. *Geology* 19, 617-620.
- Esat, K. 2011. Ankara Çevresinde Orta Anadolu'nun Neotektoniği ve Depremselliği. Doktora Tezi, Ankara Üniversitesi Fen Bilimleri Enstitüsü, 144s.
- Esat, K., Seyitoğlu, G. 2010. Neotectonics of North Central Anatolia: A strike-slip induced compressional regime. *Tectonic Crossroads: Evolving Orogens of Eurasia-Africa-Arabia*, Abstracts with Programs (14-6), p.38, Middle East Technical University, Ankara.
- Esat, K., Çıvgın, B., Kaypak, B., Işık, V., Ecevitoglu, B., Seyitoğlu, G. 2014. The 2005-2007 Bala (Ankara, central Turkey) earthquakes: a case study for strike-slip fault terminations. *Geologica Acta* 12, 1, 71-85.
- Esat, K., Kaypak, B., Işık, V., Ecevitoglu, B., Seyitoğlu, G. 2016. The Ilıca branch of the southeastern Eskişehir Fault Zone: an active right-lateral strike-slip structure in central Anatolia, Turkey. *Bulletin of the Mineral Research and Exploration* 152, 25-37.
- Esat, K., Seyitoğlu, G., Ecevitoglu, B., Kaypak, B. 2017. Abdüselam Kısırlımlı Tektonik Kaması: KB Orta Anadolu'da Daralma Rejimiyle İlişkili Bir Geç Senozoyik Yapısı. *Yerbilimleri-Bulletin for Earth Sciences* 38(1), 33-56.
- Garcia-Veigas, J., Gündoğan, İ., Helvacı, C., Prats, E. 2013. A genetic model for Na-carbonate mineral precipitation in the Miocene Beypazarı trona deposits, Ankara province, Turkey. *Sedimentary Geology*, 294, 315-327.
- Hardy, S., Ford, M. 1997. Numerical modeling of trishear fault propagation folding. *Tectonics* 16, 841-854.
- Helvacı, C. 2010. Geology of the Beypazarı trona field, Ankara, Turkey. *Tectonic Crossroads: Evolving Orogens of Eurasia-Africa-Arabia*, Ankara, Turkey. Mid-congress field excursions guide book, 1-33.
- Helvacı, C., Yılmaz, H., İnci, U. 1981. Beypazarı (Ankara) yöresi Neojen tortullarının kil mineralleri ve bunların dikey ve yanal dağılımı. *Jeoloji Mühendisliği* 32/33, 33-42.

- İnci, U. 1991. Miocene alluvial fan-alkaline playa lignite-trona bearing deposits from an inverted basin in Anatolia: sedimentology and tectonic controls on deposition. *Sedimentary Geology* 71, 73-97.
- Jabbour, M., Dhont, D., Hervouet, Y., Deroin, J-P. 2012. Geometry and kinematics of fault-propagation folds with variable interlimb angle. *Journal of Structural Geology* 42, 212-226.
- Kalafatçıoğlu, A., Uysallı, H. 1964. Beypazarı-Nallıhan-Seben civarının jeolojisi. *Maden Tetkik ve Arama Dergisi* 62, 1-11.
- Kaplan, T. 2004. Neotectonics and seismicity of the Ankara region: A case study in the Uruş area. MSc Thesis, Middle East Technical University, 84p.
- Karadenizli, L. 1995. Beypazarı havzası (Ankara batısı) üst Miyosen-Pliyosen jipsli serilerinin sedimantolojisi. [Sedimentology of the Upper Miocene-Pliocene gypsum series of the Beypazarı basin, west of Ankara, Central Anatolia, Turkey]. *Türkiye Jeoloji Bülteni*, 38, 63-74.
- Karakaş, Z., Kadir, S. 2006. Occurrence and origin of analcime in a Neogene volcano-sedimentary lacustrine environment, Beypazarı-Çayırhan basin, Ankara, Turkey. *N. Jb. Miner. Abh.* 182/3, 253-264.
- Kavuşan, G. 1993a. Beypazarı-Çayırhan kömür havzası linyitlerinin yataklanmasında tektonizmanın önemi. *Doğa-Türk Yerbilimleri Dergisi / Turkish Journal of Earth Sciences* 2, 135-145.
- Kavuşan, G. 1993b. Beypazarı-Çayırhan linyitleri hümik asitlerin IR-Spektrofotometrik incelenmesi. *Maden Tetkik ve Arama Dergisi* 115, 91-98.
- Mitra, S. 1990. Fault-propagation folds: Geometry, kinematic evolution and hydrocarbon traps. *The American Association of Petroleum Geologists Bulletin* 74, 921-945.
- Orti, F., Gündoğan, İ., Helvacı, C. 2002. Sodium sulphate deposits of Neogene age: the Kirmir Formation, Beypazarı basin, Turkey. *Sedimentary Geology* 146, 305-333.
- Özçelik, O. 2002. Beypazarı (Ankara) kuzeyinde Miyosen yaşlı bitümlü birimlerin organik jeokimyasal özellikleri. [Organic geochemical characteristics of Miocene bituminous units, north of Beypazarı (Ankara). *Türkiye Jeoloji Bülteni* 45, 1-17.
- Özçelik, O., Altunsoy, M. 2005. Organic geochemical characteristics of Miocene bituminous units in the Beypazarı basin, central Anatolia, Turkey. *The Arabian Journal for Science and Engineering* 30, 181-194.
- Özgüm, C., Gökmenoğlu, O., Erduran, B. 2003. Ankara, Beypazarı doğal soda (trona) sahası izotop hidrolojisi çalışmaları. [Isotope Hydrology studies of Beypazarı trona mine area, Ankara]. *Jeoloji Mühendisliği Dergisi* 27, 3-16.
- Özpeker, I., Çoban, F., Esenli, F., Eren, R.H. 1991. Miyosen yaşlı Hırka Formasyonundaki (Beypazarı-Ankara) dolomitlerin mineralojik özellikleri [Mineralogical features of dolomite in the Hırka Formation (Beypazarı-Ankara)]. *Türkiye Jeoloji Bülteni* 34, 23-26.
- Özsayın, E., Dirik, K. 2007. Quaternary activity of the Cihanbeyli and Yeniceoba Fault Zones: İnönü-Eskişehir Fault System, central Anatolia. *Turkish Journal of Earth Sciences* 16, 471-492.
- Özsayın, E., Dirik, K. 2011. The role of oroclinal bending in the structural evolution of the Central Anatolian Plateau: evidence of a regional changeover from shortening to extension. *Geologica Carpathica* 62, 4, 345-359.
- Pehlivanlı, B.Y., Koç, Ş., Sarı, A., Engin, H. 2014. Factors controlling low Uranium and Thorium concentrations in the Çayırhan Bituminous shales in the Beypazarı (Ankara) area, Turkey. *Acta Geologica Sinica* 88, 248-259.
- Randot, J. 1956. 1/100.000lik 39/2 (Güney kısmı) ve 39/4 nolu paftaların jeolojisi. Seben-Nallıhan-Beypazarı ilçeleri. *Maden Tetkik ve Arama Genel Müdürlüğü Rapor no: 2517, Ankara (unpublished).*
- Ring, U., Glodny, J. 2010. No need for lithospheric extension for exhuming (U)HP rocks by normal faulting. *Journal of Geological Society London* 167, 225-228.
- Reasenber P., Oppenheimer D. 1985. Fpfit, fplot, and fpage: Fortran computer programs for calculating and displaying earthquake fault plane solutions. Technical Report. Reston, VA, USA: US Geological Survey.

- Seyitođlu, G., Kazancı, N., Karadenizli, L., Ően, Ő., Varol, B., Karabıyıkogđlu, T. 2000. Rockfall avalanche deposits associated with normal faulting in the NW of ankırı basin: Implications for the post-collisional tectonic evolution of the Neo-Tethyan suture zone. *Terra Nova*, 12, 245-251.
- Seyitođlu, G., Aktuđ, B., Karadenizli, L., Kaypak, B., Ően, Ő., Kazancı, N., IŐık, V., Esat, K., Parlak, O., Varol, B., Sara, G., İleri, İ. 2009. A Late Pliocene - Quaternary Pinched Crustal Wedge in NW Central Anatolia, Turkey: A neotectonic Structure Accommodating the Internal Deformation of the Anatolian Plate. *Geological Bulletin of Turkey*, 52(1), 121-154.
- Suner, M.F. 1993. The Beypazarı trona deposits. *Földtani Közlöny*, 123/3, 271-282.
- Suppe, J. 1983. Geometry and kinematics of fault-bend folding. *American Journal of Science* 283, 684-721.
- Suppe, J. 1985. *Principles of structural geology*. Prentice-Hall Inc., Englewood Cliffs, New Jersey.
- Suppe, J., Medwedeff, D.A. 1990. Geometry and kinematics of fault-propagation folding. *Eclogae geol. Helv.* 83, 409-454.
- Őener, M. 2007. Depositional conditions of the coal-bearing Hırka Formation beneath Late Miocene explosive volcanic products in NW central Anatolia, Turkey. *Journal of Earth System Science* 116, 125-135.
- Yađmurlu, F., Helvacı, C., İnci, U., Önal, M. 1988. Tectonic characteristics and structural evolution of the Beypazarı and Nallıhan Neogene basin, central Anatolia. *METU Journal of Pure and Applied Sciences* 21, 127-143.



Bulletin of the Mineral Research and Exploration

<http://bulletin.mta.gov.tr>



STRUCTURAL FEATURES OF THE NİĞDE MASSIF IN THE ÇAMARDI (NİĞDE) DISTRICT

Ramazan DEMİRCİOĞLU^{a*} and Yaşar EREN^b

^aDisaster and Emergency Manage AKSARAY

^bSelçuk University, Dept. of Geological Eng., KONYA

Research Article

Keywords:

Çamardı, the Niğde Massif, polyphase deformation, cusped-lobate structure

ABSTRACT

In the Çamardı (Niğde) district, the Niğde Massif is composed of marbles, gneisses, quartzites and amphibolites. These rocks of the Massif have been cut by Cretaceous aged granodiorites. The Paleocene-Eocene aged low-grade metamorphic rocks constitute the autochthonous cover of the Massif. These units are tectonically overlain by the Upper Cretaceous-Paleocene aged flyschoid and island arc type rocks. The Oligocene-Quaternary aged terrestrial and volcanic rocks constitute the youngest units of the district. The metamorphites of the Niğde Massif have been subjected to at least four phase ductile deformation (D_1 , D_2 , D_3 , and D_4) and folding. Through the D_1 phase deformation, the rocks of the Massif have been folded as recumbent-isoclinal folds (F_1 - F_2 phase folding) and have gained a structure with a foliation (S_1) which is parallel to the axial planes. Owing to the isoclinal and intense folding of the bedding planes (S_0) of the rocks, bedding transposition have developed and transposed folding structures have formed. Through the D_2 phase deformation, northeast-southwest trending and both northeast and southwest dipping map scale folds (F_3 phase folding) have developed. As a result of the interference of F_1 - F_2 and F_3 phase folds, in the district, folds, generated by Type-2 folding, have formed (mushroom folds). Second phase mesoscopic folds are of tight-isoclinal geometry and display asymmetrical and inclined fold feature. In the study area, as a result of D_3 phase folding a large dome structure has developed in the district. And D_4 phase folds have formed map scale synformal and antiformal structures that are trending approximately perpendicular to D_2 phase, plunging southeast and trending northwest-southeast. Through D_4 phase deformation, the cover rocks have been deformed together with the basement rocks (F_5 phase) that they overlie. The microscopic observations show that Cretaceous-Eocene aged rocks have been subjected to low-grade metamorphism in the greenschist facies through D_4 phase deformation. The geometry of the F_3 phase folds reflects cusped-lobate structure which is the folding type peculiar to the districts where basement rocks and cover rocks have been deformed together.

Received: 07.04.2016

Accepted: 28.06.2016

1. Introduction

The study area comprises Çamardı county of Niğde province and its surroundings (Figure 1). The Kırşehir Massif is one of the most important structural elements in the geological evolution of Turkey (Ketin, 1966; Kırşehir Block, Görür et al., 1984; The Central Anatolian Crystalline Complex, Göncüoğlu et al., 1991). In the area, high grade metamorphic rocks of the Paleozoic-Mesozoic aged Niğde Massif which belongs to the Kırşehir Massif and the Late Cretaceous-aged granodioritic rocks intruded into them constitute the basement of the district (Blumenthal, 1941; Viljoen and İleri, 1973; Kleyn, 1968; Göncüoğlu, 1977; Dellaloğlu and Aksu, 1986).

Most of the studies carried out in the study area and its near surroundings are related to stratigraphy and mineral researches (Yetiş, 1978; Kuşçu, 1992). Detailed structurally weighted works have been

carried out in the other sections of the Kırşehir Massif (Seymen, 1981a,b, 1982, 1983 and Göncüoğlu, 1991, 1993). There are also some structurally weighted works that have been carried out in the Niğde Massif. Whitney and Dilek (1998) in their work, mention that the Niğde Massif, during the Alpine Orogenesis has been subjected to crustal thickening and associated with it Barrowian type metamorphism; and afterwards depending on the developed magmatism it has been subjected to high temperature-low pressure metamorphism and during this process the Massif has been subjected to extension. Whitney and Dilek (2001) in their work, have carried out studies related to the metamorphism and exhumation of the rocks belonging to Kırşehir, Akdağ, Aksaray and Niğde Blocks which constitute the Central Anatolian Crystalline Complex, and stated in their work that the rocks belonging to the Niğde Massif possess different metamorphism properties compared to the others. Gautier et al. (2002) in their work have tried to reveal the geological evidences of the pre-Eocene exhumation of the Niğde

* Corresponding author: Ramazan Demircioğlu, e-mail: ra.demircioglu@gmail.com.
<http://dx.doi.org/10.19111/bulletinofmre.304483>

Massif. Whitney et al. (2003) in their work, have tried to establish the phases of the regional metamorphism and deformation of the rocks belonging to the Niğde Massif and the emplacement mechanism of the

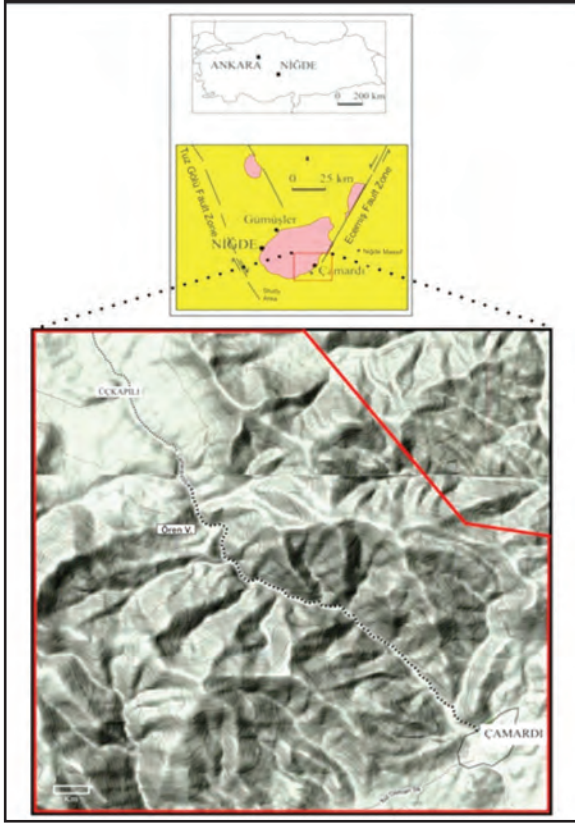


Figure1- Location map of the study area.

Üçkapılı Granodiorite and its age. And Whitney et al., (2007) in their work, have examined the Niğde Massif situated in the region between strike-slip fault zones, according to temperature-deformation properties. They mention that the regional metamorphism observed in the Niğde Massif corresponds to the same age as the other massifs (Kırşehir, etc.), however, its deformation types differ from the deformation types of the other massifs. Umhoefer et al. (2007) mention in their work that the rocks belonging to the Niğde Massif have developed under the influence of yo-yo tectonics which has developed within the region situated between the strike-slip faults and possess also a vertical component and which have given rise to the burial and exhumation of the basement and cover rocks. According to this, the rocks belonging to the Massif have been subjected to burial during Late Cretaceous era and at the same time have been subjected to metamorphism and deformation. And during pre-Tertiary era, the basement rocks have exhumed and given material to the Tertiary aged

rocks. And in the second burial phase, the basement and cover rocks have been subjected to re-burial and lower grade metamorphism. Afterward, these units have exhumed again during Miocene (17-9 my). Whitney et al. (2008) in their work have carried out fission track dating on the minerals obtained from the rocks belonging to the Niğde Massif and determined the periods of the burial and exhumation of the yo-yo tectonics. Gautier et al. (2008) mention in their work that the Niğde Massif which constitutes the south edge of the Central Anatolian Crystalline Complex is composed of two structural elements, its lower section is the section that has gained a dome structure by migmatites, and its upper section is composed of metamorphites which display lower metamorphism. They also mention that between these two sections, an extensional detachment zone has developed, and the Niğde Massif has exhumed in this way and has supplied material to the Late Maastrichtian aged units in the Ulukışla Basin which is in the form of a graben and which has developed on the hanging wall by way of southward dipping normal faults developed afterwards. The writers have stated that within the Niğde Massif, the direction of the movement observed in the slip zones which is towards south-southwest and the direction of the regional scale thrusts developed during the Alpine Orogenesis are in conformity with each other. Genç and Yürür (2010) have examined, in their work, the extensional tectonic regime developed during Cenozoic era, along the line between Konya and Yozgat, in the massifs belonging to the Central Anatolia Region. The writers have mentioned the uplift of the rocks of the Massif by the thin skin detachment faults developed in this region after Late Cretaceous era depending on the extensional tectonic regime and have tried to explain the relation of the volcanism observed in the Cappadocia region with these events. Idleman et al. (2014) in their work, have determined the burial and exhumation of the Massif according to $^{40}\text{Ar}/^{39}\text{Ar}$ analyses carried out on the muscovite and alkali feldspars obtained from the rocks of the Niğde Massif. They have stated that the first exhumation of the Massif has occurred during pre-Paleogene period and the massif and the Paleogene-aged units have been subjected to re-burial and undergone metamorphism in the greenschist facies.

2. Lithostratigraphy

In the Çamardı district, the rocks belonging to the Massif have been differentiated as Gümüşler metamorphites at the bottom, and Aşıgediği metamorphites on the top (Demircioğlu, 2001 and Demircioğlu and Eren, 2003). The rocks of the Massif

have been cut by Late Cretaceous aged Üçkapılı Granodiorites (Kleyn, 1968; Viljoen and İleri, 1973; Göncüoğlu, 1977 and 1985). The basement units which have been subjected to high grade metamorphism during pre-Paleocene era have been unconformably covered by Late Cretaceous-Eocene aged rocks that have been subjected to low-grade metamorphism, Pliocene-Quaternary aged slope debris and alluviums.

2.1. Gümüşler Metamorphites

With in the study area, the high grade metamorphic rocks that are prevalent on the south and north limbs (Figure 2) the map scale recumbent fold have been called within 'Niğde Series' by Tromp (1942), 'Lower Series' by Kleyn (1970), and 'Maden formation' by Viljoen and İleri (1973). And Göncüoğlu (1977) has named these rocks Gümüşler formation in the detailed works that he carried out in the Niğde Massif.

The gneisses that constitute the most part of the Gümüşler metamorphites display extensive outcrops in the study area. They have thicknesses ranging from several centimeters up to hundreds of meters. Their outward appearance is gray, brown, and black colored and they display distinct foliation planes. Whitney et al. (1998) state in their work that the gneisses within the rocks belonging to the Massif show sillimanite gneiss feature and indicate high grade metamorphism depending on the regional metamorphism. In Demircioğlu (2001) work, large quantities of sillimanite have been encountered during the petrographic examination carried out on the gneisses in the Gümüşler metamorphites. As Demircioğlu and Eren (2000), Demircioğlu (2001), and Eren and Demircioğlu (2003) have stated in their work, Umhoefer et al. (2007) and Idleman et al. (2014) mention in their work that the Paleocene-Eocene aged units within the study area have been subjected to low-grade metamorphism.

One of the rocks which show alternation with the gneisses and amphibolites is the marbles that possess thicknesses up to 20 meters and display various outward appearances. These marbles have been named 'Asmaca marbles' in the work of Demircioğlu (2001). The crystal sizes of the marbles having colors varying from light yellow to white range from macrocrystalline to microcrystalline. And glassy white and yellowish colored quartzites are distinguished as Alıçlıboyun quartzite (Demircioğlu, 2001). These

quartzites display alternations with the gneisses and marbles as thin bands.

2.2. Aşıgediği Metamorphites

The metamorphic rocks which crop out in the core of the recumbent fold in the middle section of the study area have been examined within Niğde series by Tromp (1942) and within Niğde Complex by Blumenthal (1952). The same unit has been named 'Upper series' by Kleyn (1970), 'Kılavuz formation' by Viljoen and İleri (1973), and 'Aşıgediği formation' by Atabey et al. (1990). Tromp (1942) has given their age as Devonian.

The marbles constitute the most predominant rocks of the Aşıgediği metamorphites which constitute the uppermost horizon of the Niğde Massif. Alternating with the marbles, metacherts, amphibolites and quartzites are also present within the unit. Demircioğlu (2001), in his work, has named these amphibolites showing alternations with the marbles 'Çingillitepe amphibolites'. They possess a highly folded structure on the map scale, too (Figure 2). They display outward appearances having colors varying from dark brown to black. Their schistosity planes are fairly conspicuous. These planes are in a position parallel to the bandings in the marbles with which they show alternation. This situation is an indication which shows that they have been subjected to the same deformations and metamorphism as the marbles. Their thicknesses range from several centimeters up to hundreds of meters. The metacherty marbles are situated at the transition zones with the Gümüşler metamorphites on each limb of the recumbent fold. The metacherty horizons can show thicknesses from 1 centimeter to 15 centimeters. They present light brown-beige colored appearances. They show competent material feature within the marbles. They have gained boudinage and pinch and swell structure feature depending on the tensions.

2.3. Üçkapılı Granodiorite

The Üçkapılı Granodiorite most prevalently crops out in Üçkapılı village and its surroundings to the north of the study area (Göncüoğlu, 1977 and 1985). In the south it is observed as smaller intrusions. Their appearance is highly fractured and they show widespread alteration. The granodiorite which cuts the metamorphites belonging to Massif is covered by Paleocene-Eocene aged rocks (Figure 2). According

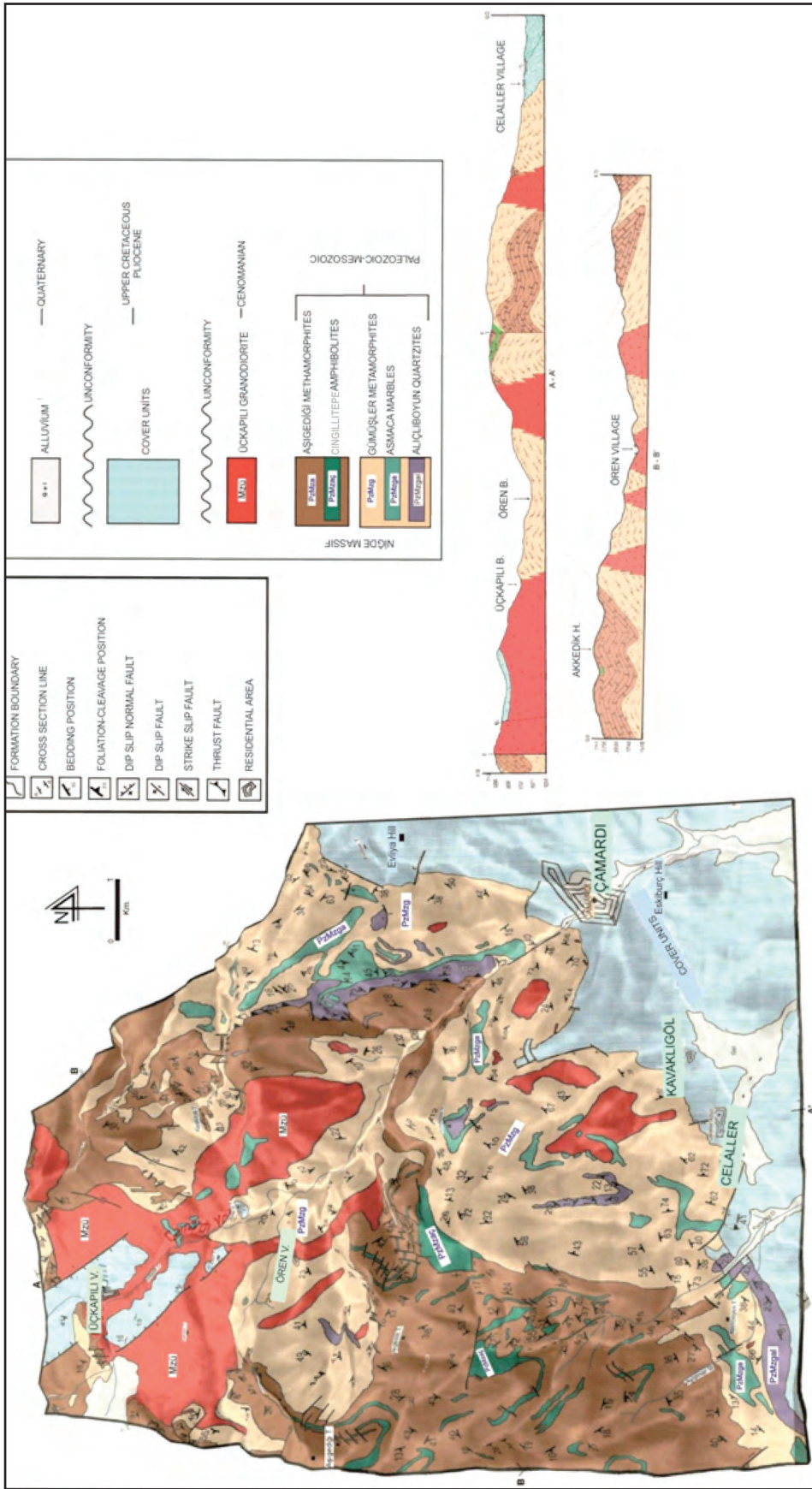


Figure 2- geological map of the study area and geologic cross sections (Demircioğlu, 2001).

to the study of Göncüoğlu (1977 and 1985) its age is Cenomanian-Maastrichtian.

2.4. Cover Units

In the study area, the Niğde Massif is unconformably covered by Late Cretaceous-Quaternary aged units. The first assemblage of the cover units is constituted by the Celaller and Eskiburç groups which have developed depending on the opening and closing of the Ulukışla Basin in the district. They unconformably cover the metamorphites belonging to the Niğde Massif and the Üçkapılı Granodiorite (Figure 3). Within the Çamardı formation there are pebbles belonging to the Üçkapılı Granodiorite.

The Paleocene-Eocene aged Celaller Group comprises the Paleocene-Eocene aged Çamardı formation and the Eocene-aged Evliyatepe formation. The Celaller Group is tectonically overlain by the Eskiburç Group in the district. The Eskiburç Group is composed of Late Cretaceous-Paleocene aged Ulukışla migmatites and Paleocene-Eocene aged Ovacık formation. They show lateral-vertical transitions with each other. These units have been subjected to low-grade metamorphism (Demircioğlu and Eren, 2000, 2001 and Demircioğlu and Eren, 2003). The above-

mentioned units are unconformably covered by the Oligocene-Quaternary aged neo-autochthonous post-orogenic rocks in the district.

3. Structural Geology

According to Göncüoğlu et al. (1981), the rocks belonging to the Niğde Massif are Paleozoic-Mesozoic aged and have been influenced by orogenic activities prior to Late Cretaceous era. Göncüoğlu (1981) states in his work that the rocks belonging to the Massif have been folded and faulted through a deformation having at least 3 phases, one of the phases solid and the other two plastic. Atabey et al. (1986) states that the Caledonian and Hercynian Orogenesis have influenced only the Niğde Massif; but, the Alpine Orogenesis have influenced both the Massif and the young units covering the Massif. Henden (1983) states in his work that the main structure in the district is constituted by dome structures depending on the granitoid intrusion.

For the detailed structural analysis of the Massif, the structural map of the district has been constructed and the area has been separated into sub-areas depending on the trend of map and mesoscopic scale structures (Figure 4). Accordingly, the study area has been separated into four sub-areas as the Ortakaya sub-area, the Akgedik sub-area, the Kartalkaya sub-area, and



Figure 3- The contact between Üçkapılı Granodiorite and Çamardı formation.

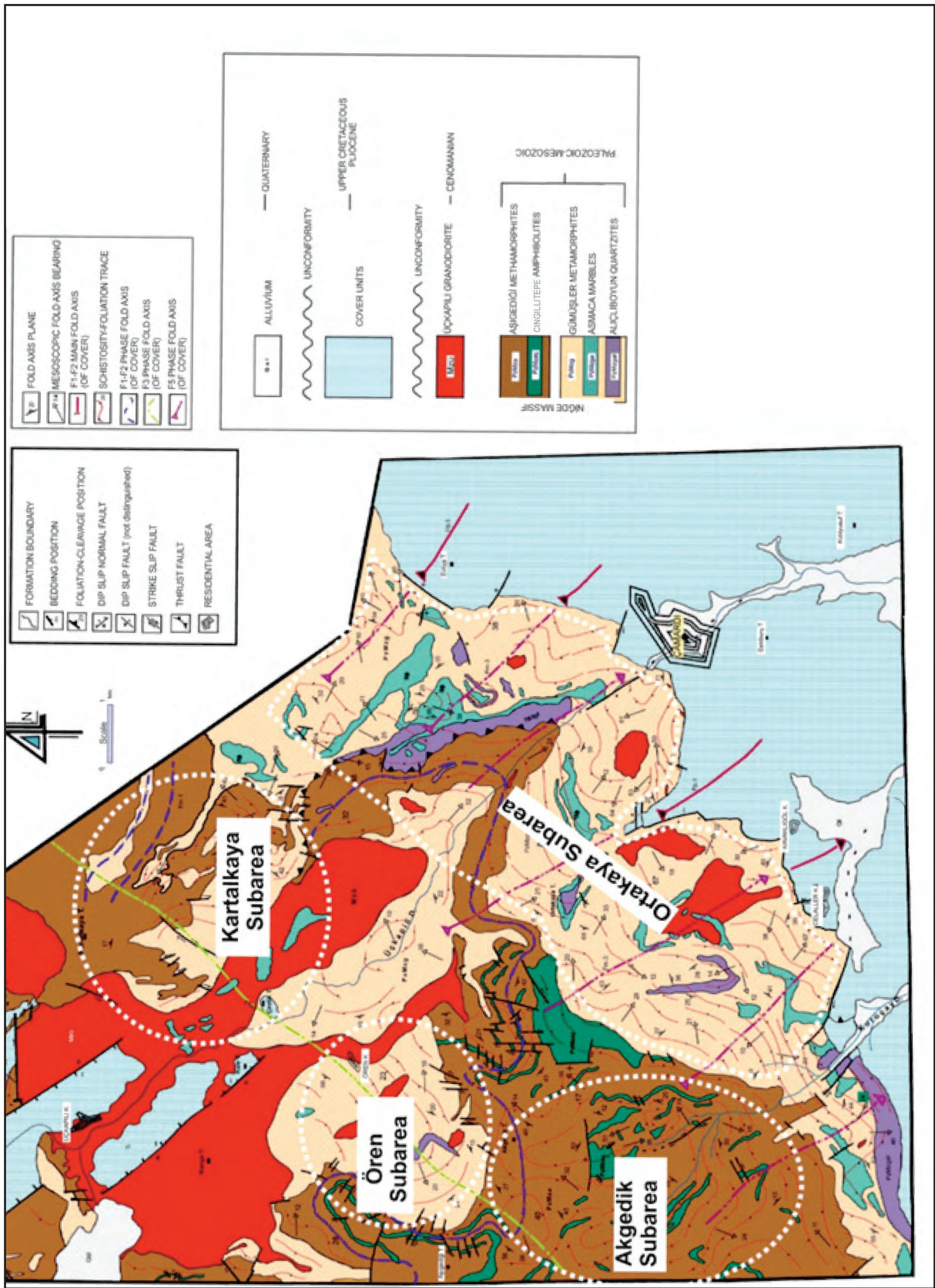


Figure 4- Structural map of the study area and sub-areas.

the Ören sub-area. Field observations and mesoscopic analyses demonstrate that the metamorphites of the Niğde Massif have been subjected to a ductile deformation (folding) having at least five phases (F_1 , F_2 , F_3 , F_4 , F_5) (Figure 4).

Through the D_1 phase deformation (F_1 phase folding), the rocks of the Massif have been subjected to map scale recumbent-isoclinal folding and have gained a structure with a S_1 -foliation (with gneissose banding) which is parallel to the fold axis planes (Figure 5a). F_1 -phase folds are encountered mostly in the sections of the study area where there is marble/metachert alternation (Figure 5b). The folds of this phase are generally in the form of recumbent-isoclinal folds and in appearance present similar fold features.

Again through D_1 phase deformation, in the district, (coaxial) Type-3 type folded folds have developed as a result of the overlying of the coaxial F_2 phase folds the F_1 phase folds (Figure 5 c, d).

During this phase, as a result of the isoclinal and intense folding of the bedding planes (S_0) and the rupture of the more competent material within the rock, bedding transposition has developed and transposed folding structures have developed (Figure 5e, f and Figure 6a). The metacherts in the marbles have gained pinch and swell structure depending on the extension during folding (Figure 6b). The metacherts occasionally display pseudo-bedding feature, too (Figure 6c). These structures prove that in the Çamardı district, notwithstanding the intense metamorphism, the primary structures have been preserved.

Through D_2 phase deformation, northeast-southwest trending and dipping both northeast and southwest map scale folds (F_3 phase folding) have developed (Figure 4).

As a result of the interference of F_1 - F_2 and F_3 phase folds, in the district, folds, generated by Type-2 folding, have formed (mushroom folds) (Figure 6b). Second phase mesoscopic folds are of tight-isoclinal geometry and display asymmetrical and inclined fold feature.

In the study area, as a result of D_3 phase folding a large dome structure has developed in the district (F_4 phase folding). This folding is most probably the result

of the deformation that the Üçkapılı Granodiorite formed while it was intruding into the rocks of the Massif. D_4 phase deformation has deformed both the Massif and the Paleocene-Eocene aged cover rocks simultaneously (Figure 4). The folds which have formed during this phase (F_5 phase folding belonging to the Massif) have formed map scale synformal and antiformal structures that are trending approximately perpendicular to F_3 phase, plunging southeast and have northwest-southeast trend.

As a result of this deformation (D_4), cusped-lobate type structures have developed which are peculiar to the districts where basement rocks and Paleocene-Middle Eocene aged cover rocks have been deformed together. As a result of the folding, the cover units have formed tight synclinals inside the rocks of the Massif, and the basement rocks have formed, towards the cover units, map scale folds having broad and round anticlinal geometry (Figure 4). The Üçkapılı Granodiorite in the area has gained meta granodiorite feature and fracture systems have developed in it.

In the study area, for the geometrical analysis of the map scale folds, foliation (gneissose banding), banding, and schistosity measurements have been taken from the rocks belonging to the Massif, and these have been evaluated on the stereographic projection depending on the sub-areas (Figure 7).

In the Kartalkaya sub-area, when the banding measurements of the Aşıgediği marbles and the banding measurements in the quartzites are jointly evaluated, fold axis trends are observed in almost every direction (probably depending on the dome structure) (Figure 4). However, the general fold axis trend in this area has been determined as N58E/20NE (Figure 7a).

In the Akgedik sub-area, when the bandings observed in the marbles and the measurements of the schistosity planes in the amphibolites are evaluated on the diagram, the general fold axis trend in this area has been determined as N44E/12SW (Figure 7b).

These fold axis trends obtained from the Kartalkaya and the Akgedik sub-areas correspond to the F_3 -phase folding phase.

It is observed that the mesoscopic fold axis trends determined in the Ören sub-area are in every direction (Figure 4). Also, when the fold axis trends measured

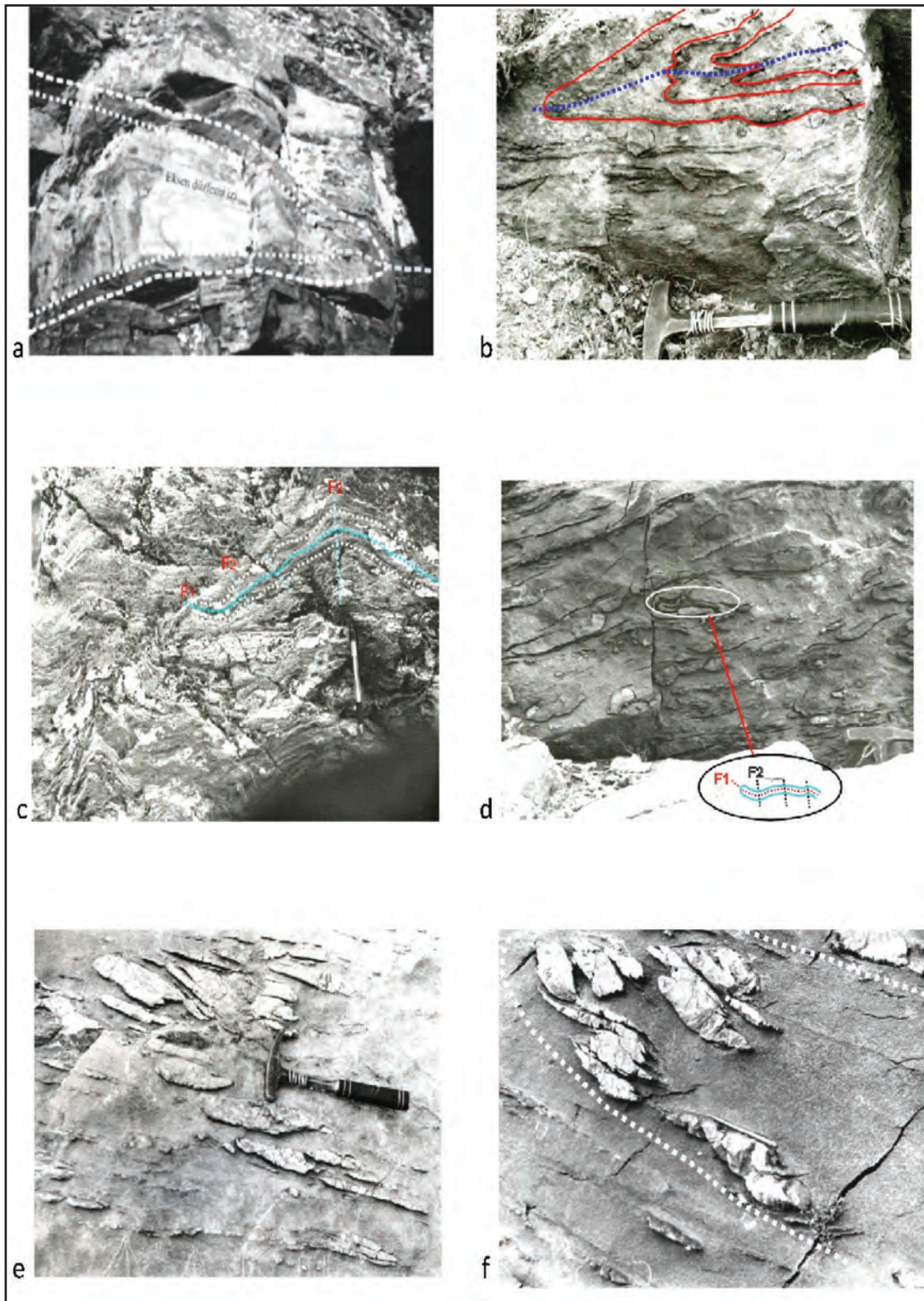


Figure 5- Folds and structural elements observed in the rocks of the Massif.

a - Recumbent-isoclinal folding and structure with S1-foliation (with gneissose banding) parallel to the fold planes
 b- F_1 phase folds in sections with marble-metachert alternation c, d - (coaxial) Type-3 type folded folds developed in the district as a result of the overlying of the coaxial F_2 phase folds the F_1 phase folds e, f - bedding transposition-transposed folding structures developed as a result of the isoclinal and intense folding of the bedding planes (S_0) and the rupture of the more competent material within the rock.

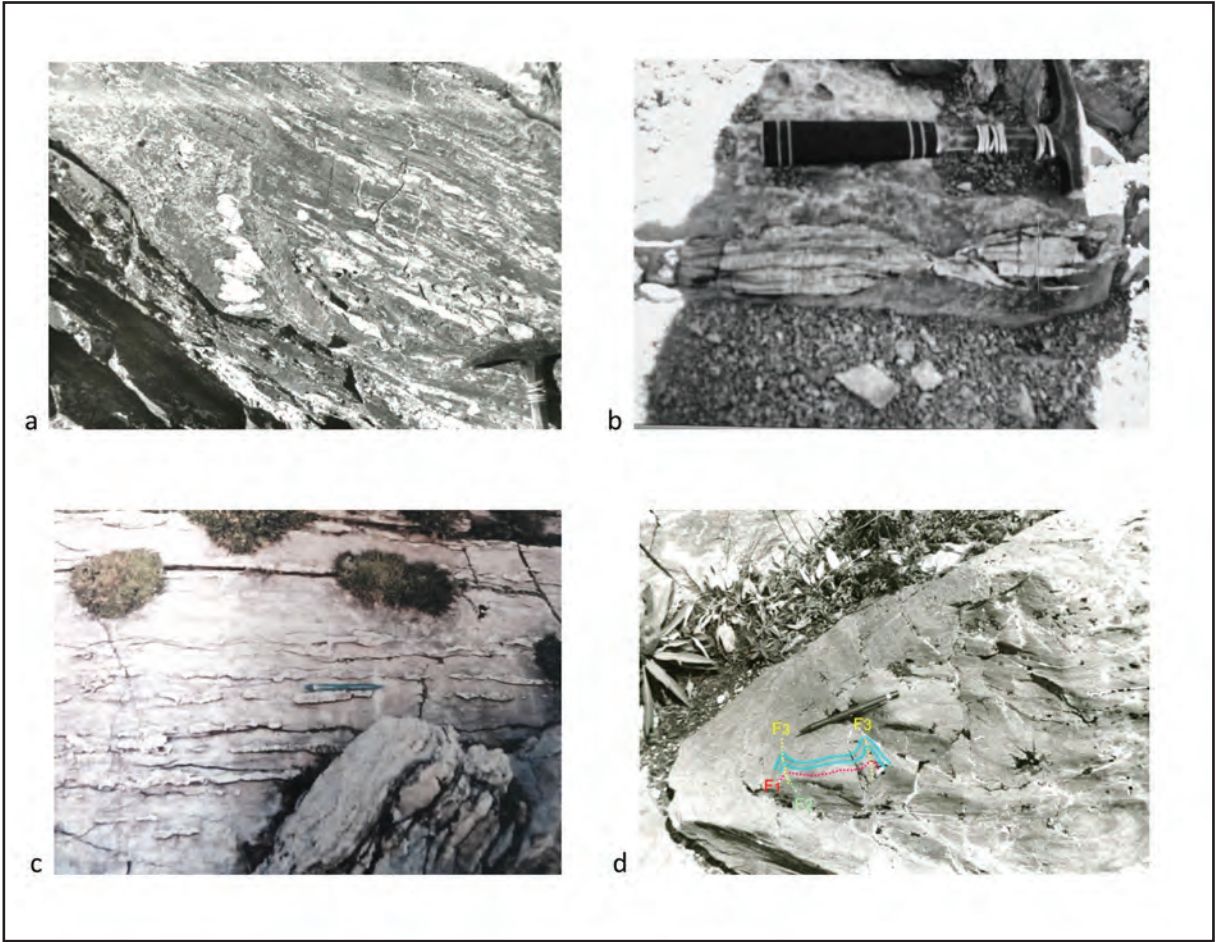


Figure 6- Structures observed in the rocks of the Massif.

- Bedding transposition and transposed fold structures observed in the gneisses within the Gümüşler metamorphites,
- In the Aşıgediği metamorphites, pinch and swell structure depending on the extension in the metacherts within the marbles,
- Pseudo-bedding observed in the metacherts,
- Type-2 type folded folds (mushroom folds) developed as a result of the interference of F_1 - F_2 and F_3 phase.

in this area are evaluated on the diagram, it has been determined that the fold axis trends are in every direction (Figure 7c). This situation can be related to the doming developed in the area depending on the intrusion of the Üçkapılı Granodiorite, and the folding developed depending on it (D_3 -phase deformation). It is thought that this doming has also caused the folding of the rocks belonging to the Massif (F_4 -phase folding).

In the Ortakaya sub-area, the general fold axis trend obtained as a result of the evaluation of the foliation measurements, taken from the gneisses belonging to the Gümüşler metamorphites, on the diagram, has been determined as N56W/14SE (Figure 7d).

When the mesoscopic fold axes measured in the same sub-area are evaluated on the diagram, it is

observed that the general trends of the fold axes are tending northwest-southeast and the plunge of these axes are toward southeast (Figure 7e). These fold axis trends give the F_5 -phase fold axis trend of the Massif, and are in conformity with the map scale fold trends obtained from the Paleocene-Eocene cover rocks (the fold axes obtained from the bedding positions measured from the formations of the Celaller Group and the Eskibuç group and belong to F_1 and F_2 phase of the cover units) (Figure 7f and Figure 7g) (Eren and Demircioğlu, 2003). As to the fold axis trends of the cover units, it has been found as N43W/28SE in the units of the Celaller group (Figure 7f) and as N46W/40SE in the units of the Eskibuç group (Figure 7g) (Eren and Demircioğlu, 2008).

When the general banding measurements obtained from the marbles and the quartzites belonging to

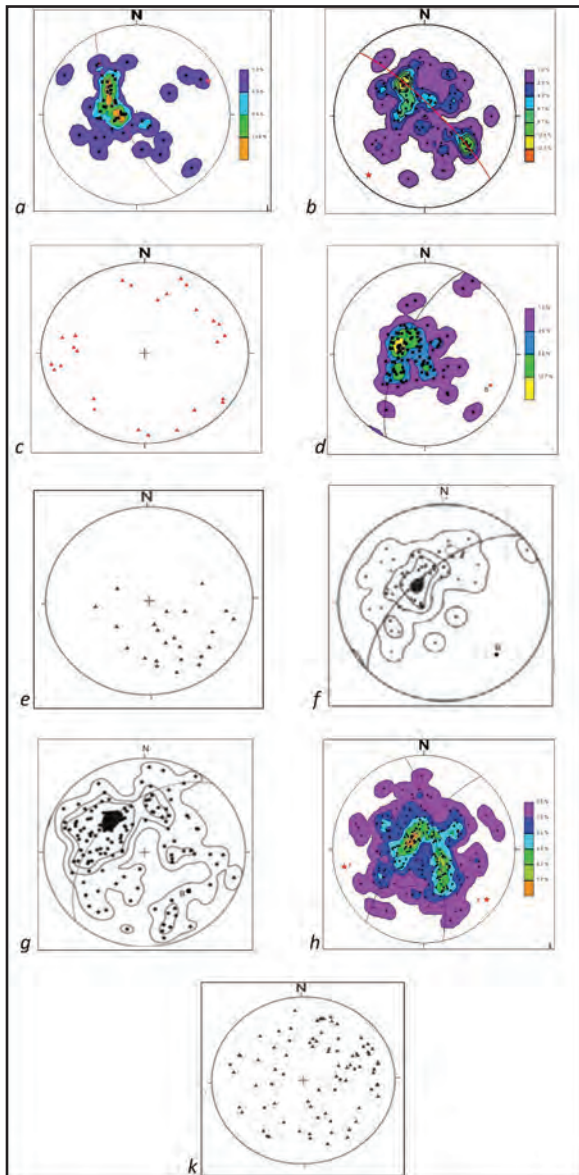


Figure 7- Lower hemisphere projection diagrams of the mesoscopic data in the study area.

the Aşığıdiği metamorphites have been evaluated on the diagram, the general fold axis trends have been determined as N52W/16SE and N78E/15SW (Figure 7h). Of these fold axis trends, the fold axis with N52W/16SE trend is in conformity with the fold axis trend obtained from the Ortakaya sub-area (F_5 phase folding). And the fold axis with N78E/15SW trend shows similarity to the fold axis trend (F_3 -phase folding) obtained from the Akgedik sub-area.

In the study area, when the mesoscopic fold axes trends measured in the rocks of the Massif are evaluated on the diagram (stereographic projection), it is observed that the fold axes trends show distribution

in every direction (Figure 7k). This situation is an indication which shows that the rocks of the Massif have been subjected to deformation in every direction and depending on it to polyphase folding.

In the study area, there are some situations showing similarities and differences with the previous studies. In the previous studies; there are differences between the geologic map used by Gautier et al. (2002, 2008), Whitney et al. (2003, 2007), Idleman et al. (2014) and the geologic map used by Demircioğlu (2001). In addition, while the studies carried out after 2000 are generally related to the burial-exhumation and the metamorphism of the Niğde Massif, this study aims to reveal the polyphase deformation of the rocks belonging to the Massif and the developed fold-fold interference types. During the burial-exhumation, yo-yo tectonics and metamorphism of the rocks belonging to the Massif, the rocks have been subjected to polyphase folding and fold interference structures have formed.

In the area, during the thin section examinations carried out on the metasandstones taken from the Paleocene-Eocene aged units, which have been mentioned in this study as cover units without giving into detail, asymmetrical pressure shadow structures have been determined that have developed in the ductile detachment zones. These structures might be the indication of a detachment fault developed after Middle Eocene. In addition, within the metasandstones of Middle Eocene aged Evliyatepe formation, the existence of outcrop scale sigmoidal veins developed in the brittle-ductile slip zones has been determined (Demircioğlu, 2001). In the rocks of the Massif, a thrust fault developed on the map scale is present. It is thought that this thrust has formed during the compressions causing map scale folding (D_4 -phase deformation).

According to this study, differing from the previous studies, in the study area, the metamorphic rocks of the Niğde Massif have been subjected to a deformation with at least 4 phases (D_1 - D_2 - D_3 - D_4). 5-phase folding (F_1 - F_2 - F_3 - F_4 - F_5) has developed in the rocks belonging to the Massif. Within the rocks of the Massif, depending on the deformations and foldings, mesoscopic fold axes have developed which are trending-plunging in every direction.

Through D_1 phase deformation, the metamorphic rocks have been subjected to recumbent-isoclinal folding and they have formed coaxial Type-3 type fold structures with the development of F_1 and F_2 phase foldings.

Through D_2 phase deformation, the rocks of the Massif have been re-folded (F_3 phase folding) and as a result of the fold interference, they have formed mushroom-shaped Type-2 type folds. According to the data obtained from the sub-areas, the general fold axis trends belonging to this phase have been found as N58E/20NE and N44E/12SW.

D_3 phase deformation has probably developed during the intrusion of the Üçkapılı Granodiorite into the rocks of the Massif and has re-folded the rocks of the Massif (F_4 phase folding). During this phase, folds have formed which are trending and plunging in every direction.

Through D_4 phase deformation, the rocks of the Massif have been subjected to folding (F_5 phase folding). The fold axis trends (N58W/21SE) obtained from the rocks of the Massif and the F_1 - F_2 phase fold axis trends (N43W/28SE and N46W/40SE) of the cover units are compatible with each other.

Again during this phase, the units of the Massif and the units of the cover have been together subjected to folding and have formed cusped-lobate structures.

References

- Atabey, E., Ayhan, A. 1986. Niğde – Ulukışla – Çamardı – Çiftehan Yöresinin Jeolojisi. Maden Tetkik ve Arama Genel Müdürlüğü Rapor No. 8064 (unpublished).
- Atabey E., Göncüoğlu M.C., Turhan N. 1990. Türkiye Jeoloji Haritaları Serisi, Kozan 119 Paftası 1:100.000. Maden Tetkik ve Arama Genel Müdürlüğü. MTA/Ankara.
- Blumenthal, M. 1941. Niğde ve Adana Vilayetleri Dahilindeki Torosların Jeolojisine Umumi Bir Bakış. Maden Tetkik ve Arama Genel Müdürlüğü Yayını, Seri B, No:6, 95s. Ankara.
- Blumenthal, M. 1952. Toroslarda Yüksek Aladağ Silsilesinin Coğrafyası, Stratigrafisi ve Tektoniği. Maden Tetkik ve Arama Genel Müdürlüğü Yayını, Seri: D, No: 6, 136s. Ankara.

- Dellaloğlu, A. A., Aksu, R. 1986. Ereğli (Konya) – Ulukışla – Çiftehan – Çamardı (Niğde) Dolayının Jeolojisi ve Petrol Olanakları. Türkiye Petrolleri Anonim Ortaklığı Rapor No. 2205. Ankara.
- Demircioğlu, R. ve Eren, Y. 2000. Çamardı (Niğde) civarında Niğde Masifi örtü birimlerinin yapısal özellikleri, N.Ü. Aksaray Mühendislik Fakültesi, Haymana-Tuzgözü-Ulukışla basenleri uygulamalı çalışma (Workshop), Bildiri özleri, s. 6. Aksaray.
- Demircioğlu, R. 2001. Çamardı (Niğde) Yöresinin Jeolojisi ve yapısal özellikleri. Yüksek Lisans Tezi, Niğde Üniversitesi, Fen Bil. Enstitüsü, 89 s. (unpublished).
- Demircioğlu, R., Eren, Y. 2003. Niğde Masifi (Çamardı-Niğde) Tersiyer yaşlı örtü kayaçlarındaki Oligosen öncesi paleogerilme konumu. Süleyman Demirel Üniversitesi Müh. Mim. Fak., 20. Yıl Jeoloji Sempozyumu. Bildiriler, s. 37.
- Eren, Y., Demircioğlu, R. 2008. Çamardı (Niğde) yöresinde Paleosen-Eosen birimlerindeki lüfisi damarlar ve yapısal yorumu. Pamukkale Üniversitesi, Mühendislik Bilimleri Dergisi, 14/2, 145-154.
- Gautier, P., Bozkurt, E., Hallot, E., Dirik, K. 2002. Pre-Eocene exhumation of the Niğde Massif, Central Anatolia, Turkey. Geological Magazine, 139/5, 559-576.
- Gautier, P., Bozkurt, E., Bosse, V., Hallot, E., Dirik, K. 2008. Coeval Extensional Shearing and Lateral Underflow during Late Cretaceous Core Complex Development in the Niğde Massif, Central Anatolia, Turkey. Tectonics, 27.TC1003–doi:10.1029/2006TC002089.
- Genç, Y., Yürür, M.T. 2010. Coeval extension and compression in Late Mesozoic Recent thin-skinned extensional tectonics in central Anatolia, Turkey. Journal of Structural Geology. 32, 623-640.
- Göncüoğlu, M.C. 1977. Geologie des Westlichen Niğde Massivs. Univ. Bonn, Ph.D. Thesis, 181s.
- Göncüoğlu, M.C. 1981. Niğde Masifi'nde Viridin Gnaysın Kökeni. Türkiye Jeoloji Kurumu Bülteni 24, 45-51.
- Göncüoğlu, M.C. 1985. Niğde Masifi Batı Yarısının Jeolojisi. Maden Tetkik ve Arama Genel Müdürlüğü Rapor No. 5883, Ankara (unpublished).
- Göncüoğlu, M.C., Toprak, G.M.V., Kuşçu, İ., Erler, A., Olgun, E. 1991. Orta Anadolu Masifi'nin Batı Bölümünün Jeolojisi, Bölüm 1: Güney Kesim. Türkiye Petrolleri Anonim Ortaklığı Rapor No. 2909. (unpublished).

- Göncüoğlu, M.C., Erler, A., Toprak, M.V., Olgun, E., Yalınız, K., Kuşçu, İ., Köksal, S., Dirik, K. 1993. Orta Anadolu Masifi'nin Orta Bölümünün Jeolojisi, Bölüm 3: Orta Kızılırmak Tersiyer Baseninin Jeolojik evrimi. Türkiye Petrolleri Anonim Ortaklığı Rapor No. 3313, 104 s. (unpublished).
- Görür, N., Oktay, F.Y., Seymen, İ., Şengör, A.M.C. 1984. Paleotectonic evolution of Tuz gölü basin complex, Central Turkey. In: Dixon, J.E., Robertson, A.H.F. (Eds.), The Geological Evolution of the Eastern Mediterranean. Special Publication of Geological Society London 17, 81-96.
- Henden, İ. 1983. Uzay Görüntülerinden Türkiye Çizgisellik Haritası ve Maden Aramaları İçin Hedef Sahaların Seçilmesi, Bölgesel Çizgiselliklerin Deprem ve Sıcak Su Kaynakları İle İlişkisi. Maden Tetkik ve Arama Genel Müdürlüğü Dergisi 95/96, 68-76.
- Idleman L., Cosca M.A., Heizler M.T., Thomson S.T., Teyssier C., Whitney D.L. 2014. Tectonic burial and exhumation cycles tracked by muscovite and K-feldspar ⁴⁰Ar/³⁹Ar thermochronology in a strike-slip fault zone, central Turkey. Tectonophysics 612-613, 134-146.
- Ketin, İ. 1966. Tectonic units of Anatolia. Bulletin of The Mineral Research and Exploration 66, 23-34.
- Kleyn, P.H. van der., 1968. Field Report on the Geological and Geochemical Prospection in the Niğde – Çamardı Massiv. Maden Tetkik ve Arama Genel Müdürlüğü Rapor No:174, Ankara (unpublished).
- Kleyn, P.H. van der. 1970. Recommendation of Expolaration for Mineralizations in the SW Part of the Niğde – Çamardı Massiv. Maden Tetkik ve Arama Genel Müdürlüğü Rapor No. 4345. (unpublished). Kuşçu, İ., 1992. Geology of the Çamardı-Niğde Region and Madsan Antimony Deposit. METU MSc. Thesis, 133 p.,
- Kuşçu, İ., Erler, A., Göncüoğlu, M.C. 1993. Geology of The Çamardı (Niğde-Turkey) Region, Geosound 23, 1-16. Seymen, İ., 1981a. Kaman (Kırşehir) dolayında Kırşehir Masifi'nin stratigrafisi ve metamorfizması. Türkiye Jeoloji Kurumu Bülteni, 24,101 - 108.
- Seymen, İ. 1981. Kaman (Kırşehir) dolayında Kırşehir Masifi'nin metamorfizması. Türkiye Jeoloji Kurumu 35. Bilimsel ve Teknik Kurultayı İç Anadolu'nun Jeolojisi Sempozyumu, 12 -15.
- Seymen, İ. 1982. Kaman Dolayında Kırşehir Masifi'nin Jeolojisi. Doçentlik Tezi, İTÜ Maden Fakültesi, İstanbul, 164 s.
- Seymen, İ. 1983. Tamadağ (Kaman-Kırşehir) çevresinde Kaman grubunun ve onunla sınırdış oluşukların karşılaştırılmalı tektonik özellikleri. Türkiye Jeoloji Kurumu Bülteni. 26, 89 – 98.
- Tromp, W., 1942. Kayseri, Niğde, Tuzgölü Arasının Jeolojisi. Maden Tetkik ve Arama Genel Müdürlüğü Rapor No: 1456, Ankara (unpublished).
- Umhoefer, P.J., Whitney, D.L., Teyssier, C., Fayon, A.K., Casale, G., Heizler, M.J. 2007. Yo-yo tectonics in a wrench zone, Central Anatolian fault zone, Turkey. GSA Special Papers 434, 35-57.
- Whitney, D. L., Dilek, Y. 1998. Metamorphism during crustal thickening and extension in central Anatolia: The Niğde metamorphic core complex. Journal of Petrology 39, 1385 – 1403.
- Whitney, D. L., Teyssier, C., Dilek, Y., Fayon, A. K. 2001. Metamorphism of the Central Anatolian Crystalline Complex, Turkey: Influence of orogen- normal collision vs. wrench dominated tectonics on P-T-t paths. Journal Metamorphic Geology 19, 411 – 432.
- Whitney, D. L., Teyssier, C., Fayon, A. K., Hamilton, M. A., Heizler M. 2003. Tectonic controls on metamorphism, partial melting, and intrusion: Timing and duration of regional metamorphism and magmatism in the Niğde Massif, Turkey. Tectonophysics 376, 37 – 60.
- Whitney, D.L., Teyssier, C., Heizler, M.T. 2007. Gneiss domes, metamorphic core complexes, and wrench zones: thermal and structural evolution of the Niğde massif central Anatolia. Tectonics 26, 1-23.
- Whitney, D.L., Umhoefer, P.J., Teyssier, C., Fayon, A.K. 2008. Yo-yo tectonics of the Niğde massif during wrenching in central Anatolia, Turkish Journal of Earth Science. 17, 209-217.
- Viljoen, R. P., İleri, S. 1973. The Geology and Mineralization of Partions in the Pozantıdağı (Niğde) Massif of South Central Turkey. Johannesburg Consolidated Investments Co. Ltd. Geological. Research Department, Unpublished Rep. No. 39, 59s.
- Yetiş, C. 1978. Çamardı (Niğde) Yakın ve Uzak Dolayının Jeoloji İncelemesi ve Ecemiş Yarılım Kuşağı'nın Maden Boğazı – Kamışlı Arasındaki Özellikleri. İÜFF Doktora Tezi., 164s. İstanbul.
- Yetiş, C. 1984. Çamardı (Niğde) alanındaki Oligosen – Miyosen Yaşlı Çökellerin Fasiyes ve Ortamsal özellikleri. Türkiye Jeoloji Kurumu Bülteni 30, 1-8.



Bulletin of the Mineral Research and Exploration

<http://bulletin.mta.gov.tr>



STRATIGRAPHY AND STRUCTURE OF THE SOUTHEASTERN PART OF PİRAMAGROON ANTICLINE, SULAIMANİ AREA, NORTHEAST IRAQ

Kamal Haji KARIM^{a*} and Polla Azad KHANAQA^b

^a Department Geology, College of Science, University of Sulaimani, New camp, Sulaimani city, Iraq

^b Institution for Strategic Studies and Scientific Research, Qrga, Sulaimani city, Iraq

Research Article

Keywords:

Gulneri Formation, Dokan Formation, Kometan Formation, Nannofossil, Pıramagroon Anticline, Stratigraphy of Sulaimani

ABSTRACT

The Pıramagroon anticline (or Pıra Magrun Mountain) elongates directly to the northwest of Sulaimani city, Northeast Iraq and its southeastern part contains two other anticlines, named Harmetool and Yakhyan anticlines in addition to their complementary synclines and many other smaller folds. The anticline has experienced intense search for oil in the last few years and a well is drilled to a depth of 3000 meters but, any evidence of oil or gas wasn't found. In the present study, the southeastern part has been studied stratigraphically and structurally and the previous studies have been critically reviewed which may help to reason about the absence of oil in the area. In this study the stratigraphy of the anticline has been determined and Kometan, Gulneri, Dokan, Balambo and Sarmord formations have been plotted on a geological map and stratigraphic column and the nannofossils have been used for the aging of intervals with undetermined ages. The thickness of the Gulneri Formation is 2-4 m and by the analysis of nannofossils its age was identified as Late Cenomanian-Early Turonian. Lithology and bedding styles of the Dokan and Upper part of the Balambo formations are very similar to Kometan Formation and they can be determined either by fossils or by using Gulneri Formation as marker bed. The outcrop of the Gulneri Formation is helpful for differentiation since it is soft and can be recognized easily in the field by its darker color. The structure of the anticline is relatively complex as it consists of asymmetrical anticlines with southwest plunge mainly in few places while it changes to overturned fold in others and is deformed by reverse fault. The anticlines are shaped by detachments on the Gulneri and Sarmord formations and by the other older soft rocks. The newly formed anticlines have the style of multi-detachment fold or multi-detachment faulted fold.

Received: 29.03.2017

Accepted: 28.07.2016

1. Introduction

The Pıramagroon anticline (or Pıramagrun Mountain) is one of the largest anticlines of Zagros Orogenic Belt in Northeast Iraq and has the length, width and elevation of about 45, 6 and 2.4 kms respectively. It is located between Sulaimani city, from southeast, and Surdash town, from northwest which coincides with the latitudes and longitudes of 35° 36' 57.30" N, 45° 22' 58.33" E and 35° 51' 33.11" N, 45° 05' 21.76" E respectively. Qamchuqa (or Balambo), Kometan, Shiranish and Tanjero Formations are exposed on and around the anticline while its core is occupied by Jurassic rocks (Figure 1). The present study is concerned with its southeastern part which includes the half of the surface area of the anticline. This part is located between Zewy valley at the northwest and Farouq Hotel inside Sulaimani city at the southeast which correspond to the latitude and longitude of 35° 44' 58.43" N, 45° 14' 57.88" E and 35° 34' 15.40" N, 45° 24' 25.17" E respectively.

This part consists of many anticlines; the largest one is called Pıramagroon anticline which plunges near Sutka village (Figure 1). The second largest one is locally famous Harmetool anticline (mountain) which is located at the east and southeast of Pıramagroon anticline.

Previously, Harmetool anticline is called Sulaimani Anticline by Ma'ala (2008) and Al-Hakari (2011). Other anticlines are Sherkuzh and Yakhyan which are located at the north and south of the Harmetool anticline with more than four smaller anticlines (Figure 1).

Very recently an oil company has drilled an oil well on the core of the anticline to the depth of 3000 meters. The well is drilled on Sarmord Formation and reached Triassic Formation without striking any trace of oil or gas. The present study is focused on the stratigraphy and structural properties of the southeastern part of Pıramagroon anticline. The

* Corresponding author: Kamal Haji Karim, kamal.karim@univsul.edu.iq
<http://dx.doi.org/10.19111/bulletinofmre.305987>

study is based on geologic mapping and structural analysis in addition to stratigraphic differentiation by nannofossils. Additionally, by this study it is planned to add more useful data and new geological results to the previous studies such as Aziz et al. (1999) (Figure 2), Ma, ala (2008), Al-Hakari (2011) (Figure 3) and Omar et al (2015).

1.1. Geological Setting

Tectonically, the studied area is part of the northeastern margin of the Arabian Plate, where the

previous Early Cretaceous platform has transformed to a foreland basin during the Late Cretaceous (Karim, 2004). According to the tectonic subdivision of Iraq by Buday and Jassim (1987), Jassim and Goff (2006) the study area is considered to be located in the High Folded Zone while it is considered to be located in the Simply Folded Zone at the classification of whole Zagros belt by Ghasemi and Talbot (2006) (Figure 1b).

In the north of the study area (Mawat-Chwarta area) a large graben is located in which ophiolites, Tertiary, and Upper Cretaceous formations are

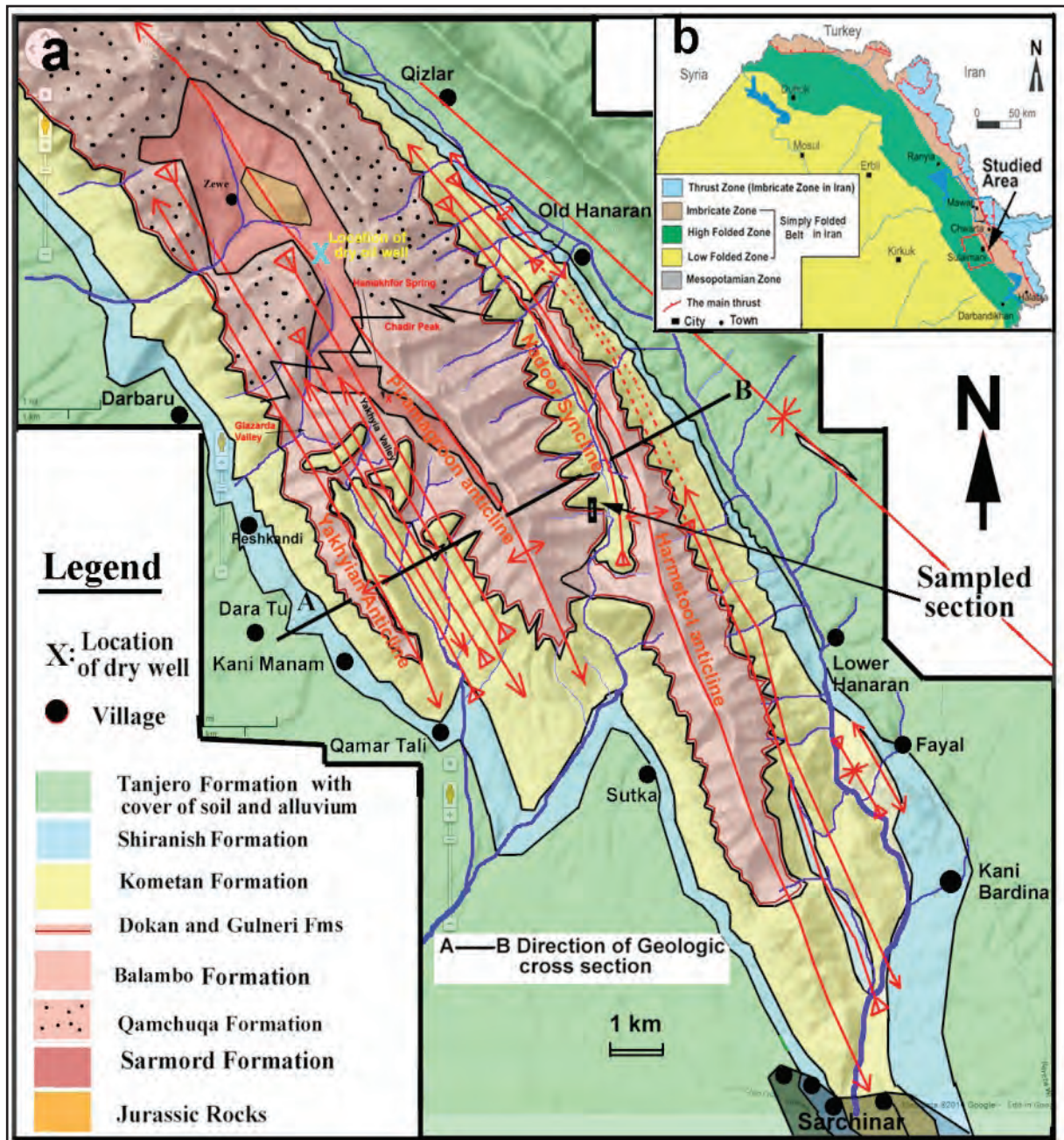


Figure 1- a) Geological and b) tectonic maps of the studied area.

outcropped. In the Graben, the Main Zagros Thrust can be observed between Qulqula Radiolarian Formation and Red Bed Series. The Upper Cretaceous Formations are Shiranish (marl), Tanjero (sandstone, marl and conglomerate) and Aqra (fossiliferous and detrital limestone) Formations (Karim, 2004; Al-Kubaysi 2008; Sadiq 2010; Özer et al. 2013; Karim and Khanaqa 2014).

Between the Graben and the study area, Azmir anticline and Chaqchaq syncline are located which are dissected by consequent valleys in which best outcrops of Cretaceous and Jurassic rocks are available for geological studies. The formations, on the anticline and in the syncline, have the same properties as those that are exposed on and around Piramagroon anticline and will be discussed in the next sections of this paper in details.

2. Result and Discussion

2.1. Stratigraphy of the Study Area

The stratigraphic study of the southeastern part of Piramagroon anticline is very important in four ways. The first one is that the study area is the zone of facies change between Qamchuqa and Balambo formations (Ameen, 2008). In this area, the thick

and massive dolomitic limestone (competent beds) of the Qamchuqa Formation, from the west, changes to well bedded limestone and marly limestone (incompetent) of Balambo Formation. Therefore, the phrase “Qamchuqa/Balambo transition or QBT” is used for the equivalent of Qamchuqa Formation in the transition zone. The second is that the transitional zone, structurally, consists of alternation of competent and incompetent beds which reflect different deformational patterns that are the combination of the two end members. The third is expanding of the urbanization of the Sulaimani city towards the study area which may cover most parts during the forthcoming decade. Fourth is that the boundary between Balambo (or its reefal equivalent of Qamchuqa Formation) and Kometan Formation (Turonian-Campanian) is well exposed in the study area.

The boundary must contain either the rocks of Cenomanian- Turonian ages or events (unconformities). Many authors (Sharland et al., 2001; Al Hussaini and Matthews, 2008; Al-Qayim et al., 2012; Lawa and Gharib, 2009 and Omar et al., 2015) have cited major unconformity in this boundary. Lawa et al. (2011 in Al-Hakari, 2011) have cited that during the early Turonian, the Qulqula Radiolarian Formation and main igneous complexes were uplifted and acted as Hinterland for Foreland basin. Buday

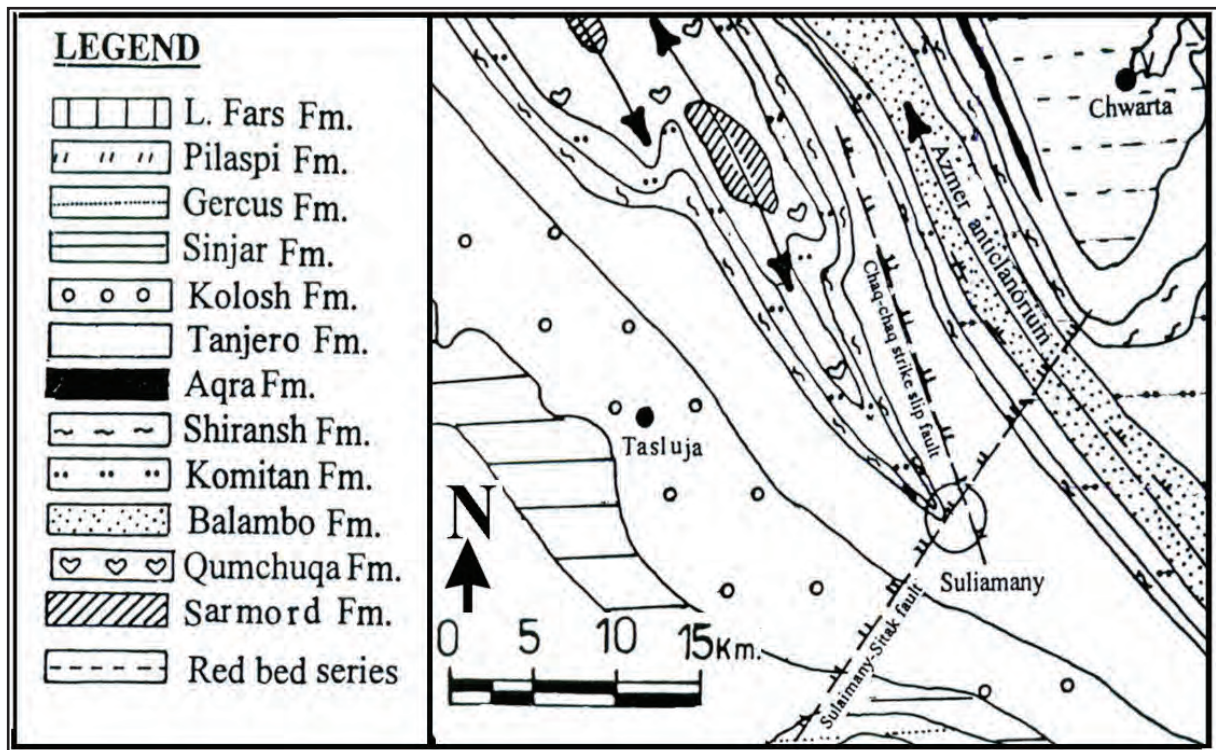


Figure 2- Geological map of the study area which shows two strike-slip faults (Aziz et al., 1999).

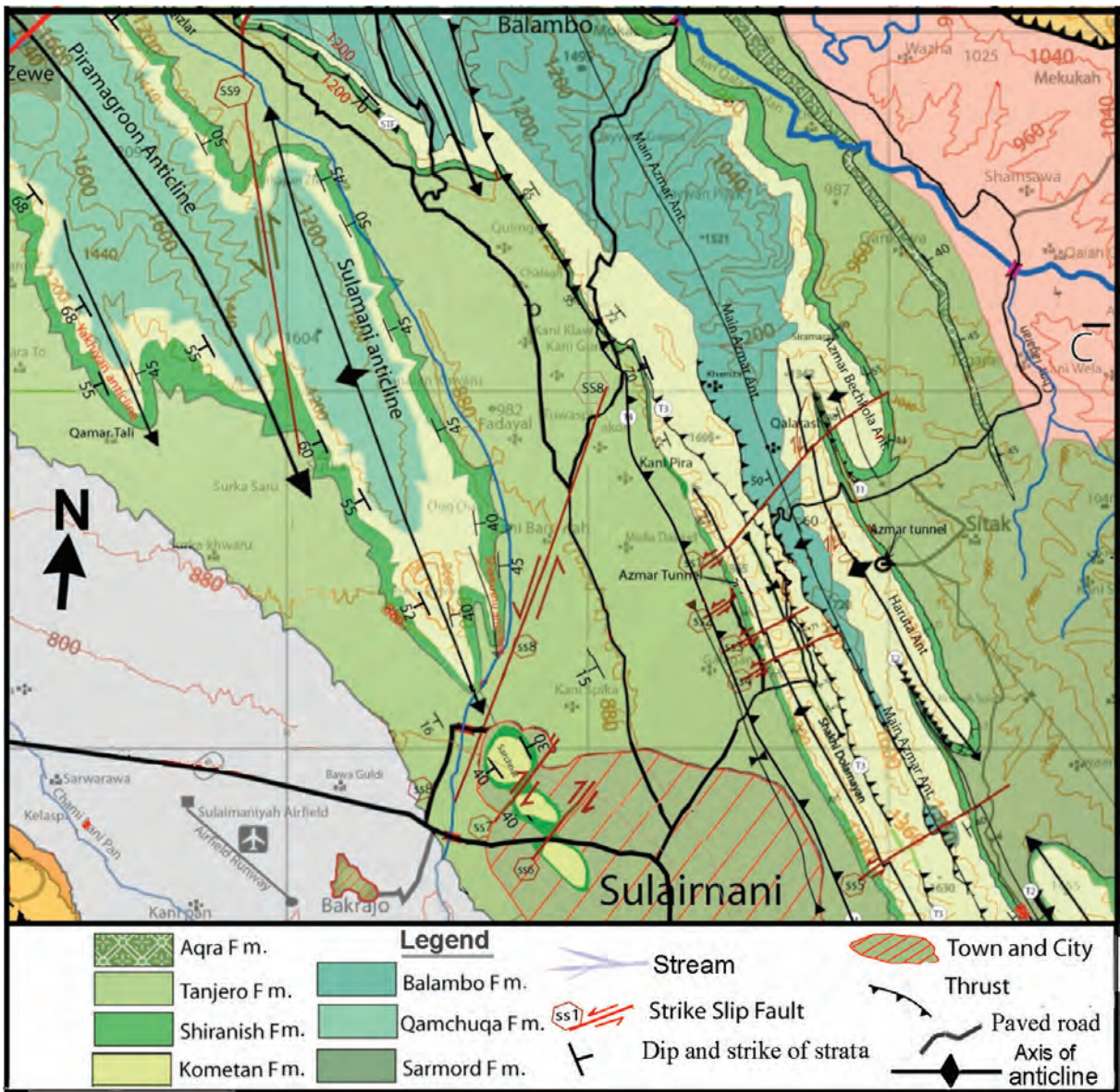


Figure 3- Geological map of the studied area (Sissakian, 2000 and Ma,ala, 2008 and modified by Al-Hakari, 2011) showing the strike slip faults that indicated by the latter authors.

(1980) and Jassim and Goff (2006) have referred that Qulqula Conglomerate Formation had deposited at the top of the Qulqula Radiolarian Formation during the Cenomanian-Turonian age. This deposition is recently referred by Ibrahim, 2009 and Al-Qayim et al. (2012).

The present study, field inspection across many sections, has not revealed any of above signatures. Moreover, the nannofossil analysis of the boundary between Qamchuqa (or Balambo) and Kometan formations showed that the Gulneri and Dokan formations exist in the boundary and unconformities are not observed (Figure 1 and 4). This result agrees

with the conclusion of the Karim and Taha (2009) who refused the unconformities that previously established at the base and at the top of the Gulneri Formation in Dokan area. The latter study concluded that the formation consist of marl and marly limestone without black shale. Karim et al. (2013) found both formations on the Azmir and Goizha anticlines and prepared a detail map of the area to the north and east of Sulaimani city which show the outcrops of the two formations.

Previously, Aziz et al. (1999), Ma,ala, (2008) and Al-Hakari, (2011) mapped the study area and

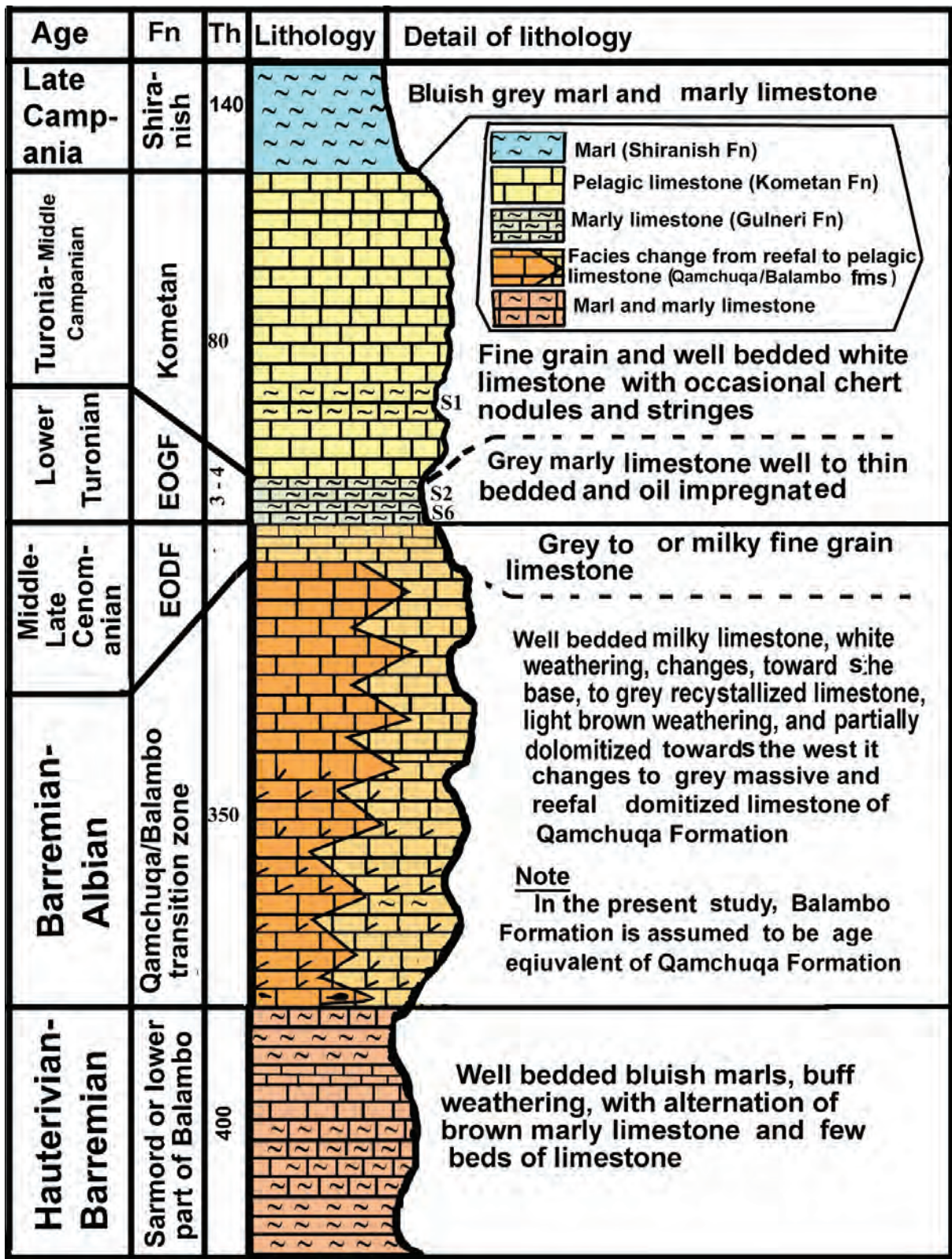


Figure 4- Stratigraphic column of the studied area drawn from the result of the present study.

indicated Qamchuqa, Kometan, Shiranish and Tanjero formations on the crest, upper and lower limbs of the anticline respectively (Figure 1 and 2). The above authors have not recorded the Gulneri and Dokan Formations. In the study area around Sulaimani City Al-Hakari (2011) and Omar et al. (2015) indicated (by stratigraphic column) that there are unconformities between Qamchuqa and Kometan formations where both Dokan and Gulneri formations are missing. About the contact between Kometan and Shiranish Formations, they showed that there is an unconformity between the two formations while the present study didn't record any unconformities and field and fossil analysis indicated conformable nature of the boundaries of the above four formations.

2.1.1. *Gulneri Formation*

The Gulneri Formation was first described by Lancaster Jones (1957) and Bellen et al. (1959) near the Dokan Dam site at the west of Sulaimani city, which consists of about 2 m black, bituminous, finely laminated, calcareous shale with glauconite and colophane at its lower part. The age of the formation is Early Turonian (Bellen et al., 1959).

The high bitumen content and dwarfed fossils indicate that the Gulneri Formation was deposited in an euxinic environment (Jassim and Buday, 1987; Jassim and Goff, 2006). The formation is separated by unconformities with both the overlying and the underlying Kometan and Dokan formations respectively (Buday, 1980). The present study found that it consists of well bedded marly limestone mainly and is laminated and oil impregnated occasionally. In all sections, shale has not been found and the observed lithology of marly limestone is same with the conclusion of Karim and Taha (2009) who reused the previous lithology (black shale) of Gulneri Formation at the type section near Dokan dam site. Karim and Taha (2009) has showed that the formation is deposited in the large basin in which Balambo and Kometan Formations are deposited, by model.

In the study area, the upper part of Balambo Formation, Dokan and Kometan formations are very similar in lithology and bedding patterns (Figure 5). They can be separated either by foraminifera study or by identifying Gulneri Formation which is located

between the two formations. The latter formation can be observed in the field which appears as a covered dark ribbon between white limestones of Kometan and Balambo Formations. The thickness of Gulneri Formation is about 2-4 m. Between Dokan and Surdash towns, it is located between Dokan and Kometan Formation and it consists of dolomitic limestone without marl and marly limestone but it is thinly bedded and due to this property, it is highly deformed as seen in Tabeen Gorge where Karim (2014) showed a photo of the formation to prove its existence. Therefore, the result of the present study refuses the presence of the Turonian unconformity in North Eastern Iraq that was mentioned before. Lawa et al. (2013) cited an unconformity and mentioned that Dokan and Gulneri formations are not present (an unconformity with duration of 4.7 m.y) in the Tabeen Gorge 4 km to the southeast of Surdash village. Similarly, Omar et al. (2015) have recorded the unconformity and they noted the absence of Dokan and Gulneri Formations (Late Cenomanian to Early Turonian age) at the top of the Balambo and Qamchuqa Formations. They attributed this absence to the reactivations of ChaqChaq fault and tectonic uplifting of the Mawat ophiolite obduction during the Turonian. They further added that the top of the latter two formations are characterized by the disappearance of planktonic foraminiferal, nannoplanktons and palynomorphs. They assigned this gap as Pre-Aruma unconformity and attributed it to ophiolite obductions. In the present study, the sediments of the Gulneri and Dokan Formations are found and they contain in many place both nannofossils and planktonic forams.

2.1.2. *Nannofossils Analysis of Gulneri Formation*

Omar et al. (2015) cited that the top of Balambo Formation is unconformity and does not contain nannofossils while at the the present study many index nannofossil species which represent the age of Gulneri and Dokan formations have been found in the formation.

In the study area, the outcrops of Gulneri Formation are mostly covered and weathered; therefore, fresh sampling is difficult. For sampling, one meter deep holes have been excavated on the outcrop of the the formation. The six samples have been sent to Romania for nannofossil analysis and age determination. A

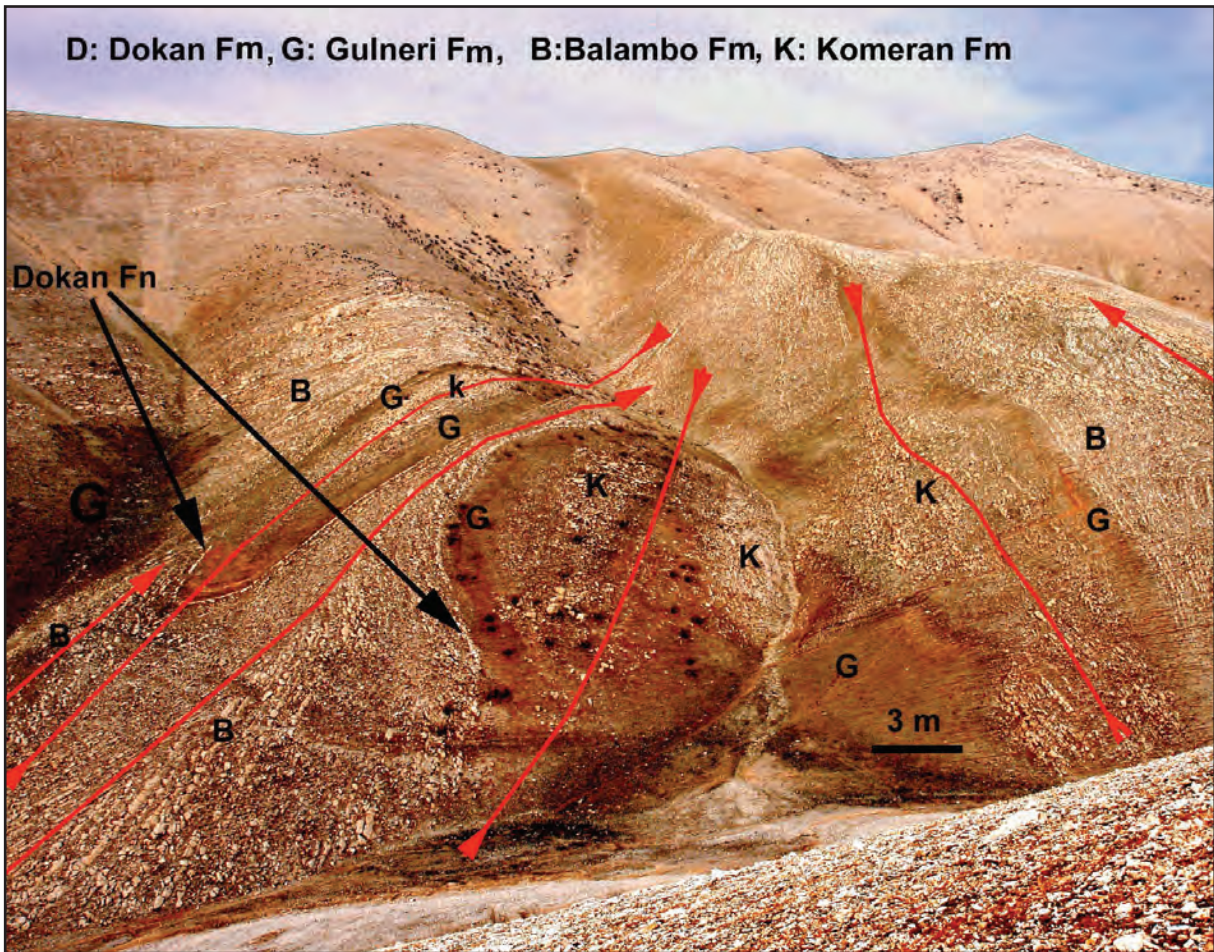


Figure 5- Southwestern side of the Nadoor valley shows the minor folding and stratigraphic differentiations.

detail report is prepared by Dr Ramona Balc (ramona.balc@ubbcluj.ro) for the nannofossils which gave the age of Late Cenomanian-Early Turonian for the sampled interval (Figure 6 and 7).

Nannofossils Species:

The age of the studied samples is given by the presence of *Corrolithion kennedyi* and *Quadrum intermedium*. The first mentioned species was identified only in one sample (sample 5). Thus, this level falls in UC3d Nannofossil Subzone (Burnett, 1998), which is Late Cenomanian in age. The top of this subzone is defined by the last occurrence (LO) of *C. kennedyi*. Next level (sample 4 and sample 3) covers the UC3d – UC5b Nannofossil Subzones, the bioevents mark the base of the UC5b which is represented by the first occurrence (FO) of *Quadrum intermedium*. The age of the above mentioned interval is Late Cenomanian. The last level (samples 2 and 1) falls in UC5c Nannofossil

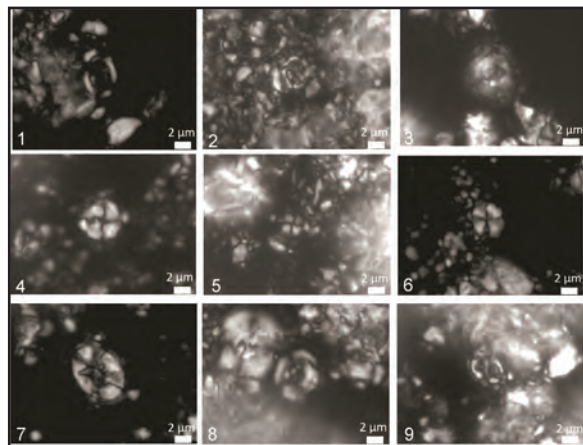


Figure 6- Species of the result of the nannofossil analysis which gives the age of Late Cenomanian-Early Turonian. Species are: 1. *Broinsonia enormis* (Sample 1); 2. *Corrolithion kennedyi* (Sample 5); 3. *Cylindralithus* sp. (Sample 5); 4. *Cylindralithus nudus* (Sample 5); 5. *Discorhabdus ignotus* (Sample 5); 6. *Eprolithus floralis* (Sample 2); 7. *Eiffelithus turriseiffelii* (Sample 2); 8. *Helenea chiastia* (Sample 5); 9. *Helicolithus trabeculatus* (Sample 5); All photos are taken under XP light.

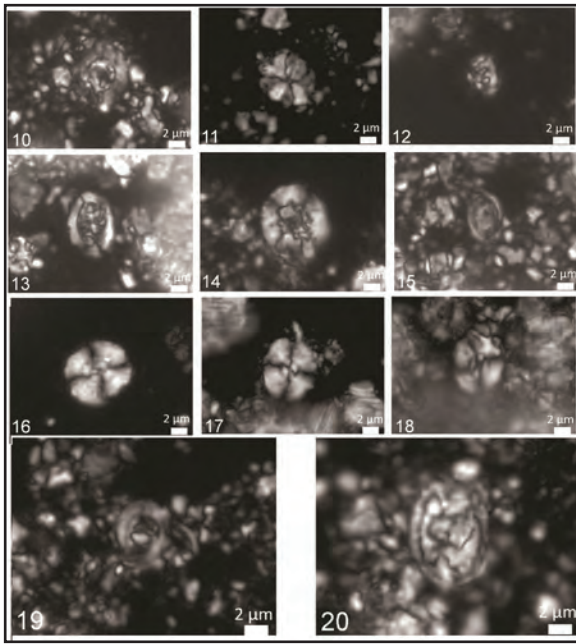


Figure 7- **10.** *Prediscosphaera cretacea* (Sample 1); **11.** *Quadrum intermedium* (Sample 3); **12.** *Rhagodiscus achlyostaurion* (Sample 5); **13.** *Rhagodiscus asper* (Sample 4); **14.** *Retecapsa crenulata* (Sample 3); **15.** *Tranolithus orionatus* (Sample 5); **16-17.** *Watznaueria barnesiae* (Sample 2); **18.** *Watznaueria ovate* (Sample 1); **19.** *Zeugrhabdotus diplogrammus* (Sample 4); **20.** *Zeugrhabdotus embergeri* (Sample 3). All photos are taken under XP light.

Subzone, the base of this subzone is defined by the FO of *Q. intermedium* (Figure 6). The age of this subzone is Late Cenomanian–Early Turonian.

2.2. Structure of the Study Area

When we examine the accurate analysis held in the preceding sections about the stratigraphy of the study area, the structure analysis kept in more update conditions is much more suitable than the previous studies.

2.2.1. Strike Slip and Reverse Faults

Aziz et al. (1999) have recorded two strike slip faults and called them Sulaimani-Sitak and Chaqchaq strike slip faults. They have indicated the two faults intersecting beneath western part of Sulaimani city ($35^{\circ} 34' 15.40''$ N and $45^{\circ} 24' 25.17''$ E) (Figure 1). They added that the facies change from reefal Qamchuqa Formation to Pelagic Balambo Formation is controlled basically by deep seated Chaqchaq strike slip fault. The same idea is accepted by Ibrahim (2009), Al-Hakari (2011) and Omar et al. (2015) but they showed it diagrammatically as normal listric fault (Figure 8).

The present study doesn't agree with the citation of the above authors about the effect of the fault on the facies change from reefal limestone to deep pelagic limestone or marl during Early Cretaceous. This disagreement is due to the fact that this facies change is not restricted to the area at north and northeast of Piramagroon anticline but exists in the whole northern Iraq. On the tectonic map of Jassim and Goff (2006), this facies change is indicated as located between the Balambo-Tanjero Zone and High Folded Zones and starts from Chachaq valley and continues to the north of Rawndoz town.

The facies changes of Qamchuqa Formation (shallow reefal limestone) to Balambo Formation (deep pelagic limestone or marl) should not to be controlled by fault because this facies change is very common on the continental margin of the present day oceans where the reefal carbonate on the shelf rapidly (relatively) changes to pelagic limestone or mud on the slope or continental rise. During Early Cretaceous the Arabian platform was part of the continental margin of the New Tethys Ocean. Ameen (2008); Ameen and Karim (2009) and Karim and Taha (2009) have discussed and indicated this facies change without connecting it with faults (Figure 9).

Al-Hakari, (2011) has found two other strike slip faults in the area to the west of the Sulaimani-Sitak fault (Figure 3). The authors of the present study, as a result of the fieldwork, have not found any evidence of these four faults at the west and northwest of the Sulaimani city. The geological mapping has not detected any shifting of the axes of the folds and the topographic features in the studied area (Figure 3). Two reverse faults were observed which have had the displacement less than 20 m, one of them cut the southwestern limb of the Piramagroon Anticline and was observed inside the Yakhyian valley (Figure 10). Another reverse fault is seen on the northeastern limb of Harmetool anticline near the mouth of the Nadoor valley (Figure 11a). These two faults may be anticline break through faults due to the fact that the anticlines are detachment folds and this type of faults are observed commonly in this type of folds.

2.2.2. Type of Anticlines

There are two main anticlines in the studied area which are named Piramagroon and Sulaimani (Harmetool in the present study) anticlines by Ma'ala,

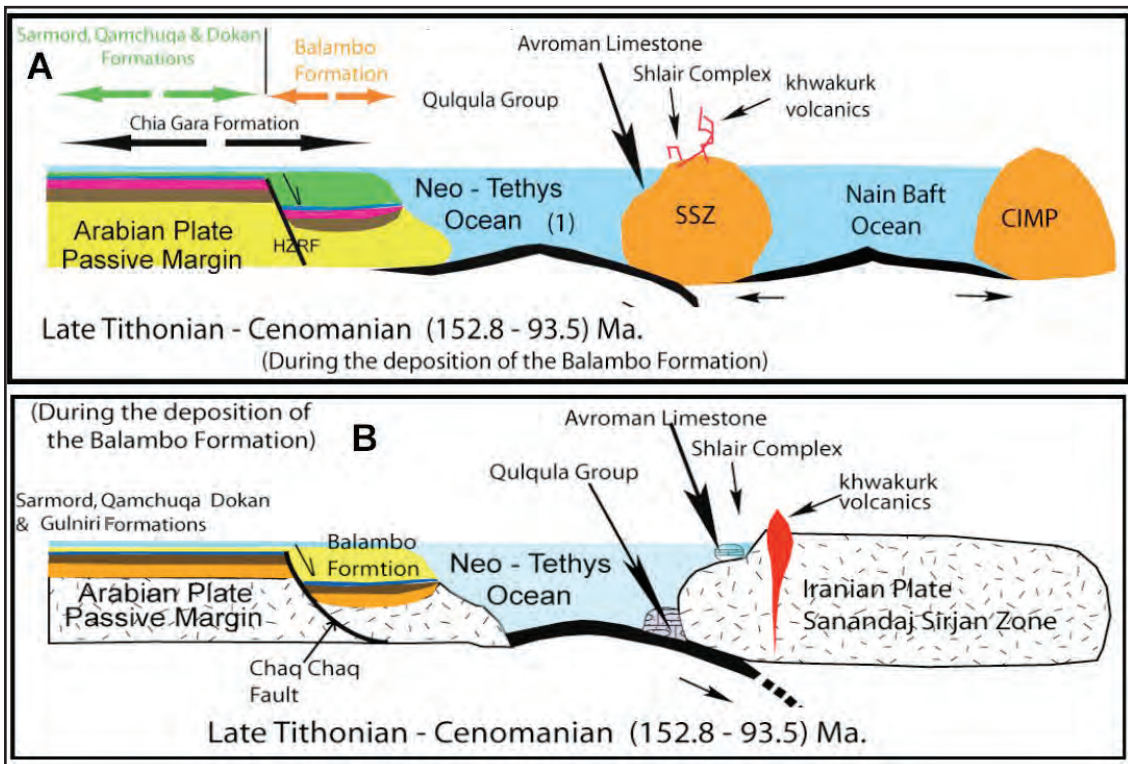


Figure 8- Paleogeography and tectonics of Late Tithonian-Cenomanian in which listric fault is indicated by: a) Ibrahim (2009), b) Al- Hakari (2009) and Omar et al. (2015).

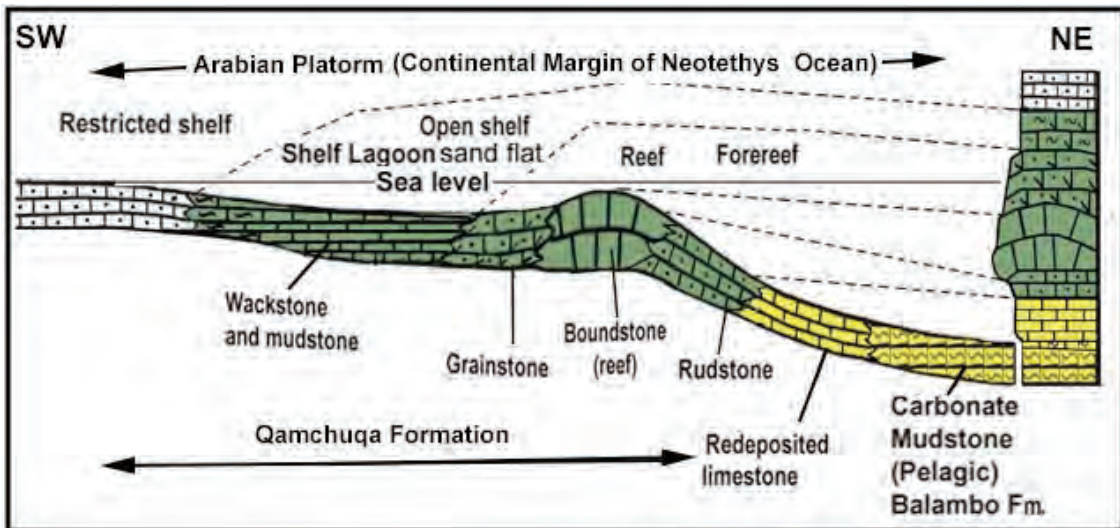


Figure 9- Paleogeography of the Arabian Platform during Early Cretaceous which shows facies changes which are not related to fault (Ameen, 2008; Karim and Ameen, 2009).

(2008) and both of them are recently mapped by Al-Hakari, (2011) who has indicated all the main anticlines as southwest vergent asymmetrical anticlines. It was observed that the above indications are true for those found inside QBT. In some cases the anticlines are reversely faulted by anticline breakthrough fault. However, the folds inside Kometan Formation

behaved more or less differently. In addition to asymmetrical anticlines, Kometan Formation contains box and recumbent anticlines (Figure 11d).

Al-Hakari (2011) and Omar et al. (2015) have assigned the anticlines in the studied area as fault propagation folds (Figure 1) but the present study

showed that it is detachment fold. The proof for detachment fold is discussed in detail for during the study of Azmir-Goizha anticline at the north of Sulaimani city by Karim and Ahmad (2014). The detachments of the anticlines occurred on the Gulneri and Sarmord formations and other older soft rocks. The anticlines which were formed are in the style of multi-detachment fold or multi-detachment faulted fold. Al-Hakari (2011) mentioned that the cores of the anticlines in the study area were occupied by Qamchuqa Formation but the present study showed that Balambo and Sarmord Formations exist in the core (Figure 2, 10 and 12).

The absence of the oil in the core of the anticline is attributed, according to the result of the present study, to refolding and intense deformation of the core of the Piramagroon anticline by detachment folding which includes rotation of both limbs and squeezing of the core of the anticline. Al-Hakari (2011) and Omar et al. (2015) assigned that this refolding (parasitic folding) and squeezing, by the above processes, has destroyed any existing reservoir (Figure 5) and its seal more intensely than previous model of fault propagation folds. The latter authors explained that, as shown in the figure 13, open folds, without parasitic folds, are much more suitable for keeping accumulated oil than detachment folds aforementioned in the present study. Another reason for the absence of oil is the

deep burial of the targeted rocks which are more than 10 km during Pliocene below Cretaceous and Tertiary rocks before exhumation. The burial temperature was so high that degraded the possible existed oil.

2.2.3. Sulaimani Anticline

This anticline is located inside the western part of Sulaimani city ($35^{\circ} 34' 15.50''$ N and $45^{\circ} 24' 25.15''$ E) and geomorphologically consists of three low hills such as UN and Farouk hills (Figure 14). The plotting of its axis indicates that this anticline, most possibly, is an independent anticline. Previously this anticline is assigned as southeastern plunge of Harmetool anticline by Ma'ala (2008), Al-Hakari (2011) (Fig.13A) and Aziz et al, (1999). The elongation of the axis of Sulaimani anticline coincides with the Sherkuzh anticline (Figure 14a). Al-Hakari (2011) had indicated two strike slip faults that cut this anticline (Figure 3). In this study, only a small strike slip fault was found that strikes nearly east-west (Figure 14b)

3. Conclusion

- 1-The equivalents of the Dokan and Gulneri Formations are found for the first time in the study area.
- 2-The unconformities below and above Kometan Formation were not found.



Figure 10- Folds in the south eastern limb of Piramagroon anticline, Yakhyian valley, 15 kms to the northwest of Sulaimani city, 3km to the north of Qamar Taly village.



Figure 11- a) Reverse faults on the northeastern limb of Harmetool anticline near the mouth of the Nadoor valley, b) The oil well about 3000 meter deep which is dry, (c) Recumbent and box folds, (d) folds in the northeastern limb of Harmetool anticline at south west of Old Hanaran village.

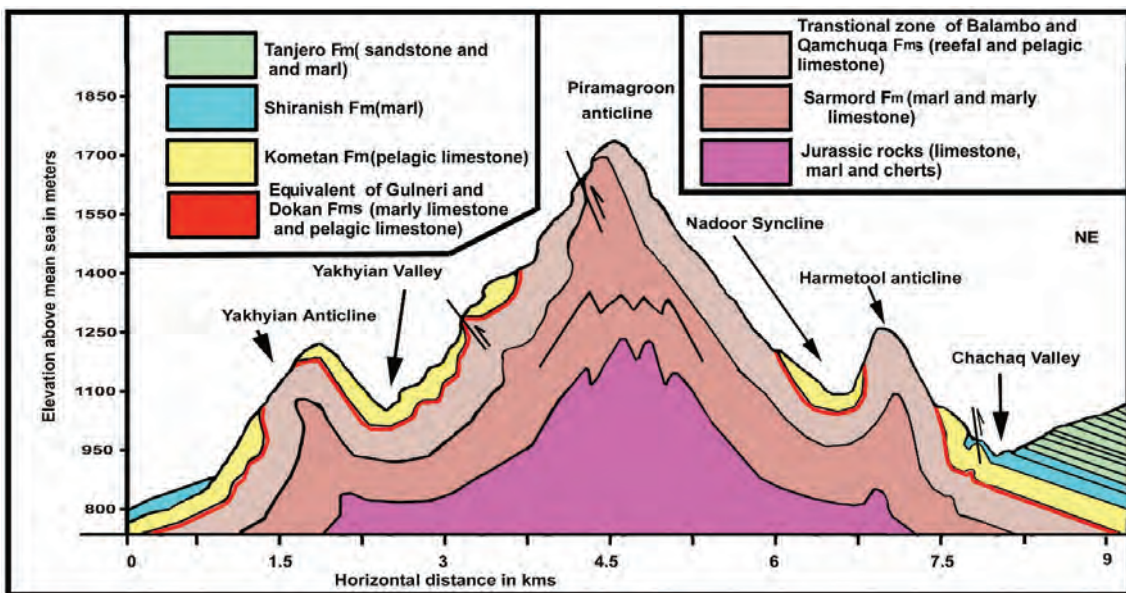


Figure 12- Geological cross section of the southeastern part of Piramagroom anticline (A---B line in the figure 1). The minor deformations are not shown.

3-The age of the Gulneri Formation is Late Cenomanian-Early Turonain

4-A new and updated geological map is drawn for the area on which all the formations are differentiated.

5-The most realistic structural analysis of the study area on which new folds and fault is recorded for the first time is revealed.

6-The folds of the area consist of detachment anticlines and synclines and detachments which occurred on marls of the Gulneri, Sarmord Formation and other older rocks.

7- The main faults are reverse faults.

8-The probable reason for the absence of oil is intense refolding and squeezing of the core of the anticline by detachment folds.

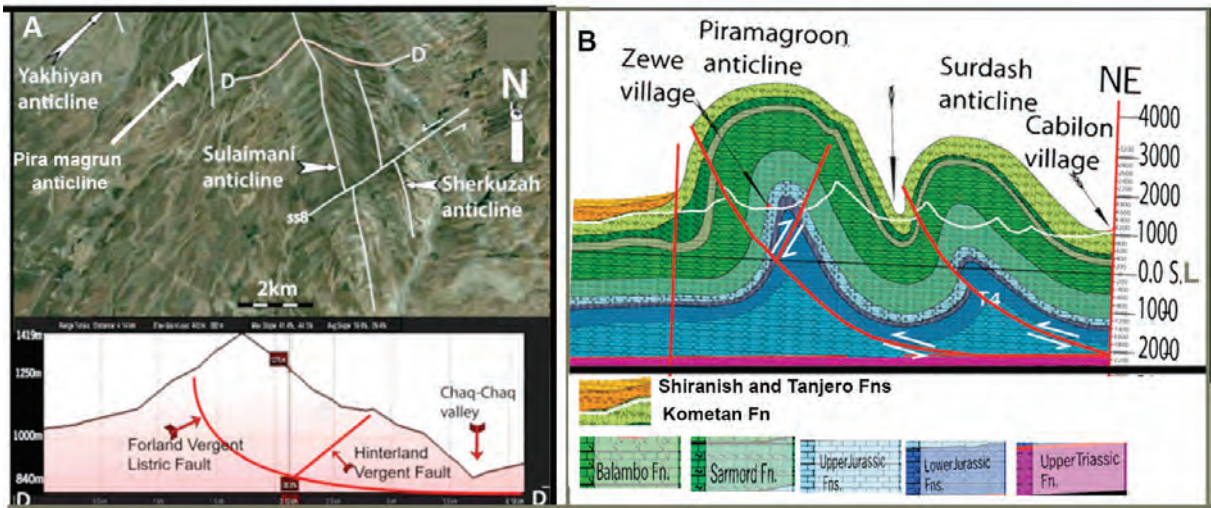


Figure 13- Two geological cross sections of A)Al-Hakari (2011) and B)Al-Hakari (2011); Omar et al.(2015) shows that they assigned the anticlines in study area as fault propagation folds which were uplifted through the reverse slipping of the hanging wall of the blind foreland vergent listric thrust fault associated with the hinterland-vergent-fault.

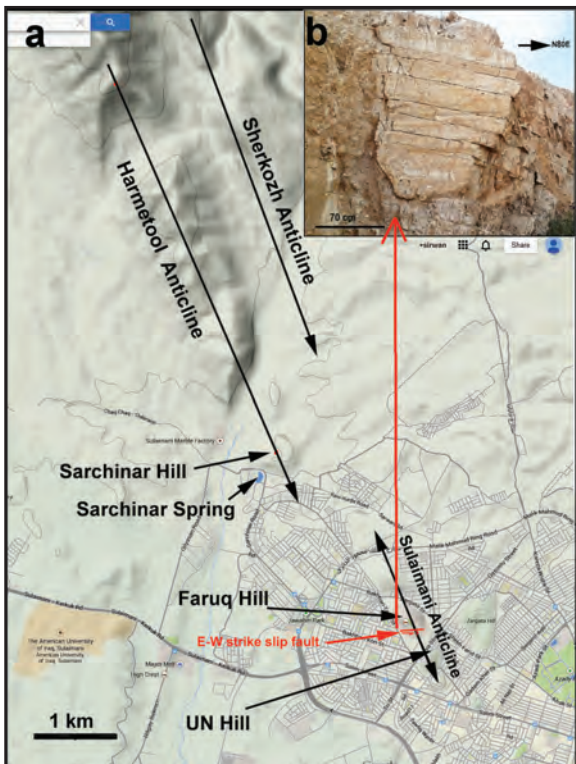


Figure 14- a) Topographic map of western part of Sulaimani city (From Google Earth) which shows the anticlines, b) Strike slip fault between the UN and Faruq hills

Acknowledgement

The authors thank to Dr. Ramona Balc (ramona.balc@ubbcluj.ro) for her effort in the nannofossil analysis and the age determination studies.

References

Al-Hakari, S.H.S. 2011. Geometric Analysis and Structural Evolution of NW Sulaimani Area, Iraq. Unpublished PhD Thesis University of Sulaimani.

Al-Kubaysi, K. N. 2008. Biostratigraphy of Aqra, Tanjero and Shiranishs Formation in Chwarta Area, Sulaimanyah Governorate, NE-Iraq. Iraqi Bulletin of Geology and Mining, Vol.4, No. 5.p.23.

Al-Qayim, B., Omar, A., Koyi, H. 2012. Tectonostratigraphic overview of the Zagros Suture Zone, Northeast Iraq, GeoArabia, 17(4) :109-156.

Ameen, B.M., 2008. Lithostratigraphy and Sedimentology of Qamchuqa Formation from NE-Iraq. Unpublished Ph D. Thesis. University Of Sulaimani.

Aziz, B.K., Lawa, F.A., Said, B.M. 1999. Sulaimani Seismic Swarm during spring 1999, NE Iraq. Journal of Zankoy Sulaimani. 4(1):87-100.

Bellen, R.C.van, Dunnington, H.V., Wetzel, R., Morton, D., 1959. Lexique Stratigraphic International. Asie, Fasc.,10a, Iraq, Paris.Buday, T. 1980. The Regional Geology of Iraq, Stratigraphy and Paleogeography, Dar AL-Kuttib Publication House. University of Mosul, Iraq.

Buday, T., Jassim, S. Z. 1987. "The Regional geology of Iraq, Tectonism Magmatism and Metamorphism". I.I. Kassab and M.J. Abbas (Eds), Baghdad.

Burnett, J.A, 1998, Upper Cretaceous, in Bown, P.R. (Ed.), Calcareous nannofossils biostratigraphy: British Micropalaeontological Society, Publications Series, Kluwer Academic, London, pp. 132-199.

- Ghasemi, A., Talbot, C. J. 2006. A new tectonic scenario for the Sanandaj-Sirjan Zone (Iran). *Journal of Asian Earth Sciences*, 26: 683-693.
- Al-Husseini, M. I., Matthews, R. K. 2008. Jurassic-Cretaceous Arabian orbital stratigraphy: The AROS-JK Chart *GeoArabia*, vol. 13
- Jassim, S.Z., Goff, T. 2006. Phanerozoic development of the northern Arabian Plate, In: Jassim SZ and Goff JC *Geology of Iraq*, publication of Dolin, Prague and Moravian Museum, Brno.
- Karim, K.H. 2004. Basin analysis of Tanjero Formation in Sulaimaniya area, NE-Iraq, Ph.D. thesis, University of Sulaimaniya, 135 p.
- Karim, K. H., Ameen, B.M. 2009. Facies Analysis of Early Cretaceous Arabian Platform from Northeastern Iraq, GERMENA III.
- Karim, K. H., Taha, Z.A. 2009. Tectonical history of Arabian platform during Late Cretaceous. An example from NE Iraq. *Iranian Journal of Earth Sciences* 1 (1): 1-14.
- Karim, K. H., Salih, A.O., Ahmad, S.H. 2013. Stratigraphic Analysis of Azmir-Goizha anticline by Nannofossils. *Journal of Zankoy Sulaimani (JZS)*, Part A, 15(2):103-124.
- Karim, K. H., Ahmad, S.H. 2014. Structural analysis of the Azmir-Goizha anticline, north and northeast of Sulaimani city, Northeast Iraq, *Journal of Zankoy Sulaimani-Part A*.16 (1):11-25.
- Karim, K. H., Khanaqa, P.A. 2014. Association of rudists and red clastic facies in the upper part of Aqra Formation, Mawat area, NE Iraq. *Arabian Journal of Geoscienc*, 8, (5) :2751-2759
- Lawa, F. A. 2004. Sequence stratigraphic analysis of the middle Paleocene –Middle Eocene in the Sulaimani District. Unpublished Ph.D. thesis, University of Sulaimani.
- Ibrahim, A.O. 2009. Tectonic style and evolution of the NW segment of the Zagros Fold – Thrust Belt, Sulaimani Governorate, NE Iraq. Unpublished Ph. D. Thesis, University of Sulaimani, College of Science, 187pp.
- Lawa, F. A., Gharib, H. 2010. Cretaceous Sequence Stratigraphy of Western Zagros Outcrops from N. Iraq. AAPG GEO 2010 Middle East Geosciences Conference & Exhibition March 7-10, 2010–Manama, Bahrain (only abstract available).
- Lawa, F.A., Koyi, H., Ibrahim, A. 2013. Tectono-stratigraphic evolution of the NW segment of the Zagros fold-thrust Belt, NE Iraq. *Journal of Petroleum Geology* 36 (1): 75–96
- Ma, ala, K.A. 2008. Geological map of the Sulaimaniyah Quadrangle, sheet N1-38-3, scale 1:20000, GEOSURV, Baghdad.
- Omar, A.A., Lawa, F.A, Sulaiman, SH. 2015. Tectonostratigraphic and structural imprints from balanced sections across the north-western Zagros fold-thrust belt, NE Iraq. *Arabian Journal of Geoscience*, DOI 10.1007/s12517-014-1682-6.
- Özer, S., Karim, K.H., Sadiq, D.M. 2013. First determination of rudists (bivalvia) from NE Iraq: Systematic palaeontology and palaeobiogeography. *Bulletin of MTA*, 147: 31-55. (Bulletin of the Mineral Research and Exploration of Turkey).
- Sadiq, D. M. 2010. Facies analysis of Aqra Formation in Chwarta-Mawat Area from NE-Iraq. Unpublished MSc thesis, College of Science, University of Sulaimani.105p.
- Sharland, P. R., Archer, R., Casey, D. M., Hall, S. H., Heward, A. P., Horbury, A. D., Simmons, M. D. (2001). *Arabian Plate sequence stratigraphy*, *GeoArabia*, special publication 2, Gulf Petrolink, Bahrain, p. 371. Sissakian, V.K . 2000. Geological map of Iraq, sheet No.1- 3-307 rd edition, *Geol. Surv. Min., Invest.*, Baghdad, Iraq.



Bulletin of the Mineral Research and Exploration

<http://bulletin.mta.gov.tr>



AN APPROACH TO COAST EDGE LINE AT THE EASTERN ANTALYA MARGINAL-MARINE SEA SIDES

Muhittin GÖRMÜŞ^{a*}, Levent BAŞAYIĞIT^b and Ahmet UYSAL^c

^aAnkara University, Engineering Faculty, Geology, Department Ankara

^bSüleyman Demirel University, Faculty of Agriculture, Soil Science Department, Isparta

^cSüleyman Demirel University, Technical Science High School, Isparta

Research Article

Keywords:

Mediterranean, Antalya, Coast Edge Line, Google Earth, Aerial Photo

ABSTRACT

In this study, geological and geomorphologic studies having the solution approaches for the coast edge line problem at the marginal-marine environments were realised. Some solutions on the matter were proposed. The eight following locations were chosen: the south of Lara Main Road (1), Aksu River Exit (2), Acısu Stream-2 (3), Ağılısu Stream Exit (4), Köprüçay Exit (5), seashore at the south of Evrenseki (6), seashore at the east of Side (7) and Kızılot (8). Past and new images of the Google Earth satellite views, topographic maps and aerial views; lithological-sedimentological observations, fauna data in sediments, plant cover, artificial structures, previous literature and related law and rules were taken into consideration. Besides the matter were also evaluated in the views of tectonics and sea level changes. From the obtained data two significant subjects are seen as important points on the matter. The first is backward date and validity period in future. The second is effective sea level in height. In fact, recent geomorphologic structure of the eastern Antalya Coasts is the result of mixed functions such as wave, river and wind dominated activities. It is also important to indicate that internal parts of the land also comprise very low elevations up to just a few meters above the sea-level. As a result it is brought out that last and future centuries as a time, observations on the sea level changes in last and future decades as a space should be taken into consideration for the coast edge line solution.

Received: 11.05.2016

Accepted: 24.06.2016

1. Introduction

Coast edge line problem is one of the main controversial problems between citizens and government institutions or organizations. This problem particularly causes some affects on the facilities of farmers and tourism sector investors who have investments in the region. In the literature, different approaches for the solution of the problem are remarkable. Differences in these approaches put forward insolubility instead of the solution. For that reason, long-term legal processes initiate to defend their rights. One of the examples showing this kind of problem is the sea sides of the Antalya coast. Determination of coast edge line around water masses such as lake and marine also seems to be main subject between citizens and government institutions. Related law and regulations which were issued for making use of the public have been changed with some additions and applied since 1982. 43 article of the 1982 basic law, 3086 numbered coastal law, 3621 numbered coastal law issued in the Official Gazette (Resmi Gazete) on

17 April 1990, cancellation decisions of the Turkish Constitution Court on some articles of the law dated on 18.09.1991, and 3830 numbered law including some changes on the 3621 coastal law are important coastal laws and their regulations. The recent applications are based on 3621 numbered coastal law with the changes of the 3830 law and regulations issued in 1992 and 1994. According to the law and regulations; Coast Line is the natural line of sea, natural and artificial lakes and rivers changing with meteorological events except floods. It extends on the combinations of the water points touched to the landmass. In the same law and regulations, Coast Edge Line (Changes: RG-Official Gazette: 30.03.1994-21890) is defined in the mentioned law and regulations as follow: In the low-flattened coastal areas, it is a border towards the landscape including beach and coastal sand dunes, gravel, rocky, stony, reeds and marshes; in the narrow-high coastal areas, it is the upper limit of the slope or cliff. It cannot be changed either when the border is altered by unnatural fillings. The area between coast line and coast edge line is known as Coast (Changes:

* Corresponding author: Muhittin Görmüş, mgormus@ankara.edu.tr
<http://dx.doi.org/10.19111/bulletinofmre.285907>

RG-Official Gazette: 30.03.1994-21890). It includes both coastal areas as narrow-high coastal areas (it has no beach and platform and ends with a narrow slope or cliff) and low-flattened areas (it comprise lagoon, beach and coastal sand dunes, gravel, rocky, stony, reeds and marshes in a flattened areas, Regulation, 2013).

The Miocene to Pliocene aged ancient marine and terrestrial sediments occur at the basement at the Antalya coasts (Figure 1). The previous literature present geological maps of the region, Quaternary geology and the ages of the formations based on foraminifera, nannofossil and other marine organisms data (Akay et al., 1985; Şenel, 1997*a-c*; Ergin et al., 2004; Avcı et al., 2008; Parlar, 2010; Kanbur, 2012; Sagular et al., 2015; İslamoğlu, 2002; İslamoğlu and Taner, 2002, 2003*a-c*).

Many places in the Eastern Antalya Coasts include low-flattened coastal areas. Many investigations explain observations and details on the coastal edge line determinations at water column such as lake and marine (Abama, 1991; Görmüş et al., 2001, 2005, 2007, 2010, Tüysüz, 2003, Tüysüz and Erturaç, 2005). As known, coast line is related to sea level changes and depends on different factors (Nummedal et al., 1987; Pluet and Pirazzoli, 1991). Among them, tectonic-eustatic, sedimentary-eustatic and glacial-eustatic ones are long-term factors while atmospheric ones (such as precipitation, wind, pressure, temperature, tidal effects) are known as short-term period factors. In the previous literature, it is reported that anthropogenic factors and global warming in the last and next century have affected the sea level up to 100 cm (Douglas et al., 2000; Climate Change, 2013). This situation means that sea level will rise at the low-flattened coastal areas and sea water column will cover in the low elevations in the region. Besides, changes in climate may affect weathering of landscape rocks. As a result of this sediment transportations may occur. All indicated events may be seen as a transgression or regression in the coastal areas. Some examples may be given from the Turkish coastal areas (Kayan, 1988; Brückner, 1997). The effects of the earthquake are also known to cause a decline in the sea sides. Ciner et al. (2009) reports the last five thousand years of the Antalya Coasts based on observations of the beach stones and ¹⁴C analysis. They state that subsidence was formed by earthquake effects. They

also emphasize the significance of tectonic control on the sea level changes. Besides Turkish National Committee For Coastal Zone Management founded in 1993 have been organising national congresses that many subjects and problems on the matter have been discussed (Akyol et al., 2010; Altın, 2010; Balas, 2010; Sesli et al., 2010; Kutoğlu et al., 2010). Among them Akyol et al., (2010) indicate that geological, agricultural and topographical engineers have more responsibilities on the determination of the coastal edge line and necessity changes on the regulations should be done. Altın (2010) explains the process of determining the coastal edge line. Sesli et al. (2010) presents some examples, particularly related to coast legal and technical aspects from the coasts of Ordu. Kutoğlu et al. (2010) concerns with changes in the Zonguldak surroundings from the 1890s to the present. In addition to these, in the literature it is also indicated that wave heights average derived from the SW winds in the eastern sea sides of the Antalya is 50 cm monthly. It changes with daily and seasonal conditions up to 2-8 meters (Özhan and Abdalla, 2002). Depending on the progress of wave heights on the landscape, sea will cover the land in different altitudes. All mentioned investigations brings out that determination of the coast edge line controlled by sea level changes will always be a problem if a limit time for the past and future, and scientific determination criteria are not taken into consideration. The beginning time of mankind history in terms of time seems to be a longer time. Many coastal changes are seen during this time. So, the aim of this study is to present last century coastal changes from the eastern Antalya shores with examples. The study mainly emphasizes that time limit is a significant parameter on the determination of the coast edge line and some changes should be done on the related law and regulations. It also deals with which kinds of scientific criteria should be added to the regulations.

2. Studied Locations and Methods

The study mainly focuses on the significance of coast edge line determination based on its limit time, progress and place. The locations comprise the following eight areas from the eastern Antalya coasts (Figure 1): Particularly it is seen that river and stream exits are more important on the coastal formation. So, river and stream exits were chosen. These are as follows: the south of the Lara Road (1),



Figure 1- A map showing the studied locations (www.googleEarth) and geological map of the area on the satellite view (travertine outcrops having narrow coastal side around the Antalya, particularly low plains at the eastern parts of the Antalya, Miocene to Pliocene aged basement geological units are seen in the region, k2m. Cretaceous ophiolitic melange, e2-3. Eocene neritic limestone, m3. Miocene aged, ancient marine siliciclastic sediments, p1. early Pliocene aged terrestrial, occasionally marine clastic sediments, Q. Quaternary alluvium, travertine-terrestrial, please see MTA geological map 1/500.000 in scale for other detail explanations of the map.

exit of the Aksu Stream (2), Acısu Stream-2 (3), exit of the Ağılısu Stream (4), exit of the Köprüçay (5), the southern shore of the Evrenseki (6), shore of the eastern Side (7) and Kızılot (8) (Figure 1).

In the study, new and old Google Earth satellite data (the dates are given on the images) and aerial photographs were used. The changes were marked in the old and new images. In the field works, observation holes were realized by auger or grap. Observations on lithology, soil, plant cover and artificial constructions were performed. Fauna observations and soil analysis in the laboratory were also realized. So, data on geological, geomorphologic, topographic, soil characteristics and plant cover features as well as previous reports and law and regulations were used for the determination of coast edge line.

3. Results and Discussion

Low-flattened eastern Antalya Coasts generally include many meandering and braided river systems arising in the Taurides and pouring to marine. Approximately northwest-northeast trending coastal margin at the south of the Isparta Angle (Gutnic et al., 1979) has a typical view for formation of marine shores. Observations about the studied areas are given as follows:

3.1. Satellite Data

Google Earth satellite data dated as 2003 and 2015 were evaluated. Some changes on the coasts are clearly seen within twelve years; even it is obvious within five years. However the views also have errors depending on pixel resolution. Figure 2 shows

vertical and horizontal differences, a few meters in distance. The reasons of that may be related to many factors such as beaming error, data difference, transformations of projection systems and corrections on the errors. Although these errors may be important, clear geomorphologic differences and changes on coastal edge line are clearer in the views. Figures 2-4 shows satellite views and changes in the studied coastal areas.

The south of Lara Main Road: Touristic constructions and buildings on the sand dunes (I), flattened area around the exit of the one of the branch of the Aksu Stream (Acısu-1) filled by beach sediments (II), change of the exit of the stream (III) and changes in the size and locations of the swampy areas (IV) are seen as the main changes (Figures 3A- B). Longer beach or shore of the sea, and shorter stream angle are seen in the 1/25.000 scaled topographical map of the area dated on 1962 (Figure 3G).

Exit of the Aksu Stream: Mankind effects at the exit of the Aksu Stream (I), changes on the coast line (II) and buildings (III) are the important changes in the area (Figures 3C-D). Changes on the coastal edge line is seen clearly in 1962 topographic map, 1/25.000 in scale (Figure 3G).

Acısu Stream-2: Left side bending at the exit of the Aksu River is seen and called as Acısu Stream in the eastern part of the river (Figure 3E-F). Although some coastal changes are seen in the area, hollow of stream parallel to sandy dunes is more or less the same during the last fifty-sixty years. Widening sandy barrier (I), differences at the exit of the stream (II) are the main changes. Standard topographical map 1/25.000 in



Figure 2- Google Earth satellite views showing illusion scale in meters in Recent and past views (it is clear that the same building is seen in different place in the 2015 satellite view, coordinates are shown in the figures).



Figure 3- Google Earth satellite views of 2003 and 2015 for the following locations A-B. South of the Lara Main Road, C-D. exit of the Aksu Stream, E-F. exit of the Acisu Stream-2, G. topographical map of these three locations in 1962, (a) south of the Lara Main Road, (b) exit of the Aksu Stream, (c) Acisu Stream-2, numbers show changes in time.

scale and dated as 1962 show a natural water channel at the exit of the Acısu Stream in the land (Figure 3G).

Ağılsu-Acısus Stream: So many differences in the nature are not seen in the area during the fifty-sixty years. The most changes are observed as human made constructions and buildings at the pouring place of the stream to the sea. Stream name is the Ağılsu in

the topographic map, 1/25.000 in scale dated as 1963. Dried channels that are related to underground water level are clearly seen at the northern sandy dunes at the new dated topographical map (Figures 4A-D).

Exit of the Köprüçay: It is called as Karaöz Stream in the standard topographical map, 1/25.000 in scale dated as 1963. Significant changes are seen around

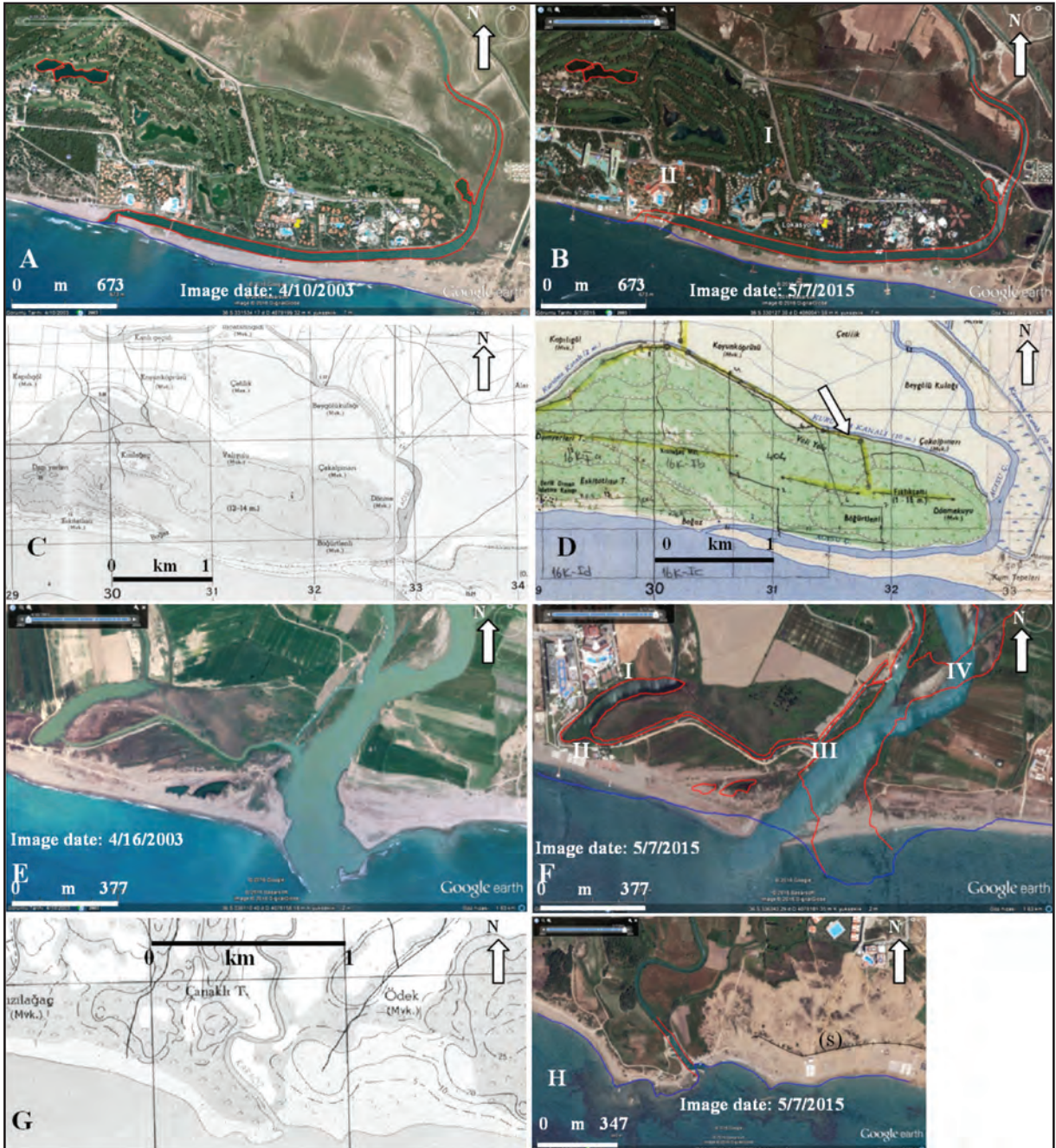


Figure 4- Google Earth satellite views of 2003 and 2015, past and recent topographic maps for the Ağılsu (A-D), Köprüçay exit-Karaöz Stream exit (E-F), Google Earth view of south of Kısalar location, black line may be thought as wave effect boundary in last decade, numbers show changes in time.

the exit of the stream. Displacement of the exit of the stream and changes in the coastal line are seen as important changes in comparing the views (Figures 4A-D).

Seaside at the southern Evrenseki: When comparing the views of 2003 and 2015 Google Earth satellite views, buildings or constructions and changes on the coastal edge line are seen clearly (Figures 5A-B).

Seaside of the eastern Side: During the last two decades, significant differences are not seen in the area when comparing the satellite views (Figures 5C-D).

Kızılot: Sheki occurred around the coast edge of the area during the last fifteen years is seen clearly in comparing of satellite views (Figures 5E-F).

3.2. Field Work Observations - Observation Holes

Sediments in the observation holes by grab and pits by hand auger were examined and analysed in the mentioned areas above as Ağılısu, seaside of the eastern Side and Kızılot. The following includes details of observation holes and pits. Besides soil characteristics and formations, past aerial views, plant cover changes in time were also indicated in the text.

Ağılısu: Figures 7-8 show faunal and lithological characteristics of the sediments in the observation holes and pits around the Ağılısu Stream (Figure 6A). In the first observation hole, the lithology changes from bottom to top as swamp muddies, ancient beach sands, soil A horizon and sand cover. Observation



Figure 5- Comparative Google Earth satellite views of 2003 and 2015 for the south of the seashore at the south of Evrenseki, seashore at the east of Side and south of Kızılot.

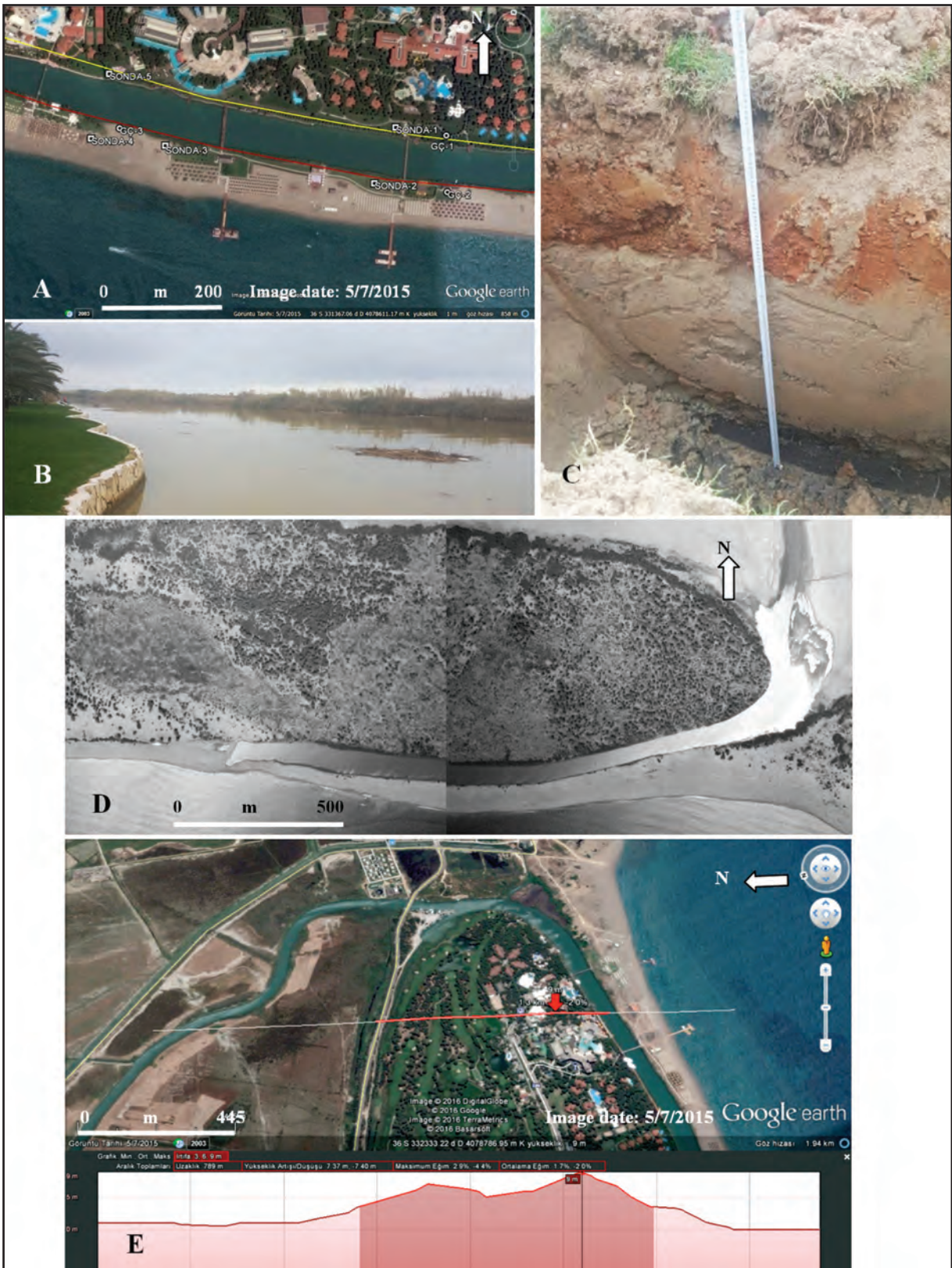


Figure 6- A view indicating of the locations of the observation holes from the Ağılısu (A), a view from the dunes that include reedy at the south of Ağılısu (B), lithologies in the observation hole (C), past aerial photographic view in 1953 (D) and a topographical cross-section showing elevations (E).

holes grapped around the beach 2 and 3 includes marine sand lithologies.

It is clearly seen that a shallow inner lake were formed around the Ağılısu area in the past aerial view, 1953 in date (Figure 6D). It could be interpreted as a lagoon. However, its formation around the exit of the stream, transportation of stream sediments and elevation values, a few meters in heights prove that it was most probable an inner lake in the land. Besides swamp occurrences, stream bending related to sandy barrier, not reaching to the sea directly, it may be assumed that inner land conditions such as river and wind were the predominant conditions during the last seventy years. In the south, 1,5 meters beach sediments in height from the sea level to Acısu Stream occur at the tidal part of the marine. However sandy dunes

reach up to 3,5 meters in height. At the northern part of the Acısu Stream, the elevation increase towards the northern landscape starting from 1, 8 meters (Figure 8).

The stream is clearly seen that it is related to a meandered river system. Formation of the stream, parallel to marine, decreasing elevation, fine terrestrial materials, swamp formation, brown in colour are also seen. Streams and river systems arising out of the Taurides mountain reach to the low altitudes and show many bendings before pouring to the sea. Materials derived from the mountains have been altered to fine sized clastics and deposited with muddy materials in flattened areas. It is seen that a sandy barrier, parallel to the Mediterranean Sea was occurred by the effects of winds and waves.

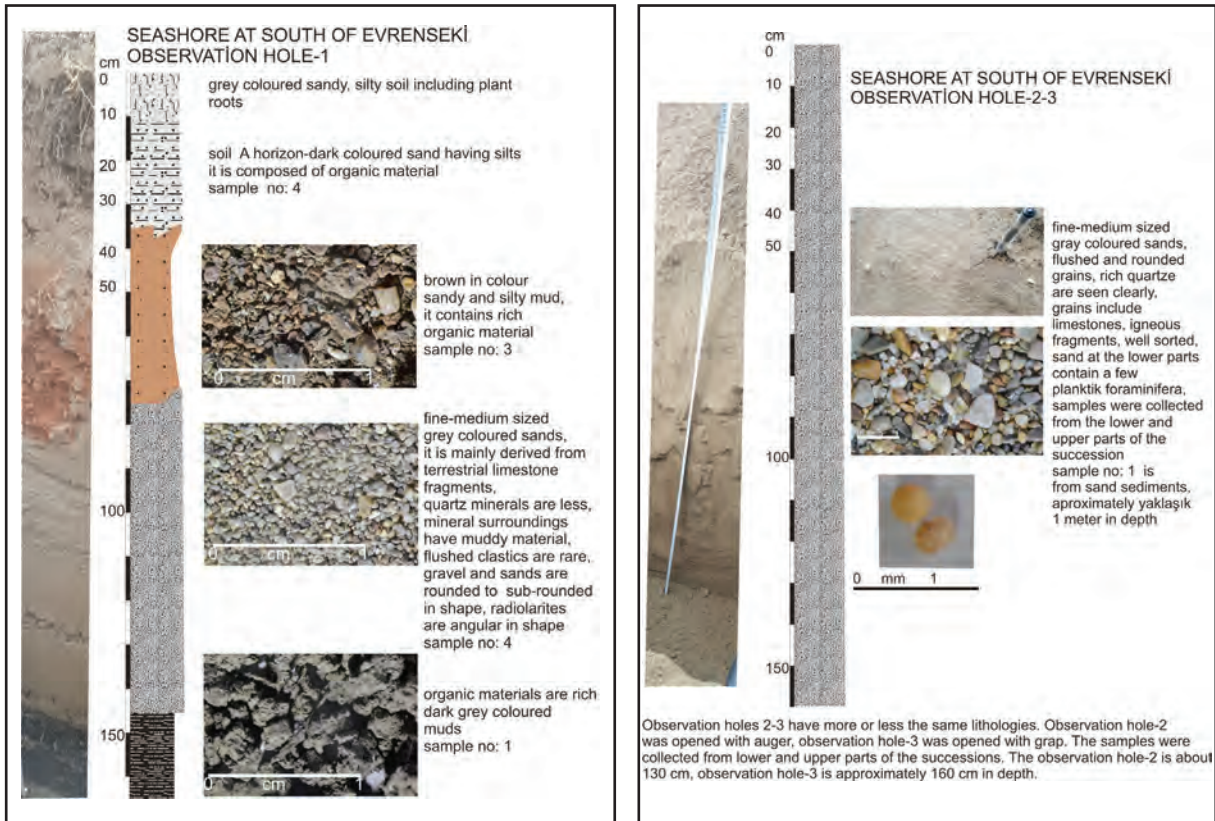


Figure 7- Stratigraphic sections of the observations holes from the Ağılısu area.

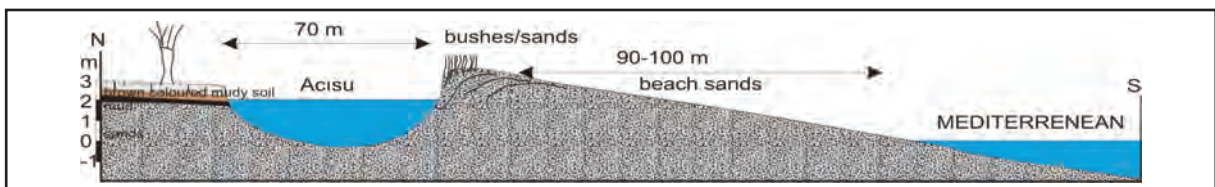


Figure 8- Topographic cross section showing the relation between marine and Acısu Stream (a sandy barrier including marine sands is interesting to notify).

Land use around the Ağılısu area: Plant cover in having the worth of agricultural usage have not been observed at the northern and the southern parts of the Ağılısu Stream. Due to the Recent landscape design to the north of the Acısu Stream, grass, palm and other landscape plants are seen in the area. In the south of the stream, sand dunes, sedge, reed, sand lily and trichome types are usual plant cover. In the past aerial views of the area, it is seen that the northern area of the stream have dwarf trees (such as pınarlılex and kermaz oak) that are typical plant cover of the area. In the same views, there have been rarely high-tall plants and forest trees (Pines). However, the southern part of the stream has more or less the same view in comparing Today's view. Formation of natural vegetation is related to soil characteristics. Durable sedge, reed types, sand lily and sea nergisi- daffodil are usual plant material at the saline and alkaline conditions while plant cover diversity and its richness, forest development comprising high-tall plants and shrubbery are seen on terrestrial soil material. Observing of plant cover at the southern part of the Ağılısu Stream from the last a few decades to Recent show that it was dried many years ago.

At the northern and the southern parts of the Ağılısu Stream, grapped observations holes that are vertical and horizontal to the stream were realized. They were also compared each other. In the first observation hole at the northern part of the stream, the sediments were divided into 5 layers. At the top artificial filling material 10 cm in thickness (0-10 cm) is a landscape design material. It is clear that these materials were filled by mankind effects. It was not taken into consideration for the last century history. Then darker topsoil material 25 cm in thickness (from 10 cm to 35 cm) follows. Analysis of topsoil material shows that they are loamy, carbonated and alkaline sands (Tables 1-2). Rich organic materials are seen. Value of EC is 260 mmhos/cm. Third layer is 35 cm in thickness (35-70 cm). Its colour is reddish brown. It is composed of clay material including sub-rounded gravels 1-2 cm in size. This soil is less alkaline and have not carbonate material. Organic content is medium. EC value is 350 mmhos/cm. Towards to bottom, light coloured fine sands, and 50 cm in thickness (70-120 cm) are seen. They have alkaline, carbonates and less organic material. EC value is around 185 mmhos/cm. Fine clastics starting from 120 cm are seen at the bottom of the sediments. 'dir. They are grey to green in colour

and include silty clay material. Carbonized plant relicts were observed. They have rich organic material and include less alkaline, carbonated material. EC value is 510 mmhos/cm. Report on the soils of the Antalya Basin in 1970, and report on the landscape of the Antalya City show that the soils in the area are alkaline character V. class Regosoller (L4-1 O Vs) type according to Forest Land Use, Land Capability Classification. In the second observation hole at the southern part of the Acısu Stream, the sediments are divided into two layers. At the top, light coloured coarse sands, 70 cm in thickness are seen. They have alkaline and carbonated characters. EC value is 60 mmhos/cm. The bottom part include light coloured sands. They have also alkaline and carbonated material. They do not include organic material. EC value is 190 mmhos/cm. Report on the soils of the Antalya Basin in 1970, and report on the landscape of the Antalya City show that the materials in the area are VIII. class Beach Sediments (SK T VIII) type according to Forest Land Use, Land Capability Classification.

It is thought that the divided layers and their irregular physical and chemical features in the first observation hole show an alluvial origin. Upper layers were formed within their settlement place with deposition of different materials transported in the Acısu Stream during the last a few decades. Occurrences of organic material and plant relicts derived from the land areas show that the soil layers were got out of the marine conditions a long time ago.

Although some marine effects are seen in northern Acısu Stream, different layer occurrences and Recent geomorphologic view were related to the stream effects. Floods have brought many materials derived from the Taurides. The different sediments were deposited within the different layers in the area. It is assumed that the area was got out of marine conditions and terrestrial soil materials were deposited around the stream during the last century.

The eastern coast of Side: One observation well by scoop, two observation holes by auger were realized within the coast of the eastern Side. Figure 9 shows lithological and faunal observations of the well. When the topographical cross sections, N-S in direction were examined, it is seen that sand dunes reaches up to 19-20 meters in heights and plane areas are around 1 meter high above the sea level. In the topographical map, a zone, 60-80 meters in width is

Table 1- Soil properties of observation hole 1.

| | pH | EC ($\mu\text{mhos/cm}$) | Carbonate CaO (%) | Organic Material (%) | Classification |
|---------------------------------|-----|----------------------------|-------------------|----------------------|----------------|
| Topsoil-surface soil (10-35 cm) | 8,6 | 260 | 12 | 1,5 | Loamy sand |
| Medium soil (35-70 cm) | 8,2 | 350 | 0,5 | 2 | Clay |
| Bottom soil (70-120 cm) | 8,5 | 185 | 8 | 0,01 | Fine sand |
| Swamp muddies (from 120 cm) | 8,2 | 510 | 16 | 4,5 | Silty clay |

Table 2- Soil properties of observation hole 2.

| | pH | EC ($\mu\text{mhos/cm}$) | Carbonate CaO(%) | Organic Material (%) | Classification |
|--------------------------------|-----|----------------------------|------------------|----------------------|----------------|
| Topsoil-surface soil (0-70 cm) | 9,4 | 60 | 6 | 0,01 | Sand |
| Bottom soil (70-150 cm) | 9,8 | 190 | 7 | 0,01 | Sand |

observed as beach sands. Northern area of the beach sands covers green belt.

Land use around the eastern coast of Side: There have not been any differences of natural plant characteristics between the area at the northern coast edge line and a belt at the southern coast edge line extending from east to west towards the sea, 10-50 meters in width. Beach sand sediments are seen 10 meters in width in the east part of the area and 50 meters in width in the western part of the area. A belt 50 meters in width at the northern and the southern parts of the coast edge line had the same plant characteristics in the past aerial photos (Figure 10).

Appearing of natural plant cover is related to soil formations. The increase of the amount and diversity of plant cover, forest having shrubs and tall pine trees are only seen in terrestrial soils while sedge and reed types, sand lily, sea daffodil plants that are resistant to sea pressure are observed within the soils formed in saline and alkali conditions. According to plant cover appearance there have not been any differences between coast edge line surrounding and a belt, 10-50 meters in width at the south. This observation show that soils were formed at both sides of the coast edge line by terrestrial effects.

Sediments in the observation hole-2 at the eastern side includes 5 layers. The topmost unit is 15 cm in thickness (0-15 cm). They include artificial materials of landscaping formed and transported by human-being. Below the first unit, dark coloured surface soil was

seen from 15 to 45 cm, 30 cm in thickness. According to soil analysis, they have sandy soils, carbonate and alkaline in character (Table 3). Organic material is poor in these soils. EC value is 65 $\mu\text{mhos/cm}$. Third layer is 15 cm in thickness (45-60 cm). It contains alluvial gravely sands. Gravels are sub rounded in shape and 1-2 cm in size. This layer is mainly composed of coarse sands. It has less carbonates, less alkaline and poor organic materials. EC values was found as 50 $\mu\text{mhos/cm}$. The section continuous with dark coloured sandy soils from 60 to70 cm. Reddish brown sandy silts are seen between 70 and 80 cm, 10 cm in thickness. It has alkaline, carbonated characters. Organic material is moderate. Value of EC is 240 $\mu\text{mhos/cm}$. The bottom layer starts from 80 cm. In the observation hole, the bottom layer is about 150 cm in thickness. Brown coloured layer is composed of fine sands. The layer including poor organic material has carbonated and alkaline characters. EC value is 90 $\mu\text{mhos/cm}$.

Report on the soils of the Antalya Basin in 1970, and report on the landscape of the Antalya City show that the soils in the area are alkaline character VI. class Regosoller (L8-2 O VIes) type according to Forest Land Use, Land Capability Classification. Report on the soils of the Antalya Basin in 1970, and report on the landscape of the Antalya City show that the materials in the belt between 30-30 meters south of coast edge line and seaside are VIII. class Beach Sediments (SK T VIII) type according to Forest Land Use, Land Capability Classification.

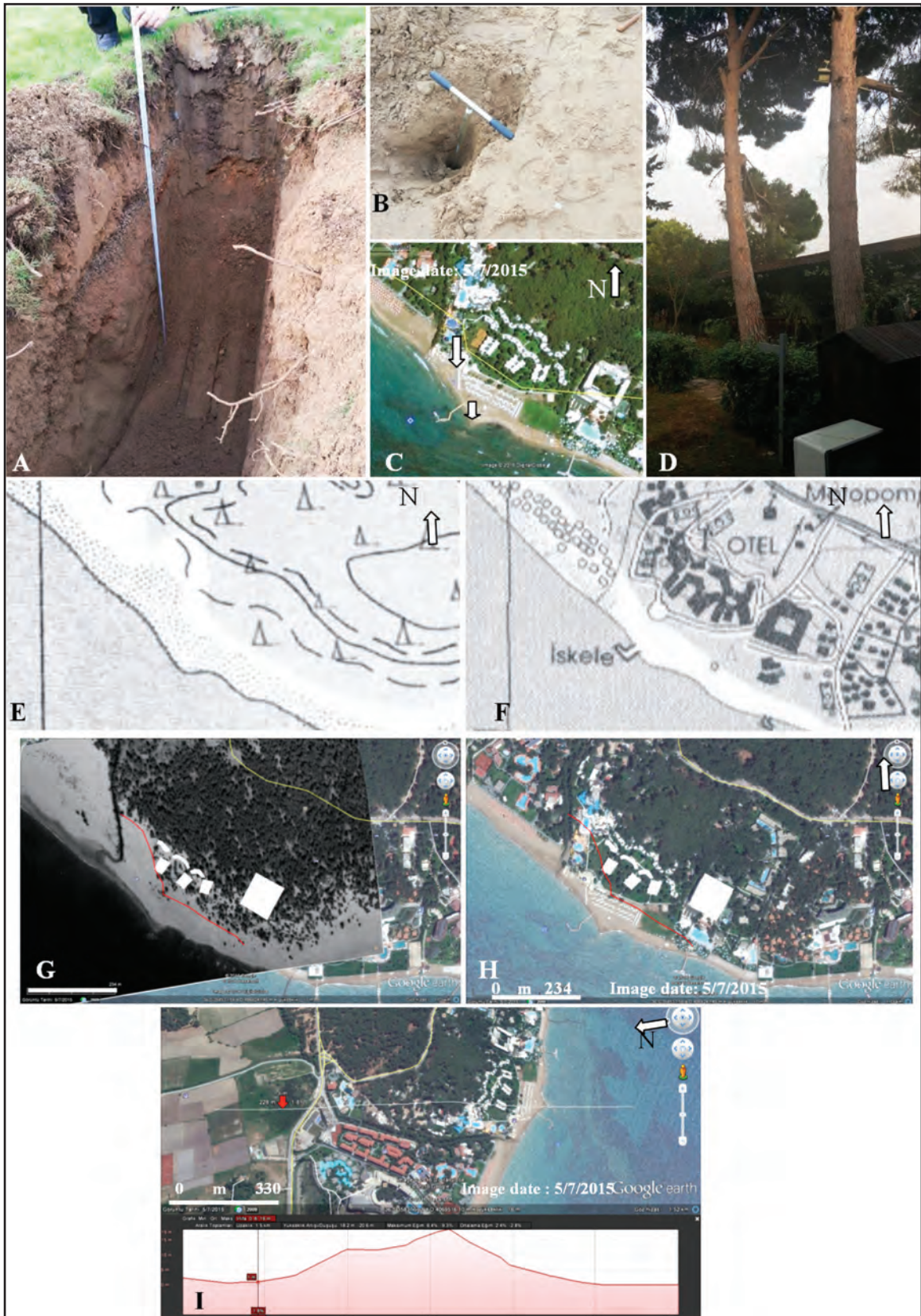


Figure 9- Views from the seashore at the east of Side. (A). Observation hole, (B). a hole digged by hand screw, (C). Google Earth view, (D). Old plant cover, (E). Topographic map in 1963, (F). Recent topographic map, (G). Aerial view in 1953, (H). 2015 Google Earth view, (I). Topographic cross-section.

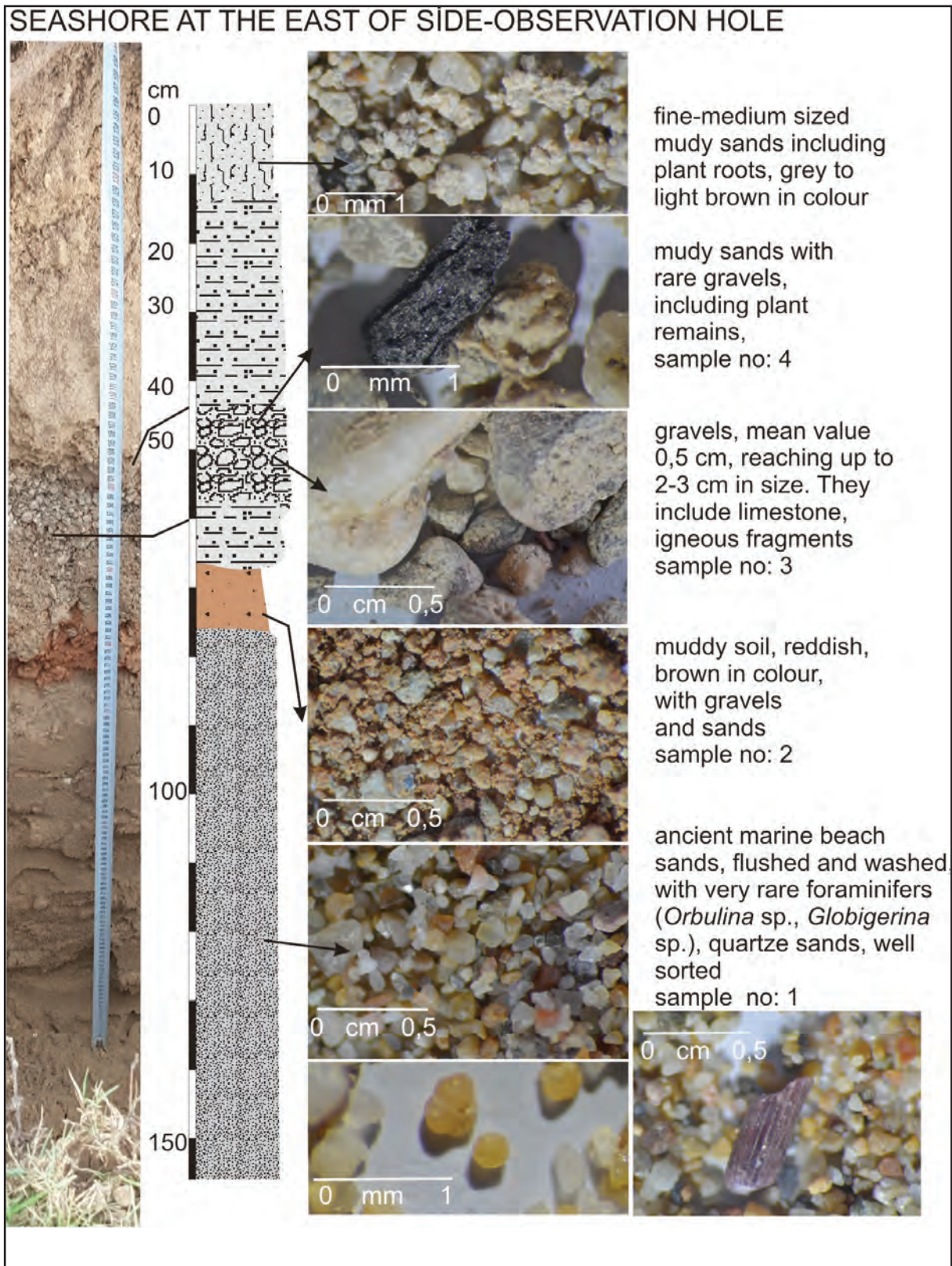


Figure 10- Stratigraphic section including observation details of the hole around seashore at the east of Side.

Layers of soils were identified based on sediment succession and their features. The layers characteristics, particularly on physical and chemical features and irregular changes show alluvial origin. The sediments were formed by surface currents and floods at the western side. Different size materials were deposited in different times. Organic contents of layers and roots of plants, 5-6 cm in diameter indicate terrestrial plant structures. The soils were under the terrestrial conditions a long time ago. High tall plants also show that soils of the area is related to land occurrences.

Around Kızılot: Coast line is parallel to beach around Kızılot. A different geomorphologic view is seen due to the Miocene aged hard rock's exposing towards the sea. It differs from the flattened plain area. Conciliated rocks such as conglomerates and sandstones have terrace elevations reaching up to approximately 10-15 meters in height. It is clear that terrace formation is related to wave effects. There have been small streams on the both sides of the area at the west and east. It is thought that terrace steps about 3-6 meters in height at the northern side of the area is also due to exposing of the Miocene aged hard rocks.

Land usage: The area has no agricultural potential. Natural plant cover divides the area into two parts. The first part has a touristic building including a garden. The garden comprise pines, 50-60 years in age and occasionally citrus fruits. The second part has also a garden including various ornament and landscape plants, and walking area with wooden structures. These area are clearly seen in the satellite view, 2003 in date. Figures 11-12 show satellite and field views. Regular palm trees are observed within the southern coast. The second part of the area in the past aerial photographs includes bushes and other small land plant cover on the coastal sands. The first part area in the past aerial photograph has more or less the same present view. Based on the past aerial photographic view, it may be said that the first part of the area has terrestrial soil occurrences and plant cover from the past to Today. However, it may be thought that the second part was under the marine effects twenty years ago. Because it's poor plant cover also supports this interpretation. The figures include field views. Based on the obtained data, it is assumed that the first part has the same Today's geomorphologic view while the second part was under the marine effects a few

decades ago. The second part turned to land and dunes were formed. First bushes and terrestrial small plants growth within the coastal sands.

The first part has a narrow slope separated from the coast. It has also semi-narrow-high coastal property. It was formed and turned to land a long time ago. The second part at the eastern part of the Kızılot has partly a flattened area. It does not show narrow-high coastal property. Artificial fillings and soil transportations may be seen. To interpret the past history, the data on morphologic, topographic, geologic and geomorphologic features are needed. Only landscape characteristics are not enough to get the past data.

4. Conclusions

Coasts of the Antalya Bay generally includes low-flattened coastal areas. Streams reaching to the sea turns to meandered type rivers at the coast plains. Different geomorphologic views have been formed by the effects of stream, waves and winds at the coastal plains. Changes on coast edge lines are seen on the stream exits related to convoluted revines towards right or left sides.

A definite past time for coast edge line is not seen on the law and regulations. For that reason, a problem appears government organizations and citizens, tourism sector investors. Our observations show that a period such as seventy and eighty years should be taken into consideration for the past history time. Because marine effects and coast edge line are seen in the inland areas in geological times. In the inland, kilometres far away from the sea, marine transgression and regression towards the land occurred within thousand years. Foraminifera and other organism relicts within the observation holes support the idea. Besides it is also assumed that a limit time of coast edge line for the feature such as seventy years or a century will be useful as acceptance time. Because sea level changes may be so different from the Today's level within thousand years. Another problem in determining of coast edge line is sea level effect towards land in height. The obtained data indicate that elevation height such as one meter or interpreting of the coast edge line from the past aerial photographs, 70 years ago (beach boundary and plant cover line towards the sea) may be a good solution for the problem. However inland areas may include

Table 3- Soil properties of observation hole 1.

| | pH | EC ($\mu\text{mhos/cm}$) | Carbonate CaO(%) | Organic Material (%) | Classification |
|-------------------------------------|-----|----------------------------|------------------|----------------------|----------------------|
| Top soil (15-45 cm) | 9,4 | 65 | 17 | 1.8 | Sand |
| Gravel interbedded layer (45-60 cm) | 8,5 | 50 | 20 | - | Gravelly coarse sand |
| Top soil continue (60-70 cm) | 9,4 | 65 | 17 | 1.8 | Sand |
| Medium soil (70-80 cm) | 9,0 | 240 | 10 | 1.2 | Sandy silt |
| Bottom soil (from 80 cm) | 9,3 | 90 | 18 | 1.0 | Fine sand |

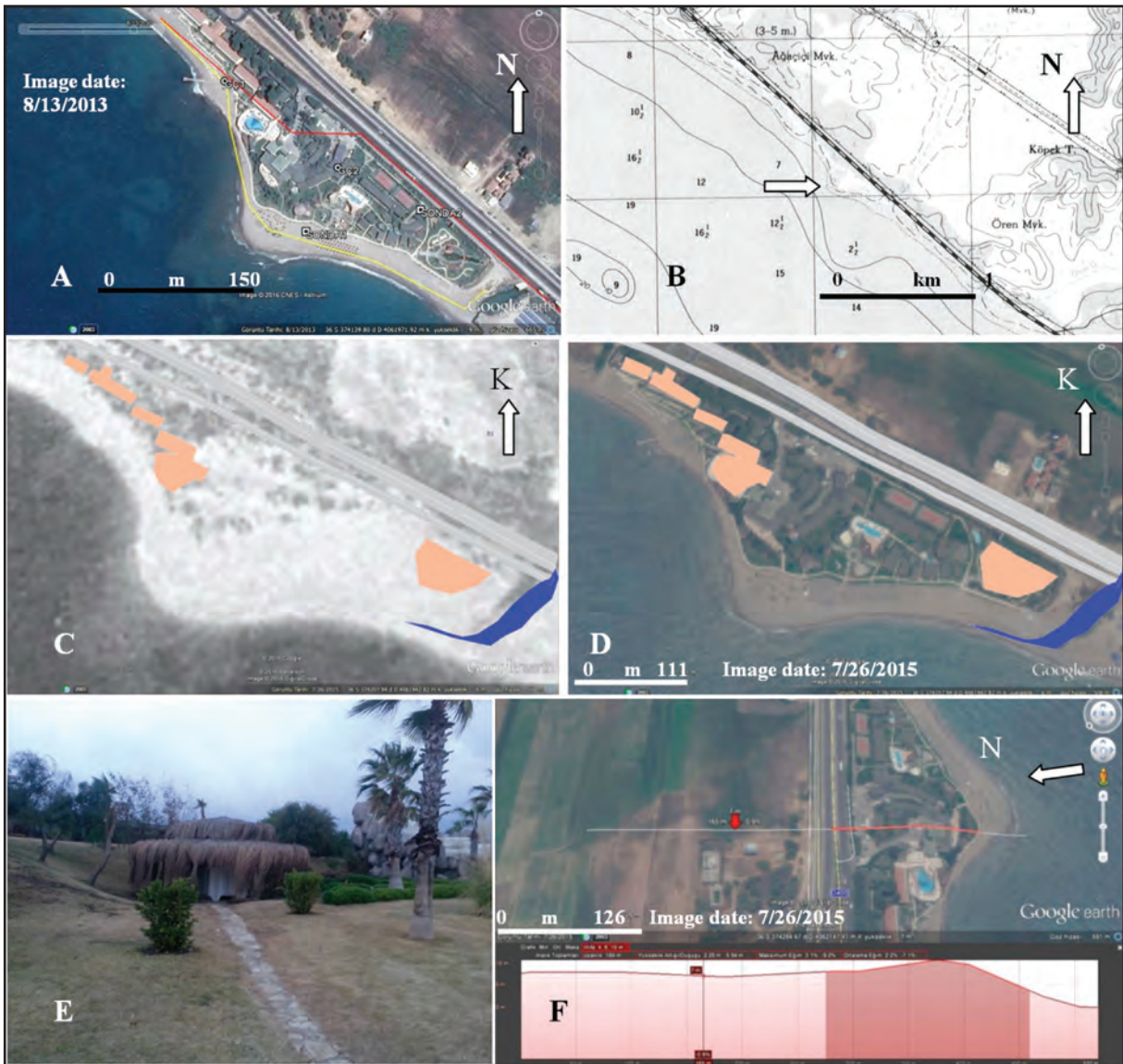


Figure 11- Google Earth view showing the investigation locations from the Kızılot area (A), topographic map (B), aerial view in 1953 (C), Google Earth view in 2015 (D), clear elevation differences (E) and topographic cross section (F).



Figure 12- A general view from the beach area (A), observation hole at the north part of the beach area (B), a view from the Miocene aged (5-10 million years) conglomerate-sandstone, carbonate sandstone lithologies (C), closer views of the siliciclastics (D, E).

low elevations, only a few meters in height behind the sand dunes. The wave effects reaching up to 2-8 meters in height should also be observed inland areas. The research results on the transgression towards the sea and depression after earthquake effects should also be taken into consideration. After all data, the elevation height may be suggested.

Although there have been no enough data on the active tectonism and its effects to coast edge line, it is clear that tsunami and tidal effects related to tectonism are not seen as big as the effects in marine conditions. If these effects happen, it is also obvious that the marine transgression may affect inland areas, kilometres far away from the sea. However all

mentioned negative occurrences are not valid in the area. So, determination of coast edge line by Today's data is thought to be solutions for the problems.

In conclusion, it is thought that clarifying of limit times for the past and future, sea level effect height and definition criteria for the coast edge line within the law and regulations should be evaluated for the solution of the problems.

Acknowledgement

The authors thank to the hotel directors and workers for helps on the observation holes, and staff in the Harita Genel Komutanlığı for obtaining of aerial views in the aims of education and research.

References

- Abama, M. 1991. Açıklamalı-Gerekçeli Kıyı Kanunu. Cansu Basın yayın Gazetecilik Ltd. Şti. Ankara, 372s.
- Akay E, Uysal S, Poisson A, Cravatte, Y., Muller, C. 1985. Stratigraphy of the Antalya Neogene Basin. Bull. Geol. Soc. Turkey, 28, 105-119.
- Akyol, N., Sesli, F.A., Gün, S. 2010. Kıyı kenar çizgisi tespitlerinde karşılaşılan problemlerin teknik yönden incelenmesi. İç: Türkiye'nin Kıyı ve Deniz Alanları VIII. Ulusal Kongresi, 27 Nisan -1 Mayıs 2010 Trabzon Bildiriler Kitabı Cilt 1, Balas, L. (ed.), 173-182.
- Altın, S. 2010. Kıyı kenar çizgisi tespiti ve kıyı kenar çizgisine bağlı uygulamalar. İç: Türkiye'nin Kıyı ve Deniz Alanları VIII. Ulusal Kongresi, 27 Nisan -1 Mayıs 2010 Trabzon Bildiriler Kitabı Cilt 1 (Ed. Balas, L.), 183-195.
- Avşar, N., Meriç, E., Alramazanoğlu, A., Dinçer, F. 2008. Antalya Körfezi (GB Turkey) Kıta Sahaneliği Bölgesi Güncel Bentik Foraminifer Toplulukları. Yerbilimleri, 29 (3), 111-136.
- Balas, L. 2010 (Editor). Türkiye'nin Kıyı ve Deniz Alanları VIII. Ulusal Kongresi, Bildiriler Kitabı, 27 Nisan -1 Mayıs 2010 Ankara, Kıyı Alanları Yönetimi Türkiye Milli Komitesi, Orta Doğu Teknik Üniversitesi Ankara CI, CII ve C3, 1619s.
- Brückner, H. 1997. Coastal changes in Western Turkey; rapid delta progradation in historical times. In: Briand, F., Maldonado, A. (eds.): Transformations and evolution of the Mediterranean coastline. CIESM Sci. Ser. 3, 63-74, Monaco.
- Climate Change, 2013. Contribution of Working Group I to the fifth assessment report of the IPCC. The Physical Science Basis. Geneva, Switzerland.
- Çiner, A., Desruelles, S., Fouache, E., Koşun, E., Dalongeville, R. 2009. Türkiye'nin Akdeniz sahillerindeki yalıtışlarının Holosen deniz düzeyi oynamaları ve tektonizma açısından önemi. Türkiye Jeoloji Bülteni, 52(3), 257-296.
- Douglas, B., Kearney, M.T., Leatherman, S.P. 2000. Sea level rise: History and consequences. Academic Press, USA, 232s.
- Ergin, M., Okyar, M., Ediger, V., Keskin, Ş., Tezcan, D., Salihoğlu, İ. 2004. Antalya Körfezi Kıta sahanlığının Geç Kuvaterner Jeolojisi: Sedimantolojik, mineralojik, jeokimyasal ve sismik araştırmalar. Proje no: YDABÇAG-199Y074.
- Görmüş, M., Caran, Ş., Çoban, H., Yılmaz, K. 2001. Bedre-Barla (Eğirdir Gölü Batısı) arasında kıyı kenar çizgisi. 1. Eğirdir Sempozyumu, 31 Ağustos-1 Eylül 2001 Eğirdir, bildiriler kitabı, 387-402.
- Görmüş, M., Çoban, H., Caran Ş., Uysal, K., Bircan, C., Tunç, İ.O. 2005. Eğirdir Gölü Batısı Pliyo-Kuvaterner Sedimanları. Türkiye Kuvaterner Sempozyumu V, 205-218.
- Görmüş, M., Yağmurlu, F., Şentürk, M., Uysal, K. 2007. Jeolojik sentez : Burdur Gölü çevresi, I. Burdur Sempozyumu, 16-19 Kasım 2005, Burdur, bildiriler kitabı, I. Cilt, Yıldız, G., Yıldırım, M.Z., Kazan, Ş. (eds.), Fakülte Kitabevi Baskı Merkezi, Isparta, 558-569, ISBN: 978-9944-729-01-7.
- Görmüş, M., Uysal, K., Uysal, A. 2010. Eğirdir Gölü kıyıları - kıyı kenar çizgisi problemi. SDUGEO (Online) 1 (2), 42-53 (www.geo.sdu.edu.tr), ISSN 1309-6656
- Gutnic, M., Monod, O., Poisson, A., Dumont, J.F. 1979. Geologies des Taurides occidentales (Turquie). Mem. Soc. Geol. France, 137, 1-112.
- <http://google.earth.com>
- İslamoğlu, Y. 2002. Antalya Miyosen havzasının mollusk faunası ve stratigrafisi (Batı- Orta Toroslar, GB Turkey). Maden ve Tetkik Arama Dergisi, 123/124, 27-58.
- İslamoğlu, Y., Taner, G. 2002. Kasaba Miyosen havzasında Uçarsu ve Kasaba formasyonlarının mollusk içeriği ve stratigrafisi. Maden ve Tetkik Arama Dergisi, 125, 31- 57

- İslamoğlu, Y., Taner, G. 2003a. Antalya ve Kasaba havzalarındaki Miyosen yaşlı mollusk faunasının paleocoğrafik ve paleoekolojik özellikleri (Batı ve Orta Toroslar). Maden ve Tetkik Arama Dergisi, 126, 11-42.
- İslamoğlu, Y., Taner, G. 2003b. Antalya Miyosen havzasının Bivalvia faunası (Batı- Orta Toroslar, GB. Turkey). Maden Tetkik ve Arama Dergisi, 127, 1- 27.
- İslamoğlu, Y., Taner, G. 2003c. Antalya Miyosen havzasının Gastropoda faunası (Batı- Orta Toroslar, GB. Turkey). Maden Tetkik ve Arama Dergisi, 127, 29- 65.
- Kanbur, S. 2012. Karaöz-Lara arasındaki Plio-Kuvaterner çökellerinin foraminiferleri ve ortamsal yorumlar. S.D.Ü. Fen Bilimleri Enstitüsü, Doktora tezi (unpublished), 289s.
- Kayan, İ. 1988. Late Holocene sea-level changes on the western Anatolian coast. Palaeogeogr., Palaeoclimatol., Palaeoecol., 68, 205-218.
- Kutoğlu, H.Ş., Akçın, H., Görmüş, K.S., Oruç, M., Öngel, S., Şimşek, Ş. 2010. 1890'lardan günümüze Zonguldak Taşkömür Havzasında endüstrileşmeye bağlı kıyı değişimlerinin incelenmesi. İç: Türkiye'nin Kıyı ve Deniz Alanları VIII. Ulusal Kongresi, 27 Nisan -1 Mayıs 2010 Trabzon Bildiriler Kitabı Cilt 1 Balas, L. (ed.), 237-244.
- MTA. 1989. Türkiye Jeoloji Haritası. 1:2.000.000 Ölçekli, Ankara.
- Nummedal, D., Pilkey, O. H., Howard, J.D. 1987. Sea-Level fluctuation and coastal evolution, SEM Spec. Publ., 41, 267p.
- Özhan, E., Abdalla, S., 2002. Türkiye kıyıları rüzgar ve derin deniz dalga atlası. Kıyı Alanları Yönetimi Türk Milli Komitesi/MEDCOAST, Orta Doğu Teknik Üniversitesi, Ankara, 445s.
- Parlar, Ş. 2010. Belek çevresinde Plio-Kuvaterner Foraminiferleri. Selçuk Üniversitesi Fen Bilimleri Enstitüsü, Doktora tezi (unpublished), 559s.
- Pluet, J., Pirazzoli, P.A. 1991. World Atlas of Holocene sea - level changes, Elsevier, Amsterdam, 299s.
- Sagular, E.K., Aydemir, A., Yavuzlar, G., Yüzcül, N.S., Uysal, K., Görmüş, M., Yıldız, A., Koşun, E. 2015. Manavgat havzasındaki genç denizel kırıntılı tortulların gerçek çökelim zamanı hangisi? Yeni nannofosil ve ascidian fosil bulgularına dayanan yeni bir stratigrafik yorum. 16.Paleontoloji-Stratigrafi Çalıştayı,25-28 Ekim 2015, Rize, Bildiriler Kitabı, Görmüş, M., Demircan, H. (eds.), Jeoloji Mühendisleri Odası Yayını, 109-116
- Sesli, F.A., Kılıçoğlu, C., Akyol, N. 2010. Kıyı kenar çizgisi tespitlerindeki problemlerin ve mülkiyetle ilişkilerinin hukuki ve teknik yönden incelenmesi. İç: Türkiye'nin Kıyı ve Deniz Alanları VIII. Ulusal Kongresi, 27 Nisan -1 Mayıs 2010 Trabzon Bildiriler Kitabı Cilt 1, Balas, L. (ed.), 197-206.
- Şenel, M., 1997a. 1:100 000 Ölçekli Türkiye Jeoloji Haritaları, Antalya L10 paftası. No 7, Maden Tetkik ve Arama Genel Müdürlüğü, Ankara.
- Şenel, M., 1997b. 1:100 000 Ölçekli Türkiye Jeoloji Haritaları, Antalya L11 paftası. No 8, Maden Tetkik ve Arama Genel Müdürlüğü, Ankara.
- Şenel, M. 1997c. 1/250.000 ölçekli Türkiye Jeoloji Haritaları, Antalya paftası. No: 3, Maden Tetkik ve Arama Genel Müdürlüğü, Ankara.
- Tüysüz, O., 2003. Kuvaterner Çalıştayı-IV. Bildiriler Kitabı, 29-30 Mayıs 2003, İTÜ-Avrasya Yerbilimleri Enstitüsü, 213s.
- Tüysüz, O., Erturaç, K. 2005. Kuvaterner Çalıştayı-V. Bildiriler Kitabı, 2-5 Haziran 2005, İTÜ-Avrasya Yerbilimleri Enstitüsü, 315s.
- Yönetmelik, 2013. Kıyı Kanununun Uygulanmasına Dair Yönetmelikte Değişiklik Yapılmasına Dair Yönetmelik. Resmî Gazete 2 Nisan 2013 Salı, Sayı: 28606.



Bulletin of the Mineral Research and Exploration

<http://bulletin.mta.gov.tr>



GRAIN SIZE, TOTAL HEAVY MINERAL AND ELEMENT DISTRIBUTION AND CONTROL FACTORS OF CURRENT SEDIMENTS ON THE FLOOR OF HISARÖNÜ AND DATÇA BAYS

Barbaros ŞİMŞEK^{a*}, Mustafa ERGİN^b, Murat EVREN^a, Özgür TÜRKMEN^b, Serkan PALAS^a, Hakan PEHLİVAN^a, Bahri Serkan AYDEMİR^a and Füsün ÖCAL^a

^aGeneral Directorate of MTA, Marine Research Department

^bAnkara University, Geological Engineering Department and River, Lake and Seas Geologic Research Center

Research Article

Keywords:

Datça, Hisarönü, Bay, Sediment, Sea

ABSTRACT

This paper presents research results for Holocene sedimentary processes and controlling factors in Datça and Hisarönü Bays located in south west Turkey. For this purpose, we collected seafloor grab samples (upper 30 cm) from 71 stations and seismic profiles (only one sample is used to explain sedimentary process) from Hisarönü and Datça Bays with the MTA-SELEN research ship. According to the seismic profile, the continental shelf edge or threshold is found at depths of -90/-120 m and displays seismic facies parameters showing sea level variations from the Quaternary period. According to radiocarbon dating calculations, the sediment samples began to be deposited 2694-14700 years before present. The seafloor sediments comprise 1-18% gravel, 7-85% sand, 2-30% silt and 6-69% clay size clastic material. Although mud of mixed silt and sand composition is the most common sediment type, there are significant sand and gravel amounts. As well as discussing regional differences in grain size distribution, the presence of residual (relict) sediments is noted. The total amount of heavy mineral-rich black sand is mostly below 2%, reaching 13% in ophiolite- and chromite-rich central and eastern regions. Inorganic geochemistry of sediments includes relatively significant amounts of ophiolitic-sourced Mg, Cu, Ni and Fe. Regional variations in river drainage system, bay morphology, terrestrial source rock lithology and marine waves and currents affect not only sediment grain size distribution, but also total heavy mineral content and the main element composition.

Received: 04.04.2016

Accepted: 06.05.2016

1. Introduction

The study area incorporates Datça and Hisarönü Bays in the southwest of Turkey located with Datça Peninsula to the north, Marmaris to the east, and Simi (Sömbeki) island to the south between the Mediterranean and Aegean Seas with oceanographic characteristics of these seas (Figure 1). The studies and available data for the region are generally related to the general geology, with insufficient study on the seafloor sediments and their characteristics. This article, prepared to research the decomposition products of source rocks on Datça Peninsula and the offshore traces of heavy mineral placer sands deposited along the current coastline, comprises sedimentologic and geochemical studies along with interpretations, partial seismic and C¹⁴ studies. As there is no previous data on studies of heavy mineral placers in the marine area south of Datça Peninsula, this study is considered to fill an important gap in the literature.

1.1. General Geology

The Aegean region is actively shaped by tectonic events (Figure 2). The region was the setting for the formation of the Aegean trench and is currently dominated by intense tectonic movements linked to subduction (Şengör and Yılmaz, 1981, Ersoy, 1991). The Upper Miocene was the period when N-S extension began in the Aegean region (Kurt, 1999). In this period the Aegean Sea, coastline and neighboring continents were one of the most seismically active regions in the world (Jackson and McKenzie, 1984; Taymaz et al., 1991; Dirik et al., 2003). Under the effect of these motions, the Aegean Sea was influenced by active extensional tectonics in the boundary system of plates around the Mediterranean (Mascle and Martin, 1990; Uluğ et al., 2005) and east-west striking grabens formed due to extensional tectonics (McKenzie, 1972, 1978; Dewey and Şengör, 1979; Angelier et al., 1981; Uluğ et al., 2005).

* Corresponding author: Barbaros ŞİMŞEK, barbaros.simsek@mta.gov.tr, 0312 201 1516
<http://dx.doi.org/10.19111/bulletinofmre.304502>

The current setting of the Datça Peninsula is closely related to a range of geologic events such as the regional emplacement of the Likya Nappes and the formation of the Gökova, Datça and Hisarönü Bays. The Likya Nappes were formed by the thrusting of oceanic crust above the Anatolide-Tauride platform during subduction along the Izmir-Ankara suture belt in the Cretaceous and the shaping of this thrust and later material accreted by subduction during the continent-continent collision in the Upper Paleocene-Lower Eocene along with allocthonous units from the Western Taurus (Brunn et al., 1971, Şengör and Yılmaz, 1981, Ersoy, 1991, Uluğ, 2005). A NW-SE striking rift system including Middle-Upper Miocene units developing due to the effect of a compressional regime and later N-S oriented systems including Plio-Quaternary units occurring during the extensional regime appear to have been effective during the formation of Gökova Bay north of Datça Peninsula (Görür et al., 1995; Uluğ et al., 2005). With the effect of slab pull beginning in the Upper Miocene, the currently submarine Hisarönü Graben formed between the Datça and Bozburun Peninsulas (Ersoy, 1991). Gravity causing extensional forces on the Datça Peninsula produced structural elements like horst and graben due to a growth fault. The most typical examples are NE-trending faults bounding the north and south of Datça Graben. The faults of the Hisarönü and Gökova Grabens cut the faults of the Datça Graben obliquely. As a result the Datça

Peninsula gained a horst structure together with the grabens between the Datça Graben (Ersoy, 1991).

Outcrop geology in the Datça Peninsula comprises the Triassic-Cretaceous age Likya Nappes including the Bodrum Nappe, Gülbahar Nappe and Marmaris Ophiolite and overlying Paleogene, Neogene and Quaternary units (Figure 3). The Bodrum Nappe comprises Middle Triassic-Upper Cretaceous dolomite, limestone, mudstone, claystone, siltstone and volcanics and represents bedrock. The Middle Triassic-Upper Cretaceous Gülbahar Nappe consisting of sandstone, mudstone, limestone and volcanic overlies these units (Şenel and Bilgin, 1997). The Jurassic-Upper Cretaceous Marmaris Ophiolite Nappe is located above the Gülbahar Nappe, and includes rock types such as limestone, cherty limestone, dolomite, radiolarite, chert and volcanics in sheared serpentinite mud with a chaotic structure. There is occasional harzburgite, dunite, gabbro, diabase and serpentinitized harzburgite and dunite in the Kızılcaadağ Melange and Olistostrome with harzburgite, occasionally serpentinitized harzburgite and dunites and occasional small diabase and gabbro masses comprising the Marmaris Peridotites (Şenel and Bilgin, 1997). Paleogene clastic units are found over the Likya Nappes above an angular unconformity with Neogene clastics and carbonates continuing above an unconformity. Unconformably lying above all units are Quaternary-age clastic sediments (slope debris, alluvium) and volcanics (Şenel and Bilgin, 1997).

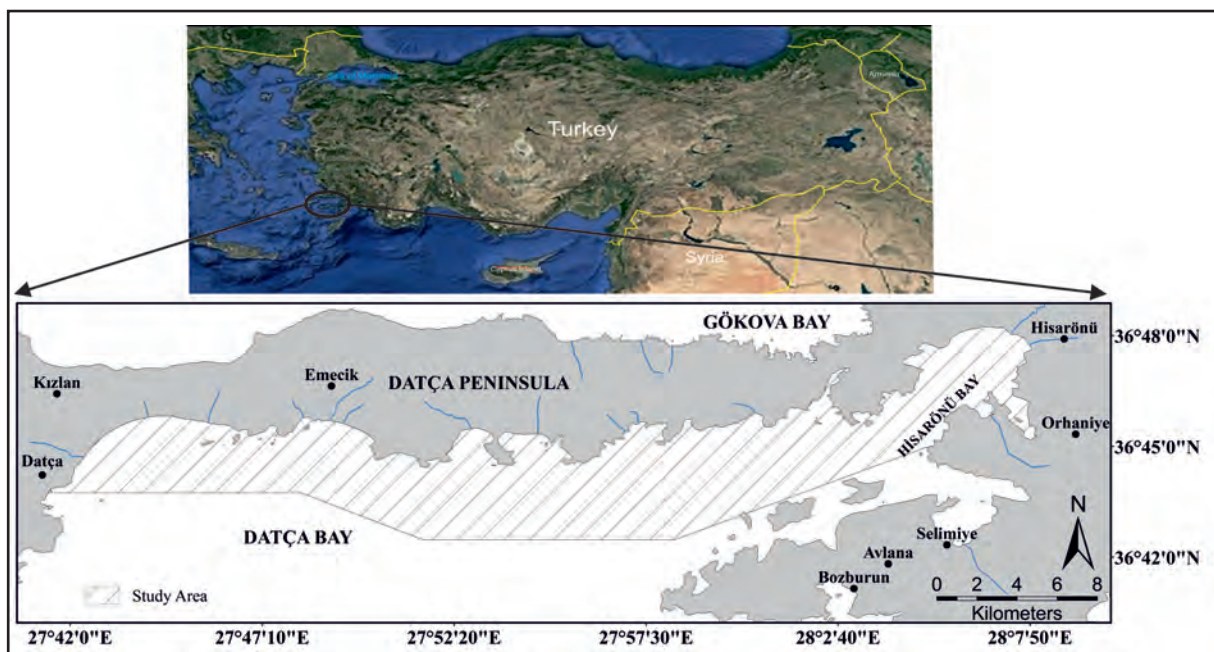


Figure 1- The study area of Datça and Hisarönü Bays and close surroundings.

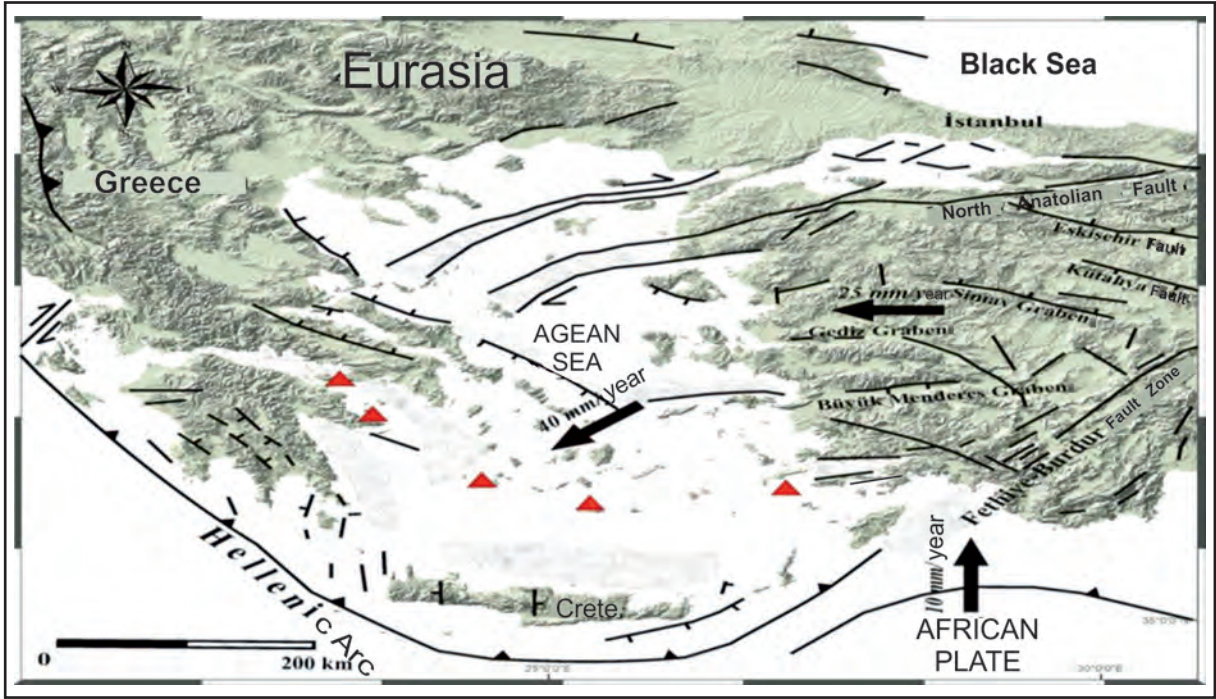


Figure 2- Tectonic map of Aegean Sea and surroundings (Large black arrows - plate movement directions, black lines - faults (Barka and Reillinger, 1997; from Kaşer, 2010, fault south of Dağça Peninsula Ersoy, 1991), red triangles - volcanos (National Observatory of Athens, from Kaşer, 2010).

1.2. Morphology, Climate and Rivers

The coastline of the Dağça Peninsula comprises mountainous morphology with generally narrow and short beaches, and small islands and submarine elevations extending from the coast into the sea (Figure 4). The highest points on the Dağça Peninsula are from west to east; Yassıdağ (408 m); Karabalık Peak (455 m); Bozdağ (1163 m); Karmanbaşı Peak (747 m) and Mount Yağlıdağ (486 m). South of the peninsula the shelf area deepens from the coast to 200 m reaching broad extension in Hisarönü Bay of ~ 22 km, with a narrow shelf of ~ 5 to ~ 8 km in Dağça Bay linked by a deepening section beginning from 200 m (Figure 4). The region has typical Mediterranean climate. Summers are hot and dry, while winters are mild and rainy. Mean annual temperature is 19.1 °C in Dağça with the hottest month of July having mean temperature of 27.1 °C and the coldest month of January having mean temperature of 12.1 °C. Mean precipitation for Dağça is 710.9 mm. Nearly all precipitation falls during the winter months (Taşlıgil, 2008).

Due to the steep morphology of the peninsula, it has many inclined short riverbeds with seasonal and irregularly flowing rivers and streams carrying material

to the coast in the region represented by Küçükakalataka Stream (1); Eksera Stream (2); Çakal Stream (3); Günuç Stream (4); Bakacak Stream (5); Alazeytin Stream (6); Akçabük Stream (7); Kızıl Stream (8); Karabük Stream (9); Koca Stream (10); Armutyanı Stream (11); İnceburun Stream (12); Zindan Stream (13); Uzunırmak Stream (14); Çakallıca Stream (15); Gökçe Stream (16); Havari Stream (17); Değirmen Stream (18); Bağlıca Stream (19); Cin Stream (20); Kurucaboğaz Stream (21); Kocaçığı Stream (22); Karacalıbükü Stream (23); Dallı Stream (24); Kazan Stream (25); Hisarönü Stream (26); Değirmen Stream (27); and Çaykuyu Stream (28) (Figure 5). Apart from streams, the Dağça Hot Spring collecting in a natural basin with temperature 27 °C is located 100 m inland west of Dağça Pier (Taşlıgil, 2008).

2. Material and Method

On the General Directorate of Mineral Research and Exploration (MTA) research ship MTA Selen, the Dağça Project voyage collected single channel shallow seismic reflection profiles, grab and core samples from Dağça and Hisarönü Bays. For shallow seismic sections, a seismic profile perpendicular to the coast in accordance with the aims and scope of the

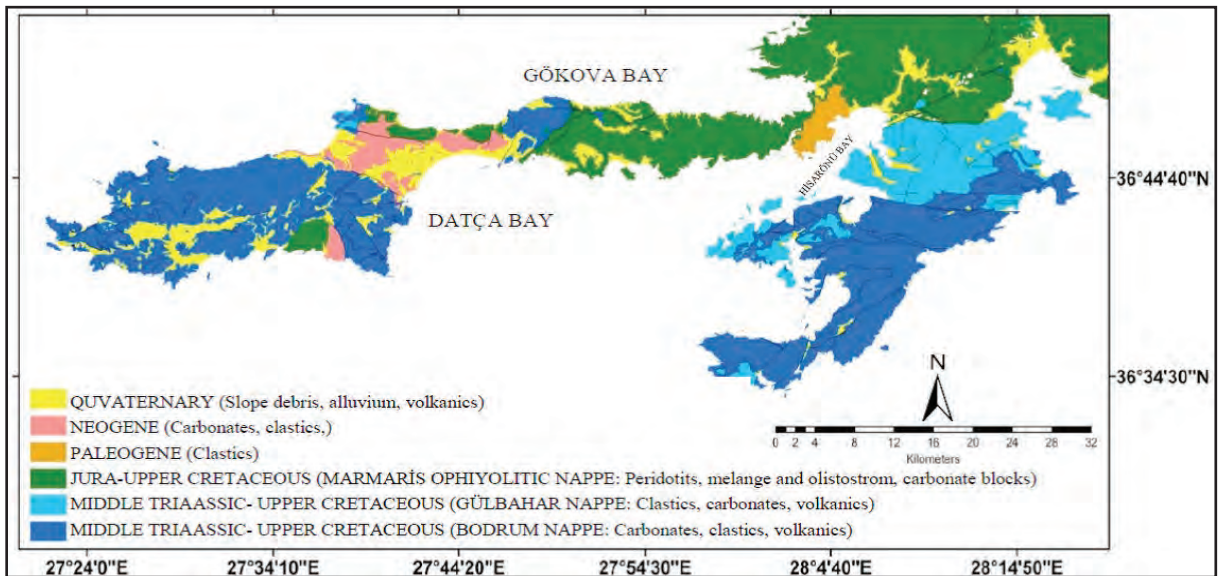


Figure 3- General geology map of Datça Peninsula and surroundings (adapted from Şenel and Bilgin, 1997).



Figure 4- Underwater morphology map of bays north and south of Datça Peninsula (adapted from TR311 Navigation Map and www.hgk.gov.tr/sayisal-uygulamalar, no scale).

project was chosen (Figure 6). Single channel seismic data were collected using a high resolution shallow seismic system (Geoacoustics) with energy source of a 175 joule boomer, listen time of 500 ms and sampling interval of 40 μ s. The data were processed with the system's Geo-Pro II data processing software to obtain seismic reflection profiles. For calculation of water and sediment depths from two way travel time (TWT) data, the acoustic wave speed was accepted as 1500 m/s. With the aim of explaining Quaternary geology, principles and methods stated in Mitchum et al. (1977) and Posamentier et al. (1988) were used for interpretation of facies analysis and parameters on seismic reflection profiles.

The study used 71 samples taken with a sediment scoop representing the top 30 cm of the seafloor (Figure 7). The majority of samples were analyzed

in the MTA laboratories, with some completed in the Geological Engineering Department of Ankara University. The sediment sample points numbered 51, 52, 53, 54 and 55 were in close proximity to the region of the number 10 seismic profile (Figures 6 and 7).

For grain size analysis, the sediment samples were washed and after sea salt was removed, they were washed above a 0.0625 mm pore size sieve to separate the sand and gravel fractions. The remaining mud fraction was separated into silt and clay grain sizes with a Malyem Mastersizer 2000 device. The samples were later dried and passed through a 0.0625 mm sieve to separate 4 mm, 2 mm, 1 mm, 0.25 mm and 0.125 mm diameter grain sizes. Grain size classification was determined according to the Wentworth scale stated by Folk (1980).

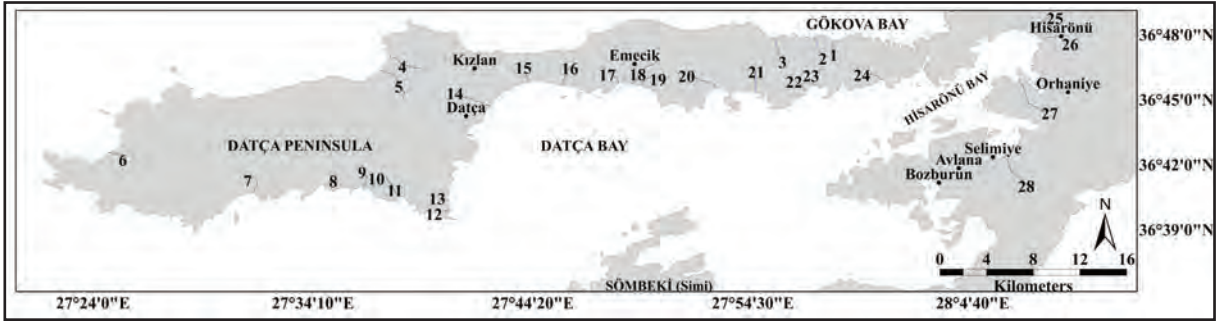


Figure 5- Irregular and seasonal streams on Datça Peninsula and surroundings (prepared from General Command of Mapping topographic maps and field observations).



Figure 6- Location of no. 10 seismic section taken in Datça Bay.

To identify the ages of the sediments, sediment samples from the upper levels of cores obtained from 8 sample points (Figure 8) were sent to the ETH (Swiss Federal Institute of Technology of Zurich) laboratory and age dating was completed with convective radiocarbon methods with results given as C^{14} BP after C^{13} correction (BP – before present).

For total heavy mineral analyses, washed and dried sediment samples with grain size from 1 mm to 0.0625 mm were separated into heavy and light mineral fractions according to standard methods with bromoform liquid with density 2.89 g/ml (Müller, 1967; Lewis, 1984; Grosz et al., 1990).

Based on total heavy mineral analyses of scoop samples from Datça and Hisarönü Bays, 21 samples were chosen for geochemical analysis (Figure 9). The dried and ground sediment samples had main and trace elements measured with a Thermo ARL XRF system (reference material UQ standart) in the Turkish Accreditation Agency-certified MTA General Directorate Laboratories for geochemical element analysis (Figure 9). Statistical methods like the Pearson correlation matrix were used to assess the analysis results.

3. Results

The assessment of data from sediment sample analyses and seismic section in Datça and Hisarönü Bays are given below.

3.1. Radiocarbon (C^{14}) Ages of Sediments

The ages of base levels of the sediments in the study (30 cm below the seafloor) were determined with calculation methods to have begun deposition 2694 years before present for station number 4 and 14,700 years before present for station number 3 with all ages obtained from the field between these values (Table 1). Calculations from other cores with 30 cm thickness found station no. 7 began deposition 11,424 years before present, station no. 8 began deposition 10,237 years before present with other stations beginning deposition between 2816 to 6112 years before present. The sediment deposition rates obtained from the ages of sediments was mean 6 cm/1000 years, with significant differences regionally (2-11 cm/1000 years) (Table 1). The highest values (10-11 cm/1000 years) were encountered in the concave, protected and relatively wide shelf at Datça Bay with fluvial inputs. The ages of scoop (surface) sediment samples in

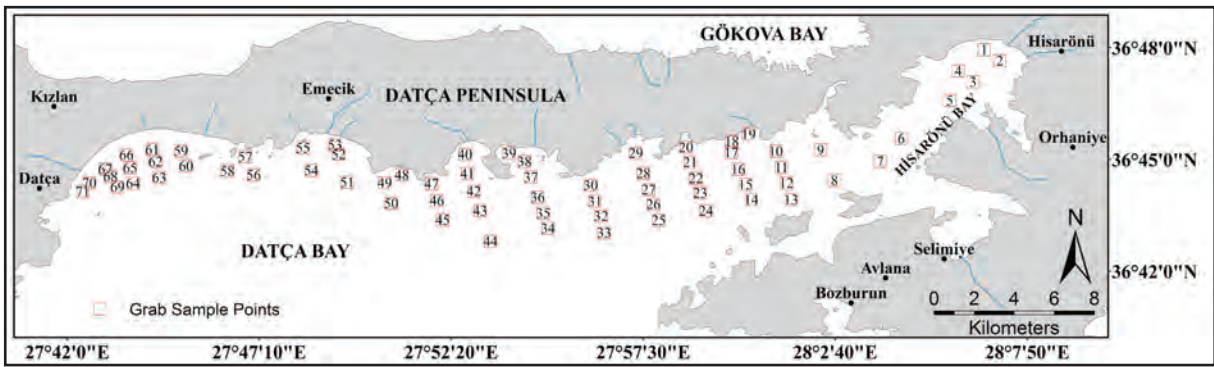


Figure 7- Surface sediment sampling stations in Datça and Hisarönü bays.

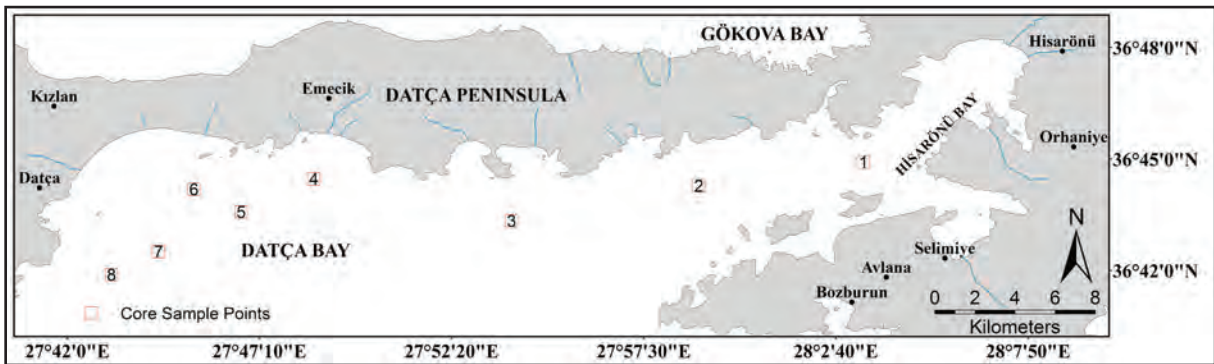


Figure 8- Core sample points chosen for radiocarbon age dating.

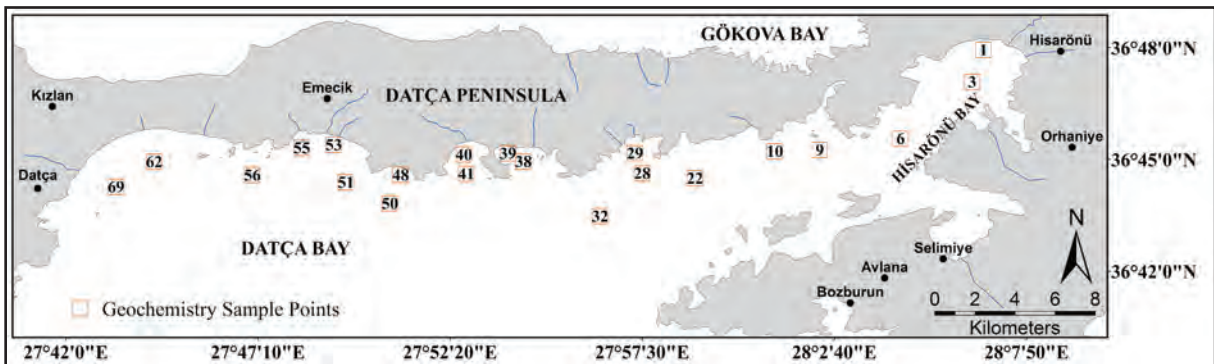


Figure 9- Grab sediment samples for geochemical analysis in Datça-Hisarönü bays.

Datça and Hisarönü Bays were assessed as varying from Upper Pleistocene to Holocene. For these bays, it was estimated that nearly 2 m of sediment may have accumulated from the beginning of the Last Glacial Maximum (LGM; 19,000 years BP, Hamann et al., 2008) and Holocene (11,700 year BP. IUGS ICS, 2016) to the present day (Table 1).

3.2. Seismic Facies Analysis

To make the seafloor, sea level changes and tectonics more comprehensible in the region, the no.

10 seismic reflection profile from east of Datça Bay was investigated (Figure 10). With approximately 410 ms listen time, no. 10 profile is equivalent to about 300 meters depth when seawater acoustic wave speed is taken as 1500 m/s. Beginning near the coast and in shallow water with 60 ms (45 m) water column depth, the section extends into open water with 270 ms (202 m) depth. The edge or threshold of the shelf is very clear on the profile at 160 ms (120 m) depth and is very much in accordance with the previously published Upper Pleistocene global sea level variation curves (Fairbanks, 1989; Siddall, 2003; Toucanne,

Table 1- Radiocarbon age (C¹⁴) distribution of core samples from Datça and Hisarönü Bays and correlation to grab samples.

| Core No | C ¹⁴ Core Depth Grab Sample Depth Holocene (LGM) Depth (cm) | C ¹³ Corrected C ¹⁴ Age (BP) | Calculated sediment deposition rate (cm/1000 years) |
|---------|--|---|--|
| 1 | 40-41 30 78 (126) | 6099 4517 11700 (19000) | 6.64 |
| 2 | 40-41 30 89 (145) | 5307 3931 11700 (19000) | 7.63 |
| 3 | 29-30 30 24 (39) | 14455 14700 11700 (19000) | 2.04 |
| 4 | 34-35 30 130 (212) | 3098 2694 11700 (19000) | 11 |
| 5 | 40-41 30 57 (93) | 8252 6112 11700 (19000) | 4.9 |
| 6 | 26-28 30 125 (202) | 2535 2816 11700 (19000) | 10.65 |
| 7 | 25-26 30 31 (50) | 9711 11424 11700 (19000) | 2.62 |
| 8 | 30-31 30 50 (81) | 10408 10237 11700 (19000) | 2.93 |
| Mean | 30 | 7054 | 6 |

2012). Again on this profile, sediment or deposition depth on the inner shelf near the coast is 20 ms (15 m) reaching 60 ms (45 m) on the outer shelf and falling to 20 ms (15 m) again on the upper slopes. Seismic facies units with continuous regular high-amplitude reflections parallel to the slope with cover-like form pass to wavy, dome-like parallel moderate-high amplitude occasionally chaotic, irregular, lenslike and progressively clinof orm units on the shelf. Especially at 160 ms depth (120 m) with clear progressive clinof orms, a sediment wedge similar to a low sea level delta and the ancient coastline from the Upper Pleistocene period shape the shelf in the study area. Investigation of available data shows that in the study area in Datça and Hisarönü Bays sea level variation and terrestrial clastic supply were among the important factors in the Upper Pleistocene and especially Holocene. The angled (normal, reverse) faults identified on the seismic profile show that the region was affected by active tectonics especially in the Miocene and later times (Figure 10).

Surface sediment samples obtained with a scoop (30 cm thick) are equivalent to 0.4 ms thickness on the seismic profile and as a result it is very difficult, if not impossible, to perform detailed seismic facies analysis with such low values (Figure 10).

3.3. Grain Size Distribution

The grain size distribution of sediment samples from 30 cm depth on the sea floor in Datça and Hisarönü Bays comprised 0-18% gravels, 7-85% sand, 2-30% silt and 6-69% clay (Figure 11). When the bays are compared, the sediments in Hisarönü Bay varied from 5-10% gravel, 25-50% sand, 10-30% silt and 25-69% clay. The sediments from Datça Bay meanwhile have distribution of 0-15% gravels, 25-85% sand, 0-30% silt and 0-69% clay (Figures 11 – 12 - 13 – 14 - 15).

According to this distribution the sediments in Datça Bay contained relatively high proportions of

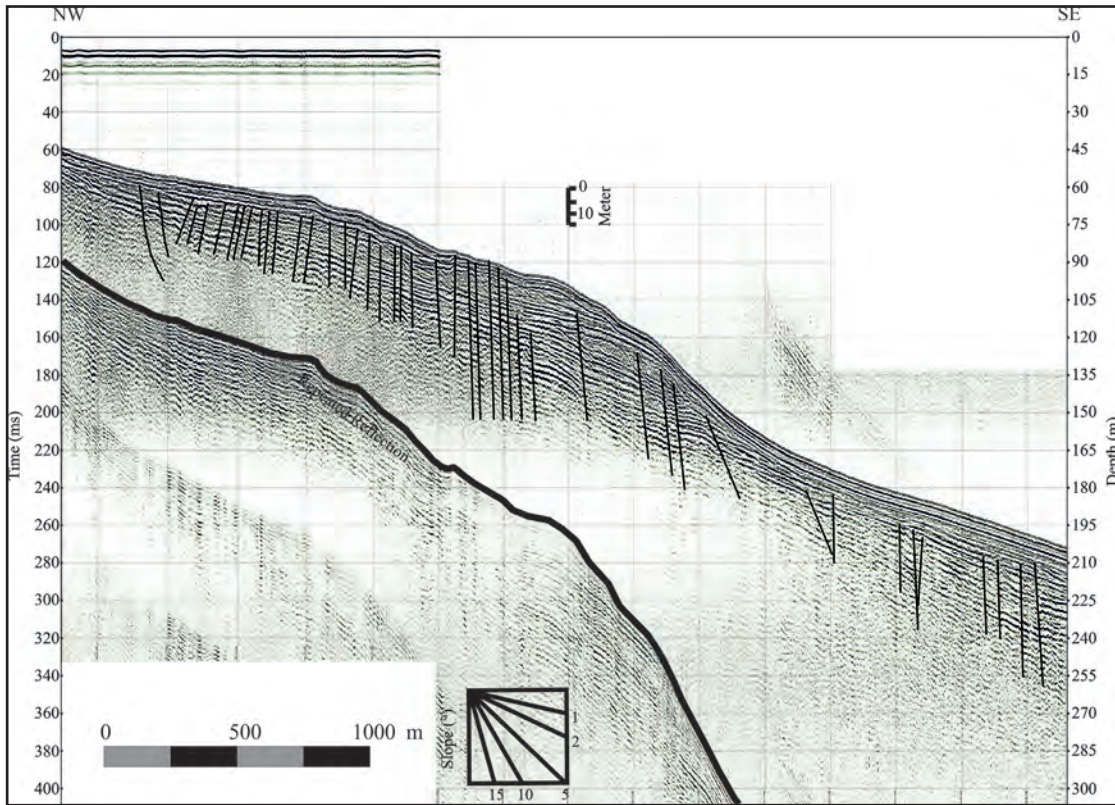


Figure 10- Seismic reflection profile no. 10 from east of Datça Bay. For section location see figure 6, interpretation in text.

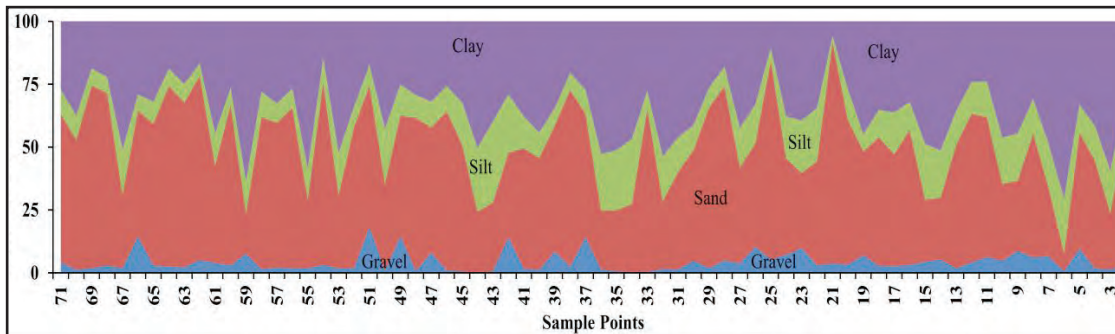


Figure 11- Grain size distribution of surface sediments in Datça and Hisarönü Bays.

sand and low proportions of clay. The relatively high gravel amounts in Datça Bay were found in the west, central and east sections in a regionally narrow area. Similarly the proportion of gravels in Hisarönü Bay has regional increases in the central and western sections. Generally the increase in gravels was encountered at the shelf edge and nearby, in front of rocky coasts and in relatively shallow waters (Figure 12). An increase in the proportion of gravels was only found near stream mouths in a few areas, with gravels in Datça Bay increasing from the interior to exterior.

Sand amounts may increase near the coast in the west and east of Datça Bay (50-85%) but also

may increase in more distal areas (Figure 13). Silt proportions generally increase from the coast (<10%) toward open waters (shelf edge) (20-30%) (Figure 14). These increases appear to be more dominant in limited regions in the eastern portion of Datça Bay and the eastern, central and western portions of Hisarönü Bay.

Clay amounts vary in the western and eastern sections of Datça Bay. In the west in areas close to the coast 50-69% clay grain size material reduces toward open water to fall below 25% and in the east increases again to reach 69% occasionally on the shelf edge (Figure 15). In the protected and secluded Hisarönü Bay, the clay amount is generally high and values of

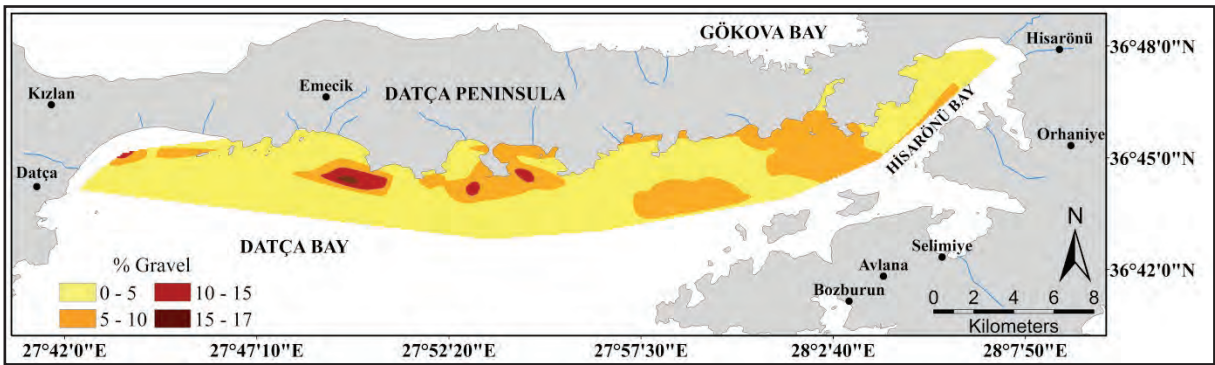


Figure 12- Distribution of gravel size material in surface sediments in Datça and Hisarönü Bays.

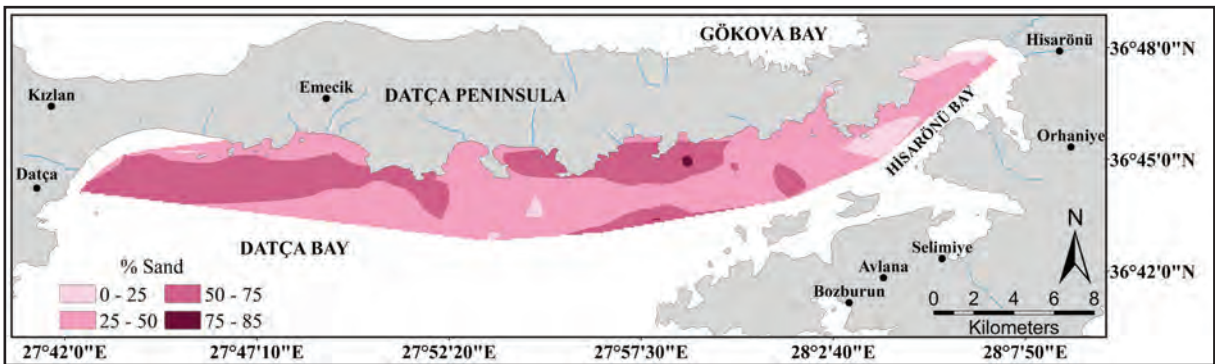


Figure 13- Distribution of sand size material in surface sediments in Datça and Hisarönü Bays.

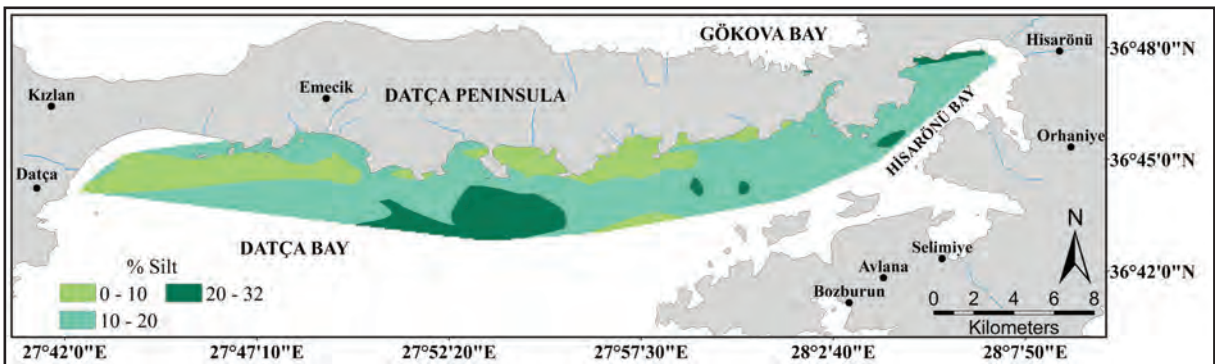


Figure 14- Distribution of silt size material in surface sediments in Datça and Hisarönü Bays.

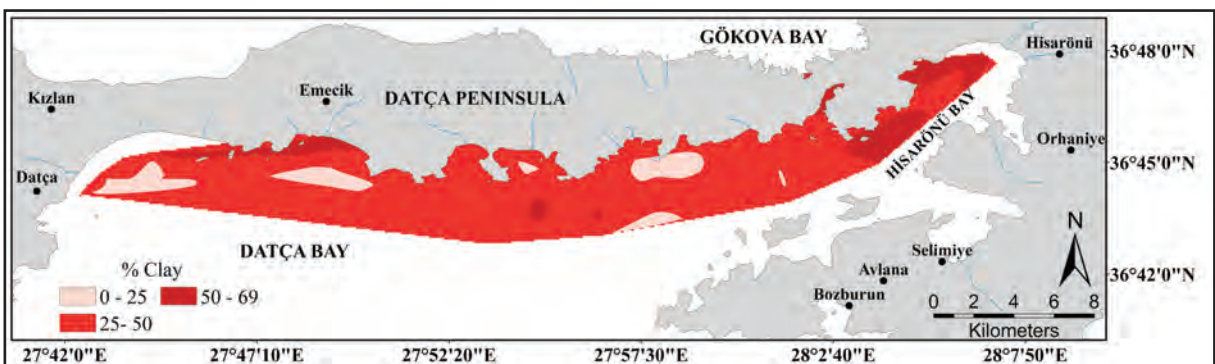


Figure 15- Distribution of clay size material in surface sediments in Datça and Hisarönü Bays.

50-69% are more common (Figure 15). Though high clay proportions are encountered near stream mouths, it appears difficult to apply this correlation to the whole study area. When sediment grain size distribution is classified according to the triangle diagram of Folk (1980) the bay sediments belong to slightly gravelly muddy sand "(g)mS", slightly gravelly sandy mud "(g)sM", gravelly muddy sand "gmS", slightly gravelly mud "(g)M", slightly gravelly sand "(g)S", gravelly mud "gM" and sandy mud "sM" with sand and mud proportions varying occasionally (Figures 16 - 17). In the field sandy and muddy units are the dominant two common sediment types and generally muddy units accumulate in Hisarönü Bay while sandy units generally accumulate in Datça Bay. In some regions and especially in the west, sediment types change from mud to sand from the coast to open water, while other regions display transition from sand to mud.

The graphic mean grain size of sediment samples varies from \emptyset 4.70 to \emptyset 8.14, with mean grain size of clay for a small area close to the coast in the interior of Hisarönü Bay, while the mean grain size for other areas of Hisarönü Bay and Datça Bay is mainly silt (Figure 18).

3.4. Total Heavy Mineral Distribution

The total heavy mineral (THM) amounts in surface sediments in Datça and Hisarönü Bays vary from <1 to 13% with values mainly lower than 2% (Figure 19). Relatively high THM amounts are encountered in the interior sections of Hisarönü Bay (10-15%) and in the tip area east of Datça Bay (5-10%) (Figure 20). Inland from the coast in the bays and especially in regions that may form source areas, it is previously known that there are ophiolitic rocks that may contain heavy minerals. In fact, ophiolitic rocks rich in heavy minerals are more common in Hisarönü Bay (Figure 3). When the total heavy mineral contents of samples are compared in terms of grain size, samples containing heavy minerals appear to have gravel percentages from 0-10% with sand 25-75%, silt 5-25% and clay 15-55% (Figure 21). Additionally it cannot be said that there was a strong direct positive correlation between total heavy mineral proportions and grain size distribution of sediments.

3.5. Element Geochemistry

The element analysis results obtained in the study (Figures 22-32, Table 2) were compared with mean

values for continental crust, sedimentary (e.g., shale, sandstone, limestone) and basic-ultrabasic (e.g., dunite, harzburgite) rocks.

When the mean values for SiO_2 , TiO_2 , Al_2O_3 , Fe_2O_3 , MnO , MgO , CaO , Na_2O , K_2O , P_2O_5 and Cr_2O_3 in study area sediments are compared with mean sedimentary, magmatic and continental crust rock values, the majority had similarities identified. The source rocks found inland from the coasts are commonly observed, forming a wide range from dunite, harzburgite, basalt, sandstone, limestone and basic-ultrabasic rocks (Figure 3). Especially the relatively high Mg, Fe and Cr amounts may be considered decomposition products from the Marmaris Ophiolite. The distribution of some elements displays regional differences (Figures 22-32). In the outer portion of Hisarönü Bay in front of Dil Headland and from sample no. 28 at the shelf edge to Datça Bay in the west and Hisarönü Pier in the east, amounts of SiO_2 , Al_2O_3 , Fe_2O_3 , and K_2O generally and clearly increase. The increasing trend toward the east is partially accompanied by TiO_2 , MgO , Na_2O and P_2O_5 . While MgO increases in the remaining area between the two bays (Figure 27), MnO values are high throughout all regions (Figure 26). CaO has an inverse distribution decreasing to the east and west from station no. 28 (Figure 28). Sampling station no. 28 is located in the region of the ~100 m depth contour in Datça and Hisarönü Bays and determines the bathymetric limit separating the bays (Figure 4). Datça Bay to the west of the sample point has a relatively narrow coast with steep slope linking 100 m to deeper areas, Hisarönü Bay to the east has a broader and relatively lower slope opening to deeper areas from 100 m (Figure 4).

Evaluation with a correlation matrix prepared from results of interelement correlations and dependence on other variables was completed taking account of correlations between elements and element associations and determined positive and high correlations for those with correlation coefficient +0.8 or more (Table 3). Accordingly SiO_2 - TiO_2 , SiO_2 - Al_2O_3 , SiO_2 - Fe_2O_3 , TiO_2 - Al_2O_3 and Al_2O_3 - K_2O have very high positive (+) correlations, with the majority of these elements directly or indirectly associated with or enriched in silicates and aluminosilicates. Coefficients varying from 0.66 to 0.91 for Cr_2O_3 , MgO , Fe_2O_3 and total heavy mineral amounts may be linked to source rocks containing chromite and peridotite in the region. Generally the effect of total heavy mineral amounts on

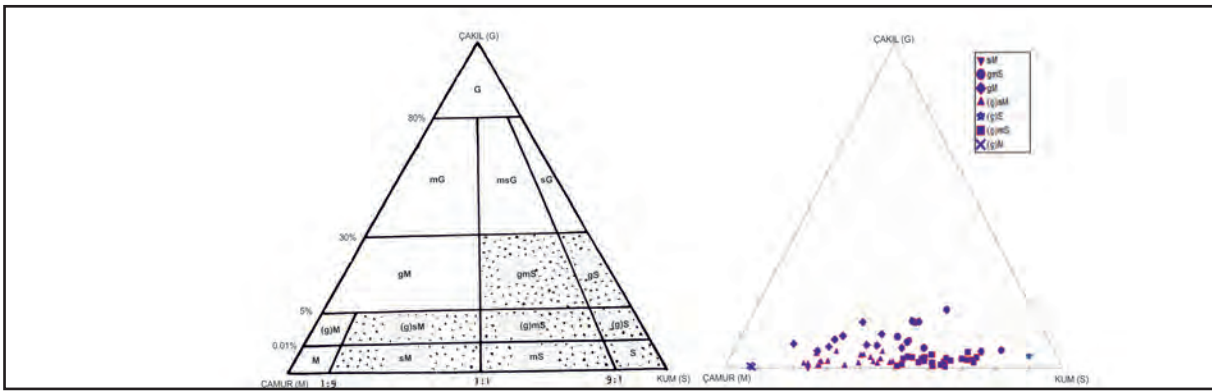


Figure 16- Classification of surface sediments in Datça and Hisarönü Bays according to Folk (1980).

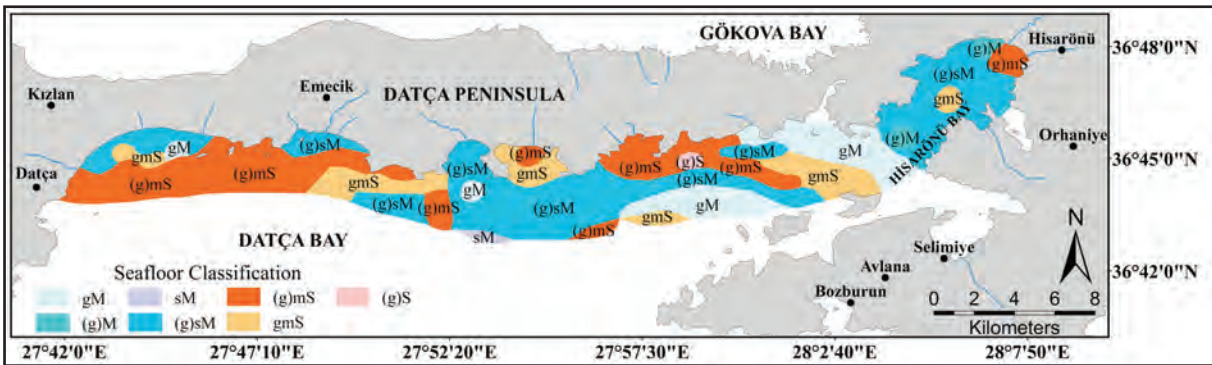


Figure 17- Distribution of surface sediments in Datça and Hisarönü Bays according to Folk's classification (1980).

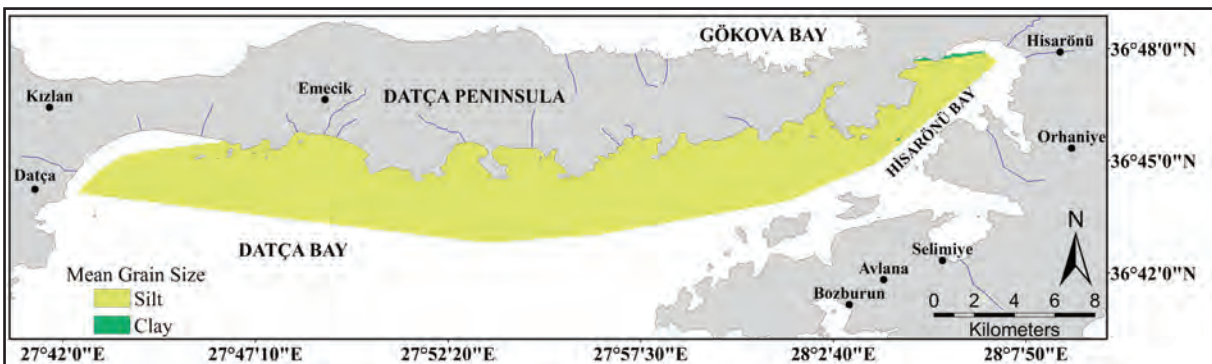


Figure 18- Mean grain size distribution of surface sediments in Datça and Hisarönü Bays.

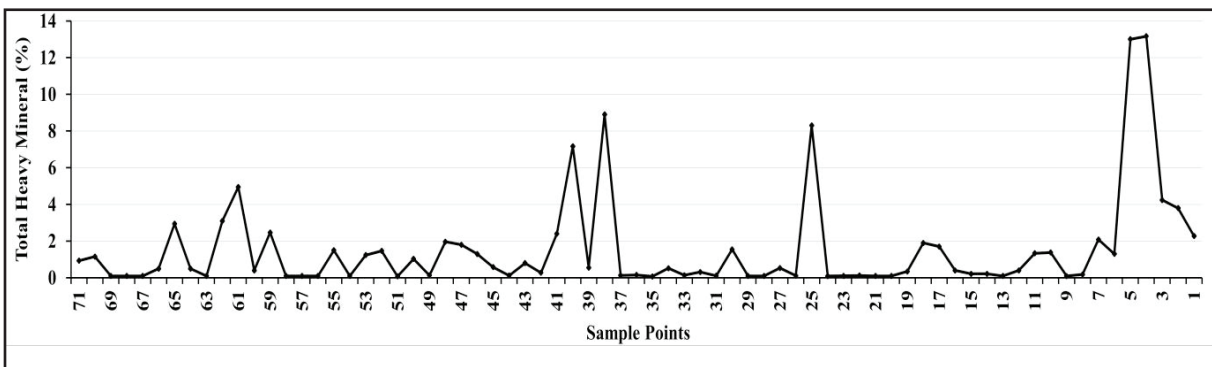


Figure 19- Total heavy mineral distribution in grab sediment samples from Datça and Hisarönü Bays.

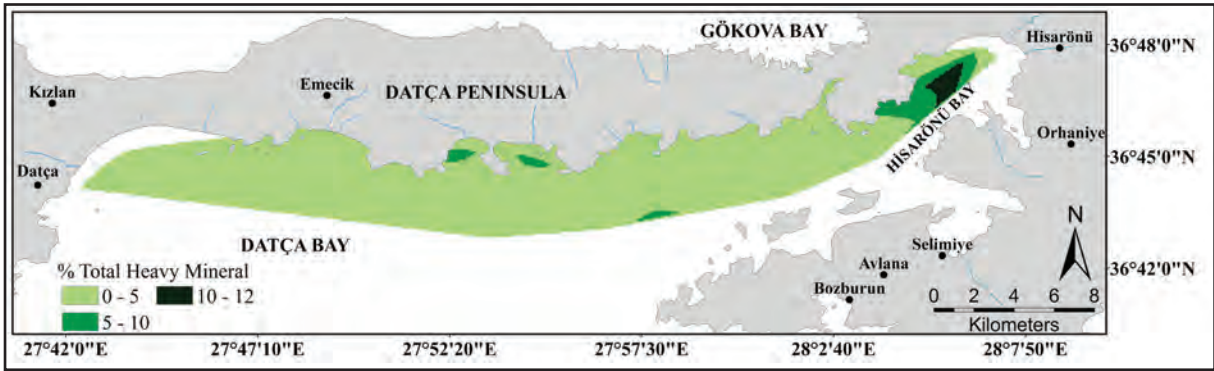


Figure 20- Total heavy mineral distribution in grab sediment samples from Datça and Hisarönü Bays.

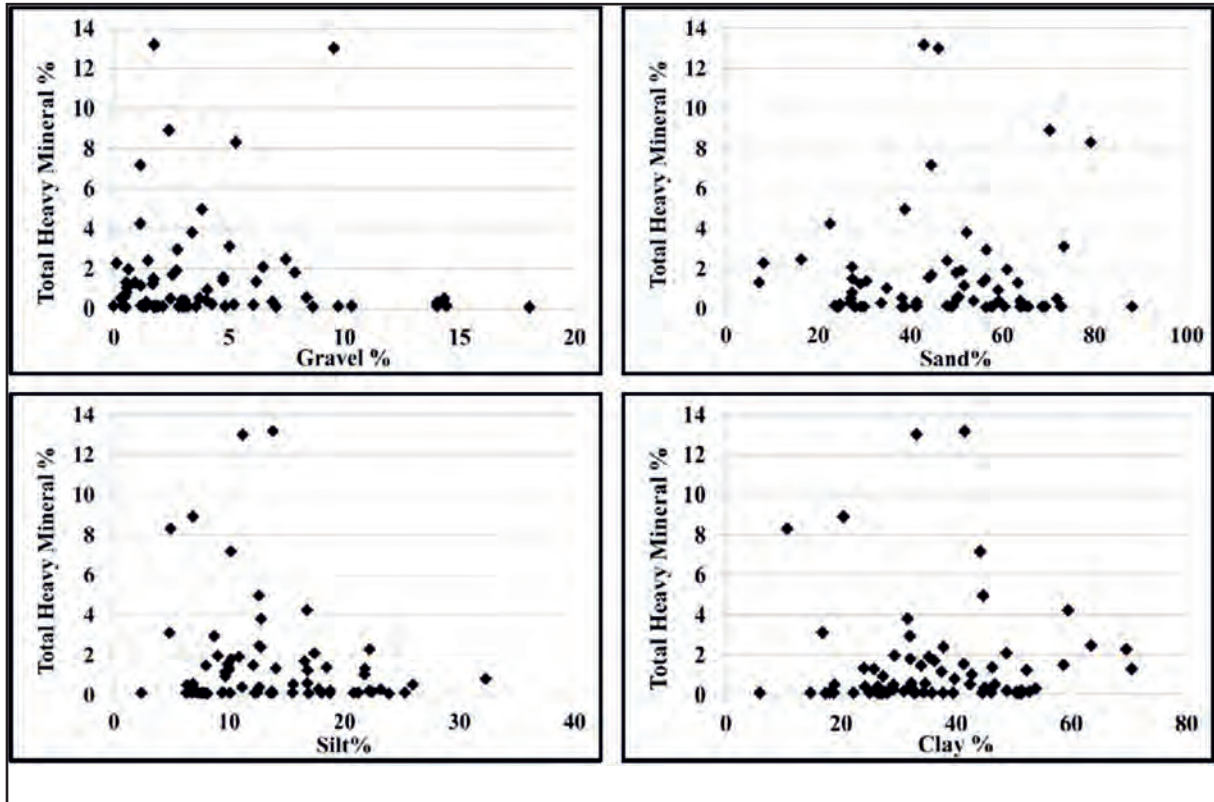


Figure 21- Correlation of total heavy minerals and grain size in samples from south of Datça Peninsula.

element distribution was very low (Table 3). No matter how sand size and clay size sediments appeared to have relatively high correlation coefficients, generally clay fractions were not enriched in elements (Table 3).

4. Discussion

Generally high resolution seismic reflection profiles provide important clues about the stages within a Quaternary-fill sedimentary basin including erosion, transportation and deposition conditions and texture and structure of accumulated sediment

(Mitchum et al., 1977; Posamentier et al., 1988). These include, especially, environment and facies types linked to high and low sea levels developing in the Upper Pleistocene period (Ergin et al., 1992; Aksu et al., 1999; Çağatay et al., 2000; Boggs, 2006). Investigation of available seismic data show that sea level variation during the Upper Pleistocene-Holocene period and supply of terrestrial clasts were among the most important factors affecting the sea floor sediments in Datça and Hisarönü Bays. The fact that the surface sediments investigated had mean thickness of 30 cm made seismic facies analysis of the

Table 2- Comparison of continental crust, shale, basalt, sandstone, limestones, ultrabasics, dunite and harzburgite geochemistry with geochemical data of samples from Datça-Hisarönü Bays.

| % Oxide | This study Min | This study Max | This Study Mean | Continental Crust (Rudnick, 2005) | Continental Crust (Gao et al., 1998) | Shale (Okumola and Idowu 2012) | Basalt (Klein 2005) | Sandstone (Turekian and Wedepohl 1961) | Limestone (Turekian and Wedepohl 1961) | Harzburgite (Uysal 2007) | Dunite (Uysal 2007) | Ultrabasic (Turekian and Wedepohl 1961) |
|--------------------------------|----------------|----------------|-----------------|-----------------------------------|--------------------------------------|--------------------------------|---------------------|--|--|--------------------------|---------------------|---|
| SiO ₂ | 7.80 | 49.00 | 23.96 | 60.60 | 64.20 | 61.26 | 50.01 | 78.71 | 5.13 | 43.64 | 41.48 | 43.85 |
| TiO ₂ | 0.10 | 0.70 | 0.25 | 0.72 | 0.80 | 1.74 | 1.11 | 0.25 | 0.07 | 0.00 | 0.00 | 0.05 |
| Al ₂ O ₃ | 1.20 | 8.40 | 3.59 | 15.90 | 14.10 | 16.88 | 16.31 | 9.44 | 1.59 | 0.49 | 0.16 | 7.56 |
| Fe ₂ O ₃ | 2.10 | 10.50 | 5.20 | 6.71 | 6.80 | 3.75 | 9.73 | 2.80 | 1.09 | 8.87 | 8.83 | 26.96 |
| MnO | <0.1 | 0.10 | 0.10 | 0.10 | 0.12 | 0.02 | 0.14 | X0.1 | 0.14 | 0.11 | 0.11 | 0.21 |
| MgO | 3.90 | 18.40 | 7.90 | 4.66 | 3.50 | 0.16 | 8.67 | 1.16 | 7.79 | 45.24 | 47.83 | 33.82 |
| CaO | 5.50 | 41.10 | 27.37 | 6.41 | 4.90 | 0.05 | 11.75 | 5.47 | 42.29 | 0.66 | 0.27 | 3.50 |
| Na ₂ O | 1.20 | 2.40 | 1.80 | 3.07 | 3.10 | 0.06 | 2.52 | 0.89 | 0.11 | 0.02 | 0.00 | 1.13 |
| K ₂ O | 0.30 | 1.40 | 0.71 | 1.81 | 2.30 | 1.39 | 0.05 | 2.58 | 0.65 | 0.00 | 0.00 | 0.01 |
| P ₂ O ₅ | <0.1 | 0.10 | 0.14 | 0.13 | 0.18 | 0.08 | 0.08 | 0.08 | 0.18 | 0.00 | 0.00 | 0.10 |
| Cr ₂ O ₃ | 0.04 | 0.52 | 0.16 | 0.01 | 0.01 | 0.01 | 0.03 | 0.01 | 0.00 | 0.14 | 0.05 | 0.47 |

X: Estimated value

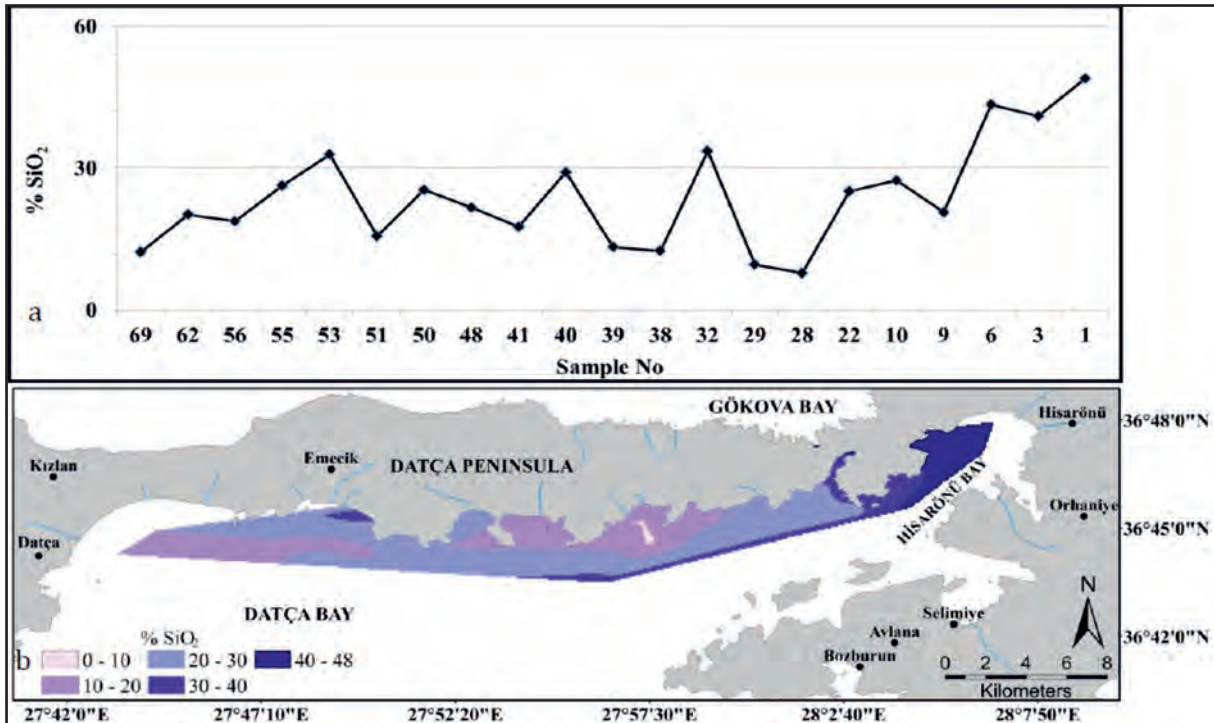


Figure 22- a) SiO₂ amounts and b) SiO₂ spatial distribution in surface sediments in Datça-Hisarönü Bays.

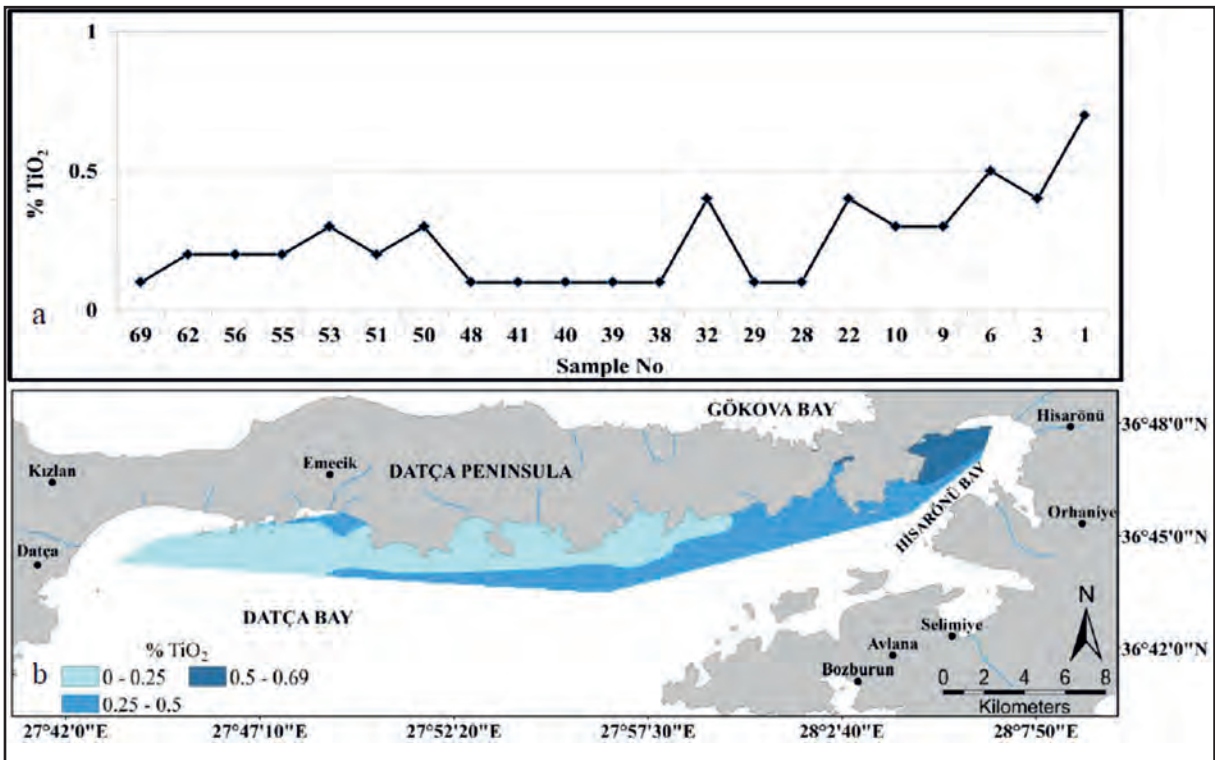


Figure 23- a) TiO_2 amounts and b) TiO_2 spatial distribution in surface sediments in Datça-Hisarönü Bays.

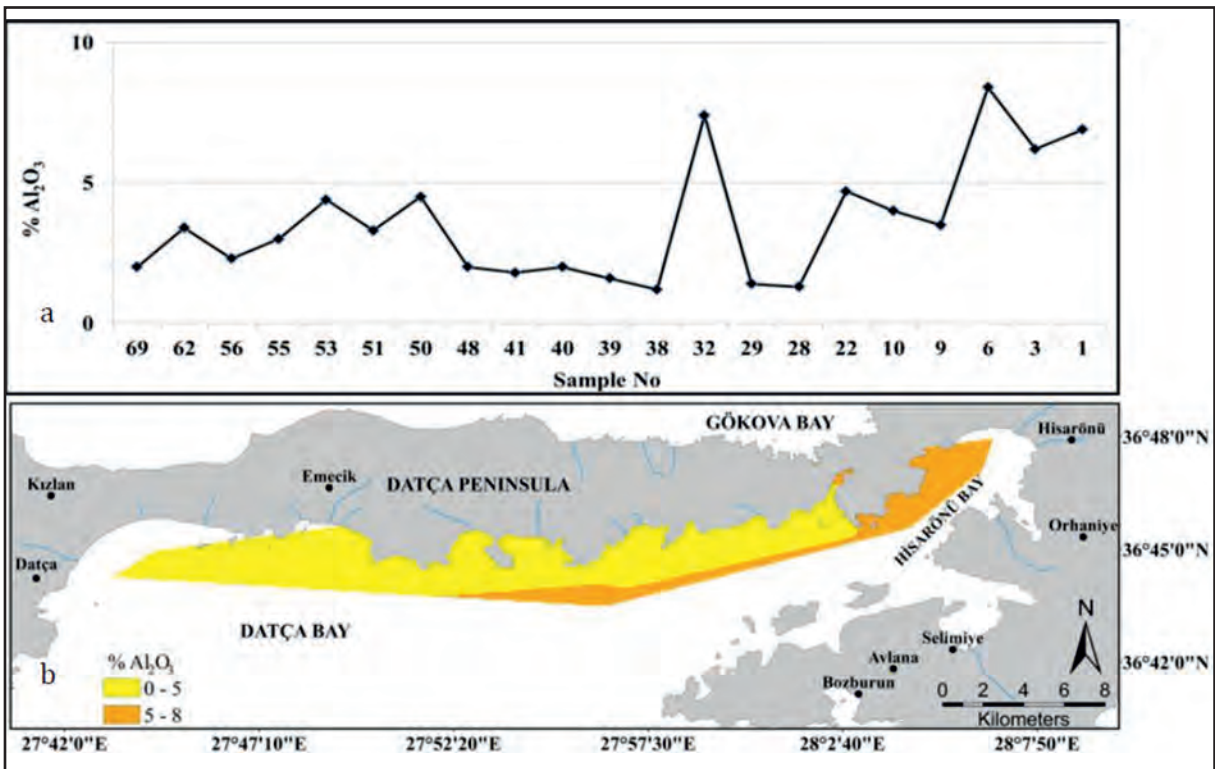


Figure 24- a) Al_2O_3 amounts and b) Al_2O_3 spatial distribution in surface sediments in Datça-Hisarönü Bays.

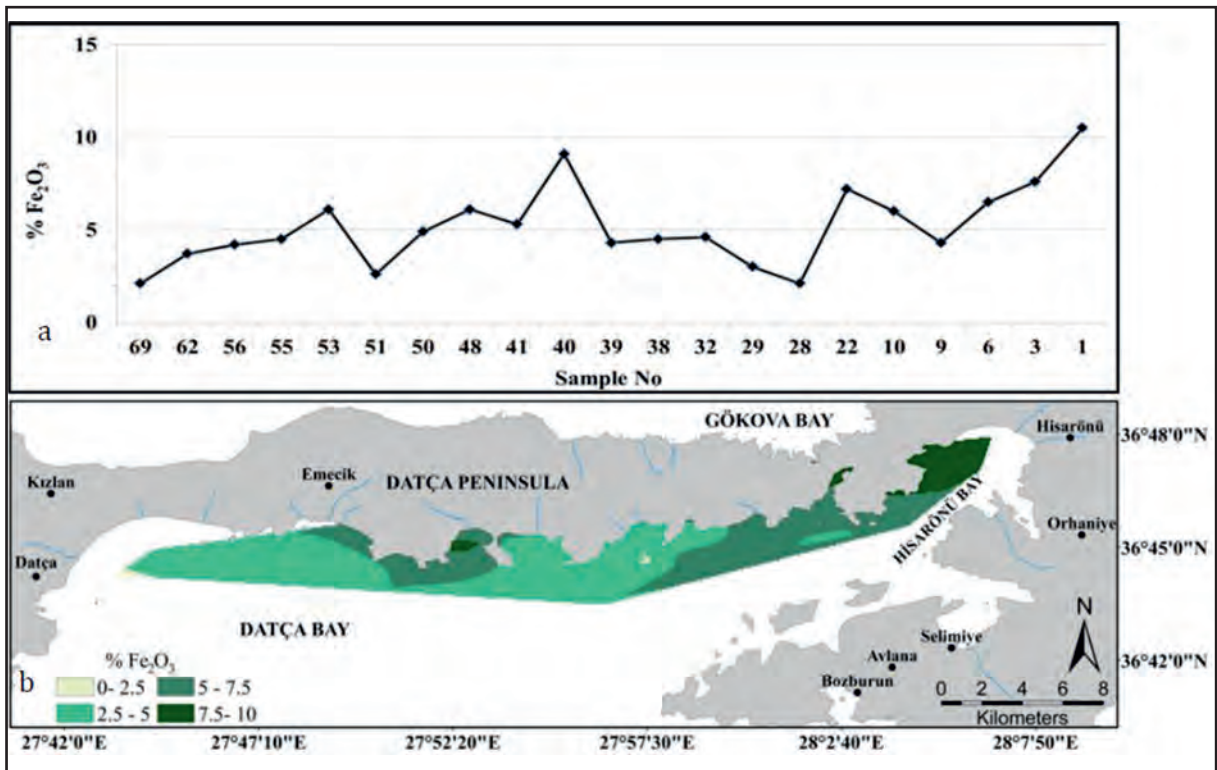


Figure 25- a) Fe₂O₃ amounts and b) Fe₂O₃ spatial distribution in surface sediments in Datça-Hisarönü Bays.

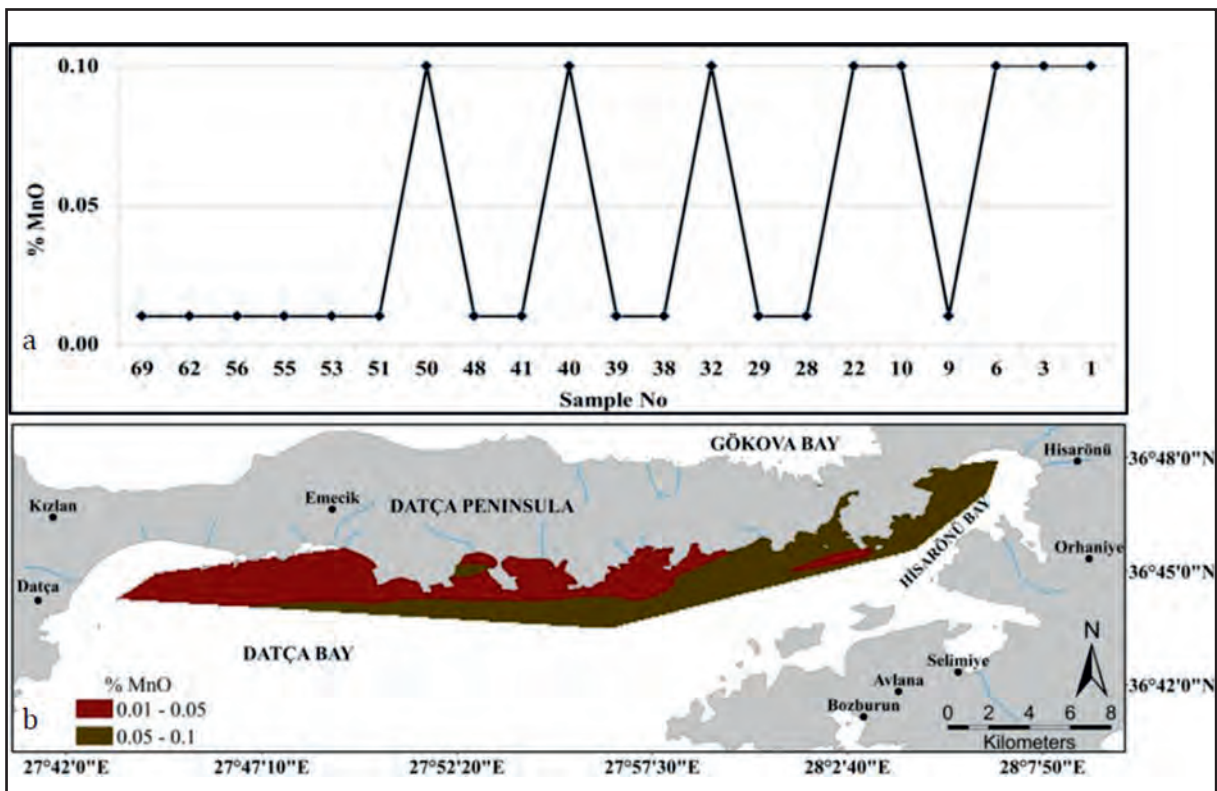


Figure 26- a) MnO amounts and b) MnO spatial distribution in surface sediments in Datça-Hisarönü Bays.

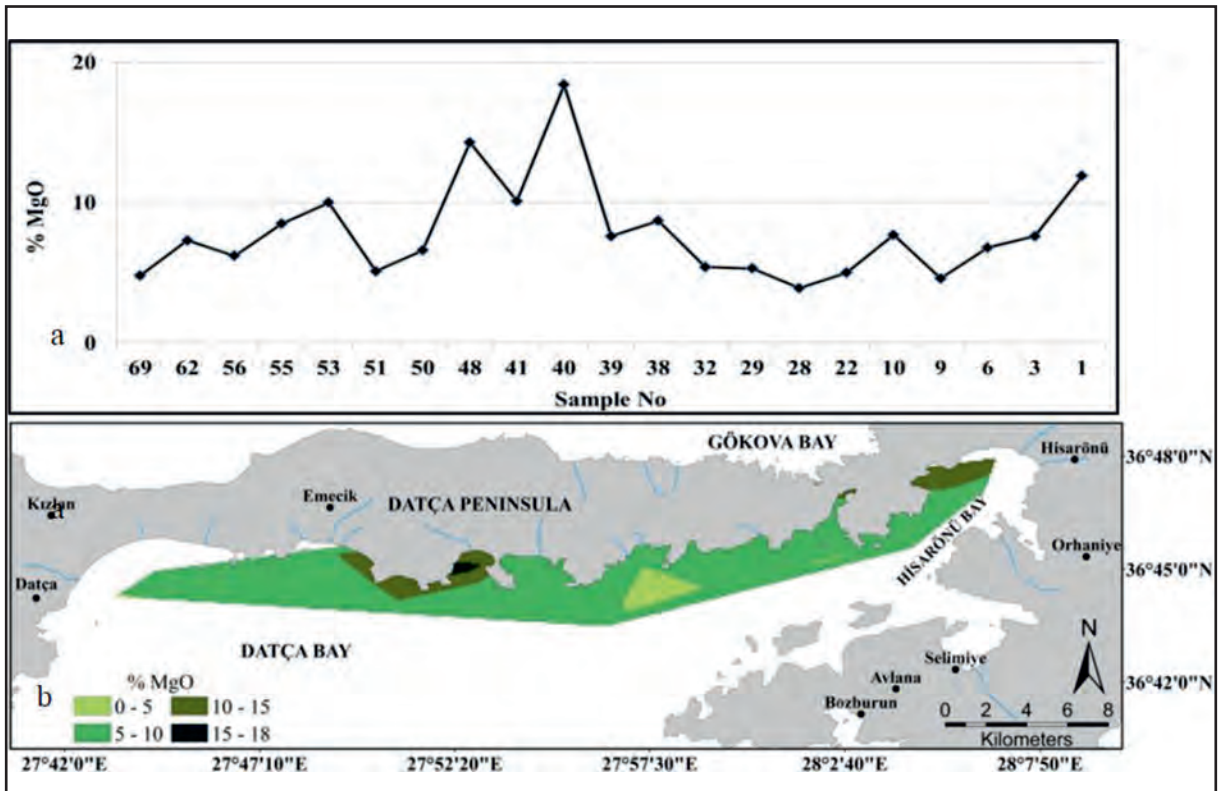


Figure 27- a) MgO amounts and b) MgO spatial distribution in surface sediments in Datça-Hisarönü Bays.

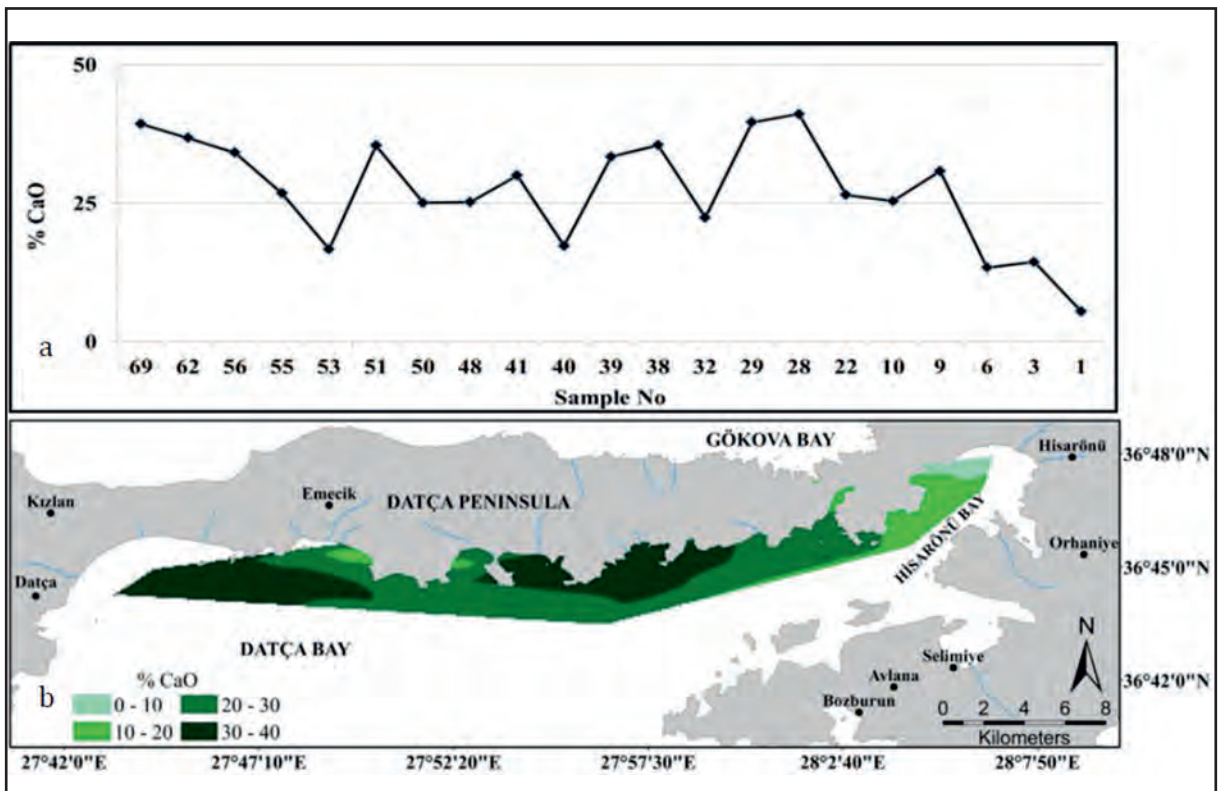


Figure 28- a) CaO amounts and b) CaO spatial distribution in surface sediments in Datça-Hisarönü Bays.

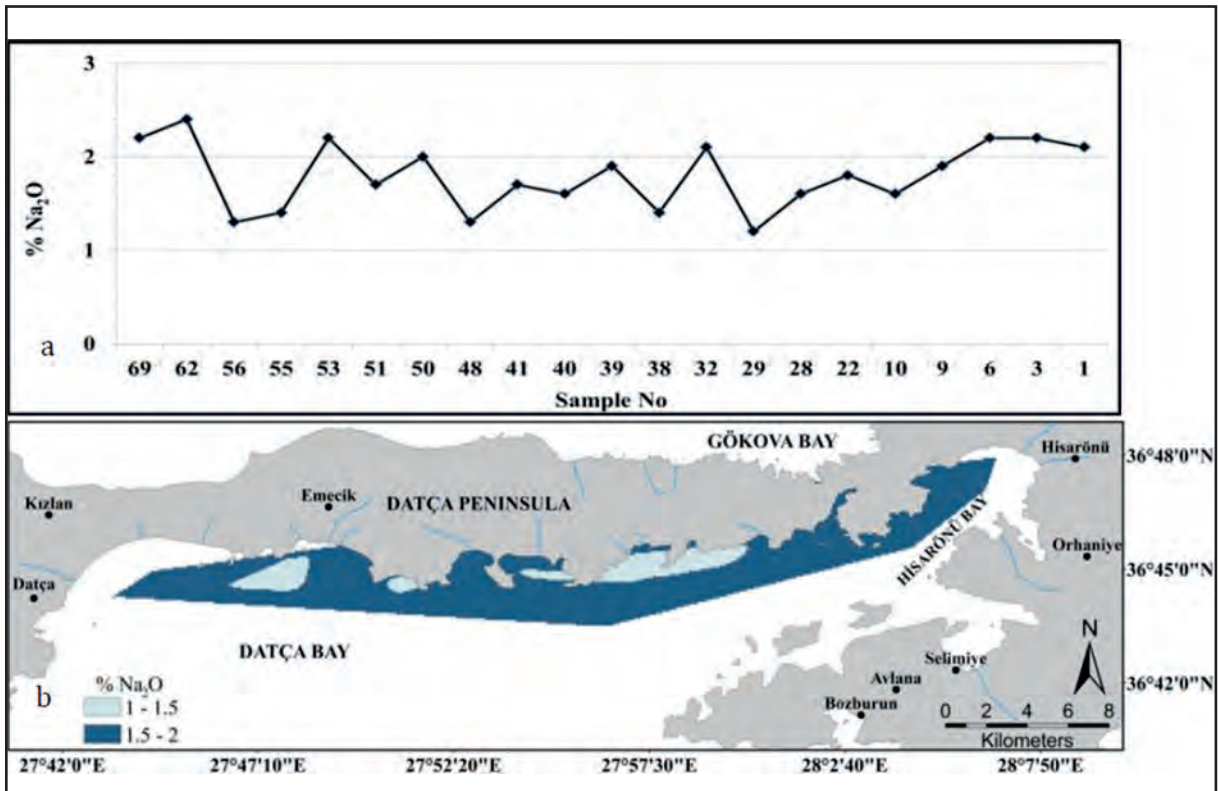


Figure 29- a) Na₂O amounts and b) Na₂O spatial distribution in surface sediments in Datça-Hisarönü Bays.

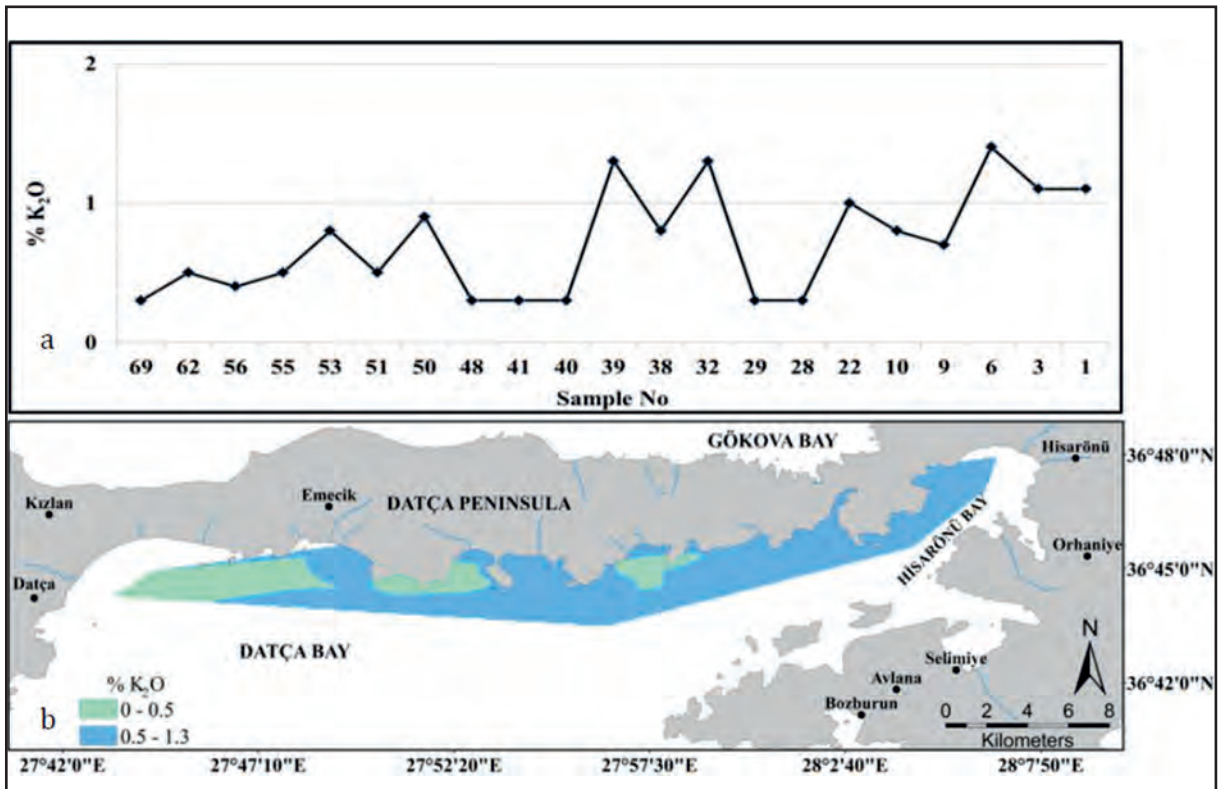


Figure 30- a) K₂O amounts and b) K₂O spatial distribution in surface sediments in Datça-Hisarönü Bays.

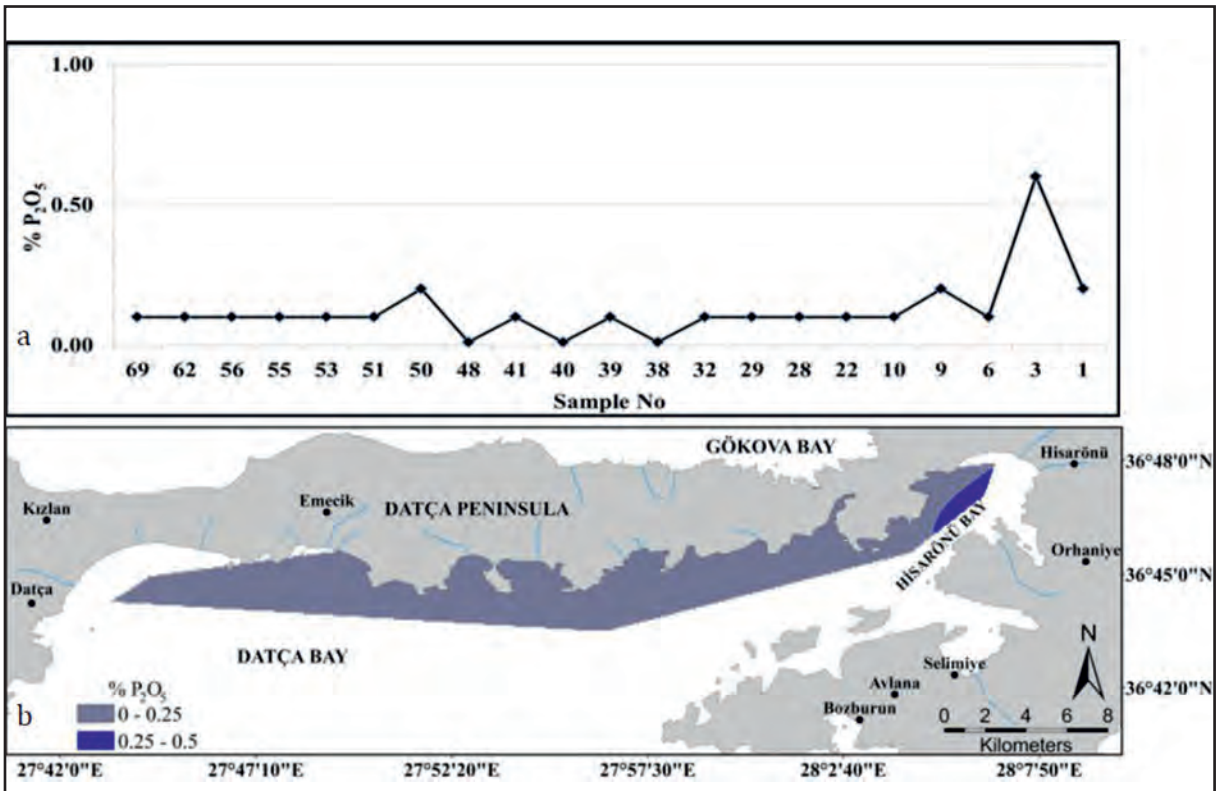


Figure 31- a) P_2O_5 amounts and b) P_2O_5 spatial distribution in surface sediments in Datça-Hisarönü Bays.

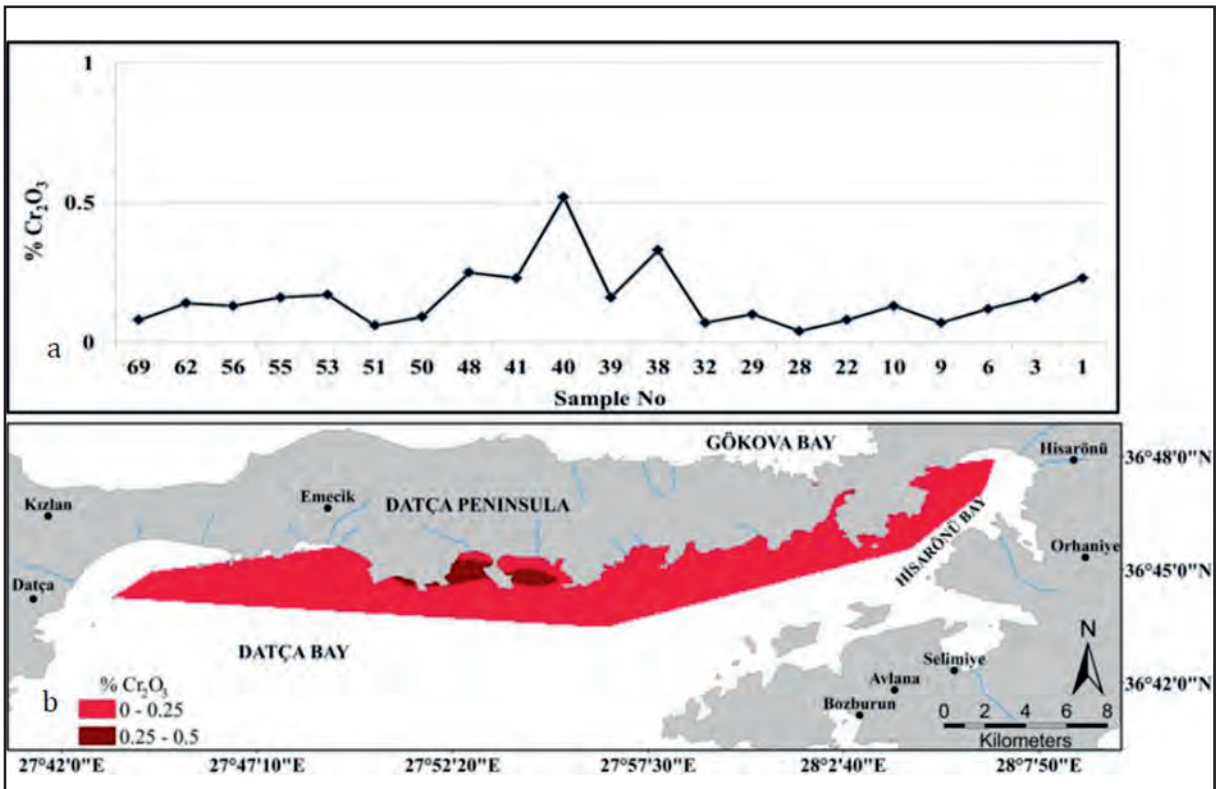


Figure 32- a) Cr_2O_3 amounts and b) Cr_2O_3 spatial distribution in surface sediments in Datça-Hisarönü Bays.

Table 3- Correlation matrix for geochemical data, sand, clay and total heavy mineral amounts in surface sediments in Datça-Hisarönü Bays.

| % | SiO ₂ | TiO ₂ | Al ₂ O ₃ | Fe ₂ O ₃ | MnO | MgO | CaO | Na ₂ O | K ₂ O | P ₂ O ₅ | Cr ₂ O ₃ | Sand | Clay | Total Heavy Mineral |
|--------------------------------|------------------|------------------|--------------------------------|--------------------------------|------|-------|-------|-------------------|------------------|-------------------------------|--------------------------------|-------|-------|---------------------|
| SiO ₂ | 1.00 | 0.87 | 0.86 | 0.80 | 0.65 | 0.30 | -0.95 | 0.42 | 0.68 | 0.37 | 0.17 | -0.78 | 0.78 | 0.35 |
| TiO ₂ | | 1.00 | 0.90 | 0.62 | 0.68 | -0.07 | -0.76 | 0.37 | 0.74 | 0.38 | -0.17 | -0.73 | 0.63 | 0.12 |
| Al ₂ O ₃ | | | 1.00 | 0.45 | 0.74 | -0.15 | -0.72 | 0.49 | 0.82 | 0.31 | -0.25 | -0.70 | 0.60 | 0.12 |
| Fe ₂ O ₃ | | | | 1.00 | 0.52 | 0.66 | -0.87 | 0.10 | 0.40 | 0.23 | 0.59 | -0.58 | 0.64 | 0.51 |
| MnO | | | | | 1.00 | 0.03 | -0.56 | 0.17 | 0.61 | 0.23 | 0.00 | -0.49 | 0.38 | 0.14 |
| MgO | | | | | | 1.00 | -0.48 | -0.12 | -0.18 | -0.17 | 0.91 | -0.16 | 0.31 | 0.46 |
| CaO | | | | | | | 1.00 | -0.41 | -0.60 | -0.30 | -0.34 | 0.79 | -0.81 | -0.40 |
| Na ₂ O | | | | | | | | 1.00 | 0.43 | 0.25 | -0.17 | -0.37 | 0.32 | 0.13 |
| K ₂ O | | | | | | | | | 1.00 | 0.27 | -0.19 | -0.63 | 0.55 | 0.16 |
| P ₂ O ₅ | | | | | | | | | | 1.00 | -0.20 | -0.36 | 0.35 | -0.02 |
| Cr ₂ O ₃ | | | | | | | | | | | 1.00 | -0.01 | 0.17 | 0.65 |
| Sand | | | | | | | | | | | | 1.00 | -0.94 | 0.03 |
| Clay | | | | | | | | | | | | | 1.00 | 0.04 |
| Total Heavy Mineral | | | | | | | | | | | | | | 1.00 |

uppermost section of the seismic profile used in this study very difficult.

According to radiocarbon age dating, the surface sediments of 30 cm thickness began to be deposited from 2694 to 14,700 years ago (BP) with sediment thicknesses from the Upper Pleistocene-Holocene boundary (11,700 BP) between 24 to 130 cm and from the Last Glacial Maximum (19,000 BP) from 39 to 212 cm in Datça and Hisarönü Bays. In other words, the scoop or surface sediment samples were generally Holocene in age. Regionally varying clastic supply, transportation and accumulation conditions are among important factors affecting deposition, ensuring sediment accumulation in different regions, at different times and thicknesses. However, it cannot be said that regional sediments are all current. The presence of different age sediments or older or relict sediments accumulating during the last glacial period and later may be interpreted.

In the study area of Datça and Hisarönü Bays with narrow and long morphology, the surface sediments covering the top 30 cm of the sea floor have grain size distribution from clay to gravel with relatively high proportions of clay and sand in sediments. Generally sand-rich areas at the coast become more clay-rich environments horizontally toward open water without clear transition. For example, regional increases in gravel and sand proportions not only occurred in high-energy shallow areas, but were found in areas close to the current shelf threshold parallel to the coast. These may be interpreted as relict deposits.

Near stream mouths in Datça Bay and in the interior section of Hisarönü Bay, the clay and silt proportions increase relatively, while increases in open water and shelf areas may indicate different sources or depositional environments. The current high clay, silt, sand and gravel proportions may indicate the presence of ancient stream channels and flood plains on the sea floor from the last glacial period. There are many factors affecting or controlling grain size of deposited clasts. Important factors controlling sediment types and distribution include varying regional climatic conditions and precipitation amounts, presence and abundance of transportation elements like rivers and ice/snow, distance from the coast and especially river mouths, morphologic properties of fluvial systems, topography of the coast and inland, underwater morphology and topography, and waves and currents along the shore and offshore (Reineck and Singh, 1975; Lewis, 1984; Leeder, 1988; Ergin et al., 1991; Ergin et al., 1998; Black and Oldman, 1999; Ergin and Bodur, 1999; Nichols, 1999; Çağatay et al., 2000; Hiscott et al., 2002; Boggs, 2006; Falco et al., 2015). Additionally there may be relict sediments carrying traces of previous deposition and last glacial/ interglacial variations on the modern seafloor (Emery 1968; Falco et al., 2015). Marine regression during the last glacial period before the Holocene (19,000 years BP and up to -120 m globally) and large-grained sediments deposited in relative shallow waters are covered by fine-grained sediments belonging to the Holocene transgression (Ergin et al., 1992; 1999; Aksu et al., 1999; Algan et al., 2007). Currently in

some shelf areas both large-grained (rich in sand and gravel) relicts and fine-grained (rich in clay and silt) current sediments are found together. In relatively high-energy coastal regions and river mouths, large-grained sediments like gravel and sand are deposited while in low-energy and open water areas silt and clay sediments commonly accumulate (Scruton, 1960; Kuehl et al., 1986; Jouanneau et al., 1989; Ergin et al., 1998; Owen, 2005). In short the study area does not just contain current sediments, but is covered by occasional relict sediments from the last glacial period. Another possibility affecting the grain size distribution in the study areas is the difference in rock types along the coast and inland in the region (Figure 3). South of Hisarönü Bay clastics, carbonates and volcanic are dominant, while ophiolites are more common in the north. While ophiolites have broad distribution in the east of Datça Peninsula, in the west clastics and carbonates are abundant. As fluvial systems in the area are short, high-energy with steep beds and seasonal-irregular flow, they may transport grains longer distances from the coast into open water.

The majority of sediments in the study area have total heavy mineral amounts below 2%, with relatively high values up to 13% common in Hisarönü Bay with heavy-mineral rich ophiolitic rocks along the coast. Between Datça and Hisarönü Bays and in the other two remaining coastal areas, total heavy minerals range from 5-10% which may be linked to previously-worked chrome mines inland and have been carried by streams. Beach sand rich in heavy minerals have been previously encountered along the south Mediterranean coasts (Ergin et al., 2013, Ergin, 2014). Generally, black sands containing varying proportions of chromite, magnetite and ilmenite forming heavy mineral placers are found on some sea coasts in the region and may even be worked as mines (Malik et al., 1987; Gujar et al., 2010).

In sediments accumulating distant from coasts, there are total heavy mineral amounts that are negligible which may indicate that sediments accumulating in the region are poor in heavy minerals and large grain sizes. Though there is generally no significant correlation between total heavy mineral amounts and grain size distribution in sediments, there is a relatively positive correlation between sediments with more than 2% total heavy mineral content and those rich in sand (Figure 21).

When the element geochemistry in study area sediments is compared with other geological reference data, the results indicate they are decomposition products of the rocks inland in the region (e.g., limestone, clay-mudstone, sandstone, peridotite, basalt, gabbro, serpentinite, radiolarite). Mean geochemistry for rocks forming the crust are given in works by Turekian and Wedepohl (1961), Gao et al. (1998), Klein (2005), Rudnick (2005) and Okunlola and Idowu (2012). Mean geochemical data for ophiolites near the study area indicated dunite and harzburgite in a doctoral study by Uysal (2007). These researchers' data and the values identified in this study are mainly in accordance, though amounts of elements like Fe, Mg and Cr are relatively high (Table 2). The presence of high concentrations of elements contained in ultramafic rocks like harzburgite and dunite support the values in this study.

5. Conclusion

Analyses completed on surface sediment samples collected with a scoop from the floors of Datça and Hisarönü Bays south of Datça Peninsula assessed the grain size distribution, geochemical components, total heavy mineral contents and seismic reflection profile in the region and the results are summarized below:

Datça Yarımadası güneyinde yer alan Datça ve Hisarönü Körfezlerinin tabanından kepçe ile alınan yüzeysel sediman örnekleri üzerinde gerçekleştirilen analizler ile bölgede elde edilen tane boyu dağılımları, jeokimyasal bileşimleri, toplam ağır mineral içerikleri ve sismik yansıma kesiti değerlendirilmiş ve elde edilen sonuçlar aşağıda özetlenmiştir:

The common sediment type in Datça and Hisarönü Bays is mud, with occasional contribution of sand and gravel. The age interval of sediment samples varies from 2694-14700 years (BP) and the sources are a variety of sedimentary and magmatic rocks outcropping along and behind the coasts indicating the Upper Pleistocene-Holocene period. The environmental characteristics developing linked to sea level changes during the last glacial and later period are very clear. Ancient coasts and shelf thresholds or edges are observed on the seismic profile at current water depths of -90/-120 m. Grain size distribution is significantly controlled by terrestrial and submarine morphology, fluvial drainage systems, geological

source differences on land and wave and current variations. Generally low total mineral amounts of 2%, but reaching up to 13%, indicate the presence and significance of the Marmaris Ophiolite. The majority of the chemical element composition and statistical interpretation of sediments is in accordance with mean crustal rock values, with Fe, Mg and Cr amounts indicating the broad distribution of partially serpentinized peridotites. Element distribution also may be correlated with regional variations of source rocks.

Acknowledgements

This study was obtained from the doctoral thesis of the first author conducted within the MTA General Directorate Datça Peninsula Southern Marine Area Geological and Geophysical Properties Research project (2013-37-14-02) and Ankara University Scientific Research Projects Datça and Hisarönü Bays Sedimentologic, Mineralogic and Geochemical Research and Submarine Traces and Effects of Ophiolitic Rocks project (AÜ-BAP project no. 13L4343008). For contributions to the project, we wish to thank Murat Cenk, Özkan Öksüz, Fatih Sertçetin, Erdem Onur Başer, Dilek Babacan, Ebru Beyribey, Ayşe Özkara, Banu Karabacak, Muhsine Kocakurt, Fatoş Kurtuluş, Nermin Kayabaşı, Güzin Avcı, Derya Öztürk, Eyüp Özbek, the crew of MTA Selen Research ship, colleagues in Ankara University River, Lake and Seas Geologic Research Center, the student group and for input into seismic profile interpretation Dr.Selim Özalp.

References

Aksu, A. E., Hiscott R. N., Yaşar D. 1999. Oscilating Quaternary water levels of the Marmara Sea and vigorous outflow into the Aegean Sea from the Marmara Sea-Black Sea drainage corridor. *Marine Geology* 153(1), 275-302.

Algan, O., Ergin, M., Keskin, Ş., Gökaşan, E., Alpar, A., Ongan, D., Kırıcı-Elmas, E. 2007. The sea-level changes during the late Pleistocene-Holocene on the southern shelves of the Black Sea. V. Yanko-Hombach, A. S. Gilbert, N.Panin, P.Dolukhanov, (Ed.). *The Black sea flood question: changes in coastline, climate, and human settlement*. Springer. Netherlands, 603-631.

Angelier, J., Dumont, J.K., Karamanderesi, H., Poisson, P., Şimşek, Ş., Uysal, S. 1981. Analysis of fault mechanisms and expansion of southwestern Anatolia since the late Miocene. *Tectonophysics* 75, T1–T9.

Barka, A.A., Reilinger, R. 1997. Active tectonics of the Mediterranean region: deduced from GPS, neotectonic and seismicity data. *Annali di Geofisica* XI. 587-610.

Black, K.P., Oldman, J.W. 1999. Wave mechanisms responsible for grain sorting and non-uniform ripple distribution across two moderate-energy, sandy continental shelves *Marine Geology* 162, 121–132.

Boggs, S. Jr. 2006. *Principles of Sedimanology and Stratigraphy* (Fourth Edition). Pearson Prentice Hall, 655 p. Brunn, J.H., Dumont, J.F., De Graciansky, P.C., Gutnic, M., Juteau, T., Marcoux, J., Monod, O., Poisson, A. 1971. Outline of the geology of the Western Taurids. Campwell, A.S. (Ed.), *Geology and History of Turkey*. Petroleum Exploration Society of Libya, 225- 255.

Çağatay M.N., Görür, N., Algan, O., Eastoe, C., Tchapylyga, A., Ongan, D., Kuhn, T., Kuşçu İ. 2000. Late Glacial–Holocene palaeoceanography of the Sea of Marmara: timing of connections with the Mediterranean and the Black Seas, *Marine Geology*, Volume 167, Issues 3–4, 191–206.

Dewey, F.J., Şengör, A.M.C. 1979. Aegean and surrounding regions: complex multiplate and continuum tectonics in a convergent zone. *Geological Society of America Bulletin* 90, 84- 92.

Dirik K., Türkmenoğlu A., Tuna N., Dirican M. 2003. Datça Yarımadası'nın neotektoniği, jeomorfolojisi ve bunların eski medeniyetlerin yerleşimi ve gelişimi üzerindeki etkisi proje raporu. Orta Doğu Teknik Üniversitesi AFP-00-07-03-13 No'lu Proje, 72 s., Ankara (unpublished).

Emery, K.O. 1968. Relict sediments on continental shelves of the world. *American Association of Petroleum Geologists Bulletin* 52, 445–464.

Ergin, M. 2014. Samandağ (Hatay, GD Turkey) deniz sahillerinde ağır mineral plaser araştırmaları: sedimentolojik, mineralojik ve jeokimyasal çalışmalar, TÜBİTAK ÇAYDAG 112Y146 nolu proje, Ankara (unpublished).

- Ergin, M., Bodur, M.N., Ediger, V. 1991. Distribution of surficial shelf sediments in the northeastern and southwestern parts of the Sea of Marmara: Strait and canyon regimes of the Dardanelles and Bosphorus. *Marine Geology* 96 (3/4), 313-340.
- Ergin, M., Okyar, M., Timur, K. 1992. Seismic stratigraphy and late Quaternary sediments in inner and mid-shelf areas of eastern Mersin Bay, Northeastern Mediterranean Sea. *Marine Geology* 104, 73-91.
- Ergin, M., Kazan, B., Eryılmaz, M., Yücesoy Eryılmaz, F., Okyar, M. 1998. Hydrographic, deltaic and benthogenic controls of sediment dispersal in the Gulf of İskenderun, SE-Turkey (E.-Mediterranean). *Estuarine Coastal and Shelf Science* 46,4, 493-502.
- Ergin, M., Bodur, M.N. 1999. Silt/clay fractionation in surficial Marmara sediments: implication for water movement and sediment transport paths in a semi-enclosed and two-layered flow system (northeastern Mediterranean Sea). *Geo-Marine Letters* 18, 225-233.
- Ergin, M., Karakaş, Z.S., Sözeri, K., Eser-Doğdu, B., Kadioğlu, Y.K., Yiğit-Faridfathi, F. 2013. Morphological, drainage and eolian controls on the microtidal Patara Beach Sediments (Eastern Mediterranean): Textural, geochemical and mineralogical investigations. *Quaternary International* 302, 135-153.
- Ersoy, Ş. 1991. Datça (Muğla) Yarımadasının stratigrafisi ve tektoniği. *Türkiye Jeoloji Bülteni C 34*, 1-14.
- Fairbanks, R.G. 1989. A 17,000-year glacio-eustatic sea-level record: influence of glacial melting rates on the Younger Dryas event and deep-ocean circulation, *Nature* 342, 637-642.
- Falco, G., Budillon, F., Conforti, A., Bitetto, M., Martino, G., Innangi, S., Simeone, S., Tonielli, R. 2015. Sorted bedforms over transgressive deposits along the continental shelf of western Sardinia (Mediterranean Sea) *Marine Geology* 359, 75-88.
- Folk, R.L. 1980. *Petrology of Sedimentary Rocks*. Hemphill Publishing Company, 184 p.
- Gao S., Luo T.-C., Zhang B.R., Zhang H.-F., Han Y.-W., Hu Y.K., Zhao Z.D. 1998. Chemical composition of the continental crust as revealed by studies in east China. *Geochimica Cosmochimica Acta* 62, 1959-1975.
- Görür, N., Şengör, A.M.C., Sakiç, M., Tüysüz, O., Akkök, R., Yiğitbaş, E., Oktay, F.Y., Barka, A., Sarıca, N., Ecevitoglu, B., Demirbaş, E., Ersoy, Ş., Algan, O., Güneysu, C., Aykol, A. 1995. Rift formation in the Gökova region, southwest Anatolia: implications for the opening of the Aegean Sea. *Geological Magazine* 132, 637-650.
- Grosz, A.E., Berquist Jr., C.R., Fisher, C.T. 1990. A procedure for assessing heavy mineral resources potential of continental shelf sediments. in: Berquist Jr., C.R. (Ed.), *Heavy-mineral studies-Virginia inner continental shelf*, Virginia Div. Min. Res. Publ., 103, 13-30.
- Gujar, A.R., Ambre, N. V. 2010. Ilmenite, magnetite and chromite beach placers from south maharashtra, central west coast of India. *Resource Geology*, Volume 60, Issue 1, 71-86.
- Hamann, Y., Ehrmann, W., Schmiedl, G., Krüger, S., Stuut, J.-B., Kuhnt, T. 2008. Sedimentation processes in the Eastern Mediterranean Sea during the Late Glacial and Holocene revealed by end-member modelling of the terrigenous fraction in marine sediments, *Marine Geology* 248, 97-114.
- HGK (Harita Genel Komutanlığı). 1998. 1/100.000 ölçekli O18-O19 paftaları, MSB Harita Genel Komutanlığı, Ankara.
- HGK (Harita Genel Komutanlığı). 1999. 1/100.000 ölçekli O20 paftası, MSB Harita Genel Komutanlığı, Ankara.
- HGK (Harita Genel Komutanlığı). <http://www.hgk.msb.gov.tr/sayisal-uygulamalar>. 05 Temmuz 2015.
- Hiscott, R.N., Aksu A.E., Yaşar D., Kaminski M.A., Mudie P.J., Kostylev V.E., MacDonald J.C., İşler F.I., Lord A.R. 2002. Deltas south of the Bosphorus Strait record persistent Black Sea outflow to the Marmara Sea since 10 ka. *Marine Geology* 190 (1-2), 95-118.
- IUGS (International Union of Geological Sciences), ICS (International Commission on Stratigraphy), <http://www.stratigraphy.org/index.php/ics-chart-timescale>. 25 Nisan 2016.
- Jackson, J.A., McKenzie, D. 1984. Active tectonics of the Alpine-Himalayan belt between western Turkey and Pakistan. *Geophysical Journal of the Royal Astronomical Society* 77, 185-264.

- Jouanneau, J.M., Weber, O., Latouche, C., Vernet, J.P., Dominik, J. 1989. Erosion, non-deposition and sedimentary processes through a sedimentological and radioisotopic study of surficial deposits from the Ouest- Girond vasiere (Bay of Biscay). *Continental Shelf Research* 9, 325– 342.
- Kaşer, N. 2010. Hisarönü Körfezi'ndeki Deniz Seviyesi Değişimi, Sedimentasyonu ve Bölgedeki Eski Çağ Kıyı Yerleşimleri Üzerindeki Etkileri. Doktora Tezi, Dokuz Eylül Üniversitesi Fen Bilimleri Enstitüsü, 135 s (unpublished).
- Klein E.M. 2005. Geochemistry of the igneous oceanic crust, Rudnick, R.L. (Ed.). *The Crust- Treatise on Geochemistry Volume 3*. Elsevier Science, 433-463.
- Kuehl, S.A., DeMaster, D.J., Nittrouer, C.A. 1986. Nature of sediment accumulation on the Amazon continental shelf. *Continental Shelf Research* 6, 209-225.
- Kurt, H., Demirbağ, E., Kuşçu, İ. 1999. Investigation of the submarine active tectonism in the Gulf Gökova, Southwest Anatolia-Southeast Aegean Sea, by Multi-Channel Seismic Reflection Data, *Tectonophysics* 305, 477-496.
- Leeder, M.R. 1988. Recent developments in Carboniferous geology: a critical review with implications for the British Isles and N.W. Europe, *Proceedings of the Geologists' Association Volume 99, Issue 2*, 73–100. Lewis, D.W. 1984. *Practical Sedimentology*, Hutchinson Ross, Stroudsburg, Pennsylvania, 227.
- Malik, T.K., Vasudevan V., Abyverghese P., Machado T. 1987. The black sand placer deposits of Kerala beach south west India. *Marine Geology* 77, 129-150.
- Masclé, J., Martin, L. 1990. Shallow structure and recent evolution of the Aegean Sea: A synthesis based continuous reflection profiles. *Marine Geology* 94 (4), 271– 299.
- McKenzie, D. 1972. Active tectonics of the Mediterranean region. *Geophys. J. R. Astron. Soc.* 30, 109– 185. McKenzie, D., 1978. Active tectonics of the Alpine Himalayan belt: the Aegean Sea and surrounding regions (tectonics of the Aegean region). *Geophys. J. R. Astron. Soc. Lond.* 55 (1), 254–271.
- Mitchum R. M. Jr., Vail P. R., Thompson S. 1977. Application of seismic reflection configuration to stratigraphic interpretation, *Seismic Stratigraphy- Applications to Hydrocarbon Exploration*. American Association of Petroleum Geologists (AAPG). Special Volume M 26, 53-62.
- Müller, G. 1967. *Methods in Sedimentary Petrology*, Schweizerbart, Stuttgart, 283 p.
- National Observatory of Athens, Aegean Tectonics, (b.t.) <http://www.gein.noa.gr/services/kythira-linkstectonics.gif>. 06 Nisan 2008.
- Nichols, G. 1999. *Sedimentology and Stratigraphy*, Second Edition, Wiley-Blackwell, 432 p.
- Okunlola O.A., Idowu O. 2012. The geochemistry of claystone-shale deposits from the Maastrichtian Patti formation, Southern Bida basin, *Earth Sciences Research Journal*, Vol. 16, No. 2, 57 – 67.
- Owen, R.B. 2005. Modern fine-grained sedimentation-spatial variability and environmental controls on an inner pericontinental shelf, Hong Kong, *Marine Geology* 214 () 1– 26.
- Posamentier, H. W., Jervy M. T., Vail, P. R. 1988. Eustatic controls on clastic deposition I - conceptual framework. Wilgus C. K., Hastings B. S., St. C. Kendall C. G., Posamentier, H. W., Ross C. A., Van Wagoner J. C. (Ed.). *Society of Economic Paleontologists and Mineralogists (SEPM)*, Special Publication vol. 42, 110–124.
- Reineck, H.E., Singh, I.B. 1975. *Depositional Sedimentary Environments: With Reference to Terrigenous Clastics*, Springer Study Edition, 439 p.
- Rudnick, R.L., Gao, S. 2005. Composition of the continental crust. Rudnick, R.L. (Ed.). *The Crust- Treatise on Geochemistry Volume 3*. Elsevier Science, 1-64.
- Scruton, P.C. 1960. Delta Building and the Deltaic Sequence, SP 21: *Recent Sediments, Northwest Gulf of Mexico*, AAPG Special Volumes, 53-62.
- Şenel, M., Bilgin, Z.R. 1997. Türkiye Jeoloji Haritaları, 1/100.000 ölçekli Marmaris O-18, O-19, O-20 Paftaları, Maden Tetkik ve Arama Genel Müdürlüğü, Ankara.
- Şengör, A. M. C., Yılmaz, Y. 1981. Tethyan evolution of Turkey: a plate tectonic approach, *Tectonophysics* 75, 181-241.

- SHOD. 1970. TR 311 Akdeniz, Ege Denizi, Türkiye Bodrum Geçidi-Marmaris Seyir Haritası. Deniz Kuvvetleri Komutanlığı Seyir, Hidrografi ve Oşinografi Dairesi Başkanlığı, İstanbul.
- Siddall, M., Rohling, E.J., Almogi-Labin, A., Hemleben, Ch., Meischner, D., Schmelzer, I. Smeed, D. A. 2003. Sea-level fluctuations during the last glacial cycle. *Nature* 423, 853-858.
- Taşlıgil, N. 2008. Datça-Bozburun özel çevre koruma bölgesi ve turizm, *Ege Coğrafya Dergisi* 17/1-2, 73-83.
- Taymaz, T., Jackson, J.A., McKenzie, D. 1991. Active tectonics of the north and central Aegean Sea. *Geophysical Journal International* 106, 433-90.
- Toucanne S., Jouet G., Ducassou E., Bassetti M.A., Dennielou B., Minto'o C.A.M., Lahmi M., Touyet N., Charlier K., Lericolais G., Mulder T. 2012. A 130000-year record of Levantine intermediate water flow variability in the Corsica Trough, western Mediterranean Sea, *Quaternary Science Reviews* 33, 55-73.
- Turekian K.K., Wedepohl K.H. 1961, Distribution of the elements in some major units of the earth's crust, *Geological Society of America Bulletin* 72, 175-192.
- Uluğ, A. 2005, Hisarönü ve Gökova Körfezleri (Güneydoğu Ege Denizi) Geç kuvarterner Evrimi: Tektonizma, Delta Sedimanasyonu ve Deniz Seviyesi Değişimi, Proje No:197Y052 (YDABÇAG-607/G), TÜBİTAK Yer Deniz ve Atmosfer Araştırma Grubu Proje Raporu, 24 s., Ankara (Yayınlanmamış).
- Uluğ, A., Duman, M., Ersoy, Ş., Özel, E., Avcı, M. 2005. Late Quaternary sea-level change, sedimentation and neotectonics of the Gulf of Gökova: Southeastern Aegean Sea, *Marine Geology* 221, 381-395.
- Uysal, İ. 2007. Muğla (GB-Turkey) Üst manto Peridotitleri ve Ofiyolitik Kromititleri'nin Petrolojileri: Mineral Kimyası, Ana Oksit-İz Element-NTE-PGE Jeokimyası, PGE Mineralojisi ve Rs-Os İzotop Sistematiği. Doktora Tezi, KTÜ Fen Bil.Ens., 470 s. Trabzon (unpublished).



Bulletin of the Mineral Research and Exploration

<http://bulletin.mta.gov.tr>



MAASTRICHTIAN - SELANDIAN PLANKTONIC FORAMINIFERA BIOSTRATIGRAPHY AND PALAEOECOLOGICAL INTERPRETATION OF AKVEREN FORMATION IN BARTIN AREA (WESTERN BLACK SEA, TURKEY)

Caner KAYA ÖZER^{a*}

^a Bozok University, Engineering and Architecture Faculty, Department of Geological Engineering, Atatürk Road, 66090, Yozgat, Turkey

Research Article

Keywords:

Maastrichtian, Paleocene, paleoecology, planktonic foraminifera

ABSTRACT

The changes in planktonic foraminifera assemblages were studied in two sections composed of clayey limestone, limestone, claystone and marl in the Akveren Formation in the Bartın Province. *Pseudoguembelina palpebra*, *Racemiguembelina fructifera*, *Abathomphalus mayaroensis* and *Pseudoguembelina hariaensis* biozones in the Maastrichtian and *Parvularugoglobigerina eugubina*, *Glomobanomalina compressa*/*Praemurica uncinata*, *Praemurica uncinata* and *Morozovella angulata* biozones in the Paleocene were determined using planktonic genus and species identified in these sections. Paleocological interpretations in this study were completed by using the relative abundances of paleoecological species identified in these biozones. The abundance of *Rugoglobigerina* spp., *Heterohelix globulosa*, *Pseudoguembelina* spp., species that tolerated changes in sea water temperature and nutrition, increased in the Maastrichtian. In the uppermost Maastrichtian, high abundance of *Racemiguembelina fructifera*, *Heterohelix globulosa* and *Rugoglobigerina* spp. show oligotrophic and warmer environmental conditions in this study. The abundance of globotruncanids are unstable due to environmental changes. The new species have smaller sizes and globular chambers emerged in the Paleocene. High abundance of *Subbotina triloculinoides* and *Parasubbotina pseudobulloides* show mesotrophic and cooler environmental conditions in the Danian. Morozovellid taxa started to dominate in the Selandian and environmental conditions changed from mesotrophic to oligotrophic.

Received: 08.01.2016

Accepted: 27.03.2016

1. Introduction

The temperature in the Late Cretaceous from Cenomanian to Maastrichtian was higher than today as determined by stable isotope studies and global climate models (Huber et al., 1995, 2002; Clarke and Jenkyns, 1999; DeConto et al., 1999; Wilson and Norris, 2001; Norris et al., 2002; Wilson et al., 2002; Bice et al., 2006; Forster et al., 2007; Bornemann et al., 2008; Friedrich et al., 2008; Shirazi et al., 2013; Kaya-Özer, 2014).

The Cretaceous climate started to cool in the Campanian and Maastrichtian (Huber et al., 1995, 2002). While the decrease reached a maximum level in the Maastrichtian (Clarke and Jenkyns, 1999; Huber et al., 2002; Miller et al., 2005), a sudden increase in temperature occurred at the end of this period (Li and Keller, 1998a,b) and surface water temperatures increased by 2-3 °C between ~65.45 and 65.1 Ma before the Cretaceous–Paleogene boundary (K–Pg) (Li and Keller 1998a,b; Barrera and Savin,

1999). Global cooling continued in the last 100 kyr of the Maastrichtian and sea surface water temperatures decreased (Thibault and Gardin, 2007).

Climatic changes caused variations in the biota of planktonic foraminifera together with most fauna (Abramovich and Keller, 2003). An important biotic event that occurred in this period is a decrease in planktonic foraminifera species richness at about 66 Ma in the South Atlantic and Tethys basins, coincident with the end-Maastrichtian global warming (Li and Keller, 1998a, b). This was also proven by oxygen isotope studies carried out on deep-sea drillings in the Atlantic, Pacific and Indian Oceans (Zachos et al., 1985, 1989; D'Hondt and Lindinger, 1994; Corfield and Norris, 1996; Barrera et al., 1997; Li and Keller, 1998a,b; Abramovich and Keller, 2003; Friedrich et al., 2012) and in the Boreal Realm (Friedrich et al., 2008).

Keller et al. (2002) noticed the faunal decline crested at the K/Pg boundary with the mass extinction

* Corresponding author: Caner Kaya Özer, c.kayaozer@gmail.com
<http://dx.doi.org/10.19111/bmre.22772>

of tropical-subtropical planktonic foraminiferal species whereas the cosmopolitan and ecologically generalist species survived into the Danian. At first, tropical species with complex, large and ornamental shells (*globotruncanids*, *racemiguembelinids*, *planoglobulinids*) and then smaller subtropical species (*pseudotextularids*, *rugoglobigerinids*) were affected during the extinction at the K/Pg boundary (Keller, 1996)

There are lots of paleoecological studies based on stable oxygen and carbon isotopes and changes in planktonic foraminifera assemblages in Maastrichtian and Paleocene sediments which were collected from deep sea drillings and several locations worldwide (Huber et al., 1995; Li and Keller, 1998a). The aim of this study is to identify planktonic foraminifera biostratigraphy in the Akveren Formation and determine the paleoecological conditions based on changes in planktonic foraminifera assemblages between Maastrichtian and lower Paleocene period using samples from Bartın Province (Western Black Sea) in Turkey. The biostratigraphic and paleoenvironmental interpretations of the composition of the planktonic foraminifers were also discussed.

2. Geological Setting and Previous Studies

The study area is in the Western Black Sea Basin in the Pontides, one of the tectonic plates in Turkey, which is a part of the Alpine Belt. There are several geological studies about Bartın province and its surrounding. The first studies in the region were about its petroleum potential (Badgley, 1959; Saner, 1981; Gedik and Korkmaz, 1984; Robinson et al., 1996; Görür and Tüysüz, 1997). There are also several studies investigating its geological and tectonic characteristics. The geological map of Cide-Kurucaşile area was drawn by Akyol et al. (1974). Geological structure, tectonic, petrographical and petrological characteristics of the region from Jurassic to Quaternary were investigated by Saner (1980), Gedik et al. (1983), Barka et al. (1983), Aydın et al. (1986), Derman et al. (1995), Derman (2002) and Tüysüz et al. (2012).

Şengör (1982) suggested that the Western Black Sea basin was opened as a back arc basin in relation to closure of the Tethys Ocean. Görür (1988) mentioned the Western Black Sea Basin as related to post rift thermal subsidence (Görür, 1988). Özçelik and Çaptuğ (1990) examined the tectonic characteristics

of the region and emphasized that sedimentation was continuous in upper Cretaceous/Tertiary units. In addition, they pointed out that the Akveren Formation is of Maastrichtian-early Paleocene age, comprises marls, calciturbiditic limestones, micrites and shale.

Akman (1992) studied the stratigraphic units between Lutetian and Permian, and named the various sediments, volcano-sedimentary, and volcanic rocks that outcrop in the region. Tüysüz (1993) investigated the Pontides in detail, classified its tectonic sections and suggested a geological evolution model. Sunal and Tüysüz (2001) studied the stratigraphy and tectonics of the region. Tüysüz (2002) stated that deposition was accompanied by strong volcanism in the Cenomanian-Maastrichtian period and this volcanism that was common on the Black Sea coast began at the end of the Campanian and ended in the Maastrichtian.

Paleontological studies completed in the study area and its surrounding are important. Dizer and Meriç (1981) defined the planktonic foraminifera zones from the upper Cretaceous to Paleocene in Gebze, Akçakoca, Devrek and Bartın areas in Northwest Anatolia. They stated that the sea had a deep sea characteristic in Bartın in the upper Cretaceous and Paleocene. Varol (1983) discussed the late Cretaceous-Paleocene calcareous nanofossils from the Kokaksu Section. Sirel (1991) defined a new species (*Cideina* n.gen.) in his study in the Cide region. Özkan-Altınar and Özcan (1999) examined the benthic and planktonic foraminifera in the units from late Cretaceous to early Tertiary in the forearc basins located in north, northwest and central Anatolia.

Şener (2007) identified *Neotrocholoid* and *Orbitolinoid* species that were benthic foraminifera in the İnaltı Formation outcropping in Amasra. Three new *Neotrocholoid* species (*Neotrocholoid amasraensis*, *N. sireli*, *N. bartinensis*) were identified, the age of the formation in the study area was defined as Cimmerian-Aptian based on these identified species.

3. Stratigraphy

The oldest unit in the area consists of Amasra Group rocks, belonging to the Yemişliçay Upper Group (Tüysüz et al., 2004). The Amasra Group, deposited in the late Santonian and Campanian, begins with a marine succession that overlaps the older units (Tüysüz et al., 2004). At the beginning of this period, pelagic limestones were deposited and then volcanics

and pyroclastics (Kazpınar Formation) developed (Tüysüz et al., 2004).

3.1. Kazpınar Formation

The name of the formation was first used by Tokay (1954/1955). This unit was studied as the Yemişliçay formation (Ketin and Gümüş, 1963), Kuruçayı formation (Akyol et al., 1974), Lüneran formation (Kaya et al., 1982/1983), Cambu formation (Şahintürk and Özçelik, 1983; Tüysüz et al., 1997) and Dinlence formation (Akman, 1992) in previous studies. Kazpınar formation widely consists of andesitic lavas, pyroclastics, volcanic sandstones, siltstones, marls and lava blocks (Tüysüz et al., 2004).

Kazpınar formation indicates volcanic activity in the deep sea environment (Akman, 1992). Turbiditic units were deposited when the volcanism lost its effect (Akman, 1992). The age of the formation was defined as Campanian according to its stratigraphic position (Tüysüz et al., 2004). In another study, it was dated as early Campanian due to genus and species of planktonic foraminifera and nanofossils that were identified in carbonate levels in this formation (Kaya-Özer, 2009).

3.2. Akveren Formation

Akveren Formation overlaps the Yemişliçay group rocks consisting of volcanic and volcanoclastic rocks (Gedik et al., 2005). The Akveren Formation was first described by Gayle (1959) as layers of clayey limestone then formally defined by Ketin and Gümüş (1963) as widespread along the western Black Sea coast.

Akveren Formation was the subject of several studies. Dobrucalı (1985) and Sarıca (1993) examined planktonic foraminifera fauna and stratigraphic position of the Akveren Formation. Kırıcı (1998) stated that the Akveren Formation includes a rich foraminifera assemblage that consists of planktonic foraminifera, small benthic foraminifera and large benthic foraminifera in Maastrichtian and dated it as late Cretaceous-Paleocene. In addition, she pointed out that it was dominated by deepening intensity flows and represented a calciturbiditic succession that reflected deposition in the open shelf environment.

Aydın (2005) studied nanoplankton biostratigraphy in detail in the units of Cretaceous-Paleogene age including the Akveren Formation northwest of İzmit. In this study, the Cretaceous-Tertiary

boundary was determined to be continuous. Güray (2006) determined the Campanian-Maastrichtian boundary by using planktonic foraminifera. While the Campanian-Maastrichtian boundary was determined as the boundary of zones of *Pseudotextularia elegans* and *Planoglobulina acervuloides* in her study, the Cretaceous/Tertiary boundary was determined by the extinction of upper Cretaceous fossils.

The Akveren Formation is initially characterized at the base by white-gray, medium to thickly bedded sandstones and greenish-gray marls that change to white-cream, thinly bedded micritic limestones and clayey limestones in the upper levels. The formation ends with white-beige, locally siliceous, thin to medium bedded limestones, claystones, and marl alternations and gradually passes into the Atbaşı Formation consisting of calcareous mudstones (Akman, 1992, Figure 1).

Thickness of the Akveren Formation was indicated as 390 m by Akyol et al. (1974) and 590 m by Akman (1992). The age of the formation was indicated as Campanian-Maastrichtian by Akman (1992), Maastrichtian by Ketin and Gümüş (1963) and Maastrichtian-Paleocene by Gedik and Korkmaz (1984). Kaya-Özer (2009), Kaya-Özer and Toker (2012) pointed out that the age of the Akveren Formation age is Campanian-Selandian based on planktonic foraminifera and nannofossil biostratigraphy.

3.3. Atbaşı Formation

The Atbaşı formation was first named by Ketin and Gümüş (1963) and different names have been used in some studies (Akyol et al., 1974; Akman, 1992). The unit consists of green and purple thin bedded, conchoidal fracture, fossiliferous siltstones, claystones and marls. Thin to medium bedded, green, greenish, gray sandstone layers and rarely white colored, thin bedded limestones are found in the unit. According to Gedik and Korkmaz (1984), its thickness is 537 m Akyol et al. (1974) named this unit the Akgüney Formation and indicated its thickness as 260 m. The age of the unit was determined as Paleocene-Early Eocene (Ketin and Gümüş, 1963), Paleocene (Akyol et al., 1974), early Eocene (Gedik and Korkmaz, 1984) and Paleocene (Tüysüz et al., 1997), in various studies. Kaya-Özer and Çakır (2015) pointed out the age of the formation was Selandian-Ypresian according to detailed planktonic foraminifera biostratigraphy.

4. Material and Method

This study is based on 37 samples from two sections in the Akveren Formation. The study area lies in the Bartın area on the Black Sea coast and is shown on the 1:25000 Zonguldak E28-c2 map (Figure 1).

The samples of planktonic foraminifera were disaggregated in 10% concentrated hydrogen peroxide soaked with water and washed through >63 µm sieve until clean foraminiferal residues were recovered. The washed samples were dried at room temperature. From each Cretaceous sample, about 300 planktonic foraminifera were picked from random sample splits (Abramovich and Keller, 2003). All Paleocene planktonic foraminifera species were picked from the samples, because they are rare. The planktonic foraminifera species were identified under a stereo

microscope (Leica zoom 2000). The important species were photographed with a scanning electron microscope (SEM-JEOL JSM-6490LV)) at the Turkish Petroleum Company (TPAO) and are presented in the plate.

Mesozoic taxonomic concepts for planktonic foraminifera identification were applied in this study according to Robaszynski et al. (1984), Caron (1985), Robaszynski and Caron (1995), Huber et al. (2008), Petrizzo et al. (2011). Cenozoic taxonomic concepts for planktonic foraminifera identification were used according to Toumarkine and Luterbacher (1985), Berggren and Norris (1997) and Olsson et al. (1999).

The percentages of planktonic foraminifera species were calculated for paleoecological interpretation and these percentages were counted according to the

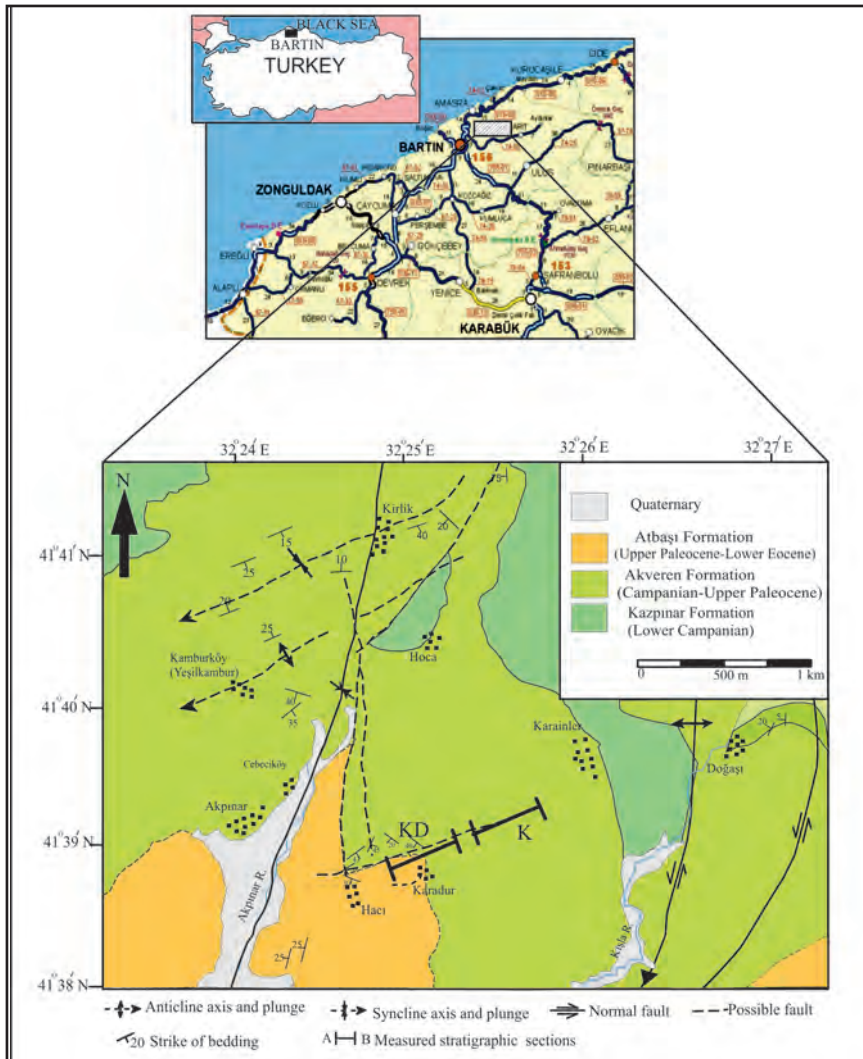


Figure 1- Location and geological map of the study area with locations of the measured sections (modified from Akman, 1992).

relative abundance of each species in the samples. The percentage abundances (%) of planktonic foraminifera are listed in table 1 and table 2.

5. Results

5.1. Stratigraphic Section

The detailed planktonic foraminiferal biostratigraphy were studied in the Karainler and Karadur areas around Bartın (Figure 1).

Karainler stratigraphic section

Measured in west of Karainler Village in the Akveren Formation, the Karainler section begins

at the coordinates 41°39'25"- 32°25'80" and ends at 41°39'15"- 32°25'50". It consists of an alternation of pink, cream-colored, thin to medium bedded clayey limestones, cream-colored, thin-bedded claystones and gray conchoidal marl at the base of the Akveren Formation (Figure 2). It passes into an alternation of gray, beige, thin to medium bedded, clayey limestones, white, thin bedded claystones and gray, green laminated marl in the upper level of the Akveren Formation. The section ends with an alternation of gray marl and thin to medium bedded limestones that include hard, partly silicified and echinoid fossils (Figure 2, 3). Total thickness of the section measured in the Akveren Formation is 140 m and the sampling intervals varied every 3-10 m in this section (Figure 3).

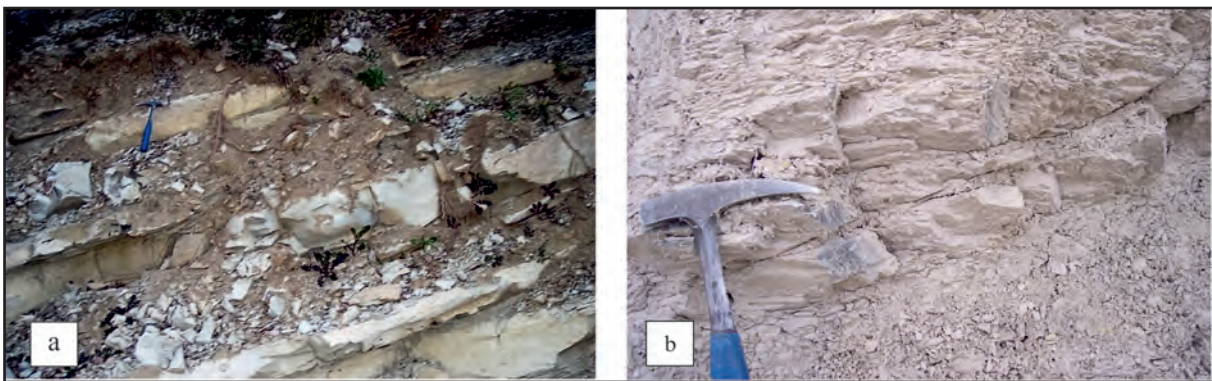


Figure 2- Field photographs of the sedimentary rocks of the Karainler stratigraphic section. (a). Alternating silicified limestones and marl in the upper Maastrichtian of the Akveren Formation, (b). interbedded gray green marls and cream clayey limestone in the lower Maastrichtian of the Akveren Formation.

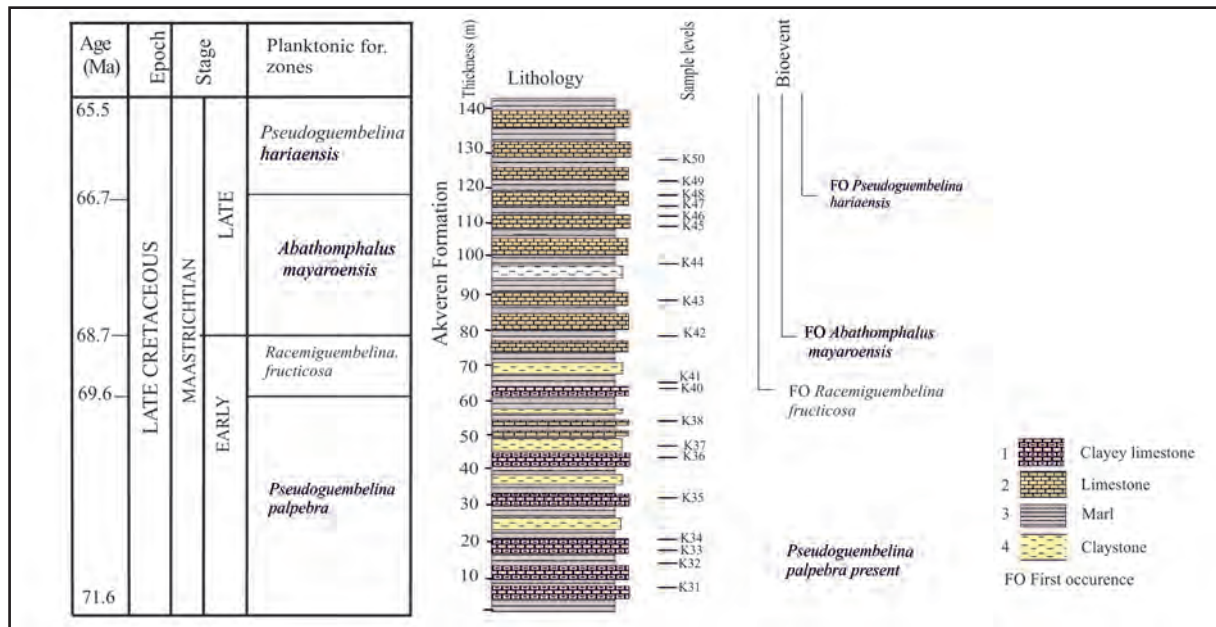


Figure 3- Karainler measured stratigraphic section showing lithostratigraphy, biostratigraphy and main planktonic foraminiferal bioevents from the Bartın area.

Karadur stratigraphic section

Measured around Karadur Village, the Karadur section begins at the coordinates 41°39'15"- 32°25'45" and ends at 41°38'80"- 32°24'95". It consists of an alternation of cream-colored, thin to medium bedded limestones, claystones and green, beige marl at the base in the Akveren Formation (Figure 4). The section continues as an alternation of partly silicified, thin to medium bedded limestones and laminated marl in the upper level of the Akveren Formation (Figure 4), it gradually passes into the Atbaşı Formation consisting of purple, green, thin to medium bedded conchoidal fracture marl in the uppermost levels (Figure 5). Total thickness of Karadur section is 23 m and the sampling intervals varied from 1-5 m in this section (Figure 5).

In the study area, the K/Pg boundary is located within the Akveren Formation. However, during the

sampling process, this boundary was missed and could not be identified.

5.2. Biostratigraphy

The standard upper Cretaceous biozonation scheme of Huber et al. (2008) and standard Paleocene biozonation scheme of Wade et al. (2011) were applied to the planktonic foraminifera data (Figure 3, 5). The important planktonic foraminifera species were shown in the plate I, II.

5.2.1. Maastrichtian Planktonic Foraminifera Zones

Pseudoguembelina palpebra Partial-range Zone: Biostratigraphic interval from the first occurrence (FO) of *Pseudoguembelina palpebra* to the FO of *Racemiguembelina fructicosa*.

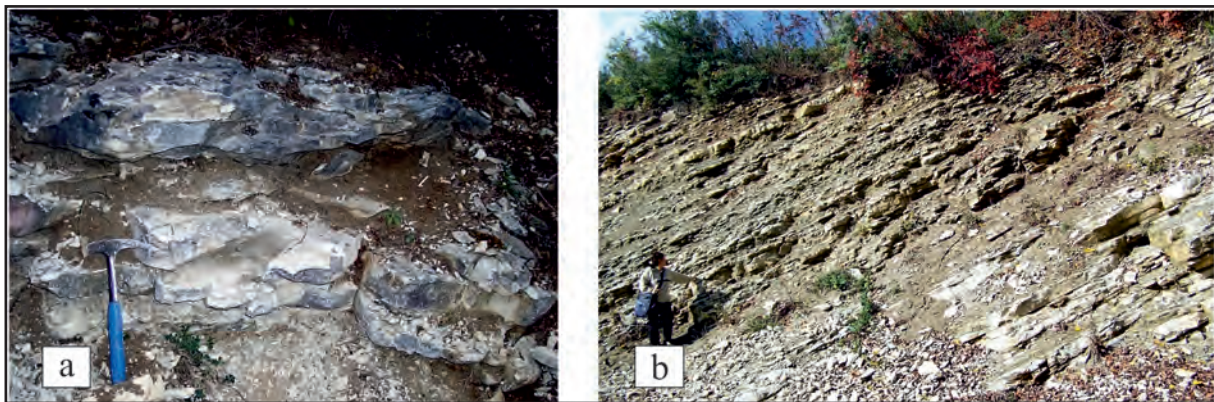


Figure 4- Field photographs of the sedimentary rocks of the Karadur stratigraphic section. (a). interbedded graygreen marls and cream silicified micritic limestones in the upper Maastrichtian of the Akveren Formation, (b). field view of Karadur stratigraphic section.

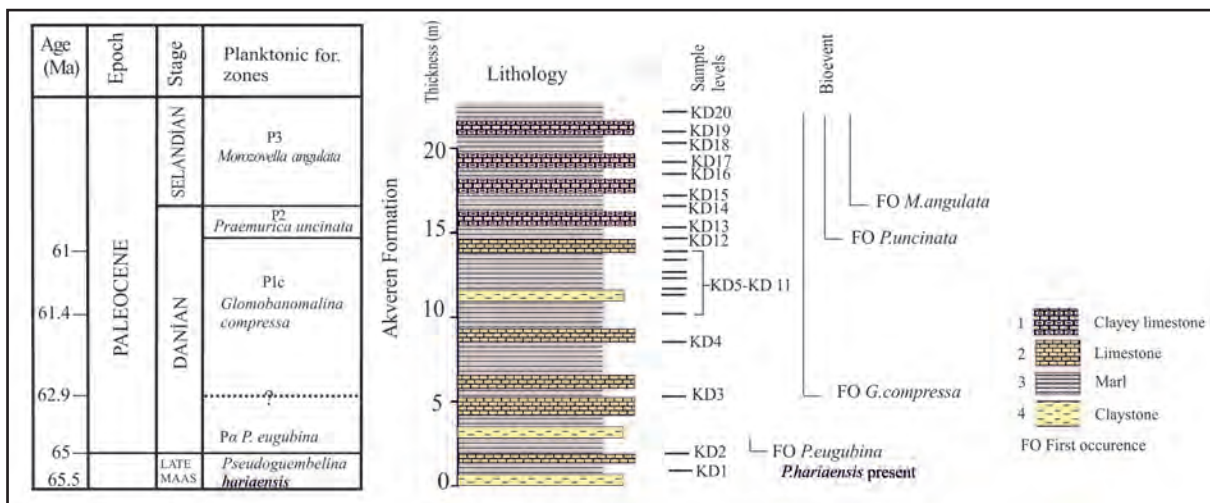


Figure 5- Karadur measured stratigraphic section showing lithostratigraphy, biostratigraphy and main planktonic foraminiferal bioevents from the Bartın area.

Author: Huber et al., 2008

Age: late Campanian-early Maastrichtian (Base 71.64 Ma, top 69.62 Ma; Huber et al. 2008).

The dominant planktonic foraminiferal species recorded in this zone include *Contusotruncana contusa*, *C. fornicata*, *C. patelliformis*, *C. plicata*, *C. plummerea*, *C. walfischensis*, *Gansserina gansseri*, *Globigerinelloides ultramicrus*, *Globotruncana arca*, *G. aegyptiaca*, *G. bulloides*, *G. falsostuarti*, *G. insignis*, *G. linneiana*, *G. mariei*, *Globotruncanella havanensis*, *G. minuta*, *G. petaloidea*, *Globotruncanita stuarti*, *G. stuartiformis*, *Heterohelix globulosa*, *Planoglobulina acervulinoides*, *P. multicamerata*, *Pseudoguembelina costulata*, *P. palpebra*, *Pseudotextularia elegans*, *Rugoglobigerina hexacamerata*, *R. macrocephala*, *R. rugosa*, *R. rotundata* (Table 1).

This zone has been identified in samples K31–K38 from the base of the Karainler stratigraphic section of the Akveren Formation (Table 1, Figure 3).

Racemiguembelina fructicosa Partial-range Zone: Biostratigraphic interval from the FO of *Racemiguembelina fructicosa* to the FO of *Abathomphalus mayaroensis*.

Author: Huber et al., 2008 (modified by Robaszynski and Caron 1995; Li and Keller 1998a, b).

Age: early Maastrichtian (Base 69.62 Ma, top 68.72 Ma; Huber et al., 2008).

The dominant planktonic foraminiferal species recorded in this zone include *Contusotruncana contusa*, *C. plicata*, *C. plummerea*, *C. walfischensis*, *Gansserina gansseri*, *Globigerinelloides ultramicrus*, *Globotruncana arca*, *G. aegyptiaca*, *G. falsostuarti*, *G. insignis*, *G. mariei*, *Globotruncanella havanensis*, *G. petaloidea*, *Globotruncanita falsocalcarata*, *G. stuarti*, *G. stuartiformis*, *Heterohelix globulosa*, *Planoglobulina acervulinoides*, *P. multicamerata*, *Pseudoguembelina costulata*, *P. palpebra*, *Pseudotextularia elegans*, *Racemiguembelina fructicosa*, *Rugoglobigerina hexacamerata*, *R. macrocephala*, *R. rugosa*, *R. Rotundata*.

This zone has been identified in samples K40 and K41 of the Karainler section (Table 1, Figure 3).

Abathomphalus mayaroensis Partial-range Zone: Biostratigraphic interval from the FO of *Abathomphalus mayaroensis* to the FO of *Pseudoguembelina hariaensis*.

Author: Huber et al., 2008, modified by Robaszynski and Caron (1995).

Age: late Maastrichtian (Base 68.72 Ma, top 66.78 Ma; Huber et al., 2008).

The dominant planktonic foraminiferal species recorded in this zone include *Abathomphalus mayaroensis*, *Contusotruncana contusa*, *C. patelliformis*, *C. plicata*, *C. plummerea*, *C. walfischensis*, *Gansserina gansseri*, *Globigerinelloides ultramicrus*, *Globotruncana arca*, *G. aegyptiaca*, *G. bulloides*, *G. falsostuarti*, *G. insignis*, *G. mariei*, *Globotruncanella havanensis*, *G. minuta*, *G. petaloidea*, *Globotruncanita falsocalcarata*, *G. stuarti*, *G. stuartiformis*, *Heterohelix globulosa*, *Planoglobulina acervulinoides*, *P. multicamerata*, *Pseudoguembelina costulata*, *P. palpebra*, *Pseudotextularia elegans*, *Racemiguembelina fructicosa*, *Rugoglobigerina hexacamerata*, *R. macrocephala*, *R. rugosa*, *R. rotundata*.

This zone has been identified in samples K42–K47 of the Karainler section of the Akveren Formation (Table 1, Figure 3).

Pseudoguembelina hariaensis Partial-range Zone: Biostratigraphic interval from the FO of the nominate species to the extinction of most Cretaceous planktonic foraminifera at the Cretaceous-Paleogene boundary.

Author: Robaszynski and Caron (1995).

Age: latest Maastrichtian (Base 66.78 Ma, top 65.50 Ma; Huber et al., 2008).

Toward the end of the Maastrichtian, globotruncanids decreased and high abundances of biserial heterohelicids, pseudoguembelinids, and rugoglobigerinids are recorded. The most characteristic elements recorded in this zone are *Abathomphalus mayaroensis*, *Contusotruncana contusa*, *C. plicata*, *C. plummerea*, *C. walfischensis*, *Gansserina gansseri*, *Globigerinelloides ultramicrus*, *Globotruncana arca*, *G. aegyptiaca*, *G. falsostuarti*, *G. mariei*, *Globotruncanella havanensis*, *G. petaloidea*,

Table 1- Percentage abundances (%) of planktonic foraminifera are represented against sample position of the Karainler stratigraphic section in the Maastrichtian.

| Maastrichtian | | | | | | | | | | | | | Stage | | | | | |
|-------------------|-----|------|---------------------|-----|----------------------|-----|------|-----|-----|--------------------|------|-----|-------------------------------|-----|-----|-----|---------------------------------------|--|
| <i>P.palpebra</i> | | | <i>R.fructicosa</i> | | <i>A.mayaroensis</i> | | | | | <i>Phariaensis</i> | | | Planktonic Foraminifera Zones | | | | | |
| K31 | K33 | K34 | K35 | K36 | K38 | K40 | K41 | K42 | K43 | K44 | K45 | K46 | K47 | K48 | K49 | K50 | SAMPLES | |
| 0 | 0 | 0 | 0 | 0 | 3.5 | 0 | 0 | 0.1 | 0 | 0 | 0 | 0 | 0.1 | 0 | 0 | 0 | <i>Abathomphalus mayaroensis</i> | |
| 0 | 0.4 | 0.3 | 0 | 0 | 0 | 0 | 0.3 | 1.1 | 0 | 0 | 0 | 0.2 | 0.2 | 0 | 0.1 | 0 | <i>Contusotruncana contusa</i> | |
| 17 | 5.3 | 0 | 0 | 0 | 0 | 0 | 0 | 0 | 0 | 0 | 0 | 0 | 0 | 0 | 0 | 0 | <i>Contusotruncana fornicata</i> | |
| 0.6 | 0 | 0.1 | 0 | 0 | 0 | 0 | 0 | 0.1 | 0 | 0.1 | 0.1 | 0.1 | 0.1 | 0 | 0 | 0 | <i>Contusotruncana patelliformis</i> | |
| 2.1 | 0.9 | 0.1 | 0 | 0 | 0 | 0.1 | 0.2 | 0.4 | 0.5 | 0.5 | 0.2 | 0.2 | 0.1 | 0.1 | 0.1 | 0.1 | <i>Contusotruncana plicata</i> | |
| 0 | 0 | 0.6 | 0 | 0 | 5.6 | 0.1 | 0.6 | 0.6 | 0 | 0.1 | 0.5 | 0.3 | 0.2 | 0.3 | 0.1 | 0.1 | <i>Contusotruncana plummerea</i> | |
| 0 | 0 | 0.2 | 0 | 0 | 14 | 0 | 0.3 | 0.2 | 0 | 0.3 | 0.3 | 0.2 | 0.2 | 0.1 | 0.1 | 0 | <i>Contusotruncana walfischensis</i> | |
| 0.6 | 1.1 | 0.3 | 0 | 0 | 2.1 | 0 | 0.2 | 0.3 | 0 | 0.2 | 0.2 | 0.1 | 0.2 | 0.2 | 0.1 | 0.1 | <i>Gansserina gansseri</i> | |
| 2.5 | 0.7 | 0 | 0 | 0 | 0 | 0 | 5 | 0.9 | 1.1 | 1.1 | 3.5 | 1.1 | 1.5 | 0 | 0 | 0 | <i>Globigerinelloides ultramicrus</i> | |
| 3.2 | 14 | 0.5 | 0.3 | 0.1 | 9.2 | 0.5 | 0 | 0.3 | 0.1 | 0.3 | 0.1 | 0.1 | 0.1 | 0.2 | 0.1 | 0.1 | <i>Globotruncana aegyptiaca</i> | |
| 13 | 8.8 | 1.5 | 1.4 | 1.2 | 7 | 0.4 | 1.7 | 1.5 | 1.2 | 0 | 1.3 | 1.2 | 1.5 | 0.8 | 0.6 | 0.5 | <i>Globotruncana arca</i> | |
| 0 | 0 | 0 | 0.1 | 0 | 0 | 0 | 0 | 0.1 | 0.1 | 0 | 0 | 0.1 | 0 | 0 | 0 | 0 | <i>Globotruncana bulloides</i> | |
| 0 | 0 | 0.1 | 0.3 | 0.2 | 14 | 0.2 | 0.1 | 0.1 | 0.2 | 0.2 | 0.1 | 0.2 | 0.1 | 0.1 | 0.1 | 0.1 | <i>Globotruncana falsostuarti</i> | |
| 0 | 0.4 | 0 | 0 | 0.1 | 0 | 0.5 | 0.2 | 0.3 | 0 | 0.5 | 0.1 | 0.1 | 0 | 0 | 0 | 0 | <i>Globotruncana insignis</i> | |
| 16 | 3.5 | 1.2 | 2.5 | 3.6 | 0 | 0 | 0 | 0 | 0 | 0 | 0 | 0 | 0 | 0 | 0 | 0 | <i>Globotruncana linneiana</i> | |
| 2.5 | 1.6 | 0 | 0.3 | 0.3 | 3.5 | 0.3 | 0 | 0 | 0 | 0 | 0 | 0.4 | 0.3 | 0.5 | 0.2 | 0.2 | <i>Globotruncana mariei</i> | |
| 0 | 5.3 | 0.5 | 8 | 17 | 0 | 2.9 | 3.1 | 2.2 | 2.7 | 4.9 | 1.9 | 2.2 | 0.2 | 0.1 | 0.2 | 0.1 | <i>Globotruncanella havanensis</i> | |
| 4.8 | 2.7 | 1.2 | 1.5 | 1.7 | 0 | 0 | 0 | 0 | 0 | 0 | 0 | 0.1 | 0.1 | 0 | 0 | 0 | <i>Globotruncanella minuta</i> | |
| 3 | 1.6 | 1.5 | 2.3 | 1.9 | 0 | 3.8 | 12 | 13 | 14 | 11 | 11 | 10 | 9 | 16 | 17 | 16 | <i>Globotruncanella petaloidea</i> | |
| 0 | 0 | 0 | 0 | 0 | 0 | 0.1 | 0.8 | 0 | 0 | 0.6 | 0.1 | 0.1 | 0.1 | 0.6 | 0.3 | 0.5 | <i>Globotruncanita falsocalcarata</i> | |
| 0.4 | 0 | 0.1 | 0 | 0.1 | 0 | 0.2 | 0.6 | 0.4 | 0.3 | 0.2 | 0.4 | 0.6 | 1.2 | 0.1 | 0.1 | 0.1 | <i>Globotruncanita stuarti</i> | |
| 1.3 | 0.5 | 0.4 | 1.1 | 0.2 | 0 | 1.1 | 0.8 | 0.8 | 0.5 | 0.4 | 0.8 | 0.4 | 0 | 0.1 | 0.2 | 0.1 | <i>Globotruncanita stuartiformis</i> | |
| 4.7 | 2.1 | 14 | 10 | 16 | 4.2 | 6.1 | 6.7 | 6.7 | 7.3 | 6.5 | 6 | 4.5 | 9.4 | 13 | 16 | 16 | <i>Heterohelix globulosa</i> | |
| 0.6 | 0.2 | 0.1 | 0 | 0.3 | 0 | 2.3 | 1.1 | 0.9 | 0 | 1.6 | 1 | 1.5 | 2.5 | 3.4 | 2.7 | 2.7 | <i>Planoglobulina acervulinoides</i> | |
| 0.2 | 0 | 0.1 | 0 | 0 | 0 | 0.5 | 0.9 | 0.5 | 0.6 | 0.9 | 0.7 | 0.5 | 0.2 | 1.3 | 1.3 | 1.3 | <i>Planoglobulina multicamerata</i> | |
| 4.6 | 4 | 13.5 | 10 | 3.5 | 4.3 | 12 | 16.6 | 16 | 18 | 17.2 | 17.6 | 19 | 19 | 7 | 4 | 4 | <i>Pseudoguembelina costulata.</i> | |
| 0 | 0 | 0 | 0 | 0 | 0 | 0 | 0 | 0 | 0 | 0 | 0 | 0 | 0 | 4.5 | 2.2 | 8 | <i>Pseudoguembelina hariaensis</i> | |
| 3 | 1.8 | 1.5 | 2 | 2.5 | 2 | 8 | 5.4 | 10 | 11 | 9.8 | 6.4 | 8 | 3 | 7.5 | 5.3 | 4 | <i>Pseudoguembelina palpebra</i> | |
| 1.3 | 1.8 | 4 | 2.6 | 1.2 | 2.8 | 3.8 | 6.9 | 6 | 9.4 | 4.8 | 6.7 | 8 | 3.5 | 1.8 | 2.1 | 2.1 | <i>Pseudotextularia elegans</i> | |
| 0 | 0 | 0 | 0 | 0 | 0 | 0.3 | 12 | 14 | 8 | 11 | 14 | 16 | 12 | 8.3 | 10 | 10 | <i>Racemiguembelina fructicosa</i> | |
| 5.5 | 2.1 | 16 | 14 | 3.9 | 0 | 29 | 9.7 | 14 | 13 | 12 | 13 | 14 | 16 | 11 | 9.6 | 9.6 | <i>Rugoglobigerina hexacamerata</i> | |
| 0.6 | 0 | 6.9 | 7.5 | 5.1 | 0 | 3.4 | 4.2 | 4.3 | 4.8 | 5.5 | 2.1 | 2.8 | 5.1 | 5.3 | 5.5 | 5.5 | <i>Rugoglobigerina macrocephala</i> | |
| 9.7 | 8.8 | 20 | 17 | 9 | 18 | 23 | 9 | 5.1 | 6.7 | 8.2 | 7.9 | 6.4 | 1.3 | 16 | 19 | 19 | <i>Rugoglobigerina rugosa</i> | |
| 1.9 | 4.5 | 15 | 19 | 12 | 35 | 0.6 | 0.8 | 0.9 | 1.2 | 1.6 | 1.3 | 1 | 1.5 | 2 | 1.6 | 1.6 | <i>Rugoglobigerina rotundata</i> | |

Globotruncanita falsocalcarata, *G. stuarti*, *G. stuartiformis*, *Heterohelix globulosa*, *Planoglobulina acervulinoides*, *P. multicamerata*, *Pseudoguembelina palpebra*, *P. costulata*, *P. palpebra*, *Pseudotextularia elegans*, *Racemiguembelina fructicosa*, *Rugoglobigerina hexacamerata*, *R. macrocephala*, *R. rugosa*, *R. rotundata*.

This zone has been identified in the Akveren Formation in samples K48–K50 of the Karainler section (Table 1, Figure 3), as well as in sample KD1 from the lowermost levels of the Karadur section (Table 2, Figure 5).

Plummerita hantkeninoides Zone is absent from all the Bartın sites which evolved within the last 300 k.y. of the Maastrichtian (Abramovich and Keller, 2002). The markers species of this zone is apparently preferred to live in eutrophic shelfal to upper-slope continental margin environments (e.g., Abramovich et al. 1998; Abramovich and Keller, 2002; MacLeod et al., 2007) and has not been reported from open-ocean pelagic carbonate sediments (Huber et al., 2008).

The Cretaceous-Paleogene transition is within the Akveren Formation. Any lithological changes were not seen in this region. Consequently, this boundary was estimated with changes of planktonic foraminifera species of this area.

K/Pg boundary are defined planktonic foraminiferal zone *Guembelitra cretacea* (P0) followed by the *Parvularugoglobigerina eugubina* Zone (P1a) (Smit, 1982). Abramovich et al. (2010) studied the distribution of the *Guembelitra* genera in detail in the uppermost Maastrichtian. They mentioned that whereas *Guembelitra* genera bloomed in the uppermost surface water primarily above shelf and slope environments, it appears to have failed to reach the open ocean.

5.2.2 Paleocene Planktonic Foraminifera Zones

Parvularugoglobigerina eugubina Taxon-range Zone (Pα): Biostratigraphic interval characterized by the total range of the nominate taxon *Parvularugoglobigerina eugubina*.

Author: Luterbacher and Premoli Silva, 1964.

Age: 64.97–64.8 Ma; Danian (early Paleocene).

The most characteristic assemblage recorded in this zone includes *Eoglobigerina eobulloides*, *Globoconusa conusa* and *Parvularugoglobigerina eugubina*.

This zone has been identified in sample KD2 of the Karadur section of the Akveren Formation (Table 2, Figure 5).

Parasubbotina pseudobulloides Partial-range Subzone (P1a) and *Subbotina triloculinoides* Lowest Occurrence Subzone (P1b) were not determined in this study area (Table 2, Figure 5).

Glomobanomalina compressa/*Praemurica uncinata* Lowest Occurrence Subzone (P1c): Biostratigraphic interval between the FO of *Glomobanomalina compressa* and/or *Praemurica inconstans* and the FO of *Praemurica uncinata*.

Author: Berggren and Miller, 1988.

Age: 62.87–61.37 Ma; early Paleocene (mid-late Danian).

The characteristic assemblage recorded in this zone includes *Globoconusa conusa*, *Parasubbotina pseudobulloides*, *Eoglobigerina eobulloides*, *Subbotina triloculinoides*, *Praemurica inconstans*, *Morozovella trinidadensis* and *Glomobanomalina compressa*.

This zone has been identified in sample KD3-KD11 of the Karadur section (Table 2, Figure 5).

Praemurica uncinata Lowest Occurrence Zone (P2): Biostratigraphic interval between the FO of *Praemurica uncinata* and the FO of *Morozovella angulata*.

Author: Berggren and Miller, 1988.

Age: 61.37–61.0 Ma; late early Paleocene (late Danian).

Associated species of the nominate taxon are *Globoconusa conusa*, *Parasubbotina pseudobulloides*, *Subbotina triloculinoides*, *Praemurica inconstans*, *Morozovella trinidadensis*, *Glomobanomalina compressa* and *Praemurica uncinata*.

This zone has been identified in sample KD12-

Table 2- Percentage abundances (%) of planktonic foraminifera are represented against sample position of the Karadur stratigraphic section from Maastrichtian to Selandian.

| Maastr. | Danian | | | | | | | | | | Selandian | | | | | Stage | | | | | | |
|--------------------|--------------------|------------|------------|------------|------------|------------|------------|-------------|-------------|-------------|-------------------|-------------|-------------|-------------|-------------|-------------------------------|-----|-----|-----|-----|-----|--|
| | <i>G.compressa</i> | | | | | | | | | | <i>M.angulata</i> | | | | | Planktonic Foraminifera Zones | | | | | | |
| <i>Phanerozois</i> | | | | | | | | | | | | | | | | Samples | | | | | | |
| <i>Pseudobina</i> | | | | | | | | | | | | | | | | | | | | | | |
| <i>KD1</i> | <i>KD2</i> | <i>KD3</i> | <i>KD4</i> | <i>KD5</i> | <i>KD6</i> | <i>KD8</i> | <i>KD9</i> | <i>KD10</i> | <i>KD11</i> | <i>KD12</i> | <i>KD13</i> | <i>KD14</i> | <i>KD15</i> | <i>KD17</i> | <i>KD19</i> | <i>KD20</i> | | | | | | |
| 0.5 | 2.1 | 0.6 | 0.3 | 0.5 | 2.2 | 0.7 | 1.3 | 0.6 | 0.3 | 4.2 | 0.2 | 0.7 | 4.5 | 3.2 | 1.0 | 3.4 | 1.1 | 4.7 | 2.6 | 4.2 | 4.7 | <i>Abathomphalus mayaroensis</i> |
| | | | | | | | | | | | | | | | | | | | | | | <i>Contusotruncana contusa</i> |
| | | | | | | | | | | | | | | | | | | | | | | <i>Contusotruncana plummerea</i> |
| | | | | | | | | | | | | | | | | | | | | | | <i>Contusotruncana walfischensis</i> |
| | | | | | | | | | | | | | | | | | | | | | | <i>Gansserina gansseri</i> |
| | | | | | | | | | | | | | | | | | | | | | | <i>Globigerinelloides ultramicrus</i> |
| | | | | | | | | | | | | | | | | | | | | | | <i>Globotruncana aegyptiaca</i> |
| | | | | | | | | | | | | | | | | | | | | | | <i>Globotruncana arca</i> |
| | | | | | | | | | | | | | | | | | | | | | | <i>Globotruncana falsostuarti</i> |
| | | | | | | | | | | | | | | | | | | | | | | <i>Globotruncanella havanensis</i> |
| | | | | | | | | | | | | | | | | | | | | | | <i>Globotruncanella petaloidea</i> |
| | | | | | | | | | | | | | | | | | | | | | | <i>Globotruncanita stuarti</i> |
| | | | | | | | | | | | | | | | | | | | | | | <i>Globotruncanita stuartiformis</i> |
| | | | | | | | | | | | | | | | | | | | | | | <i>Heterohelix globulosa</i> |
| | | | | | | | | | | | | | | | | | | | | | | <i>Planoglobulina acervulinoides</i> |
| | | | | | | | | | | | | | | | | | | | | | | <i>Pseudoguembelina costulata.</i> |
| | | | | | | | | | | | | | | | | | | | | | | <i>Pseudoguembelina hariaensis</i> |
| | | | | | | | | | | | | | | | | | | | | | | <i>Pseudoguembelina palpebra</i> |
| | | | | | | | | | | | | | | | | | | | | | | <i>Racemiguembelina fruticososa</i> |
| | | | | | | | | | | | | | | | | | | | | | | <i>Rugoglobigerina hexacamerata</i> |
| | | | | | | | | | | | | | | | | | | | | | | <i>Rugoglobigerina macrocephala</i> |
| | | | | | | | | | | | | | | | | | | | | | | <i>Rugoglobigerina rugosa</i> |
| | | | | | | | | | | | | | | | | | | | | | | <i>Parvularugoglobigerina eugubina</i> |
| | | | | | | | | | | | | | | | | | | | | | | <i>Eoglobigerina eobulloides</i> |
| | | | | | | | | | | | | | | | | | | | | | | <i>Globoconusa conusa</i> |
| | | | | | | | | | | | | | | | | | | | | | | <i>Parasubbotina pseudobulloides</i> |
| | | | | | | | | | | | | | | | | | | | | | | <i>Subbotina triloculinoides</i> |
| | | | | | | | | | | | | | | | | | | | | | | <i>Glomobanomalina compressa</i> |
| | | | | | | | | | | | | | | | | | | | | | | <i>Praemucira inconstans</i> |
| | | | | | | | | | | | | | | | | | | | | | | <i>Morozovella trinidadensis</i> |
| | | | | | | | | | | | | | | | | | | | | | | <i>Praemurica uncinata</i> |
| | | | | | | | | | | | | | | | | | | | | | | <i>Morozovella angulata</i> |
| | | | | | | | | | | | | | | | | | | | | | | <i>Morozovella conicotruncana</i> |
| | | | | | | | | | | | | | | | | | | | | | | <i>Igorina pusilla</i> |
| | | | | | | | | | | | | | | | | | | | | | | <i>Morozovella velascoensis</i> |
| | | | | | | | | | | | | | | | | | | | | | | <i>Acarinina primitiva</i> |
| | | | | | | | | | | | | | | | | | | | | | | <i>Planorotalites chapmani</i> |

KD13 of the Karadur section (Table 2, Figure 5) of the Akveren Formation.

Morozovella angulata Lowest Occurrence Zone (P3): Biostratigraphic interval between the FO of *Morozovella angulata* and the FO of *Globanomalina pseudomenardii*.

Author: Berggren and Miller, 1988.

Age: 61.0–59.4 Ma; early late Paleocene (Selandian).

Associated species of the nominate taxon in the studied section are *Globoconusa conusa*, *Parasubbotina pseudobulloides*, *Subbotina triloculinoides*, *Praemurica inconstans*, *Morozovella trinidadensis*, *M. angulata*, *M. conicotruncana*, *M. velascoensis*, *Glomobanomalina compressa*, *Praemurica uncinata*, *Acarinina primitiva*, *Igorina pusilla* and *Planorotalites chapmani*.

This zone has been identified samples KD14–KD20 of the Akveren Formation (Table 2, Figure 5).

5.3. Planktonic Foraminifera Assemblages

5.3.1. Composition of the Planktonic Foraminifera Assemblages in the Maastrichtian

The Maastrichtian is represented by small-sized biserial and low trochospiral spired planktonic foraminifera in the study area. The most dominant species in the Maastrichtian is small-sized *Rugoglobigerina* (*Rugoglobigerina rugosa*, *R. hexacamerata*, *R. macrocephala*) with low trochospiral shell. Within the foraminifera assemblages, *Rugoglobigerina* spp. is the most dominant species with 10-55% enrichment (Table 1, Figure 6). *Rugoglobigerina rotundata* with

higher trochospiral shell is the only dominant species in the lower Maastrichtian with abundance of 45% in sample K33 and 35% in sample K38. Although it has abundance between 2% and 45% in the lower Maastrichtian, the species is rare in the upper Maastrichtian (0.4-2%). *Pseudoguembelina* spp. is the second most dominant species (6-27%) (Table 1, Figure 6).

The third dominant species is *Heterohelix globulosa* with abundance of 2-16%. The other small-sized and low trochospiral shell species *Globotruncanella petaloidea* is another dominant species (2-17%). *Pseudotextularia elegans* is observed as a less common species (1-7%). In the upper Maastrichtian, *Racemiguembelina fructicosa* is the second common species (8-14%) together with *Rugoglobigerina* spp., with the exception of sample K40 (Table 1, Figure 6).

5.3.2. Composition of the Planktonic Foraminifera Assemblages in the Paleocene

Planktonic foraminifera species appearing just after the K/Pg boundary are small sized with globular chambers. The first Danian genera are *Parvularugoglobigerina eugubina*, *Eoglobigerina eobulloides* and *Subbotina triloculinoides*. In the lower Danian, *Globoconusa conusa*, *Parasubbotina pseudobulloides*, *Glomobanomalina compressa* and *Praemurica inconstans* are also observed together with *P. eugubina*, *E. eobulloides* and *S. triloculinoides* (Table 2, Figure 7).

Beginning from upper Danian, *Morozovella* spp. species appear (Table 2, Figure 7). The life time of *P. eugubina* and *E. eobulloides*, which are the initial species appearing in the Danian, is short. They are observed only in a few samples (Figure 7). The most dominant species of the Danian is *S. triloculinoides*

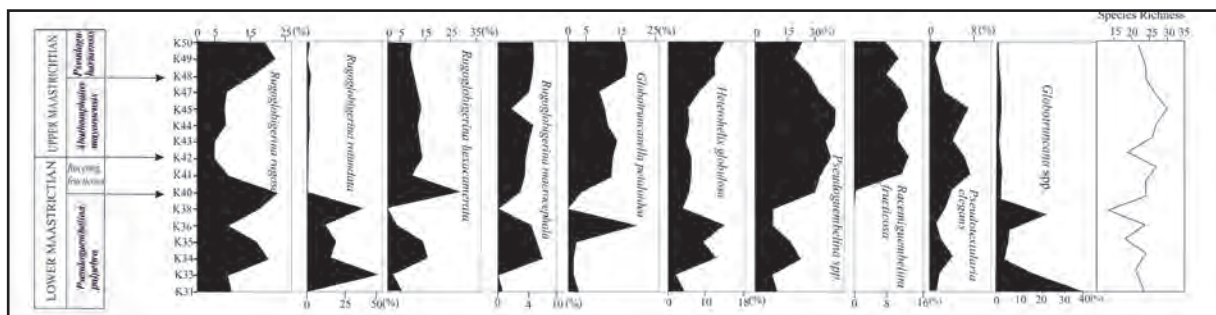


Figure 6- Species richness, percentage distributions of selected planktonic foraminifera of the Karainler stratigraphic section in the Maastrichtian.

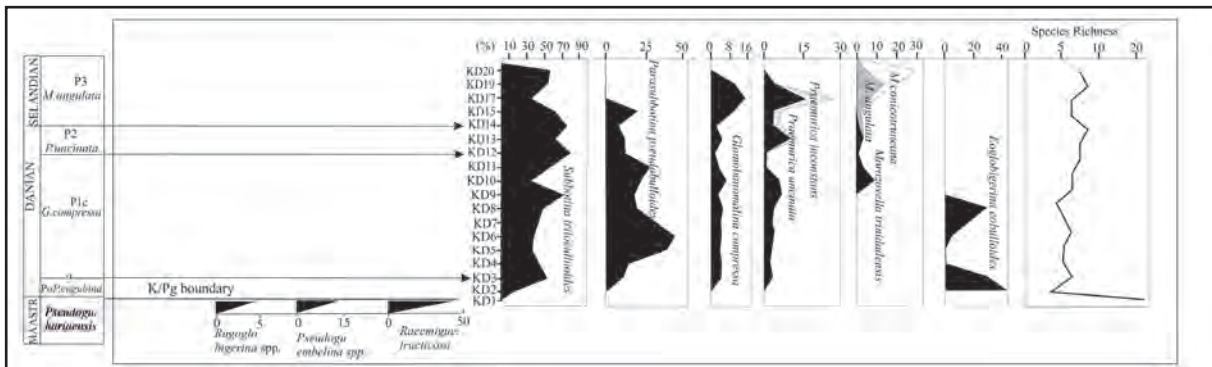


Figure 7- Species richness, percentage distributions of selected planktonic foraminifera of the Karadur stratigraphic section from Maastrichtian to Selandian.

with 14-79% abundance. *P. pseudobulloides* is the other dominant species with 8-43% abundance (Table 2, Figure 7).

Less dominant species are *G. compressa* (2-14%), *P. inconstans* (3-21%), *G. conusa* (2-7%), *Morozovella trinidadensis* (1-9%), *Praemurica uncinata* (1-14%), *Morozovella angulata* (2-7%) and *Morozovella conicotruncana* (10-15%). In the Selandian, *S. trilocolinoides* (53-57%) and *Morozovella* species are dominant (Table 2, Figure 7).

5.4. The Paleocology of Planktonic Foraminifera in the Maastrichtian

Planktonic foraminifera are defined as sensitive recorders of the upper part of the water column, reflecting changes in primary productivity, sea surface water temperature and the degree of water column stratification (Leckie, 1987; Schiebel and Hemleben, 2000). In the Bartin area, abundance of *Globotruncana* spp. (*Globotruncana arca*, *G. linneiana*, *G. aegyptiaca*, *G. mariei*, *G. bulloides*, *G. falsostuarti*, *G. ventricosa* and *G. insignis*) is rare and shows a decrease in the Maastrichtian (Table 1, Figure 6). Abramovich and Keller (2003) indicated that the abundance of globotruncanids decreased under biotic stress in the Maastrichtian. In this study area, decrease in the abundance of globotruncanids may reflect the changes in environmental conditions.

In the lower Maastrichtian, the abundance of *Rugoglobigerina* taxa increased when abundances of globotruncanids decreased. Genus *Rugoglobigerina* are widely observed from lower Maastrichtian to upper Maastrichtian (Table 1, Figure 6). This genus was proposed to live in tropical-mid latitudes and

warm climates in previous studies and the abundance of *Rugoglobigerinids* arrive at maximum levels in climatic warming periods (Malmgren, 1991; Nederbragt, 1991, 1998; Li and Keller, 1998a). Abramovich and Keller (2003) stated that decreases in the relative abundance of tropical-subtropical *Pseudoguembelina costulata*, *Rugoglobigerina rugosa* and several keeled globotruncanids (including *Contusotruncana* species) coincide with the warm event and their decline suggests unfavorable environmental conditions.

Pseudoguembelina and *Heterohelix globulosa* are dominant in the upper Maastrichtian fauna in the study area (Table 1, figure 6). Abramovich et al. (2003) and Keller (2004) suggest that the domination of small biserial ecological species and low trochospiral species (*Rugoglobigerina*, *H. globulosa*, *Pseudoguembelina*, *Pseudotextularia*) and also the low diversity of the species indicates the presence of highly stressed environmental conditions.

Heterohelix globulosa is evaluated as tolerant of the changes in salinity, temperature, oxygen and the amount of nutrition (Keller, 2004). *Heterohelix globulosa* continued to live without being affected by changes in environmental conditions. Ashckenazi-Polivoda et al. (2011) stated that Heterohelicids display high abundance in a variety of marine environments, indicate unsuitable environmental conditions and an ability to adjust to a wide range of water column conditions. In this study, increasing abundance of *Heterohelix globulosa* and *Pseudoguembelina* spp. shows that they are resistant and tolerant of the changes in environmental conditions such as nutrition and temperature, exhibiting compatibility with global climate changes before the K/Pg boundary.

Racemiguembelina, which is common in the upper Maastrichtian assemblages, were defined as photosymbiotic (Houston and Huber, 1998; D'Hondt and Zachos, 1998; Houston et al., 1999). *Racemiguembelina* is defined as an oligotrophic genus in the open ocean (Abramovich et al., 2010). In the uppermost Maastrichtian, high abundance of *Racemiguembelina fructicosa*, *Heterohelix globulosa* and *Rugoglobigerina* spp. can be interpreted as the presence of oligotrophic and warmer environmental conditions in this study (Table 1-2, Figure 6-7).

Kaya-Özer (2014) investigated nanofossil assemblages, carbon and oxygen stable isotope data in this stratigraphic section and suggested that environmental conditions changed from eutrophic to oligotrophic during the Maastrichtian. Diversification of planktonic foraminifera species indicate the same environmental conditions in this study.

In the upper Maastrichtian in the Bartın area, the increasing abundance of *Globotruncanella petaloidea* is coherent with increasing abundance of the species which are tolerant of changes in nutrition and temperature (Table 1, Figure 6). It is possible that these species are able to live in similar environments.

5.5. The Paleocology of Planktonic Foraminifera in the Paleocene

Small, unornamental and primitive Paleogene species began to be seen just above K/Pg boundary in this study area. *Parasubbotina pseudobulloides* and *Subbotina triloculinoidea* are the dominant species in the Danian (Table 2, Figure 7). In the upper Danian, together with these species, the abundance of *Praemurica* species also increased. However, in the Selandian, *Morozovella* species start to dominate (Table 2, Figure 7).

Quillevère and Norris (2003) suggested that different depth habitats played an important role in the diversification of planktonic foraminifera, related to the initiation of photosymbiosis as a trophic strategy. Subbotinids lived within or below the thermocline whereas morozovellids and igorinids dwelled in the surface mixed-layer (Shackleton et al., 1985; Pearson et al., 1993; D'Hondt et al., 1994; Van Eijden, 1995; Lu et al., 1998; Quillevère and Norris, 2003).

Subbotina and *Parasubbotina* preferred cold water, asymbiotic living and mesotrophic environmental

conditions (Boersma and Premoli-Silva, 1991; Pearson et al., 1993; Norris, 1996; Berggren and Norris, 1997; Guasti et al., 2005). Also, *Parasubbotina* and *Subbotina* taxa shared a similar trophic strategy and living position within the thermocline (Guasti et al., 2005). Guasti et al. (2005) stated that increased productivity through enhanced input of nutrients from land may favor the thermocline dweller *Parasubbotina*. In the study area, during the Danian, high abundance of *Parasubbotina* and *Subbotina* can be considered as indicating mesotrophic and cooler environmental conditions.

Stable isotope values indicate that subbotinids lived in cooler, deeper waters than morozovellids (Boersma and Premoli Silva, 1991; Norris, 1996). Positive $\delta^{18}\text{O}$ values show *Morozovella* and later *Acarinina* species have a deeper habitat (Berggren and Norris, 1997; Quillevère et al., 2000; Quillevère and Norris, 2003). Most morozovellids, acarininids and igorinids were accepted as photosymbiotic species (D'Hondt et al., 1994; Norris, 1996; Berggren and Norris, 1997; Quillevère and Norris, 2003). Acarininids and morozovellids thrive in low-nutrient water masses in the global ocean during the late Paleocene (Norris, 1996; Quillevère and Norris, 2003). *Praemurica inconstans* was accepted as a photosymbiotic species (Kelly et al., 1996).

Morozovella adapted to warm water and oligotrophic environmental conditions (Pearson et al., 1993; Norris, 1996; Berggren and Norris, 1997; Quillevère and Norris, 2003). In this study, in the Selandian, *Morozovella* started with common taxa with *Subbotina* and *Parasubbotina* (Table 2, Figure 7). Increasing abundance of *Morozovella* taxa which lived in low nutrition waters, indicates mesotrophic-oligotrophic and warmer environmental conditions in the Selandian. Kaya-Özer (2014) suggested similar environmental conditions in the Paleocene based on $\delta^{13}\text{C}$ values.

6. Conclusion

The Akveren Formation represents open sea characteristics in the Maastrichtian-Selandian period based on planktonic foraminifera species. In the Maastrichtian, planktonic foraminifera assemblages in the study area are dominated by small, simple morphotypes, opportunists, generalists and high-stress specialist morphologies. Increased abundance

of small-sized, biserial and low trochospiral planktonic foraminifera species (*Rugoglobigerina* spp., *Heterohelix globulosa*, *Pseudoguembelina* spp., *Pseudotextularia elegans*) show variable and unstable environmental conditions in the Western Black Sea basin during the Maastrichtian. In the uppermost Maastrichtian, high abundance of *Racemiguembelina fructifera*, *Heterohelix globulosa* and *Rugoglobigerina* spp. indicates oligotrophic and warmer environmental conditions.

In the lower Paleocene, high abundance of *Parasubbotina* and *Subbotina* shows mesotrophic and cooler environmental conditions. In the Selandian, increasing abundance of *Morozovella* taxa indicates mesotrophic- oligotrophic and warmer environmental conditions.

Acknowledgements

I would like to thank the Editor-in-Chief of the Journal and anonymous reviewers for their valuable corrections and comments.

References

- Abramovich, S., Almogi-Labin, A., Benjamini, C. 1998. Decline of the Maastrichtian pelagic ecosystem based on planktic foraminifera assemblage changes: Implication for the terminal Cretaceous faunal Crisis. *Geology* 26, 63-66.
- Abramovich, S., Keller, G. 2002. High stress late Maastrichtian paleoenvironment: Inference from planktonic foraminifera in Tunisia, *Palaeogeography, Palaeoclimatology, Palaeoecology* 178, 145-164.
- Abramovich, S., Keller, G. 2003. Planktonic foraminiferal response to the latest Maastrichtian abrupt warm event: a case study from South Atlantic DSDP Site 525A. *Marine Micropaleontology* 48, 225-249.
- Abramovich, S., Keller, G., Stüben, D., Berner, Z. 2003. Characterization of late Campanian and Maastrichtian planktic foraminiferal depth habitats and vital activities based on stable isotopes. *Palaeogeography, Palaeoclimatology, Palaeoecology* 202, 1-29.
- Abramovich, S., Yovel-Corem, S., Almogi-Labin, A., Benjamini C. 2010. Global climate change and planktic foraminiferal response in the Maastrichtian. *Paleoceanography* 25, 1-15.
- Akman, Ü. 1992. Amasra-Arıt arasının jeolojisi. Doktora Tezi, Ankara Üniversitesi, 209 s. Ankara, (unpublished).
- Akyol, Z., Arpat, E., Erdoğan, B., Göğür, E., Güner, Y., Şaroğlu, F., Şentürk, İ., Tütüncü, K., Uysal, Ş. 1974. 1/50.000 ölçekli Türkiye Jeoloji haritası serisi, Zonguldak E29a, E29b, E29c, E29d, Kastamonu E30a, E30d. Maden Tetkik ve Arama Genel Müdürlüğü Yayınları, Ankara.
- Ashkenazi-Polivoda, S., Abramovich, S., Almogi-Labin, A., Schneider-Mor, A., Feinstein, S., Puttmann, W., Berner A. 2011. Paleoenvironments of the latest Cretaceous oil shale sequence, Southern Tethys, Israel, as an integral part of the prevailing upwelling system. *Palaeogeography, Palaeoclimatology, Palaeoecology* 305, 93-108.
- Aydın, A. 2005. İzmit kuzeybatısı Geç Kretase-Paleojen nannoplankton biyostratigrafisi. Yüksek lisans tezi, Ankara Üniversitesi, 237 s. Ankara, (unpublished).
- Aydın, M., Şahintürk, Ö., Serdar, H.S., Özçelik, Y., Akarsu, İ., Üngör, A., Çokuğraş, R., Kasar, S. 1986. Ballıdağ-Çangaldağ (Kastamonu) arasındaki bölgenin jeolojisi. *Türkiye Jeoloji Kurumu Bülteni* 29, 1-16.
- Badgley, P.C. 1959. Sinop Havzasının petrol olanakları. Petrol işleri Genel Müdürlüğü arşivi, Ankara.
- Barka, A., Sütçü, Y. F., Tekin, F., Gedik, İ., Karabıyıkoglu, M., Saraç, G. Önal, Ö., Arel, E., Özdemir M. 1983. Sinop Yarımadasının jeolojisi ve tektonik evrimi. *Türkiye Jeoloji Kurumu Bülteni* 4, 24.
- Barrera, E., Savin, S.M., Thomas, E., Jones, C.E. 1997. Evidence for thermohaline circulation reversals controlled by sea-level change in the latest Cretaceous. *Geology* 25, 715-718.
- Barrera, E., Savin, S.M. 1999. Evolution of late Campanian-Maastrichtian marine climates and oceans. Barrera, E., Johnson, C.C. (Ed.). *Evolution of the Cretaceous Ocean-Climate System. Geological Society of America Special Paper* 332, 245-282.
- Berggren, W.A., Norris, R.D. 1997. Biostratigraphy, phylogeny and systematics of Paleocene trochospiral planktic foraminifera. *Micropaleontology* 43, 1-116.

- Berggren, W.A., Miller, K.G. 1988. Paleocene tropical planktonic foraminiferal biostratigraphy and magneto biochronology. *Micropaleontology* 34, 4, 362-380.
- Bice, K.L., Birgel, D., Meyers, P.A., Dahl, K., Hinrichs K, U., Norris, R.D. 2006. A multiple proxy and model study of Cretaceous upper ocean temperatures and atmospheric CO2 concentrations. *Paleoceanography* 21, 1-17.
- Boersma, A., Premoli Silva, I. 1991. Distribution of Paleogene planktonic foraminifera analogies with Recent? *Palaeogeography, Palaeoclimatology, Palaeoecology* 83, 29-48.
- Bornemann, A., Norris, R.D., Friedrich, O., Beckmann, B., Schouten, S., Sinninghe Damste, J.S., Vogel, J., Hofmann, P., Wagner, T. 2008. Isotopic evidence for glaciation during the Cretaceous supergreen house. *Science* 319, 189-192.
- Caron, M. 1985. Cretaceous planktic foraminifera. Bolli H.M., Saunders J.B., Perch-Nielsen, K. (Ed.). *Plankton Stratigraphy*. Cambridge University Press, London, 1032 p.
- Clarke, L.J., Jenkyns, H.C. 1999. New oxygen isotope evidence for long-term Cretaceous climatic change in the Southern Hemisphere. *Geology* 27, 8, 699-702.
- Corfield, R.M., Norris, R.D. 1996. Deep water circulation in the Paleocene ocean. Knox R., Corfield, R.M., Dunay, R.E. (Ed.). *Correlation of the early Paleogene in Northwest Europe*. Geological Society of London Special Publication 101, 443-456.
- Deconto, R.M., Hay, W.W., Thompson, S.L., Berggren, J. 1999. Late Cretaceous climate and vegetation interactions: Cold continental interior paradox. Barrera, E., Johnson, C.C. (Ed). *Evolution of the Cretaceous Ocean-Climate System*. Boulder, CO: Geological Society of America Special Paper 332, 391-406.
- Derman, A. S. 2002. Karadeniz'in açılma istifleri (Black Sea rift sequences). *Turkish Association of Petroleum Geologists Bulletin* 14, 37-66.
- Derman, A.S., Alişan, C., Özçelik, Y. 1995. Himmetpaşa Formation: new palynological age data and its significance. Erler, A., Ercan, T., Bingöl, E., Örçen, S. (Eds). *Geology of the Black Sea region*. General Directorate of Mineral Research and Exploration and Chamber of Geological Engineers 99-103.
- D'Hondt, S., Lindinger, M. 1994. A stable isotopic record of the Maastrichtian oceanclimate system: South Atlantic DSDP Site 528. *Palaeogeography, Palaeoclimatology, Palaeoecology* 112, 363-378.
- D'Hondt, S., Zachos, J.C., Schultz, G. 1994. Stable Isotopic signal and Photosymbiosis in late Paleocene Planktic foraminifera. *Paleobiology* 30, 3, 391-406.
- D'Hondt, S., Zachos, J. 1998. Cretaceous foraminifera and the evolutionary history of planktic photosymbiosis. *Paleobiology* 24, 512-523.
- Dizer, A., Meriç, E. 1981. Kuzeybatı Anadolu'da Üst Kretase-Paleosen biyostratigrafisi. *Maden Tetkik ve Arama Dergisi* 95-96, 149-163.
- Dobrucalı, S. 1985. Akveren Formasyonu (Sinop-Gerze) planktonik foraminifer faunası ve stratigrafik konumu. Yüksek lisans tezi, Karadeniz Teknik Üniversitesi, 56, Trabzon, (unpublished).
- Forster, A., Schouten, S., Moriya, K., Wilson, P.A., Sinninghe Damste, J.S. 2007. Tropical warming and intermittent cooling during the Cenomanian/Turonian oceanic anoxic event 2: Sea surface temperature records from the equatorial Atlantic. *Paleoceanography* 22, 1-14.
- Friedrich, O., Erbacher, J., Moriya, K., Wilson, P.A., Kuhnert, H. 2008. Warm saline intermediate waters in the Cretaceous tropical Atlantic Ocean. *Nature Geoscience* 1, 453-457.
- Friedrich, O., Norris, R.D., Erbacher, J. 2012. Evolution of middle to Late Cretaceous oceans-A 55 m.y. record of Earth's temperature and carbon cycle. *Geology* 40, 107-110.
- Gayle, R.B. 1959. Sinop Yöresi ile ilgili çalışma. *Petrol işleri, Rapor no.17*, Ankara.
- Gedik, A., Ercan, T., Korkmaz, S. 1983. Orta Karadeniz (Samsun-Sinop) havzası jeolojisi ve volkanik kayaların petrolojisi. *Maden Tetkik ve Arama Dergisi* 99-100, 34-51.
- Gedik, A., Korkmaz, S. 1984. Sinop Havzasının jeolojisi ve petrol olanakları. *Jeoloji Mühendisleri Odası Dergisi* 19, 53-79.
- Gedik, I., Timur, E., Duru, M., Pehlivan, S. 2005. 1:50.000 Ölçekli Türkiye Jeoloji Haritaları (İstanbul F22 c, d; F23 c, d; Bursa G22 a, b; G23 a, b), Maden Tetkik ve Arama Genel Müdürlüğü Jeoloji Etütleri Dairesi, No: 10-17, Ankara.

- Görür, N. 1988. Timing of opening of the Black Sea basin. *Tectonophysics* 147, 247-262.
- Görür, N., Tüysüz, O. 1997. Petroleum geology of the southern continental margin of the Black Sea. Robinson, A. G. (Ed). *Regional and petroleum geology of the Black Sea and surrounding region*. American Association of Petroleum Geologists (AAPG) Memoirs 68, 227-240.
- Guasti, E., Speijer, R. P., Fornaciari, E., Schmitz, B., Kroon, D., Gharaibeh, A. 2005. Transient biotic change within the Danian-Selandian transition in Egypt and Jordan. In: *Early Paleogene environmental turnover in the Southern Tethys as recorded by foraminiferal and organic-walled dinoflagellate cysts assemblages*. *Berichte aus dem Fachbereich Geowissenschaften der Universität Bremen*, 241, 75-110.
- Güray, A. 2006. Campanian-Maastrichtian planktonic foraminiferal investigation and biostratigraphy (Kokaksu section, Bartın, NW Anatolia): remarks on the Cretaceous paleoceanography based on quantitative data. Yüksek lisans tezi, Orta Doğu Teknik Üniversitesi, 244, Ankara, (unpublished).
- Houston, R.M., Huber, B.T. 1998. Evidence of photosymbiosis in fossil taxa? Ontogenetic stable isotope trends in some late Cretaceous planktonic foraminifera. *Marine Micropaleontology* 34, 29-46.
- Houston, R.M., Huber, B.T., Spero, H.J. 1999. Size-related isotopic trends in some Maastrichtian planktonic foraminifera: methodological comparisons, intraspecific variability and evidence for photosymbiosis. *Marine Micropaleontology* 36, 169-188.
- Huber, B.T., Hodell, D.A., Hamilton, C.P. 1995. Middle-Late Cretaceous climate of the southern high latitudes: Stable isotopic evidence for minimal equator-to-pole thermal gradients. *GSA Bulletin* 107, 1164-1191.
- Huber, B.T., Macleod, K.G., Norris, R.D. 2002. Abrupt Extinction and Subsequent Reworking of Cretaceous Planktonic Foraminifera across the Cretaceous-Tertiary Boundary: Evidence from the Subtropical North Atlantic. *Geological Society of America* 356, 277-289.
- Huber, B.T., Macleod, K.G., Tur, N.A. 2008. Chronostratigraphic framework for Upper Campanian-Maastrichtian sediments on the Blake Nose (Subtropical North Atlantic). *Journal of Foraminiferal Research* 38, 162-182.
- Kaya, O., Dizer, A., Tansel, İ., Meriç, E. 1982/1983. Ereğli (Zonguldak) alanının Kretase stratigrafisi. *Maden Tetkik ve Arama Dergisi* 99/100, 19-33.
- Kaya-Özer, C. 2009. Bartın-Kurucaşile yöresi Geç Kretase birimleri planktonik foraminifer ve nannoplankton biyostratigrafisi. Doktora Tezi, Ankara Üniversitesi, Fen Bilimleri Enstitüsü, 371, Ankara (unpublished).
- Kaya-Özer, C. 2014. Calcareous Nannofossil Assemblages Changes and Stable Isotope Data from Maastrichtian to Selandian in the Akveren Formation, Western Black Sea, Turkey. *Arabian Journal of Geosciences* 7, 1233-1247.
- Kaya-Özer, C., Toker, V. 2012. Calcareous Nannoplankton Biostratigraphy of the Bartın Province, Western Black Sea, Turkey. *Acta Geologica Sinica - English Edition* 86, 6, 1434-1446.
- Keller, G. 1996. The K/T mass extinction in planktic foraminifera biotic constraints for catastrophe theories. MacLeod, N., Keller, G., (Ed.) *The Cretaceous-Tertiary mass extinction: Biotic and environmental events*, Norton Press New York 63-100.
- Keller, G. 2004. Low-diversity, Late Maastrichtian and Early Danian planktonic foraminiferal assemblages of the Eastern Tethys. *Journal of Foraminiferal Research* 34, 1, 49-73.
- Keller, G., Adatte, T., Stinnesbeck, W., Luciani, V., Karoui-Yaakoub, N., Zaghbib-Turki, D. 2002. Paleoecology of the Cretaceous-Tertiary mass extinction in planktonic foraminifera. *Palaeogeography, Palaeoclimatology, Palaeoecology* 178, 257-297.
- Kelly, C. D., Arnold, A. J., Parker, W. C. 1996. Paedomorphosis and the origin of the Paleogene planktonic foraminiferal genus *Morozovella*. *Paleobiology* 22, 2, 266-281.
- Ketin, İ., Gümüş, A. 1963. Sinop-Ayancık arasında III. Bölgeye dahil sahalarnın jeolojisi. TPAO, Rapor no. 288. Ankara.

- Kırcı, E. 1998. Cide (Kastamonu) yöresinde Kretase-Tersiyer geçişinin biyostratigrafisi. Yüksek lisans tezi, İstanbul Üniversitesi, 77, İstanbul, (unpublished).
- Leckie, R.M. 1987. Paleoecology of mid-Cretaceous planktonic foraminifera: A comparison of open ocean and epicontinental sea assemblages. *Micropaleontology* 33, 264-276.
- Li, L., Keller, G. 1998a. Maastrichtian climate productivity and faunal turnovers in planktic foraminifera in South Atlantic DSDP Sites 525A and 21. *Marine Micropaleontology* 33, 55-86.
- Li, L., Keller, G. 1998b. Diversification and extinction in Campanian-Maastrichtian planktic foraminifera of Northwestern Tunisia. *Ecl. Helv* 91, 75-102.
- Lu, G., Adatte, T., Keller, G., Ortiz, N. 1998. Abrupt climatic, oceanographic and ecologic changes near the Paleocene-Eocene transition in the deep Tethys basin: The Alamedilla section, southern Spain. *Eclogae geol. Helv.* 91, 293-306.
- Luterbacher, H.P., Premoli Silva, I. 1964. Biostratigrafi a del limite cretaceo-terziario nell' appennino centrale. *Riv Ital Paleontol Stratigr* 70,67-128.
- Macleod, K.G., Whitney, D.L., Huber, B.T., Koeberl, C. 2007. Impact and extinction in remarkably complete Cretaceous-Tertiary boundary sections from Demerara Rise, tropical western north Atlantic. *Geological Society of America, Bulletin* 119, 101-115.
- Malmgren, B.A. 1991. Biogeographic patterns in terminal Cretaceous planktonic foraminifera from Tethyan and warm transitional waters. *Marine Micropaleontology* 18, 73-99.
- Miller, K.G., Wright, J.D., Browning, J.V. 2005. Visions of ice sheets in a greenhouse world. *Marine Geology* 217, 215-231.
- Nederbragt, A.J. 1991. Late Cretaceous biostratigraphy and development of Heterohelicidae (planktic foraminifera). *Micropaleontology* 37, 329-372.
- Nederbragt, A.J. 1998. Quantitative biogeography of late Maastrichtian planktic foraminifera. *Micropaleontology* 44, 385-412.
- Norris, R.D. 1996. Symbiosis as an Evolutionary Innovation in the radiation of Paleocene planktic foraminifera. *Paleobiology* 22, 4, 461-480.
- Norris, R.D., Bice, K.L., Magno, E.A., Wilson, P.A. 2002. Jiggling the tropical thermostat in the Cretaceous hothouse. *Geology* 30, 299-302.
- Olsson, R.C., Hemleben, C., Berggren, W.A., Huber, B.T. 1999. Atlas of Paleocene planktonic foraminifera. *Smithsonian Contributions to Paleobiology* 85, 1-252
- Özçelik, Y., Çaptuğ, A. 1990. Amasra doğusu-Cide arasında kalan alanda yapılan saha gözlemleri ve revizyon çalışmaları. Türkiye Petrolleri Anonim Ortaklığı, Rapor No:2789, Ankara.
- Özkan-Altın, S., Özcan, E. 1999. Upper Cretaceous planktonic foraminiferal biostratigraphy from NW Turkey: calibration of the stratigraphic ranges of larger benthonic foraminifera. *Geological Journal* 34, 287-301.
- Pearson, P.N., Shackleton, N.J., Hall, M.A. 1993. Stable isotope paleoecology of middle Eocene planktonic foraminifera and multi-species isotope stratigraphy, DSDP Site 523, South Atlantic. *Journal of Foraminiferal Research* 23, 2, 123-140.
- Petrizzo, M.R., Falzoni, F., Premoli Silva, I. 2011. Identification of the base of the lower-to-middle Campanian *Globotruncana ventricosa* zone: comments on reliability and global correlations. *Cretaceous Research* 32, 387-405.
- Quillevère, F., Norris, R.D., Berggren, W.A., Aubry, M.P. 2000. 59.2 Ma and 56.5 Ma: two significant moments in the evolution of acarininids (planktonic foraminifera). *GFF Early Paleogene warm climates and biosphere Dynamics* 122, 131-132.
- Quillevère, F., Norris, R.D. 2003. Ecological development of acarininids (planktonic foraminifera) and hydrographic evolution of Paleocene surface waters. S.L. Wing et al. (Ed.) *Causes and consequences of globally warm climates in the early Paleogene*. The Geological Society of America, Boulder, Colorado 369, 223-238.
- Robaszynski, F., Caron, M., Gonzales-Donoso, J.M., Wonders, A.A.H. 1984. The European Working Group on Planktonic Foraminifera. Atlas of Late Cretaceous globotruncanids. *Revue Micropaleontology* 26, 145-305.

- Robaszynski, F., Caron, M. 1995. Foraminifères planctoniques du Cretace; commentaire de la zonation Europe-Mediterranee Bulletin de la Societe Geologique de France 166, 681-692.
- Robinson, A.G., Rudat, J. H., Banks, C. J., Wiles, R. L.F. 1996. Petroleum geology of the Black Sea. Marine and Petroleum Geology 13, 195-223.
- Saner, S. 1980. Batı Pontidlerin ve komşu havzaların oluşumlarının levha tektoniği kuramıyla açıklanması, Kuzeybatı Türkiye. Maden Tetkik ve Arama Dergisi 93-94, 1-19.
- Sarıca, N. 1993. Gökçeada (Kastamonu) yöresinde Kretase/Tersiyer sınırının planktik foraminiferlerle biyostratigrafik incelemesi. Türkiye Jeoloji Kurumu Bülteni 8, 329-345.
- Schiebel, R., Hemleben, C. 2000. Interannual variability of planktic foraminiferal populations and test flux in the eastern North Atlantic Ocean (JGOFS). Deep Sea Research Part II: Topical Studies in Oceanography 47, 9-11, 1809-1852.
- Shackleton, N.J., Corfield, R.M., Hall, M.A. 1985. Stable isotope data and the ontogeny of Paleocene planktonic foraminifera. Journal of Foraminiferal Research 15, 4, 321-336.
- Shirazi, M.P.N., Shams, P., Bahrami, M. 2013. Biostratigraphy and paleoecology of Maastrichtian sediments in the Zagros Basin, Iran. Acta Geologica Sinica (English Edition) 87, 5, 1387-1395.
- Sirel, E. 1991. Cide Bölgesi (Kuzey Turkey) Maastrichtiyende bulunan yeni bir foraminifer cinsi: Cideina n.gen. Maden Tetkik ve Arama Dergisi 112, 149-154.
- Smit, J. 1982. Extinction and evolution of planktonic foraminifera after a major impact at the Cretaceous/Tertiary boundary. Silver, L.T., Schultz, P.H. (Ed.) In Geological implications of impacts of large asteroids and comets on the Earth. Special Papers. Geological Society of America 190, 329-352.
- Sunal, G., Tüysüz, O. 2001. Batı Pontidler'de Tersiyer yaşlı çarpışma sonrası sıkışmalı yapıların özellikleri. Türkiye Petrol Jeologları Derneği Bülteni 13, 1-26.
- Şahintürk, O., Özçelik, Y. 1983. Zonguldak-Bartın-Amasra-Kurucaşile-Cide dolaylarının jeolojisi ve petrol olanakları. Türkiye Petrolleri Anonim Ortaklığı, Rapor No:1816, Ankara.
- Şener, S. 2007. Amasra yöresi (Batı Karadeniz) Üst Jura-Alt Kretase İnalıtı kireçtaşlarının bentik foraminifer paleontolojisi, Yüksek lisans tezi, Ankara Üniversitesi, 76, Ankara, (unpublished).
- Şengör, A.M.C. 1982. Ege'nin neotektonik evrimini yöneten etkenler, Batı Anadolu'nun genç tektoniği ve volkanizması paneli. Türkiye Jeoloji Kurultayı 59-71.
- Thibault, N., Gardin, S. 2007. The late Maastrichtian nannofossil record of climate change in the South Atlantic DSDP Hole 525A. Marine Micropaleontology 65, 163-184.
- Tokay, M. 1954/1955. Filyos çayı ağızı-Amasra-Bartın-Kozcağız-Çaycuma bölgesinin jeolojisi. Maden Tetkik ve Arama Dergisi 46/47, 58-74.
- Toumarkine, M., Luterbacher, H. 1985. Paleocene and Eocene planktic foraminifera. Bolli, H.M., Saunders, J.B., Perch-Nielsen, K. (Ed.) Plankton Stratigraphy. Cambridge University Press 87-154.
- Tüysüz, O. 1993. Karadeniz'den Orta Anadolu'ya bir Jeotravers: Kuzey Neo-Tetisin tektonik evrimi. Türkiye Petrol Jeologları Derneği Bülteni 5, 1-33.
- Tüysüz, O. 2002. Upper Cretaceous red pelagic limestones in the Pontides, northern Turkey and their significance on the geological evolution of Black Sea. Inaugural Workshop of IGCP 463, 30.
- Tüysüz, O., Kırıcı, S., Sunal, G. 1997. Cide-Kurucaşile dolayının jeolojisi. Türkiye Petrolleri Anonim Ortaklığı, Rapor No. 3736, Ankara.
- Tüysüz, O., Aksay, A., Yiğitbaş, E. 2004. Batı Karadeniz bölgesi litostratigrafi birimleri. Stratigrafi komitesi litostratigrafi birimleri serisi-1. Maden Tetkik ve Arama Genel Müdürlüğü Yayınları, Ankara.
- Tüysüz, O., Yılmaz, İ.Ö., Svabnicka, L., Kırıcı, S. 2012. The Unaz Formation: a key unit in the western Black Sea region, N Turkey. Turkish Journal of Earth Sciences 21, 1009-1028.
- Van Eijden, A.J.M. 1995. Morphology and relative frequency of planktic foraminiferal species in relation to oxygen isotopically inferred depth habitats. Palaeogeography, Palaeoclimatology, Palaeoecology 113, 267-301.

- Varol, O. 1983. The Cretaceous-Paleocene calcareous nannofossils from the Kokaksu section (Zonguldak, Northern Turkey). *Geol. Palaont. Abh.*166, 431-460.
- Wade, B.S., Pearson, P.N., Berggren, W.A., Palike, H. 2011. Review and revision of Cenozoic tropical planktonic foraminiferal biostratigraphy and calibration to the geomagnetic polarity and astronomical time scale. *Earth-Science Reviews* 104, 111–142.
- Wilson, P.A., Norris, R.D. 2001. Warm tropical ocean surface and global anoxia during the mid-Cretaceous period. *Nature* 412, 425-429.
- Wilson, P. A., Norris, R. D., Cooper, M. J. 2002. Testing the Cretaceous greenhouse hypothesis using glassy foraminiferal calcite from the core of the Turonian tropics on Demerara Rise. *Geology* 30, 607–610.
- Zachos, J.C., Arthur, M.A., Thunell, R.C., Williams, D. F., Tappa, E.T. 1985. Stable isotope and trace element geochemistry of carbonate sediments across the Cretaceous/Tertiary boundary at Deep Sea Drilling Project Hole 577. *Initial Reports of the Deep Sea Drilling Project* 86, 513-532.
- Zachos, J.C., Arthur, M.A., Dean, W.E. 1989. Geochemical evidence for suppression of pelagic marine productivity at the Cretaceous/Tertiary boundary. *Nature* 337, 61-64.

PLATES

PLATE I

Figure 1- *Abathomphalus mayaroensis* (Bolli), Spiral view, Sample K41.

Figure 2- *Abathomphalus mayaroensis* (Bolli), Umbilical view, Sample K41.

Figure 3- *Contusotruncana contusa* (Cushman), Spiral view, Sample K41.

Figure 4- *Gansserina gansseri* (Bolli), Side view, Sample K39.

Figure 5- *Rugoglobigerina rugosa* (Plummer), Spiral view, Sample K48.

Figure 6- *Heterohelix globulosa* (Ehrenberg), Side view, Sample K32.

Figure 7- *Planoglobulina multicamerata* (De Klasz), Side view, Sample K48.

Figure 8- *Pseudoguembelina hariaensis* Nederbragt, Side view, Sample K48.

Figure 9- *Pseudoguembelina hariaensis* Nederbragt, Side view, Sample K48.

Figure 10- *Pseudoguembelina palpebra* Bronnimann and Brown, Sample K36.

Figure 11- *Racemiguembelina fructicosa* (Egger), Side view, Sample K42.

Figure 12- *Pseudotextularia elegans* (Rzehak), Side view, Sample K48.

PLATE I

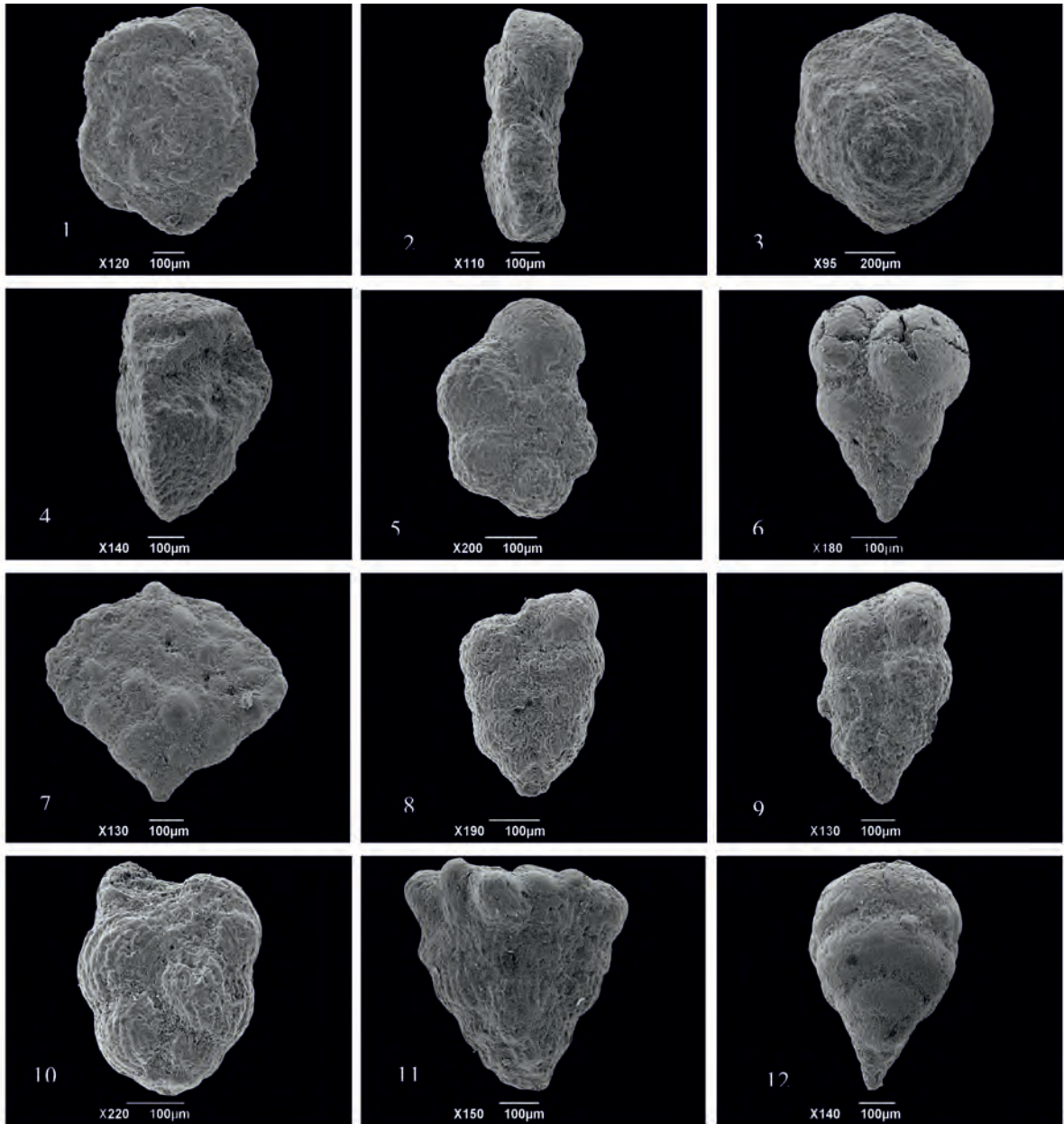


PLATE II

Figure 13- *Parvularugoglobigerina eugubina* (Luterbacher and Premoli Silva), Umbilical view, Sample KD3.

Figure 14- *Parasubbotina pseudobulloides* (Plummer), Spiral view, Sample KD6.

Figure 15- *Parasubbotina pseudobulloides* (Plummer), Side view, Sample KD15.

Figure 16- *Igorina pusilla* (Bolli), Spiral view, Sample KD20.

Figure 17- *Subbotina triloculinoides* (Plummer), Spiral view, Sample KD16.

Figure 18- *Subbotina triloculinoides* (Plummer), Umbilical view, Sample KD20.

Figure 19- *Praemurica uncinata* (Bolli), Spiral view, Sample KD13.

Figure 20- *Morozovella angulata* (White), Side view, Sample KD19.

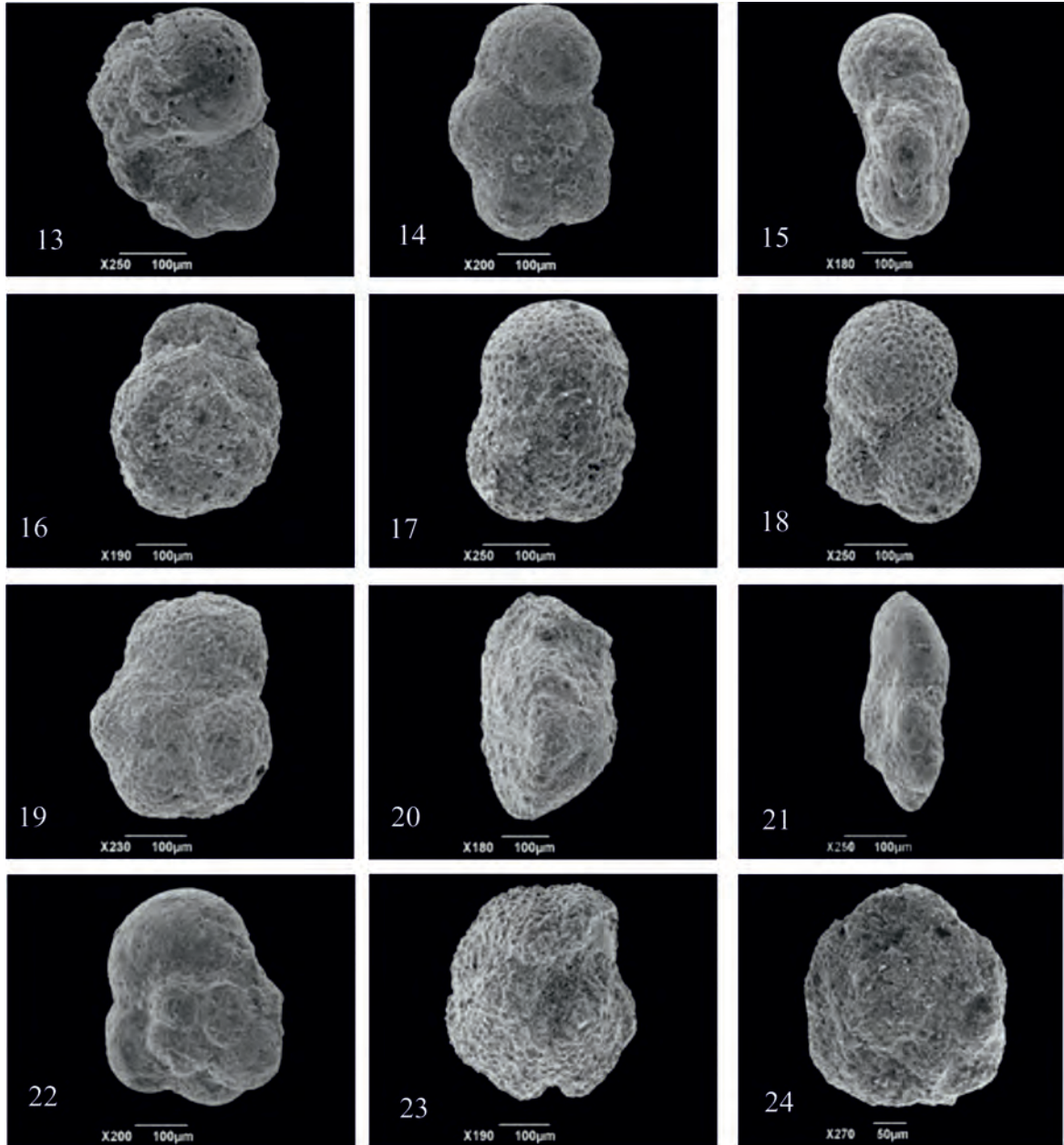
Figure 21- *Globanomalina compressa* (Plummer), Side view, Sample KD12.

Figure 22- *Globoconusa conusa* Khalilov, Spiral view, Sample KD6.

Figure 23- *Morozovella velascoensis* (Cushman), Umbilical view, Sample KD19.

Figure 24- *Morozovella conicotruncana* (Subbotina), Spiral view, Sample KD19.

PLATE II





Bulletin of the Mineral Research and Exploration

<http://bulletin.mta.gov.tr>



SEDIMENTOLOGY, MINERALOGY AND ORIGIN OF THE FIRST DISCOVER MAGNESITE-DOLOMITE BELT IN MA'RIB DISTRICT, SW ARABIAN PENINSULA

Sa'ad Zeki A.kader AL-MASHAIKIE^a

^aDept. of Earth Sciences, Collage of Sciences, University of Baghdad, Al-Jadriyah, Baghdad, IRAQ

Research Article

Keywords:

Magnesite, Dolomite, Metamorphic belt, Al-Thanyiah, Yemen.

ABSTRACT

Magnesite mineralization of high purity was discovered and described herein for the first time from metamorphosed folded belt from Al-Thanyiah locality in Rub'Al-Khali sector, 360 km east of Sana'a City, northwest Yemen. The magnesite-metamorphic belt, belonging to the Precambrian/Neoproterozoic age? comprises thrust belt, which trends generally N-S direction. Magnesite mineralization was identified in an extended carbonate-metamorphic belt for several tens of kilometers cf. 31 km and occurred in association with 8 stratigraphic units. The thicknesses of pure magnesite bearing units are variable and ranges from 20 to 60 m, associated with dark green chlorite-schist with intersecting huge ultrabasic intrusions. Geochemical, mineralogical and petrographic analyses show that the magnesite concentrations in the stratigraphic units are ranging from 78% up to high purity of 99.6% cf. 35 to 48.9% MgO, with minor dolomite and calcite respectively. Little to rare content of talc and brucite were also recognized. Two thick, productive and high purity magnesite beds, the first is of 40 m thick and the second is 60 m in thickness, which reveals more than 95% MgCO₃ and considered to be economic. The suggested origin of the magnesite mineralization is coming from high stress of regional metamorphism associated with ultramafic intrusions cf. amphibolite and harzburgite associated with diagenetic solutions rich in Mg²⁺, associated with the heat of magma. The alteration of dolomite to magnesite was formed by multiple phases to transform calcite and/or dolomite to magnesite.

Received: 18.05.2016

Accepted: 23.06.2016

1. Introduction

Magnesite beds in Al-Thanyiah metamorphic belt are unusual formations in the Arabian Peninsula. The magnesite beds are very thick and of high purity in composition. The belt is lying 360 km east of Sana'a Capital City and 130 km from Ma'rib city. It is extended for more than 31 km in a belt, which is formed by metamorphosed carbonates interbedded with thick green schist beds (Al-Mashaikie, 2006) (Figure 1 and 2).

It is not well understood how the Mg-rich carbonates of Al-Thanyiah area formed and they have attracted the attention of the author because: i) they are among the oldest carbonates preserved in the southern Arabian Peninsula as well as in Yemen, ii) they contain more than one magnesite bearing thick horizons (Al-Mashaikie, 2006, 2007, 2008) and, iii) they record a complex diagenetic history, which may be useful in understanding the mechanisms that resulted in the formation of similar deposits elsewhere in the world.

Magnesite precipitates in the modern coastal and continental environments (Pueyo and Inglés, 1987; Schroll, 2002) as well as in ancient sedimentary sequences (Zachmann, 1989). The formation of magnesite in sedimentary conditions is always considered to be secondary and as a typical product of advanced diagenesis (Müller et al., 1972; Tucker and Wright, 1990). Pohl (1990) distinguished two types of economically important magnesite deposits: 1) cryptocrystalline magnesite with Mg sourced by ultramafic magmatic host rocks (Pohl, 1989), and 2) stratabound lenses of coarse crystalline magnesite, which are associated with marine platform environments such as those examined in this paper.

The magnesite deposits are present as extended thick beds in Al-Thanyiah area without any lens like strata. The magnesite beds are interbedded with dolomite beds as well as thick green schist horizons.

The origin of the second type of magnesite is controversial and there are two main models postulated for its formation. In the first model, magnesite

* Corresponding author: Sa'ad Zeki A.kader Al-Mashaikie, magnesite2006@gmail.com

<http://dx.doi.org/10.19111/bmre.82662>

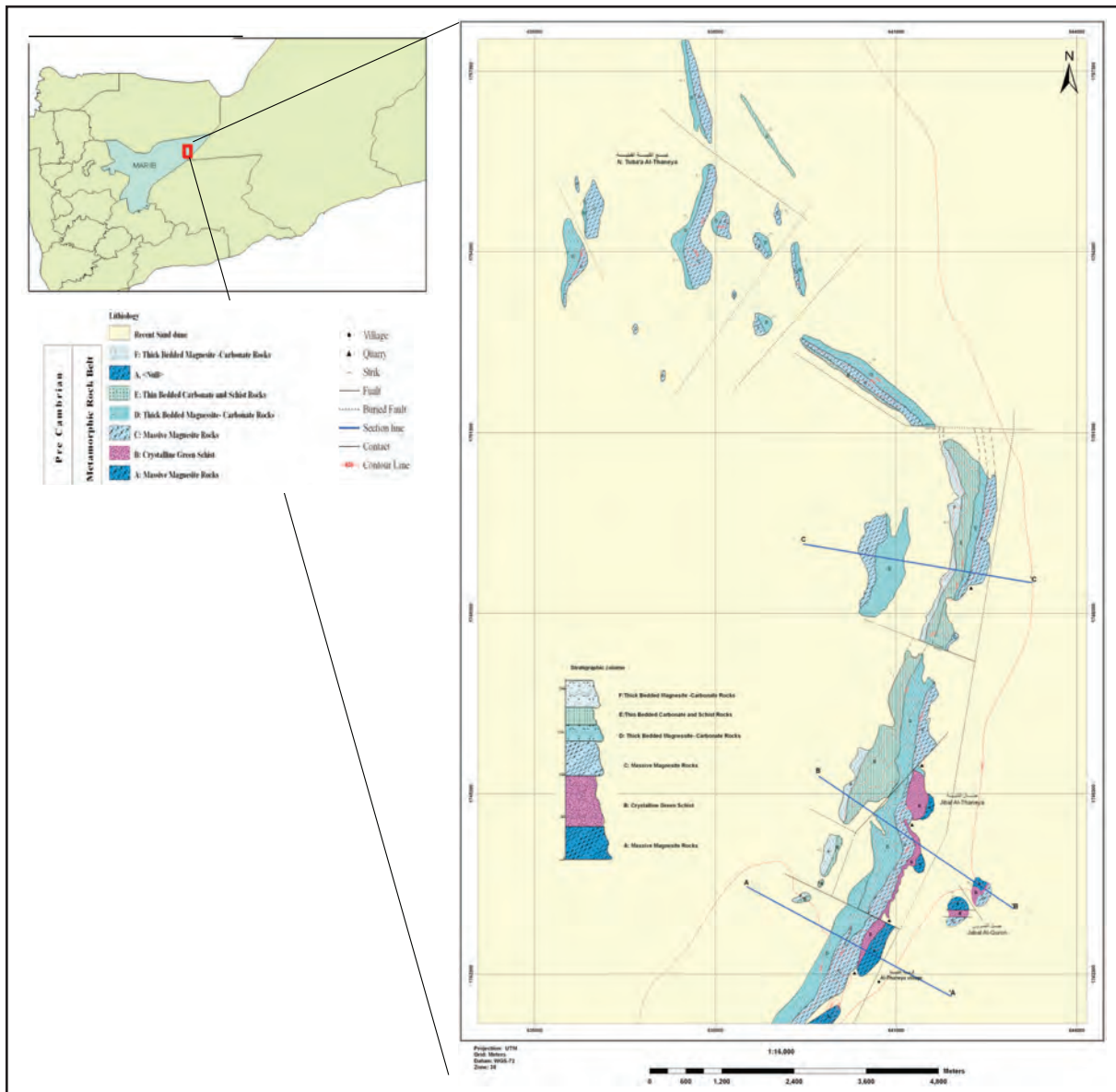


Figure 1- The geological map of the Al-Thanyiah Belt shows the stratigraphic units of the major belt (the map constructed by the author Al-Mashaikie (2006)).

is considered to be a product of syndimentary processes related to evaporitic conditions or to early diagenetic transformations of carbonates (Pohl, 1990; Tucker and Wright, 1990; Melezhik et al., 2001). Magnesite precipitation has been suggested to occur in evaporitic sabkha-type environments (Quemeneur, 1974) or from Mg-concentrated brines originated by early diagenetic compaction of clays (Siegl, 1984).

The second model considers an epigenetic origin, which involves hydrothermal/ metasomatic replacement of dolostones during thermal events (Tucker, 1982; Dulski and Morteany, 1989; Zachmann

and Johannes, 1989; Lugli et al., 2000; Machel and Lonnee, 2002; Kiliyas et al., 2006).

Al-Mashaikie (2006) was discovered and recorded the magnesite rocks belt first time ever. The chemical analysis of collected rock samples show that the percentages of magnesite in these rocks range from 78.22% up to 97.78% with MgO percentages vary from 35.22% up to 47.65%.

Geomine Company (1984-1985) was working in the areas in NW Yemen in the proximity of border of Yemen Arab Republic with Saudi Arabia. They

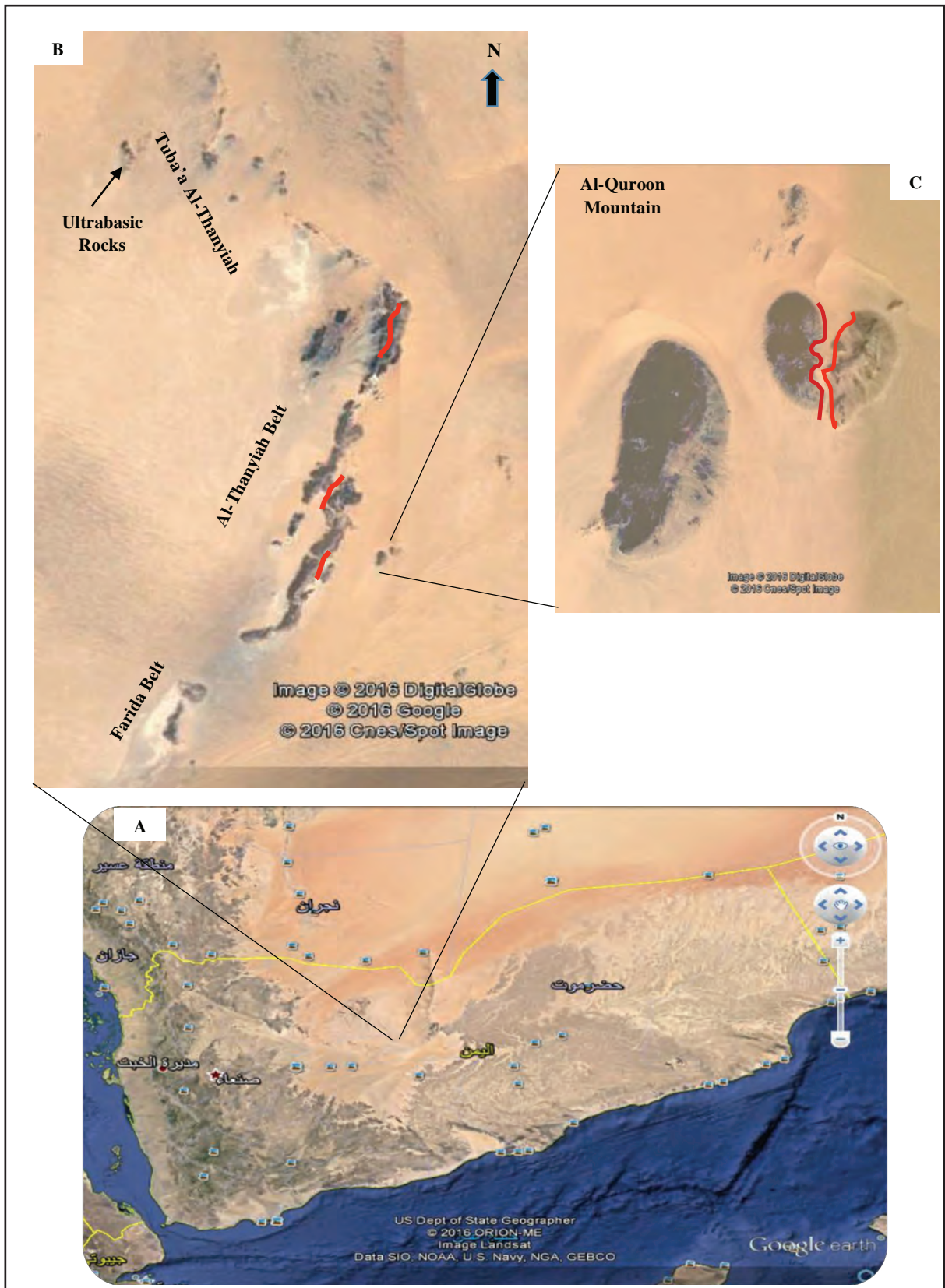


Figure 2- Satellite images show (A) general map of Yemen, (B) The Al-Thanyiah Belt with subdivisions of Fariedah, AL-Thanyiah and Tuba'a Al-Thanyiah belts with the ultrabasic intrusion (the red lines, and (C) Al-Quroon Mountain show large ultrabasic intrusion in between the red lines.

reported several hills amounting about 12 km length and a part as 300m width, and 25-50 m height trending north – south and dip 60-70 ° to the west. They are consisted of marbles (crystalline limestone, dolomitic limestone and dolomites) of various colors including white–gray, gray–yellowish, black–colored with intermediate hues. The rocks have crystalline, granular and granoblastic structures, compact texture, sometimes with vacuoles and irregular breaks (Geomine Company, 1984-1985). Beydoun et al. (1998) referred to rock successions in Al-Thanyiah area as unknown rock units of Cambrian age.

In this paper, we discuss the origin of the magnesite and dolostone of the Neoproterozoic (Ediacaran?) deposits of the Al-Thanyiah metamorphosed belt (Al-Mashaikie, 2006). Sedimentology, petrology, diagenesis and geochemical analyses permit to establish a dataset that characterize magnesite deposits formed under hydrothermal conditions. This model is useful to understand the genesis of similar magnesian deposits in other parts of the world and offers an alternative explanation for magnesite deposits that have been interpreted as products of evaporation processes.

2. Geological Setting

The Neoproterozoic (?) bed rocks are crop out in the Rub'Al-Khali Sector of Northwest Yemen. This area is characterized by extensive exposure of high grade metamorphosed sedimentary series of the Ediacaran (?) schist-greywacke-carbonate complex. Al-Thanyiah Belt surrounded by recent sand dunes of the Rub'Al-Khali Desert (Figure 1 and 2).

The Metamorphic Belt is composed of interbedded thick horizons of magnesite, magnesite/dolomite, dolomite, and green schist (Figure 3). These successions are most probably deposited on a mixed carbonate–siliciclastic platform. These rocks are exposed in an over-thrust fold intersected with several reverse faults. These rocks are not described or recorded previously, and the age is still unknown. The main thrust belt trends almost N-S direction. The geological age suggested herein is according to the stratigraphic correlation with the Oman and Ethiopia (Brasier et al., 2011).

The Neoproterozoic (?) carbonate platform was never reported previously in Yemen. Only a

preliminary report was written after detailed field work and lab analyses for the collected samples (Al-Mashaikie, 2006).

The major belt of Al-Thanyiah outcrops is intersected by major thrust fault forming overturned fold e.g. both structures trend N-S direction. The upthrow part represents the out crop successions e.g. the western part of the mountain, while the eastern down throw part is sinking under the recent sand dunes (Figure 1). All these features are the result of complex tectonic evolution. These magnesite-carbonate metamorphic belt is cut by huge ultrabasic intrusions.

The area is subjected to intense regional metamorphism as the major tectonic event that affected the Precambrian basement rocks in Yemen (Beydoun et al., 1998). This magnesite-carbonate metamorphic belt most probably represents cap carbonate rocks that followed the Ediacaran main glacial period in Yemen.

3. Methodology

Conventional petrography analyses were performed on selected 50 thin sections cut perpendicular to the bedding plane to present all mineralogical constituent and variations in the rock sample, following the procedure listed in Tucker (1988). Polarizing microscope type Leitz-LABOURLUX 12 Pol was used for the petrographic examinations.

Powdered samples (18) were mineralogically examined using Philips PW-1710 X-ray diffraction (XRD) system operating at 40 kV and 40 mA, and employing mono-chromated CuK α radiation. The XRD spectra obtained from 2 to 66° 2 θ . XRD analysis were carried out in the labs of Natural Resources Authority, Amman-Jordan.

Moreover, geochemical analysis were carried out to determine the MgO% and CaO% contents to determine the magnesite concentration in the rocks. The X-ray fluorescence technique was employed a Bruker Tiger S-6 XRF instrument to analyze 23 samples for their major element contents. Both XRD and XRF analyses were carried out in the labs of the Natural Resources Authority in the Hashemite Kingdom of Jordan and labs of University of Beijing in China.

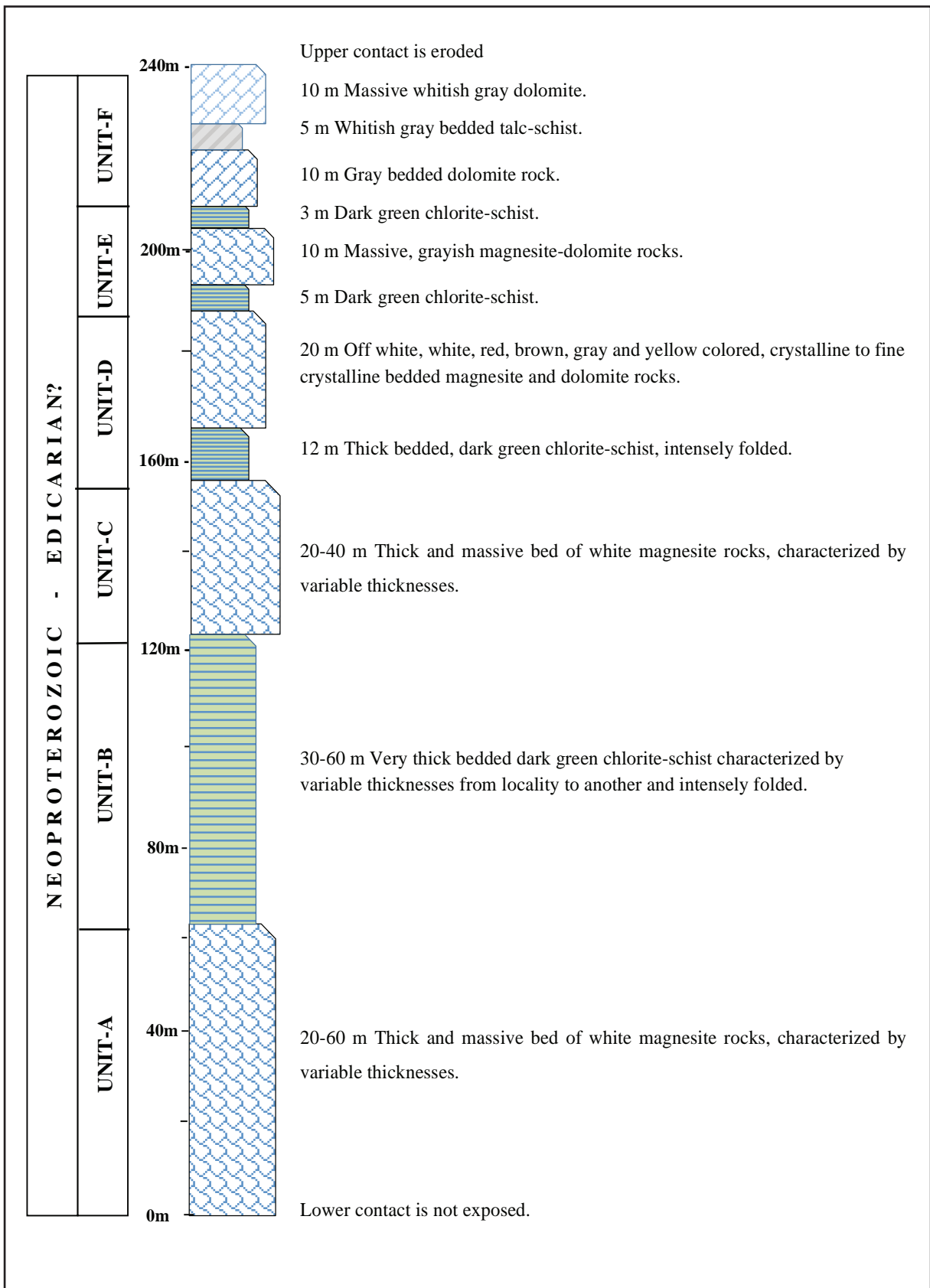


Figure 3- Stratigraphic section of the Al-Thanyiah Belt Rocks presents different stratigraphic units of magnesite, dolomite, chlorite-schist and talc-schist, which are cropping out in the studied area.

4. Field Characteristics of Magnesite Belt

Detailed and comprehensive field works were carried out to examine and define Al-Thanyiah magnesite belt:

Stratigraphic Name: Al-Thanyiah Group is suggested as a new name for this new stratigraphic unit to introduce in the geological column of Yemen, where there is no previous record for it.

Geologic Age: The previous works was not defining the age of Al-Thanyiah belt. Field observations suggest that these rocks are of Neoproterozoic-Ediacaran age, in which the rock successions are underlain by glaciogenic rocks. Moreover, the rocks are intensely tectonized where any fossils were observed.

Morphotectonic: Al-Thanyiah region comprises a carbonate-metamorphic major belt trends generally N-S and surrounded by recent sand dunes. The major belt composed essentially of three belts e.g. southern Fariedah, middle Al-Thanyiah and north Tuba'a Al-Thanyiah. These belts are separated by strike-slip faults, which tends to tilt the south Fariedah toward SE and the Tuba'a Al-Thanyiah toward NW (Figure 2). Two major tectonic events are reported in the Al-Thanyiah belt, overturned fold and the thrusting reverse fault (both are dipping more than 120°). The thrusting reverse fault is intersected the Fariedah and Al-Thanyiah belts along the fold axis and from the eastern side, while the Tuba'a Al-Thanyiah is intersected along the fold axis and from the western side. Several minor normal and over-thrust faults are intersected the bed rocks. The morphotectonic represented by series of low elevation mountains standing up sand dunes of the Yemeni side of the Rub'Al-Khali Desert.

The width of the Al-Thanyiah belt ranges from 0.5 to 1.35 km and extended for more than 31 km the general height ranges from 90 to 135 m above the land surface and the whole area is elevated for 800-900 m above sea level (a.s.l.).

The south Fariedah is extended for about 3 km, middle Al-Thanyiah belt is 17 km and Tuba'a Al-Thanyiah for about 11 km. The geology of the belt reflects some complications due to intense tectonism. According to intense thrusting the eastern limb of Al-Thanyiah major fold was subducted under the sand dunes.

Thickness: The thickness of the whole successions reaches more than 240 m including green schist beds. The magnesite-bearing units attain a part as 15 m up to 60 m thick, while the schist beds are ranging from 6 m up to 70 m in thickness. The intersecting ultra-basic rocks range from 10 m up to 50 m thick.

Boundaries: The upper surface of the carbonate rocks was eroded and sometimes not exposed and the bottom are buried under the sand dunes of the desert.

Sedimentology: The magnesite and dolomite rocks examined here appear in six distinct units at the Al-Thanyiah area. The lower Unit-A was studied in the three main belts of Fariedah, Al-Thanyiah and Tuba'a Al-Thanyiah, sections (Plate I). Carbonate units (magnesite and dolomite rocks) are about 240 m thick and are separated by intercalations of metamorphosed thick and thin siliciclastic beds of most probably sandstones and shales (Plate I, photo 3,6,7, plate II, photo 5,6). The rocks are mostly crystalline, and in places the magnesite crystals reach about 0.1 to 0.3 m in size (Plate II, photo 1).

The successions of the rocks are composed of magnesite, magnesite-dolomite, chlorite-schist, talc-schist, talc, and ultra-basic rocks. These rocks are developed in the areas of the Precambrian basement rocks e.g. granite, schist, talc, ultra-basic igneous rocks, and amphibolite overlies with magnesite-dolomite successions. The basement rocks are intensely tectonized. In the field, the magnesite rocks are white, off-white, gray, red, yellow and black in color with intermixing of white and pink colors. While the dolomite rocks are mostly of gray color.

The six magnesite-carbonate units show similar features although most of their primary structures and textures have been erased by magnesitization and dolomitization processes.

i) Magnesite rocks appear as massive and bedded and sometimes laminated. The massive beds are very thick and attain more than 20 m in thickness (Plate I, photo 2,3,6). These beds consist of coarse mosaic magnesite crystals with little brucite, and talc crystals (Plate III, photo 1-4). Another identified magnesite rocks appears as thin beds. These beds exhibit porphyritic texture represented by coarse crystals surrounded with small crystal (Plate III, photo 5).

ii) Dolomites appear as both massive and thinly bedded/laminated beds. Massive dolomites occur in beds ranging from 0.5 to 2 m in thickness (Plate I, photo 6, Plate II, photo 7). These beds consist of coarse mosaic dolomite including ghosts of dark cloudy twining laminae. In addition, there are undulated laminations that is thought as stromatolite laminations (Dragastan and Richter, 2011; Perri et al., 2012) also confirming the shallow nature of the depositional environment.

iii) Intensely metamorphosed siliciclastic deposits formed by thin (mm-cm) alternations of sandstones and shales (Plate I, photo 3,6). These rocks comprise chlorite-schist and talc-schist, dark green, black, and grayish white in color. The architectural facies arrangement is that characteristic of a mixed carbonate-siliciclastic platform environment, which has been developed during Ediacaran (?) time (IUGS, 2009). The suggested depositional environment was characterized by carbonate deposits that would represent the shallower inter to supratidal facies, whereas the clastic deposits correspond to deeper and higher energy environments (subtidal).

5. Petrography

The magnesites and dolomites of the Al-Thanyiah Group comprises magnesite-carbonate successions intercalated with metamorphosed siliciclastic deposits. The most extensive cases are the formation of magnesite, which shows different textures. In all of Al-Thanyiah three belts, magnesitization advanced through fractures, faulting, cavities, and bedding planes; it was pervasive and totally replaced the dolomitic rocks.

The Al-Thanyiah Belt is intersected with several dikes and intrusive bodies of ultrabasic igneous rocks of peridotite and hornblendite compositions. The peridotite rocks composed of majority olivine and pyroxene with minor anorthite, while the hornblendite is composed totally of hornblende mineral.

In the studied sections of southern Farieda, middle Al-Thanyiah and northern Tuba'a Al-Thanyiah belts (Plate I, photo 1-5), replacement mostly advanced totally for the magnesite-productive beds. The main dominant mineral is magnesite with minor dolomite, calcite, talc, brucite and rarely forsterite.

Magnesite

Magnesite was identified as four different diagenetic textural phases termed M1, M2, M3 and M4.

1. Magnesite 1 (M1) is composed of unimodal, euhedral, planar boundary and mosaic very coarse crystals with strong undulatory extinction. Crystal size ranges from mm to several centimeters. M1 is free of Fe-minerals (Plate III, photo 2) and associated with minor talc and brucite minerals. No relics exist of the previous texture of the rock. This magnesite initially occurs along cavities, fracture and fault planes (Plate II, photo 1,5,6,8), and ultimately totally replace the previous dolomite rocks to form a massive beds of magnesite.
2. Magnesite 2 (M2) is composed of bimodal, subhedral, planar and irregular boundary crystals with strong undulatory extinction. Crystal size ranges from mm to several centimeters. M2 is also free of Fe compounds (Plate III, photo 3) and associated with minor talc and brucite minerals. No relics exist of the previous texture of the rock. This magnesite initially occurs along cavities, fracture and fault planes and ultimately totally replace the previous dolomite rocks to form a massive beds of magnesite.
3. Magnesite 3 (M3) is composed of unimodal, anhedral, non-planar boundary crystals with undulatory extinction. Crystal size ranges from mm to several centimeters. M3 is free of Fe-minerals crystals (Plate III, photo 4) and associated with minor talc and brucite minerals. No relics exist of the previous texture of the rock. This magnesite initially occurs along cavities, fracture and fault planes and ultimately completely replace the previous dolomite rocks to form a massive beds of magnesite.
4. Magnesite 4 (M4) is composed of porphyritic bimodal, subhedral planar to non-planar boundary crystals with undulatory extinction. M4 is totally free of Fe-minerals (Plate III, photo 5) and associated with minor dolomite, talc and brucite minerals. No relics exist of the previous texture of the rock. This magnesite initially occurs along cavities, fracture and

fault planes and ultimately totally replace the previous dolomite rocks to form a massive beds of magnesite.

Dolomite: Two different dolomite textures were identified (D1 and D2):

1. Dolomite 1 (D1) is characterized by non-planar, anhedral closely packed with subhedral crystals (0.01 to 0.3 mm) with undulatory extinction (Plate III, photo 5). The dolomite crystals are with cloudy shades.
2. Dolomite 2 (D2) consists of mosaic of coarser, 0.1 to 1 mm size crystals. Most crystals are clear and mostly have planar and non-planar crystal boundaries. The crystals are characterized by bands of cloudy shades (Plate III, photo 6). D1 and D2 textures are of low percentages in the magnesite-productive units. This is identified from the petrographic examination and confirmed by the XRD and XRF analyses.

Talc: Talc appears as scattered euhedral to subhedral laths and was recognized in all of the studied beds. Talc is commonly associated with coarse magnesite crystals along fractures or between the boundaries of the crystals. It is almost lath like shape and sometimes present as aggregates (Plate III, photo 5,6).

Brucite: Brucite is recognized in all of the studied rock samples and associated with magnesite mineral. It was identified as single crystal appears in the boundaries between magnesite and dolomite crystals, and along the fractures and micro-fault planes. It attains prismatic or irregular crystal shapes (Plate III, photo 3).

Other diagenetic minerals: Calcite was identified as fine crystals and rare to minor mineral in some of the studied samples. It is most probably of late diagenetic origin. Moreover, some clay minerals cf. montmorillonite, were identified due to diagenetic alteration of talc and brucite minerals.

6. Mineralogy

The XRD analyses were performed for selected samples collected from different localities across the Al-Thanyiah Belt. The results showed that the majority of the samples are magnesite with minor dolomite, talc, brucite, calcite, and sometimes montmorillonite clays (Table 1 and 2, Figure 4). Table 2 shows that 5 samples comprise magnesite productive horizons, which are composed of MgO % from 75 to 95%. The other samples are dolomitic magnesite, dolomites and two samples are marble rocks

7. Geochemistry

Geochemical analyses were carried out using XRF technique to define and confirm the presence of magnesite deposits and to differentiate the associated dolomite and calcite minerals and rocks. The results of XRF analyses are listed in table 3. These results are coincided with the XRD analyses.

Element composition: Average composition of the major oxides in the studied samples is listed in table 3. The XRF analyses reveal four productive units containing magnesite with high MgO wt. % concentrations. The MgO concentrations in these beds range from 43.69 % up to 45.6 %, while the CaO

Table 1- The XRD results of selected rock samples from Al-Thanyiah region shows the relative abundance of the mineralogical constituents of essential magnesite, calcite and dolomite minerals with minor talc, brucite and quartz (Labs of Authority of natural resources Amman-JORDAN).

| Sample no | Calcite | Quartz | Muscovite | Dolomite | Magnesite | Smectite | Brucite | Talc | Kaolinite | Ilmenite |
|-----------|---------|--------|-----------|----------|-----------|----------|---------|------|-----------|----------|
| S-1 | * | - | - | * | *** | * | - | * | - | - |
| N-3 | *** | ** | * | - | - | * | - | - | - | * |
| N-4/3 | - | - | - | *** | - | * | * | - | - | - |
| N-5 | * | - | - | *** | *** | * | * | - | - | - |
| N-8 | - | - | - | *** | - | * | * | * | * | - |
| N-7 | - | *** | - | *** | * | - | - | * | - | - |
| N-2 | - | *** | - | *** | - | * | * | - | - | - |
| N-7/2 | - | - | - | *** | * | * | * | * | - | - |
| N-4 | * | - | - | * | *** | * | * | * | - | - |
| G-M | *** | * | * | ** | - | * | * | - | - | - |

Major *** Minor ** Trace *

Note: All of the samples are form carbonate rocks e.g. magnesite, dolo-magnesite, dolomite and marble (calcite).

Table 2- XRD results of selected rock samples from Al-Thanyiah region shows the mineralogical constituents includes essential magnesite, dolomite and calcite minerals with minor talc, brucite and quartz (Analysis was carried out in the University of Beijing-CHINA).

| Örnek no. | Mineralogical constituent % | | | | | | | | | | | |
|-----------|-----------------------------|---------|--------|------|--------|----|----------|---------------|-----------|----------|--------|--------|
| | Manyezit | Dolomit | Kalsit | Talk | Brusit | Q | Feldspat | Mika-Muskovit | Serpantin | Periklas | Klorit | Toplam |
| N4-L1 | 95 | 1 | | 4 | 1 | | | | | | | 100 |
| N5 | 94 | | | 6 | | | | | | | | 100 |
| N6-L1 | 85 | 1 | | 13 | | 1 | | | | | | 100 |
| N7-L1 | 86 | | | 14 | | | | | | | | 100 |
| N3-L1 | | 98 | | 2 | | | | | | | | 100 |
| N8-L1 | 75 | 22 | | 3 | | | | | | | | 100 |
| N9-L2 | 68 | 28 | | 4 | | | | | | | | 100 |
| R1-3 | 60 | 32 | | 8 | | | | | | | | 100 |
| R1-2 | 51 | 42 | | 6 | 1 | | | | | | | 100 |
| R2-2 | 39 | 52 | | 8 | 1 | | | | | | | 100 |
| R2-4 | 1 | 94 | | 5 | | | | | | | | 100 |
| N4-L3 | 2 | 94 | | | 1 | | | | 3 | | | 100 |
| N10-L1 | | 98 | | | | | 2 | | | | | 100 |
| N6-L2 | | 83 | 1 | 16 | | | | | | | | 100 |
| N7-L3 | | 82 | 1 | | | | 13 | | | 4 | | 100 |
| N2-L1 | 8 | 73 | | 14 | | 5 | | | | | | 100 |
| N10-L2 | | | 98 | | | 2 | | | | | | 100 |
| N10-L4 | | | 67 | | | 23 | | 10 | | | | 100 |

R=Fariedah Belt N 1-8 =Al-Thanyiah Belt N10 = Tuba'a Al-Thanyiah samples

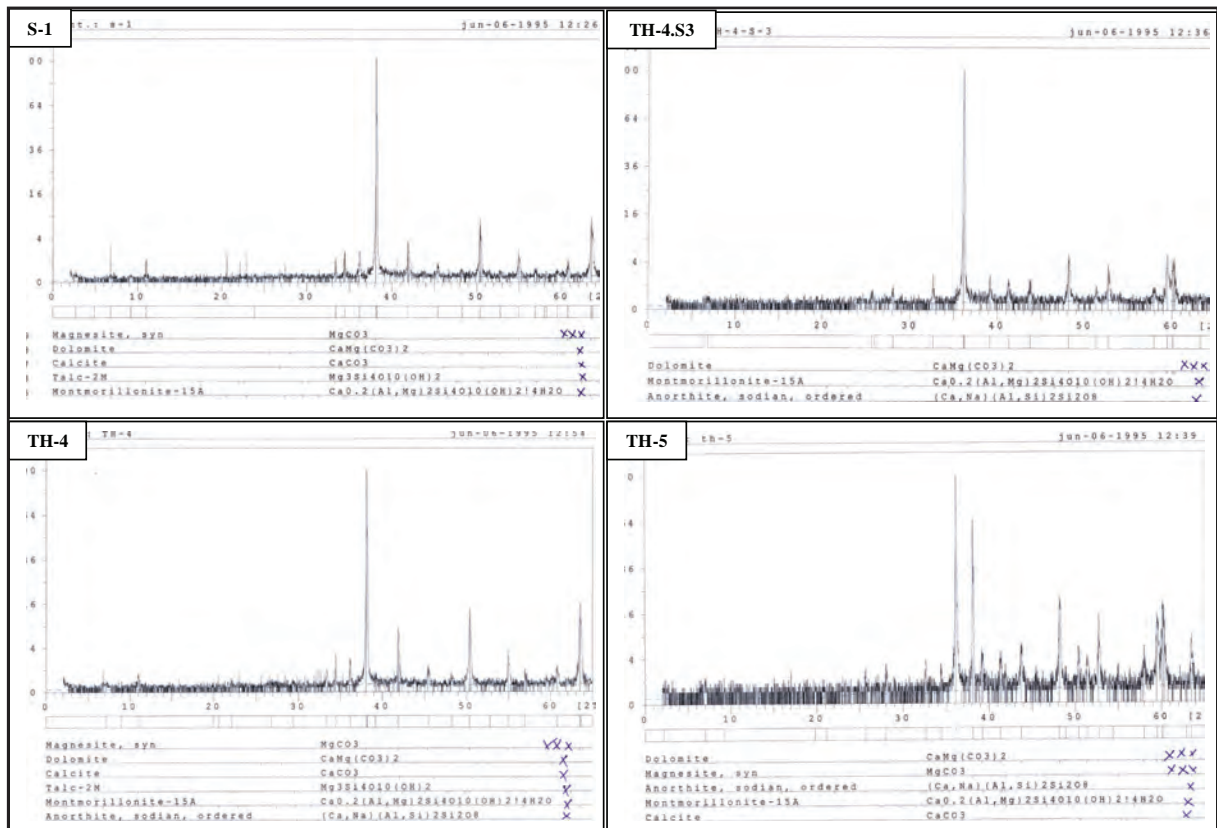


Figure 4- XR-Diffractograms of selected sample shows the majority of magnesite mineral in the productive beds with minor dolomite and rare calcite and talc minerals.

concentrations in the same beds are 0.09 % to 0.54 % respectively. Otherwise, the XRF analyses show six beds composed of almost pure dolomites, with two marble beds composed of pure calcite.

Three of magnesite phases are similar M1, M2 and M3 e.g. N4-L1, N5, N6-L1, while N7-L1 is differ in MgO% (45.6, 45.39, 43.76wt. %), FeO (0.37, 0.38, 0.3wt. %), and MnO % (0.007, 0.002, 0.012), respectively, while M4 e.g. N7-L1 has MgO % (43.69), FeO % (0.19) and MnO % (0.014).

8. Discussion

The critical examination of the different textures observed in the outcrop and thin section studies and their relationships, along with the geochemical characteristics permit to establish the sequence of diagenetic events that lead to the formation of the phases previously described (Figure 5).

A. First Dolomitization Event: The pre-existing limestones which was deposited in a mixed siliciclastic-carbonate platform is undergone intense dolomitization (Figure 5). Dolomitization processes only partially preserved the original depositional texture of the priory limestone. D1 and D2 are the result of replacement processes via the circulation of Mg²⁺ rich solutions, most probably created by progressive evaporation of marine waters within the peritidal environment (sabkha dolomitization model) (Morse and MacKenzie, 1990). Moreover, during the field works, the stromatolite algae were preserved in some examined beds, which refers to the formation of symsedimentary dolomites in the presences of microbial math cf. microbialites, in shallow marine setting (Prasannakumar et al., 2002; Teedumäe et al., 2006; Wacey et al., 2007; Spadafora et al., 2010; Herrero et al., 2011; Nash et al., 2011; Meister et al., 2013). The textural and geochemical evidences do not evoke a clear dolomitization mechanism due to intense tectonism and the rocks components

Table 3- XRF-Geochemical analysis results of selected samples from Al-Thanyiah region (Analysis was carried out in the University of Beijing-CHINA).

| Sample no. | Major oxides % | | | | | | | | | | | |
|------------|----------------|-------|-------|-------|------|-------|------|-------|-------|-------|-------|-------|
| | Al2O3 | CaO | MgO | Fe2O3 | SiO2 | MnO | Na2O | K2O | P2O5 | TiO2 | LOI | Total |
| N4-L1 | 0.34 | 0.54 | 45.6 | 0.37 | 3.21 | 0.007 | 0.22 | 0.01 | 0.005 | 0.014 | 49.55 | 99.86 |
| N6-L1 | 0.28 | 1.34 | 43.76 | 0.3 | 5.98 | 0.012 | 0.18 | 0.01 | 0.016 | 0.013 | 47.99 | 99.88 |
| N7-L1 | 0.28 | 0.09 | 43.69 | 0.19 | 4.84 | 0.014 | 1.94 | 0.01 | 0.003 | 0.014 | 48.74 | 99.81 |
| N3-L1 | 0.39 | 30.51 | 19.27 | 0.2 | 2.8 | 0.038 | 0.65 | 0.01 | 0.011 | 0.01 | 46.02 | 99.91 |
| N8-L1 | 0.28 | 9.28 | 38.09 | 0.39 | 3.38 | 0.001 | 0.01 | 0.01 | 0.005 | 0.015 | 48.43 | 99.88 |
| N9-L2 | 0.22 | 16.96 | 30.73 | 0.28 | 4.25 | 0.002 | 0.91 | 0.01 | 0.001 | 0.013 | 46.48 | 99.86 |
| R1-3 | 0.45 | 15.83 | 31.77 | 0.17 | 5.33 | 0.001 | 0.19 | 0.01 | 0.003 | 0.014 | 46.12 | 99.87 |
| R1-2 | 0.28 | 20.88 | 27.86 | 0.32 | 4.71 | 0.002 | 0.5 | 0.01 | 0.005 | 0.014 | 45.3 | 99.87 |
| R2-2 | 0.32 | 21.11 | 27.44 | 0.31 | 3.67 | 0.003 | 0.76 | 0.01 | 0.003 | 0.014 | 45.95 | 99.89 |
| R2-4 | 0.27 | 30.05 | 20.09 | 0.41 | 2.87 | 0.01 | 0.81 | 0.01 | 0.011 | 0.14 | 45.34 | 99.88 |
| N4-L3 | 0.22 | 30.62 | 20.42 | 0.2 | 2.7 | 0.059 | 0.24 | 0.01 | 0.007 | 0.013 | 45.48 | 99.81 |
| N10-L1 | 0.32 | 30.82 | 19.39 | 0.08 | 1.99 | 0.05 | 0.49 | 0.01 | 0.003 | 0.013 | 46.78 | 99.9 |
| N6-L2 | 0.15 | 30.09 | 20.15 | 0.33 | 4.66 | 0.002 | 0.84 | 0.01 | 0.002 | 0.012 | 43.66 | 99.89 |
| N7-L3 | 1.52 | 29.46 | 18.48 | 0.58 | 5.24 | 0.086 | 0.59 | 0.16 | 0.015 | 0.031 | 43.76 | 99.9 |
| N2-L1 | 0.31 | 26.33 | 21.26 | 0.37 | 9.85 | 0.004 | 0.39 | 0.01 | 0.001 | 0.013 | 41.37 | 99.89 |
| N10-L2 | 0.71 | 51.86 | 0.31 | 0.3 | 4.79 | 0.007 | 0.79 | 0.21 | 0.011 | 0.008 | 40.9 | 99.88 |
| N10-L4 | 0.97 | 50.58 | 1.9 | 0.3 | 5.18 | 0.009 | 0.93 | 0.32 | 0.006 | 0.001 | 39.68 | 99.88 |
| N4-L2 | 0.011 | 29.9 | 21.9 | 0.54 | 1.98 | 0.081 | 0.05 | 0.007 | 0.007 | 0.002 | 45.5 | |
| N3 | 0.85 | 50.8 | 1.54 | 0.33 | 5.02 | 0.02 | 0.02 | 0.669 | 0.013 | 0.022 | 40.1 | |
| N4 | 0.00 | 1.25 | 47.6 | 0.028 | 2.14 | 0.001 | 0.00 | 0.08 | 0.00 | 0.00 | 49.0 | |
| N5 | 0.4 | 0.48 | 45.39 | 0.38 | 3.59 | 0.002 | 0.11 | 0.01 | 0.003 | 0.014 | 49.49 | 99.86 |
| N7 | 0.00 | 11.6 | 11.7 | 0.25 | 57.1 | 0.023 | 0.01 | 0.001 | 0.018 | 0.00 | 19.2 | |
| N8 | 0.56 | 27.1 | 23.6 | 0.944 | 6.5 | 0.085 | 0.05 | 0.002 | 0.015 | 0.019 | 41.1 | |

R=Fariedah Belt N 1-8 =Al-Thanyiah Belt N10 = Tuba'a Al-Thanyiah samples


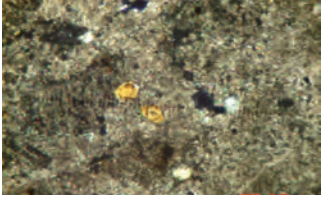

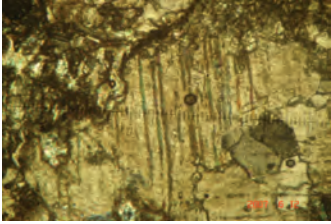


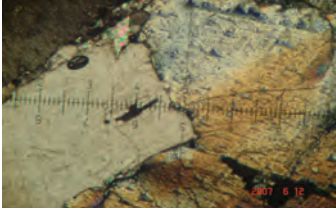
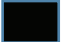
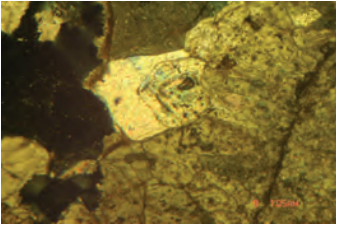

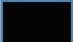

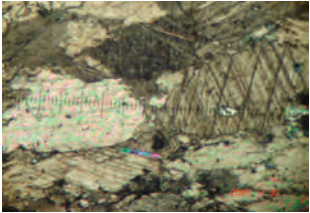
| DIAGENETIC PHASE | EXPOSED TO SHALLOW BURIAL | INTERMEDIATE TO DEEP BURIAL | UPLIFT | TEXTURAL RELATIONSHIPS |
|------------------------|---|---|---|---|
| DOLOMITIZATION |  | | |  |
| FRACTURE I | |  | |  |
| STYLOLITE | |  | | |
| HYDROTHERMAL MAGNESITE | |  | |  |
| FRACTURE II | | |  |  |
| BRECCIATION | | |  | |
| HYDROTHERMAL DOLOMITE | | |  | |
| LATE CALCITE | | |  |  |

Figure 5- Diagenetic sequence inferred for the Al-Thanyiah Group carbonates in the study area. Bars indicate the relative depths of different diagenetic events. The transition between shallow burial and intermediate-to-deep burial is interpreted as the onset of stylolization; the transition from burial to uplift is defined by the initiation of the retrograde thermal history.

were metamorphosed. The fact that the sedimentary structures are preserved may indicate a dolomitization process in a not too advanced diagenetic stage. Dolomites seem to be the dominant carbonates within the Precambrian sedimentary record (Tucker and Wright, 1990; Melezhik et al., 2001; Prasannakumar et al., 2002; Melezhik and Fallick, 2003; Herrero et al., 2011).

The origins of these rocks have been widely disputed (Tucker, 1982), though there are data to suggest that in that time, the physical conditions (T and P_{CO_2}) and Mg^{2+}/Ca^{2+} ratios would promote dolomitization processes whereby preexisting calcite was replaced by dolomite.

In the upper Proterozoic and lower Paleozoic, the $\delta^{18}O$ signature of marine carbonate material was significantly lower than those deposited later on (Allan and Wiggins, 1993). D1 and D2 dolomite phases were probably formed at this time period, where low temperature dolomite acquired this low $\delta^{18}O$ signature during formation (Allan and Wiggins, 1993). These dolomites were later on totally recrystallized during burial and metamorphism and this might further lower the $\delta^{18}O$ values (Allan and Wiggins, 1993). The recrystallization is also confirmed by the coarser crystal size of dolomite and other components when it replaces either mud dominated carbonates or grain dominated carbonates. Later recrystallization of these dolomitic rocks during burial and subsequent metamorphism caused an increase in crystal size and homogenization of geochemical signatures (Sibley and Gregg, 1987; Morse and Mackenzie, 1990; Moore, 2001; Prasannakumar et al., 2002; Herrero et al., 2011).

The absence of stylolites affecting magnesite cf. M1-M4 and dolomite D1 and D2 is an indication of the burial and chemical compaction as well as intense tectonic activities in that these magnesites and dolomites subjected. Accordingly, this replacement event should represent burial and metamorphism stages or, as interpreted above, the resetting by recrystallization of initial geochemical signatures.

B. Genesis and Origin of The Magnesite Belt: The main requirements for magnesite formation through dolomite replacement include an increase in the Mg^{2+}/Ca^{2+} ratio and P_{CO_2} . Compaction, metamorphism

and ultra-basic rocks intrusion during burial of the Al-Thanyiah Group affected siliciclastic deposits, specifically shales, which supplied water enriched in Mg^{2+} , as well as hydrothermal solutions rich in Mg^{2+} comes from ultra-basic intrusions.

In addition, during diagenesis, fluids enriched in Mg^{2+} may have been formed by Mg-liberating reactions resultant of the formation of chloritization (Morteani et al., 1982; Lugli et al., 2002). This water increased the Mg^{2+}/Ca^{2+} ratio and contributed to magnesite precipitation (Möller, 1989). Experimental work (Franz, 1989) suggests that the stability field of magnesite ranges from very low temperatures and pressures (sedimentary environment) to extremely high temperature conditions (upper mantle). A higher temperature shifts the mineral stability from the dolomite stability field to the magnesite field (Johannes, 1970; Kralik et al., 1989; Prasannakumar et al., 2002; Herrero et al., 2011). Hence, processes such as Mg^{2+} enriched hydrothermal fluid circulations could both enhance Mg^{2+}/Ca^{2+} ratios in fluids and contribute to increase temperature conditions (Siegl, 1984; Herrero et al., 2011). Magnesite appears in outcrop replacing both the dolomite and the dolomitic limestone rocks. The replacement front is appreciable in the field and the textural relationship of the magnesite to fractures, fault planes, large cavities and vugs and bedding planes reveals that the hydrothermal fluids used them as conduits to pass through the rocks (Lugli et al., 2000). The extent and distribution of replacement was controlled by the location of fractures, the nature of the precursor rock and the permeability and the capacity of the solution to pass through (Smith and Davies, 2006).

Magnesite formation is possible at both low and high contents of CO_2 in the fluid phase (Möller, 1989). However, an increase in CO_2 pressure favors the precipitation of magnesite (Möller, 1989) at moderate temperatures. Hydrothermal fluids would increase the CO_2 pressure, similarly to the increase of CO_2 volume produced by metamorphism of calcareous sequences by emplacement of igneous intrusions (Morad, 1998).

The formation of magnesite with iron rich rims (M2), has been explained by Johannes (1970) to be due to retrograde metamorphism. In M2, the decrease in Fe and Mn as the Mg content increases is the outcome

of iron and manganese being usually incorporated into the solid phase, whereas magnesium, strontium and barium are preferentially left in the fluid. This leads to a distinct zoning of magnesite, with more Fe-poor cores and Fe-rich rims as temperature decreases (Johannes, 1970). As magnesite precipitates, residual fluids are enriched in calcium.

According to the field observations and petrographic examination of the magnesite-bearing horizons, the magnesite formation took place during hydrothermal fluid circulation events derived from the ultra-basic intrusions associated with intense tectonic events. It could also be modified in response to water-rock interactions or by contributions of oxidized carbon with meteoric waters (Souza et al., 1995).

The studied rocks have undergone several diagenetic processes associated with metamorphic alteration events e.g. thermal metamorphism by intrusion of ultra-basic magma, rather than resulting from interactions with later post-depositional diagenetic fluids.

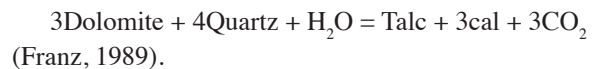
Magnesites are most probably interpreted as a result of heating up the circulating and related formational and diagenetic fluids, which have reacted with the original dolomites and metamorphic rocks, and probably associated with meteoric waters and/or reactions with underlying basement rocks e.g. schist and granitic rocks (Veizer, 1989).

Magnesite appears to have formed subsequently to stylolitization of the first dolomite rocks (D1 and D2). At least 500 m of burial is required for stylolite formation in limestones (Fabricius, 2000). Brecciation and boxwork vugs structures (which is observed in the field) are attributed to hydro-fracturing (Davies, 2004; Smith and Davies, 2006) produced when the fluids were expelled along high permeability faults and fractures into the surrounding strata. The fluids were injected into the sequence, causing brecciation and fracturing of the host rock by pressure release (Prasannakumar et al., 2002; Smith and Davies, 2006; Herrero et al., 2011).

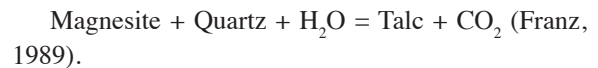
When the pore size is large enough to be appreciable at outcrop scale e.g. as it is observed in the field, it is observed that they appear aligned to faults and bedding planes and in close relation to the magnesite formation front. Therefore, dolomite

is interpreted to have been formed postdating the magnesitization event, and that the dolomitizing fluids entered though the rocks using similar pathways, where dolomite formed due to magnesite replacement caused by interaction with hydrothermal fluids (Lugli et al., 2000; Kiliyas et al., 2006). It is most probably suggested that both dolomite and magnesite rocks are formed under the influence of the same evolving hydrothermal fluids comes from ultra-basic intrusions.

Talc appears in the boundaries between the crystals of magnesite and dolomite and in joints, fractures and stylolites within the magnesite and later dolomite phases. The reaction assumed for the main stage of talc mineralization within dolomite rocks is:



The reaction of talc formation from magnesite is:



The latter reaction may even occur at low temperatures (Winkler, 1988). Bucher and Frey (1994) described the formation of talc through decarbonation reactions of magnesite at temperatures lower than 500 °C and from fluids of low P_{CO_2} .

The formation of talc from dolomites occurs at temperatures between 300 °C and 400 °C. Therefore, the presence of talc related to D1 and D2 implies that these dolomites underwent temperatures as high as 400 to 500 °C.

The presence of forsterite associated to the magnesite provides additional clues to interpret the interaction of the studied rocks with hydrothermal fluids. Experimental work has shown that by rising total fluid pressure and P_{CO_2} , and decreasing temperature, forsterite can form through the reaction of talc and magnesite (Franz, 1989).

$\text{Talc} + \text{Magnesite} = \frac{1}{4} \text{Forsterite} + \text{CO}_2 + \text{H}_2\text{O} \dots$ at almost 400-500°C associated with high compressional pressure

Dolomite and talc probably formed under the influence of hydrothermal fluid, and the later should be cooling of this fluid and varying chemical composition led to the formation of forsterite.

The brucite appears in the fractures, boundaries between magnesite crystals or embedded in the magnesite crystals. The brucite is most probably formed by hydration of magnesite mineral during diagenetic phases (Keer, 1975).

C. Late Calcite Cement: Calcite appears as a late diagenetic phase filling intracrystalline pores, displaying consistent Fe zoning. This Low-Mg calcite suggests that the rocks were exhumed and subjected to surficial diagenetic processes (Moore, 2001). This idea confirms the inferred oxidation conditions in a meteoric surface environment interpreted for the increase in Fe⁺² contents (Pierson, 1981). This late diagenetic calcite reduces porosity and permeability in outcrop.

9. Conclusion

The detailed analysis of the magnesite and dolomite phases in newly introduced Al-Thanyiah Group permits to constrain the model of formation and conditions that accounted for their development. Detailed sedimentological, petrographic and geochemical analyses of the magnesite-carbonate rocks that most probably belong to Neoproterozoic-Ediacaran (?) succession reveals a complex paragenetic evolution. The studied area located 360 km east of Sana'a City and 130 km east of Ma'rib city.

Based on facies association analyses and their vertical and lateral stacking pattern, the sequence is interpreted as a mixed siliciclastic-carbonate platform. The age of the succession suggested as Ediacaran based on the regional stratigraphic correlation with the Oman and Ethiopia, where there are no any fossils content observed. These rocks have suffered from intense metamorphism and associated transformations. Magnesite, dolomite and minor traces of talc, brucite and very rare forsterite together with geochemical data and outcrop observations reveal that the principal processes that affected these rocks were related to burial diagenesis, ultrabasic intrusions e.g. peridotite and hornblendite. and associated up heated diagenetic fluids circulation. Two early dolomite phases (D1 and D2) appear as crystalline replacive dolomite, which formed through dolomitization of the original peritidal limestones under evaporative conditions. Crystal sizes variations between D1 and D2 depend on the texture of the precursor limestone. The recrystallization of these dolomites took place during burial. Cross-checking

the field observations together with petrographic examinations indicate that the magnesite (M1, M2 and M3) were formed through the replacement of D1 and D2 by Mg⁺² enriched fluids that entered the system via stylolite, vugs, faults, fractures and bedding planes. The enriched Mg⁺² in the fluids were probably sourced by compaction of lateral detrital sediments and the transformation of clays into chlorites. These are basically associated with intense tectonism and metamorphism.

In addition, possible Mg⁺² enriched up heated fluids e.g. heat comes from introduced ultrabasic rocks, may have contributed to increase the Mg⁺²/Ca⁺² ratio and temperature. The absence of zoning of the magnesite phases into an initial iron-poor phase reflects variations towards lower temperature conditions. Talc, brucite, forsterite and the late dolomites formed in relation to hydrothermal fluids. Talc associated with dolomite could have formed through de-carbonation of magnesite at temperatures lower than 500 °C. Forsterite formed through the reaction of talc and magnesite, probably as the fluids cooled down probably at temperature more than 500 °C.

A late diagenetic calcite phase appears in some samples replacing magnesite and dolomite phases. This low-Mg calcite was precipitated during telodiagenesis, when the rocks interacted with surficial fluids of meteoric origin.

Although some questions such as the precise temperature and the mechanisms of circulation of the up heated fluids remain unclear, our study reveals that the occurrence of magnesite deposits within the Al-Thanyiah Group is the result of complex diagenetic and heated processes associated with intense tectonism and metamorphism e.g. compressional pressure. Both the prior dolomites and the presence of siliciclastic beds suggest an important role for these deposits in the formation of magnesitization fluids. The textural characterization both in the field and in thin section analysis of the magnesite and dolomite as well as their geochemical signatures permits to develop a model of their origin and mechanism of formation that supports the hydrothermal origin of spary magnesite by replacement of precursor dolomites, similarly to those described in other magnesite deposits like those of the Eugui or Rubian deposits in Spain (Lugli et al., 2000; Kiliyas et al., 2006).

References

- Allan, J.R., Wiggins, W.D. 1993. Dolomite reservoirs; geochemical techniques for evaluating origin and distribution: American Association of Petroleum Geologists Continuing Education Course Note Series 36, 129p.
- Al-Mashaikie, S. Z. 2006. Preliminary Report; Petrography and geochemistry of Al-Thanyiah magnesite-carbonate belt in Ma'rib District, NW Yemen. Geological Survey and Mineral Resource Board, Ministry of Oil, Sana'a, Yemen, 34p.
- Al-Mashaikie, S. Z. 2007. Petrography, geochemistry and technical report of the Carbonate - Magnesite rocks belt in Al-Thanyiah region NE YEMEN, Unpublished Geological Research. Geological Survey and Mineral Resource Board, Ministry of Oil, Sana'a, Yemen, 82p.
- Al-Mashaikie, S. Z. 2008. Geochemistry, mineralogy and industrial evaluation of the first discover of Magnesite – Carbonate belt rocks, in Yemen. 8th conference of Mineral resources in the Arabian Countries, Amman, Jordan, 32p.
- Beydoun, Z.R., As-Sururi, M., El-Nakhal, H., Al-Ganad, I., Baraba, R., Nani, A., Al-Awah, M. 1998. International Lexicon of stratigraphy, vol., Asia, Fascicule 3(10b2), Republic of Yemen. IUGS publication No. 34, 245p. Sedimentary cover. *Z.geol. Wiss.*, 26(5/6) 517-529 Berlin.
- Brasier, D. Martin, Allen, A Phillip, Leather, J. 2011. Chapter 20, The Abu Mahara Group (Ghubrah and Fiq formations), Jabal Akhdar, Oman. Geological Society, London, *Memoirs* 36, 251-262.
- Bucher, M., Frey, M. 1994. Petrogenesis of Metamorphic Rocks. Springer-Verlag, 318p.
- Davies, G.R. 2004. Hydrothermal (thermobaric) dolomitization: rock fabric and organic petrology support for emplacement under conditions of thermal transients, shear stress, high pore fluid pressure with abrupt pressure transients, hydrofracturing, episodic rapid fluid flow, and instantaneous cementation by saddle dolomite. In: Davies, G.R., Packard, J., McAuley, R. (Ed.), Dolomite Seminar and Core Conference. Canadian Society of Petroleum Geologists, Calgary, 20p.
- Dragastan, O.N., Richter, D.K. 2011. Stromatolite and calcareous algae of Munder Formation (Tithonian- Berriasian) From NW Germany. *Acta Palaeontologica Romaniae* 7, 139-168.
- Dulski, P., Morteany, G. 1989. Magnesite formation by CO₂ metasomatism during regional metamorphism of the ultrabasic rocks of the Ochsner serpentinite (Zillertaler Alpen, Tyrol, Austria). Monograph Series on Mineral deposits, 28. Borntraeger, Berlin-Stuttgart, 95–104.
- Fabricius, I.L. 2000. Interpretation of burial history and rebound from loading experiments and occurrence of microstylolites in mixed sediments of Caribbean sites 999 and 1001. In: Leckie, R.M., Sigurdsson, H., Acton, G.D., Draper, G. (Ed.), Proceedings of the Ocean Drilling Program, scientific results 165: College Station, Texas, Ocean Drilling Program, 177–190.
- Franz, G. 1989. Stability of magnesite in carbonate–silicate assemblages; a review. Monograph Series on Mineral deposits, 28. Borntraeger, Berlin-Stuttgart, 259–268.
- Geomine Company 1984-1985. Preliminary Report; Industrail rocks and minerals in Ma'rib District. Unpublished report, Geological Survey and Mineral Resources Board, Romaine, 210p.
- Herrero, M.J., Martín-Pérez, A., Ana M. Alonso-Zarza, Gil-Peña, I., Meléndez, A., Martín-García, R. 2011. Petrography and geochemistry of the magnesites and dolostones of the Ediacaran Ibor Group (635 to 542 Ma), Western Spain: Evidences of their hydrothermal origin. *Sedimentary Geology* 240, 71-84.
- IUGS, 2009. International Stratigraphic Chart. International Commision on Stratigraphy. <http://www.stratigraphy.org/2009>.
- Johannes, W. 1970. Zur entstehung von magnesitvorkommen. *Neues Jahrbuch für Mineralogie Abhandlungen* 113, 274–325.
- Kralik, M., Aharon, P., Schroll, E., Zachmann, D. 1989. Carbon and oxygen isotope systematics of magnesites: a review. In: Moller, P. (Ed.). Magnesite, Monograph Series on Mineral deposits, 28. Berlin-Stuttgart, Borntraeger, 197–224.

- Kilias, S.P., Pozo, M., Bustillo, M., Stamatakis, M.G., Calvo, J.P. 2006. Origin of the Rubian carbonate-hosted magnesite deposit, Galicia, NW Spain: mineralogical, REE, fluid inclusion and isotope evidence. *Mineralium Deposita* 41, 713–733.
- Lugli, S., Torres–Ruiz, J., Garuti, G., Olmedo, F. 2000. Petrography and geochemistry of the Eugui magnesite deposit (Western Pyrenees, Spain): evidence for the development of a peculiar zebra banding by dolomite replacement. *Economic Geology* 95, 1775–1791.
- Lugli, S., Morteani, G., Blamart, D. 2002. Petrographic, REE, fluid inclusion and stable isotope study of magnesite from the Upper Triassic Burano Evaporites (Secchia Valley, northern Apennines): contributions from sedimentary, hydrothermal and metasomatic sources. *Mineral Deposits* 37, 480–494.
- Machel, H.G., Lonnee, J. 2002. Hydrothermal dolomite: a product of poor definition and imagination. *Sedimentary Geology* 152, 163–171.
- Melezhik, V.A., Fallick, A.E., Medvedev, P.V., Makarikhin, V.V. 2001. Palaeoproterozoic magnesite: lithological and isotopic evidence for playa/sabkha environments. *Sedimentology* 48, 379–397.
- Melezhik, V.A., Fallick, A.E. 2003. $\delta^{13}\text{C}$ and $\delta^{18}\text{O}$ variations in primary and secondary carbonate phases: several contrasting examples from Palaeoproterozoic ^{13}C -rich dolostones. *Chemical Geology* 201, 213–228.
- Meister, P., Judith A. McKenzie, J., Bernascon, S. M., Brack, P. 2013 Dolomite formation in the shallow seas of the Alpine Triassic. *Sedimentology* 60, 270–291.
- Morse, J.V., Mackenzie, F.T. 1990. Geochemistry of sedimentary carbonates. *Developments in Sedimentology*, 48. Elsevier Scientific Publication Co, New York, 696p.
- Moore, C.H. 2001. Carbonate reservoirs: porosity evolution and diagenesis in a sequence stratigraphic framework. *Developments in Sedimentology* 55, 444.
- Morad, S. 1998. Carbonate cementation in sandstones: distribution patterns and geochemical evolution. In: Morad, S. (Ed.). *Carbonate Cementation in Sandstones: Distribution Patterns and Geochemical Evolution: International Association of Sedimentologists Special Publication* 26, 1–26.
- Morteani, G., Möller, P., Schley, F. 1982. The rare earth element contents and the origin of the sparry magnesite mineralizations of Tux-Lanersbach, Entachen Alm, Spiessnägel, and Hochfilzen, Austria, and the lacustrine magnesite deposits of Aiani-Kozani, Greece, and Bela Stena, Yugoslavia. *Economic Geology* 77, 617–631.
- Möller, P. 1989. Minor and trace elements in magnesite. In: Moller, P. (Ed.). *Magnesite, Monograph Series on Mineral deposits*, 28. Berlin–Stuttgart, Borntraeger, 173–196.
- Müller, G., Irion, G., Förstner, U. 1972. Formation and diagenesis of inorganic Ca–Mg carbonates in the lacustrine environment. *Naturwissenschaften* 59, 158–164.
- Nash, M. C., Troitzsch, U., Opdyke, B. N., Trafford, J. M., Russell, B. D., Kline, D. I. 2011. First discovery of dolomite and magnesite in living coralline algae and its geobiological implications. *Biogeosciences* 8, 3331–3340.
- Prasannakumar, V., Vikas, C., Kumar, S.N. 2002. Constraints on the origin of south indian magnesite deposits. *Boletim Paranaense de Geociências* 50, 15–20.
- Perri, E., Manzo, E., Maurice E., Tucker, M. E. 2012. Multi-scale study of the role of the biofilm in the formation of minerals and fabrics in calcareous tufa. *Sedimentary Geology* 263–264, 16–29.
- Pierson, J. 1981. The control of cathodoluminescence in dolomite by iron and manganese. *Sedimentology* 28, 601–610.
- Pohl, W. 1989. Comparative geology of magnesite deposits and occurrences. In: Moller, P. (Ed.). *Magnesite, Monograph Series on Mineral deposits*, 28. Berlin–Stuttgart, Borntraeger, 1–14.
- Pohl, W. 1990. Genesis of magnesite deposits — models and trends. *Geologische Rundschau* 79, 291–299.
- Pueyo, J.J., Inglés, M. 1987. Magnesite formation in recent playa lakes, Los Monegros, Spain. In: Marshall, J.D. (Ed.). *Diagenesis of Sedimentary Sequences, Geological Society Special Publication*, 119–122.
- Quemeneur, J.M. 1974. Les gisement de magnesite du Pays Basque: Cadre géologique et sédimentologique; genese de la magnesite en milieu sédimentaire. *Diss. Univ. Paris VI*, (unpublished), 210p.

- Schroll, E. 2002. Genesis of magnesite deposits in the view of isotope geochemistry. *Boletim Paranaense de Geociências*, UFPR 50, 59–68.
- Sibley, D.F., Gregg, J.M. 1987. Classification of dolomite rock textures. *Journal of Sedimentary Petrology* 57, 967–975.
- Siegl, W. 1984. Reflections on the origin of sparrymagnesite deposits. In: Wauschkuhn, A., Kluth, C., Zimmermann, R.A. (Eds.), *Syngeneses and Epigenesis in the Formation of Mineral Deposits*. Springer-Verlag, Berlin, 177–182.
- Smith, L.B., Davies, G.R. 2006. Structurally controlled hydrothermal alteration of carbonate reservoirs: introduction. *American Association of Petroleum Geologists Bulletin* 90, 1635–1640.
- Souza, R.S., De Ros, L.F., Morad, S. 1995. Dolomite diagenesis and porosity preservation in lithic reservoirs, Carmópolis Member, Sergipe–Alagoas Basin, Northeastern Brazil. *American Association of Petroleum Geologists Bulletin* 79, 725–748.
- Spadafora, A., Perri, E., Judith, A., McKenzie, J.A., Vasconcelos, C. G. 2010. Microbial biomineralization processes forming modern Ca:Mg carbonate stromatolites. *Sedimentology* 57, 27–40.
- Teedumäe, A., Shogenova, A., Kallaste, T. 2006. Dolomitization and sedimentary cyclicity of the Ordovician, Silurian, and Devonian rocks in South Estonia. *Proceedings of the Estonian Academy of Sciences, Geology* 55 (1), 67–87
- Tucker, M.E. 1982. Precambrian dolomites: petrography and isotopic evidence that they differ from Phanerozoic dolomites. *Geology* 10, 7–12.
- Tucker, M.E. 1988. *Technique in Sedimentology*. Blackwell scientific publication: 394 p.
- Tucker, M.E., Wright, P. 1990. *Carbonate Sedimentology*. Blackwell Scientific Publications, London, 482p.
- Veizer, J. 1989. Strontium isotopes in seawater through time. *Annual Review of Earth and Planetary Science* 17, 141–167.
- Wacey, D., Wright, D.T., Boyce, A.J. 2007. A stable isotope study of microbial dolomite formation in the Coorong Region, South Australia. *Chemical Geology* 244 155–174
- Winkler, H.G.F. 1988. *Petrogenesis of Metamorphic Rocks*. Narosa Publishing House, New Delhi, 348p.
- Zachmann, D.W. 1989. Mg-carbonate deposits in freshwater environment. In: Moller, P. (Ed.). *Magnesite, Monograph Series on Mineral Deposits*, 28. Berlin-Stuttgart, Borntraeger, 61–94.
- Zachmann, D.W., Johannes, W. 1989. Cryptocrystalline magnesite. In: Moller, P. (Ed.). *Magnesite, Monograph Series on Mineral Deposits*, 28. Berlin-Stuttgart, Borntraeger, 15–28.

PLATES

PLATE I- Field photographs show the Al-Thanyiah major belt and the stratigraphic units in the Al-Thanyiah area.

Figure 1- General view of the Al-Thanyiah Mountain Belt.

Figure 2- The middle Fariedah Mountain which is situated in the southern part of the Al-Thanyiah Belt, shows the major productive Unit-A of magnesite rocks.

Figure 3- The northern Fariedah Mountain which is situated in southern part of the Al-Thanyiah Belt and shows the stratigraphic Units of A, B and C.

Figure 4- General view shows Fariedah Al-Thanyiah Mountain belts.

Figure 5- General view shows Tuba'a Al-Thanyiah, which is situated in the northern part of the Al-Thanyiah Belt.

Figure 6- General view of the Al-Thanyiah major belt shows the major stratigraphic unit (A, B and C).

Figure 7- Stratigraphic Unit D, E and F which is identified in the major the Al-Thanyiah Mountain.

Figure 8- Stratigraphic Unit E and F which is identified in the major the Al-Thanyiah Mountain.

PLATE I

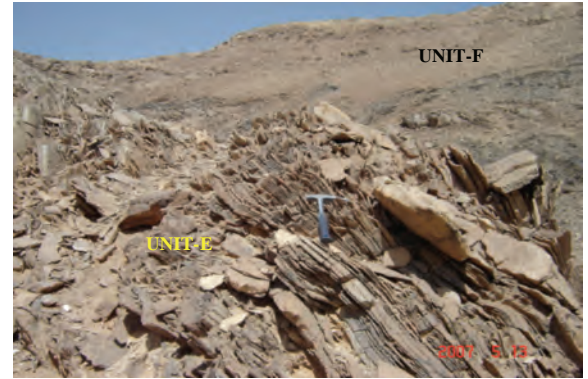
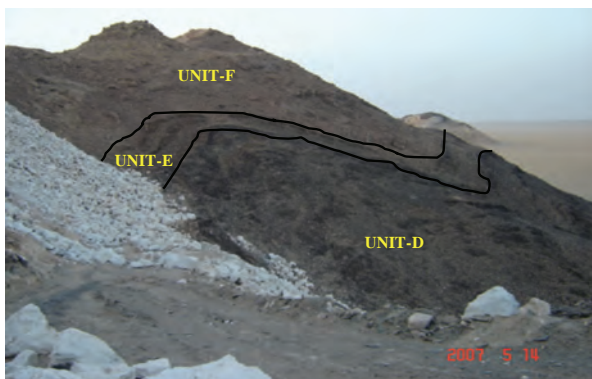
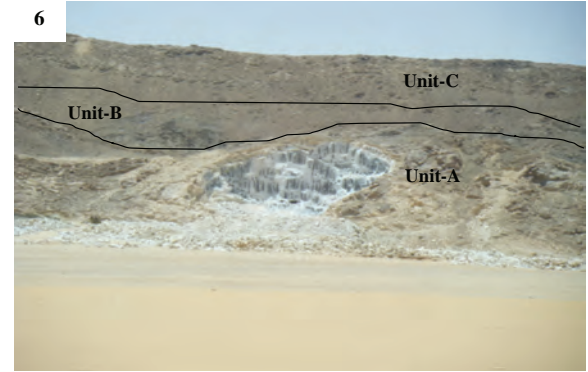
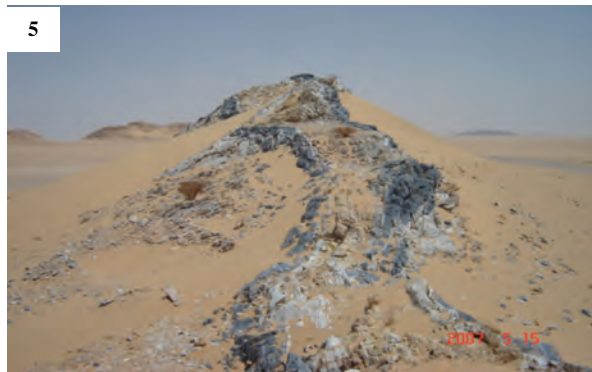
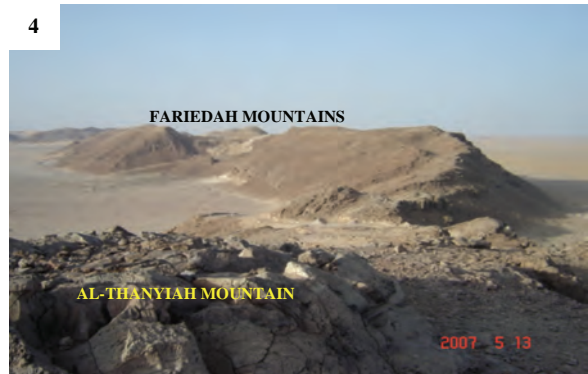
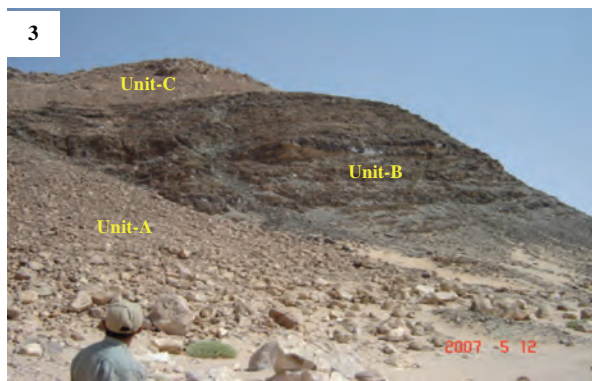
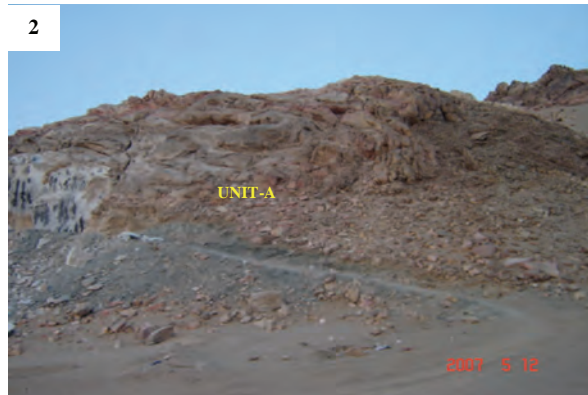
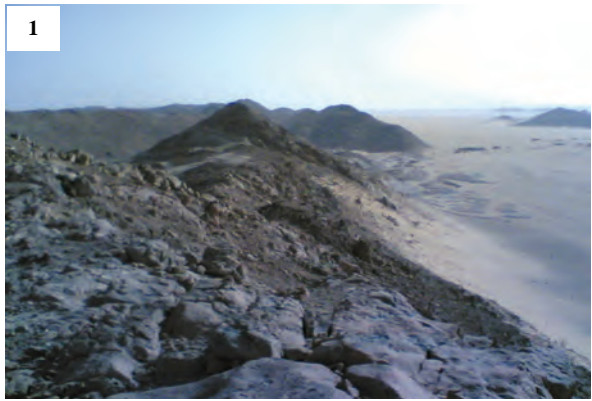


PLATE II- Field photographs show the Al-Thanyiah major belt and the stratigraphic units in Al-Thanyiah area.

Figure 1- Very large crystal of magnesite, which was recognized in the Al-Thanyiah Major Belt.

Figure 2- Hydrothermal solution effect shows in the Tuba'a Al-Thanyiah Belt in the northern limit,

Figure 3- Black magnesite rocks which was recognized at the top of the Al-Thanyiah Major Belt.

Figure 4- Red magnesite rocks which was recognized at the bottom of the Al-Thanyiah Major Belt.

Figure 5- Talc-schist rocks which was recognized at the top of the Al-Thanyiah Major Belt.

Figure 6- Talc-schist and magnesite rocks which were recognized at the top of the Al-Thanyiah Major Belt. Note the effect of intense folding and thrusting in the rock successions.

Figure 7- Dolomite-marble rocks which was recognized in the northern limit of the Tuba'a Al-Thanyiah Belt.

Figure 8- Large ultra-basic igneous intrusion, which was recognized intersecting the Jabal Al-Quroon Mountain in front of Major the Al-Thanyiah Belt.

PLATE II



PLATE III- Photomicrographs show the mineralogical constituents and the textures of magnesite in Al-Thanyiah Belt. (Mg) magnesite, (Dl) dolomite. (Br) brucite, and (Tl) talc.

Figure 1- Phenocrysts of magnesite with undulose extinction form the main magnesite-bearing horizon (CNx40X).

Figure 2- Euhedral magnesite crystals with undulose extinction (CNx40X).

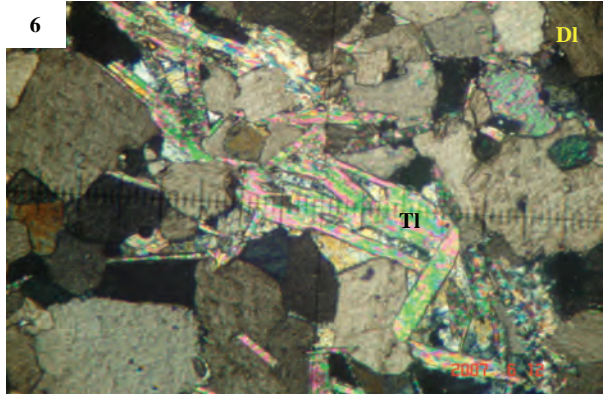
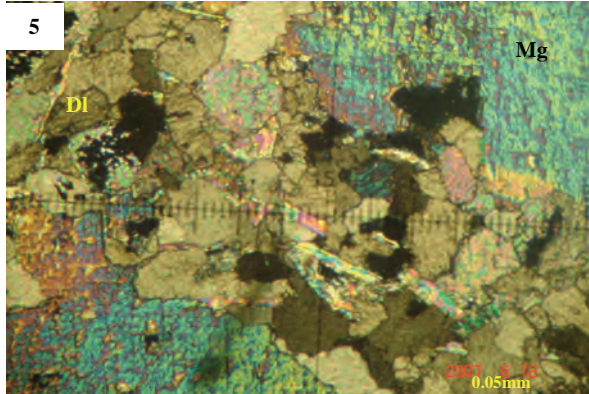
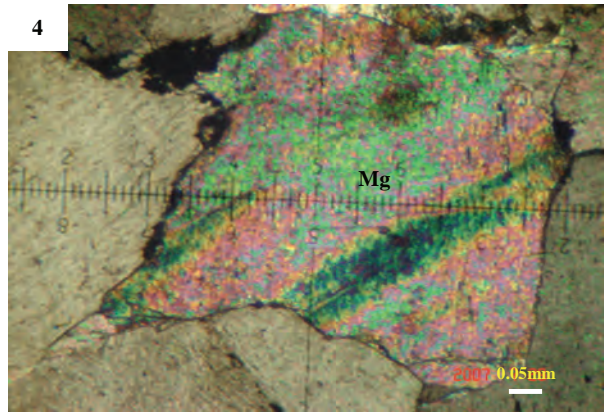
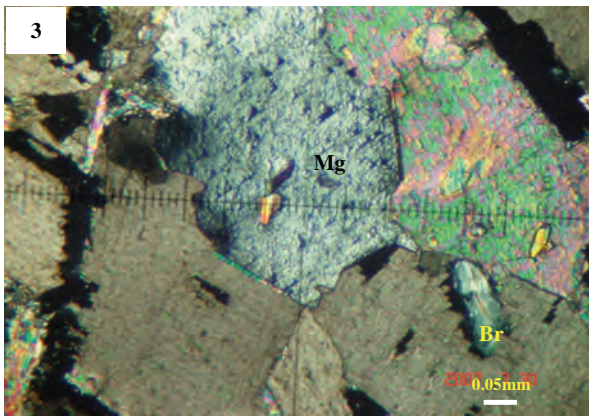
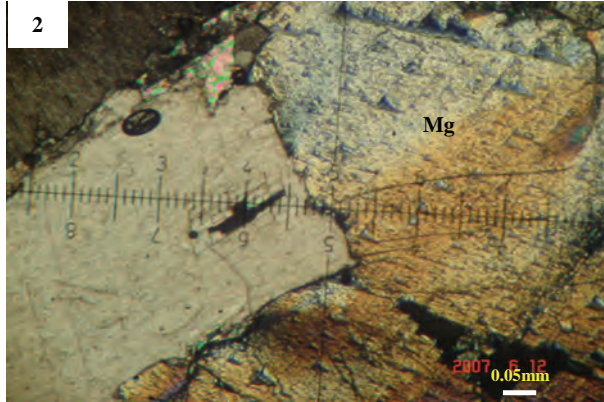
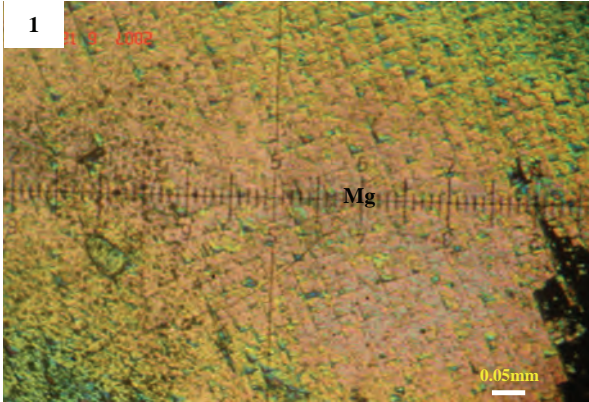
Figure 3- Subhedral magnesite crystals with undulose extinction (CNx40X).

Figure 4- Anhedral magnesite crystals with undulose extinction. Note the brucite crystal in lower left of the photo (CNx40X).

Figure 5- Porphyritic texture of magnesite phenocrysts surrounded with small crystals. Note the green flakes of talc crystals (CNx40X).

Figure 6- Flakes of green talc embedded within magnesite crystals (CNx40X).

PLATE III





Bulletin of the Mineral Research and Exploration

<http://bulletin.mta.gov.tr>



SODIUM SULFATE (GLAUBERITE-BLOEDITE) - HALITE ASSOCIATION in the TERTIARY (UPPER MIOSENE-PLIOCENE) KATRANDEDETEPE FORMATION, EREĞLİ-BOR BASIN, TURKEY

Gökhan KADINKIZ^{a*}, Memet PEKGÖZ^a, Mustafa KARAKAŞ^b and Abdurrahman MURAT^c

^aGeneral Directorate of Mineral Research and Exploration (MTA), Department of Mineral Research and Exploration, Ankara, Turkey

^bGeneral Directorate of Mineral Research and Exploration (MTA), Konya Regional Directorate, Konya, Turkey

^cTurkish Coal Enterprises, Ankara, Turkey

Research Article

Keywords:

Ereğli-Bor Basin,
Katrandedetepe Formation,
halite, glauberite, bloedite.

ABSTRACT

This study covers the investigations related to the glauberite-halite minerals detected in Neogene deposits of the Ereğli-Bor Basin in the Central Anatolia. The basin consists of Paleozoic basement rocks, the unconformably overlying Paleocene-Eocene-Oligocene marine sedimentary and volcano-sedimentary rocks, and the Lower Miocene-Pliocene lake deposits at the top which unconformably overlie all underlying layers. In the study, core drillings related to the determination of geological characteristics and investigation of the mineral potential of buried salt deposits were carried out in the Ereğli-Bor basin. As a result of drillings carried out, glauberite-bloedite, halite and bituminous shale horizons, which possess significant thickness and grade values, were cut for the first time in the Konya-Ereğli-Bor basin. Glauberite minerals were observed in three different structures as; 1- the Glauberite Mineral intercalated with High Graded, Bedded Clays, 2- the Glauberite Mineral with Disseminated Rosette Type in Low Graded Clays and 3- the Prismatic High Graded Glauberite Mineral intercalated with Halites. Bloedite minerals are mostly observed with halite. It was detected that the economical evaporitic formations in the Konya-Ereğli-Bor Basin had occurred within the Upper Miocene-Pliocene Katrandedetepe formation which represents the playa-lake environment.

Received: 08.05.2016

Accepted: 23.06.2016

1. Introduction

The purpose of the study is to explore probable burial type evaporitic industrial raw material deposits in the Ereğli-Bor Basin and their affordability.

As it is known, evaporitic basins are natural chemical deposits and accepted as the source of various industrial raw material. The Ereğli-Bor Basin is an important basin when the characteristics of geological and depositional environments are taken into consideration in terms of chemical sedimentary raw materials (sodium sulfate, halite, gypsum/anhydrite etc.) and other raw materials (lignite, bituminous shale etc.). Therefore; several investigations have been carried out in the region.

Studies, which are generally related to the investigation of the regional geology in the basin, were carried out by Türkünal, 1972; Oktay, 1982; Yoldaş, 1973; Demirtaşlı et al., 1986; Ayhan et al., 1986 and Ercan et al., 1992. The preliminary study in this region on evaporites belongs to Özgüner et al. (1989). The

authors mentioned about 20 billion tons of apparent operable pure anhydrite reservoirs in their studies, which they had carried out to explore evaporitic salt, and related sedimentary sulfide deposits in the Ereğli-Bor Basin. The investigators also stated that the hydrothermal fluids, which were the final products of the Upper Eocene island arc volcanism during the formation of anhydrite, provided ions that would supply salts to the depositional environment, and also the cherts located within these anhydrites had supported this formation. Later, Murat (1996) studied the distribution and the economic potential of celestines located in the limestone lenses among Ereğli-Ulukışla Tertiary units.

Other studies have also been carried out in Turkey in similar Tertiary basins. Helvacı et al. (1987), stated that the Neogene deposits in the Western Anatolia consisted of significant lignite, bituminous shale, uranium and borate deposits. Altay (2010) studied the mineralogical-geochemical features of the Neogene sedimentary units in Bor-Ulukışla Basin. Önal et

* Corresponding author: Sa'ad Zeki Akader Al-Mashaikie, magnesite2006@gmail.com

<http://dx.doi.org/10.19111/bulletinofmre.298685>

al. (2004) specified that the trona occurrences were intercalated with bituminous shale, mudstone and tuffs inside the Terzioğlu Member of the Gürün formation, in the article of “The Geology and the Trona Potential of the Middle Miocene Gürün Basin (Sivas) in the Central Anatolia”. The similar studies have been carried out also in the Beypazarı Basin (İnci et al., 1998; Helvacı et al., 1988; Yağmurlu and Helvacı, 1994; Helvacı, 1998; Gündoğan and Helvacı, 2005).

The most significant one of the similar basins in the world is the Green River Basin located in the northwest of Wyoming and hosts the biggest trona deposit of the world. According to Burnside and Culbertson (1979), trona deposits are located within the Wilkins Peak member of the Eocene Green River Formation. They emphasized that this member was composed bituminous shale, marl, claystone, trona, trona-halite, limestone and tuffs. Orti et al. (2007) on the other hand, who investigated Eocene-Lower Oligocene lacustrine evaporites in the southeast of the Ebro basin in NW Spain, implied that the shallow lake environment was controlled by a series of factor such as; 1- tectonical structure, 2- meteoric waters, 3- semi-arid climate and 4- alluvial fans.

1.1. Study Area

The study area is located in the Ereğli-Bor Neogene Basin, the southern and southeastern parts of the Tuz Gölü Basin in the Konya province (Figure 1).

1.2. Method of Study

Evaporite minerals easily dissolve and do not generally crop out at the surface. They should be embedded and preserved by cover deposits (clays) in order to form a deposit.

Among the material and methods for embedded mineral exploration, the drilling method was used to explore evaporite deposits which do not crop out in the Ereğli-Bor Neogene Basin. The geological map (1/25000 scale) of the basin was generated using previous studies. Using satellite data of M32 and M33 sheets (1/100 000 scale), the basin margin faults were investigated extracting lineaments of the basin.

Both previous local and foreign geophysical-geological investigations carried out in the region, the

cuts excavated for various purposes and drilling wells were studied on the site. Oil, irrigation and potable water drillings made by TPAO, DSI and private people were correlated with drill logs in the project, and environments of the basin were interpreted. The age and chemical contents of volcanic activities in the basin and their contact relationships with lake units were studied, so the basin was interpreted by correlating with the Beypazarı basin. All drillings in the basin were carried out at right angle. Both clastic and cored advances were made in drills and put into plastic drilling boxes. Samples were taken from the mineralized zone (halite, glauberite, tenardite, bloedite, bituminous shale), evaporitic zone (gypsum, anhydrite) and non-mineralized both for general and detailed analyses. Samples were collected by the radioactive decay method from drills both for mineralized and evaporitic zones, and the remaining samples were left in the drill box. Solid samples were dried under the temperature of 105°C. Samples were analyzed under the salt program of RIX 3000 model XRF device (Rigaku brand). The other samples were studied under IQ+ (nonstandard program) of the AXIOS model XRF device (Philips brand).

The polygon method was used as the reservoir estimation method. The polygon method is an important reservoir estimation method especially used in the formation of sedimentary deposits, and it generally gives reliable results. The reliability of the method increases depending on the number and interval of drillings performed on the field. The coordinates of drillings performed on the field in order to calculate the sodium sulfate reservoir in the study area were plotted on 1/10 000 scale map, then low angle triangles were formed from drill locations, which are close to each other. Polygons were then formed by drawing the centroid of each triangle. The polygonal area of each drilling was estimated and the reservoir amount of each polygon was separately calculated being multiplied by the mineral thickness, density and factor of safety. The estimated reservoirs were then summed up and total apparent reservoir was obtained.

In grade estimations, Na₂O and NaCl values were taken as the basis for glauberite and halite, respectively. As it is understood from drillings carried out, the rock salt and sodium sulfate transitions are present in the field. Therefore, the percent amount of

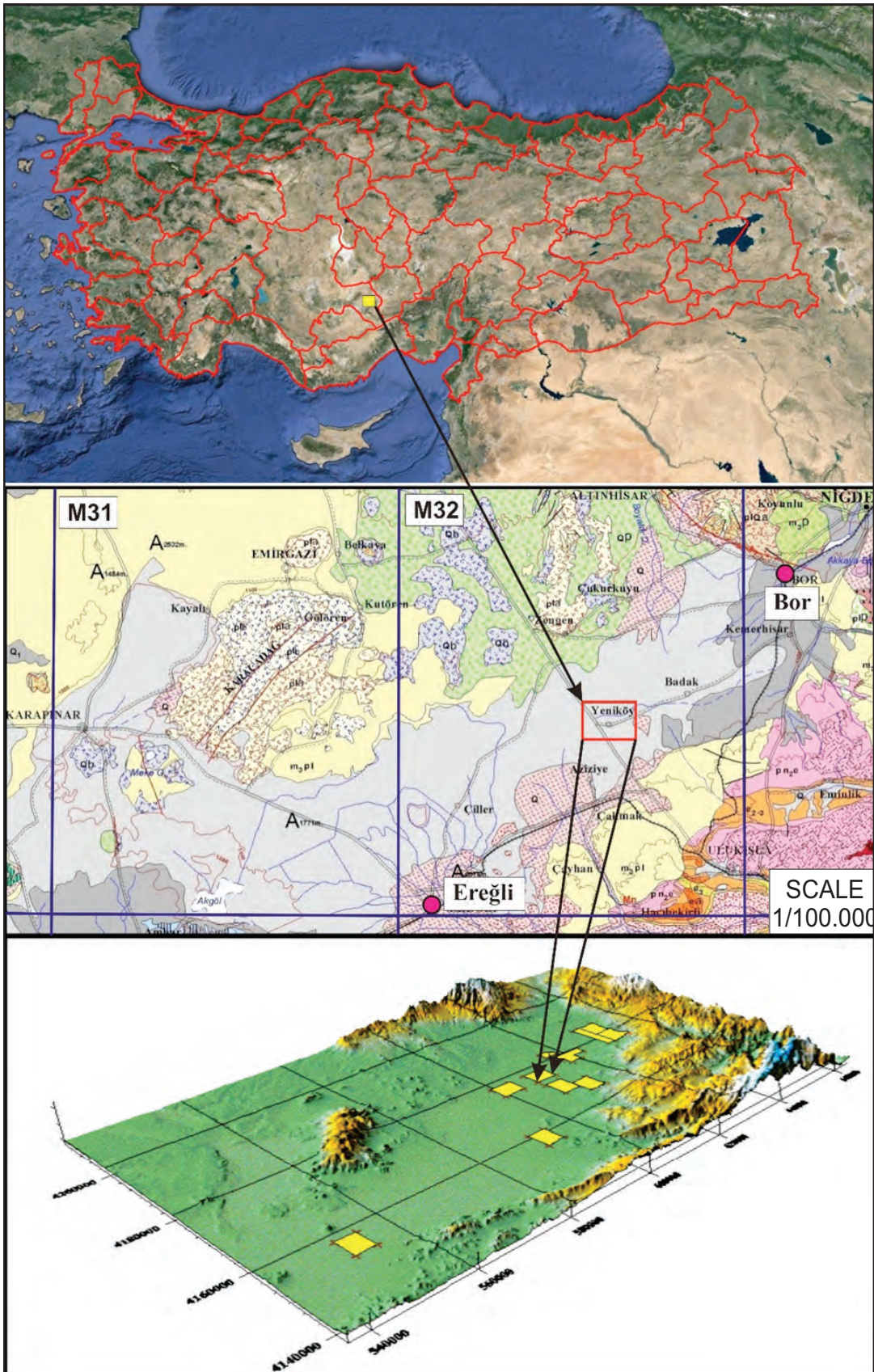


Figure 1- Location map of the study area.

sodium in the body, which combines with chlorine and sulfate, were detected one by one using basically their stoichiometric coefficients. Later on, the grade of Na_2SO_4 was estimated by multiplying the constant of 2.29 which is the stoichiometric coefficient of the percent Na_2O value that combines with sulfate.

2. Regional Geology

The oldest units of the region, where the Ereğli-Bor Neogene basin is located, are formed by the metamorphic rocks of the Lower Paleozoic Niğde massive (Figure 2). The metamorphics of the Niğde massive, which is generally represented by gneiss, marble, quartzite and amphibolites, were separated as Gümüşler, Kaleboynu, Aşıgediği formations and gathered under the name of “Niğde Group” by being interpreted as group (Atabey and Ayhan, 1986). The Gümüşler formation is composed of units of gneiss, quartzite, calc-silicate, marble and biotitic gneiss. The Kaleboynu formation consists of marble, quartzite and gneiss units. However, the Aşıgediği formation is formed by coarse crystallized marble units with amphibolite, gneiss and quartzite bands. The rocks of the Niğde group were occasionally cut by the Upper Cretaceous Sineksizyayla Metagabbro (varying from amphibolite to gabbroic pegmatite) and Üçkapılı Granodiorite (granite with aplitic and pegmatitic veins) (Göncüoğlu, 1981*a,b*).

The basement units are overlain by the Paleocene-Eocene Ulukışla-Çamardı Group in the region (Atabey and Ayhan, 1986). The volcanics are represented by agglomerate, pillow lava, tuff, dacites, syanite and trachy andesite, and they are occasionally composed of limestones blocks. The Sansartepe formation consists of Upper Paleocene monzonitic shallow intrusions (trachy andesite) and pillow lavas with compositions of basalt-olivine-dolerite and sporadically consists of thin limestone interlayers. The Serenkaya formation is composed of shale, conglomerate, siltstone, sandstone with volcanic materials and blocky coarse conglomerates in places, and it overlies the Sansartepe formation (Figure 3). This formation is cut by the Köyderesitepe trachyte. The Upper Paleocene-Eocene (Reefal nummulitic limestone) Başmakçı limestone overlies the Serenkaya formation. All these units are cut by the Lower Eocene Cehritepe syanite.

This unit is then overlain by the nummulitic limestone with coral, gastropod and lamellibraches (much fossiliferous) (Karatepe limestone) (Oktay, 1982). The volcanic activity ended in Middle Lutetian, and the Güney formation began to deposit (Figure 3). The bottom of the Güney formation begins with mudstone and continues with the alternation of gray claystone, beige-brown fine-thick layered calciturbiditic sandstone with volcanic elements and shale in upward. The orogenic movements,

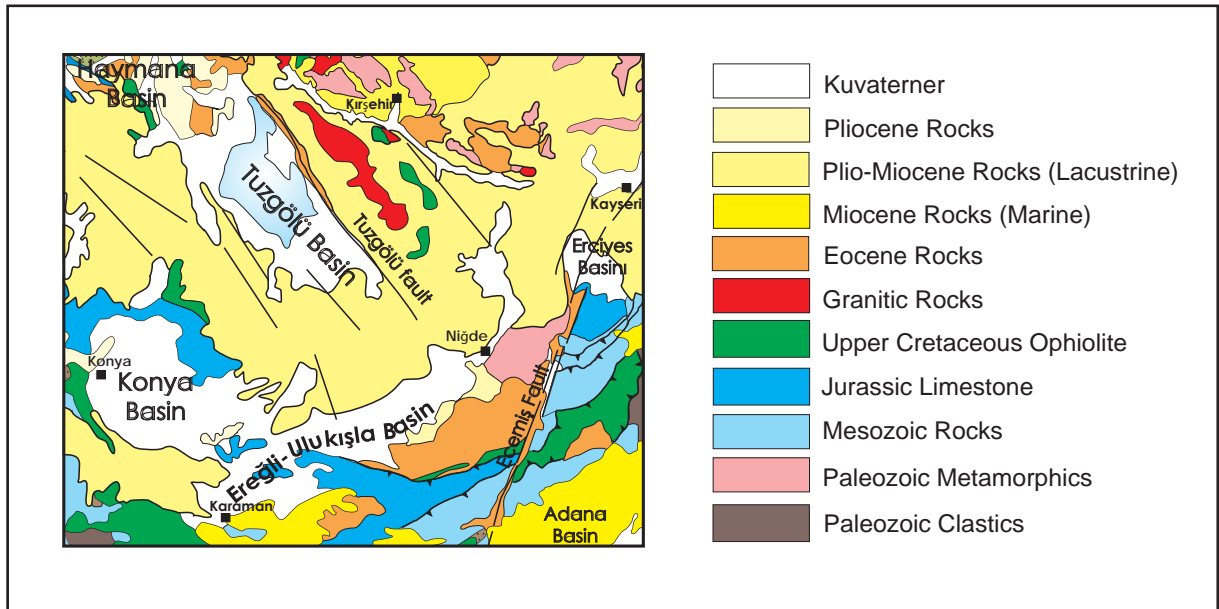


Figure 2- Regional geological map of the Ereğli-Bor Neogene Basin (modified from 1/500.000 scale geological map of MTA).

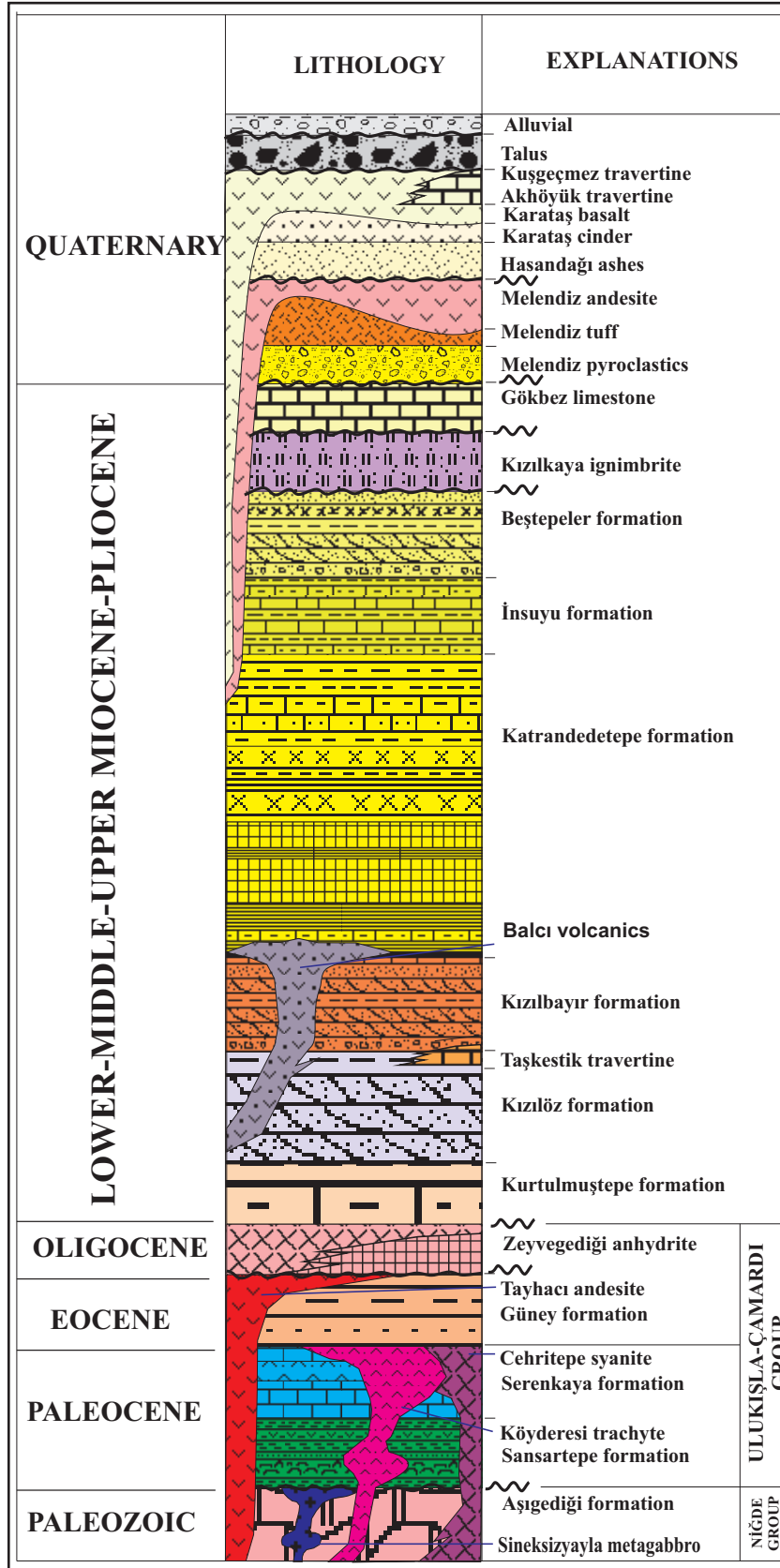


Figure 3- The generalized stratigraphical section of the Ereğli-Bor basin (modified from Oktay, 1982) (not to scale).

which developed in Upper Lutetian, form an angular unconformity between these rocks and overlying units.

In the Upper Eocene-Oligocene basin, the Zeyvedediği anhydrite, which forms an evaporitic succession (the product of a shallow marine-lagoon environment) was deposited. The Zeyvedediği anhydrites begin with white and layered anhydrite at the bottom (Figure 3), and then continue with brown, thin layered sandstone-limestone and green marl in upward. It is composed of white, layered anhydrite and brown clayey gypsums. Lacustrine units were deposited following the evaporitic succession.

Orogenic movements that developed in Middle Miocene form an angular unconformity between the units deposited in the Middle-Upper Miocene lake and evaporitic and molasses type deposits. The Kızılbayır formation was formed by clastic materials which had been transported from eastern and southern parts, and it is in the form of alternation of red and green sandstone and claystone. Inside, gypsum veins, which were created by the gypsum bearing groundwaters are present (Oktay, 1982). It begins with red, green, pebbly clays in the Kızılbayır locality and then continues with lensoidal-cross bedded sandstone-conglomerate interlayers. It then grades into Katrandetepe formation with the increase of marl and limestone in upwards (Figure 3). Later on; the formation is overlain by fine clastics and limestone-marl alternation due to the deepening of lake waters.

The abundance of living creatures in this period has caused much organic material to be transported into the lake. The transported organic materials have generated bituminous shales in the anaerobic environment where the lake becomes deep (Katrandetepe formation). The Katrandetepe formation begins with green, white marls and is generally alternates with clayey limestone and marl. It sometimes consists of bituminous shale layers which intercalate with evaporitic units.

Clayey limestones are white to dirty white, hard, fine and regularly bedded. However, marls overlying the clayey limestone are greenish gray, with mussel shell fragments. Coarse clastics such as; conglomerate and sandstone, were formed by the re-shallowing of the lake (Beştepeler formation) (Oktay, 1982). The formation, which begins with green sandstone intercalating with conglomerate, is in the form of

alternation of sandstone-claystone-conglomerate intercalated with clayey limestone. The uppermost part is represented by the coarse limestone and pebbly conglomerate. Sandstones are occasionally in the form of lenses within conglomerate layers. These were followed by vertical movements affected in Pliocene.

In north, a series of volcanic activities have occurred over the sediments of the Tuz Gölü Basin starting from Upper Miocene-Pliocene to Quaternary and affected the basin in terms of salinity. The calcalkaline type Melendiz and Hasandağı volcanisms, which developed along big tectonical lines in Upper Miocene-Pliocene, form heights on the plain. Augite-Andesite, Pyroxene-Andesite type lavas of the Melendiz volcanics were followed by the Hasandağı volcanism in Andesite-Basalt type in Quaternary and finally by the alkaline type volcanism on the plain (Dönmez et al., 2003).

3. Geology of the Study Area

The study area, which is located within basin, has a flat topography and is formed by thick Neogene lacustrine deposits and covered by Quaternary alluvial deposits (Figure 4). The Katrandetepe formation outcropping in south, which was determined as the target formation for chemical salt explorations, is buried by deep seated fault on basin margins on the plain. Lithological characteristics of formations determined by the study of outcrops and the cores of drills in the study area are given below.

3.1. Güney Formation (Tg)

The Güney formation was first defined by Oktay (1982) as a formation, and it is observed in the Güney village, the southern part of the study area and in its close vicinity. It corresponds to the Koçak Formation of Ketin and Akarsu (1965) and the Bozbeltepe member of the Hasangazi formation of Demirtaşlı et al. (1986). It outcrops in southern and southeastern parts of the study area, around Güney, Altay, Kolsuz, Eminlik and Başmakçı villages, between Gökbez-Karacaören villages, in Karakaya Tepe and Bozbel Tepe. It mainly strikes in the form of bands in E-W directions. The unit laterally exhibits different thicknesses and developed concurrently from north to south. Therefore, it is observed in different facies and ages in its type locality and southeast of Ulukışla. The bottom of the unit begins with mudstone and

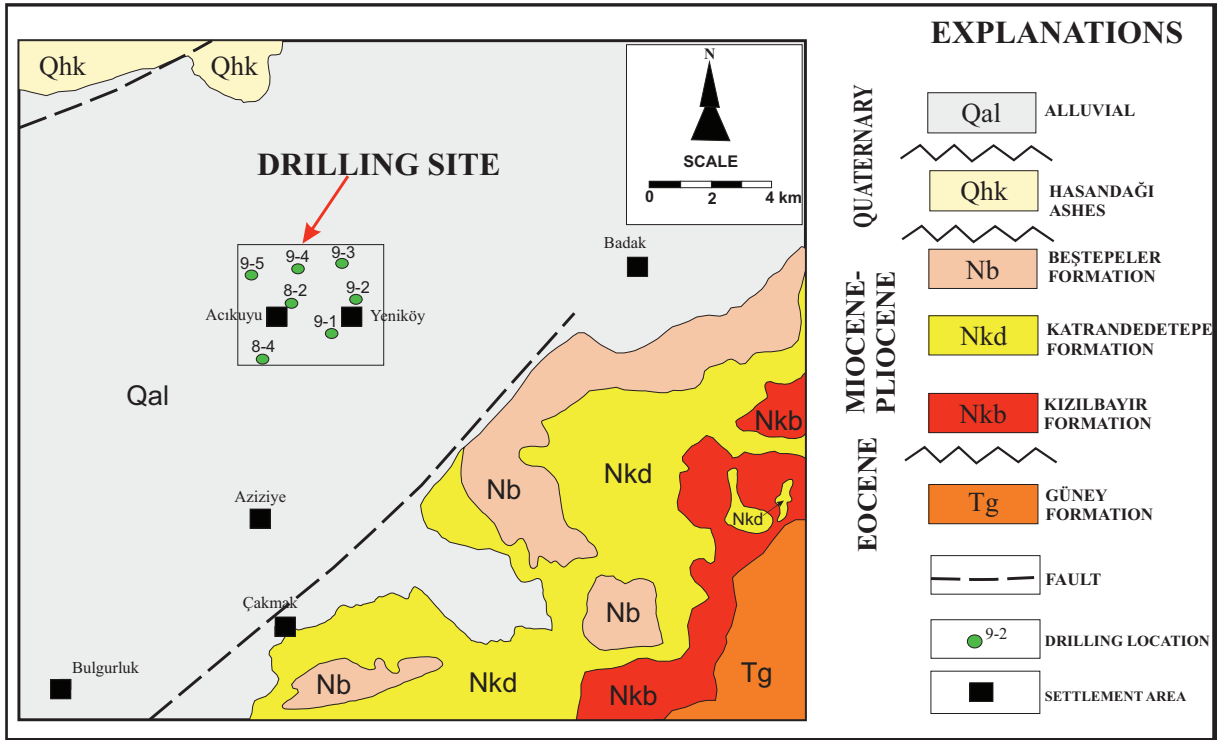


Figure 4- Geological map of the study area.

then continues with alternation of gray claystone, beige to brown, fine to thick layered calciturbiditic sandstone with volcanic materials and shale. To these regions, the clastic material, which was derived due to the erosion of sections of volcanic islands above water and erosion of the land in west of the basin, was rapidly deposited (Oktay, 1982). The Güney formation conformably overlies the Serenkaya formation around Güney village. It is cut by Tayhacı andesite and Dikmenderetepe trachyte, which are the final stage products of the Ulukışla island arc volcanism outside the study area in southwest. It is overlain by fluvial and lake deposits, which was formed by three conformable lithostratigraphical units in lake environment, with an angular unconformity.

The age of the formation was given as Lutetian due to the presence of *Globorotalia* cf., *Discocyclus* sp., *Orbitolites* sp., *Assilina* sp., *Alveolina* sp., *Locharitia* sp., *Halkyardia* sp., *G. mekana*, *G. aragonensi*, *Globogerina* sp., *Globorotalia* fossils described in different lithological units within the Güney formation by many investigators, who carried out several studies in the study area and its close vicinity (Demirtaşlı et al., 1986; Oktay, 1982; Ketin and Akarsu, 1965; Çevikbaş and Öztunalı, 1992).

3.2. Kızılbayır Formation (Nkb)

This formation was first defined by Oktay (1982) and its type locality is the Kızılbayır locality in SW of the Altay village. It is the first sedimentary deposit which extends in NE-SW directions between Hacibekirli and Altay villages and formed under lacustrine and fluvial conditions. It exhibits a wide distribution around Gelinkayaları in north of Hacibekirli, east of Katrandetepe, south of Bohcadikmentepe, east of Şahingüzmesi Ridge and Altay village (Oktay, 1982).

It begins to deposit with red to green, coarse pebbly clays in Kızılbayır locality and continues with lensoidal, cross bedded sandstone-conglomerate interlayers. It then grades into the Katrandetepe formation with the increase in marl and limestones in upward (Figure 5).

In the Hacıhüseyinler Obası locality (M32-c4), it begins to deposit with red to green pebbly clays, loose cemented, pink, white to black conglomerate layers which consists of recrystallized limestone and volcanic pebbles at the bottom. It is then overlain by the alternation of brown colored, by mostly cross bedded sandstone and red to green claystone.

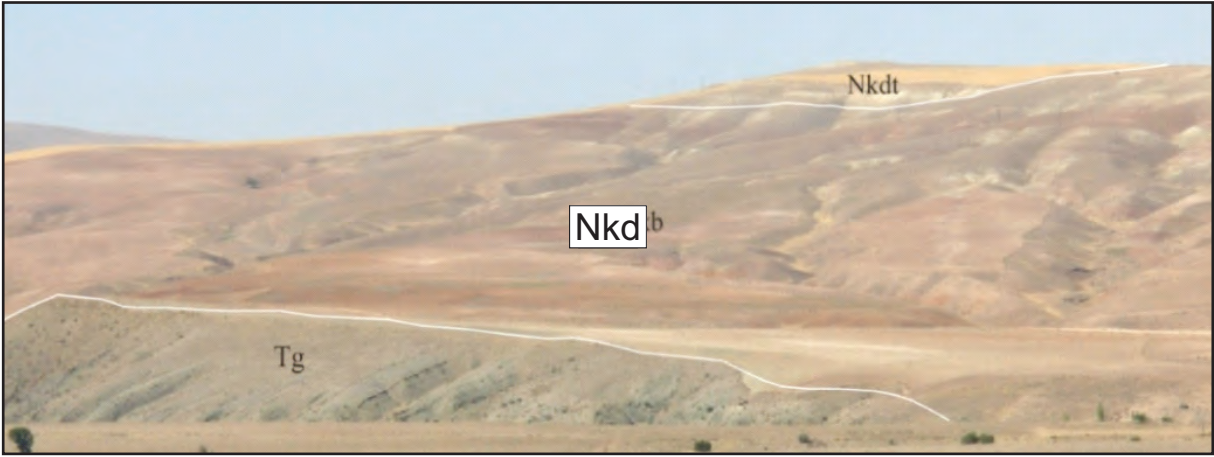


Figure 5- The contact relationships of the Güney formation (Tg), Kızılbaş formation (Nkb) and the Katrandetepe formation (Nkd).

Within this deposit, coal layers with thicknesses varying between 0-20 cm are observed between 3-5 m thick to medium bedded limestone layers. However, this layer is lensoidal and has not any lateral continuity. Claystones inside the formation are unlayered and fragmented in the form of mussel shell. The thickness is approximately 200-250 m. It discordantly overlies Zeyvedeği anhydrites at the bottom. However, there is a tectonical contact relationship with the Serenkaya formation in east of Altay village. It is conformably overlain by the Katrandetepe formation.

The grains in the Kızılbaş formation, which formed in lake and fluvial environments, are poorly sorted and not well-rounded, as the environment is tidal and transportation is in short distance. There was not found any paleontological data to age the Kızılbaş formation. However, the conformably overlying Katrandetepe formation to be in Upper Miocene makes us consider that this formation could be Middle-Upper Miocene, too. The thickness of the formation is nearly 300 meters according to drillings carried out in the study area.

3.3. Katrandetepe Formation (Nkd)

Its type locality is the Katrandetepe location in Tepeköy village (Niğde-Ulukışla). That is why it was named under this nomenclature (Oktay, 1982). It corresponds to the Ulukışla formation of Yoldaş (1973). The formation can easily be distinguished by its dirty white color over the red-green Kızılbaş formation. It spreads in the form of banding parallel to the Kızılbaş formation.

To the north; it outcrops in east of Güçük Tepe (M32-c2), in Boztepe, the north of Çakmaktepe, around Beştepeler, and to the south; in Karakayatepe, Katrandetepe (M32-c3) and Tozlu Tepe (M32-c4), then it wedges out in Çayhan Valley in west of Hacıbekirli.

The formation starts to deposits with green to white marls and generally alternates with clayey limestone and marl. It also includes bituminous shales in occasion (Figure 6). Bituminous shale layers alternate with evaporites. Clayey limestones are white to dirty white, hard and horizontal bedded. The marls overlain by clayey limestones are greenish gray colored with fragments of mussel shell. The evaporite ore minerals such as; halite, bloedite, loweite, tenardite in the basin were formed within this formation.

In places, where the bituminous content of the formation increases, the color becomes dark brown, blackish and laminated. The maximum thickness measured on the outcrop is 200 m. However, it was determined that the formation thickness varied in between 235-1400 meters in drillings performed and the thickness increased due to the sinking of the basin.

Many trenches excavated within bituminous shales were studied, and it was observed that these alternated occasionally with dolomites and green illitic clays. It was seen that bituminous shales turned into the view of wet carton when they dried up losing their moisture. The Katrandetepe formation conformably overlies the Kızılbaş formation and underlies the Beştepeler formation and remains below the Ereğli-Bor plain with a gentle slope.



Figure 6. View from units of the Katrandedetepe formation in a trench excavated in Ulukışla-Tepeköy-Karakaya Tepe.

Yoldaş (1973) dated the formation definitely as Upper Miocene according to spores and pollens in samples collected from bituminous layers. Oktay (198) dated the unit as Lower Pontian according to Ostracoda fauna present in green marls underlying the unit. The age of the formation was accepted most probably as Upper Miocene due to *Ostracoda* and *Gastropoda* shells and *Chara* sp in samples collected from clayey limestones. The Katrandedetepe formation has the characteristics of lacustrine-playa environment because of evaporitic interlayers it includes. The thickness of the formation is approximately 350 meters according to drillings carried out in the study area.

3.4. Beştepeler Formation (Nb)

It is best observed in Beştepeler locality that is why it was named under this nomenclature (Oktay, 1982). This is the last formation deposited in fluvial and lake environments in the Ereğli-Bor Basin and overlies the Karadedetepe formation with a distribution in NE-SW directions. It spreads over a very wide area in north starting from Güçük Tepe-Bögelek Tepe, Beştepeler (M32-c2), southeast of Tepeköy (M32-c4), Şeyhomerli, Çayhan, north of Hacıomerli and north of Bozdağ to the plain.

The formation, which begins to deposit with green sandstones intercalated with pebbles in

north, is in the form of sandstone-conglomerate alternation intercalating with clayey limestone. It is fully represented by loose conglomerates at the top and continues with alternation of clayey limestone-conglomerate in north of Hacıbekirli and around Çayhan. The sandstones are occasionally in the form of lenses within conglomerate layers. The conglomerates are fine to medium in north, medium to thick in west and are loose cemented. It easily disperses since it is loose cemented, and forms pebble piles. Pebbles are well rounded. The formation is conformably overlies the Katrandedetepe formation and remains below the alluvial of the Ereğli-Bor plain with a gentle slope. There was not encountered any fossils to date the formation. As the age of the Katrandedetepe formation, which conformably underlies the formation, is Upper Pliocene the age of this formation is considered to be Upper Pliocene-Miocene or younger in age. The depositional environment of the formation is fluvial and fresh water lake. The dominant fragmental material indicates that this formation formed in shallow and energetic environment. The thickness of the formation is approximately 300 meters in the study area according to drillings performed.

3.5. Hasandağı Ashes (Qhk)

It is observed as widespread in northwest of the study area. It is grayish white, beige, gray and milky white colored. Volcanic rock fragments are observed

in ash and tuff. Dönmez et al. (2003) dated the unit as the Lower Quaternary.

3.6. Alluvial (Qal)

Quaternary deposits, which outcrops in east-west directions in the central part and in wide regions in northwest of the study area, are formed by alluvial (Qal) and talus (Qym). Alluvial deposits mainly consist of pebble, sand and clayey materials. However, talus consists of angular limestone talus in variable sizes belonging to the Güneydağı formation (Tg) in western part of the Güneydağı. In drilling carried out in the Ereğli-Bor Basin the thickness of the alluvial cover was determined between 3-18 meters. The alluvial thickness in the study area is approximately 10 meters according to the drillings made.

4. Economical Geology

Yeniköy sodium sulfate deposit is located in 30 km northeast of Ereğli (Konya), approximately 25 km northwest of Ulukışla (Niğde), 27 km southwest of

Bor (Niğde). Ankara-Adana auto road passes through the study area.

The major mineral of the sodium sulfate deposit is glauberite and it is a burial chemical sedimentary type deposit. Another sodium sulfate mineral, which is frequently encountered in the deposit, is the bloedite mineral that accompanies with halite (Figure 7). The sodium sulfate deposition alternates with bituminous shale and rock salt within evaporite zone of the Upper Miocene-Pliocene Katrandetepe formation, and it is formed from the association of glauberite, halite, magnesite, bloedite and anhydrite.

Below the sodium sulfate deposition the grayish black, laminated bituminous shale, which generates liquid petroleum, is encountered. However, inside the deposition the alternation of pale gray siltstone-claystone which consists of fiber like gypsum and nodules of anhydrite and dolomitic layers in occasion are observed (Figure 8).

Above the sodium sulfate bearing zone, again grayish black, laminated bituminous shale, in which



Figure 7- Bloedite-halite alternation cut in the drilling KEY-09/05 excavated in Konya-Ereğli-Yeniköy study (x: 4177106, y: 612493).



Figure 8- Bituminous shale core with liquid petroleum indications cut at 462 m in Yeniköy drilling KEY-08/02 (x: 4176100, y: 613550).

between laminae the liquid petroleum generates, anhydrite and dolomitic layers, in which pores and fractures are occasionally filled with liquid petroleum, are located (Figure 9).

Sodium sulfate bearing zone generally begins with gray, discoidal gypsum, liquid petroleum bearing dolomite and thin laminated bituminous shales at the bottom. Within bituminous shales, prismatic, layer like glauberite crystals with 2-3 cm in size are much observed. The thickness of glauberite crystals increases much more in upper layers. Pale gray – dirty white glauberite minerals disintegrate in the air and are broken into small pieces like flavor by whitening and swelling. The thickness of glauberites, which are

the major mineral of the deposit, varies between 0.60 – 14.40 m. The number of glauberite bearing layers shows variation between 4 to 11 (Table 1).

In drillings KEY-09/02 and KEY-09/03 carried out in the eastern part of the study area two glauberite zones were cut as being different than other drills. In both drillings glauberite minerals in the upper zone are located in halite-anhydrite alternation with interlayers of siltstone-dolomite between 407-429 m. However, the glauberite zones located below were deposited within alternation of oil producing shale-halite and anhydrite as it had been in other drillings.



Figure 9- Liquid petroleum infilling the pores of dolomites cut in Yeniköy drill KEY-08/04 (371 m).

Table 1- The mineralization characteristics of the Yeniköy sodium sulfate deposit.

| Drilling No | Mineralization Interval (m) | Number of layer | Total Thickness (m) |
|-------------|-----------------------------|-----------------|---------------------|
| KEY-08/02 | 447,30-572,70 | 8 | 30,95 |
| KEY-08/04 | 403,40-438,80 | 4 | 19,90 |
| KEY-09/01 | 437,00-510,80 | 8 | 16,30 |
| KEY-09/02 | 407,00-601,00 | 5+5 | 16,70 |
| KEY-09/03 | 407,00-676,30 | 3+8 | 19,80 |
| KEY-09/04 | 499,30-629,80 | 5 | 30,00 |
| KEY-09/05 | 518,60-668,40 | 4 | 27,70 |
| Mean | 403,40-676,30 | Different | 23,05 |

Sodium sulfate deposit is at the depth of 404-528 m from the surface and in the form of a zone of which its thickness varies between 16.30-30.95 m (Table 2). As a result of drillings made in the study area, it was detected that the sodium sulfate deposit dispersed over a wide area (13.59 km²) and generally possessed a sub-horizontal slope.

Determined grades of the Yeniköy sodium sulfate deposit vary between 27.39% and 42.16% Na₂SO₄. On the other hand; the mean sodium sulfate grade of the deposit was determined as; 33.34% Na₂SO₄, bloedite grade as; 28.19% Na₂SO₄, and halite grade as; 80.25% NaCl.

5. Mineralization

5.1. Ore Minerals and Mineral Association

NaCl salt is obtained in nature in two different ways as; marine and terrestrial environments. The

main economical source of the salt is oceans in the world. On lands, it is obtained from rock salts and salt lakes. However, mainly the rock salt (halite), anhydrite, gypsum and glauberite were observed in drillings in the study area (Table 4). Major ore minerals though in fewer amounts are accompanied by magnesite, dolomite, hydro glauberite, quartz, illite/mica group clays, starkeyit, zeolite group (clinoptilolite, heulandite and analcim-C) minerals, chlorite group minerals and amorph materials.

In addition that sodium sulfate salts form many minerals in nature, its most significant minerals are mirabilite, tenardite, glauberite, bloedite and glaserite in terms of economy and workability. These salts are deposited in contemporary alkaline lakes and playa lakes. Ereğli-Yeniköy sodium sulfate deposit is also a playa type deposit and covers wide areas. In drillings made in this basin, glauberite-bloedite and halite minerals were cut. The correlation of the mineralized zone based on drillings is shown in figure 10.

Table 2- Yeniköy sodium sulfate deposit (Mineralization thicknesses with respect to drillings)

| Drilling No | Drilling Name | Mineral | Total Thickness (m) | Mean Tenure (% Na ₂ SO ₄) and (% NaCl) |
|-------------|---------------|------------|---------------------|---|
| 1 | KEY-08/02 | GLAUBERITE | 30,95 | 35,66 |
| | | BLOEDITE | 6,00 | 18,08 |
| | | HALITE | 16,00 | 89,29 |
| 2 | KEY-08/04 | GLAUBERITE | 19,90 | 42,16 |
| | | BLOEDITE | | |
| | | HALITE | | |
| 3 | KEY-09/01 | GLAUBERITE | 16,30 | 27,39 |
| | | BLOEDITE | 3,75 | 36,85 |
| | | HALITE | 17,05 | 93,07 |
| 4 | KEY-09/02 | GLAUBERITE | 16,70 | 31,97 |
| | | BLOEDITE | 2,60 | 43,66 |
| | | HALITE | 21,10 | 45,50 |
| 5 | KEY-09/03 | GLAUBERITE | 19,80 | 35,39 |
| | | BLOEDITE | | |
| | | HALITE | 31,30 | 64,15 |
| 6 | KEY-09/04 | GLAUBERITE | 30,00 | 28,03 |
| | | BLOEDITE | | |
| | | HALITE | 35,80 | 85,50 |
| 7 | KEY-09/05 | GLAUBERITE | 27,70 | 20,05 |
| | | BLOEDITE | | |
| | | HALITE | 45,40 | 93,08 |

Table 3- Grade and reservoir conditions of the Yeniköy sodium sulfate deposit.

| Drilling No | Reservoir Based Polygon Areas (m ²) | Mineralization Thickness (m) | Specific Gravity (ton/m ³) | Factor of Safety | Apparent Reservoir (Ton) | GLAUBERITE | | | | | | | | | | |
|--|---|------------------------------|--|------------------|--------------------------|--------------------------------------|-------|-------------------|-----------------|------|--------------------------------|------------------|------------------|-------|--------------------------------|---------------------------------|
| | | | | | | Values of Weighted Mean Analysis (%) | | | | | | | | | | |
| | 1 | 2 | 3 | | 5=1x2x3x4 | Na | Cl | Na ₂ O | SO ₃ | MgO | Fe ₂ O ₃ | SiO ₂ | K ₂ O | CaO | Al ₂ O ₃ | Na ₂ SO ₄ |
| KEY-08/02 | 2.840.000 | 30,95 | 2,77 | 0,7 | 170.434.222 | 13,96 | 3,72 | 18,82 | 40,23 | 5,72 | 0,83 | 4,69 | 0,21 | 15,86 | 1,08 | 35,66 |
| KEY-08/04 | 2.140.000 | 19,90 | 2,77 | 0,7 | 82.574.254 | 13,76 | 0,16 | 18,55 | 42,87 | 5,80 | 0,61 | 5,18 | 0,17 | 16,53 | 1,15 | 42,16 |
| KEY-09/01 | 2.640.000 | 16,30 | 2,77 | 0,7 | 83.439.048 | 10,71 | 2,84 | 14,43 | 44,72 | 7,98 | 0,09 | 5,00 | 2,60 | 8,64 | 1,15 | 27,39 |
| KEY-09/02 | 2.150.000 | 16,70 | 2,77 | 0,7 | 69.619.795 | 13,27 | 4,49 | 17,88 | 37,61 | 7,89 | 0,68 | 4,72 | 0,24 | 16,64 | 1,31 | 31,97 |
| KEY-09/03 | 1.670.000 | 19,80 | 2,77 | 0,7 | 64.114.974 | 13,62 | 3,33 | 18,36 | 38,54 | 7,41 | 0,18 | 4,49 | 0,23 | 17,44 | 1,26 | 35,39 |
| KEY-09/04 | 2.150.000 | 30,00 | 2,77 | 0,7 | 125.065.500 | 10,30 | 1,88 | 13,88 | 44,32 | 6,45 | 0,77 | 3,48 | 0,15 | 19,43 | 0,86 | 28,03 |
| | | TOTAL | | | 595.247.793 | | | | | | | | | | | |
| VALUES OF WEIGHTED MEAN ANALYSES (FIELD) | | | | | | 12,59 | 2,76 | 16,97 | 41,60 | 6,64 | 0,59 | 4,53 | 0,53 | 15,95 | 1,10 | 33,34 |
| | | | | | | | | | | | | | | | | |
| Drilling No | Reservoir Based Polygon Areas (m ²) | Mineralization Thickness (m) | Specific Gravity (ton/m ³) | Factor of Safety | Apparent Reservoir (Ton) | BLOEDITE | | | | | | | | | | |
| | | | | | | Values of Weighted Mean Analysis (%) | | | | | | | | | | |
| | 1 | 2 | 3 | | 5=1x2x3x4 | Na | Cl | Na ₂ O | SO ₃ | MgO | Fe ₂ O ₃ | SiO ₂ | K ₂ O | CaO | Al ₂ O ₃ | Na ₂ SO ₄ |
| KEY-08/02 | 2.840.000 | 6,00 | 2,25 | 0,7 | 26.838.000 | 23,72 | 27,58 | 31,98 | 28,40 | 6,60 | 0,02 | 0,23 | 0,01 | 0,64 | 0,07 | 18,08 |
| KEY-09/01 | 2.640.000 | 3,75 | 2,25 | 0,7 | 15.592.500 | 13,34 | 2,16 | 17,98 | 51,58 | 9,48 | 0,01 | 0,95 | 0,02 | 3,44 | 0,28 | 36,85 |
| KEY-09/02 | 2.150.000 | 2,60 | 2,25 | 0,7 | 8.804.250 | 28,27 | 21,80 | 38,10 | 32,10 | 7,40 | - | 0,20 | 0,20 | - | - | 43,66 |
| | | TOTAL | | | 51.234.750 | | | | | | | | | | | |
| VALUES OF WEIGHTED MEAN ANALYSES (FIELD) | | | | | | 21,34 | 18,85 | 28,77 | 36,09 | 7,61 | 0,01 | 0,44 | 0,04 | 1,38 | 0,12 | 28,19 |
| | | | | | | | | | | | | | | | | |
| Drilling No | Reservoir Based Polygon Areas (m ²) | Mineralization Thickness (m) | Specific Gravity (ton/m ³) | Factor of Safety | Apparent Reservoir (Ton) | HALITE | | | | | | | | | | |
| | | | | | | Values of Weighted Mean Analysis (%) | | | | | | | | | | |
| | 1 | 2 | 3 | 4 | 5=1x2x3x4 | Na | Cl | Na ₂ O | SO ₃ | MgO | Fe ₂ O ₃ | SiO ₂ | K ₂ O | CaO | Al ₂ O ₃ | NaCl |
| KEY-08/02 | 2.840.000 | 16,00 | 2,17 | 0,7 | 69.023.360 | 35,06 | 54,18 | 47,25 | 7,95 | 2,00 | 0,10 | 0,26 | 0,10 | 0,45 | 0,10 | 89,29 |
| KEY-09/01 | 2.640.000 | 17,05 | 2,17 | 0,7 | 68.373.228 | 36,22 | 56,48 | 48,82 | 1,39 | 0,19 | 0,04 | 0,21 | 0,01 | 0,52 | 0,13 | 93,07 |
| KEY-09/02 | 2.150.000 | 21,10 | 2,17 | 0,7 | 68.909.435 | 27,81 | 27,61 | 37,49 | 23,51 | 2,04 | 0,12 | 0,69 | 0,10 | 6,64 | 0,19 | 45,50 |
| KEY-09/03 | 1.670.000 | 31,30 | 2,17 | 0,7 | 79.399.649 | 28,18 | 38,93 | 37,98 | 11,50 | 2,80 | 0,20 | 0,40 | 0,03 | 0,91 | 0,13 | 64,15 |
| KEY-09/04 | 2.150.000 | 35,80 | 2,17 | 0,7 | 116.917.430 | 23,10 | 51,88 | 31,13 | 10,27 | 2,05 | 0,11 | 0,83 | 0,07 | 2,67 | 0,23 | 85,50 |
| KEY-09/05 | 1.760.000 | 45,40 | 2,17 | 0,7 | 121.374.176 | 36,22 | 56,48 | 48,82 | 1,39 | 0,19 | 0,04 | 0,21 | 0,01 | 0,52 | 0,13 | 93,08 |
| | | TOTAL | | | 523.997.278 | | | | | | | | | | | |
| VALUES OF WEIGHTED MEAN ANALYSES (FIELD) | | | | | | 30,82 | 48,70 | 41,53 | 8,68 | 1,50 | 0,10 | 0,45 | 0,05 | 1,86 | 0,16 | 80,25 |

Table 4- The distribution of ore minerals and paragenesis of the Yeniköy sodium sulfate deposit based on drillings.

| Drilling No | Mineralization Interval (m) | Zone Thickness (m) | Mineral Paragenesis |
|-------------|--------------------------------|-----------------------|--|
| KEY-08/02 | 447,30-572,70 | 125,40 | Glauberite halite magnesite bloedite anhydrite |
| KEY-08/04 | 403,40-438,80 | 35,40 | Glauberite anhydrite magnesite gypsum |
| KEY-09/01 | 437,00-510,80 | 73,80 | Glauberite halite magnesite |
| KEY-09/02 | 407,00-429,00 519,00-601,00 | 22 + 82=104,00 | Glauberite halite bloedite dolomite |
| KEY-09/03 | 404,20-429,70 547,00-676,30 | 25,50+ 129,30= 154,80 | Glauberite anhydrite halite magnesite |
| KEY-09/04 | 499,30-629,80 | 130,50 | Glauberite anhydrite halite magnesite |
| KEY-09/05 | 518,60-668,40 | 149,80 | Glauberite anhydrite halite magnesite |
| MEAN | 403,40-676,30 | Variable | Glauberite halite magnesite bloedite anhydrite |

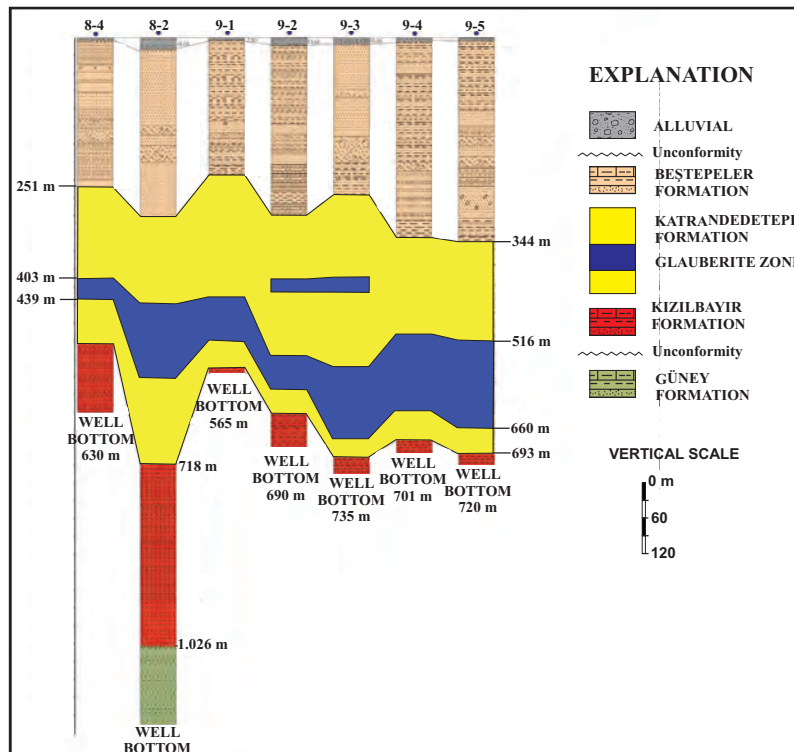


Figure 10- Drilling correlation of the Yeniköy sodium sulfate deposit.

5.2. Mineralization and the Factors Controlling the Mineralization

The Ereğli-Bor Neogene Basin is located in north of the Central Taurus belt, west of the Ecemiş Fault and in southeast part of the Tuzgölü Basin. At the basement structural elements are dominant. These elements were formed by the Alpine orogeny, which caused the closure of the Southern Neotethys Sea and affected in the form of N-S directing compression starting from Upper Cretaceous to Upper Miocene (Şengör and Yılmaz, 1983). The Niğde Fault Zone, which restricts the basin from south, continues until Karaman in the form of discontinues branches. The Niğde fault zone is approximately 170 km long, 5-8 km wide, left lateral strike slip fault with a strike of NE-SW and dipping in NW direction (Koçyiğit, 2000). The northeastern border of the Ereğli-Bor basin is controlled by the branches of the Tuzgölü fault zone (Figure 11).

Central Anatolia is divided into two neotectonic regions. These are; 1- Konya-Eskişehir neotectonic region and 2-Kayseri-Sivas neotectonic region

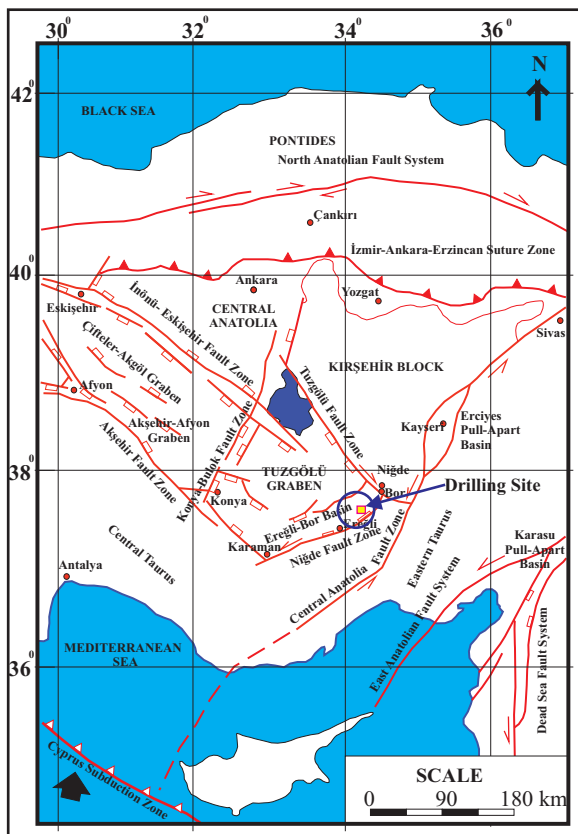


Figure 11- Simplified neotectonic map of the Central Anatolia and its close vicinity (modified from Koçyiğit, 2000).

(Figure 11). Konya-Eskişehir neotectonic region is the first neotectonic region that remains between the Kesikköprü fault that extends between Kırıkkale in north and Niğde in south, and the area to the east of Tuzgölü fault zone. Konya-Eskişehir neotectonic region is the eastern continuation of the West Southwest Anatolia and the Turkish Lake Land (Göller Bölgesi) horst graben system and characterized by extensional tectonic regime and oblique slip normal faulting. The starting age of the neotectonic regimes characterizing the Central Anatolia is the post-Pliocene (Koçyiğit, 2000). The Ereğli-Bor basin is located in the first neotectonic region, too. This basin has the characteristics of being a semi-graben type depositional basin which developed in and after the Upper Miocene as a result of the pressure release which occurred in the region following the Miocene compressional tectonism (Şengör and Yılmaz, 1983).

In the formation of the Ereğli-Bor Basin, which is a closed lake basin, it is considered that tectonically; an extensional regime became effective and tectonical factors causing the development of basin mediated a volcanic activity in the same period (Middle-Upper Miocene). It was observed that volcanism (Balçı volcanism) derived solutions and other volcanic materials were supplied into the lake environment as the sinking in the basin synchronously occurred with sedimentation (Kadınkız and Pekgöz, 2015).

Tectonic and volcanic activities effective in the basin development, beyond the occurrence of the extensional region, have provided significant volcanism derived solutions that would cause economical mineralization especially to the lake environment. Besides; the Zeyvegediği anhydrite (Upper Eocene-Oligocene) has a great importance for ion supplement into the basin (Figure 12). As sedimentation in the lake environment continues, it is considered that Na, Ca and SO_4 bearing solutions mix into lake water by means of fracture systems (Kadınkız et al., 2015).

Most of the lake deposits exhibit especially well developed bedding, lamination and frequently lateral lithology and color variations. Fresh water carbonates, thin dolomite layers, bituminous shales and evaporites are particular stages and types characterizing the lake environment (Einsele, 1992). It is probable to encounter one or several such rock salts in many lake deposits

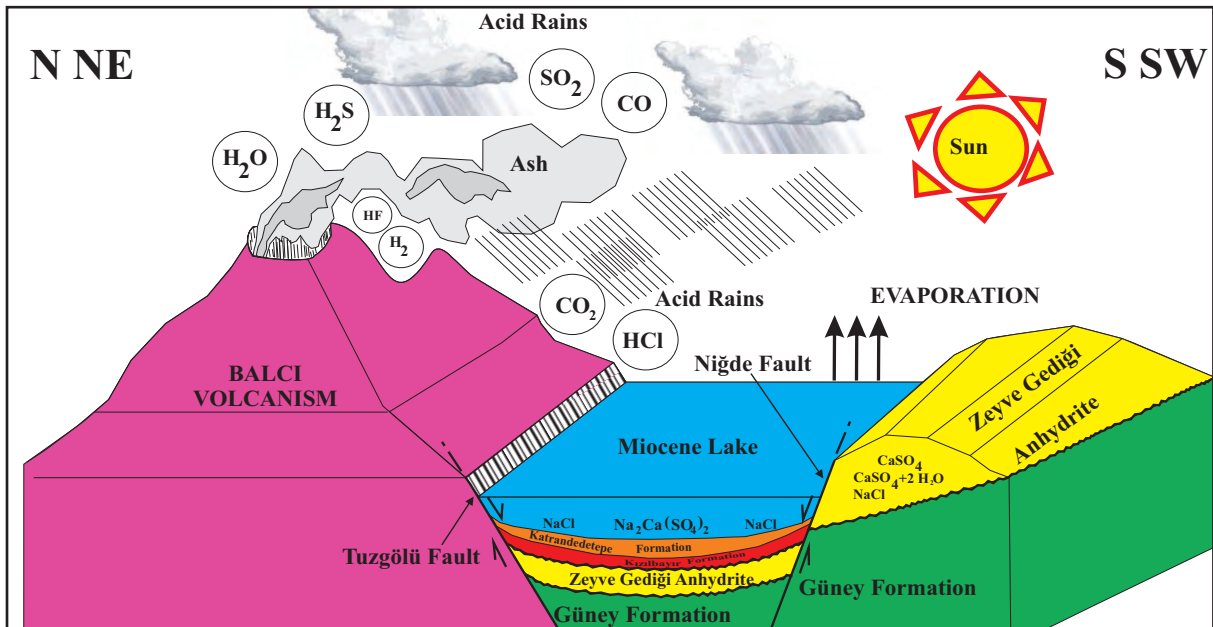


Figure 12- Schematic model showing the glauconite deposition in the Ereğli-Bor Neogene Basin in Miocene.

(İnci et al., 1998; Helvacı et al., 1988; Yağmurlu and Helvacı, 1994; Helvacı, 1998; Gündoğan and Helvacı, 2005). When significant salt formation types in closed lake systems are taken into consideration, it is seen that gypsum, halite, glauconite and bloedite minerals in sulfate lakes in which sulfate, chlorine and calcium rich waters are effective, are deposited.

The presence of thin lignite layers located at the bottom indicates that the primary lake bottom started to shape and the environment was a marsh land rich in plant and tree remnants in the first period when the Ereğli-Bor Basin began to open. Parallel to the gradual deepening and the enlargement of the basin, the sediment transportation and depositional process also began to develop. Marl-carbonate and lignite occurrences in the form of thin layers are encountered in sediments deposited in this period. Besides; sodium sulfate and rock salt layers observed within the Katrandetepe formation and bituminous shales, which form a thick succession in the form of alternations, were deposited in the basin (Kadınkız et al., 2005) (Figure 10).

Bituminous shales deposited in the closed saline lake system of the Ereğli-Bor basin are also important. The presence of bituminous shales alternating with evaporite minerals in the basin shows that some planktonic organisms and plants may increase if there will be high temperature and enough food

support although high salinity waters are not rich in organisms. In such environments phytoplankton production and the occurrence of algal accumulations could reach important amounts. However, a few part of this production were deposited with sediments while most of them decayed. These kerogen rich bituminous shales indicate high lake altitude and humid phase. Sodium sulfate minerals and halite layers on the other hand were deposited in a playa lake environment in which organic poor and more arid climate had developed. Bituminous shales have generated liquid petroleum in significant amount and frequency. Bituminous shales of which their kerogen types are suitable to generate petroleum have produced oil by the effect of temperature and pressure that increases with embedding, and by the temperature which increase as a result of hydrothermal solutions originating from Plio-Quaternary Melendiz Mountain volcanisms in the basin. Thus, the primary migration of the petroleum has occurred by the petroleum generation from bituminous shales which are source rocks for petroleum.

When relationships between the bituminous or oily shales and evaporites are studied, it is seen that there is an active transgressive-regressive system in which bituminous shale deposition is followed by the evaporite deposition (Eugster, 1985). It was also determined in late diagenetic stages of highly alkaline isolated saline lakes that siliceous and



Figure 13- Glauberite mineralization alternated with high graded clays.



Figure 14- Disseminated, rosette type glauberite mineralization within low graded clays.



Figure 15- Prismatic, high graded glauberite mineralization alternated with halites.

The mineralization is reached at depth of approximately 400 meters from the surface in the Yeniköy sodium sulfate deposit. The approximate thickness of the glauberite mineralization varies between 17-31 meters. Thickness of the halite mineralization on the other hand is in between 16-45 meters. It was observed that the sodium sulfate mineralization decreased towards south but increased towards north.

Besides; there were also detected oil producing thick bituminous shales with approximate thicknesses varying between 40-85 meters in the study area. The correlations of drillings were lithologically made, and the level distribution of sodium sulfate, rock salt and bituminous shale, and layer and thickness variations with depth were shown in Figure 16.

According to the correlation of drillings, it was observed that zones of sodium sulfate and halite took place in major part of the study area and thickened northward (Figure 16).

To make comparison, the reservoir of the Çayırhan sodium sulfate deposit is totally 190 million tons with 33% grade. Sodium sulfate zone is located at depths of 75-100 meters with thicknesses varying between 1.85-20.05 meters. The major mineral of the Çayırhan sulfate deposit is glauberite. The sodium sulfate zone is formed by the association of glauberite-tenardite-gypsum-Brugnatellite ($Mg_6Fe^{3+}(CO_3)(OH)_{13} \cdot 4(H_2O)$ (Çelik et al., 1987).

Total of 1.8 million tons of sodium sulfate is present in Acıgöl, Tersakan and Bolluk lakes (Alkim AŞ, 2010, oral). According to lake sizes, volumes of water and chemical analyses, our sodium sulfate reservoir in three lakes is estimated at least as 50 million tons (Gündoğan et al., 1995).

However; it was estimated that the Ereğli-Yeniköy sodium sulfate deposit became an important ore deposit in worldwide with its apparent reservoir of 646.482.543 tons. The approximate sodium sulfate and halite grades of the deposit were estimated as; 33.34% Na_2SO_4 and 80.25% NaCl, respectively (Kadınkız et al., 2015).

Acknowledgement

This study was carried out within the framework of “Tuz Gölü Endüstriyel Hammadde Aramaları Projesi” in the Department of Mineral Research and Exploration of MTA. We would like to thank to Erdoğan Yiğit (Geol. Eng., MSc) and to Hasan Topsakal (Geol. Eng., MSc) in field studies.

We are thankful to A. Servet Şanver (Geol. Eng.), Hamdi Kırbaş (Mine Eng., MSc) and to Oya Yücel (Geol. Eng.) from staffs of the Department of the Feasibility Researches.

We appreciate to Prof. Cahit Helvacı and Selahattin Kadir, who contributed a lot for the development of this article, for their supportive critics and suggestions.

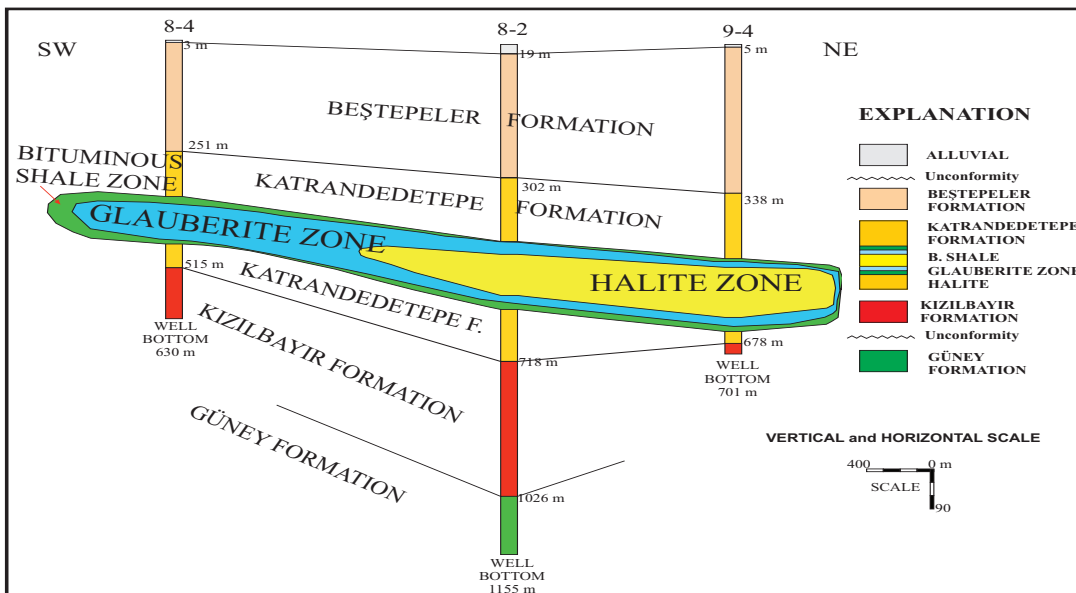


Figure 16- The correlations of drillings 8-4, 8-2 and 9-4 and the locations of mineralization zones.

References

- Altay, T. 2010. Bor-Ulukışla Arasındaki Neojen Yaşlı Sedimanter Birimlerin Minerolojik-Jeokimyasal Özelliklerinin İncelenmesi ve Endüstriyel Hammadde Potansiyelinin Araştırılması, Doktora Tezi, Selçuk Üniversitesi, Konya, 284s (unpublished).
- Arakel, A.V., Cohen, A. 1991. Deposition and Early Diagenesis of Glauberite in the Karinga Creek Playas, Northern Territory, Sediment. Geol., 70,41-59.
- Ayhan, A., Sevin, M., Altun, İ.E. 1986, Karapınar-Ereğli (Konya)-Ulukışla (Niğde) civarının Jeolojisi, Maden Tetkik ve Arama Genel Müdürlüğü Derleme No: 8090 (unpublished).
- Biricik, A.S. 1978. Konya Ereğlisi Akhüyük Travertenleri ve Kükürtlü Suları. Jeomorfoloji Dergisi, 7, 55-61.
- Burnside, M.J., Culbertson, W.C. 1979. Trona deposits in The Green River Basin, sweetwater, Uinta, and Lincoln Counties, Wyoming, open-file report, 79-737.
- Çelik, E., Kartalkanat, A., Kayakıran, S. 1987. Çayırhan Doğal Sodyum Sülfat Yatağı Maden Jeolojisi Raporu ve Dünyada Sodyum Sülfat. Maden Tetkik ve Arama Genel Müdürlüğü Rapor No: 8206 (unpublished).
- Çevikbaş, A., Öztunalı, Ö. 1991, Ulukışla-Çamradı (Niğde) Havzasının Maden Yatakları. Jeoloji Mühendisliği, 39, 22-40, Ankara.
- Demirtaşlı, E., Selim, M., Turan, N., Bilgin, A. Z., Erenler, F., Işıklar, S., Sanlı, D. 1973. Bolkardağlarının Jeolojisi. Cumhuriyetin 50. yılı Yerbilimleri kongresi tebliğler, Maden Tetkik ve Arama Genel Müdürlüğü yayını.
- Demirtaşlı, E., Turan, N., Bilgin A. Z. 1986. Bolkardağları ile Ereğli - Ulukışla Havzasının Genel Jeolojisi. Maden Tetkik ve Arama Genel Müdürlüğü Rapor No: 8097, Ankara (unpublished).
- Dönmez, M., Türkecan, A., Akçay., A. E. 2003. Kayseri-Niğde-Nevşehir Yöresi Tersiyer Volkanitleri, Maden Tetkik ve Arama Genel Müdürlüğü Rapor No: 10.574, Ankara (unpublished).
- Einsele, G. 1992. Sedimentary basins: Evolution, facies, and sediment budget: New York, NY, Springer-Verlag, 628 p.
- Eugster, H., P., Hardie, L.A. 1978, Salina Lakes, Lerman, A. (edi), Lakes; chemistry, geology, physics, New York, NY, Springer-Verlag, 237-293.
- Eugster, H., P. 1985, Oil shales, evaporites and ore deposites, Geochimica et Cosmochimica, Acta, 49, 619-635.
- Ercan, T., Tokel, S. Can, B., Fişekci, A., Fujitani, T., Notsu, K., Selvi, Y., Ölmez, M., Matsuda, J., I., Ui, T., Yıldırım, T., Akbaşlı, A. 1990, Hasandağı – Karacadağ (Orta Anadolu) dolaylarındaki Senozoyik yaşlı volkanizmanın kokeni ve evrimi, Jeomorfoloji Dergisi, 18, 39-54 (unpublished).
- Erol, O. 1969. Tuzgözü Havzasının jeolojisi ve jeomorfolojisi. Tübitak araştırma raporu. (unpublished).
- Göncüoğlu, M. C. 1981a, Niğde Masifinin Jeolojisi: İç Anadolunun Jeolojisi Sempozyu, TJK yayını, Ankara.
- Göncüoğlu, M. C. 1981b, Niğde Masifinde viridinli gnaysın kökeni. T.J.K. Bül. 24/1: 45-50, Ankara.
- Grokhovskii, L.M. 1978, Glauberite as a source of Sodium sulfate, Lithol. Mineral Resour, 12, 356-360.
- Gündoğan, İ., Mordoğan, H., Helvacı, C. 1995. Türkiye'deki Acı Güllerden Sodyum Sülfat Üretimi, Endüstriyel Hammaddeler Sempozyumu, İzmir, Türkiye, 21-22 Nisan 1995.
- Gündoğan, İ., Helvacı, C. 1996. Geology, Hydrochemistry, Mineralogy and Economic Potential of the Bolluk Lake (Cihanbeyli-Konya) and the Adjacent Area, Turkish Journal Of Earth Sciences, (5),91-104.
- Gündoğan, İ., Helvacı, C. 2005. Mineralogy, petrography and diagenetic aspects of the Beypazarı trona deposit, Middle Miocene, Turkey. 44-45 (IESCA-2005, İzmir (Turkey), Abstracts book).
- Hardie, L. A. 1968. The Origin of the Nonmarine Evaporite Deposit of Salina Valley, California, Geochim. Cosmochim Acta, 32, 1270-1301.
- Hardie, L. A. 1984. Evaporites: marine or non marine? Am. J. Sci, 284, 193-249.
- Helvacı, C. 1998. The Beypazarı trona deposit. Ankara Province, Turkey. Proceedings of the First International Soda Ash Conference, Rock Springs, Wyoming, Wyoming State Geological Survey Public Information Circular 40, pp. 67- 103.

- Helvacı, C., İnci, U., Yağmurlu, F., Yılmaz, H. 1987. Batı Anadolu'nun Neojen Stratigrafisi ve Ekonomik Potansiyeli. Akdeniz Üniversitesi Isparta Mühendislik Fakültesi Dergisi, 3, 31-45.
- Helvacı, C., Yılmaz, H., İnci, U. 1988. Beypazarı (Ankara) yöresi Neojen tortullarının kil mineralleri ve bunların dikey ve yanıl dağılımı. Jeoloji Mühendisliği, Sayı 32-33, 33-42.
- Helvacı, C., İnci, U., Yılmaz, H., Yağmurlu, F. 1989. Geology and Neogene trona deposit of the Beypazarı region, Turkey. Turkish Journal of Engineering and Environmental Sciences 13 (2), 245-256.
- Helvacı, C., Alçıçek, M.C., Gündoğan, İ., Gemici, Ü. 2012. Acıgöl Sığ-Kalıcı, Playa-Göl Havzasının Tektono Sedimenter Çatısı ve Ortamsal Gelişimi, GB Anadolu, Türkiye, 65. Türkiye Jeoloji Kurultayı, 2-6 Nisan.
- Helvacı, C., Alçıçek, M.C., Gündoğan, İ., Gemici, Ü. 2013. Tectonosedimentary Development and, Palaeoenvironmental Changes in the Acıgöl Shallow-Perennial Playa-Lake Basin, SW Anatolia, Turkey. Turkish J Earth Sci, 22: 173-190.
- İnci, U., Helvacı, C., Yağmurlu, F. 1988. Stratigraphy of Beypazarı Neogene basin, Central Anatolia, Turkey. Newsl. Stratigr. 18, 165- 182.
- Kadınkız, G., Karakaş, M., Murat, A. 2015. Ereğli-Bor Havzası (Konya-Ereğli-Yeniköy AR: 20056105 No'lu Çalışma Sahası Maden Jeolojisi Raporu. Maden Tetkik ve Arama Genel Müdürlüğü Rapor no: 45567 (unpublished).
- Kadınkız, G., Pekgoz, M. 2015. Yeniköy (Konya-Ereğli) 311 33 13 Erişim nolu ruhsat sahasının (ar: 2011 00 384) buluculuğa esas maden jeolojisi raporu. Maden Tetkik ve Arama Genel Müdürlüğü Rapor No: 45600, (unpublished).
- Kartalkanat, A. 1985. Beypazarı-Çayırhan Sodyum Sülfat Olanakları. Maden Tetkik ve Arama Genel Müdürlüğü Rapor No: 7840 (unpublished).
- Ketin, İ. 1966. Anadolu'nun tektonik birlikleri, Maden Tetkik ve Arama Dergisi, 66, 20-34.
- Ketin, İ., Akarsu, I. 1965. Ulukışla Tersiyer Havzasının jeolojik etüdü hakkında rapor: TPAO, No.: 339, Ankara.
- Koçyiğit, A. 2000. Orta Anadolu'nun genel neotektonik özellikleri ve deprenselliği, TPJD, Workshop, 9-11 Ekim 2000, 1-26.
- Murat, A. 1996. Ereğli (Konya) - Ulukışla (Niğde) Sölestin Zuhurları Maden Jeolojisi Raporu. Maden Tetkik ve Arama Genel Müdürlüğü Rapor No: 9926 (unpublished).
- Last, W.M. 1999. Geolimmology of the Great Plains of western Canada, p. 23-53. In D. S. Lemmon and R. E. Vance [eds.], Holocene climate and environmental change in the Palliser Triangle: A geoscientific context for evaluating the impacts of climate change on the southern Canadian Prairies. Geological Survey of Canada.
- Oktay, F. 1982. Ulukışla ve çevresinin stratigrafisi ve jeolojik evrimi. Türkiye Jeol, Kur, Bül., 25, 15-24.
- Önal, M., Helvacı, C., Ceyhan, F. 2004. Geology and trona potential of the Middle Miocene Gürün (Sivas) basin, Central Anatolia, Turkey: Carbonates and Evaporites, 19 (2), 118-132.
- Orti, F., Gündoğan, I., Helvacı, C. 2002. Sodium sulphate deposits of Neogene age: the Kirmir Formation, Beypazarı Basin, Turkey, Sedimentary Geology 146 (2002) 305- 333
- Orti, F., Rosell L., Ingles, M., Playa, E. 2007. Depositional models of lacustrine evaporites in the SE margin of the Ebro Basin (Paleogene, NE Spain). Geologica Acta, 5 (1), 19-34.
- Özgüner, A., Büyüktemiz, M., Atilla, A., Erdem, E., Mutlu, H., Karatosun, H., Yumuşak, S. 1989. Ereğli (Konya) - Bor (Niğde) havzası kimyasal Tuz yatakları maden jeolojisi raporu. Maden Tetkik ve Arama Genel Müdürlüğü rapor No: 8829 (unpublished).
- Özgüner, A, M., Büyüktemiz, M., Murat, A. 1993. Konya-Karapınar (Sultaniye Ovası) graben çevresi jeolojisi ve Yeraltı tuzlu su seviyelerinin sodyum sülfat tuzu imkanları. Maden Tetkik ve Arama Genel Müdürlüğü, Ankara (unpublished).
- Pampal, S., Meriç, E. 1990. Ereğli (Konya) güneybatısındaki Tersiyer yaşlı tortulların stratigrafisi, Türkiye Jeoloji Bülteni, 33, 39 - 45.
- Rondot, J. 1956. 1/100000'lik 39/2 (güney kısım) ve 39/4 nolu paftaların jeolojisi Maden Tetkik ve Arama Genel Müdürlüğü Rapor No: 2517 (unpublished),

- Sonel, N., Sarı, A. 2004. Ereğli-Ulukışla (Konya-Niğde) Havzasının Hidrokarbon Potansiyelinin incelenmesi. Gazi Üniv, Müh, Mim, Fak, Der, 19(4), 393-403.
- Sevim, M., Altun, İ. 1986. Karapınar Ereğli Konya ve Ulukışla Niğde civarının jeolojisi. Maden Tetkik ve Arama Genel Müdürlüğü Rapor No: 8090 (unpublished).
- Sheppard, R. A., Simandi, G.J. 1999. Closed-basin Zeolites; in Selected British Columbia Mineral Deposit Profiles, Volume 3, Industrial Minerals, G.J. Simandi, Z.D. Hora and D.V. Lefebure, Editors, British Columbia Ministry of Energy and Mines, Open File 1999-10.
- Sinha, R., Raymahashay, B.C. 2004. Evaporite mineralogy and geochemical evolution of the Sambhar Salt Lake, Rajasthan, India, *Sedimentary Geology*, 166, 59-71.
- Smoot, J.P., Lowenstein, T.K. 1991. Depositional environments of non marine evaporites, Melvin, J.D. (edi), *Evaporites, petroleum, and mineral resources*, Elsevier Science, *Developments in Sedimentology*, 189-347.
- Şengör, A. M. C. 1980. Türkiye'nin Neotektoniğinin esasları, Türkiye Jeoloji Kurumu Konferans serisi, 2.
- Şengör, A.M.C., Yılmaz, Y. 1983. Türkiye'de Tethis'in Evrimi, Levha Tektoniği Açısından bir yaklaşım. Türkiye Jeoloji Kurumu yayını no: 1, 75s.
- TPAO AŞ Genel Müdürlüğü TG-10 petrol Sondajı Kompozit logu (unpublished).
- Türkunal, S. 1972. Doğuda Karaisalı, Batıda Konya Ereğlisi ilçeleri boylamları, Güneyde Akdeniz sahili Kuzeyde Ovacık Köyü enlemi ile sınırlı bölgenin jeolojisi. Maden Tetkik ve Arama Genel Müdürlüğü Rapor no: 5552 (unpublished).
- Uyanık, E. 2004. Tuzgözü tuzlarında ham tuz üretimi, *Evaporitler Tuzlar Semineri JMO yayını No:81*.
- Uygun, A. 1982. Tuzgözü havzasının jeolojisi. Maden Tetkik ve Arama Genel Müdürlüğü Rapor No:7188 (unpublished).
- Yağmurlu, F., Helvacı, C. 1994. Sedimentological characteristics and facies of the evaporite-bearing Kirmir Formation (Neogene), Beypazari Basin, central Anatolia, Turkey. *Sedimentology* 41, 847-860.
- Yoldaş, R. 1973. Niğde-Ulukışla bitümlü şist alanının jeolojisi ve ekonomik olanakları. Maden Tetkik ve Arama Genel Müdürlüğü Rapor No: 8097 (unpublished).



Bulletin of the Mineral Research and Exploration

<http://bulletin.mta.gov.tr>



PERMEABILITY OF SAVCIBEY DAM (BİLECİK) AXIS LOCATION AND DESIGN OF GROUT CURTAIN

Mustafa Can CANOĞLU^a and Bedri KURTULUŞ^b

^a Sinop University, Engineering and Architecture Faculty, Department of Environmental Engineering, Sinop

^b Muğla Sıtkı Koçman University, Department of Geological Engineering, Muğla

Research Article

Keywords:

Savcibey Dam, Lugeon Test, falling head permeability test, design of grout curtain hole

ABSTRACT

This study comprise the design of the planned grout curtain in Savcibey Dam (Söğüt/Bilecik) in order to provide impermeability along the dam axis. Within the context of field studies, engineering geology map was generated, ground investigation drilling was realized and permeability tests were performed. Within the field studies, the joint conditions of the geological units (Triassic aged Bozüyük Metamorphic schists) under the dam axis and its effect on permeability was observed considering the positions of the discontinuities with regard to the dam axis location. Orientation of discontinuities generally have strikes changing between N – S and NNE – SSW. 5 boreholes on dam axis, 2 boreholes on cofferdam, 3 boreholes on diversion tunnel and 2 boreholes on spillway total 245 m ground investigation borehole were drilled. In order to determine the permeability profile of dam axis and design the grout curtain, Lugeon tests in Bozüyük Metamorphic units observed in dam axis, falling head permeability tests in alluviums observed in thalveg and slope debris observed in right abutment were performed. Lugeon tests realized in Bozüyük Metamorphic units show that the unit is generally permeable and partly low permeable. Alluvium and slope debris are highly permeable. In addition, drilling works realized in dam axis shows that the augmentation of the weathering degree cause an increase of permeability in Triassic aged Bozüyük Metamorphic schists. As a result of these studies information about the permeability of Savcibey Dam was collected and the grout curtain hole was designed. Accordingly, it is predicted that approximately 40 m depth of grout curtain from the stripping excavation with the depth of 1.50 m would prevent the possible leakages.

Received: 15.01.2015

Accepted: 02.08.2016

1. Introduction

Depending upon the population increase, dams make a significant contribution to the national economy in terms of energy need, potable water supply, agricultural irrigation, flood protection, fishery, recreation and many more purposes. Engineering geology and hydrogeology studies realized during planning stage are crucial to minimize the potential problems during construction stage and to exploit these dams safely. These constructions are studied by many researchers from different perspectives such as geotechnics, hydrogeology, landsliding, liquefaction, resistance to earthquake, etc. (Lombardi, 1985; Nonveiller, 1989; Karagüzel and Kılıç, 2000; Tunar et al., 2013; Eryılmaz Türkkın and Korkmaz, 2015; Aldemir et al., 2015). Lombardi (1985) studied about the cementation properties of grout and grout curtain designed for the impermeability of dams and underlined that the cohesion of the grout increase the viscosity and grout can not penetrate into the

discontinuities. Nonveiller (1989) studied about the different techniques for the construction of grout curtain. Aksoy and Ercanoğlu (2006) and (2007) studied about landsliding. Ulusay et al. (2007) studied about the liquefaction in dams and reservoirs. Tunar et al. (2013) studied about tailings dam stability. Eryılmaz and Korkmaz studied the determination of hydraulic conductivity with in-situ tests. Aldemir et al. (2015) studied about analysis techniques utilized in earthquake behaviours of concrete dams. Karagüzel and Kılıç (2000) researched the effect of alteration in permeability of an ophiolitic melange in terms of grouting efficiency and grout take amount. In addition, Karagüzel and Kılıç (2000) expressed mathematically the relation between the water loss in Lugeon test and grout take amount with the use of statistical analysis. Moreover, permeability of rock masses is analysed by many researchers (Ewert, 2003; Foyo et al., 2005; Şekercioğlu, 2007; Coli et al., 2008; Li et al., 2008; Gürocak and Alemdağ, 2012; Kayabaşı et al., 2015). Foyo et al. (2005) determined

* Corresponding author: Mustafa Can Canoğlu, e-mail: mccanoglu@sinop.edu.tr

<http://dx.doi.org/10.19111/bmre.00419>

a secondary permeability index for the rock masses in dam foundations with Lugeon tests. Rock mass permeability properties are analysed numerically and empirically in the study realized by Gürocak and Alemdağ (2012). Kayabaşı et al. (2015) evaluated the relation between the Lugeon values and discontinuity properties of rock masses with the utilization of nonlinear regression analysis. For the determination of grout curtain depth the empiric method proposed by Şekercioğlu (2007). However, as this method is an empiric method, grout curtain depth is determined using with the engineering judgement considering the hydraulic head of the foundation rock.

The aim of this work in general is, design of the grout curtain and to determine the permeability characteristics of Savcıbey Dam axis location. For this purpose, the depth of the grouting works is determined. Project area is located in Bilecik Province, Söğüt County (Figure 1). Savcıbey Dam is planned to construct on Yol River by DSİ 3. Regional Directorate for the irrigation of agricultural lands which is approximately 164 ha and belonging to Savcıbey Village. Dam axis is located in 1/25,000 scaled Eskişehir “İ24-a2” topographic map and transport is provided by asphalt road (Figure 1).

2. Geology

This study comprises office works, site works and laboratory works. In context of office works, literature review about the study area and its near environ is done and the studies realized by General Directorate of State Hydraulic Works (DSİ) and General Directorate of Mineral Research and Exploration (MTA) are investigated. Site works are consist of geological mapping, drilling, and in-situ permeability tests. Laboratory works are performed on the core samples

handled from the drilling operations. 5 boreholes and 200 m depth for dam axis, 2 boreholes and 25m depth for cofferdam, 3 boreholes and 30m depth for diversion tunnel, 2 boreholes and 20m depth for spillway, total 275m of drilling works realized within the field works. The boreholes drilled for axis location, diversion tunnel and cofferdam are shown on figure 2 and 3. The permeability characteristics of ruck units under different hydraulic heads are determined by the Lugeon tests performed in the boreholes drilled along dam axis. Hydraulic conductivity of the alluvium and slope debris is specified by the falling head permeability tests.

Dip and dip direction of the discontinuities in metamorphic rocks is the most important parameter for the permeability of dam axis location. Therewithal, infilling material, weathering degree, aperture, spacing are the factors effecting the dam permeability also. Any negative provision is detected in terms of permeability in dam axis location based on the observations realized according to the field prestudies. In addition, dip directions are generally towards upstream, even if schistosity strikes cross the dam axis with 90° and the discontinuities are infilled with clay. For these reasons, any permeability problem is waiting based on the observations.

Schists belonging to Bozüyük Metamorphics are dominated in project area and its surroundings but marbles of same formation crop out locally. Quaternary aged alluvium (Qal) and slope debris (Qym) overly the Bozüyük Metamorphics discordantly. Study area is located in second degree earthquake zone and approximately 50 km far from North Anatolian Fault Zone which is the one of main active tectonic fault system. Geological units of dam location and surroundings is explained below and generalized stratigraphic columnar section of study area and its surrounding is given in figure 4.

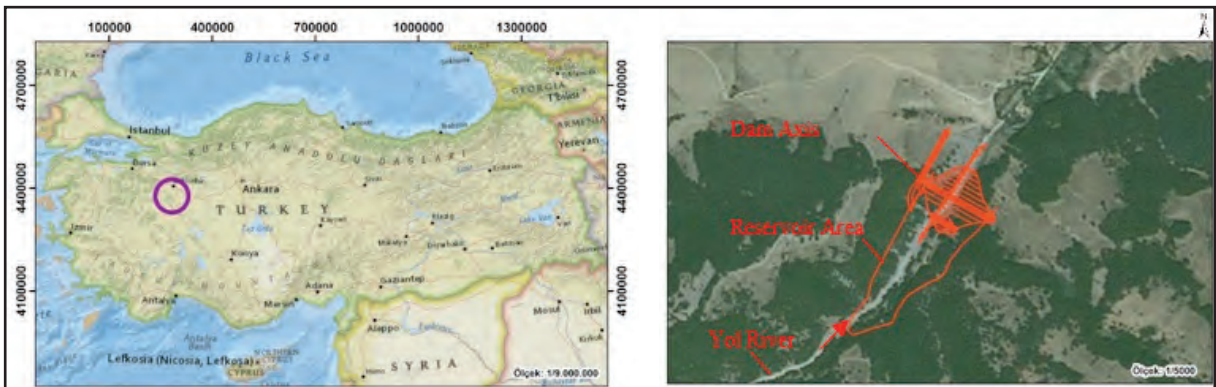


Figure 1- Site location map of study area.

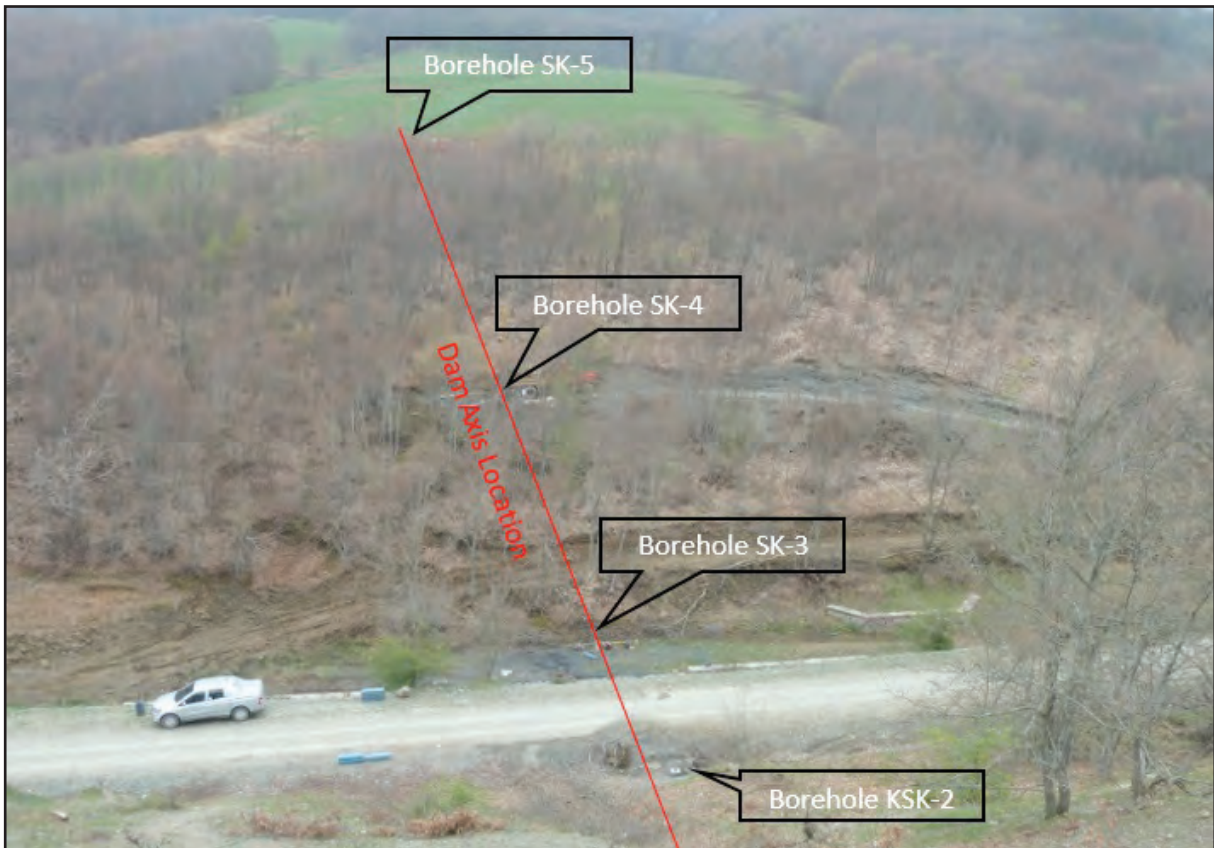


Figure 2- View to right abutment from borehole SK -1 (left abutment) in Savcıbey Dam axis location.

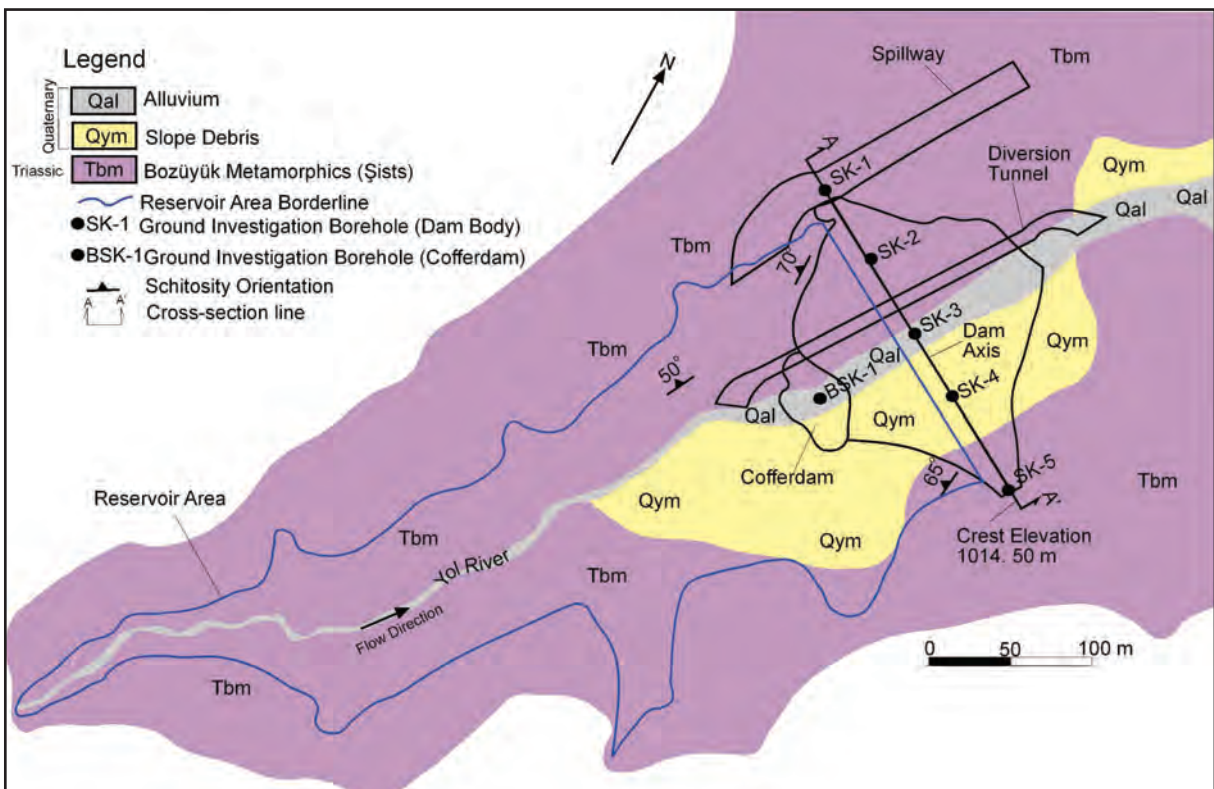


Figure 3- Engineering geology map of Savcıbey Dam axis location and reservoir area.

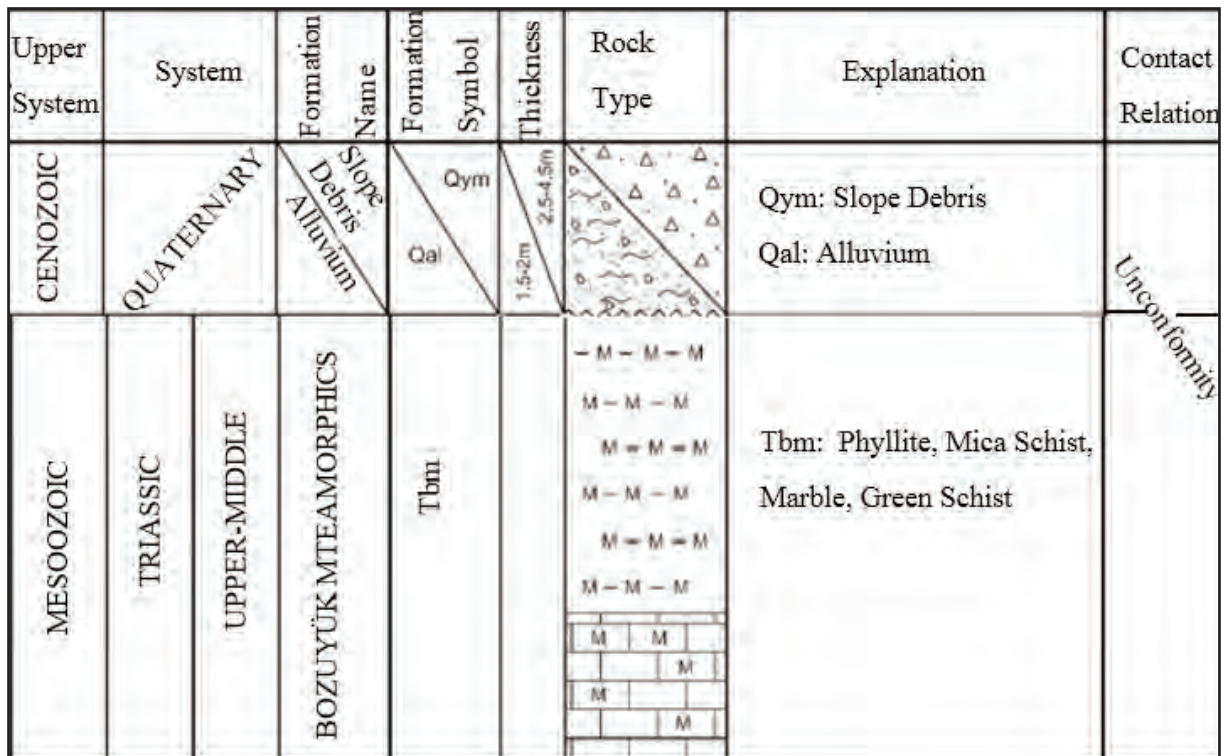


Figure 4- Generalized stratigraphic columnar section of dam location and its surrounding.

2.1. Bozüyük Metamorphics (Tbm)

Bozüyük Metamorphics are exposed over large areas in the region. This unit is investigated by many researchers and aged as Triassic (Yılmaz, 1979; Yılmaz and Koral, 2007; Ayaroğlu, 1979; Kayadibi et al., 1994). Quaternary aged alluvium (Qal) and slope debris (Qym) overly the Bozüyük Metamorphics discordantly. Rock units of this formation are phyllite, mica schist, green schist, talk schist, chloride schist, amphibole schist, microscaled glaucophane schist, graphite schist, ortho gneiss, quartzite, marble, serpentinite, peridotite, gabbro, metadiabase and metabasalt (Yılmaz, 1979). Initially, carbonates with clay and sand sized materials and products of a granitic intrusion are effected from metamorphism of green schist facies conditions and became actual petrographic properties (Ayaroğlu, 1979). Green schists belonging to Bozüyük Metamorphics are dominated in project area and its near environ but local marble masses are also observed. However, any marble mass is encountered on the ground of dam body as seen in figure 5. However, Triassic aged this units are subjected to tectonic effect of during many geological times and due to this effect the schistosity planes have different orientations. Schistosity plane

strikes are towards NE-SW direction and their dips are changing between 50° and 70° based on the orientations surveyed on the outcrops in dam axis, left and right abutments. General dip direction of schistosity planes are surveyed as NW.

First folding is started with Hersinian movement in study area and its near environ. Paleozoic aged schists are folded severely and intrusion activity is started through the faults in faulting stage. Acidic intrusives are settled into the schists during this stage. Then aplites are setted into these intrusives trough the NE-SW directed faults. This aplite mass is transformed to E-W direction with the Alpine movements (Yılmaz, 1979). But, any of this aplites are encountered in dam location. Fracture system which are formed by the paleotectonic activities are generally infilled with clay. The mean spacing of the fractures is 2m, aperture is changing between 1 cm and 30 cm based on the information handled from the line investigation along the road cut.

Accordingly, the relation between the Quaternary aged alluvium and slope debris overlying the Bozüyük Metamorphics is shown on figure 5 with the ground investigation borehole locations which is represented with A-A' cross section of figure 3.

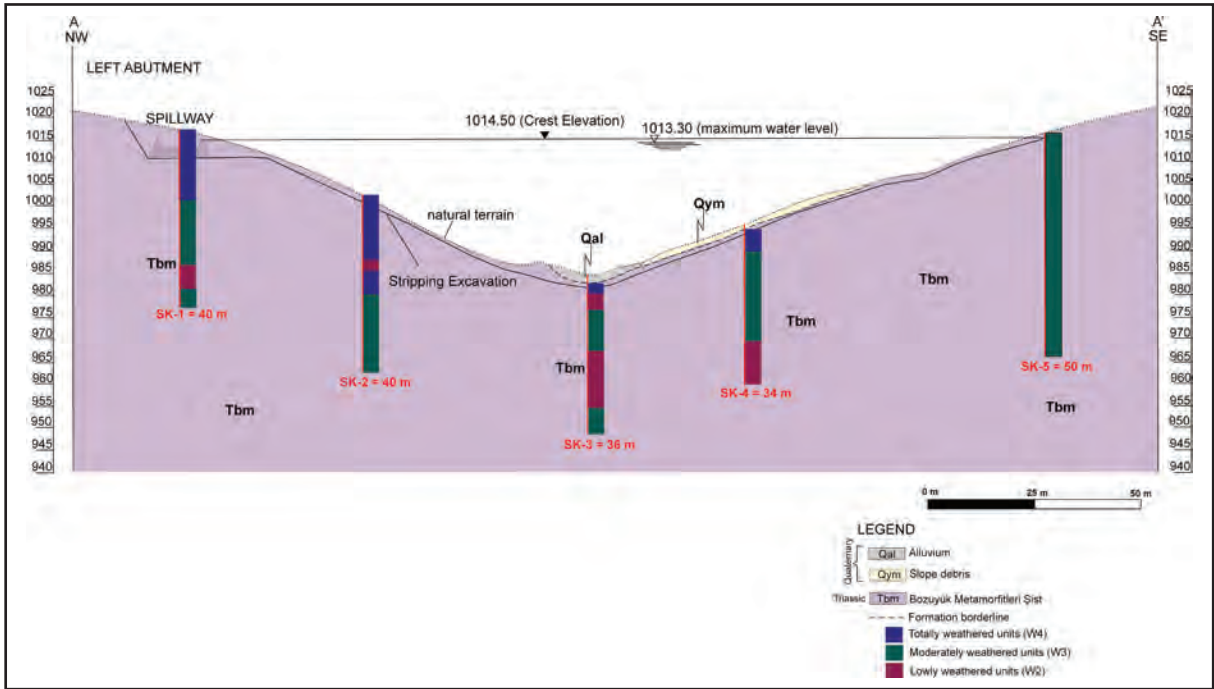


Figure 5- Engineering geology cross section of dam body (A - A' section).

2.2. Alluvium (Qal)

Quaternary aged alluviums are located along the Yol River bed (Figures 3 and 5). This unit, which is formed by erosion transportation and deposition, is constituted by gravel, sand, silt and clay sized material. According to the drilling works, the thickness of the alluvium is changed between 1.50 - 2.00 m. The width of the alluvium can be reach up to 10 m locally.

2.3. Slope Debris (Qym)

Blocky structured slope debris are formed by the weathered bedrock and transported to piedmont. For this reason slope debris is constituted by coarse gravel and clay sized material and cementation is observed. The drilling works realized in right abutment shows that the slope debris thickness can be reach up to 1.0 m.

3. Engineering Geology

Savcıbey Dam body is projected as clay cored rock-filled dam, its height from thalveg is 31.15 m and from foundation is 36.15 m. Crest length of dam body is 189.67 m, thalveg elevation is 985.64 m and minimum water elevation of reservoir is 995.75 m,

maximum water elevation of reservoir is 1013.3 m. Sluice outlet is designed as concrete jacket penstock pipe type in left abutment with inlet elevation of 988.50 m and outlet elevation of 978.50 m. Spillway is projected in left abutment with water stilling basin.

According to the criteria of weathering degree of rock masses proposed by ISRM (2007), the core samples obtained from drilling works are generally totally weathered (W4) and moderately weathered (W3), but locally lowly weathered (W2) units are encountered.

4. Permeability of Dam Axis Location

The principal aim of this study is design of grout curtain and for this purpose, to determine the permeability of alluvium, slope debris and bedrock falling head permeability test and Lugeon tests have been performed. These tests are realized in ground investigation boreholes drilled on dam axis location.

Lugeon test is an in-situ test applied in a borehole with the purpose of hydraulic conductivity determination of rock masses under different hydraulic heads. This test is realized generally with test levels changing between 2 – 5 m. Test level

length is designate based upon the physical and structural properties of rock mass. In an uniform and impermeable rock mass test level can be applied with 5 – 10 m test zone and in a permeable rock mass which has variable physical properties, this test zone can be reduced until 1 m (Akyüz, 2010). Test method proposed by Lugeon (1933), 1 Lugeon is defined as the water amount pumped to the 1 meter length of test zone under 10 atm hydraulic pressure in 1 minute. The pressure applying to the test zone is also specified by engineering judgement depending on the physical properties of rock but general application in Turkey is using 2, 4, 6, 8, 10 kg/cm² of test pressures. Each pressure stage applied to the rock during 10 minutes and the water leakages are recorded each 5 minutes. Then, 9, 7, 5, 3, 1 kg/cm² of test pressures are applied and water leakages are recorded.

Lugeon value (LU) is calculated by the equation below.

$$LU = (Q \times 10) / (P \times L) \quad (\text{equation 1})$$

In this expression, LU is Lugeon value (lt/min/m), Q is water amount given to the rock formation (lt/min), P is hydraulic head applied to the test zone (kg/cm²) and L is test length (m). The permeability class

corresponding to the Lugeon values is presented in table 1.

Table 1- Permeability classification based on the Lugeon values of rock masses

| Lugeon Values | Permeability Class |
|---------------|--------------------|
| <1 Lugeon | Impermeable |
| 1 - 5 Lugeon | Low Permeable |
| 5 - 25 Lugeon | Permeable |
| >25 Lugeon | Highly Permeable |

A grout curtain is planned along the dam axis to avoid the probable leakage from Savcibey Dam and to accumulate the water more efficiently. To design the grout curtain and to predict the approximate grout amount for each grout stage, Lugeon (1933) tests are performed in total 6 boreholes, 5 boreholes (SK-1, SK-2, SK-3, SK-4 and SK-5) drilled along dam axis and 1 borehole (BSK-1) drilled for cofferdam (Figure 3).

Under homogeneous and isotropic conditions 1 Lugeon is equivalent to a hydraulic conductivity of 1.3x10⁻⁵ cm/s proposed by Fell et al. (2005). In the table proposed by Fell et al. (2005), the relation between Lugeon values and hydraulic conductivity is shown on figure 6.

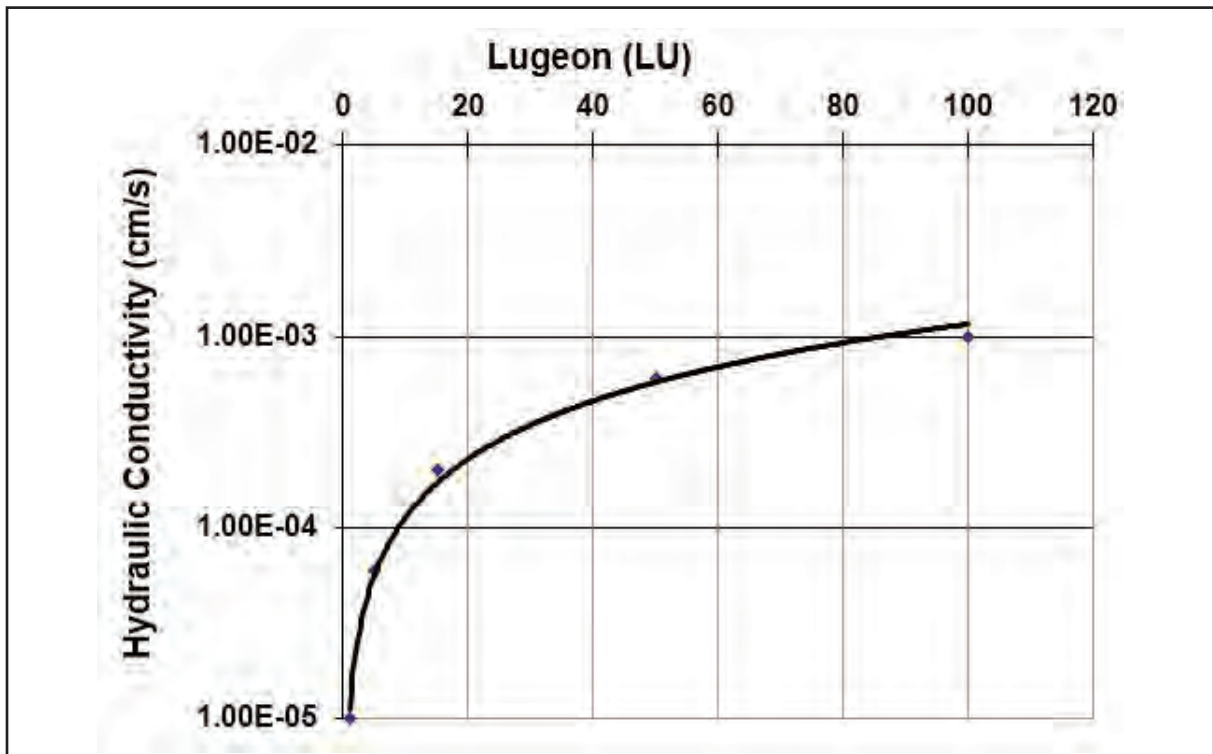


Figure 6- Relation between Lugeon values and hydraulic conductivity (modified from Fell et al., 2005).

Hydraulic conductivity values corresponding to Lugeon values of figure 6 can be represented by the expression given in equation 2.

$$K = 1 \times 10^{-5} \times (LU)^{1.0082} \quad (\text{equation 2})$$

The coefficient of correlation between hydraulic conductivity (K) and Lugeon values (LU) expressed in equation 2 is determined as $R^2=0.9954$. The coefficient of correlation converging to 1 indicates the higher relationship between the Lugeon and hydraulic conductivity values expressed in equation 2. In other words, R^2 converging to 1 shows that equation 2 reflects the reality. The Lugeon values obtained from the Lugeon tests which are performed for the determination of the permeability characteristics of Savcıbey Dam foundation under variable hydraulic heads, are transformed to hydraulic conductivity with the use of equation 2. Minimum, mean and maximum hydraulic conductivity values are shown on table 2.

In addition, the variation of Lugeon values with the depth is shown on figure 7 for the boreholes drilled in left abutment SK-1 and SK-2, thalveg SK-3 and BSK-1 and right abutment SK-4 and SK-5.

5. Falling Head Permeability Tests

Falling head permeability tests are performed in alluvium and slope debris to specify the permeability characteristics of Savcıbey Dam soil foundation. Each test stage is set as 2 m. This test is realized in weathered parts of Bozüyük Metamorphics in 0 – 4 m stage of SK-1, 0 – 2 m stage of SK-2 and alluviums in 0 – 8 m stage of BSK-1. Falling head permeability test cannot be applied to the boreholes SK-3, SK-4 and SK-5 due to the use of casing for unstable borehole walls during drilling operation. Permeability of alluvium sampled

from the borehole SK-3 is predicted by the test results of the borehole BSK-1.

Falling head permeability tests realized in boreholes SK-1 and SK-2 show that the weathered and highly jointed parts of Bozüyük Metamorphics are permeable in terms of hydraulic conductivity ($K \approx 10^{-4}$ cm/s). And the falling head permeability tests realized in the borehole BSK-1 shows that the alluviums are highly permeable in terms of hydraulic conductivity ($K \approx 10^{-3}$ cm/s). Under this circumstance, excavation of alluvium units under the Savcıbey Dam axis is important with regard to the permeability and stability of dam body. Considering the groundwater level and the hydraulic conductivity of the excavated soil, it is predicted that a water income to the excavation pit with 3,2 lt/s flow rate (SuYapı, 2013). In this case, the water income to the excavation pit should be dewatered with suitable pumps.

6. Determination of Grout Curtain Depth

There are many methods for the determination of grout curtain depth (h') (Bureau of Indian Standard, 1993; Pettersson and Molin, 1999; Ewert, 2003; Şekercioğlu, 2007; Schleiss and Pougatsch, 2011). This methods in which the grout curtain depth is a function of dam height (h), are expressed as equation 3, 4, 5, 6 and 7.

According to Bureau of Indian Standard (1993) $h' = \left\{ \frac{2}{3} \right\} h + 8$ (equation 3);

According to Pettersson ve Molin (1999) $h' = \left\{ \frac{3}{4} \right\} h$ (equation 4);

According to Ewert (2003) $h' = h$ (equation 5);

According to Schleiss ve Pougatsch (2011) $h' = \left\{ \frac{2}{3} \right\} h$ (equation 6);

According to Şekercioğlu (2007) $h' = \left\{ \frac{1}{2} \right\} h + 15$ (equation 7);

Table 2- Minimum, mean and maximum hydraulic conductivity (cm/s) of each borehole.

| | Hydraulic Conductivities (cm/s) | | | | | |
|---------|---------------------------------|---------|---------|---------|---------|---------|
| | SK-1 | SK-2 | SK-3 | SK-4 | SK-5 | BSK-1 |
| Minimum | 4.1E-05 | 4.1E-05 | 3.1E-05 | 3.6E-05 | 8.4E-06 | 8.8E-05 |
| Mean | 1.4E-04 | 2.2E-04 | 7.6E-05 | 1.3E-04 | 1.1E-04 | 7.5E-04 |
| Maximum | 3.6E-04 | 5.4E-04 | 1.8E-04 | 1.9E-04 | 2.3E-04 | 1.8E-03 |

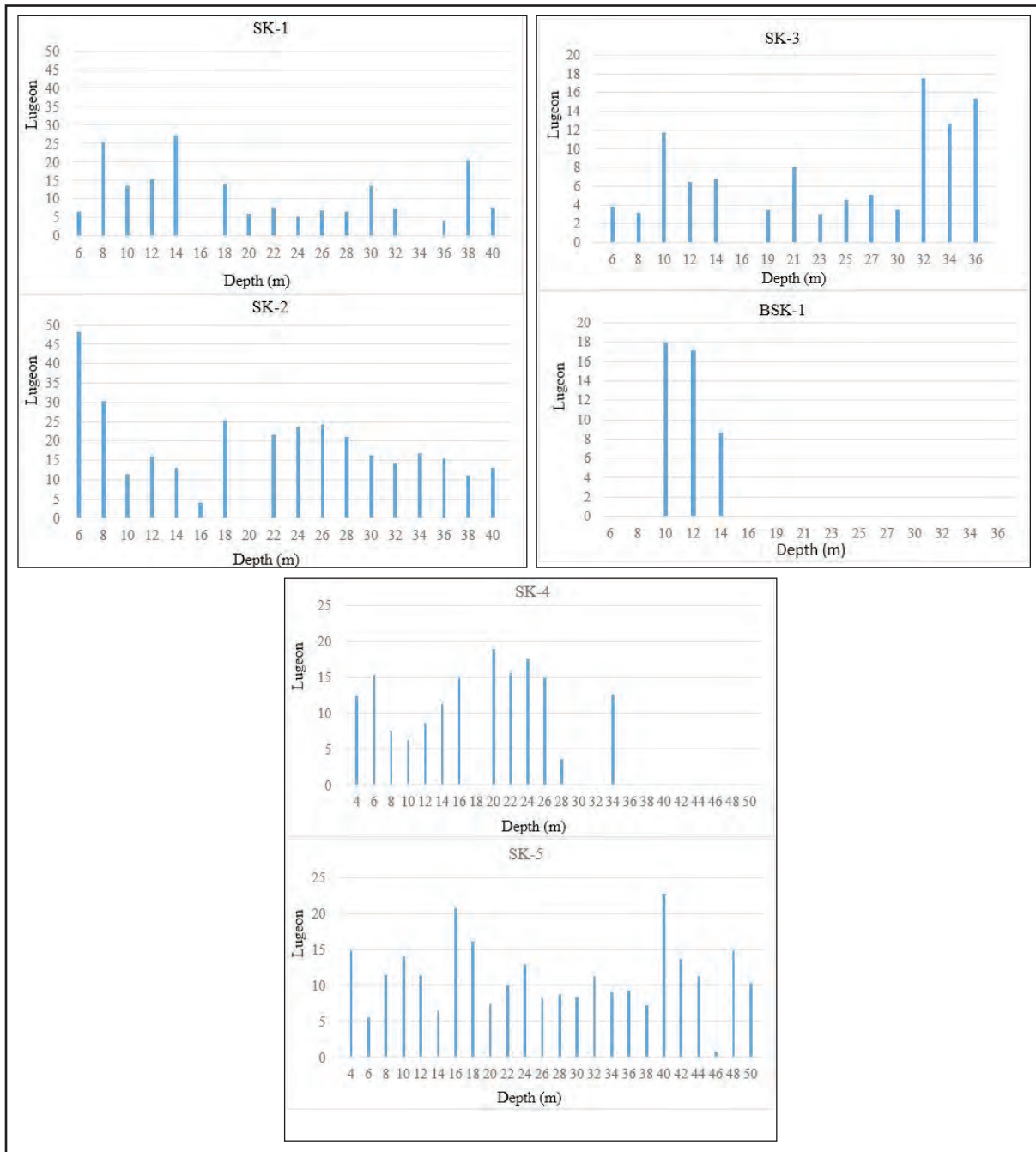


Figure 7- Lugeon value variations with depth for left abutment (SK- 1 and SK-2), thalveg (SK – 3 and BSK – 1) and right abutment (SK -4 and SK -5).

Grout curtain depth (h') calculation is compared using with the equation 3 proposed by Bureau of Indian Standard (1933) and the equation 7 proposed by Şekercioğlu (2007) for Savcıbey Dam thalveg area. Hereunder, h' is calculated 30.575 m from equation 7 and 28.77 m from equation 3. It is seen that both of methods proposed for the grout curtain depth are close. In this study, grout curtain depth for Savcıbey Dam is calculated based on the equation 7 proposed

by Şekercioğlu (2007) but on behalf of to be in safe side same grout curtain depth is predicted for the abutments considering the engineering judgement.

In addition, grout curtain depth is designed considering the height of dam body from thalveg (31.15 m) and the extra hydraulic head on the bedrock of dam foundation. Moreover, grout curtain is prolonged through the reservoir area in order to

avoid small-scale leakages. It is thought that small-scale leakages would be avoided and impermeability would be provided by the grout curtain represented in figure 7. Groundwater Levels (GWL) and hydraulic conductivity values are considered for the design of the grout curtain. GWL surveys realized after drilling operation shows that GWL of the borehole SK-1 is 13.20 m and SK-2 is 13.60 m. GWL of the borehole SK-3 drilled for thalveg is 0 m. GWL of the boreholes SK-4 and SK-5 drilled for right abutment are 3.00 m and 0.60 m respectively. Comparison of the GWL of the boreholes drilled along the dam axis indicates that GWL movement is through river for both of abutments (Figure 8). This GWL conditions demonstrates that river is fed by both of the abutments and any of water flux trough the abutments by the river elevation.

It is aimed to avoid the potential leakages and provide the impermeability with the grout curtain represented in figure 8. Accordingly, grout curtain depth of left abutment is changing between 35 and 40 m. Augmentation of hydraulic head on the formation will also increase the hydrostatic pressure and favour the leakages. For this reason, due to the most of the hydraulic head will be on thalveg, grout curtain depth is increased approaching trough thalveg. Grout curtain depth is calculated as 40 m along thalveg. As a result of the calculations, approaching to right abutment from thalveg the grout curtain depth is 45 m from

the stripping excavation due to the augmentation of permeability.

7. Results and Suggestions

The results obtained from the Lugeon tests performed in 5 boreholes drilled on dam axis and 1 borehole drilled on cofferdam are evaluated for thalveg, right abutment and left abutment separately. Evaluation is realized based on the permeability classes stated in table 1. Accordingly, permeability of the boreholes SK-1 and SK-2 drilled for left abutment are changing between permeable and highly permeable until 14 m depth. Permeability of the borehole SK-1 is changing between lowly permeable and permeable between the depths 14 – 40 m and the rock mass of the borehole SK-2 is permeable – highly permeable especially for the depths 18 – 28 m between 28 – 40 m formation is permeable (Figure 7).

Lugeon values obtained from the boreholes SK-3 and BSK-1 drilled for thalveg indicates the existence of local highly permeable levels. Due to the water income from the borehole entrance during the Lugeon test, the test is failed for the 6 – 8m and 8 – 10 m test levels considering depth of alluvium is more than 5 m in the borehole BSK-1 and the Lugeon test can be performed only in 10 – 12 m, 12 – 14 m, 14 – 16 m test levels. For these test levels rock mass is evaluated

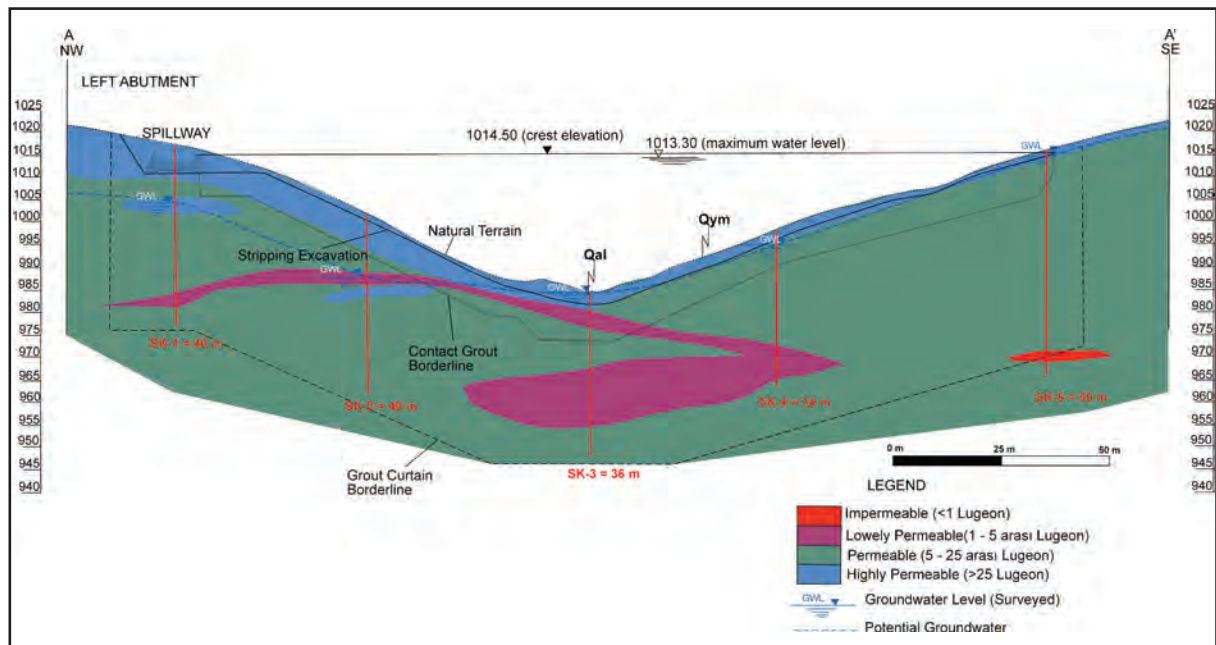


Figure 8- Microzonation of dam axis based on the Lugeon values and grout curtain borderline.

as permeable. However, 6 – 10 m and 23 – 32 m test levels of the borehole SK-3 can be evaluated as lowly permeable. The other test levels are permeable (Figure 7). The boreholes SK-4 and SK-5 drilled in right abutment are generally permeable – lowly permeable and some local impermeable levels are remarked (Figure 7).

Permeability variations based upon the depth in figure 7 is evaluated as follow considering the permeability classes corresponding to Lugeon values given in table 1;

- In the borehole SK-1, 6 – 8 m and 12 – 14 m test levels are highly permeable, 4 – 6 m, 18 – 20 m, 22 – 24 m and 34 – 36 m test levels are lowly permeable and other test levels are permeable.
- In the borehole SK-2, 4 – 8 m test level is highly permeable, 14 – 16 m test level is lowly permeable and other test levels are permeable.
- In the borehole SK-3, 4 – 8 m, 16 – 19 m, 21 – 25 m and 28 – 30 m 12 – 14 m test levels are lowly permeable and other test levels are permeable.
- In the borehole BSK-1, 8 – 14 m test levels are permeable.
- In the borehole SK-4, 26 – 28 m test level is lowly permeable and other test levels are permeable.
- In the borehole SK-5, 44 – 46 m test level is impermeable 4 – 6 m test level is lowly permeable and other test levels are permeable.

This unit can be defined as moderately (W3) – completely (W4) weathered based on the data obtained from ground investigation boreholes and the observations considering the weathering degree definition criteria of rock masses proposed by ISRM (2007). Additionally, lowly weathered (W2) units are observed during drilling operations. Comparison of the figures 5 and 8 indicates the effect of weathering degree to permeability. Accordingly, it is observed that completely weathered (W4) units are more permeable than moderately (W3) and lowly weathered (W2) units. And it is remarked that the Lugeon test levels which are failed due to the water income from the borehole entrance are completely weathered (W4). In this case, it can be said that permeability increases with

the augmentation of weathering degree in Bozüyük Metamorphics.

Foundation rock unit of dam location Bozüyük Metamorphics can be evaluated as lowly permeable – permeable. It is approved that 1.5 – 2 m thick alluvium and 1 m thick slope debris existing in dam axis will be removed by stripping excavation. The results of geological observations and Lugeon tests performed in boreholes are evaluated and it is deduced that after removing the alluvium and slope debris there will not be any permeability problem except some levels in thalveg and abutments. Considering these, water movement from upstream to downstream will be avoided with the grout curtain, in other words, the targeted impermeability will be provided.

Bozüyük Metamorphics which constitute foundation rock of the dam axis location and its near environ is observed as mica schist, graphite schist and talc schist. The units belonging to Bozüyük Metamorphics observed in dam location and its near environ are generally greenish brown – grey with schistosity. Triassic aged this metamorphic units are subjected to tectonic effect of during many geological times and due to this effect the schistosity planes have different orientations. However, any negative provision is detected in terms of permeability in dam axis location due to the dip direction of schistosities are generally towards upstream. In addition, slope debris and alluvium located in dam body will be stripped and it is planned to construct the dam on the bedrock. During this operation water income to the excavation area can be awaited but discharging of this water with the suitable pumps is possible. Any stability problem is awaited for dam axis considering the stress-strain characteristics of bedrock.

8. Acknowledgement

This work is realized in context of “Sakarya: Pamukova Çilekli, Kemaliye and Turgutlu, , Merkez-Beşevler, Kütahya: Pazarlar-Orhanlar, Tavşanlı-Kışlademirli, Bilecik ili: Söğüt-Savcıbey Dams Planning Engineering Services” project belonging to Turkish Republic Ministry of Forestry and Water Works, General Directorate of State Hydraulic Works, Eskişehir 3. Regional Directorate with the contribution of SuYapı Engineering and Consulting Co.

Authors thank to SuYapı Engineering and Consulting Co. for their information share and to State Hydraulic Works, Eskişehir 3. Regional Directorate staff especially Hayrettin Baysal, Şeref Dağdelen, Feridun İnce, Osman Çakır, Engin Kaplan and Hüseyin Yavuz.

In addition, authors thank sincerely to SuYapı Engineering and Consulting Co. family especially to Department of Geology and Geotechnics who finance for this article and share their engineering experiences with their scientific support.

References

- Aksoy, H., Ercanoğlu, M. 2006. Determination of the rockfall source in an urban settlement area by using a rule-based fuzzy evaluation. *Natural Hazards and Earth System Science* 6, 941-954.
- Aksoy, H., Ercanoğlu, M. 2007. Fuzzified kinematic analysis of discontinuity-controlled rock slope instabilities. *Engineering Geology* 89, 206-219.
- Akyüz, S. 2010. Kargı baraj yeri (Çorum) litolojik birimlerin geçirgenlik özellikleri yönünden incelenmesi. Çukurova Üniversitesi, Fen Bilimleri Enstitüsü, Jeoloji Mühendisliği Anabilim Dalı, Yüksek Lisans Tezi, 134s.
- Aldemir, A., Yılmaztürk, S.M., Yücel, A.R., Binici, B., Arıcı, Y., Akman, A. 2015. Beton barajların deprem davranışlarının incelenmesinde kullanılan analiz metotları. *İMO Teknik Dergi* 6943-6968.
- Ayaroğlu, H. 1979. Bozüyük metamorfiklerinin (Bilecik) petrokimyasal özellikleri. *Türkiye Jeoloji Bülteni* 22/1, 101-107.
- Bureau of Indian Standard, 1993. "Guidelines for the Design of Grout Curtain: Part 2: Masonry and Concrete Gravity Dams".
- Coli, N., Pranzini, G., Alfı, A., Boerio, V. 2008. Evaluation of rock-mass permeability tensor and prediction of tunnel inflows by means of geostructural surveys and finite element seepage analysis. *Engineering Geology* 10, 174-184.
- Eryılmaz Türkkın, G., Korkmaz, S. 2015. Kuyu ve akifer testlerinde uygulanan analitik ve sayısal yöntemlerle hidrolik iletkenliğin belirlenmesi. *İMO Teknik Dergi* 6969-6991.
- Ewert, F.K. 2003. Discussion of Rock Type Related Criteria for Curtain Grouting. *Proceedings of the Third International Conference on Grouting in Rock and Ground Improvement*, ASCE Special Publication No. 120.
- Fell, R., MacGregor, P., Stapledon, D., Bell, G. 2005. *Geotechnical Engineering of Dams*. Taylor and Francis. London. UK.
- Foyo, A., Sanchez, M. A., Tomillo, C. 2005. A proposal for a secondary permeability index obtained from water pressure tests in dam foundations. *Engineering Geology* 77, 69-82.
- Gürocak, Z., Alemdağ, S. 2012. Assessment of permeability and injection depth at the Atasu dam site (Turkey) based on experimental and numerical analyses. *Bulletin of Engineering Geology and the Environment* 71, 221-229.
- ISRM (International Society for Rock Mechanics). 2007. *Rock Characterization, Testing and Monitoring. International Society of Rock Mechanics Suggested Methods*, Pergamon Press, Oxford, 211 p.
- Karagüzel, R., Kılıç, R. 2000. The effect of the alteration degree of ophiolitic melange on permeability and grouting. *Engineering Geology* 57, 1-12.
- Kayabaşı, A., Yeşiloğlu-Gültekin, N., Gökçeoğlu, C. 2015. Use of non-linear prediction tools to assess rock mass permeability using various discontinuity parameters. *Engineering Geology* 185, 1-9.
- Kayadibi, Ö., Aydal, D., Kadioğlu, Y. K. 1994. Bilecik-Söğüt altın mineralizasyonunun incelenmesi. *Türkiye Jeoloji Kurultayı Bülteni* 9, 252-259.
- Li, P., Lu, W., Long, Y., Yang, Z., Li, J. 2008. Seepage analysis in a fractured rock mass: the upper reservoir of Pushihe pumped storage power station in China. *Engineering Geology* 97, 53-62.
- Lombardi, G. 1985. The Role of Cohesion in Cement Grouting of Rock, 15. *ICOLD-Congress*, Lausanne, 3, 235-261.
- Lugeon, M. 1933. *Barrage et Géologie*. Dunod. Paris.
- Nonveiller, E. 1989. *Grouting Theory in Practice*. Elsevier, Tokyo.

- Pettersson, S.A., Molin, H. 1999. "Grouting and Drilling for Grouting: Purpose, Application, Methods with Emphasis on Dam and Tunnel Projects". Atlas Copco. 6991 1019 01
- Schleiss, A. J. Pougatsch, H. 2011. "Les Barrages: Du projet à la mise en service. Presses Polytechniques Universitaires Romandes, 17, 714p.
- Suyapı, 2013. Savcıbey Göleti, mühendislik jeolojisi planlama raporu rev.1. DSİ 3. Bölge Müdürlüğü, Eskişehir.
- Şekercioğlu, E. 2007. Yapıların projelendirilmesinde mühendislik jeolojisi. JMO yayınları, 28, 4. Baskı, s.117.
- Tunar, N.Ö., Ulusay, R., Işık, N.S. 2013. A study on geotechnical characterization and stability of downstream slope of a tailings dam to improve its storage capacity (Turkey). Environmental Earth Sciences 69, 1871-1890.
- Ulusay, R., Tuncay, E., Hasağebi, N. 2007. Liquefaction assessments by field-based methodologies for the foundation soils at a dam site in northeast Turkey. Bulletin of Engineering Geology and the Environment 66 (3), 361-375.
- Yılmaz, M., Koral, H. 2007. Yenişehir Havzası'nın (Bursa) neotektonik özellikleri ve jeolojik gelişimi. İstanbul Üniversitesi Mühendislik Fakültesi Yer Bilimleri Dergisi, 20, 21-32.
- Yılmaz, Y. 1979. Söğüt-Bilecik bölgesinde polimetamorfizma ve bunların jeoteknik anlamı. Türkiye Jeoloji Bülteni 22/1, 85-100.



Bulletin of the Mineral Research and Exploration

<http://bulletin.mta.gov.tr>



THE IMPORTANCE OF AMOUNT OF SETTLEMENT IN DETERMINING THE BEARING CAPACITY OF SOILS

Selçuk ALEMDAĞ^{a*}, Ashlan CİNOĞLU^b and Elif GACENER^a

¹Gümüşhane University, Geological Engineering Department, 29000, Gümüşhane, Turkey

²Gümüştaş Mining and Trade Inc., 29000, Gümüşhane, Turkey

Research Article

Keywords:

Geophysics Methods,
Numerical Analysis,
Seismic Velocity, Bearing
Capacity, Soil, Settlement

ABSTRACT

In this study, it is aimed to determine safe bearing capacity of soils, which are out cropped around Tamzi and Akcakale villages located in Gumushane, providing allowable settlement conditions for an optimum foundation design. To define the geotechnical properties of soils, three trenches were dug and two seismic refraction with two Multichannel Spectral Analysis of Surface Waves (MASW) were carried out in each research area. Sieve analyses, shear box tests, triaxial compression tests were carried out on disturbed and undisturbed samples taken from the trenches. Seismic velocities of the soils are determined by seismic refraction and MASW methods. While determining the safe bearing capacity; the equations proposed by Terzaghi, Meyerhof, Kurtuluş, Tezcan and Özdemir, Türker, Keçeli were used and the obtained safe bearing capacity values were compared to each other. After, the soils were modeled numerically by using finite elements method and safe bearing capacities providing allowable settlement conditions were determined. According to the results, safe bearing capacity values obtained from empirical equations are not satisfactory to have an optimum foundation design. For the optimum foundation design, safe bearing capacity should be accepted as 190 kN/m² for clayey soil (CL) and 485 kN/m² for the clayey sand (SC).

Received: 11.05.2016

Accepted: 07.08.2016

1. Introduction

For engineering studies to be reliably and economically designed the use of different methods to determine design parameters and comparison of results obtained from these methods is a basic principle of engineering studies. The most important of these engineering parameters is soil bearing capacity and is very important in terms of structural statics. To date researchers (Terzaghi, 1943; Meyerhof, 1963; Keçeli, 1990; Richards et al., 1993; Keçeli, 2000; Kurtuluş, 2000; Türker, 2004; Çinicioğlu, 2005; Keçeli, 2010; Tezcan et al., 2010; Uzuner et al., 2000; Tezcan and Özdemir, 2011) have recommended many empirical equations to determine soil bearing capacity. When these empirical equations are investigated, they appear to use different engineering properties of soils. Some researchers (Terzaghi, 1943; Skempton, 1951; Meyerhof, 1963) have noted basic dimensions of the physical and mechanical properties of soils, while other researchers (Keçeli, 1990; Richards et al., 1993; Keçeli, 2000; Kurtuluş, 2000; Türker, 2004; Çinicioğlu, 2005; Önalp and Sert, 2006; Keçeli, 2010; Tezcan et al., 2010; Uzuner et al., 2000; Tezcan

and Özdemir, 2011) have used dynamic property parameters of soils. These empirical equations are commonly chosen by researchers and engineers to determine bearing capacity of soils (Alemdağ and Gürocak, 2006; Alemdağ et al., 2008; Kayabaşı and Gökçeoğlu, 2012; Uyanık and Gördesli, 2013; Alemdağ, 2015). However, for the design to be sound, the equation to be used should be chosen well and it is important that the design is made by comparing the results of different equations. Additionally, checking the results of the empirical equations with numerical analyses is necessary for comparison of results and the structure design.

Another important situation to be considered during determination of bearing capacity of soils after the design is completed by noting the bearing capacity value determined empirically is that the settling and compression amount that will occur in the soil as a result of stress transmitted to the ground by the structure foundations should be within acceptable limits. This situation is ignored the majority of the time and it is assumed the settling amount is within acceptable limits. However, a significant amount of

* Corresponding author: Selçuk Alemdağ, e-mail: selcukalemdag@gmail.com

<http://dx.doi.org/10.19111/bulletinofmre.298630>

settling and compression will occur in soils with high compressibility and these settling and compression values exceeding acceptable limits may cause severe damage to the structure. As a result, the bearing capacity values obtained from empirical equations become important for determination of the amounts of settling and compression caused in soils.

This study determined the bearing capacity of soils comprising disintegration products from Gümüşhane granitoid complex and the Şenköy formation in Akçakale and Tamzı villages (Figure 1) in Gümüşhane province using empirical equations recommended by different researchers. The amount of settlement and compression caused in soils with these bearing strength values were determined by numerical analysis and an attempt was made to determine the empirical equations producing results appropriate for design.

2. Field and Laboratory Studies

To determine the bearing capacity of soils comprising the disintegration products of the Early Carboniferous-age Gümüşhane granitoid complex (Topuz et al., 2010; Dokuz, 2011; Kaygusuz et al., 2012; Karlı et al., 2017) outcropping in Akçakale village and the Early Jurassic-age Şenköy formation (Kandemir and Yılmaz, 2009) outcropping in Tamzı village, both field and laboratory studies were completed. Field studies include two line studies in each area (Figure 2) using seismic refraction and multi-channel analysis of surface wave (MASW) measurements to determine the V_p and V_s wave velocities of soil layers (Table 1). This study obtained the V_p wave velocity from the seismic refraction method and the V_s wave velocity from the MASW method. Additionally, three trial pits were dug in each

study area and disturbed and undisturbed samples were taken for laboratory experiments.

To determine the dynamic parameters of soils in the study areas, seismic refraction and MASW methods were used to obtain V_p and V_s velocities, and the elasticity module, slip module and Poisson ratio were determined using the empirical equations of Bowles (1988) with density determined according to the equation by Keçeli (2012) (Table 2).

$$\rho = 0.44V_s^{0.25} \quad (1)$$

$$\nu = (V_p^2 - 2V_s^2) / 2(V_p^2 - V_s^2) \quad (2)$$

$$\mu = \rho V_s^2 / 100 \quad (3)$$

$$E = \mu (3V_p^2 - 4V_s^2) / (V_p^2 - V_s^2) \quad (4)$$

In these equations, V_p : compressional wave velocity (m/s), V_s : shear wave velocity (m/s), ρ : density (gr/cm^3), ν : Poisson ratio, μ : shear modulus (kg/cm^2), and E_m is the elasticity modulus (kg/cm^2).

Sieve analysis experiments in laboratory studies of the disturbed samples taken from the trial pits were completed according to ASTM D 422-63 (2003) standards. For undisturbed samples, shear box tests (ASTM, 2011) and triaxial compression tests (ASTM D 4767-95, 2003) were completed to determine soil resistance parameters with the aid of shear stress-normal stress graphs (Figure 3). Combined soil classification of samples from the Akçakale area was clayey sand (SC) while soils in Tamzı village had low plasticity clay (CL) properties. The results for the engineering properties of the investigated soils are given in table 3.

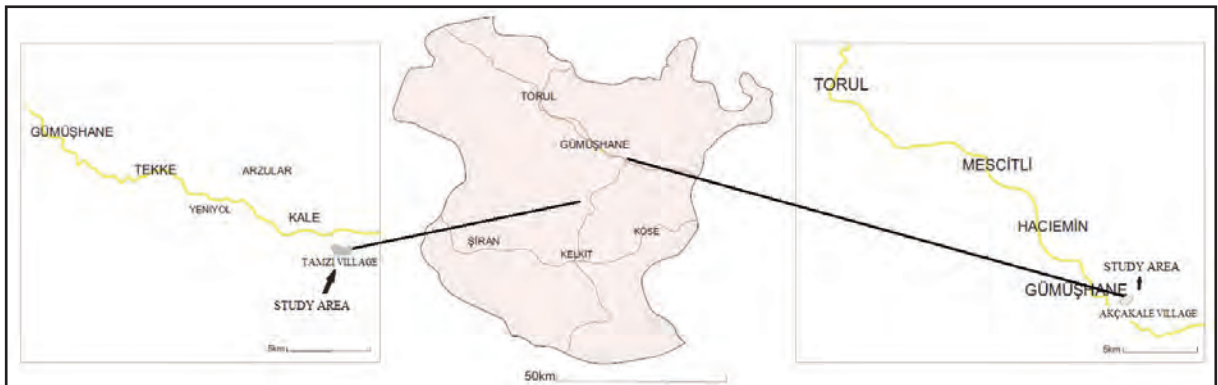


Figure 1- Location map of the study area.

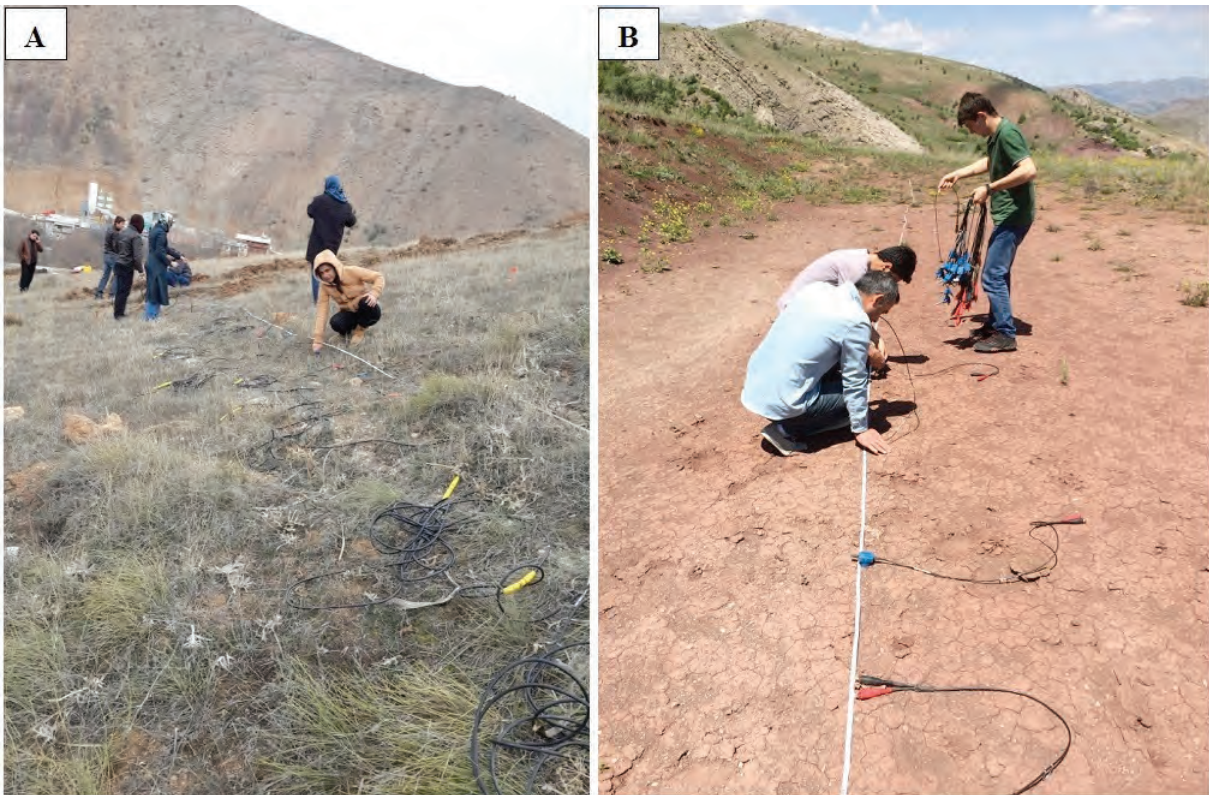


Figure 2- Geophysical studies in Akçakale (A) and Tamzı (B) villages.

Table 1- V_p and V_s wave velocities obtained with seismic refraction and MASW methods.

| AKÇAKALE VILLAGE | | | | | TAMZI VILLAGE | | |
|------------------|----------|-----------|---------------------------|---------------------------|---------------|---------------------------|---------------------------|
| Measurement No | Layer No | Depth (m) | V_p Wave Velocity (m/s) | V_s Wave Velocity (m/s) | Depth (m) | V_p Wave Velocity (m/s) | V_s Wave Velocity (m/s) |
| Line 1 | 1 | 7.5 | 452.4 | 184 | 7.5 | 516.9 | 213 |
| | 2 | 13.5 | 763.0 | 224 | 13.5 | 883.7 | 349 |
| | 3 | - | 2510.3 | 288 | 21 | 2423 | 394 |
| Line 2 | 1 | 7.5 | 320.8 | 143 | 7.5 | 585.6 | 235 |
| | 2 | 13.5 | 800.5 | 215 | 13.5 | 996.9 | 391.5 |
| | 3 | 21 | 2506.2 | 304 | 21 | 2058.5 | 573.7 |

Table 2- Dynamic parameters of soils.

| Study Line No | USC | ρ (gr/cm ³) | V_p (m/s) | V_s (m/s) | μ (kg/cm ²) | Poisson Ratio | E_m (kg/cm ²) |
|------------------|-----|------------------------------|-------------|-------------|-----------------------------|---------------|-----------------------------|
| Tamzı Village | | | | | | | |
| 1 | CL | 1.68 | 516.9 | 213 | 762.62 | 0.39 | 2131.9 |
| 2 | CL | 1.72 | 585.6 | 235 | 951.38 | 0.40 | 2671.5 |
| Akçakale Village | | | | | | | |
| 1 | SC | 1.62 | 452.4 | 184 | 548.65 | 0.40 | 1537.2 |
| 2 | SC | 1.52 | 320.8 | 143 | 311.14 | 0.38 | 856.3 |

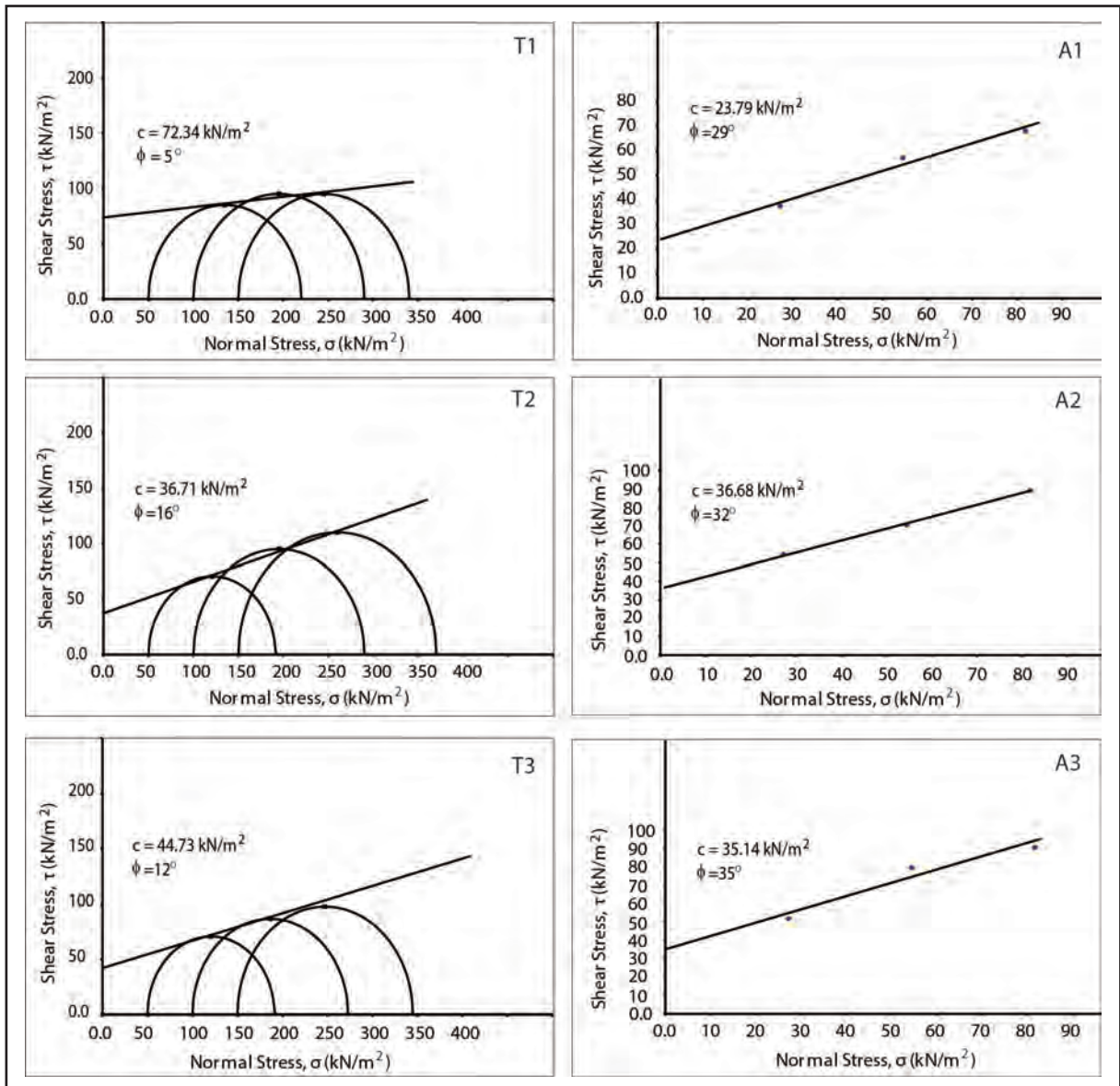


Figure 3- Shear stress (t)-normal stress (s) graphs for the soils.

Table 3- Resistance parameters and classification of soils in the study area.

| Research Trench | Retained in 4 No. sieve (%) | Passing 200 No. Sieve (%) | LL (%) | PL (%) | PI (%) | c (kN/m ²) | ϕ (°) | g_p (kN/m ³) | USC |
|-----------------|-----------------------------|---------------------------|--------|--------|--------|--------------------------|------------|----------------------------|-----|
| T1 | 12 | 90.55 | 42 | 17 | 25 | 72.34 | 5 | 18.96 | CL |
| T2 | 10.65 | 76.50 | 38 | 20 | 18 | 36.71 | 16 | 18.44 | CL |
| T3 | 8.23 | 71.20 | 26 | 15 | 11 | 44.73 | 12 | 19.22 | CL |
| A1 | 10.05 | 18 | 22 | 12 | 10 | 23.79 | 29 | 19.81 | SC |
| A2 | 8.50 | 15.6 | 28 | 10 | 18 | 36.68 | 32 | 19.62 | SC |
| A3 | 11.30 | 13 | 26 | 14 | 12 | 35.14 | 35 | 18.53 | SC |

T 1-2-3: Tamzı Village

A 1-2-3: Akçakale Village

c : Cohesion; ϕ : Internal Friction Angle; g_p : Unit Volume Weight

3. Determination of Bearing Capacity with Empirical Equations

The results of the seismic studies and laboratory experiments on soils outcropping in Tamzı and Akçakale villages were used in the empirical equations recommended by Terzaghi (1943), Meyerhof (1963), Kurtuluş (2000), Türker (2004), Keçeli (2010) and Tezcan and Özdemir (2011) and bearing capacity for strip footing was determined.

3.1. Bearing Capacity According to Terzaghi's (1943) Equation

The bearing capacity equation recommended by Terzaghi (1943) is one of the equations commonly used for geotechnical studies in many fields today. This equation is recommended for different foundation types with strip footing assessed in this study.

$$q_u = K_1 c N_c + \gamma D_f N_q + K_2 \gamma B N_\gamma \quad (5)$$

$$q_{net} = q_u - \gamma D_f \quad (6)$$

$$q_{em} = q_{net} / G_s + \gamma D_f \quad (7)$$

In these equations; q_u : final bearing capacity, q_{net} : net bearing capacity, q_{em} : safe bearing capacity, K_1, K_2 : coefficients linked to the foundation type, c : cohesion, D_f : foundation depth (3m), G_s : reliability number (3), B : foundation width (2 m), γ : unit volume weight, and N_c, N_q, N_γ : bearing strength factors, calculated from the following equations.

$$N_q = e^{(\pi \tan \phi)} \tan^2 [45 + (\phi/2)] \quad (8)$$

$$N_c = (N_q - 1) \cot \phi \quad (9)$$

$$N_\gamma = 1.8 (N_q - 1) \tan \phi \quad (10)$$

According to equation 7 above, the safe bearing capacity values for soils in the study area are given in table 4.

3.2. Bearing Capacity According to Meyerhof's (1963) Equation

The bearing capacity equation produced by Meyerhof (1963) includes the parameters depth (d) and shape (s) different from Terzaghi (1943). Here a rectangular foundation type was used.

$$q_u = c N_c s_c d_c + \gamma D_f N_q s_q d_q + 0.5 \gamma B N_g s_g d_\gamma \quad (11)$$

In this equation; $B=2, L=4, D_f=3,$ and $G_s=3$ were used.

$$K_p = \tan^2(45 + \phi/2) \quad (12)$$

$$s_c = 1 + 0.2 K_p (B/L) \quad (13)$$

$$d_c = 1 + 0.2 K_p^{0.5} (D_f/B) \quad (14)$$

$$s_q = s_\gamma = 1 + 0.1 K_p (B/L) \quad (15)$$

$$d_q = d_\gamma = 1 + 0.1 K_p^{0.5} (D_f/B) \quad (16)$$

$$N_q = e^{\pi \tan \phi} \tan^2 (45 + \phi/2) \quad (17)$$

$$N_c = (N_q - 1) \cot \phi \quad (18)$$

$$N_\gamma = (N_q - 1) \tan(1.4\phi) \quad (19)$$

The safe bearing capacity values for soils in the study area according to Meyerhof's (1963) bearing capacity equation are given in table 5.

Table 4- Bearing capacity of soils according to Terzaghi's (1943) equation.

| Parameters | Trial Pits | | | | | |
|--------------------------------|------------|-------|-------|-------|-------|-------|
| | T1 | T2 | T3 | A1 | A2 | A3 |
| c (kN/m ²) | 72.3 | 36.7 | 44.7 | 23.8 | 36.7 | 35.1 |
| ϕ (°) | 5 | 16 | 12 | 29 | 32 | 35 |
| g_n (kN/m ³) | 18.96 | 18.44 | 19.22 | 19.81 | 19.62 | 18.53 |
| N_c | 6.5 | 11.6 | 9.28 | 27.8 | 35.4 | 46.1 |
| N_q | 1.57 | 4.33 | 2.97 | 16.4 | 23.2 | 33.3 |
| N_γ | 0.09 | 1.72 | 0.75 | 15.4 | 24.9 | 40.6 |
| K_1 | 1 | 1 | 1 | 1 | 1 | 1 |
| K_2 | 0.5 | 0.5 | 0.5 | 0.5 | 0.5 | 0.5 |
| q_u (kN/m ²) | 561 | 693 | 604 | 1943 | 3151 | 4220 |
| q_{net} (kN/m ²) | 504 | 637 | 547 | 1884 | 3093 | 4165 |
| q_{em} (kN/m ²) | 225 | 267 | 240 | 687 | 1090 | 1444 |
| USC | CL | CL | CL | SC | SC | SC |

Table 5- Bearing capacity of soils according to Meyerhof's (1963) equation.

| Parameters | Trial Pits | | | | | |
|--------------------------------|------------|--------|-------|--------|--------|--------|
| | T1 | T2 | T3 | A1 | A2 | A3 |
| c (kPa) | 72.34 | 36.71 | 44.73 | 23.79 | 36.68 | 35.14 |
| ϕ (°) | 5 | 16 | 12 | 29 | 32 | 35 |
| g_n (kN/m ³) | 18.96 | 18.44 | 19.22 | 19.81 | 19.62 | 18.53 |
| N_c | 6.5 | 11.6 | 9.3 | 27.8 | 35.4 | 46.1 |
| N_q | 1.6 | 4.3 | 3.0 | 16.4 | 23.1 | 33.3 |
| N_γ | 0.1 | 1.4 | 0.6 | 13.2 | 22.0 | 37.1 |
| q_u (kN/m ²) | 810.7 | 1039.3 | 894.3 | 3064.5 | 5306.5 | 7362.1 |
| q_{net} (kN/m ²) | 754 | 984 | 837 | 3005 | 5248 | 7307 |
| q_{em} (kN/m ²) | 308 | 383 | 337 | 1061 | 1808 | 2491 |
| USC | CL | CL | CL | SC | SC | SC |

3.3. Bearing Capacity According Kurtuluş's (2000) Equation

The shear and compression wave velocities obtained for the zone forming the foundation level (first layer) near the surface as a result of seismic refraction and MASW tests from study lines in the study areas were used in the final bearing capacity equation of Kurtuluş (2000) to determine the soil bearing capacity of soils in Akçakale and Tamzı villages (Table 6). In the equation recommended by Kurtuluş, the wave velocities of soil, are used together with a unitless P constant, foundation width (B) and foundation depth (D) parameters to determine safe bearing capacity of soils. Additionally to determine the safe bearing capacity the reliability coefficient was taken as the velocity ratio ($F_s = V_p/V_s$).

$$q_u = (PV_s)/200 \text{ (kg/cm}^2\text{)} \quad (20)$$

$$q_{em} = q_u/F_s \quad (21)$$

$$P = 1 + 0.33 D/B \quad (22)$$

$$\rho = 0.31 V_p^{0.25} \text{ (gr/cm}^3\text{)} \quad (23)$$

3.4. Bearing Capacity according to Türker's (2004) Equation

Türker accepted the dominant soil vibration period (T) as 0.33 seconds and recommended the following equation for final bearing capacity. For safe bearing capacity, the reliability coefficient (G_s) was taken as 3.

$$q_u = (V_s g T)/40 + (\gamma D_f)/10 \text{ (kg/cm}^2\text{)} \quad (24)$$

$$q_{em} = q_u/G_s \quad (25)$$

$$\rho = 0.31 V_p^{0.25} \text{ (gr/cm}^3\text{)} \text{ (Kurtuluş, 2000)} \quad (26)$$

Using the velocities obtained from seismic measurements of soils in the study areas, the safe bearing capacity values are given in table 7.

Table 6- Soil bearing capacity according to Kurtuluş's (2000) equation.

| Study Line No | B (m) | D _f (m) | ρ (gr/cm ³) | V_p (m/s) | V_s (m/s) | P | F (V _p /V _s) | q_u (kN/m ²) | q_{em} (kN/m ²) | USC |
|------------------|-------|--------------------|------------------------------|-------------|-------------|-------|-------------------------------------|----------------------------|-------------------------------|-----|
| Tamzı Village | | | | | | | | | | |
| 1 | 2 | 3 | 1.48 | 516.9 | 213 | 1.495 | 2.43 | 156.13 | 64.25 | CL |
| 2 | 2 | 3 | 1.52 | 585.6 | 235 | 1.495 | 2.49 | 172.25 | 69.18 | CL |
| Akçakale Village | | | | | | | | | | |
| 3 | 2 | 3 | 1.43 | 452.4 | 184 | 1.495 | 2.46 | 134.87 | 54.83 | SC |
| 4 | 2 | 3 | 1.31 | 320.8 | 143 | 1.495 | 2.24 | 104.82 | 46.79 | SC |

Table 7- Soil bearing capacity according to Türker's (2004) equation.

| Study Line No | D _f (m) | γ (gr/cm ³) | V _p (m/s) | V _s (m/s) | q _u (kN/m ²) | q _{em} (kN/m ²) | USC |
|------------------|--------------------|-------------------------|----------------------|----------------------|-------------------------------------|--------------------------------------|-----|
| Tamzı Village | | | | | | | |
| 1 | 3 | 1.48 | 516.9 | 213 | 298.19 | 99.40 | CL |
| 2 | 3 | 1.52 | 585.6 | 235 | 334.78 | 111.59 | CL |
| Akçakale Village | | | | | | | |
| 3 | 3 | 1.43 | 452.4 | 184 | 254.88 | 84.96 | SC |
| 4 | 3 | 1.31 | 320.8 | 143 | 190.37 | 63.46 | SC |

3.5. Bearing Capacity According to Keçeli's (2010) Equation

The bearing capacity equation recommended by Keçeli only used the wave velocities, and appears not to consider the dimensions of the foundation. The safe bearing capacity of soils in the study areas were determined by using the following equations, with results given in table 8.

$$q_u = rV_s / 100 \text{ (kg/cm}^2\text{)} \quad (27)$$

$$q_{em} = (rVs^2/Vp) / 100 \text{ (kg/cm}^2\text{)} \quad (28)$$

$$\rho = 0.44 V_s^{0.25} \text{ (gr/cm}^3\text{)} \quad (29)$$

3.6. Bearing Capacity According to Tezcan and Özdemir's (2011) Equation

In addition to the wave velocities, to determine safe bearing capacity of soils Tezcan and Özdemir developed a α coefficient representing foundation

width. In this study the foundation width was taken as B=2 m and the following equations were used.

On condition that $1.2 \leq B \leq 3.0m$;

$$\alpha = 1.13 - 0.11B \quad (30)$$

$$\gamma = 4.3 V_s^{0.25} \text{ (kN/m}^3\text{)} \quad (31)$$

$$q_u = 0.1gV_s \alpha \text{ (kN/m}^2\text{)} \quad (32)$$

With the condition $V_s \leq 750$ as $n=4$ is accepted as, n (reliability coefficient)

$$q_{em} = 0.025gV_s \alpha \text{ (kN/m}^2\text{)} \quad (33)$$

Using the bearing capacity equation of Tezcan and Özdemir, the soil bearing capacities of soils in Tamzı and Akçakale villages were determined (table 9).

The safe bearing capacity values calculated using empirical equations for soils outcropping in Tamzı and Akçakale villages are given in table 10.

Table 8- Soil bearing capacity according to Keçeli's (2010) equation.

| Study Line No | ρ (gr/cm ³) | V _p (m/s) | V _s (m/s) | q _u (kN/m ²) | q _{em} (kN/m ²) | USC |
|------------------|-------------------------|----------------------|----------------------|-------------------------------------|--------------------------------------|-----|
| Tamzı Village | | | | | | |
| 1 | 1.68 | 516.9 | 213 | 351.09 | 144.67 | CL |
| 2 | 1.72 | 585.6 | 235 | 396.99 | 159.31 | CL |
| Akçakale Village | | | | | | |
| 3 | 1.62 | 452.4 | 184 | 292.39 | 118.92 | SC |
| 4 | 1.52 | 320.8 | 143 | 213.36 | 95.11 | SC |

Table 9- Soil bearing capacity according to Tezcan and Özdemir's (2011) equation.

| Study Line No | B (m) | ρ (kN/m ³) | V _p (m/s) | V _s (m/s) | a | n | q _u (kN/m ²) | q _{em} (kN/m ²) | USC |
|------------------|-------|------------------------|----------------------|----------------------|------|---|-------------------------------------|--------------------------------------|-----|
| Tamzı Village | | | | | | | | | |
| 1 | 2 | 16.43 | 516.9 | 213 | 0.91 | 4 | 318.41 | 79.60 | CL |
| 2 | 2 | 16.84 | 585.6 | 235 | 0.91 | 4 | 360.03 | 90.01 | CL |
| Akçakale Village | | | | | | | | | |
| 3 | 2 | 15.84 | 452.4 | 184 | 0.91 | 4 | 265.17 | 66.29 | SC |
| 4 | 2 | 14.87 | 320.8 | 143 | 0.91 | 4 | 193.50 | 48.37 | SC |

Table 10- Safe bearing capacity values for soils.

| Researcher | Tamzı (CL) q_{em} (kN/m ²) | Akçakale (SC) q_{em} (kN/m ²) |
|--|--|---|
| Terzaghi (1943) | 225 | 687 |
| | 267 | 1090 |
| | 240 | 1444 |
| Meyerhof (1963) | 308 | 1061 |
| | 383 | 1808 |
| | 337 | 2491 |
| Kurtuluş (2000) | 64.25 | 54.83 |
| | 69.18 | 46.79 |
| Türker (2004) | 99.40 | 84.96 |
| | 111.59 | 63.46 |
| Keçeli (2010) | 144.67 | 118.92 |
| | 159.31 | 95.11 |
| Tezcan and Özdemir (2011) | 79.60 | 66.29 |
| | 90.01 | 48.37 |
| CL: Low Plasticity Clay, SC: Clayey Sand | | |

When the safe bearing capacity results in Table 10 are assessed, the clays (CL) outcropping in Tamzı village have carrying capacity according to Terzaghi (1943) equation varying from 225-267 kN/m², while the clayey sand (SC) outcropping in Akçakale village varies from 687-1444 kN/m². According to Meyerhof's (1963) equation, the clays (CL) have bearing capacity of 308-383 kN/m², while the clayey sand (SC) have bearing capacity of 1061-2491 kN/m².

When the safe bearing capacity results obtained from geophysical methods are investigated, the bearing capacity of clays (CL) in Tamzı village are from 64-159 kN/m², while the clayey sand (SC) in Akçakale village have bearing capacities varying from 47-119 kN/m².

3.7. Determination of Settlement Amounts with Numerical Analysis

Acceptable settlement values for soils are predicted as ≤ 7.5 cm for clayey soils and ≤ 5 cm for sandy soils.

The stress values which provide these settlement amounts are defined as the maximum vertical stress that can be applied to the soils. As a result using the bearing capacity values obtained from empirical equations is important to determine whether the settlement values for the soils are within acceptable limits.

To determine which vertical stress values provide acceptable amounts of settling in the clay (CL) and clayey sand (SC) soils investigated in this study, numerical analysis was completed with the finite element method (FEM). Noting the condition of two-dimensional plane deformation, the strain-deformation behavior of the material was modeled with a finite element network showing linear behavior. The modeling used the Phase² v6.0 (Rocscience, 2006) finite element-based computer program and under Mohr Coulomb failure conditions, settling that will occur in a vertical direction was determined. The values of parameters used in the numerical analysis of clay and clayey sand soils are given in table 11.

Table 11- Values of parameters used in numerical analysis.

| USC | γ (kN/m ³) | ϕ (°) | c (kN/m ²) | Poisson Ratio (ν) | E_m (MN/m ²) | P (kN/m ²) |
|-----------------------------------|----------------------------------|---------------|-----------------------------|-------------------------|----------------------------|---------------------------|
| CL | 18.87 | 11 | 51.26 | 0.39 | 213 | 190 |
| SC | 19.32 | 32 | 31.87 | 0.38 | 85.6 | 485 |
| P: Uniform stress applied to soil | | | | | | |

Taking note of the acceptable vertical settling for construction foundations in clay (CL) and clayey sand (SC) soils in the model sections (clay soils ≤ 7.5 cm, sands ≤ 5 cm) and the safe bearing capacity for strip footing geometry obtained from empirical equations (3 m foundation depth, 2 m foundation width), each soil was separately evaluated under uniform load.

According to the numerical analysis results, uniform vertical strains causing acceptable settling conditions were determined as 190 kN/m^2 for clay soils (CL) and 485 kN/m^2 for clayey sand (SC) (Figures 4-5). Under this uniform vertical strain the amount of vertical settling in clay soils is 6.40-7.20 cm (Figure 4). When clayey sand is assessed in this situation, the vertical settling amount varies from 3.75-4.75 cm under 485 kN/m^2 uniform vertical stress (Figure 5).

When the uniform vertical stress values ensuring acceptable settling conditions obtained from numerical analysis are compared with the bearing capacity values obtained from empirical equations, it is possible to see that the safe bearing capacity values obtained from the

empirical equations recommended by Terzaghi (1943) and Meyerhof (1963) for clay (CL) and clayey sand (SC) soils are higher than the values obtained from the numerical analysis.

The empirical equation recommended by Keçeli (2010) calculated a safe bearing capacity value that ensured acceptable settling values only for clay soils (CL). The values obtained from equations recommended by Kurtuluş (2000), Türker (2004), and Tezcan and Özdemir (2011) were determined to cause much less settling compared to the acceptable settlement conditions.

4. Results and Discussion

This study calculated the safe bearing capacity of clay and clayey sand soils in Tamzı and Akçakale villages in Gümüşhane using bearing capacity equations recommended by several researchers and attempted to determine which values obtained from these empirical equations ensured acceptable settlement conditions for the soils. With this aim

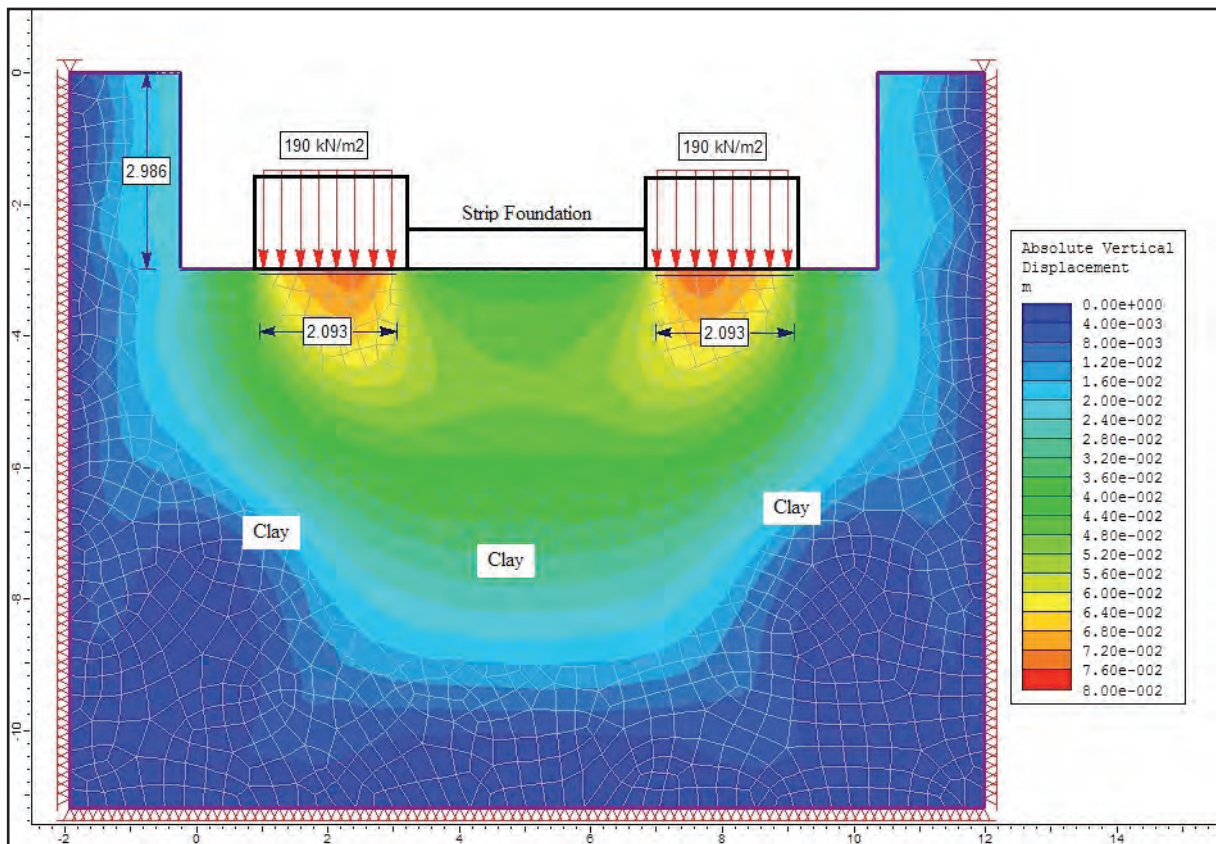


Figure 4- Numerical analysis model of vertical settling of clays (CL) under uniform stress.

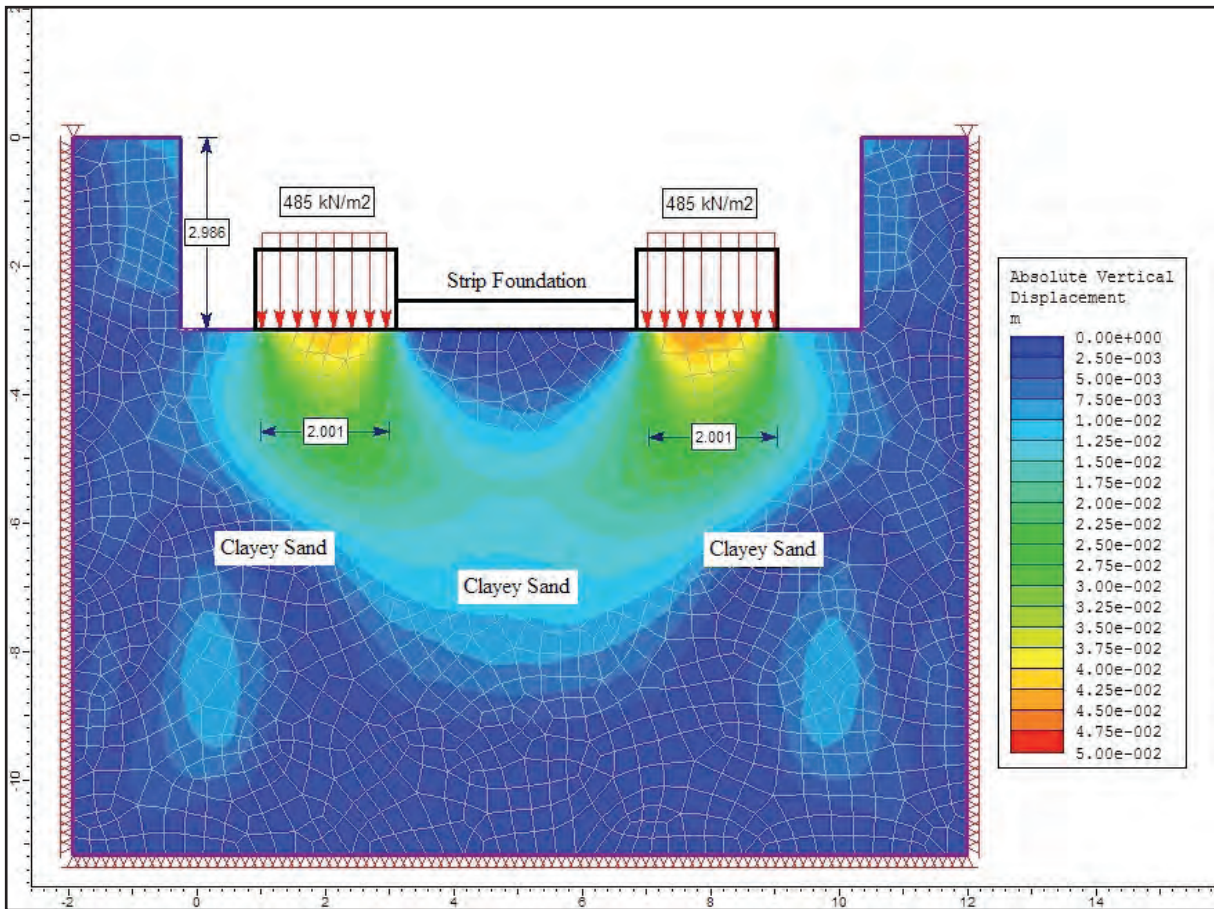


Figure 5- Numerical analysis model of vertical settling of clayey sand (SC) under uniform stress.

values obtained from field and laboratory studies were used to complete numerical analysis. The results obtained from the study are summarized below.

1. The safe bearing capacity values calculated from empirical equations based on geophysical methods showed great differences both compared with each other and with the safe bearing capacity values obtained from laboratory experiments. Using geophysical methods, the safe bearing capacity was 64.25-159.31 kN/m² for clay soil (CL) and 46.79-118.92 kN/m² for clayey sand (SC). Bearing capacity values calculated from empirical equations based on laboratory data varied from 225-383 kN/m² for clay soil (CL) and from 687-2491 kN/m² for clayey sand (SC).
2. When parameters obtained from laboratory tests are noted and the bearing capacity equations of Terzaghi (1943) and Meyerhof (1963) are used, there were significant differences in the values obtained from these two equations.

According to the equation recommended by Meyerhof (1963), bearing capacity for both clays (CL) and clayey sand (SC) had higher values. Similarly, when geophysical data are used the safe bearing capacity values obtained using the empirical equations recommended by Kurtuluş (2000), Türker (2004), Keçeli (2010) and Tezcan and Özdemir (2011) presented very different values.

3. When the numerical analysis of soils are assessed, the uniform vertical strain value ensuring acceptable settlement conditions was determined as 190 kN/m² for clay (CL) and 485 kN/m² for clayey sand (SC). These values are the optimum safe bearing capacity values for the soils and if more stress is applied to these soils, the settlement values in the soils will exceed acceptable limits. If less stress is applied than these values, there will be less than the necessary stress applied and optimum design will not ensue.

4. When the safe bearing capacity values calculated with the aid of different empirical equations for clay (CL) and clayey sand (SC) soils are compared with the uniform vertical stress obtained from numerical analysis and ensuring acceptable settlement conditions, the values obtained from the empirical equations recommended by Terzaghi (1943) and Meyerhof (1963) provide higher settling above the limits of acceptable settlement in both soil types (clay soils ≤ 7.5 cm, sands ≤ 5 cm). The values obtained from the empirical equations of Kurtuluş (2000), Türker (2004), Keçeli (2010) and Tezcan and Özdemir (2011) cause much less settling. These results show that the safe bearing capacity values obtained from all empirical equations are not appropriate for optimum design. As a result, to complete optimal foundation design, the safe bearing capacity values should be taken as 190 kN/m² for clay soil (CL) and 485 kN/m² for clayey sand (SC),
5. The study shows that determination of whether empirical calculation of safe bearing capacity of soils ensures acceptable settlement conditions is very important for optimum design. Thus, it is fundamental to apply the maximum stress that the soil can bear in foundation design while keeping the settlement amount caused by this stress within acceptable limits. As a result, during foundation design, it is necessary to note not only the soil safe bearing capacity but also the settling amount that will occur in soils.

Acknowledgements

We thank Assoc. Prof. Dr. Nafiz Maden for his efforts during field application and evaluation of geophysical methods and our students for their contributions to field studies. Additionally we offer our gratitude to our esteemed colleague Prof. Dr. Zülfü Gürocak for his constructive criticism during manuscript development.

References

- Alemdağ, S. 2015. Assessment of Bearing Capacity and Permeability of Foundation Rocks at the Gumustas Waste Dam Site, (NE Turkey) Using Empirical and Numerical Analysis. *Arabian Journal of Geosciences* 8, 1099-1110.
- Alemdağ, S., Gürocak Z. 2006. Atasu (Trabzon) Baraj Yerindeki Bazaltların Taşıma Gücü. *Fırat Üniversitesi Fen ve Mühendislik Dergisi*, 18, 3, 285-396.
- Alemdağ, S., Gürocak, Z., Solanki, P., Zaman, M. 2008. Estimation of Bearing Capacity of Basalts at Atasu Dam Site, Turkey. *Bulletin of Engineering Geology and the Environment* 67, 1, 79-85.
- ASTM D 422-63, 2003. Standard Test Method for Particle-Size Analysis of Soils, In: *Annual Book of ASTM Standards*, Volume 04.08, Philadelphia, PA, pp. 93-99.
- ASTM D 4767-95, 2003. Standard test method for consolidated-undrained triaxial compression test for cohesive soils. *Annual Book of ASTM standards*. Volume 04.08, West Conshohocken, PA, pp.924-934.
- ASTM, 2011. Standard test method for direct shear test of soils under consolidated drained conditions. *Annual Book of ASTM Standards*, ASTM D3080, Philadelphia, USA.
- Bowles, J.E. 1998. *Foundation Analysis and Design*, 6th ed., Mc Graw-Hill, 56799 9346, Newyork, USA.
- Çinicioğlu, S. F. 2005. Zeminlerde statik ve dinamik yükler altında taşıma gücü anlayışı ve hesabı, *Seminer*, IMO İstanbul Şubesi.
- Dokuz, A. 2011. A slab detachment and delamination model for the generation of Carboniferous high-potassium I-type magmatism in the Eastern Pontides, NE Turkey: the Köse composite pluton. *Gondwana Research*, 19, 926-944.
- Kandemir, R., Yılmaz, C. 2009. Lithostratigraphy, facies, and deposition environment of the lower Jurassic Ammonitico Rosso type sediments (ARTS) in the Gümüşhane area, NE Turkey: implications for the opening of the northern branch of the Neo-Tethys Ocean. *Journal of Asian Earth Sciences*, 34, 586-598.
- Karşlı, O., Dokuz, A., Kandemir, R. 2017. Subduction-related Late Carboniferous to Early Permian Magmatism in the Eastern Pontides, the Camlik and Casurluk plutons: Insights from geochemistry, whole-rock Sr-Nd and in situ zircon Lu-Hf isotopes, and U-Pb Geochronology. *Lithos*, <http://dx.doi.org/10.1016/j.lithos.2016.10.007>.

- Kayabaşı, A., Gökçeoğlu, C. 2012. Taşıma Kapasitesi ve Oturma Miktarının Hesaplanmasında Yaygın Kullanılan Yöntemlerin Mersin Arıtma Tesisi Temeli Örneğinde Uygulanması, *Jeoloji Mühendisliği Dergisi* 36 (1), 1-22.
- Kaygusuz, A., Arslan, M., Siebel, W., Sipahi, F., Ilbeyli, N. 2012. Geochronological evidence and tectonic significance of Carboniferous magmatism in the southwest Trabzon area, eastern Pontides, Turkey. *International Geology Review*, 54, 1776–1800.
- Keçeli, A. 1990. Sismik yöntemlerle mücade edilebilir dinamik zemin taşıma kapasitesi ve oturmasının saptanması, *Jeofizik* 4, 83-92.
- Keçeli, A. 2000. Sismik Yöntemlerle Kabul Edilebilir veya Emniyetli Taşıma Kapasitesi Saptanması, *Jeofizik* 14, 61-72.
- Keçeli, A. 2010. Sismik Yöntem ile Zemin Taşıma Kapasitesi ve Oturmasının Saptanması. *Jeofizik Bülteni* 22(63), 65-76.
- Keçeli A. 2012. Soil parameters which can be determined with seismic velocities. *Jeofizik* 16(1), 17-29.
- Kurtuluş, C. 2000. Sismik Yöntemle Belirlenen Ampirik Taşıma Gücü Bağlantısı ve Uygulaması. *Uygulamalı Yerbilimleri Dergisi*, 6, 51-59.
- Meyerhof, G.G. 1963. Some recent research on the bearing capacity of foundations. *Canadian Geotechnical Journal* 1(1), 16-26.
- Önalp, A., Sert, S. 2006. *Geoteknik Bilgisi-III, Bina Temelleri*, Birsen Yayınevi, İstanbul, 375 s.
- Richards, R., Elms, D.G., Budhu, M. 1993. Seismic bearing capacity and settlements of foundations. *Journal of Geotechnical Engineering* 116 (5), 662-674.
- Rocscience, 2006. Phase2 v6.0, 2D finite element program for calculating stresses and estimating support around the underground excavations. *Geomechanics Software and Research*, Rocscience Inc., Toronto, Ontario, Canada.
- Skempton, A.W. 1951. The bearing capacity of clays. *Proceedings, Building Research Congress*, London.
- Terzaghi, K. 1943. *Theoretical Soil Mechanics*. Wiley Publishing, New York, USA.
- Tezcan, S. S., Keçeli, A., Özdemir, Z. 2010. Zemin ve Kayaçlarda Emniyet Gerilmesinin Sismik Yöntem ile Belirlenmesi, *Tübvav Bilim Dergisi* 3 (1), 1-10.
- Tezcan, S., Özdemir, Z. 2011. A Refined Formula for the Allowable Soil Pressure Using Shear Wave Velocities. *The Open Civil Engineering Journal* 5, 1-8.
- Topuz, G., Altherr, R., Siebel, W., Schwarz, W.H., Zack, T., Hasözbeke, A., Barth, M., Satır, M., Şen, C. 2010. Carboniferous high-potassium I-type granitoid magmatism in the Eastern Pontides: The Gümüşhane pluton (NE Turkey). *Lithos* 116, 92–110.
- Türker, E. 2004. Computation of Ground Bearing Capacity from Shear Wave Velocity. *Continuum Models and Discrete Systems* Kluwer Academic Publisher, Netherland, 173-180.
- Uyanık, O., Gördesli, F. 2013. Sismik Hızlardan Taşıma Gücünün İncelenmesi. *SDU International Journal of Technologic Sciences* 5(2), 78-86.
- Uzun, B. A., Bektaş, F., Moroğlu, B. 2000. Kumda Merkezi ve Eksantrik Yüklü Şerit Temellerde Taban Gerilmelerinin Dağılımları, Zemin Mekaniği ve Temel Mühendisliği Sekizinci Ulusal Kongresi, İstanbul Teknik Üniversitesi, 32-38.



Bulletin of the Mineral Research and Exploration

<http://bulletin.mta.gov.tr>



INVESTIGATION OF GÜLLÜK (MUĞLA) WETLAND USING STABLE ISOTOPES ($\delta^{18}\text{O}$, δD)

Melis A. SOMAY^{a*}

^a Dokuz Eylül University, Faculty of Engineering, Geological Engineering Department, Tinaztepe Campus 35160, Buca, İzmir.

Research Article

Keywords:

Güllük, Wetland, Stable Isotope, Salt water intrusion, Hydrogeology.

ABSTRACT

Wetlands play an important role in the hydrologic cycle. This investigation was completed to determine the origin of waters and recharge-discharge areas using stable isotopes ($\delta^{18}\text{O}$ and δD) which are fingerprints of the water in Güllük (Muğla) wetland. This area is important both economically and in terms of aquaculture environment in Turkey. Sample locations were selected from not only wetlands but also the possible recharge area that consists of karstic springs and streams. EC (Electrical Conductivity) of the waters range between 5080-41000 $\mu\text{S}/\text{cm}$, except streams. $\delta^{18}\text{O}$ and δD contents of the samples ranged from -6.00‰ to 0.50‰ and from -29.1‰ to 2.1‰, respectively. In general, samples plotted between Global and Local Meteoric Water line with waters also plotted on the seawater mixing line. The sources of salinity were evaluated by $\delta^{18}\text{O}-\text{Cl}$ in and around the wetland. Streams are under the influence of "Evaporation"; samples from Avşar and Koruköy are under the influence of "Both Evaporation and Seawater Mixing"; İçme and Ekinambarı springs, and Limni Lake are under the influence of "Seawater Mixing"; and Savran spring and Tuzla Lake are under the influence of "Dissolution of Salts-Leaching" processes. The fact that Savran source plotted in this area raises the question of whether the current sea water is the source of salinity. The recharge area of the wetland consists of karstic formations, sea water, streams and precipitation in the Güllük area.

Received: 11.03.2016

Accepted: 22.03.2016

1. Introduction

Wetlands are complicated and very sensitive ecologic locations involving many biological, hydrological and hydrogeological elements. They have a very important place in terms of fresh water supply within the hydrological water cycle. The presence, attributes, quality and potential of water are significant factors directly affecting the wildlife and plant cover in wetlands (Somay and Gemici, 2012). As such for groundwater recharge by wetlands (surface waters filtered by soil and rocks mixing with underground water), hydrogeology, hydrogeochemistry and water-rock interaction are important (Somay and Filiz, 2005). Hydrogeology, hydrogeochemistry and environmental isotopes aid in the determination of water types, recharge-discharge limits, and water storage capacities of wetlands (Somay and Filiz, 2006). The water quality in wetlands is linked to rock types, mineralogy, and distance from the sea, industry-agriculture and settlement areas. Lithology controls major ion exchanges and which minerals saturate the water (Somay and Filiz, 2005). The major/minor ion contents and environmental isotope values of water indicate how waters arrived at which source. There are

some hydrogeological and hydrogeochemical studies completed on some important coastal wetland areas in western Anatolia (Gediz Delta, Küçük Menderes Coastal Wetland, Büyük Menderes Coastal Wetland) (Somay and Filiz, 2003; Somay et al., 2008; Somay and Gemici, 2009; Somay and Gemici, 2012). Additionally as the studied region is an important karstic area, there are many hydrogeological and hydrogeochemical studies on karstic areas in the western Aegean and Mediterranean (Öztan et al., 2004; Yüce, 2005; Ekmekçi et al., 2008; Özyurt, 2008; Bayarı et al., 2011; Günay et al., 2015).

One of Turkey's important wetlands of Güllük (Muğla) and Tuzla-Boğaziçi Lake is a significant region contributing to the country's economy with aquaculture in addition to tourism and cultural heritage (Figure 1). The region in the south of Milas county in Muğla also houses an active airport. The Republic of Turkey Ministry of Forestry and Water Management began the Tuzla Lake and Güllük Delta Wetland Management Plan Project and Tuzla Lake and Güllük Delta Wetlands Sub-basin Biodiversity Research Subproject as the area is an important wetland. With depth varying from 0.5-5.0 m covering

* Corresponding author: Melis A. Somay, e-posta: melis.somay@deu.edu.tr
<http://dx.doi.org/10.19111/bulletinofmre.298595>

2500 decares, the area covered by Güllük lagoon is linked to Güllük Bay with a canal (Egemen et al., 1999). One of the first and largest fishtraps in Turkey is Güllük Lagoon northeast of Milas-Güllük covering the mouth of Sarıçay, with seawater access from the Aegean Sea through Güllük Bay while freshwater input comes from drainage channels collecting water from tobacco and cotton fields surrounding the trap dug by the General Directorate of State Hydraulic Works (DSI). Topics like whether the chemical balance is preserved or not, which regions the wetland is recharged by and the water-rock interaction have not been determined. The majority of studies in the area have focused on seafood, geography and partial agricultural applications (e.g., Dalman et al., 2006; Demirak et al., 2006; Tuna et al., 2007; Kaymakçı et al., 2010; Yücel-Gier et al., 2013 Kalkan and Altuğ, 2015; Altınşaçlı et al., 2015). Additionally the karstic areas around Milas were studied by Barut et al. (2001), while the geology of the region was studied by Yılmaz et al. (2002) Aksoy and Aksarı, (2008) and Arslan et al. (2013).

Oxygen and hydrogen isotope ratios vary linked to different factors such as precipitation in the region, evaporation amounts and geographic conditions (Clark et al., 1997). Temperature plays an important role in the variation of isotopic ratios. As temperature increases, evaporation increases and increased evaporation leads to depletion of light isotopes and enrichment of heavy isotopes in the ratio. Thus, heavy isotopic compositions are dominant (Clark and Fritz, 1997). Surface and underground water which are not affected by a significant degree of evaporation are located on the global meteoric water line. Spring and summer rains and precipitation at lower elevations have slightly positive $\delta^{18}\text{O}$ and $\delta^2\text{H}$ values above the global meteoric water line. In contrast, autumn and winter rains and precipitation at high elevations have more negative $\delta^{18}\text{O}$ and $\delta^2\text{H}$ values (Coplen et al., 2000). Environmental isotopes in the study area are used to determine distribution of recharge areas, source of water, evaporation rates, mixing rates of seawater, fresh water and geothermal waters and rock-water interactions.

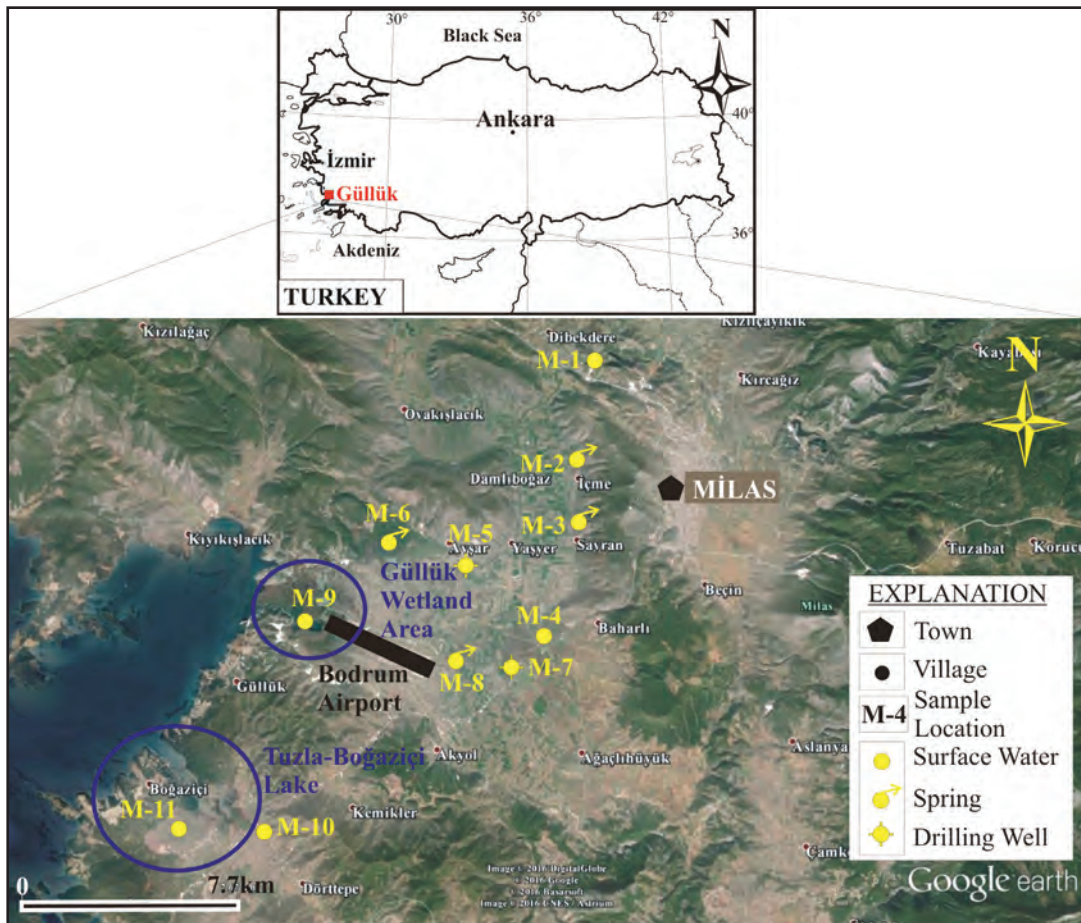


Figure 1- Location of the study area and sample locations.

In this way, the recharge-discharge and water-rock interaction are important in terms of continuity and sustainability of the naturally, culturally and economically important Güllük wetland. Within this study environmental isotope analyses of samples with important representative capacity were completed with the aim of researching the recharge and sources of water within and around the wetland area.

2. Climate Characteristics

The long term meteorological data (1950-2014) were obtained from the Turkish State Meteorological Service linked to the Republic of Turkey Ministry of Forestry and Water Management (Table 1). The lowest monthly mean temperature in the region is 5.5 °C for the month of January with highest monthly mean temperature of 26.3 °C for the month of July. The annual mean precipitation amount for Muğla province was measured as 811.3 mm. Using the 64-year meteorological data, the evapotranspiration values for the region were calculated using the “Thornthwaite” (1948) method with the EVAPO (Birsoy and Ölgem, 1991) program (Table 1). According to the Thornthwaite method, the study area has climate type “B3,B’2,s2,b’3 (Humid, Mesothermal, Water deficit in summer and strong, summer evaporation rate: 54%)”. The Etp (potential evapotranspiration) was calculated with the method as follows:

$$Etp = 1.6 \left(\frac{10t}{I} \right)^a \quad \text{(Equation 1)}$$

In this formula Etp: potential evapotranspiration (mm); t: monthly mean temperature (°C); I: total temperature indice and a: $6.75 \cdot 10^{-7} I^3 - 7.71 \cdot 10^{-5} I^2 + 1.79 \cdot 10^{-2} I + 0.492$. The meteorological data were used in the EVAPO computer program with the Etp formula and the values obtained are shown in Table 1 and from these a “Evapotranspiration Graph” was drawn (Figure 2). In table 1, PE is potential evapotranspiration, CPE is corrected evapotranspiration and ETR is real evapotranspiration. In calculations the soil-moisture reserve (beneficial water reserve) was conceptually taken as 100 mm. When the table is examined, in January, February and March precipitation appears to be greater than Etp and as a result Etp is equivalent to Etr (real evapotranspiration). Some of the surplus precipitation feeds rivers while some recharges groundwater. In the months of April, May and June, the water shortage occurring due to precipitation being less than Etp is compensated by the soil-moisture reserve conceptually assumed to be 100 mm. Thus from June to October, an agricultural water shortage (water deficit) occurs. Between July to October, the Etr value is written as the mean monthly precipitation values for the region. As precipitation is once again greater than Etp in November and December, it is equal to Etr. Here the surplus precipitation recharges the consumed soil-moisture reserve. The remaining precipitation surplus feeds surface and groundwater.

Table 1- Thornthwaite Water Balance Table (T: temperature-°C; TI: temperature indices; PE: potential evapotranspiration-mm; CF: Correction Factor; CPE: Corrected PE-mm; P: precipitation-mm; SC: Storage Change; S: Storage; ETR: Real evapotranspiration (mm); WD: Water Deficiency; EW: Excessive Water; RO: Runoff-mm; MR: Moisture Ratio).

| Data | January | February | March | April | May | June | July | August | September | October | November | December | Total |
|------|---------|----------|-------|-------|------|-------|-------|--------|-----------|---------|----------|----------|--------|
| T | 5.5 | 6.1 | 8.5 | 12.5 | 17.6 | 22.9 | 26.3 | 26.1 | 21.7 | 15.9 | 10.5 | 7.0 | |
| TI | 1.2 | 1.4 | 2.2 | 4.0 | 6.7 | 10.0 | 12.3 | 12.2 | 9.2 | 5.8 | 3.1 | 1.7 | 69.8 |
| PE | 10.9 | 12.9 | 21.9 | 40.6 | 70.1 | 106.7 | 133.1 | 131.5 | 97.9 | 59.6 | 30.7 | 16.1 | 732.2 |
| CF | 0.9 | 0.8 | 1.0 | 1.1 | 1.2 | 1.2 | 1.3 | 1.2 | 1.0 | 1.0 | 0.9 | 0.8 | |
| CPE | 9.3 | 10.9 | 22.6 | 44.7 | 86.2 | 132.3 | 166.4 | 153.9 | 101.9 | 57.2 | 25.8 | 13.4 | 824.5 |
| P | 235.3 | 174.7 | 117.6 | 66.3 | 48.8 | 22.5 | 7.5 | 7.2 | 17.0 | 66.5 | 136.8 | 259.0 | 811.3 |
| SC | 0 | 0 | 0 | 0 | 37.4 | 62.6 | 0 | 0 | 0 | 9.3 | 90.7 | 0 | |
| S | 100 | 100 | 100 | 100 | 62.6 | 0 | 0 | 0 | 0 | 9.3 | 100 | 100 | |
| ETR | 9.3 | 10.9 | 22.6 | 44.7 | 86.2 | 85.1 | 7.5 | 7.2 | 17.0 | 57.2 | 25.8 | 13.4 | 386.8 |
| WD | 0 | 0 | 0 | 0 | 0 | 47.2 | 158.9 | 146.7 | 84.9 | 0 | 0 | 0 | 437.66 |
| EW | 226.0 | 163.9 | 95.0 | 21.6 | 0 | 0 | 0 | 0 | 0 | 0 | 111.0 | 245.7 | 863.1 |
| RO | 113.0 | 194.9 | 129.4 | 58.3 | 10.8 | 0 | 0 | 0 | 0 | 0 | 55.5 | 178.3 | 740.3 |
| MR | 24.3 | 15.1 | 4.2 | 0.5 | -0.4 | -0.8 | -1.0 | -1.0 | -0.8 | 0.2 | 4.3 | 18.4 | |

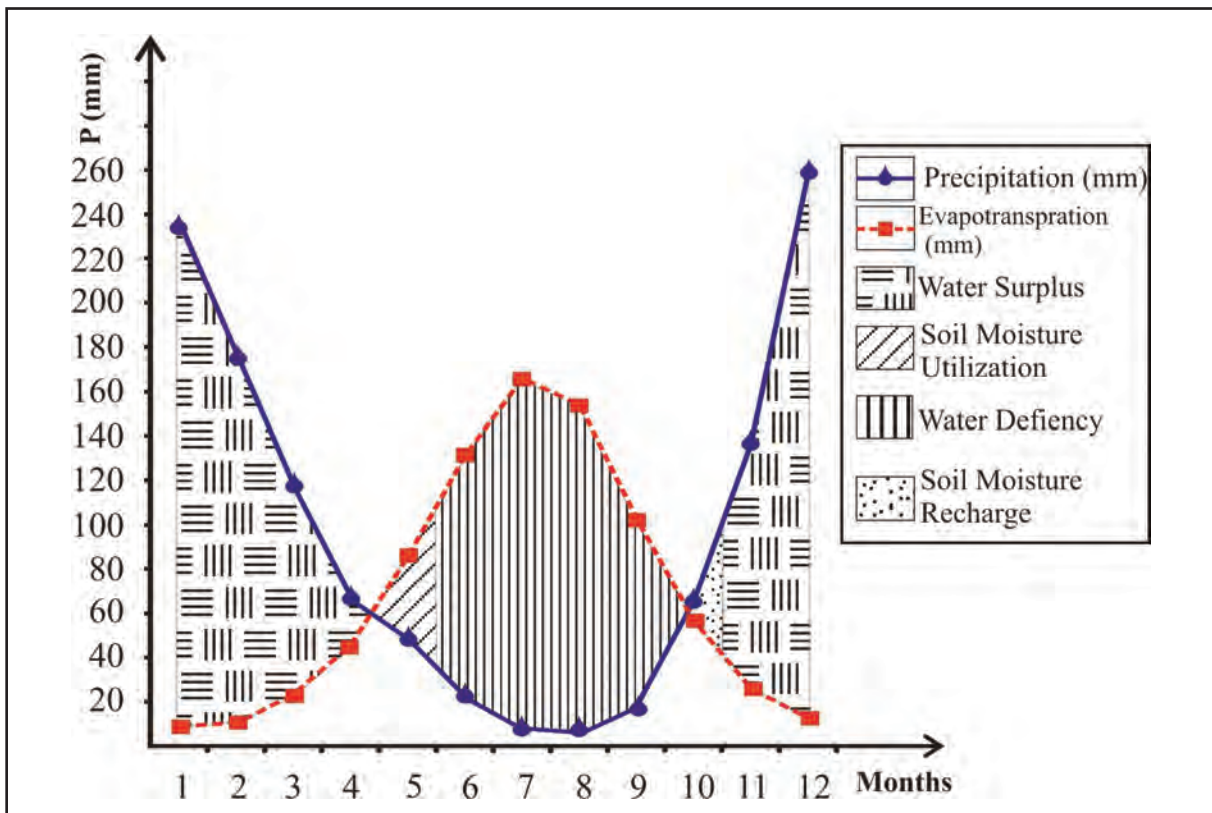


Figure 2- Thornthwaite graph for the study area.

3. Sampling and Analysis

In March 2014, 11 water samples were taken from the study area; 5 surface water samples from rivers and lakes, 4 from springs and 2 from underground water in drill holes (Figure 1). At all these points, water temperature, electrical conductivity (EC) and pH measurements were completed with a WTW brand multimeter device and water was sampled for oxygen-18 ($\delta^{18}\text{O}$) and deuterium (δD) analyses. Samples were collected in 50 ml PE plastic bottles and were not filtered.

$\delta^{18}\text{O}$ and δD isotope analyses were completed with a GVI Optima isotope mass spectrometer (SIRMS) at California University Davis Stable Isotope Laboratory. Vienna Standard Mean Ocean Water (VSMOW) was used as standard and the measurement sensitivity for this standard was determined as 0.25‰ for $\delta^{18}\text{O}$ and 3‰ for δD .

4. Geological and Hydrogeological Characteristics

The study area is located at the SW of the Menderes Massif at the contact with the Likya Nappes (Figure

3). There are three stratigraphic sequences described in the region. These are autochthonous Menderes Massif rocks, allochthonous emplaced Likya Nappe rocks and the young sediments overlying these two rock assemblages (MTA, 2002).

From older to younger the units forming the lithologies in the Menderes Massif comprising the bedrock are; metamorphic basement, Milas formation and Kalınağıl formation (Barut et al., 2001). The metamorphic basement comprises gneiss, schist, quartzite and marbles. The age of the basement rocks was estimated to be Precambrian by Akat (1975). The clayey schist, mica schist, chlorite schist, quartzite, calcschist and marble lenses in this unit are impermeable. Large areas with transitions from marbles to schists may be assessed as local karstic aquifers (Eroskay et al., 1992). However, in general schist and quartzite is impermeable basement (Barut et al., 2001). With broad distribution in the study areas, the concordant Milas Formation above the schists comprises dolomitized limestone (Eroskay et al., 1992). Generally these are permeable and have very karstic character. Karstic springs emerge from the impermeable schist contact at the base of

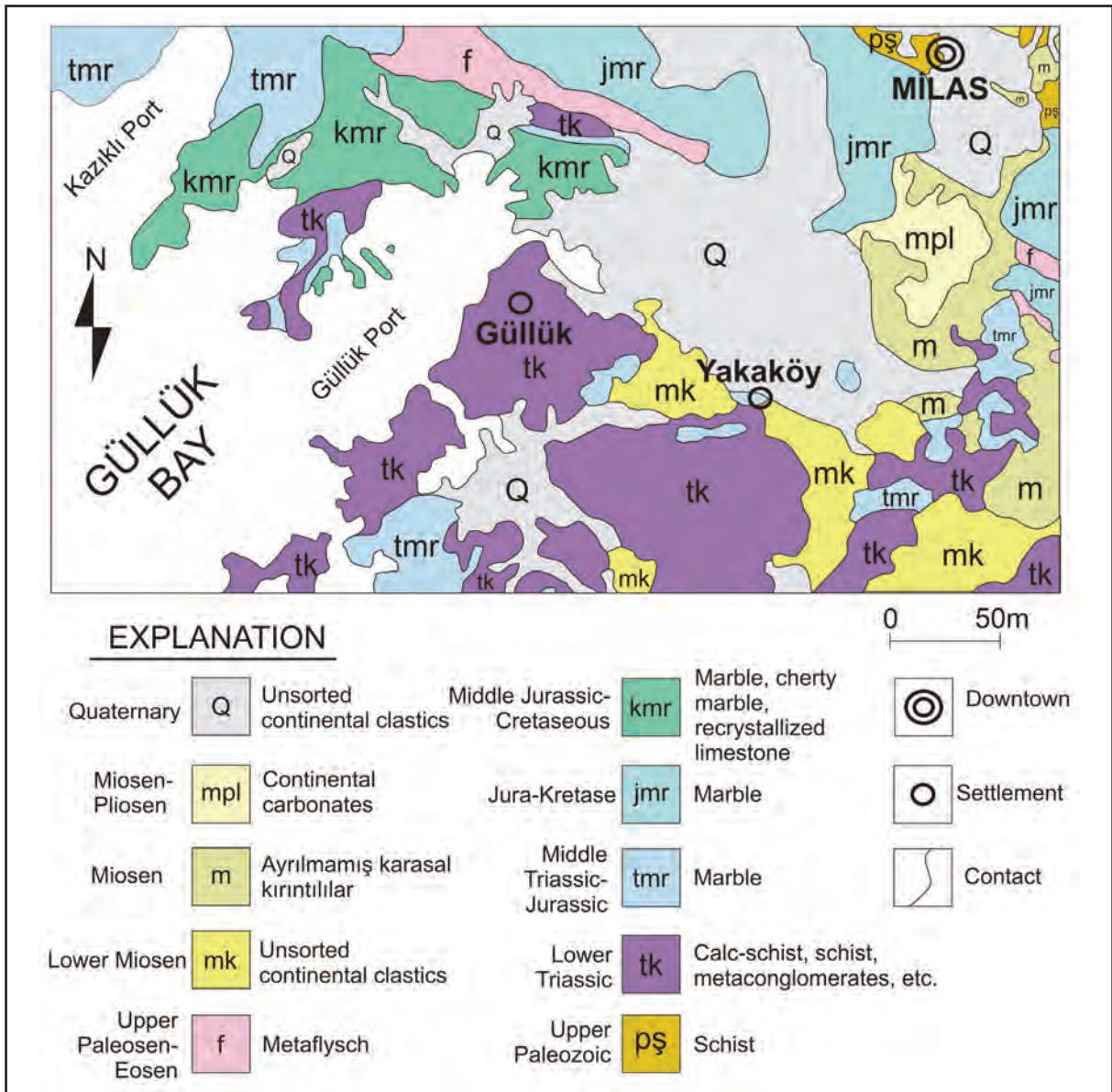


Figure 3- General geological map of the study area (MTA, 2002).

the formation (Barut et al., 2001). The Kalnağlı formation (Eroskay et al., 1992) overlies the Milas formation and is counted as cover on the Menderes Massif and the uppermost unit in the autochthonous sequence. The age of the formation was determined as Maastrichtian-Paleocene (Çağlayan et al., 1980) or Late Paleocene (Akat, 1975). Located at the top of the autochthonous sequence, the formation comprises breccia-structured red limestones, and cherty micritic limestone levels that have karstic permeability. The shale, marl and siltstone levels found at the upper levels of the formation are impermeable. The regions where the limestones from lower levels

are exposed have karstic structure. As a result they may be accepted as locally permeable in terms of hydrogeology (Barut et al., 2001). The overthrusts Likya Nappes are internally organized. From bottom to top, this sequence starts with clastic sediments and continues with limestones and repeated clastics above. From younger to older this allochthonous sequence comprises the Gökova formation, allochthonous limestones, Güllük formation and tectonic melange (Barut et al., 2001). The Güllük formation is the lowest in the allochthonous sequence. It comprises initially conglomerate followed by sandstone, shale layers and limestone lenses of varying sizes (Barut

et al., 2001). The age of the Güllük formation is Late Permian-Early Triassic (Çağlayan, 1980). Due to its lithological properties, it is generally impermeable. It forms a barrier to underground water movements (Eroskay et al., 1992). In sections near the base of the formation, the limestone under sandstone and shale has karstic character. In the study area the Kızıkkışlacık, Ekinambarı and Yaykın springs emerge from karstic limestone (Barut et al., 2001). According to fossil finds, the age of the sediments is Late Triassic-Liassic (Akat, 1975). According to Barut et al. (2001), the allochthonous sequence above the Güllük formation is a permeable unit. The transitional surfaces with the Güllük formation are impermeable. Levels transformed to dolomite and calcites are permeable and have karstic character. This sequence is composed of rocks such as conglomerate, sandstone, shale, mudstone, limestone, etc. (Barut et al., 2001). The Yatağan formation is formed of lacustrine and river sediments comprising gray, cream-colored sandstone, conglomerate, siltstone, marl, claystone and limestone with occasional coal beds (Barut et al., 2001). These Neogene sediments are covered with alluvium in Milas plain between Ekinambarı and Ağaçalhöyük. In this formation, a neo-autochthonous sequence, the clays, marls and coal levels are impermeable. There are sorted sandy and pebble levels forming generally locally impermeable cover sediments (Barut et al., 2001). In the study area Quaternary-age alluvium and slope debris are most common on plains between Milas, Ekinambarı, Savran and Hisarcık-Ovakışlacık. Due to active tectonism and linked uplift in the study area, depression areas are commonly filled with broad and thick alluvium sediments (Barut et al., 2001). The alluvial cover is generally permeable. However, upper levels in these sediments containing clay have impermeable character. Karst is observed within slope debris along the Milas-Bodrum road. As a result, in terms of hydrogeology, the alluvium and slope debris are generally accepted as being permeable (Barut et al., 2001).

5. Results and Discussion

The EC values of water samples from the study area were generally very high with values varying from 5080-41000 $\mu\text{S}/\text{cm}$, apart from the Sarıçay-Dibekdere (M-1) sample in the north and the Maziçayı (M-10) sample in the south (Table 2). The highest value was measured in Tuzla Lake in the south of the study area.

This value was close to the EC value of 50000 $\mu\text{S}/\text{cm}$ measured in seawater during the study by Barut et al. (2001). Another lake forming an important element of Güllük wetland, Limni Lake, had EC value recorded as 15330 $\mu\text{S}/\text{cm}$. The mean EC value of karstic springs in the basin was 17310 $\mu\text{S}/\text{cm}$.

The pH values of waters in the study area varied from 7.27 to 9.15. Sodium concentrations had a wide interval from 18-11450 mg/l. Calcium amounts were 34-435 mg/l, while Mg amounts were 6-920 mg/l. The dominant anion in the region was Cl and distribution was 15-19600 mg/l. Apart from surface waters, the remaining water samples were Na-Cl water facies type according to IAH (1979) classification.

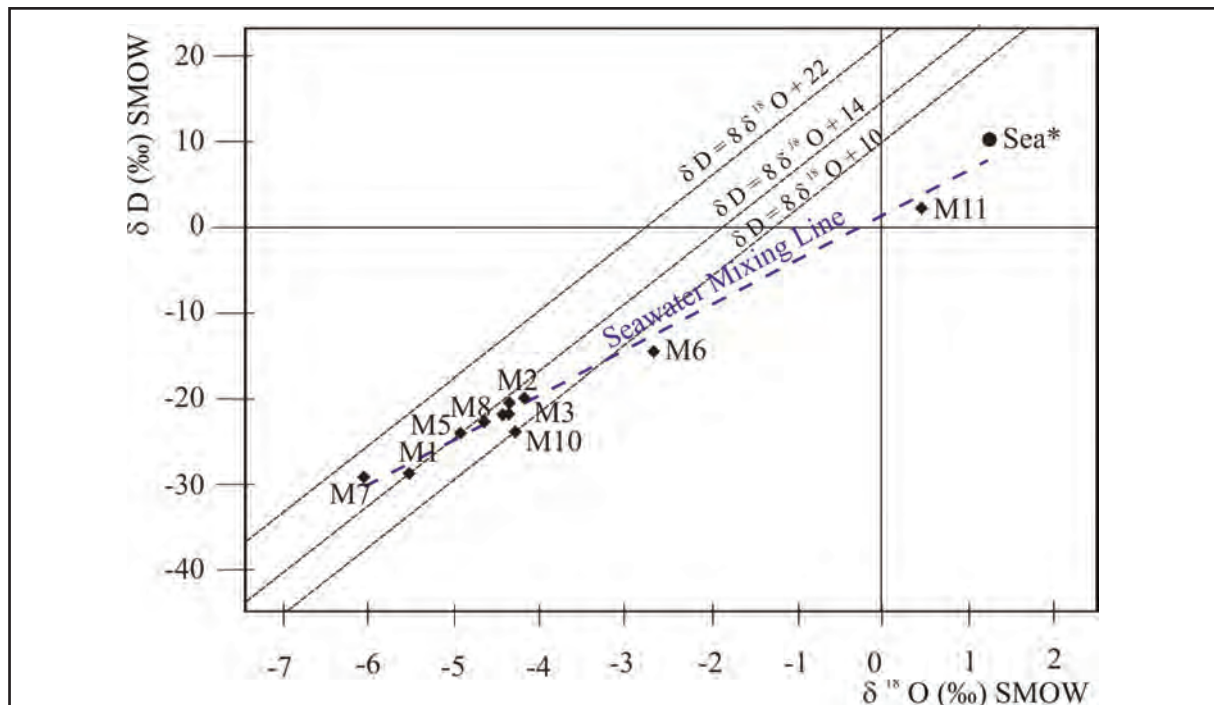
In a study by Barut and Gürpınar (2005) based on Cl values, the contribution of seawater to karstic springs in the region was calculated as 13% in Ekinambar and Avşar, 35% in Savran and 37% in İçme. This indicates that moving from the sea toward inland, the contribution of seawater increases.

The $\delta^{18}\text{O}$ and δD values of samples taken from the study area were between -6.00‰ to 0.50‰ and -29.1‰ to 2.1‰, respectively (Table 2, Figure 4).

Using the formula $d = \delta\text{D} - 8 \cdot \delta^{18}\text{O}$, the deuterium excess for samples from the study area was calculated to vary from 6.49 to 18.87‰ (Table 2). When the deuterium excess is examined, the samples with lowest deuterium excess had evaporation effects (M6, M10, M11). The highest deuterium excess was from a sample taken from Koruköy dug-well (M7); it was depleted in heavy isotopes compared to other samples and determined to be a sample discharging from higher elevations with no evaporation effect. As given in table 2, when the spring discharge elevation is examined, it is noted that springs discharging from higher elevations are depleted in heavy isotopes. Samples placed along the Global Meteoric Water Line (GMWL: $\text{D} = 8 \cdot \delta^{18}\text{O} + 10$; Craig, 1961) and the Mediterranean Meteoric Water Line (MMWL: $\delta\text{D} = 8 \cdot \delta^{18}\text{O} + 22$; Gat and Carmi, 1970). In terms of representing the region, the Local Meteoric Water Line (LMWL: $\delta\text{D} = 8 \cdot \delta^{18}\text{O} + 14$; Barut et al., 2001) calculated from precipitation in the region was used. The samples with relatively more negative values on the diagram are probably fed from more continental and higher elevations. In light of this knowledge, the most depleted samples in terms of heavy isotopes in

Table 2- Temperature, electrical conductivity and environmental isotope values from the study area (*Sea water values taken from Barut et al. (2001)).

| Sample | Location | Distance from Sea (km) | Elevation above sea level (m) | T (°C) | pH | EC ($\mu\text{S/cm}$) | Cl (mg/l) | δD (‰) | $\delta^{18}\text{O}$ (‰) | D – excess (‰) |
|--------|---------------------|------------------------|-------------------------------|--------|------|-------------------------|-----------|----------------------|---------------------------|----------------|
| M-1 | Sarıçay-Dibekli | 14 | 27 | 12.7 | 8.07 | 276 | 15 | -28.7 | -5.47 | 15.05 |
| M-2 | İçme Spring | 12 | 16 | 20.1 | 7.41 | 18830 | 6900 | -20.5 | -4.31 | 9.97 |
| M-3 | Savran Spring | 11 | 13 | 20.0 | 7.60 | 19240 | 8100 | -19.8 | -4.13 | -1.89 |
| M-4 | River-Avşar | 9 | | 21.2 | 7.92 | 17250 | 6450 | -21.7 | -4.33 | 14.02 |
| M-5 | Drilling Well-Avşar | 7 | | 21.1 | 7.35 | 7190 | 2600 | -24.0 | -4.88 | 13.24 |
| M-6 | Avşar Spring | 4 | 2 | 26.2 | 8.18 | 7480 | 2750 | -14.5 | -2.63 | 12.97 |
| M-7 | Dug Well-Koruköy | 9 | | 19.2 | 7.27 | 5080 | 1650 | -29.1 | -6.00 | 15.07 |
| M-8 | Ekinambarı Spring | 7 | 11 | 17.3 | 7.60 | 13860 | 6100 | -22.6 | -4.60 | 6.49 |
| M-9 | Limni Lake | 1 | | 21.2 | 8.19 | 15330 | 6750 | -21.8 | -4.37 | 18.87 |
| M-10 | Mazı Stream | 5 | | 16.5 | 7.80 | 799 | 71 | -23.9 | -4.24 | 14.22 |
| M-11 | Boğaziçi-Tuzla Lake | 3 | | 17.2 | 8.34 | 41000 | 19600 | 2.1 | 0.50 | 13.07 |
| Sea* | Sea water | | | | | 50000 | | 9.9 | 1.30 | -0.50 |

Figure 4- Relationship between $\delta^{18}\text{O}$ and δD .

the study area are Koruköy dug-well (M7) and Sarıçay River (M1), with these fed by precipitation falling at higher elevations compared to samples from other locations.

The M6, M10 and M11 samples from the region deviated from the meteoric water line (Figure 4). This deviation may be due to different processes such as evaporation, condensation and water-rock interaction, or CO_2 effects (Clark and Fritz, 1997; Mook, 2001).

As mentioned by Clark and Fritz (1997) and Coplen et al. (2000), mixed waters are located on a line with lower slope under the meteoric line. To identify which of these processes caused the deviation, the Cl- $\delta^{18}\text{O}$ diagram recommended by Mook (2001) was used for the study area (Figure 5). The sample closest to the fresh water end component was sample M1. Accordingly the dominant processes are shown in figure 5.

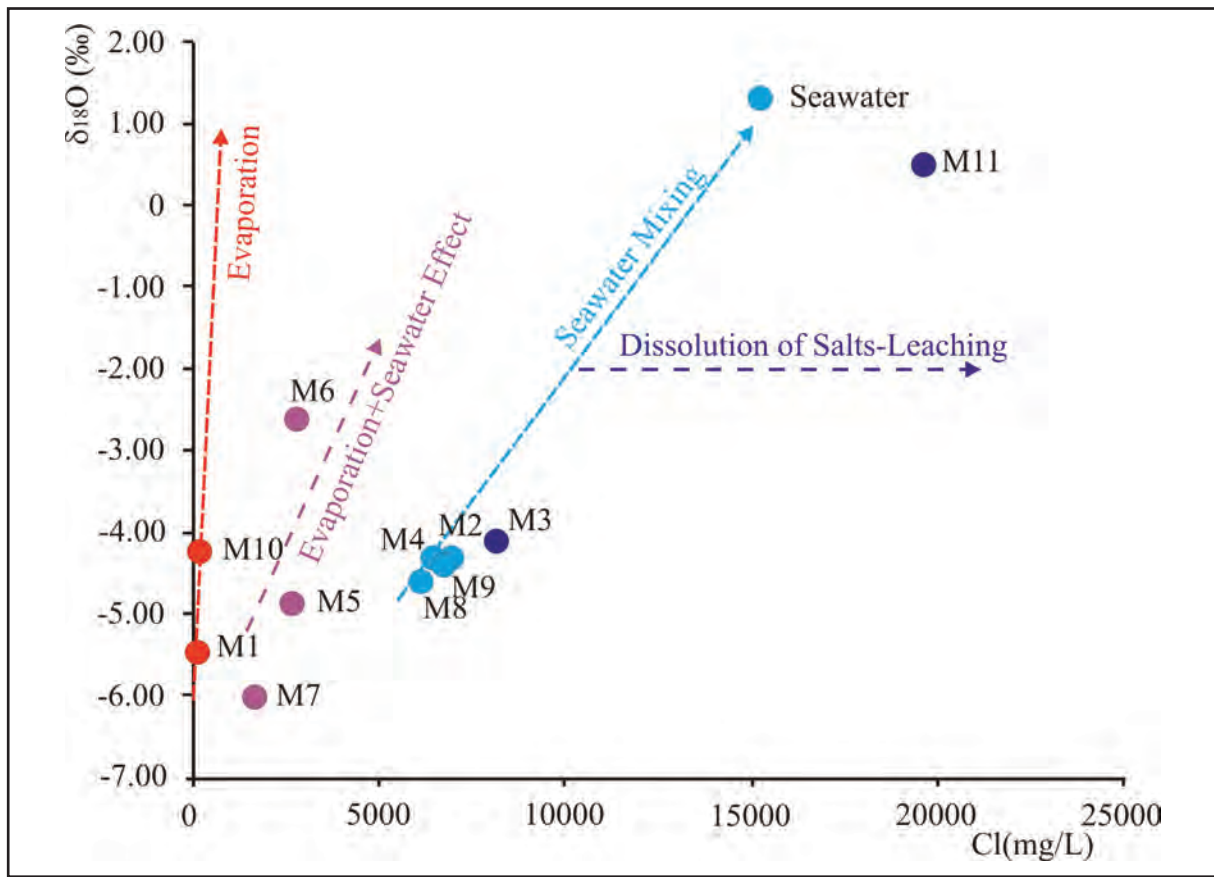


Figure 5- Relationship between Cl and $\delta^{18}\text{O}$.

Sea water with nearly 14000 mg/l Cl content and 1.3‰ $\delta^{18}\text{O}$ isotope values is located at the top portion of the graph. Relatively more fresh waters with Cl varying from 15-71 mg/l and $\delta^{18}\text{O}$ isotopic ratios varying from -5.47 to -4.24 ‰ are located in the left lower corner of the graph. According to figure 5, the surface waters from Sarıçay River (M1) and Mazıçay (M10) are more affected by “evaporation”; samples from Avşar drill hole (M5), Avşar spring (M6) and Koruköy dug-well (M7) are affected by “both evaporation and seawater mixing”; İçme spring (M2), Avşar drainage channel (M4), Ekinambarı spring (M8) and Limni Lake (M9) are affected by “seawater mixing”; and Savran spring (M3) and Tuzla Lake (M11) samples are affected by “dissolution of salts-leaching”.

6. Conclusions

Environmental isotope research was completed on one of Turkey’s most important aquaculture areas of Güllük wetland. Limni Lake and surrounding karstic springs forming the Güllük wetland comprise a salt-water ecosystem. Seawater continuously advances

toward the interior sections of the limestone and feeds İçme and Ekinambarı springs and the lakes (Figure 6). According to Erol (1991), in the last 4000-5000 years a total of 3-4 m uplift has occurred along coasts in Western Anatolia. Additionally, according to Ekmekçi et al. (2008), due to the saltwater wedge geometry in karstic aquifers commonly observed on the south coasts of Turkey and irregular variation of sea levels linked to paleoclimatic conditions, the estimation of equations developed for isolated aquifers is generally difficult. The seawater contribution to spring discharge 11-12 km inland may be explained in this way. The Savran spring discharging 11 km from the sea does not appear to support the current seawater mixing model. Savran spring and Tuzla Lake were defined within the “dissolution of salts-leaching” area and have brine character. The results of comparing analyses from the early 2000s with the isotope analyses of the same springs in this study showed no significant change in the $\delta^{18}\text{O}$ and δD values of İçme and Savran springs and they appear stable.

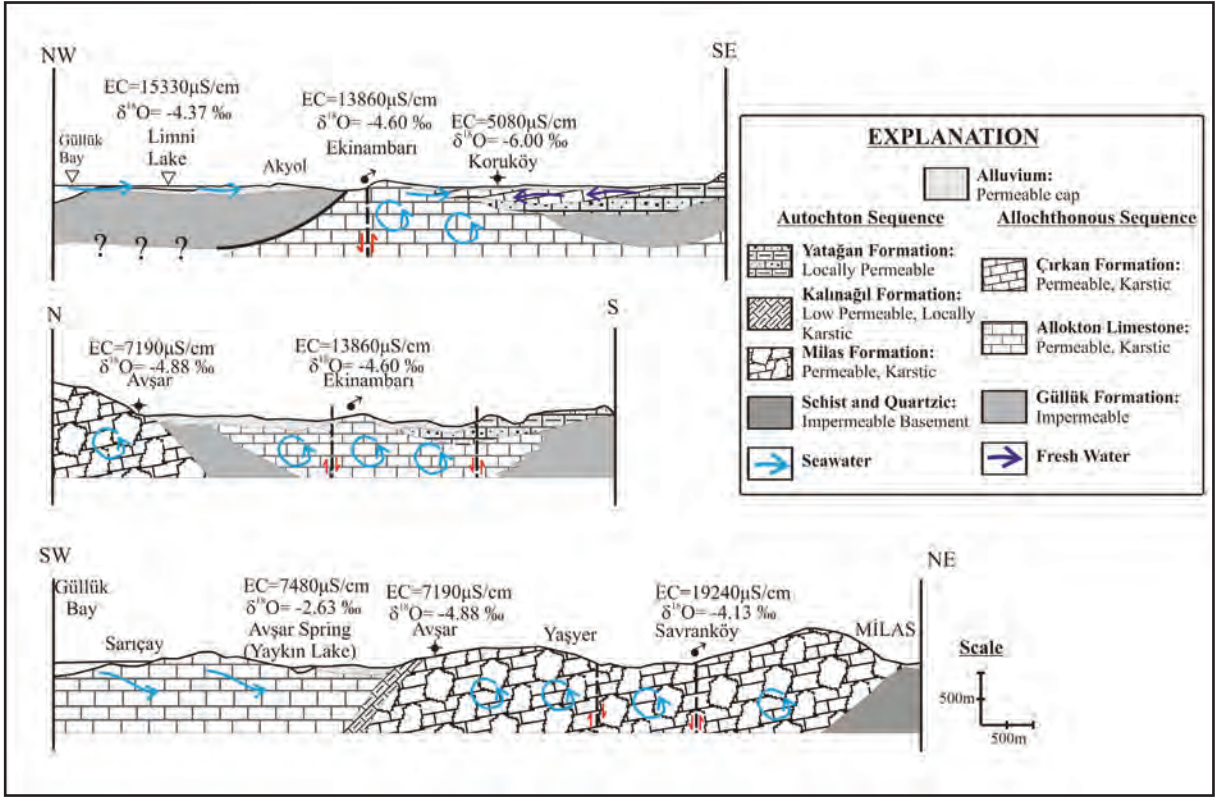


Figure 6- Water circulation model for the study area (Cross sections taken from Barut et al., 2001).

Other sources recharging the wetland are Sarıçay and Mazı Çayı freshwater springs. According to isotope values, these are recharged from high elevations and generally affected by evaporation. The water from Avşar and Koruköy are affected by both seawater mixing and evaporation. Though Koruköy waters, especially, were salty, based on the $\delta^{18}\text{O}$ and δD values as it is recharged from the NE Çirkan Formation and relatively high sections, mixing with fresh water is predicted (Figure 6).

Different karstic formations, current and non-current seawater, freshwater streams and precipitation ensure the Güllük wetland is recharged. Currently both fresh and salt water ecosystems appear to be balanced, but in the future the sustainability of these ecosystems should be monitored.

Acknowledgements

I acknowledge a debt of thanks to Prof.Dr. Nilgün Güleç, Prof.Dr. Halim Mutlu and Yrd.Doç.Dr. Füsün Tut Haklıdır for their great contributions to shaping the final manuscript. Additionally I thank Geological Engineers Ulvi İbrahim Soyuçok, Sibel Çakır, Okan

Barbaros and Ali Kal for support given during field studies.

References

- Aksoy, R., Aksarı, S. 2008. Elmalı (Antalya, Batı Toroslar) Kuzeyinde Likya Naplarının Jeolojisi. S.Ü. Müh.-Mim. Fak. Dergisi 23:2, 45-59.
- Akat, U. 1975. Menderes Masifi Güneyi GB Toros Kuşağı İlişkisi, (Ön Rapor), Maden Tetkik ve Arama Genel Müdürlüğü Raporu, No. 5488, 58s, Ankara (unpublished).
- Altınşanlı, S., Altınşanlı, S., Paçal, F.S. 2015. Diversity, species composition and habitat preferences of Ostracoda (Crustacea) in seven karstic springs of varying salinity in Milas (Muğla, Turkey). International Journal of Fisheries and Aquatic Studies 3(2): 374-390.
- Arslan, A., Güngör, T., Erdoğan, B., Pisschier, C.W. 2013. Tectonic transport directions of the Lycian nappes in southwest Turkey constrained by kinematic indicators. Journal of Asian Earth Sciences 64, 198-209.

- Barut, İ., Eroskay, O., Özer, N. 2001. Milas-Ekinambarı ve Savran Tuzlu Karst Kaynaklarının Hidrojeokimyasal Araştırılması. Tübitak Araştırma Projesi. Proje No: YDABÇAĞ-588/A.
- Barut, İ., Gürpınar, O. 2005. Milas (Muğla) Havzasının Tuzlu Karst Kaynaklarının Hidrojeolojik Dolaşım Modeline Bir Yaklaşım. İstanbul Üniv. Müh. Fak. Yerbilimleri Dergisi 18 1-22.
- Bayarı, C.S., Özyurt, N.N., Öztan, M., Bastanlar, Y., Varanlıoğlu, G., Koyuncu, H., Ülkenli, H., Hamarat, S. 2011. Submarine and coastal karstic groundwater discharges along the southwestern Mediterranean coast of Turkey, *Hydrogeology Journal* 19: 399–414.
- Birsoy, Y., Ölgün, M.K. 1991. Thorntwaite İklim Sınıflandırması ve Su Bilançosunun Belirlenmesinde Bilgisayar Kullanımı. *Ege Coğrafya Dergisi*. 6, 153-179.
- Clark, I., Fritz, P. 1997. *Environmental Isotopes in Hydrogeology*. CRC Press, 342 s.
- Clark, J.F., Stute, M., Schlosser, P., Drenkard, S. 1997. A tracer study of the Floridan aquifer in southeastern Georgia: implications for groundwater flow and paleoclimate. *Water Resources Research* 33, 281–289.
- Coplen, T.B., Herczeg, A.L., Barnes, C. 2000. *Isotope Engineering, Using Stable Isotopes of the Water Molecule to Solve Practical Problems, Environmental Tracers in Subsurface Hydrology* (editors. P.G. Cook and A. L. Herczeg), Kluwer Academic Publishers, Australia, pp: 529.
- Craig, H. 1961. Isotopic variations in meteoric waters. *Science* 133, pp: 1702-1703.
- Çağlayan, M.A. 1980. Menderes Masifi Güneyine Ait Bulgular ve Yapısal Yorum. *Jeoloji Mühendisliği Dergisi* 10: 9-17.
- Dalman, Ö., Demirak, A., Balcı, A. 2006. Determination of heavy metals (Cd, Pb) and trace elements (Cu, Zn) in sediments and fish of the Southeastern Aegean Sea (Turkey) by atomic absorption spectrometry. *Food Chemistry* 95, 157–162.
- Demirak, A., Balcı, A., Tüfekçi, M. 2006. Environmental Impact of the Marine Aquaculture in Güllük Bay, Turkey. *Environmental Monitoring and Assessment* 123, 1–12.
- Egemen, Ö., Önen, M., Büyükkışık, B., Hoşsucu, B., Sunlu, U., Gökınar, Ş., Cirik, S. 1999. Güllük Lagünü (Ege Denizi, Turkey) Ekosistemi, *Tr. J. of Agriculture and Forestry* 23:3, 927-947.
- Ekmekçi, M., Tezcan, L., Kurttaş, T., Yüzereroğlu, S., Açikel, Ş. 2008. Gökova (Muğla) Kıyı Karst Kaynaklarında Deniz Suyu Karışımının Hidrojeokimyasal ve Duraylı Çevresel İzotop Yöntemleriyle İncelenmesi. III.Hidrolojide İzotop Teknikleri Sempozyumu. Sf: 294-305.
- Erol, O. 1991. Türkiye kıyılarında deniz düzeyi değişimleri ve bir çevre sorunu olarak İstanbul için önemi, *Uluslararası Çevre Sorunları Sempozyumu Tebliğleri*, İstanbul.
- Eroskay, S.O, Gürpınar, O., Gözübol, A.M., Şenyuva, T. 1992. Muğla-Gökova ile Milas-Savran ve Ekinambarı Karst Kaynaklarının Jeolojik ve Hidrojeolojik İncelemesi, *Sonuç Raporu*, DSİ Genel Müdürlüğü (unpublished), Ankara.
- Gat, JR., Carmi, I. 1970. Evolution of the isotopic composition of atmospheric waters in the Mediterranean Sea area. *Journal of Geophysical Research* 75: doi: 10.1029/JC075i015p03039. issn: 0148-0227.
- Günay, G., Güner, N., Törk, K. 2015. Turkish karst aquifers, *Environ Earth Science* 74:217–226, doi 10.1007/s12665-015-4298-6.
- IAH (International Association of Hydrogeologists) 1979. *Map of mineral and thermal water of Europe, Scale 1:500000*, International Association of Hydrogeologists, United Kingdom
- Kalkan, S., Altuğ, G. 2015. Bio-indicator bacteria & environmental variables of the coastal zones: The example of the Gulluk Bay, Aegean Sea, Turkey. *Marine Pollution Bulletin* 95, 380-358.
- Kaymakçı Başaran, A., Aksu, M., Egemen, Ö. 2010. Impacts of the fish farms on the water column nutrient concentrations and accumulation of heavy metals in the sediments in the eastern Aegean Sea (Turkey). *Environ Monit Assess*, 162:439–451.
- Mook, W.G. 2001. *Environmental isotopes in the hydrological cycle*. IHPV, Tech Doc in Hydrology 39 (1). Paris UNESCO.
- MTA, 2002. *Türkiye Jeoloji Haritası – Denizli Paftası*. MTA Genel Müdürlüğü, Ankara.

- Öztan, M., Baştanlar, Y., Varinlioğlu, G., Hamarat, S., Ülkenli, H., Özyurt, N., Bayarı, S. 2004. Patara-Kekova tatlı su boşalıklarının ve deniz altı mağaralarının araştırılması, Türkiye Kıyıları 04-Türkiye'nin Kıyı ve Deniz Alanları V. Ulusal Konferansı, 4-7 Mayıs 2004 Adana, Bildiriler Kitabı (Editörler: E.Özhan, H. Evliya) Cilt 2, 815-824.
- Özyurt, N.N. 2008. Analysis of drivers governing temporal salinity and temperature variations in groundwater discharge from Altug Submarine Karst Cave (Kas-Turkey), *Environ Geology* 54:731-736.
- Somay, M. A., Filiz, Ş. 2003. Hydrology, hydrogeology and hydrogeochemistry of wetlands: a case study in Izmir Bird Paradise, Turkey. *Environmental Geology* 43, 825-835.
- Somay, M.A., Filiz, Ş. 2005. The importance of hydrogeology and hydrogeochemistry in the wetlands. *Int Earth Sci Coll on the Aegean Region (IESCA 2005) Abstracts*, p.211, İzmir.
- Somay, M.A., Filiz, Ş. 2006. Küçük menderes nehri kıyı sulak alanının hidrojeokimyasal değerlendirilmesi. *Geosound Adana*.
- Somay, M.A., Gemici, U., Filiz, Ş. 2008. Hydrogeochemical investigation of Küçük Menderes River coastal wetland, Selçuk-İzmir, Turkey. *Environmental Geology* 55, 149-164. doi:10.1007/s00254-007-0972-7.
- Somay, M. A., Gemici, Ü. 2009. Assessment of the salinization process at the coastal area with hydrogeochemical tools and geographical information systems (GIS): Selçuk Plain, Izmir, Turkey. *Water, Air, and Soil Pollution*, 201, 55-74. doi:10.1007/s11270-008-9927-1.
- Somay, M. A., Gemici, U., Akar, T. 2009. Water quality of the important coastal wetlands of western Turkey. *HydroEco 2009 Proceedings*. Pp: 167-170. Vienna.
- Somay M. A., Gemici Ü. 2012. Groundwater Quality Degradation in the Buyuk Menderes River Coastal Wetland, Water, Air, and Soil Pollution, v:223/pp:15-27
- Thorntwaite, W.C. 1948. An approach toward a rational classification of climate. *Geographical Review* 38:55-94.
- Tuna, A., Levent, Yılmaz, F., Demirak, A., Özdemir, N. 2007. Sources and distribution of trace metals from sarıca stream basin in southwestern Turkey. *Environmental Monitoring and Assessment*. 125:47-57.
- Yılmaz, Y., Altunkaynak, Ş., Genç, Ş.C., Gürer, Ö. F., Karacık, Z., Bozcu, M., Yılmaz, K. 2002. Güllük Körfezi ve Dolayının Jeolojik-Tektonik Gelişimi ve Bu Bölgenin Kale-Tavas Havzası ile İlişkilerinin Araştırılması. Tübitak YDABÇAĞ Projesi. Proje No: 199Y073.
- Yüce, G. 2005. Determination of the recharge area and salinization degree of karst springs in the Lamas Basin (Turkey), *Isotopes in Environmental and Health Studies*, 41:4, 391-404, DOI: 10.1080/10256010500384747.
- Yücel-Gier, G., Pazı, İ., Küçüksezgin, F. 2013. Spatial Analysis of Fish Farming in the Gulluk Bay (Eastern Aegean). *Turkish Journal of Fisheries and Aquatic Sciences* 13: 737-744.



Bulletin of the Mineral Research and Exploration

<http://bulletin.mta.gov.tr>



ASSESSMENT OF GROUNDWATER METAL-METALLOID CONTENT USING GEOSTATISTICAL METHODS IN KARABAĞLAR POLJE (MUĞLA, TURKEY)

Bedri KURTULUŞ^{a*}, Çağdaş SAĞIR^a and Özgür AVŞAR^a

^a T. C. Muğla Sıtkı Koçman University, Geological Engineering Department, 48000 Mentеше, Muğla, Turkey.

Research Article

Keywords:

Groundwater, Heavy Metal, Muğla, Karst, Geostatistic

ABSTRACT

In this research, heavy metals (Ti, Cr, Mn, Fe, Co, Ni, Cu, Zn, Mo, Cd, Ba, Pb) and a metalloid (As) sampled from 84 wells used for drinking water and irrigation in Karabağlar Karstic Polje (Muğla, Turkey) were analyzed. The results were evaluated by different statistical methods in order to investigate the interaction between elements. Ti, Mn, Fe, Zn, Mo and Pb were detected in many wells. According to findings, the strongest correlation is between As and Cu ($R=0.832$). As-Ni ($R=0.789$) and Cu-Ni ($R=0.776$) are the other strong correlations. The relationship between these elements were also shown by Cluster Analysis (CA). With respect to CA, the closest proximity distance matrix are found for these three elements. Also, elements examined composed 3 main clusters in dendrogram created from CA result matrix. These clusters match up with the findings of Principal Component Analysis (PCA) too. PCA gathers all elements up in 3 components: As, Cu and Ni at the first component; Mo and Cd at the second; Cr and Ba at the third. The accumulation of the elements studied were investigated by Kruskal-Wallis and Mann-Whitney U tests. According to the results, the least and the most common elements are Cu and Ba, respectively. The differences in the amount of all elements except Ni and Mo were statistically significant ($p<0.05$). In addition, both the amount of the elements and some water quality parameters were compared with EPA (U. S. Environmental Protection Agency) and Turkish inland water quality classes and no hazardous situation has been found.

Received: 03.01.2016

Accepted: 05.04.2016

1. Introduction

Since surface waters have very low resistance to external factors, the use of groundwater in many parts of the world is increasing day by day. The fact that city network water cannot reach everywhere and that people can use groundwater free of charge by opening wells to their land increases the importance of underground water resources. For these reasons, groundwater has become an alternative to surface waters as a source of drinking water (Girish et al., 2013). People use groundwater daily and in field irrigation. This raises the importance of knowing the pollution status, especially heavy metal pollution and the quality of groundwater. Studies have shown that metal pollution in groundwater, particularly in urban areas, is often not noticed and remains confidential (Huang et al., 2014). Metal contamination of waters can occur both by natural means and by human origin. Many metals such as Cu, Fe, Zn, Mn and Ni are essential for the survival of life. Metals such as Cd, Pb and As are not essential, but they are highly poisonous even at low concentrations. However, whether or not

it is essential or not, each metal has a toxic effect above a certain threshold value (Pavlovic et al., 2014). The accumulation properties, permanence and toxic effects of metals make them the most important common contaminants to the world's genera (Okbah et al., 2014).

Karabağlar Plate (polje), which is selected as the study area, is located in Muğla province (Turkey) (Figure 1). The study area is about 40 km² and the altitude ranges from 606 to 717 meters except for the surrounding hills. Karabağlar Plate is an active settlement area located in the center of Mentеше district of Muğla province. Typical Mediterranean climate prevails in the region, with hot and dry summers and warm and abundant rains in the winters, with an average annual rainfall of 1185 mm which is above the Turkish average. These rains cause floods and material damage every year in the spring season. In addition to being one of the most important tourism centers of Turkey, Muğla also contributes very much to the regional economy through its wide agricultural land. The dense population and intensive agricultural activities in the

* Corresponding author: Bedri Kurtuluş, bkurtulus@mu.edu.tr
<http://dx.doi.org/10.19111/bulletinofmre.304493>

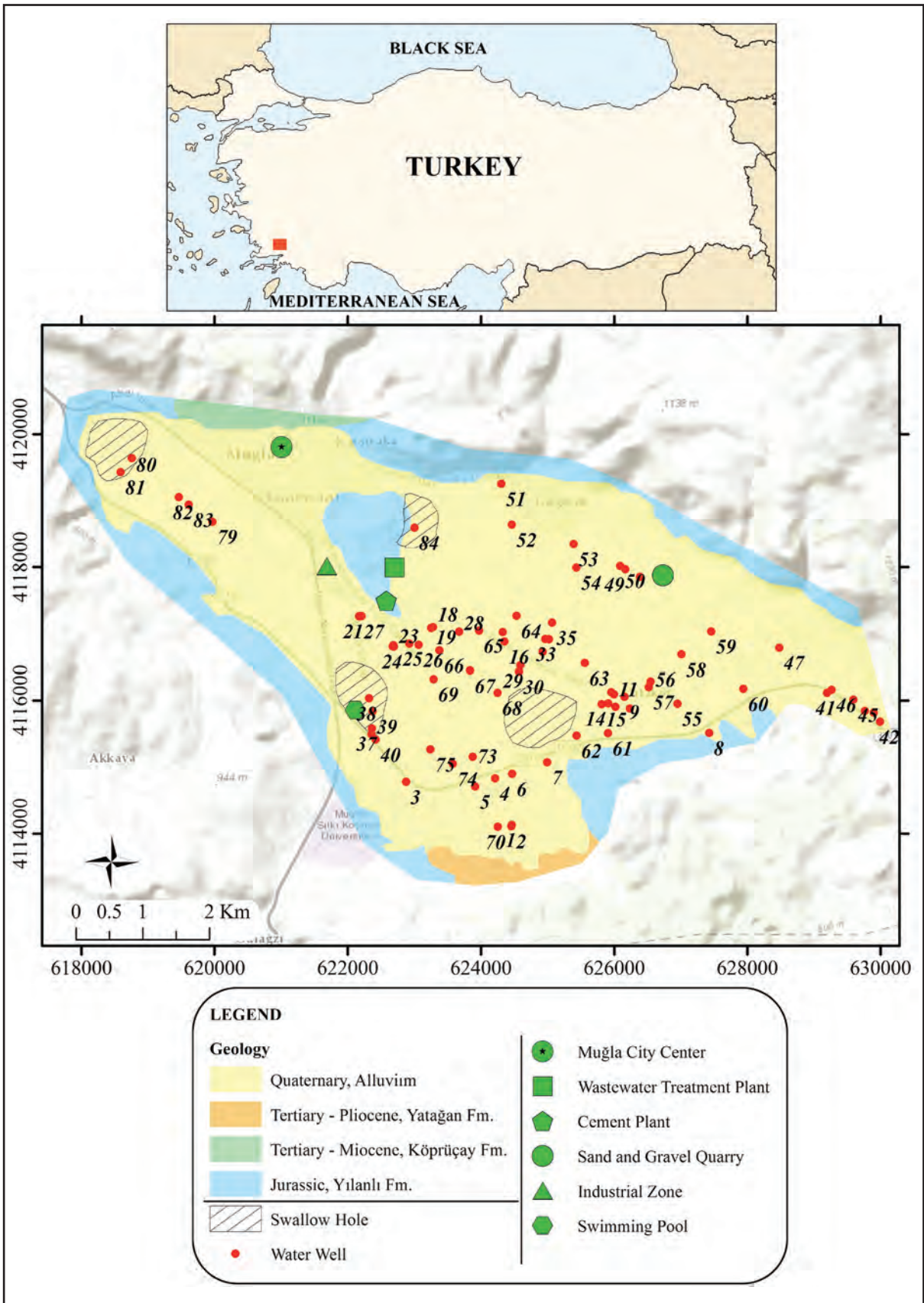


Figure 1- Geological map of Karabağlar Polje and the studied wells (MTA, 2002).

study area cause the underground waters to be used extensively in the direction of irrigation and domestic purposes and cause undesirable pollution to be found in the groundwater. For this reason, the importance of determining and regularly monitoring the metal content of the groundwater in the region is increasing. Because these elements accumulate intensively in the plants that grow on agricultural land, which is irrigated with heavy metals contaminated waters. An example is the arsenic pollution that occurs in rice fields in Bangladesh (Alam et al., 2003, Polizzotto et al., 2013). This accumulation in the plants poses a danger to all living beings consuming these plants (Kafadar and Saygıdeğer, 2010). Determination of the amount of metal in the region was carried out by Yıldıztekin and Tuna (2011). This study was conducted seasonally at 20 wells in February-November 2006 and it was researched whether these wells were suitable for irrigation purposes. Yıldıztekin and Tuna (2011) have shown that the wells investigated do not pose a risk for irrigation, but the importance of long run monitoring including the other wells, has been emphasized.

The studied wells which are water samples taken from are shallow and the depths vary between 8-20 meters. The geology of the study area is given in figure 1 and all wells sampled are within the Quaternary alluvium unit. The thickness of this unit varies between 80 and 100 m (Atalay, 1980). Alluvial deposits cover the Jurassic Yılanlı Formation (Jkmu) in much of the land. Kurttaş (1997) stated that this formation consists of dolomite-dolomitic limestone and limestone. It is estimated that the Yılanlı Formation is the most important karstic unit in the region and that the most important karstic structures in the region have developed in this unit (Ekmekçi et al., 2012; Açıkel, 2003). As a result of the field studies, water sinks were determined and it was also determined that these structures drained the flood waters accumulated in the field during the high flow period in the spring to the karst system (Figure 1). Ekmekçi et al. (2012) and Açıkel (2003) have formed a detailed hydrogeological conceptual model of the region and the broader region with the studies they have conducted and have shown that the studied area is in the drainage basin of Gökova sources.

Tertiary-Miocene Köprüçay formation (Tk) is found in the south of the study area. Ekmekçi et al. (2012) stated that this formation consists of

conglomerate and limestone formed by very large limestone pebbles bonding with a carbonate cement. Tertiary-Pliocene Yatağan formation (Tya) is found in the northwest of the study area. This unit consists of sandstone, conglomerate, siltstone, marl, claystone, limestone and coal deposits (Ekmekçi et al., 2012).

Examination of metal content of groundwater, investigation of the interaction between the metals by different statistical methods, determination whether the current situation poses a risk in terms of ecosystem and public health and determination of possible sources of pollution were aimed in the present study carried out in Karabağlar Polje, Muğla.

2. Method

Within the scope of the field study conducted in April 2013, water samples were taken from 84 different wells to perform chemical analyzes. In addition, the specific electrical conductance (SPC), total dissolved solid (TDS), salinity, pH and ammonium (NH₄-N) values of the samples were determined.

2.1. Chemical Analyzes

Elemental analyzes were performed for ⁴⁷Ti, ⁵²Cr, ⁵⁵Mn, ⁵⁶Fe, ⁵⁹Co, ⁶⁰Ni, ⁶⁵Cu, ⁶⁶Zn, ⁷⁵As, ⁹⁵Mo, ¹¹¹Cd, ¹³⁷Ba and ²⁰⁸Pb by using ICP-MS (Inductively Coupled Plasma – Mass Spectrometer). The values of ⁴⁷Ti, ⁵⁵Mn, ⁵⁶Fe, ⁶⁶Zn, ⁹⁵Mo and ²⁰⁸Pb were not included in the results because they were below the detection limits in most of the analyzes performed. The detection limits for the elements are 0.1, 0.5, 0.06, 0.9, 0.1, 0.1, 0.01, 1.4, 1.2, 0.04, 0.04, 3 and 0.04 ppb, respectively. ICP-MS measurements were performed at Bilkent UNAM Laboratories with the devices; Thermo Scientific X-Series II and Cetac Asx-260 Autosampler. Water samples were first filtered (pore size 0.22 μm) and then acid treated (%65 HNO₃) to both increase mobility and solubility of elemental ions and equate acidity of the samples to the medium of the instrument (which is about 2% HNO₃). Ultra-pure distilled water was used. High Purity Standards branded QCS-27 series standard reference material with 27 elements was used in order to preparing of calibration curves. Calibration curves for all elements were determined as the correlation coefficient is higher than 0.99 by taking account of the element concentrations of samples and keeping the searching

metal concentration on the calibration curve. 10 ppb ^{209}Bi was used as internal standard. Number of main run was assigned 3 as the analyses parameters. Sample drawing and washing periods were decided as 60 seconds by the consideration of tubing length.

2.2. Statistical Analyzes

All the statistical analyses were carried out by SPSS 19.0 (IBM, USA).

2.2.1. Comparison of Quantity Difference Between Metals (Mann-Whitney U)

This test was used to determine which of the studied metals in the region had accumulated more. Shapiro Wilk test was used to determine whether the data normally distributed or not. No data appeared to be normally distributed. On this, nonparametric Kruskal Wallis and Mann-Whitney U tests were preferred in the comparison of the averages (Tunca et al., 2013a).

2.2.2. Correlation Analysis

Correlation Analysis was used to determine whether there were correlations between amounts of metal quantity change in all samples collected during the study. Spearman's Correlation Analysis was chosen as the correlation analysis to be applied, because it was determined that the data were not normally distributed with the Shapiro Wilk Test (Tunca et al., 2013b).

2.2.3. Principal Component Analysis (PCA)

PCA, one of the most frequently used factor analyzes, is used to collect data in common components, depending on the relationships of the data with each other. For his study, this means collecting elements whose variabilities are statistically similar to each other in a common component. The PCA applied within the scope of this study was performed according to Varmuza and Filzmoser (2009) method.

2.2.4. Cluster Analysis (CA)

CA is an analysis that classifies similar features in dense data by proximity matrix. Moreover, the created dendrogram makes it easier to understand the relations visually. From here, it was desired to cluster samples according to the variations of elements quantities. In the proximity matrix, the shorter the distance

between the elements, it means that the variations in the amounts of those elements are so similar. The analysis was carried out with the "Z-score" correction in the Euclidean distance according to Ward's method (Lopez et al., 2004).

3. Results and Discussion

In this study carried out at the Karabağlar Polje in Muğla province, water samples from a total of 84 wells were taken for metal-metalloid analysis and some principal parameters (SPC, TDS, salinity, pH and ammonium) of these wells were determined (Figure 2). The metal-metalloid values of 23 from these wells were below the measurement detection limits and were therefore excluded from the study. In this study; ^{47}Ti , ^{52}Cr , ^{55}Mn , ^{56}Fe , ^{59}Co , ^{60}Ni , ^{65}Cu , ^{66}Zn , ^{75}As , ^{95}Mo , ^{111}Cd , ^{137}Ba and ^{208}Pb parameters were determined. ^{47}Ti , ^{55}Mn , ^{56}Fe , ^{66}Zn , ^{95}Mo and ^{208}Pb were not included because their values were below the detection limits for the majority of the wells investigated. The spatial distributions of the assessed elements and the water quality parameters are given in figure 3.

Statistical relationships of elements with each other were investigated by Correlation Analysis, CA and PCA. These are generally very reliable methods which are frequently used in studies related to both the environment and the earth sciences, to clarify the relationships between variables (metal-metalloid in this case). Therefore, they are frequently preferred in many studies (Tsai et al., 2003; Gergen and Harmanescu, 2012; Pandey et al., 2014).

According to Correlation Analysis, the strongest correlation is between As and Cu ($R=0.832$) (Table 1). From these elements, arsenic can be mixed with groundwater by natural processes, pesticides, industrial activities and industrial wastes. As is carcinogenic to humans as well as can lead to chronic-acute diseases, kidney and liver disorders and anemia (Fatrorini et al., 2006; Thorsen et al., 2009; Rodriguez-Sosa et al., 2013). Copper found in groundwater can be originated from metal coatings, industrial & domestic waste and mining. Cu is essential for all known organisms and serves as the cofactor for many different enzymes (Franco et al., 2009). It even enters the structure of the hemocyanin, the oxygen carrier protein, in the crustaceans (Tunca et al., 2013a, b). Cu can cause stomach, intestinal, liver, kidney and anemia diseases. Although copper is an extremely vital element, there

are many studies showing toxic effects in different organisms; in mice (Wang et al., 2014), in fungus (Klimek and Niklinska, 2007), in bacteria (Wang et al., 2009), in aquatic floating plants (Üçüncü et al., 2013), in rooted plants (Wodala et al., 2012), in crustaceans (Luis Gama-Flores et al., 2009), in mollusks (Ramakritinan et al., 2012) and in mammals (Matos et al., 2010).

Correlation of As-Ni is also very strong ($R=0.789$). Ni is one of the vital elements like Cu (Serafim et al., 2012). Nickel can be found naturally in soil, groundwater and surface water, and is used in the coating of stainless steel and alloy products. Nickel

can be toxic to mammals and can lead to heart and liver disorders (Gathwan et al., 2013).

Other strong correlations were found between Cu-Ni ($R = 0.776$) and Mo-Cu ($R = 0.726$). Besides these, moderate correlations were observed between Mo-As and Mo-Ni. Molybdenum is not only naturally found in low concentrations in groundwater, but it can also cause acute diseases in humans, although it is one of the vital elements that can be sourced from long-term domestic waste storage areas, mine tailings and sewerage (Alonso et al., 2004). But its role in metabolism and the interaction with other elements are not yet fully understood.

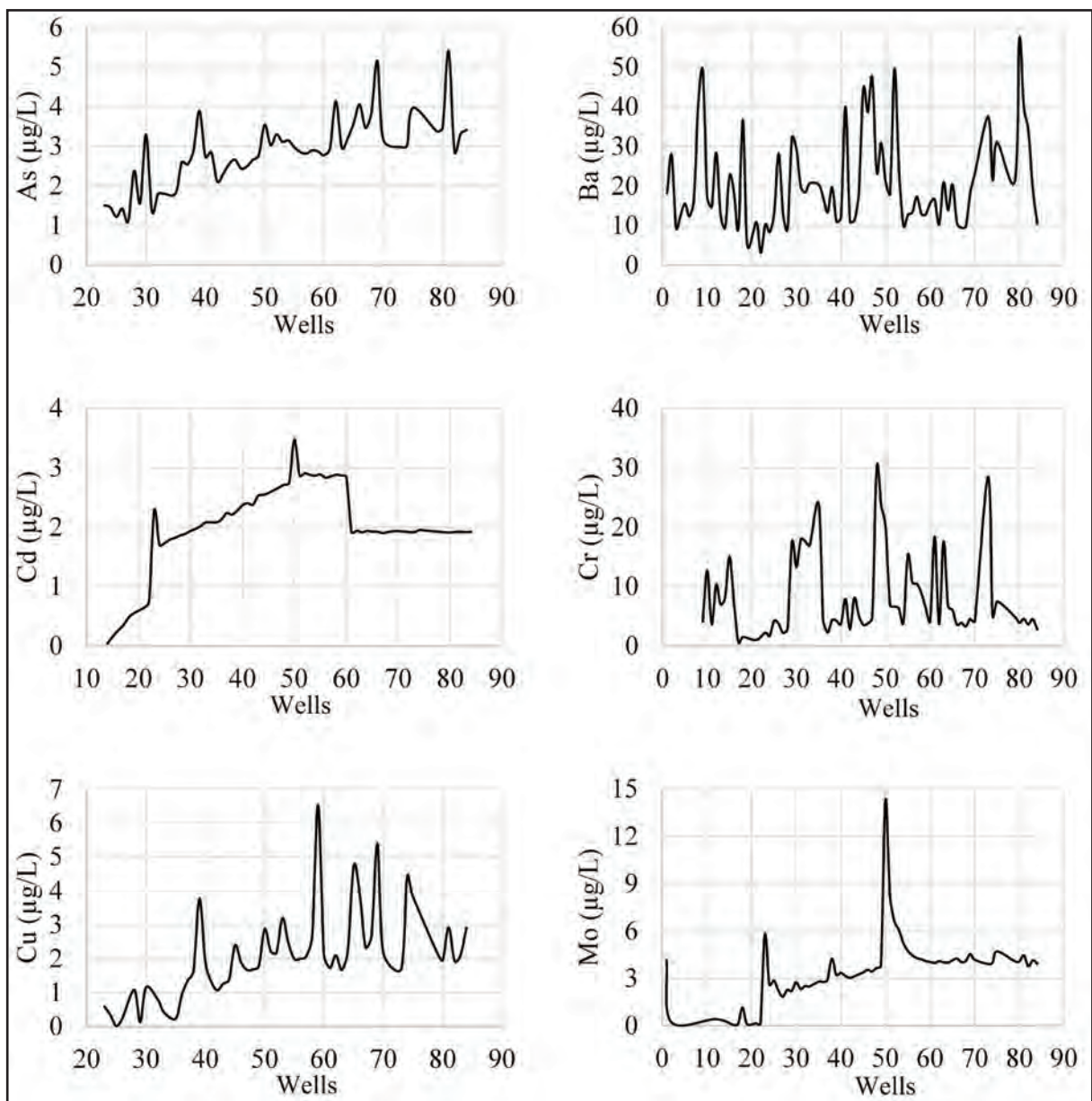


Figure 2 a- Analysis and in-situ measurement results; The amounts of ^{75}As , ^{137}Ba , ^{111}Cd , ^{52}Cr , ^{65}Cu and ^{95}Mo .

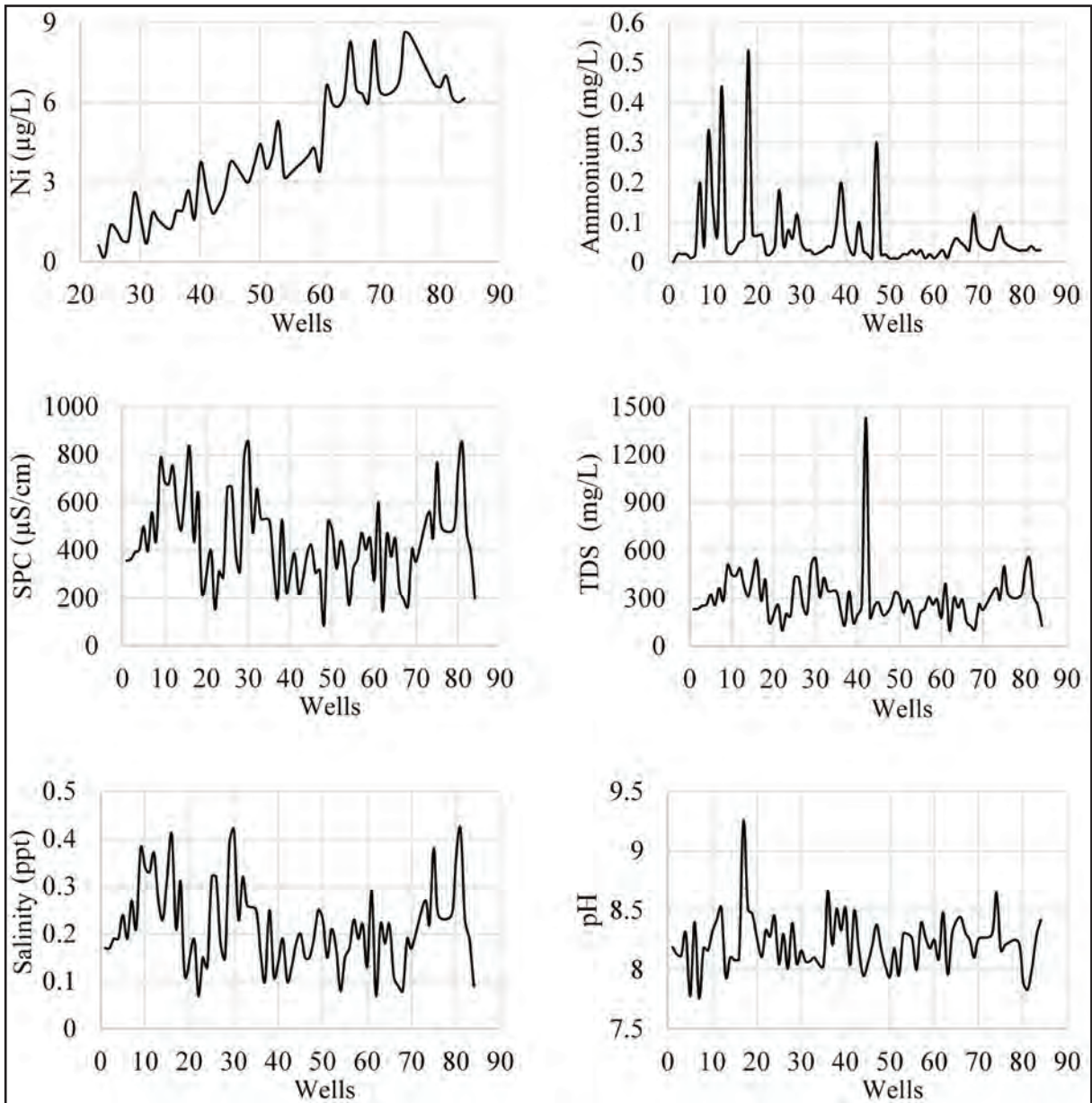


Figure 2 b- Analysis and in-situ measurement results; The amount of ^{60}Ni and the values of water quality parameters; ammonium, SPC, TDS, salinity and pH.

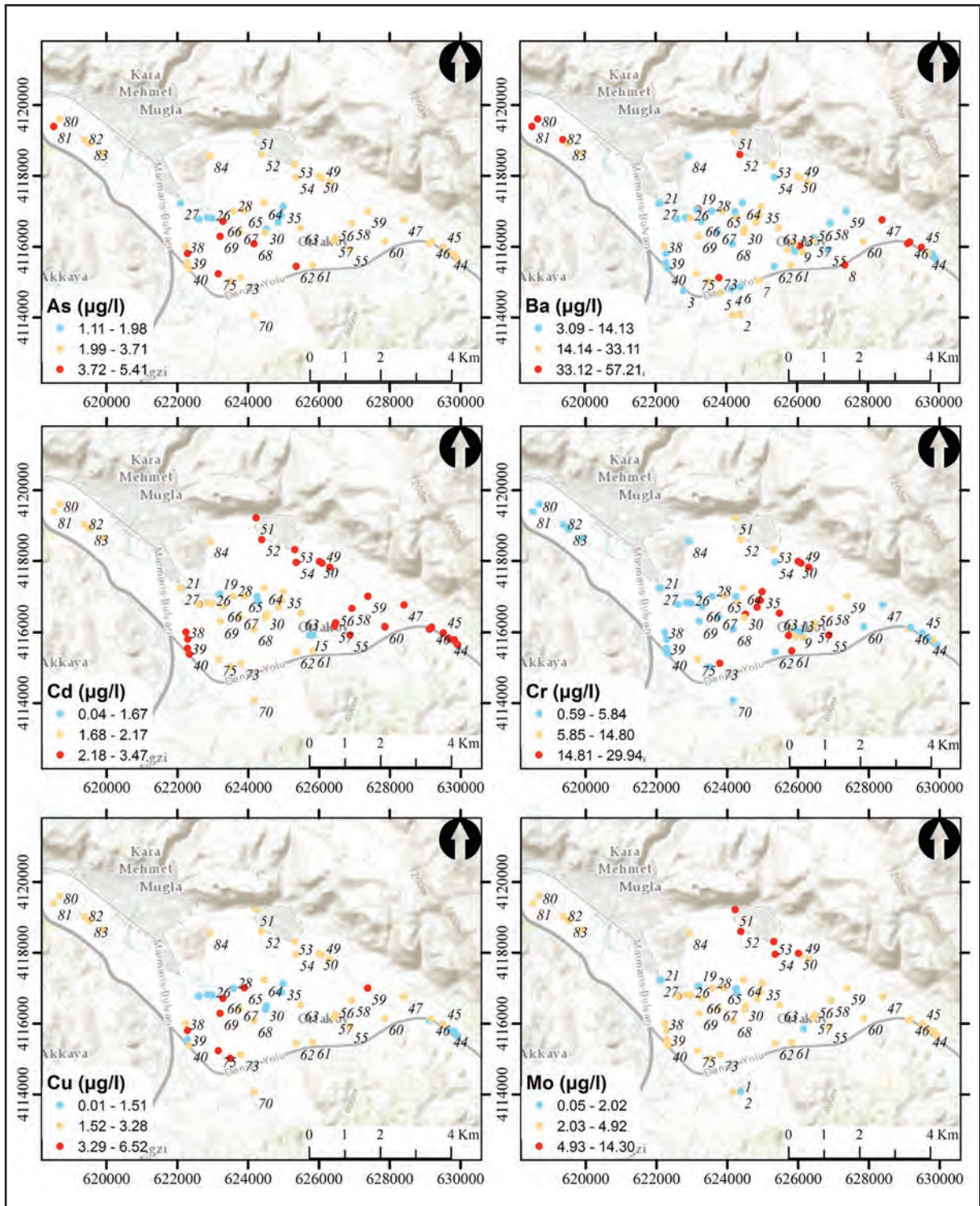


Figure 3 a- Spatial display of analysis and in-situ measurement results; The values of ⁷⁵As ¹³⁷Ba, ¹¹¹Cd, ⁵²Cr, ⁶⁵Cu and ⁹⁵Mo.

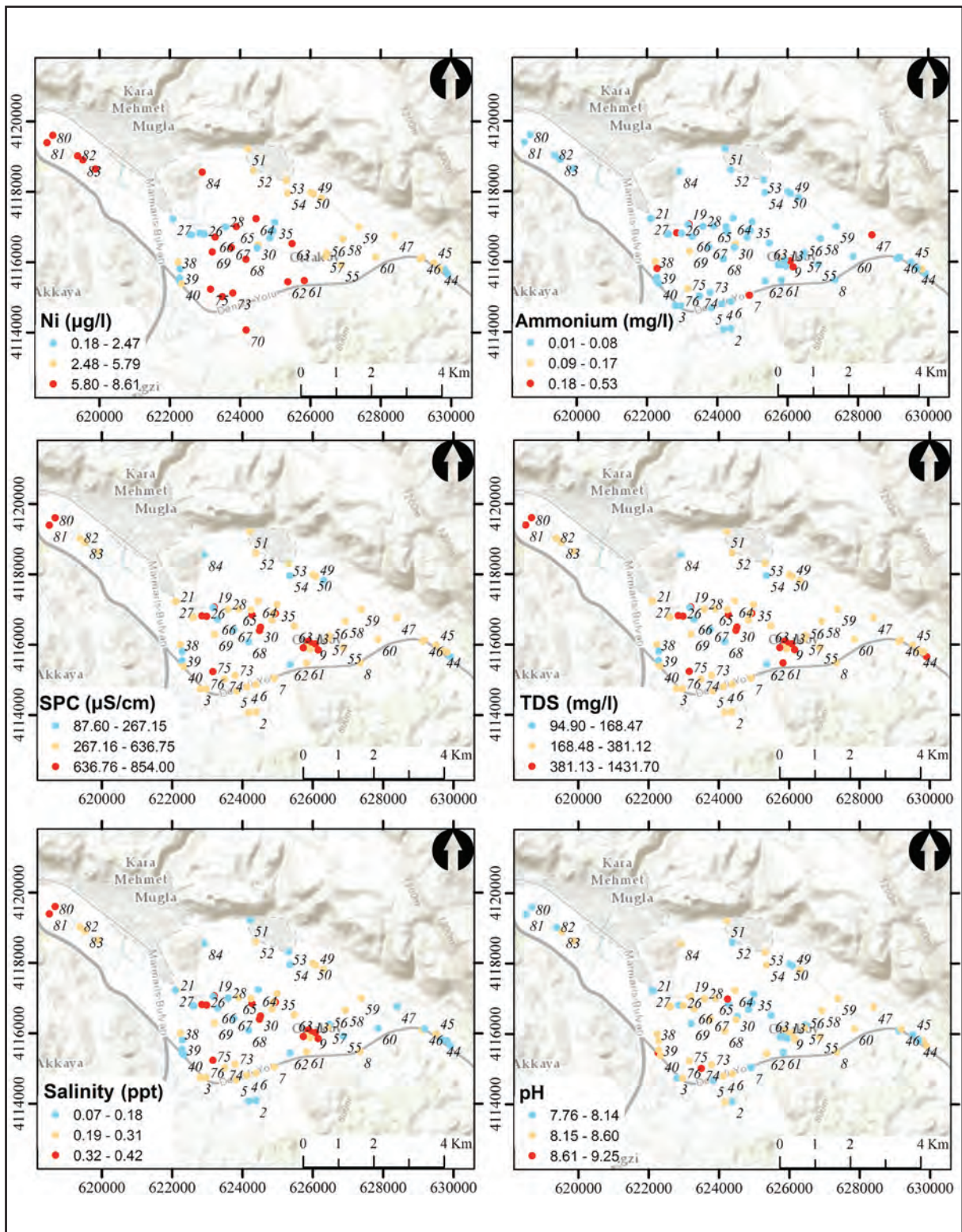


Figure 3 b- Spatial display of analysis and in-situ measurement results; The values of ⁶⁰Ni and water quality parameters; ammonium, SPC, TDS, salinity and pH.

Table 1- Correlations of elements.

| | As | Ba | Cd | Cr | Cu | Mo | Ni |
|----|---------|---------|---------|--------|---------|---------|-------|
| As | 1.000 | | | | | | |
| Ba | 0.049 | 1.000 | | | | | |
| Cd | -0.003 | 0.067 | 1.000 | | | | |
| Cr | 0.011 | 0.399** | 0.312* | 1.000 | | | |
| Cu | 0.832** | -0.013 | 0.252 | -0.048 | 1.000 | | |
| Mo | 0.679** | -0.003 | 0.412** | 0.079 | 0.726** | 1.000 | |
| Ni | 0.789** | 0.259 | -0.093 | 0.092 | 0.776** | 0.606** | 1.000 |

* Correlation is significant at 0.05 (2-tailed).

** Correlation is significant at 0.01 (2-tailed).

Table 2- CA proximity matrix.

| | As | Ba | Cd | Cr | Cu | Mo | Ni |
|----|--------|--------|--------|--------|-------|-------|-------|
| As | 0.000 | | | | | | |
| Ba | 9.827 | 0.000 | | | | | |
| Cd | 10.284 | 10.167 | 0.000 | | | | |
| Cr | 11.280 | 9.656 | 9.552 | 0.000 | | | |
| Cu | 5.357 | 10.628 | 9.328 | 11.526 | 0.000 | | |
| Mo | 8.238 | 10.257 | 6.877 | 9.967 | 8.405 | 0.000 | |
| Ni | 5.154 | 9.375 | 11.338 | 10.836 | 5.762 | 8.841 | 0.000 |

These strong correlations between Cu, Ni and As observed in Correlation Analysis are also noted in other methods in which relations between elements are investigated. The Euclidean distance between these 3 elements is closest to each other in the proximity matrix in CA (Table 2). However, unlike the Correlation Analysis, the nearest in the matrix, that is, the strongest relationship, appears between As and Ni (As-Ni=5.154 Euclidean distance). Then Cu-As (5.357 Euclidean distance) and Ni-Cu (5.762 Euclidean distance) stand out.

PCA findings also support Correlation Analysis and CA outcomes (Figure 4 and Table 3). The elements assessed in this study were collected in 3 different groups according to PCA results. These 3 components cover 77.89% of all data. The first component contains Cu, Ni and As, while the second component contains Mo and Cd. Cadmium dissolves in rocks with acidic water and can mix with groundwater at low concentrations. Other sources are industrial-mining waste, metal waste, water pipes, batteries and paints. Cd is one of the elements that are not essential for living things, which can cause liver, kidney, anemia and hypertension diseases in humans (Gallego et al., 2012). In addition, EPA has incorporated the Cd into the B1 class, which includes possible carcinogens for humans. The third component consists of Cr and Ba. The source of chromium content in groundwater can be represented by old mining operations, fossil fuel

consumption and cement plant waste. Cr is an element which can be found in different valences from -2 to +6 but trivalent and hexavalent valences are more common (Ergül-Ülger et al., 2014). Especially, hexavalent form is extremely important. Hexavalent Cr is not vital for the living creatures and has a high toxic effect (Bankar et al., 2009). Chromium is mutagenic and carcinogenic to humans and can lead to liver, kidney, internal bleeding, respiratory, skin inflammation and ulcer disorders (Mishra and Doble, 2008). Barium is an element that can be found naturally in some limestones, sandstones and soils, and whose concentration in the soil can be relatively higher than other metals (Suwa et al., 2008). It does not have a known biological function, but certain forms may cause heart, digestive and hypertension disorders, while showing a highly toxic effect (Llugany et al., 2000).

Table 3- PCA rotated component matrix.

| | Components | | |
|----|------------|-------|-------|
| | 1 | 2 | 3 |
| As | 0.911 | | |
| Cu | 0.847 | | |
| Ni | 0.920 | | |
| Cd | | 0.916 | |
| Mo | | 0.803 | |
| Ba | | | 0.822 |
| Cr | | | 0.674 |

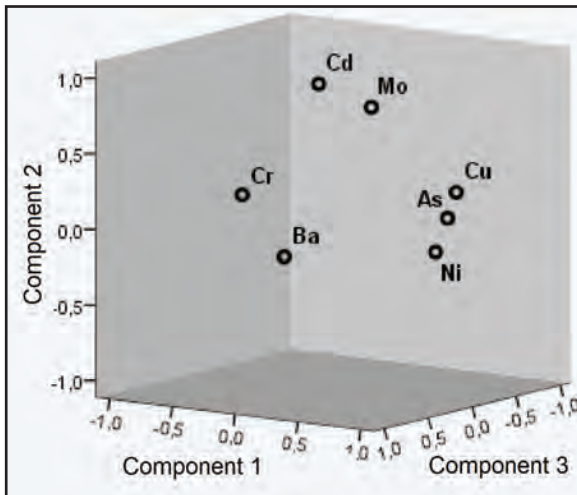


Figure 4- Components of PCA.

The PCA results also coincide with the CA results. In the dendrogram formed by CA matrix, it is seen that the elements constitute 3 main clusters (Figure 5). The element distributions of these clusters are similar to those of PCA.

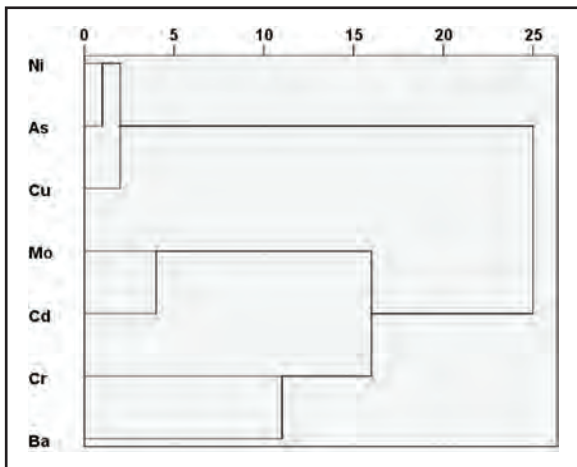


Figure 5- The dendrogram formed by CA matrix.

The accumulation of the elements has also been revealed (Figure 6). Nonparametric Kruskal Wallis and Mann-Whitney U tests were used to compare the amount of the elements, since the data was not normally distributed. This test combination is one of the most frequently used non-parametric comparison tests (Blazewicz et al., 2013; Farmaki et al., 2014). According to the results, Cu is the least common element and Ba is the most common element in the study area ($p < 0.05$). The amounts of all the elements except Ni and Mo are statistically significant. There is no statistically significant difference only between the amounts of Ni and Mo ($p > 0.005$).

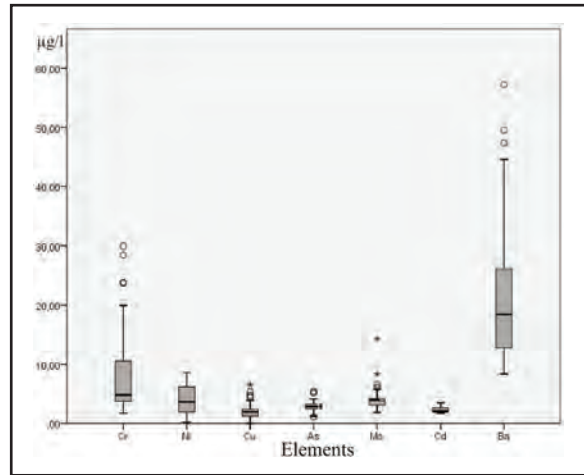


Figure 6- Box plots of studied elements.

When the relations of the elements studied in this paper are evaluated as holistic, the highest statistical relationship was found between As and Cu, followed by As-Ni, Ni-Cu, Cd-Mo, Cu-Mo, As-Mo, Mo-Ni and Cr-Ba. When the statistical relationships and the spatial distributions shown in figure 3 are evaluated together in order to determine the common sources of the elements studied, the main sources of the elements in the region are the mine and the industrial activities. In addition, household waste, agricultural activities and rock dissolution can be considered as potential sources.

The values of all metal and metalloids studied do not exceed EPA's limits for drinking water (EPA, 2012). The total dissolved matter (TDS), one of the water quality parameters, is compared by considering EPA and Turkish inland water quality classifications. The upper limit determined by EPA as 500 mg/l corresponds to the 2nd class water quality group from 4 different level found in the Turkish inland water quality classification. (ÇOB, 2004). The TDS values of the water in the examined wells were generally less than 500 mg/l and were included in the 1st and 2nd grade Turkish quality groups. A few values above 500 mg/l are point-based and do not represent a specific area. The TDS measurements determined above this value are in 3rd grade group according to the Turkish inland water quality classifications. Again according to this classification, no wells in 4th grade class were found in the study area. The range determined by EPA for pH is 6.5-8.5. This range corresponds to the 1st and 2nd degree quality groups according to the Turkish inland water quality classifications. Only 3 of the wells

examined in the study are not within this range. In terms of ammonium, most of the water samples are in the 1st degree class according to Turkish classification. Only a few of them are at the limits of the 2nd degree class. No water samples in 3rd or 4th degree classes were found. None of the parameters examined constitute health risk by the standards of the United States and Turkey and no pollution could be mentioned for the groundwater in the region. In addition, the quantities of the parameters studied do not exceed the natural limits for the water (Hem, 1985).

Yıldıztekin and Tuna (2011) obtained similar findings in the same study area. However, due to the fact that Yıldıztekin and Tuna (2011) did not specify the locations of the sampling wells in the study they performed, time-based and well-based comparisons could not be done, only general comparisons were performed.

Sampling and in situ measurements made in April, the rainy season for the region, are more likely to result in rare values due to the high water content from the rainfall. For this reason, it is recommended that the same field studies be carried out again in August, which is an arid period for the region, in order to be able to monitor and evaluate each parameter more accurate.

If the values of the elements and the other parameters examined in the study increase to the level that can be considered as "pollution", the source or sources of this pollution should be determined urgently and necessary precautions should be taken. In this context, actively operated waste water treatment plant, cement plant, sand and gravel quarry, industrial site, swimming pool and agricultural activities can be predicted as potential sources of pollution. Furthermore, it is important that the region be monitored in a stable manner, as the probability of a certain and continuous source of pollutants will increase pollution over time.

4. Conclusion

Within the scope of the study, heavy metal and metalloid analyzes of 84 water wells used for drinking and irrigation in Karabağlar Polje (Muğla, Turkey) were made and water quality parameters were measured. No evidence has been identified to threaten human health and ecosystem in terms of metals

and metalloids studied. Water quality parameters measured in place do not indicate the presence of any pollution in the area. However, the high interaction and correlations found in the context of statistical evaluation of the relationship between metal and metalloids have shown that some elements may have common sources.

Acknowledgement

This study was funded by Muğla Sıtkı Koçman University Scientific Research Project Office (12/124) and TÜBİTAK and ERANETMED (GRECPIMA and Project No: 115Y843). The authors offer their gratitude to Assoc. Dr. Evren Tunca and Dr. Esra Üçüncü Tunca who do not spare any kind of support. The authors also thank Res. Asst. Göksu Uslular for his contributions to field works.

References

- Açikel, Ş. 2012. Gökova-Azmaç (Muğla) karst kaynaklarının akım ve tuzlu su karışımı dinamiğinin kavramsal modellenmesi. Doktora Tezi, Hacettepe Üniversitesi, 140p. Ankara (unpublished).
- Alam, M. G. M., Snow, E. T., Tanaka, A. 2003. Arsenic and heavy metal contamination of rice, pulses and vegetables grown in Samta village, Bangladesh. *Arsenic Exposure and Health Effects* V 5, 103.
- Alonso, M.L., Montana, F.P., Miranda, M., Castillo, C., Hernandez, J., Benedito, J.L. 2004. Interactions between toxic (As, Cd, Hg and Pb) and nutritional essential (Ca, Co, Cr, Cu, Fe, Mn, Mo, Ni, Se, Zn) elements in the tissues of cattle from NW Spain. *Biometals* 17, 389-397.
- Atalay, Z. 1980. Muğla – Yatağan ve yakın dolay karasal Neojen'inin stratigrafi araştırması. *Türkiye Jeoloji Kurumu Bülteni* 23, 93-99.
- Bankar, A.V., Kumar, A.R., Zinjarde, S.S. 2009. Removal of chromium (VI) ions from aqueous solution by adsorption onto two marine isolates of *Yarrowia lipolytica*. *Journal of Hazardous Materials* 170, 487-494.
- Blazewicz, A., Klatka, M., Astel, A., Partyka, M., Kocjan, R. 2013. Differences in trace metal concentrations (Co, Cu, Fe, Mn, Zn, Cd, and Ni) in whole blood, plasma, and urine of obese and nonobese children. *Biological Trace Element Research* 155(2), 190-200.

- ÇOB. 2004. Su Kirliliği Kontrolü Yönetmeliği. Çevre ve Orman Bakanlığı, Ankara.
- Ekmekçi, M. Tezcan, L., Kurttaş, T. 2012. Gökova-Azmacık (Muğla) Karst kaynaklarında tuzlu su karışımının oluşum ve dinamiğinin duraylı izotop ve karışım hücreleri modelleme teknikleriyle belirlenmesi. TÜBİTAK, ÇAYDAG Project No: 109Y302, 158p. Ankara (unpublished).
- EPA. 2012. Edition of the Drinking Water Standards and Health Advisories. U.S. Environmental Protection Agency, Washington DC.
- Ergül-Ülger, Z., Özkan, A.D., Tunca, E., Atasagun, S., Tekinay, T. 2014. Chromium(VI) biosorption and bioaccumulation by live and acid-modified biomass of a novel morganella morganii isolate. Separation Science and Technology 49, 907-914.
- Farmaki, E.G., Thomaidis, N.S., Pasias, I.N., Baulard, C., Papaharisis, L., Efstathiou, C.E. 2014. Environmental impact of intensive aquaculture: Investigation on the accumulation of metals and nutrients in marine sediments of Greece. Science of the Total Environment 485, 554-562.
- Fatrorini, D., Notti, A., Regoli, F. 2006. Characterization of arsenic content in marine organisms from temperate, tropical, and polar environments. Chemistry and Ecology 22, 405-414.
- Franco, R., Sanchez-Olea, R., Reyes-Reyes, E.M., Panayiotidis, M.I. 2009. Environmental toxicity, oxidative stress and apoptosis: Menage a Trois. Mutation Research-Genetic Toxicology and Environmental Mutagenesis 674, 3-22.
- Gallego, S.M., Pena, L.B., Barcia, R.A., Azpilicueta, C.E., Lannone, M.F., Rosales, E.P., Zawoznik, M.S., Groppa, M.D., Benavides, M.P. 2012. Unravelling cadmium toxicity and tolerance in plants: Insight into regulatory mechanisms. Environmental and Experimental Botany 83, 33-46.
- Gathwan, K.H., Al-Karkhi, I.H.T., Al-Mulla, E.A.J. 2013. Hepatic toxicity of nickel chloride in mice. Research on Chemical Intermediates 39, 2537-2542.
- Gergen, I., Harmanescu, M. 2012. Application of principal component analysis in the pollution assessment with heavy metals of vegetable food chain in the old mining areas. Chemistry Central Journal 6-156.
- Girish, G., Resmi, T.R., Seralathan, P. 2013. Assessment of groundwater quality in Kavaratti Island in the Lakshadweep Archipelagos. Chemistry and Ecology 29, 309-319.
- Hem, J.D. 1985. Study and interpretation of the chemical characteristics of natural water. U.S. Geological Survey Water-Supply Paper 2254. Washington (unpublished).
- Huang, G.X., Chen, Z.Y., Sun, J.C. 2014. Water quality assessment and hydrochemical characteristics of groundwater on the aspect of metals in an old town, Foshan, south China. Journal of Earth System Science 123, 91-100.
- Kafadar, F.N., Saygıdeğer, S. 2010. Gaziantep İlinde Organize Sanayi Bölgesi Atık Suları ile Sulanan Bazı Tarım Bitkilerinde Kurşun (Pb) Miktarlarının Belirlenmesi. Ekoloji 19, 41-48.
- Klimek, B., Niklinska, M. 2007. Zinc and copper toxicity to soil bacteria and fungi from zinc polluted and unpolluted soils: A comparative study with different types of biotest plates. Bulletin of Environmental Contamination and Toxicology 78, 102-107.
- Kurttaş, T. 1997. Gökova (Muğla) karst kaynaklarının çevresel izotop incelemesi. Doktora Tezi, Hacettepe Üniversitesi, 220p. Ankara (unpublished).
- Llugany, M., Poschenrieder, C., Barcelo, J. 2000. Assessment of barium toxicity in bush beans. Archives of Environmental Contamination and Toxicology 39, 440-444.
- Lopez, F.J.S., Garcia, M.D.G., Vidal, J.L.M., Aguilera, P.A., Frenich, A.G. 2004. Assessment of metal contamination in Donana National Park (Spain) using crayfish (*Procambarus clarkii*). Environmental Monitoring and Assessment 93, 17-29.
- Luis Gama-Flores, J., Sarma, S.S.S., Nandini, S. 2009. Combined effects of exposure time and copper toxicity on the demography of *Moina macrocopia* (Crustacea: Cladocera). Journal of Environmental Science and Health Part B 44, 86-93.

- Matos, R.C., Vieira, C., Morais, S., Pereira, M.L., Pedrosa, J. 2010. Toxicity of chromated copper arsenate: A study in mice. *Environmental Research* 110, 424-427.
- Mishra, S., Doble, M. 2008. Novel chromium tolerant microorganisms: Isolation, characterization and their biosorption capacity. *Ecotoxicology and Environmental Safety* 71, 874-879.
- MTA, 2002. 1/500.000 scale Turkey Geological Maps (Denizli Section), Editor, Konak, N., Şenel, M., MTA Publisher, Ankara
- Okbah, M.A., Nasr, S.M., Soliman, N.F., Khairy, M.A. 2014. Distribution and Contamination Status of Trace Metals in the Mediterranean Coastal Sediments, Egypt. *Soil and Sediment Contamination* 23, 656-676.
- Pandey, B., Agrawal, M., Singh, S. 2014. Assessment of air pollution around coal mining area: Emphasizing on spatial distributions, seasonal variations and heavy metals, using cluster and principal component analysis. *Atmospheric Pollution Research* 5, 79-86.
- Pavlovic, A.N., Laketic, T.J., Mitic, S.S., Savic, M.J., Totic, S.B., Dordevic, M.S. 2014. Multielement determination using inductively coupled plasma optical emission spectrometry for metal characterization of water from artesian wells in Semberija region: Multivariate analysis of data. *Hemijaska Industrija* 68, 247-256.
- Polizzotto, M. L., Lineberger, E. M., Matteson, A. R., Neumann, R. B., Badruzzaman, A. B. M., Ali, M. A. 2013. Arsenic transport in irrigation water across rice-field soils in Bangladesh. *Environmental Pollution* 179, 210-217.
- Ramakritinan, C.M., Chandurvelan, R., Kumaraguru, A.K. 2012. Acute Toxicity of Metals: Cu, Pb, Cd, Hg and Zn on Marine Molluscs, *Cerithedia cingulata* G., and *Modiolus philippinarum* H. *International Journal of Mathematics and Statistics* 41, 141-145.
- Rodriguez-Sosa, M., Garcia-Montalvo, E.A., Maria Del Razo, L., Vega, L. 2013. Effect of Selenomethionine Supplementation in Food on the Excretion and Toxicity of Arsenic Exposure in Female Mice. *Biological Trace Element Research* 156, 279-287.
- Serafim, A., Company, R., Lopes, B., Rosa, J., Cavaco, A., Castela, G., Castela, E., Olea, N., Bebianno, M.J. 2012. Assessment of essential and nonessential metals and different metal exposure biomarkers in the human placenta in a population from the south of Portugal. *Journal of Toxicology and Environmental Health Part A* 75, 867-877.
- Suwa, R., Jayachandran, K., Nguyen, N.T., Boulenouar, A., Fujita, K., Saneoka, H. 2008. Barium toxicity effects in soybean plants. *Archives of Environmental Contamination and Toxicology* 55, 397-403.
- Thorsen, M., Perrone, G.G., Kristiansson, E., Traini, M., Ye, T., Dawes, I.W., Neran, O., Tamás, M.J. 2009. Genetic basis of arsenite and cadmium tolerance in *Saccharomyces cerevisiae*. *BMC Genomics* 10-105.
- Tsai, L.J., Ho, S.T., Yu, K.C. 2003. Correlations of extractable heavy metals with organic matters in contaminated river sediments. *Water Science and Technology* 47, 101-107.
- Tunca, E., Üçüncü, E., Kurtuluş, B., Özkan, A.D., Atasagun, S. 2013a. Accumulation trends of metals and a metalloid in the freshwater crayfish *Astacus leptodactylus* from Lake Yeniçağa (Turkey). *Chemistry and Ecology* 29, 754-769.
- Tunca, E., Üçüncü, E., Özkan, A.D., Ülger, Z.E., Tekinay, T. 2013b. Tissue Distribution and Correlation Profiles of Heavy-Metal Accumulation in the Freshwater Crayfish *Astacus leptodactylus*. *Archives of Environmental Contamination and Toxicology* 64, 676-691.
- Üçüncü, E., Tunca, E., Fikirdesici, S., Özkan, A.D., Altındag, A. 2013. Phytoremediation of Cu, Cr and Pb Mixtures by *Lemna minor*. *Bulletin of Environmental Contamination and Toxicology* 91, 600-604.
- Varmuza, K., Filzmoser, P. 2009. Introduction to Multivariate Statistical Analysis in Chemometrics. CRC Press, 336p.
- Wang, W., Lampi, M.A., Huang, X.D., Gerhardt, K., Dixon, D.G., Greenberg, B.M. 2009. Assessment of Mixture Toxicity of Copper, Cadmium, and Phenanthrenequinone to the Marine Bacterium *Vibrio fischeri*. *Environmental Toxicology* 24, 166-177.

Wang, X., Wang, H., Li, J., Yang, Z., Zhang, J., Qin, Z., Wang, L., Kong, X. 2014. Evaluation of Bioaccumulation and Toxic Effects of Copper on Hepatocellular Structure in Mice. *Biological Trace Element Research* 159, 312-319.

Wodala, B., Eitel, G., Gyula, T.N., Oerdoeg, A., Horvath, F. 2012. Monitoring moderate Cu and Cd toxicity by chlorophyll fluorescence and P-700 absorbance in pea leaves. *Photosynthetica* 50, 380-386.

Yıldıztekin, M., Tuna, A.L. 2011. Muğla karabağlar yöresi kuyu sularının sulama suyu kalitesi yönünden araştırılması. *Ege Üniversitesi Ziraat Fakültesi Dergisi* 48, 1-10.



Bulletin of the Mineral Research and Exploration

<http://bulletin.mta.gov.tr>

| BULLETIN OF THE MINERAL RESEARCH AND EXPLORATION | |
|--|--|
| Ömürden GENÇ* | AN INVESTIGATION ON SINGLE-PARTICLE IMPACT BREAKAGE FUNCTIONS OF A GOLD ORE BY DROP-WEIGHT TECHNIQUE |
| | Research Article |

AN INVESTIGATION ON SINGLE-PARTICLE IMPACT BREAKAGE FUNCTIONS OF A GOLD ORE BY DROP-WEIGHT TECHNIQUE

Ömürden GENÇ^{a*}

^aMuğla Sıtkı Koçman University Department of Mining Engineering 48000, Muğla, Turkey

Research Article

Keywords:

Gold Ore, Comminution, Modelling, Breakage Function, Drop-Weight Test

ABSTRACT

Impact breakage functions for a gold ore from Bergama region (Turkey) was estimated based on the single-particle impact breakage distributions of particles obtained from drop weight tests. For this purpose, a modified manual version of a JK Tech drop-weight test device was used. Effect of specific comminution energy (Ecs) on impact breakage distributions were investigated. Relationship between specific comminution energy and impact breakage product fineness (t10) parameter was established. Ecs-t10 model given in the literature was successfully fitted to the breakage test results. Ecs-t10 impact breakage model for the gold ore was proposed to be used in breakage function estimation. t-family curve approach was applied to estimate single particle breakage functions of the gold ore. For this purpose, t-family curves were modelled and variations of empirical breakage functions for the gold ore were estimated on different impact energy levels for comminution process modelling.

Received: 27.02.2016

Accepted: 24.03.2016

1. Introduction

Comminution circuit design, simulation and optimization studies can only be achieved if the reliable models of the comminution equipment are built based on the actual breakage data. Models of comminution equipment (Napier Munn et al., 2005) require the determination of breakage distribution function which can be determined by using different methods such as single particle breakage test (Narayanan, 1985), one-size fraction batch grinding test, back-calculation using continuous grinding test data (Genç, 2002). Although many methods are suggested in the literature for the experimental measurement of breakage distributions, it is usually difficult to represent the breakage of materials by a standart method due to the mathematical formulation and non-normalizable breakage. Specific breakage function of materials is usually assumed to be independent of initial particle size, process conditions (Austin and Luckie, 1971; Austin, 1982; Narayanan, 1986; Weller et al., 1988; Zhang et al., 1988) and input energy level (Austin and Weller, 1982) to ease the comminution modelling work. Many other researchers proved the opposite case (Hukki, 1961; Yashima, 1987; Schönert, 1988; 1991; Taveres and King, 1998; Weedon, 2001). Man (2000)

showed that, particle size dependency of breakage distribution function changes from material to material.

Twin-pendulum and drop-weight devices were used to develop standard procedures for the calculation of breakage functions (Narayanan, 1985; 1986; Awachie, 1983; Leung, 1987; Narayanan, 1987; Morrell and Man, 1997). Specific breakage function can be estimated by using the relationship between specific comminution energy (kWh/t) and t10 breakage parameter and t-curve approach which were described by Narayanan (Narayanan, 1985; 1986; 1987). t-curve approach normalizes the effect of particle size. Different breakage energy levels were proposed for the estimation of breakage distribution function in the literature. According to Narayanan (1985), an input energy level of 41.788 kg-cm gives the appropriate characteristic breakage distribution function on the Ecs-t10 curve and proposed to be used in wet ore ball mill modelling. Morrell and Man (1997) suggested an arbitrary energy level of 1kWh/t. Zhang et al. (1988) used an energy range of 1.25-1.5 kWh/t for the estimation of breakage distribution functions of cement clinkers. Genç (2002) proposed 1kWh/t as a standard energy level for the breakage of cement clinker particles to estimate breakage functions.

* Corresponding author: Ömürden Genç, ogenc@mu.edu.tr
<http://dx.doi.org/10.19111/bmre.78208>

In this study, it was aimed to evaluate the variations in the breakage distributions of different size fractions of a gold ore by drop-weight technique at different specific impact energy levels and normalize the size effect by using the t-curve approach in estimating the breakage functions. Ecs-t10 model (Napier Munn et al., 2005) was validated for the breakage test results. The model was also validated size by size. Established overall relationship between specific comminution energy and breakage distribution parameter (t10) was used to estimate breakage functions at different specific comminution energy levels. Breakage function reconstructions models (t10-tn models) were proposed for gold ore comminution modelling.

2. Materials and Methods

2.1. Drop-Weight Test Device

Drop-weight test device which was used in this study was previously described by Genç et al., (2004; 2014). It mainly comprises a steel anvil made from steel alloy, plate shape drop weight head, an electromagnet through which an electromagnetic field is formed so that weights can be hold or released from the desired heights (Genç et al., 2004; 2014). A photograph of the drop weight device is given in figure 1.

Impact energy level supplied by the plate shaped weight was calculated by Equation (1). Specific comminution energy level was calculated by Equation (2) (Napier Munn et al., 2005).

$$E_i = m_d g (h_i - h_f) \quad (1)$$

where,

E_i : Impact breakage energy (m²kg/sec²)

m_d : Mass of drop weight head (kg)

h_i : Initial height of the drop-weight above the anvil (m)

h_f : Final height of the drop-weight above the anvil (m)

$$Ecs = \frac{E_i}{m_p} \quad (2)$$

where,

Ecs : Specific comminution energy (kWh/t)

mp : Mean particle mass (g)

2.2. Sample and Laboratory Studies

Run-of-mine test sample was provided from the Bergama region in Turkey. Contained gangue mineral in the ore was mainly quartz. Tests were conducted on the selected narrow particle size fractions at different specific comminution energy levels (kWh/t). For this purpose, samples were dry sieved to the desired narrow size fractions and representative samples were

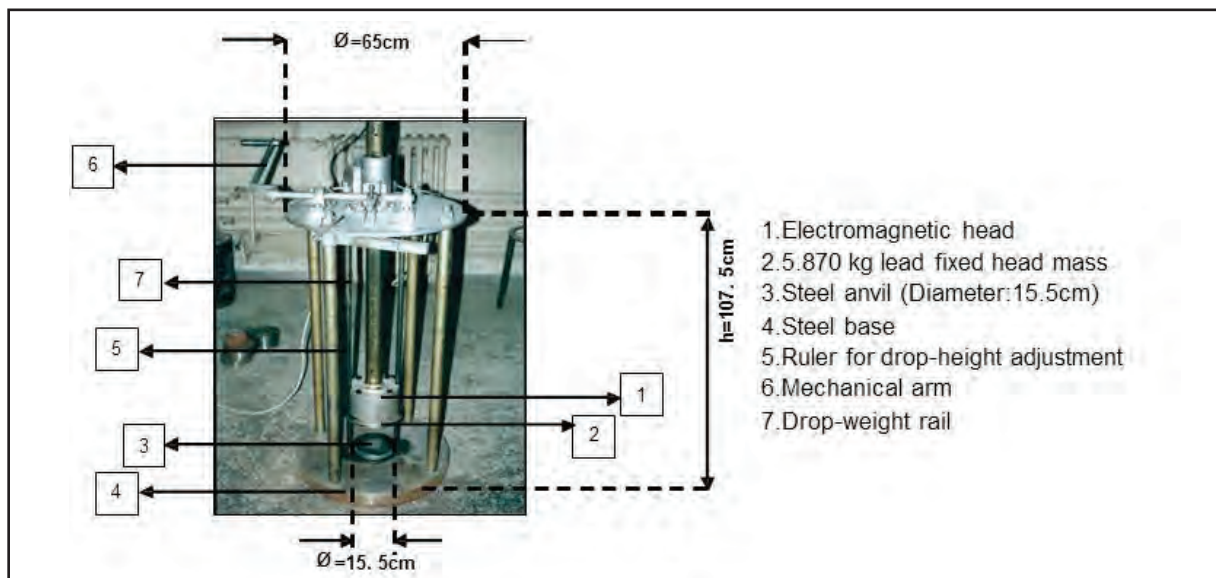


Figure 1- Drop-weight test device.

taken from each size fraction by using a riffler for each breakage energy level. Number of particles in each test size fraction was counted to determine the mean mass of the particles. Appropriate height and drop weights were calculated to achieve the desired specific comminution energy levels. Impact energy supplied by the plate shaped weight is calculated from the equations given by Napier Munn et al. (2005). Single particle breakage tests were carried out on each sample at the required energy levels. Broken fragments were collected from each breakage test, and dry sieved on $\sqrt{2}$ sieve series in a ro-tap sieve shaker for 15 minutes. Finally, particle size distributions of the broken gold ore samples were determined from the top size down to 0.038mm. Test size fractions, specific comminution energy levels (Ecs) in kWh/t and number of particles broken per energy level are tabulated in table 1.

3. Discussion

3.1. Impact Particle Size Distributions

Particle size distributions of the broken ore particles are given in figure 2 to 5 for different impact energy levels.

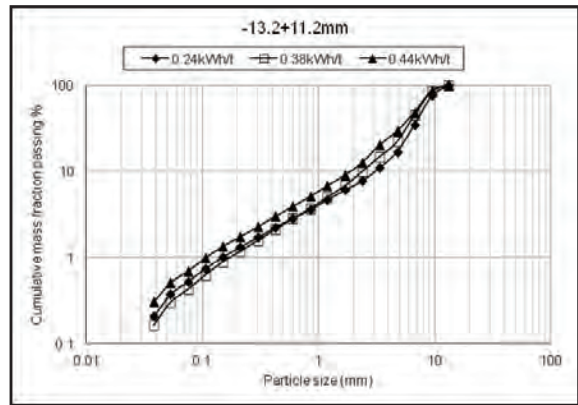


Figure 2- Size distributions of product particles from the breakage of -13.2+11.2mm at different impact energy levels.

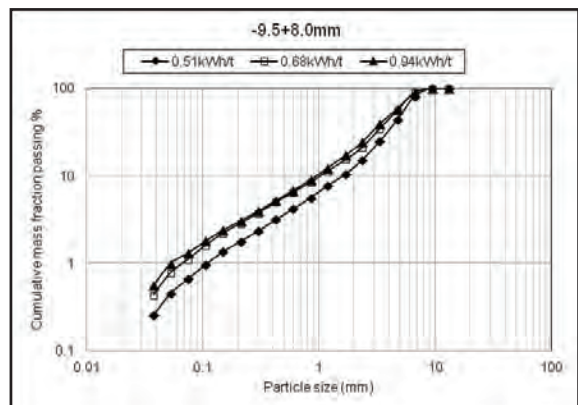


Figure 3- Size distributions of product particles from the breakage of -9.5+8mm at different impact energy levels.

Table 1- Drop-weight test specifications

| Test size fraction (mm) | Nominal test size (mm) | Ecs (kWh/t) | Number of particles broken per energy level |
|-------------------------|------------------------|-------------|---|
| -13.2+11.2 | 12.16 | 0.24 | 80 |
| | | 0.38 | 80 |
| | | 0.44 | 80 |
| -9.5+8.0 | 8.72 | 0.51 | 100 |
| | | 0.68 | 100 |
| | | 0.94 | 100 |
| -8+6.7 | 7.32 | 0.86 | 150 |
| | | 1.32 | 150 |
| | | 1.77 | 150 |
| -5.6+4.75 | 5.16 | 2.51 | 250 |
| | | 5.28 | 250 |

Particle size distributions of the breakage products in the breakage event of coarsest test size fraction -13.2+11.2mm indicated that finer particle size distribution could be achieved as the level of impact breakage energy was increased. It was observed that, breakage product size distributions did not change significantly although the energy level was increased by approximately 0.4kWh/t. This condition could be observed from the size distributions of product particles from the breakage of -8+6.7mm particles broken at energy levels of 1.32kWh/t and 1.77kWh/t (Figure 4). It became difficult to break particles by impact as the particle size got finer. For example, closely similar breakage product size distributions were observed in the breakage event of particles within the size fraction of -5.6+4.75 although the impact energy level was increased by about 3 kWh/t (Figure 5). This condition indicated that no more considerable size reduction would occur. More comminution energy is needed or the type of comminution mechanism should be changed for further breakage of gold ore particles.

3.2. Ecs-t10 Size Reduction Model

The value of t10 was traditionally accepted as the fineness or breakage index number. t10 was quantitatively defined as the amount of material passing 1/10th of the geometric mean of the broken size fraction. The value of t10 distribution parameter indicates the fineness of the broken particle size fraction for different energy consumption levels. Impact breakage behaviour of materials can be characterized and compared through a single distribution parameter at any specific comminution energy level on the particle size basis by using t10 value. When the relationship between t10 and specific comminution energy level

is established, specific energy consumption required to achieve the desired particle size distribution can be predicted using t-curves. Ecs-t10 model is given in equation (3). The product of model parameters A and b is the slope of the Ecs-t10 relation at 'zero' input energy. Axb parameter can be used to characterize the hardness of the ore. Lower value of Axb indicates that more energy is needed for an equivalent amount of breakage (Napier Munn et al., 2005).

$$t_{10} = A \times [1 - \exp(-b \times Ecs)] \tag{3}$$

In this comminution model;

A, b : material impact parameters

Ecs : specific comminution energy (kWh/t)

Impact breakage model for the gold ore is given by Equation (4). A and b values were determined by non-linear regression using SPSS statistical program. R² of the overall model fit was 0.92. Axb value was determined as 15.72.

$$t_{10} = 14.56 \times [1 - \exp(-1.08 \times Ecs)] \tag{4}$$

Overall relationship between specific comminution energy and t10 parameter is given in figure 6. Experimental values were plotted as compared to model calculated values (model fit). Sufficiently good agreement between the experimental and model fitted values were observed which showed the validation of the Ecs-t10 model for the gold ore. Non-linear regression analysis was performed on the test results of each test size fraction to establish the Ecs-t10 relationship by particle size. Experimental and model fitted values are compared for different particle size

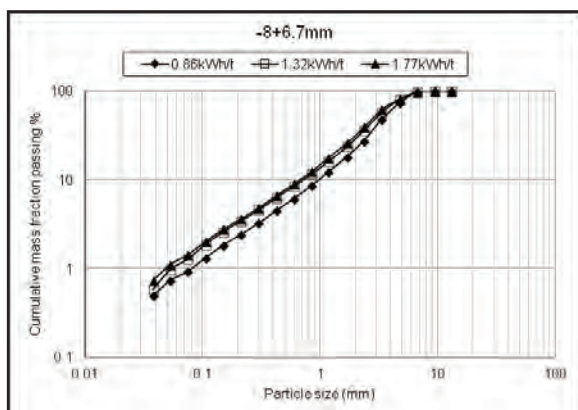


Figure 4- Size distributions of product particles from the breakage of -8+6.7mm at different impact energy levels.

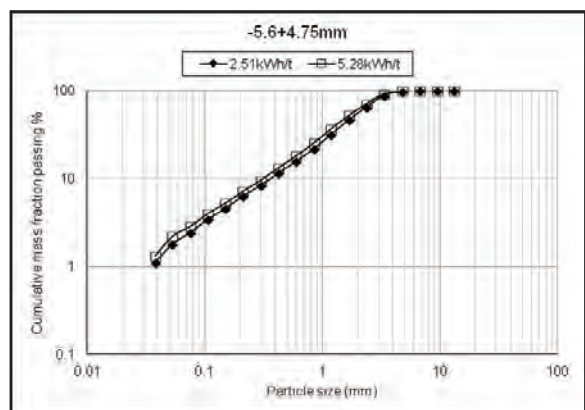


Figure 5- Size distributions of product particles from the breakage of -5.6+4.75mm at different impact energy levels.

fractions in figure 7. Model validation results for different particle size fractions are tabulated in Table 2. Ecs-t10 model could not be validated for the particle size fraction of -5.6+4.75mm as there was only two experimental results. A linear relationship was found to exist between particle size and Axb parameter. This relationship provided comparison between the hardness of different particle sizes (Figure 8). Findings also indicated that, Ecs-t10 relationships of ore particles vary by particle size for a constant level of specific comminution energy which may be linked to the probable differences in microstructure, mineralogical and chemical composition of different particle sizes.

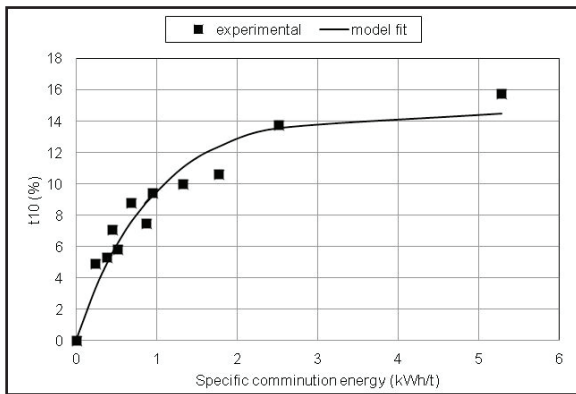


Figure 6- Overall relationship between specific comminution energy and t10% for the gold ore sample.

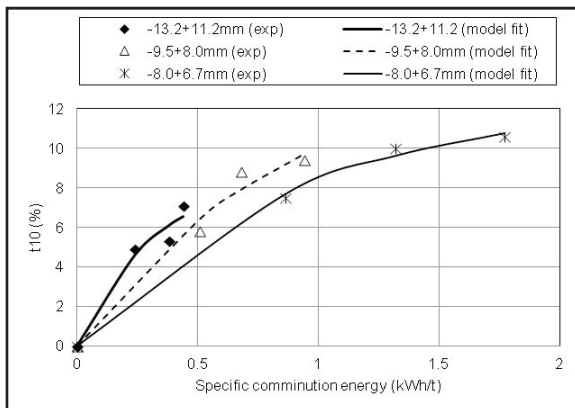


Figure 7- Relationships between specific comminution energy and t10% for different size fractions of the gold ore sample.

Table 2- Estimated model parameters for different particle size fractions.

| Size fraction (mm) | A | b | R ² | Axb |
|--------------------|-------|------|----------------|-------|
| -13.2+11.2 | 8.86 | 3.06 | 0.96 | 27.16 |
| -9.5+8.0 | 15.29 | 1.07 | 0.98 | 16.38 |
| -8.0+6.7 | 12.58 | 1.10 | 1.00 | 13.85 |

3.3. t-family Curves and Models

t-family curve approach (Narayanan, 1985) was used to determine breakage functions of the gold ore. t10-tn relationships are given in Figure 9 for breakage function reconstruction. Description of the t-curve approach which normalizes the effect of particle size was given in the literature (Narayanan, 1985; 1986; 1987). Distribution parameter, t10 was used which represents the amount of material at fine size ranges thus provides more information on the fragmentation at fine sizes. According to this approach, particle size distribution data obtained after the breakage of test samples was plotted and the size distribution parameters t2, t4, t10, t25, t50, and t75 correspondingly expressing the cumulative per cent passing size of y/2, y/4, y/10, y/25, y/50, y/75 were determined. y is the geometric mean of the size fraction of the test particles. t10 versus other distribution parameters are plotted to obtain t-family curves through which the product size distribution resulting from the breakage of the considered size fraction at any specific comminution energy level can be established. t10-tn family curves for the gold ore are given in Figure 9. Regression equations of the t-curves are tabulated in Table 3. Single particle impact breakage functions of the gold ore were estimated for different specific

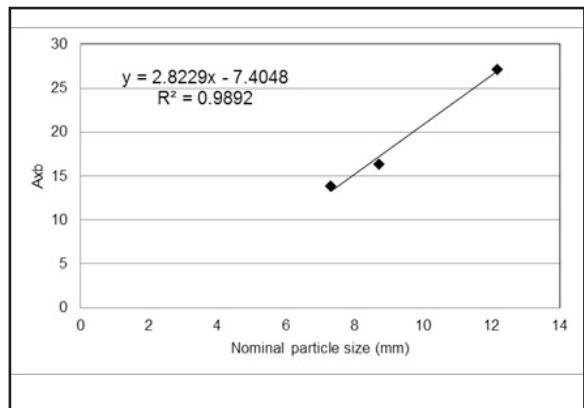


Figure 8- Relationship between particle size and Axb.

energy levels using the regression equations in table 3 and given in figure 10. It was observed that, gold ore particles started to exhibit similar breakage functions at impact energy levels higher than 1 kWh/t which indicated that no more considerable size reduction could be achieved at energy levels higher than 1kWh/t by impact mechanism.

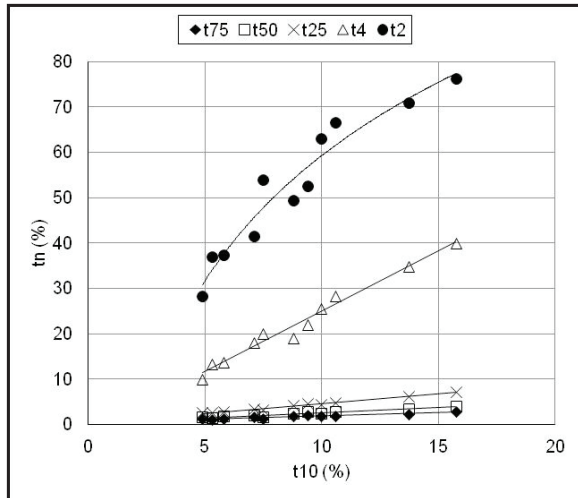


Figure 9- t10-tn family relationships for the gold ore.

Table 3- Normalized breakage function re-construction models.

| Equation | R ² |
|---------------------------|----------------|
| $t2=39.86\ln(t10)-32.516$ | 0.94 |
| $t4=2.6571(t10)-1.6486$ | 0.98 |
| $t25=0.4267(t10)+0.3636$ | 0.99 |
| $t50=0.2309(t10)+0.3403$ | 0.95 |
| $t75=0.1495(t10)+0.3738$ | 0.93 |

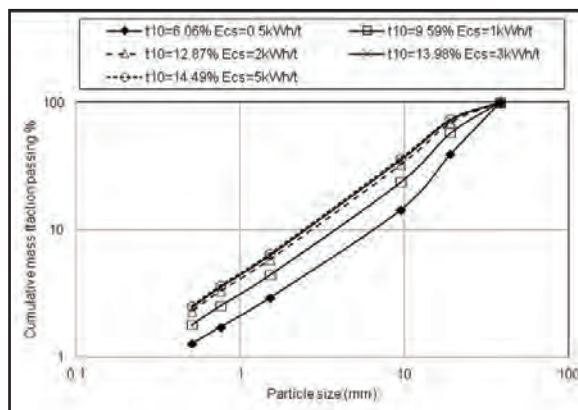


Figure 10- Typical impact breakage functions for different specific comminution energy levels.

4. Conclusion

Relationship between specific comminution energy and t10 breakage distribution parameter for the gold ore was found to be successfully fitted to the Ecs-t10 model given in the literature (Napier Munn et al., 2005). Impact breakage of gold ore particles were found to be size dependent. A linear relationship was found to exist between particle size and Axb impact breakage parameter. t-curves for the gold ore were modelled and proposed to reconstruct breakage functions which can be used in modelling of gold ore comminution. Variation in normalized breakage distribution functions were determined for different energy levels. Impact breakage distribution function was found to not change considerably at energy levels higher than 1kWh/t. Breakage function reconstruction models were proposed to be used in comminution modelling and simulations of size reduction machines operating on the basis of the impact mechanism in the processing of the related gold ore.

Acknowledgements

Author would like to acknowledge to Prof. Ş. Levent Ergün from the Mining Engineering Department of Hacettepe University.

References

Austin, L.G., Luckie, P.T. 1971. Methods for determination of breakage distribution parameters. Powder Technology 5, 45-52.

Austin, L.G., Weller, K.R. 1982. Simulation and scale-up of wet ball mills. XIV International Mineral Processing Congr., Toronto, Canada, 8.1-8.24.

Awachie, S.E.A. 1983. Development of crusher models using laboratory breakage data. PhD Thesis. The University of Queensland, JKMRRC, Australia.

Genç, Ö. 2002. An investigation of the breakage distribution functions of clinker and additive materials. MSc Thesis. Hacettepe University, Mining Engineering Department, Turkey.

Genç, Ö., Benzer, A.H., Ergün, Ş.L. 2004. Single particle breakage characterization of materials by drop weight testing. Physicochem. Probl. Miner. Process. Poland, 38, 241-255.

- Genç, Ö., Benzer, A.H., Ergün, Ş.L. 2014. Analysis of single particle impact breakage characteristics of raw and HPGR-crushed cement clinkers by drop weight testing. *Powder Technology* 259, 37-45.
- Hukki, R.T. 1961. Proposal for a Solomonic settlement between the theories of von Rittinger, Rick and Bond. *Trans SME/AIME*, 220, 403-408.
- Leung, K. 1987. An energy based ore specific model for autogenous and semiautogenous grinding. PhD Thesis. The University of Queensland, JKMR, Australia.
- Man, Y.T. 2000. A Model-based scale-up procedure for wet, overflow ball mills. PhD Thesis. Julius Kruttschnitt Mineral Research Centre, Department of Mining, Minerals and Materials Engineering, The University of Queensland, Australia.
- Morrell, S., Man, Y.T. 1997. Using modelling and simulation for the design of full scale ball mill circuits. *Minerals Engineering* (10) 12, 1311-1327.
- Napier Munn, T.J., Morrell, S., Morrison, R.D., Kojovic, T. 2005. *Mineral Comminution Circuits Their Operation and Optimization*. JKMR Monograph Series in Mining and Mineral Processing, No.2, The University of Queensland, Brisbane, Australia.
- Narayanan, S.S. 1985. Development of a laboratory single particle breakage technique and its application to ball mill modelling and scale-up. PhD Thesis. Julius Kruttschnitt Mineral Research Centre, The University of Queensland, Australia.
- Narayanan, S.S. 1986. Single particle breakage tests: A review of principles and applications to comminution modeling. *Bull Proc. Australas. Inst. Min. Metall.* 291, 4, 49-58.
- Narayanan, S.S. 1987. Modelling the performance of industrial ball mills using single particle breakage data. *International Journal of Mineral Processing* 20, 211-28.
- Schönert, K. 1988. *Fundamentals of particle breakage*. Course notes. University of Witwatersrand, Division of Continuing Engineering Education, Johannesburg, Section F6.
- Schönert, K. 1991. Advances in comminution fundamentals and impacts on technology. *Aufbereit.-tech.* 32, 487-494.
- Tavares, L.M., King, R.P. 1998. Single-particle fracture under impact loading. *International Journal of Mineral Processing* 54 (1), 1-28.
- Weedon, D.M. 2001. A perfect mixing matrix model for ball mills. *Minerals Engineering* 14, 10, 1225-1236.
- Weller, K.R., Sterns, U.J., Artone, E., Bruchard, W.J. 1988. Multicomponent models of grinding and classification for scale-up from continuous small or pilot scale circuits. *International Journal of Mineral Processing* 22, 19-147.
- Yashima, S., Kanda, Y., Sano, S. 1987. Relationships between particle size and fracture energy or impact velocity required to fracture as estimated from single particle crushing. *Powder Technology* 51, 277-282.
- Zhang, Y.M., Napier Munn, T.J., Kavetsky, A. 1988. Application of comminution and classification modelling to grinding of cement clinker. *Trans. IMM.* 97, C207-C214.



Bulletin of the Mineral Research and Exploration

<http://bulletin.mta.gov.tr>



Opinions on the article of “Investigation of the Seismic Velocity Distribution and Crustal Structure of Turkey by means of Gravity Data”

THE REACTION OF PHYSICAL TRANSFORMATION OF THE GRAVITY DATA AND LINEARITY DILEMMA

Ertan TOKER^{a*}

^a General Directorate of Mineral Research and Exploration, Department of Geophysical Researches

Discussion

Keywords:

Gravity, seismic, Bouguer, velocity, crust

ABSTRACT

This paper consists of opinions on the article entitled as “Investigation of the Seismic Velocity Distribution and Crustal Structure of Turkey by means of Gravity Data” which was published on the page 185 of the 153rd issue of the Bulletin of Mineral Research and Exploration. Within this context, it was aimed at defining some dilemmas encountered in the article, which was targeted in the exploration of the crustal structure in plate scale by means of data sets, and informing the reader. Here, the interactive relationships of Gravity and Seismic methods of which each one are discipline of expertise will be studied within scope of the mentioned article.

Received: 29.11.2016

Accepted: 25.01.2017

1. Introduction

As a result of physical transformation made by using the apparent gravity linear filter and data set of Turkey, the distribution related to the Conrad discontinuity was investigated. During this study, the velocity model based on the seismic data set generated by the gravity data was taken as a basis. In doing so; it was aimed at illuminating the crustal structure of Turkey (Akın, 2016). Therefore; the subject has a great importance.

The velocity distribution obtained is based on an empirical conversion (Barton, 1986). The gravity depth variation has been estimated by a linear filter. Here, the density continuously increases with depth. However; it is not possible in everywhere. Salt fields can be regarded as an example. The variation of the gravity with depth has been obtained by not considering the lower depth of blocky structures, which are located between the upper and lower crusts and dominate the gravitational effect (Simeoni and Brückl, 2009). Conrad is a vertical discontinuity and some difficulties are encountered when monitored by dynamic parameters. The place, where the density

and seismic velocity increases are the most, is defined as 16 km's, the upper crust (estimating by using the empirical relationship obtained by Barton (1986) in Northern Sea, so far away from our country). However; the characteristics of seismic wave and the gravity effect do not linearly disperse in crust.

1.1. Linearity Dilemma

The resulting paragraph of the Barton's (1986) article, quoted for each value of the empirical conversion (valid under some circumstances), titled as “The relationship between seismic velocity and density in continental crust – a useful constraint?”, which forms the backbone of the article, is as follows;

Conclusion: Calculated gravity profiles for the continental crust show that, due to the range of Densities possible for rocks of each seismic velocity and vice versa, the use of a seismic velocity measurement of a rock as the only indication of its density does not provide a useful constraint when attempting to reproduce observed gravity variations.

It is understood from the paragraph that, the author has answered the question of “usability of the method”

* Corresponding author: Ertan Toker, ceyhanertan.toker@mta.gov.tr
<http://dx.doi.org/10.19111/bulletinofmre.306006>

as given on title of the article and reached the result that “the rock density is not usable as the “single indicator” for seismic velocity conversion”.

In this case, to the contrary of the source article, which has been used during the preparation of the article criticized, there has not been used any other indicator. Furthermore; a transformation from gravity data to seismic data has been made with an inverse method.

When theoretical and empirical trials reach the success, industrial sectors would follow and benefit from these methods. This article has handled a subject, which saves time and money, but it is seen that this subject has not been taken seriously in sectorial basis from 1986 to recent.

It is known that the single indicator is not useful except for reconstruction studies by means of seismic and gravity data conversion. However; the studies in which the single indicator is used are mainly based on the correlation of drilling data. The medium velocities of P and S waves are sensitive to temperature and pressure changes. The physical meaning of this statement is as follows; the velocities do not linearly vary with depth. Besides; the elements such as; the compressibility and attenuation losses, which determine the seismic quality of the environment, are the factors affecting the seismic velocity. These factors do not disperse uniformly in underground, and the reason of the anomaly, which we often search for, is the non-availability of this uniform dispersion.

When these indicators are not taken into consideration, the result of data transformation is almost one to one related with primary data. When the output obtained in this article are studied, it is seen that the velocity distribution and Conrad distribution maps, which their scale change and show the same distributions with the Bouguer gravity map, were achieved (see figure 4 and 6 from Akın, 2016).

The whole Turkey has been selected for the study area and Bouguer gravity data set has been used. However; quite large areas are observed, where the data transformation is not valid, within the boundaries of this study area.

Çankırı and Salt lake basins are some of these areas. Large scale salt structures take place on these

fields. Salt structures may rise up due to the excess load of the overlying sediments in sedimentary environments. That is; these structures are very low compressible structures, and their volumes and structures can dramatically change under pressure. Although the densities are 2-2.2 gr/cm³, their seismic velocities are very high (4.5- 5 km/s). That is; the response of these formations to parameter conversion, which is the topic of this article, is false. For example; the Thrace basin is very deep and the block structures, which are mentioned that dominate the upper crust, are in minority. Similarly; sedimentary basins of which have thicknesses that continue for kilometers are present. Physical transformation on these fields is regarded as inconvenient.

It is not mentioned any exception or an exceptional area about data and conversions used in the study. Velocity losses have not been considered. Seismic discontinuities based on the apparent density anomaly are investigated by acquiring apparent velocities using increases of apparent density. If this was a valid approach, it would be possible to estimate layers and discontinuities only by gravity data. It would even be a preferable way in order to get rid of the application cost of seismic methods.

Mathematical and logical acceptations can be done for the resolution of underground structures. These acceptances are sometimes compulsory in order to solve the problem or make it solvable. When Barton (1986) investigated, whether this conversion was useful or not, he made a modelling with a transformation into gravity using an empirical relationship by the seismic method. This can give information about the formation in vertical direction and its layer thickness can be estimated, and an empirical acceptance for a model construction. Seismic velocities are measured in time scale as they do not disperse linearly. Therefore; the nature of the problem is not linear.

In addition; the inverse of it is not valid. That is; the transformation into seismic data to make discontinuity calculation from the gravity method, which its layer thickness cannot be estimated (which does not homogenously disperse in layer), cannot be qualified as a meaningful acceptance.

Simeoni and Brückl (2009) wrote the conditions of velocity-density conversions in their studies. They

stated under what giga pascal (gpa) pressure and what temperature (°C) conditions the conversions had been made and in which velocity interval the relation of conversion had been valid.

Seismic velocities in crust size are measured by traversing the mantle. We may get seismic signals where the crust is thick. Despite that; there are situations when we cannot achieve contrast by effects such high temperature and metamorphism. Similarly; density values are also influenced by the high temperature and metamorphism. The problem is the same. The method followed here does not obscure the problem. However; its effect on the conversion is not known either.

The zone, where the velocity information changes, decreases or increases is normally the anomaly region. The gravity-seismic transformation at these depths will not give a reliable anomaly zone because of temperature and pressure conditions. That is; the differences, which should be solved the first would not affect the estimation and unnoticed, have not been investigated. The Conrad, which is difficult to monitor also by seismic methods in which the vertical variation of seismic waves with respect to time are observed, is a weak discontinuity zone.

2. Technical Dilemmas

Opinions on “acquiring the density from seismic velocities and the seismic velocity from densities”, which are applied in the article, are as follows;

The contrast between the lower and upper crusts in line 16 of the page 3 is given as 0,3 gr/cm³ based on Simeoni and Brückl (2009) on page 186. However; it is mentioned about 300 kg/m³ contrast between the lower crust and upper mantle. The author, here has misunderstood the contrast between the lower and upper crusts and the contrast between the lower crust and mantle. This is a big difference. Thus; accepting such a big difference forms an equal confusion of accepting that the Conrad discontinuity can be monitored across Turkey. The excessively discontinuous and tectonically active structure of Turkey already makes the monitoring of this zone impossible.

On page 189 of the article, the “apparent” density by means of linear method is calculated by formula (1)

as given below, using gravity Bouguer data of which its first term is based on the parameter prediction of (ρ_o), but the conditions of the prediction are not explained;

$$\rho(x,y) = \rho_o + (1/2\pi G) F^{-1}\{(\omega / 1-e^{-\omega h}) \cdot \Delta g(u,v)\} \quad (1)$$

In doing so; the seismic velocity from “density” has been obtained making an empirical and linear relationship using the density values suggested by Barton (1986).

Woollard (1959) clearly stated that there had not always been a linear relationship between seismic velocities and gravity.

Barton (1986), in figure 1 of his article used a method which has not any formula, but was defined by a linear relationship with indefinite coefficient of relationships. He predicates the method on the linear interpretation of laboratory calculations in Nafe and Drake (1970) and the offset of these values. Velocities (5,7 km/s) were taken as the base for massif continental crust in such a way to correspond to 2,8 gr/cm³. However; this is an acceptance, too. Despite that; the velocity was transformed from apparent density by the transformation, which Barton had used, instead of the conversion from velocities into density in the article mentioned. Here; the method of re-calculation by empirical method had been edited from previously made empirical calculation.

The increasing depth negatively affects the downward analytical continuation signal, but it does not affect the apparent density relationship. If the effect has been removed then it should be explained. The density continues to increase linearly. The relationship works at the center of the earth, too. The prediction of “ ρ_o ” has been expressed as a background value. In formula (1), the “ ρ_o ” value is constant and prediction value. The condition of the second term to be zero should be analyzed and with what respect the prediction has been made should be explained. It also has not been explained what had been meant by “ ω ” symbol.

The gravity senses the total effect and is not sensitive to the calculation of layer information in vertical due to the block lower depth, as the “lateral change” is estimated basically in this method. In spite

of this; seismic waves are lithology sensitive and anisotropic. Seismic velocities are valid in the location where the measurement is made. Seismic waves are transmitted on the boundaries of solid particle and have identities both in shear and pressure.

On page 189, in table 1, seismic velocities corresponding to scale increase of the densities have been written, but their identities explaining whether velocities (V_p or V_s) are pressure or shear wave velocities have not been indicated (Akın, 2016). Whereas; the identity affects the result.

On page 198, in figure 8, profile images in different directions and lengths take place (Akın, 2016). The profile passing through Turkey in W-E directions in profile E and the profile, which has approximately half length in NE-SW direction in profile F, have been displayed as in the length. The vertical exaggeration for both profiles are different and therefore; it causes some confusions in interpretations.

Seismic waves are energy extinct and dynamic facts. Seismic waves in the article are directionless, continuous, point based and have no identity. In velocity maps obtained from active-passive source seismology studies, the magnitudes of velocity are the time dependent magnitudes that have pre and post.

The density is under the control of temperature and pressure, and this effect is not linear. It is inconvenient to apply a linear transformation to a fact which depends on non-linear parameters in the mass and in an environment where the mass non-linearly disperses. The first term of the transformation formula is estimated by prediction method. Thus; the scientific quality of the transformation made is in debate.

If calculations made were handled within scope of approach then the valid interval if available should be stated. A certain velocity distribution map is introduced in the article. The obtained model has been formed bearing several negativities in its body.

3. Result

Earth science studies are multi-disciplinary in terms of their effects and results, and are problem focused investigations that should be solved by the combination of information and experiences decomposed from different educations. Only

qualitative or only quantitative approaches in the solution of problem negatively affect the productivity. Analytical thinking and creativity make both approaches valuable and necessitate both of them to be handled together, but the transitions between them should be based on scientific facts with no doubts.

Bulletin of Mineral Research and Exploration is a publication which has an access via internet, worldwide and organizational characteristic. It fulfills an important emptiness beyond its great role in the area of earth science in Turkey. Its contribution to scientific studies in our country has reached a significant level. The bulletin has a body recording recent professional developments rather than being a magazine. Therefore; it was needed to express opinions in order to ease the scientific sight about the article discussed above.

The author thanks to the editorial board for providing to express his opinions.

References

- Akın, U. 2016. Investigation of the Seismic Velocity Distribution and Crustal Structure of Turkey by Means of Gravity Data. Bulletin of the Mineral Research and Exploration 153, 185-202.
- Barton, P.J. 1986. The relationship between seismic velocity and density in the continental crust - a useful constraint? Geophys. J. R. astr. SOC. 87,195-208.
- Woollard, G.P. 1959. Crustal Structure from Gravity and Seismic Measurements. J. Geophys. Res., 64 (10), 1524-1544.
- Simeoni, O., Brückl, E. 2009. The Effect of Gravity Stripping on the Resolution of Deep Crustal Structures in the Eastern Alps and Surrounding Regions. Austrian Journal of Earth Sciences Volume 102/2 p.157 – 169 Vienna.



Bulletin of the Mineral Research and Exploration

<http://bulletin.mta.gov.tr>



RESPONSE TO THE “REACTION OF THE PHYSICAL TRANSFORMATION OF THE GRAVITY DATA AND LINEARITY DILEMMA”

Uğur AKIN^{a*}

^aGeneral Directorate of Mineral Research and Exploration, Department of Geophysical Researches

Reply

Received: 13.03.2017

Accepted: 22.03.2017

There is not any filter such as the “apparent gravity linear filter”, which is mentioned by the criticizer, in the literature of geophysical potential methods.

The “apparent density filter” was used in the study. As the name implies; the crustal structure of Turkey was investigated in the article of “Investigation of the Seismic Velocity Distribution and the Crustal Structure of Turkey” (Akın, 2016). So; the article had different findings. The “Conrad discontinuity” has been one of the findings of this article. Or else; the distribution related to the Conrad discontinuity has not been the main topic of the article as it had been understood by the criticizer. In this study, the density and seismic velocity took their highest values within first 20 km’s of the continental crust as; 2.74 gr/cm³ and 5.86 km/s, respectively. This zone was considered at the same time as the Conrad discontinuity between the lower and upper crusts, and it had an approximate depth of 16 km.

The statement of “Although their densities are 2-2.2 gr/cm³, the velocities are very high (4.5-5 km/s). That is; the response given to the parameter transformation by these formations, which is the subject of the article, is false” made by the criticizer is rather thought-provoking.

Therefore; the article was reviewed. However; the density of 2-2.2 gr/cm³ and the corresponding velocity

of 4,5-5 km/s mentioned by the criticizer were not encountered in the article. The article has not been carefully read by the criticizer.

Density and velocity maps in this publication were prepared for depths of 20 m as emphasized in figure captions. The apparent density map of Turkey for depth of 20 m in figure 4 in the article showed variation within intervals of 2.55-2.98 gr/cm³. Also; the seismic velocity values of Turkey for 20 km depth in Figure 6 were estimated within intervals of 4.91-6,78 km/s. Basins mentioned by the criticizer by giving examples for Çankırı and Lake Salt is considered as very shallow structures.

Apart from the example basins, which the criticizer mentions about, there are many basins in many places of Turkey. The investigations regarding these basins can surely be carried out by me or by other investigators in the future. However; it can never anticipated personally to answer for some basins in this article.

Therefore; in this study the gravity apparent density data were estimated and different characteristics of the crustal structure were investigated. Besides; simple relationships between the tectonic units and structural zones were utilized. As the name of the article implies, this study was performed in Turkey scale, however; the interpretations of shallow and small scale basins or

* Corresponding author: Uğur Akın, ugurakin11@gmail.com
<http://dx.doi.org/10.19111/bulletinofmre.306030>

other geological structures as the criticizer mentions have never been targeted in this article.

Simeoni and Brückl (2009), applied power spectrum on to gravity Bouguer data. The data of $0,3 \text{ gr/cm}^3 = 300 \text{ kg/m}^3$, which is mentioned in the article, was given as the reference of previous information. The criticizer thought that the density information here had entered into estimations or interpretations. Thus, he completely misunderstood the article. Besides; the information about the Conrad discontinuity have come up due to the abnormal increase in the gravity apparent density at mentioned depth in the article.

The description of “ ω ” symbol, which is said to have not been explained in formula in the article, is already present. The article has not been carefully read by the criticizer.

$$\rho(x,y) = \rho_o + (1/2\pi G) F^{-1}\{(\omega / 1 - e^{-\omega h}) \cdot \Delta g(u,v)\}$$

ω : total number of waves

The formula in the article is in medium of wave number. However; the estimation of prediction value of “ ρ_o ” between the values of 2.7-3.3 gr/cm^3 were continued with 0,1 gr/cm^3 increments until the mean value of the crust is attained. As a result of the estimation, the lowest and the highest densities at different levels of Turkey were obtained as; 2.23 gr/cm^3 and 3 gr/cm^3 , respectively. Nevertheless; the mean density value were estimated as; 2.698 gr/cm^3 .

It is also stated by the criticizer for Figure 8 that, the vertical exaggerations are different and caused confusions in interpretations. Nonetheless; the vertical axes of all sections shown in figure 8 are in the same scale. Almost all sections have different lengths from each other. Therefore; depths and distances on vertical and horizontal axes in interpretations were already described on sections in order to prevent any misunderstanding. The article has been carefully read by the criticizer.

The author would like to thank the criticizer for taking the time to read the article during his very intensive work.

As the general assessment, I could say that the article, which is called the “Investigation of the Seismic Velocity Distribution and Crustal Structure of Turkey by means of Gravity Data”, is a significant

research topic. I also believe that the article findings will enlight the solution of earth science problems from a different point of view. Every researches are open to conceptual contributions and renovations. Therefore; this investigation too will be developed and remediated more as it is in all other research topics by the supports of related earth scientists.

References

- Akın, U. 2016. Gravite verilerinden Türkiye'nin sismik hız dağılımı ve kabuk yapısının ortaya çıkartılması. MTA Dergisi, 153, 185-202.
- Simeoni, O., Brückl, E. 2009. The Effect of Gravity Stripping on the Resolution of Deep Crustal Structures in the Eastern Alps and Surrounding Regions. Austrian Journal of Earth Sciences, Vol 1002/2, 157-169.

BULLETIN OF THE MINERAL RESEARCH AND EXPLORATION NOTES TO THE AUTHORS

1. Aims

The main aims of the journal are

- To contribute to the providing of scientific communication on geosciences in Turkey and the international community.
- To announce and share the researches in all fields of geoscience studies in Turkey with geoscientists worldwide.
- To announce the scientific researches and practices on geoscience surveys carried out by the General Directorate of Mineral Research and Exploration (MTA) to the public.
- To use the journal as an effective media for international publication exchange by keeping the journal in high quality, scope and format.
- To contribute to the development of Turkish language as a scientific language

2. Scope

At least one of the following qualifications is required for publishing the papers in the Bulletin of Mineral Research and Exploration.

2.1. Research Articles

2.1.1. *Original Scientific Researches*

- This type of articles covers original scientific research and its results related to all aspects of disciplines in geoscience.

2.1.2. *Developmental Researches*

- The studies using new approaches and methods to solve any problems related to geosciences and/or the researches by using new approaches and methods to solve any problems related to the science of engineering performed in the General Directorate of Mineral Research and Exploration.

2.1.3. *Review articles*

- This type of papers includes comprehensive scholarly review articles that summarize and

critically assess previous geoscience research with a new perspective and it also reveals a new approach.

2.2. Discussion/Reply

- This type of article is intended for discussions of papers that have already been published in the latest issue of the *Bulletin*.
- The discussion/reply type articles that criticize all or a part of a recently published article, are published in the following first issue, if it is submitted within six months after the distribution of the *Bulletin*.
- The discussions are sent to the corresponding author of the original paper to get their reply, before publication. So that, the discussion and reply articles can be published at the same time, if they can be replied within the prescribed period. Otherwise, the discussion is published alone. Re-criticising of the replies is not allowed. The authors should keep the rules of scientific ethics and discussions in their discussion/reply papers. The papers in this category should not exceed four printed pages of the journal including figures and tables etc. The format of the papers should be compatible with the "Spelling Rules" of the *Bulletin*.

2.3. Short Notes

- Short notes publishing in the *Bulletin* covers short, brief and concisely written research reports for papers including data obtained from ongoing and/or completed scientific researches and practices related to geoscience and new and/or preliminary factual findings from Turkey and worldwide.
- The short notes will follow a streamlined schedule and will normally be published in the following first or second issue shortly after submission of the paper to the *Bulletin*. To meet this schedule, authors should be required to make revisions with minimal delay.
- This type of articles should not exceed four printed pages of the journal including figures, tables and an abstract.

3. Submission and Reviewing of Manuscripts

Manuscript to be submitted for publishing in the Journal must be written clearly and concisely in Turkish and/or English and it should be prepared in the Bulletin of Mineral Research and Exploration style guidelines. All submissions should be made online at the <http://bulletin.mta.gov.tr> website.

- The manuscript submitted for reviews must not have been partially or completely published previously; that it is not under consideration for publication elsewhere in any language; the publication must have been approved by all-co-authors
- The rejected manuscripts are not returned back to author(s) whereas a letter of statement indicating the reason of rejection is sent to the corresponding author.
- Submitted manuscripts must follow the Bulletin style and format guidelines. Otherwise, the manuscript which does not follow the journals' style and format guidelines, is given back to corresponding author without any reviewing.
- Every manuscript which passes initial Editorial treatise is reviewed by at least two independent reviewers selected by the Editors. Reviewers' reports are carefully considered by the Editors before making decisions concerning publication, major or minor revision or rejection.
- The manuscript that need to be corrected with the advices of reviewer(s) is sent back to corresponding author(s) to assess and make the required corrections suggested by reviewer(s) and editors. Authors should prepare a letter of well-reasoned statement explaining which corrections are considered or not.
- The Executive editor (Editorial Board) will inform the corresponding author when the manuscript is approved for publication. Final version of text, tables and figures prepared in the Bulletin of Mineral Research and Exploration style and format guidelines, will need to be sent online and the corresponding author should upload all of the manuscript files by following the instructions given on the screen. In the absence of online submission conditions, the corresponding author should send

four copies of the final version of the manuscript including one original hard copy, and CD by post-mail. The files belonging to manuscript should be clearly and separately named as "Text", "Figures" and "Tables" at the CD.

- To be published in the Bulletin of Mineral Research and Exploration, the printed length of the manuscript should not exceed 30 printed pages of the journal including an abstract, figures and tables. The publication of longer manuscripts will be evaluated by Editorial Board if it can be published or not.

4. Publication Language and Periods

- The Bulletin of Mineral Research and Exploration is published at least two times per year, each issue is published both in Turkish and English.
- Thus, manuscripts are accepted in Turkish or English. The spelling and punctuation guidelines of Turkish Language Institution are preferred for the Turkish issue. However, technical terms related to geology are used in accordance with the decision of the Editorial Board.

5. Spelling Draft

- Manuscripts should be written in word format in A4 (29.7 x 21 cm) size and double-spaced with font size Times New Roman 10-point, margins of 25 mm at the sides, top and bottom of each page. Authors should study carefully a recent issue of the Bulletin of Mineral Research and Exploration to ensure that their manuscript corresponds in format and style.
- The formulas requiring the use of special characters and symbols must be submitted by the symbols part of the Microsoft Office Word Program on computer.
- Initial letters of the words in sub-titles must be capital. The first degree titles in the manuscript must be numbered and left-aligned, 10 point bold Times New Roman must be used. The second degree titles must be numbered and left-aligned, they must be written with 10 point normal Times New Roman. The third degree titles must be numbered and left-aligned, they must be written

with 10 point italic Times New Roman. The fourth degree titles must be left-aligned without having any number; 10 point italic Times New Roman must be used. The text must continue placing a colon after the title without paragraph returns (See:Sample article: <http://bulletin.mta.gov.tr>).

- Line spacing must be left after paragraphs within text.
- Paragraphs must begin with 0.5 mm indent.
- The manuscript must include the below sections respectively;

- Title Page
- Abstract
- Key Words
- Introduction
- Body
- Discussion
- Conclusion
- Acknowledgements
- References

5.1. Title Page

The title page should include:

A short, concise and informative title

The name(s) of the author(s)

The affiliation(s) and address(es) of the author(s)

The e-mail address, telephone and fax numbers of the corresponding author

The title must be short, specific and informative and written with capital letters font size Times New Roman 10-point bold. The last name (family name) and first name of each author should be given clearly. The authors' affiliation addresses (where the actual work was done) are presented below the names and all affiliations with a lower-case superscript letter is indicated immediately after the author's name and in

front of the appropriate address. Provide the full postal address of each affiliation, including the country name and, if available, the e-mail address of each author.

The author who will handle correspondence at all stages of refereeing and publication, also post-publication are to be addressed (the corresponding author) should be indicated and the telephone, FAX and e-mail address given.

Please provide a running title of not more than 50 characters for both Turkish and English issue.

5.3. Abstract

- The article must be preceded by an abstract, which must be written on a separate page as one paragraph, preferably. Please provide an abstract of 150 to 200 words. The abstract should not contain any undefined or non-standard abbreviations and the abstract should state briefly the overall purpose of the research, the principle results and major conclusions. Please omit references, criticisms, drawings and diagrams.
- Addressing other sections and illustrations of the text or other writings must be avoided.
- The abstract must be written with 10-point normal Times New Roman and single-spaced lines.
- "Abstract" must not be given for the writings that will be located in "Short Notes" section.
- English abstract must be under the title of "Abstract".

5.4. Key Words

Immediately after the abstract, please provide up to 5 key words and with each word separated by comma. These key words will be used for indexing purposes.

5.5. Introduction

- The introduction section should state the objectives of the work, research methods, location of the study area and provide an adequate and brief background, by avoiding a detailed literature survey.

- Non-standard or un-common classifications or abbreviations should be avoided but if essential, they must be defined at their first mention and used consistently thereafter.
- When pre-information is needed for facilitating the understanding of the text, this section can also be used (for example, statistical data, bringing out the formulas, experiment or application methods, and others).

5.6. Body

- In this chapter, there must be data, findings and opinions that are intended to convey to the reader about the subject. The body section forms the main part of the article.
- The data used in the other sections such as “Abstract”, “Discussions”, and “Results” is caused by this section.
- While processing subject, care must be taken not to go beyond the objective highlighted in “Introduction” section. The knowledge which do not contribute to the realization of the purpose of the article or are useless for conclusion must not be included.
- All the data used and opinions put forward in this section must prove the findings obtained from the studies or they must be based on a reference by citation.
- Guidance and methods to be followed in processing subjects vary according to the characteristics of the subjects dealt with. Various topic titles can be used in this section as many as necessary.

5.7. Discussions

- This section should state the significance of the results of the work, not repeat them. This must be written as a separate section from the results.

5.8. Conclusions

- The main conclusion of the study provided by data and findings of the research should be stated concisely and concretely in this section.

- The subjects that are not mentioned sufficiently and/or unprocessed in the body section must not be included in this section.
- The conclusions can be given in the form of substances in order to emphasize the results of the research and be understandable expression.

5.9. Acknowledgements

Acknowledgement of people, grants, funds, etc should be placed in a separate section before the reference list. While specifying contributions, the attitude diverted the original purpose of this section away is not recommended. Acknowledgements must be made according to the following examples.

- This study was carried out under the.....project.
- I/we would like to thank to for contributing the development of this article with his/her critiques.
- Academic and / or authority names are written for the contributions made because of requirement of ordinary task requirement.

For example:

“Prof. Dr. İ. Enver Altınlı has led the studies”.

In order to determine the chemistry of chromium minerals, the comments and suggestions of Dr. Tandoğan Engin’s has been considered.

- The contributions made out of the requirement of ordinary task:

For example:

“I would like to thank to Professor Dr. Melih Tokay who gives the opportunity to benefit from unpublished field notes”; “I would like to thank to State Hydraulic Work 5. Zone Preliminary-Plan Chief Engineer Ethem Göğer.” Academic and /or task-occupational titles are indicated for this kind of contributions.

- The contributions which are made because of requirement of ordinary task but do not necessitate responsibility of the contributor must be specified.

For example:

- Such sentences as “I would like to thank to our General Manager, Head of Department or Mr. / Mrs. Presidentwho has provided me the opportunity to research” must be used.

5.10. References

- All references cited in the text are to be present in the reference list.
- The authors must be sure about the accuracy of the references. Publication names must be written in full.
- Reference list must be written in Times New Roman, 9-point type face.
- The reference list must be alphabetized by the last names of the first author of each work.
- If an author’s more than one work is mentioned, ranking must be made with respect to publication year from old to new.
- In the case that an author’s more than one work in the same year is cited, lower-case alphabet letters must be used right after publication year (for example; Saklar, 2011*a, b*).
- If the same author has a publication with more than one co-author, firstly the ones having single author are ranked in chronological order, then the ones having multiple authors are ranked in chronological order.
- In the following examples, the information related to works cited is regulated in accordance with different document/work types, considering punctuation marks as well.
- If the document (periodic) is located in a periodical publication (if an article), the information about the document must be given in the following order: surnames of the author/authors, initial letters of author’s/ authors’ first names. Year of publication. Name of the document. Name of the publication where the document is published, volume and/ or the issue number, numbers of the first and last pages of the document.

For example:

- Pamir, H.N. 1953. Türkiye’de kurulacak bir hidrojeoloji enstitüsü hakkında rapor. Türkiye Jeoloji Bülteni 4, 1, 63-68.
- Barnes, F., Kaya, O. 1963. İstanbul bölgesinde bulunan Karbonifer’in genel stratigrafisi. Maden Tetkik ve Arama Dergisi 61,1-9.
- Robertson, A.H.F. 2002. Overview of the genesis and emplacement of Mesozoic ophiolites in the Eastern Mediterranean Tethyan region. Lithos 65, 1-67.

- If more than one document by the same authors is cited, firstly the ones having single name must be placed in chronological order, then the ones having two names must be listed in accordance with chronological order and second author’s surname, finally the ones having multiple names must be listed in accordance with chronological order and third author’s surname.
- If the document is a book, these are specified respectively: surnames of the author/authors, initial letters of author’s/authors’ first names. Year of publication. Name of the book (initial letters are capital). Name of the organization which has published the book, name of the publication where the document is published, volume and/ or the issue number, total pages of the book.

For example

- Meric, E. 1983. Foraminiferler. Maden Tetkik ve Arama Genel Müdürlüğü Eğitim Serisi 23, 280p.

- Einsele, G. 1992. Sedimentary Basins. Springer-Verlag, p 628.

- If the document is published in a book containing the writings of various authors, the usual sequence is followed for the documents in a periodic publication. Then the editor’s surname and initial letters of their name/names are written. “Ed.” which is an abbreviation of the editor word is written in parentheses. Name of the book containing the document (initial letters are capital). Name of the organization which has published the book. Place of publication, volume number (issue number, if any) of the publication where the document is published, numbers of the first and last page of the document.

For example:

Göncüoğlu, M.C., Turhan, N., Şentürk, K., Özcan, A., Uysal, Ş., Yalınz, K. 2000. A geotraverse across northwestern Turkey. Bozkurt, E., Winchester, J.A., Piper, J.D.A. (Ed.). Tectonics and Magmatism in Turkey and the Surrounding Area. Geological Society of London Special Publication 173, 139-162.

Anderson, L. 1967. Latest information from seismic observations. Gaskell, T.F. (Ed.). The Earth's Mantle. Academic Press. London, 335-420.

- If name of a book where various authors' writings have been collected is specified, those must be indicated respectively: book's editor/editors' surname/surnames, and initial letters of their name/names. "Ed." which is an abbreviation of the editor word must be written in parentheses. Year of Publication. Name of the book (initial letters are capital). Name of the organization which has published the book, total pages of the book.

For example:

Gaskel, T.F.(Ed.)1967. The Earth's Mantle. Academic Press, 520p.

- If the document is an abstract published in a Proceedings Book of a scientific activity such as conference/symposium/workshop ...etc. , information about the document must be given in the following order: surnames of the author/authors, initial letters of author's/authors' first names. Year of publication. Title of the abstract. Name, date and place of the meeting where the Proceedings Book is published, numbers of the first and last pages of the abstract in the Proceedings Book.

For example:

Yılmaz, Y. 2001. Some striking features of the Anatolian geology. 4. International Turkish Geology Symposiums 24-28 September 2001, London, 13-14.

Öztunalı, Ö., Yenyol, M. 1980. Yunak (Konya) yöresi kayaçlarının petrojenezi. Türkiye Jeoloji Kurumu 34. Bilim Teknik Kurultayı, 1980, Ankara, 36

- If the document is one of the unpublished documents as report, lecture notes, and so on., information about the document must be given by writing the word "unpublished" in parentheses to the end of information about the document after it is specified in accordance with usual order which is implemented for a document included in a periodic publication.

For example:

Özdemir, C. Biçen, C. 1971. Erzincan ili, İliç ilçesi ve civarı demir etütleri raporu. *General Directorate of Mineral Research and Exploration Report No: 4461*, 21 p. Ankara (unpublished).

Akyol, E. 1978. Palinoloji ders notları. EÜ Fen Fakültesi Yerbilimleri Bölümü, 45 p., İzmir (unpublished).

- The followings must be specified for the notes of unpublished courses, seminars, and so on: name of the document and course organizer. Place of the meeting. Name of the book, corresponding page numbers.

For example:

Walker, G. R. Mutti, E. 1973. Turbidite facies and facies associations. Pacific Section Society for Sedimentary Geology Short Course. Anaheim. Turbidites and Deep Water Sedimentation, 119-157.

- If the document is a thesis, the following are written: surname of the author, initial letter of the author's first name. Year of Publication. Name of the thesis. Thesis type, the university where it is given, the total number of pages, the city and "unpublished" word in parentheses.

For example:

Seymen, İ. 1982. Kaman dolayında Kırşehir Masifi'nin jeolojisi. Doçentlik Tezi, İTÜ Maden Fakültesi, 145 s. İstanbul (unpublished).

- Anonymous works must be regulated according to publishing organization.

For example:

MTA. 1964. 1/500.000 ölçekli Türkiye Jeoloji Haritası, İstanbul Paftası. Maden Tetkik ve Arama Genel Müdürlüğü, Ankara.

- The date, after the name of the author, is not given for on-printing documents; “in press” and / or “on review” words in parenthesis must be written. The name of the article and the source of publication must be specified, volume and page number must not be given.

For example:

Ishihara, S. The granitoid and mineralization. *Economic Geology 75th Anniversary* (in press).

- Organization name, web address, date of access on web address must be indicated for the information downloaded from the Internet. Turkish sources must be given directly in Turkish and they must be written with Turkish characters.

For example:

ERD (Earthquake Research Department of Turkey). <http://www.afad.gov.tr>. March 3, 2013.

- While specifying work cited, the original language must be used; translation of the title of the article must not be done.

6. Illustrations

- All drawings, photographs, plates and tables of the article are called “illustration”.
- Illustrations must be used when using of them is inevitable or they facilitate the understanding of the subject.
- While selecting and arranging the illustrations’ form and dimensions, page size and layout of the Bulletin must be considered, unnecessary loss of space must be prevented as much as possible.
- The pictures must have high quality, high resolution suitable for printing.
- The number of illustrations must be proportional to the size of the text.
- All illustrations must be sent as separate files independent from the text.
- While describing illustrations in the text, abbreviations must be avoided and descriptions

must be numbered in the order they are mentioned in the text.

- Photographs and plates must be given as computer files containing EPS, TIFF, or JPEG files in 600 dpi and higher resolutions (1200 dpi is preferred) so that all details can be seen in the stage of examination of writing.

6.1. Figures

- Drawings and photos together but not the plate in the text can be evaluated as “Figure” and they must be numbered in the order they are mentioned in the text.
- The figures published in the Bulletin of Mineral Research and Exploration must be prepared in computer environment considering the dimensions of single-column width 7.4 m or double-column width 15.8 cm. Figure area together with the writing at the bottom should not exceed a maximum 15.8x21.
- Figures must not be prepared in unnecessary details or care must be taken not to use a lot of space for information transfer.
- Figures must be arranged to be printed in black-and-white or colored. The figure explanations being justified in two margins must be as follows:
- Figure 1 -Sandıklı Town (Afyon); a) Geological map of the south-west, b) general columnar section of the study area (Seymen 1981), c) major neotectonic structures in Turkey (modified from Koçyiğit 1994).
- Drawings must be drawn by well-known computer programs painstakingly, neatly and cleanly.
- Using fine lines which can disappear when figures shrink must be avoided. Symbols or letters used in all drawings must be Times New Roman and not be less than 2 mm in size when shrink.
- All the standardized icons used in the drawings must be explained preferably in the drawing or with figure caption if they are very long.
- Linear scale must be used for all drawings. Author’s name, figure description, figure number must not be included into the drawing.

- Photos must have the quality and quantity that will reflect the objectives of the subject.

6.2. Plates

- Plates must be used when needed a combination of more than one photo and the publication on a special quality paper.
- Plate sizes must be equal to the size of available magazine pagespace.
- Figure numbers and linear scale must be written under each of the shapes located on the Plate.
- The original plates must be added to the final copy which will be submitted if the article is accepted.
- Figures and plates must be independently numbered. Figures must be numbered with Latin numerals and plates with Roman numerals (e.g., Figure1, Plate I).
- There must be no description text on Figures.

6.3. Tables

- Tables must be numbered consecutively in accordance with their appearance in the text.
- All tables must be prepared preferably in word format in Times New Roman fonts.
- Tables together with table top writing must not exceed 15x8 cm size.
- The table explanations being justified in two margins must be as follows:

Table 1- Hydrogeochemical analysis results of geothermal waters in the study area.

7. Nomenclature and Abbreviations

- Non-standard and uncommon nomenclature abbreviations should be avoided in the text. But if essential, they must be described as below: In cases where unusual nomenclatures and unstandardized abbreviations are considered to be compulsory, the followed way and method must be described.
- Full stop must not be placed between the initials of words for standardized abbreviations (MER, SHW, etc.).

- Geographical directions must be abbreviated in English language as follows: N, S, E, W, NE ...etc.

- The first time used abbreviations in the text are presented in parenthesis, the parenthesis is not used for subsequent uses.

- The metric system must be used as units of measurement.

- Figure, plate, and table names in the article must not be abbreviated. For example, “as shown in generalized stratigraphic cross-section of the region (Figure 1.....)”

7.1. Stratigraphic Terminology

Stratigraphic classifications and nomenclatures must be appropriate with the rules of International Commission on Stratigraphy and/or Turkey Stratigraphy Committee. The formation names which have been accepted by International Commission on Stratigraphy and/or Turkey Stratigraphy Committee should be used in the manuscript.

7.2. Paleontologic Terminology

- Fossil names in phrases must be stated according to the following examples:

a. For the use of authentic fossil names:

e.g. Calcareous sandstone with *Nummulites*

b. When the authentic fossil name is not used.

e.g. nummulitic Limestone

c. Other examples of use;

e.g. The type and species of *Alveolina/ Alveolina* type and species

- Taxonomic ranks must be made according to following examples:

- The names of the fossils should be stated according to the rules mentioned below:

| | |
|--|--|
| Super family: Alveolina Ehrenberg, 1939 Family: Borelidae Schmarda, 1871 Type genus: <i>Borelis</i> de Montfort, 1808 Type species: <i>Borelis melenoides</i> de Montfort, 1808; <i>Nautilus melo</i> Fitchel and Moll, 1789 | <i>Not reference, Not stated in the Reference section</i> |
| <i>Borelis vonderschmitti</i> (Schweighauser, 1951) (Plate, Figure, Figure in Body Text) | Schweighauser, 1951 not reference |
| 1951 <i>Neoalveolina vonderschmitti</i> Schweighauser, page 468, figure 1-4 | Cited Schweighauser (1951), stated in the Reference section. |
| 1974 <i>Borelis vonderschmitti</i> (Schweighauser), Hottinger, page, 67, plate 98, figure 1.7 | Cited Hottinger (1974), stated in the Reference section. |

- a. For the first use of the fossil names, the type, species and the author names must be fully indicated

Alveolina aragoensis Hottinger

Alveolina cf. *aragoensis* Hottinger

Alveolina aff. *aragoensis* Hottinger

- b. When a species is mentioned for the second time in the text:

A. aragoensis

A. cf. aragoensis

A. aff. aragoensis

- c. It is accepted as citation if stated as *Alveolina aragoensis* Hottinger (1966)

- The statement of plates and figures (especially for articles of paleontology):

- a. for statement of the species mentioned in the body text

Borelis vonderschmitti (Schweighauser, 1951).

(plate, figure, figure in the body text).

- b. When citing from other articles

1951 *Neoalveolina vonderschmitti* Schweighauser, page 468, figure 1-4, figure in body text

1974 *Borelis vonderschmitti* (Schweighauser), Hottinger, page 67, plate 98, figure 1-7

For the citation in the text

(Schweighauser, 1951, page, plate, figure, figure in the body text)

(Hottinger, 1974, page, plate, figure 67, plate 98, figure 1-7, figure in the bodytext.)

8. Citations

All the citations in the body text must be indicated by the last name of the author(s) and the year of publication, respectively. The citations in the text must be given in following formats.

- For publications written by single author:

- It is known that fold axial plain of Devonian and Carboniferous aged units around Istanbul is NS oriented (Ketin, 1953, 1956; Altınlı, 1999).

- Altınlı (1972, 1976) defined the general characteristics of Bilecik sandstone

- For publications written by two authors:

- The upper parts of the unit contain Ilerdian fossils (Keskin and Turhan, 1987, 1989).

- For publications written by three or more authors:

According to Caner et al. (1975) Alicı formation reflects the fluvial conditions.

The unit disappears wedging out in the East direction (Tokay et al., 1984).

- If reference is not directly obtained but can be found in another reference, cross-reference should be given as follows:

- It is known that Lebling has mentioned the existence of Lias around Çakraz (Lebling, 1932: from Charles, 1933).

9. Reprints

The author(s) will receive 2 two hard copies of the related issues.

10. Copyright and Conditions of Publication

- It is a condition of publication that work submitted for publication must be original, previously unpublished in whole or in part.
- It is a condition of publication that the authors who send their publications to the Bulletin of Mineral Research and Exploration hereby accept the conditions of publication of the Bulletin in advance.
- All copyright of the accepted manuscripts belong to MTA. The author or corresponding author on behalf of all authors (for papers with multiple authors) must sign and give the agreement under the terms indicated by the Regulations of Executive Publication Committee. Upon acceptance of an article, MTA can pay royalty to the authors upon their request according to the terms under the “Regulations of Executive Publication Committee” and the “Regulations of Royalty Payment of Public Office and Institutions”

All the information and forms about the Bulletin of Mineral Research and Explorations can be obtained from <http://bulletin.mta.gov.tr>